

OPG's DEEP GEOLOGIC

REPOSITORY

FOR LOW & INTERMEDIATE LEVEL WASTE

Supporting Technical Report

Phase I Hydrogeologic Modelling

November 30, 2008

Prepared by:

J.F. Sykes, E.A. Sykes, S.D. Normani,

Y. Yin and Y.-J. Park

University of Waterloo

OPG 00216-REP-01300-00009-R00



OPG's DEEP GEOLOGIC

REPOSITORY

FOR LOW & INTERMEDIATE LEVEL WASTE

Supporting Technical Report

Phase I Hydrogeologic Modelling

November 30, 2008

Prepared by:

J.F. Sykes, E.A. Sykes, S.D. Normani,

Y. Yin and Y.-J. Park

University of Waterloo

OPG 00216-REP-01300-00009-R00

DOCUMENT HISTORY

EXECUTIVE SUMMARY

A Deep Geologic Repository (DGR) for Low and Intermediate Level (L&IL) Radioactive Waste has been proposed by Ontario Power Generation (OPG) for the Bruce site near Tiverton, Ontario Canada. This report presents hydrogeologic modelling and analyses at the regional-scale and site-scale that were completed as part of the Phase 1 Geosynthesis DGR work program. As envisioned, the DGR is to be constructed at a depth of about 680 m below ground surface within the argillaceous Ordovician limestone of the Cobourg Formation. The objective of this report is to develop a geologic conceptual model for the DGR site and to describe modelling using FRAC3DVS-OPG and analyses that illustrate the influence of conceptual model, parameter and scenario uncertainty on predicted long-term geosphere barrier performance. The modelling also provides a framework for hydrogeologic and geochemical investigations of the DGR. It serves as a basis for exploring potential anthropogenic and natural perturbations of the sedimentary sequence beneath and in the vicinity of the Bruce site. The modelling framework also provides a basis for examining the long-term stability of the site's deep groundwater system.

Within the geologic setting of southern Ontario, the Bruce site is located west of the Algonquin Arch within the Bruce Megablock, positioned along the eastern edge of the Michigan Basin. Well logs have been used to define the structural contours at the regional and site-scale of the up to 31 bedrock units/formation/groups that may be present above the Precambrian crystalline basement. In this Phase 1 study, all units/formation/groups are assumed to be water saturated. The regional-scale domain is restricted to a region extending from Lake Huron to Georgian Bay. From a hydrogeologic perspective, the domain can be subdivided into three horizons: a shallow zone characterized by the units of the Devonian and extending to the base of the Bass Islands Formation; an intermediate zone that includes the low permeability units of the Salina and the more permeable Niagaran Group and extends from the base of the Bass Islands Formation to the Manitoulin Formation; and a deep groundwater domain or zone that extends from the base of the Manitoulin to the Precambrian and which includes the Ordovician shales and carbonates, such as the Cobourg Formation, with water with high total dissolved solids (TDS) concentrations that range up to 300 g/L. The deep zone also includes the permeable Cambrian Formation. The conceptual model of the Bruce DGR site required the development of constitutive models that relate the fluid density and viscosity to the fluid total dissolved solids and pressure.

Sensitivity analyses can be computationally intensive, particularly for large scale dynamic problems that couple flow and mass transport. The analyses are therefore iterative beginning with the investigation of the postulated most important parameters, and as the study progresses, resolving issues related to parameters that are deemed to be of lesser importance. The development and listing of scenarios and site attributes in a hierarchical manner based on importance facilitated the development of a parameter sensitivity analysis. Also important in the sensitivity analysis was the selection of the performance measure used to evaluate the system. The traditional metric of average water particle travel time is inappropriate for geologic units where solute transport is controlled by diffusion. The use of lifetime expectancy and the related groundwater age is a more appropriate metric for such a system. Lifetime expectancy can be estimated by determining the time required for a water particle at a spatial position in a groundwater system to reach a potential outflow point. Groundwater age of a water particle at a spatial position can be determined by the time elapsed since the water particle entered the system from a boundary condition. The variables for both age and lifetime expectancy are

random variables and as such their behaviour can be characterized by that of a probability density function (PDF) describing the distribution of water particles with respect to time. The mean age or mean life expectancy (MLE) can be determined by taking the first moment of the PDF solution for the travel time of a particle.

The groundwater velocities are density-dependent and hence a fully-coupled transient flow and brine transport analysis is required for their estimation. A pseudo-equilibrium solution was determined at 1 million years after the imposition of an initial total dissolved solids distribution in the regional domain. The boundary conditions for the base-case analysis were time invariant while the hydrologic parameters are based, in part, on measurements from borehole tests at the Bruce site. For the base-case analysis, the Mean Life Expectancy in the Cobourg Formation in the vicinity of the proposed repository was conservatively estimated to be more than 8.9 million years. A density-independent analysis that used the base-case parameters and the same boundary conditions as the density-dependent analyses yielded paths from the DGR that are different than those of the base-case density-dependent analysis. The travel time estimates for the average water particles are not indicative of solute transport migration time as the estimates do not include the impact of either diffusion or mechanical dispersion. The Mean Life Expectancies for both the density-dependent and density-independent cases were similar, reflecting the dominance of diffusion for solute transport in the Ordovician units.

The environmental head profile from the assumed TDS concentrations and measured pressures at the composite DGR-1 and DGR-2 borehole indicate that the Cambrian is over-pressured relative to the elevation of the surface while the Ordovician shale and limestone units are significantly under-pressured. The Cambrian pinches out east of the DGR site and west of the Algonquin Arch. An essential requirement of the abnormal pressures of the Cambrian is overlying extensive low vertical hydraulic conductivity strata. The low pressures in the Ordovician may be the result of stress relief as a result of significant removal of mass through erosion, that was at a rate that is greater than that of water influx to these low permeability units from the over- and under-lying units with higher pressure; the pressure distribution is still evolving. The low pore fluid pressures also may indicate the presence of a trapped non-wetting gas phase that would result in an effective hydraulic conductivity that is significantly less than the corresponding saturated hydraulic conductivities for the units. Consistent with both interpretations is the requirement of vertical hydraulic conductivities that are on the order of 1×10^{-14} m/s or lower for the Ordovician units.

The impact of glaciation and deglaciation on the groundwater system was investigated in a paleoclimate scenario. The model results indicate that basal meltwater does not penetrate below the units of the Salina at the DGR site. The most significant consequence of glacial loading is the generation of higher pressures throughout the rock column, with the level dependent on the one-dimensional loading efficiency of the rock mass. The estimation of the pressures during glaciation was undertaken assuming saturated flow conditions; the presence of a possible gas phase in the Ordovician would result in a different pressure distribution.

The analyses to examine the time frame for the transient dissipation of the observed elevated pressures in the Cambrian and low pressures in the Ordovician units indicate that the effective vertical hydraulic conductivity for the Ordovician units is on the order of 1×10^{-14} m/s and possibly lower. The simulations of the paleoclimate scenario support the conclusion that it is unlikely that the environmental head profile at the composite DGR-1/DGR-2 borehole is related to

stress loading during glaciation and stress relief during deglaciation as a result of the time of ice-sheet loading relative to the duration of load relief. It also is concluded that the profile is related to a state that is different from the state observed at the present and as characterized by the geological framework model and boundary conditions. In either an equilibrium or a disequilibrium model, the profile is a result of past boundary conditions and stresses that are different from those observed today and used in the base-case analysis. Regardless of whether a gas phase is present, in the equilibrium model the pressures in the Cambrian and Ordovician are static and the pore waters essentially stagnant. In the disequilibrium model, the pressures are slowly evolving, in a geologic time sense, to a distribution that is compatible with the boundary conditions and stresses of the currently observed state; flow will be converging on the Ordovician from the overlying Niagaran and the underlying Cambrian. From a solute transport perspective, regardless of state, the analyses and interpretation of this study indicate that migration of solutes in the Ordovician units is diffusion dominant.

ACKNOWLEDGEMENTS

This work of this report has been undertaken with valuable guidance and insight from Bob Leech of Gartner Lee Limited and Mark Jensen of Ontario Power Generation. The support of Ed Sudicky is also acknowledged.

CONTENTS

| | Page |
|---|-------------|
| EXECUTIVE SUMMARY | v |
| ACKNOWLEDGEMENTS | ix |
| 1. INTRODUCTION | 1 |
| 1.1 Geological Framework | 4 |
| 1.2 Regional-Scale Conceptual Model | 6 |
| 1.3 Scope and Objectives | 8 |
| 2. GEOLOGICAL AND GEOCHEMICAL FRAMEWORK | 12 |
| 2.1 DGR Phase 1 Site Investigation | 12 |
| 2.2 Geological Units | 14 |
| 2.3 Geological Reconstruction | 16 |
| 2.3.1 Preliminary Geologic Framework Model | 16 |
| 2.3.2 The GLL00 Geologic Framework Model | 18 |
| 2.3.3 Incorporating the GLL00 Model in the Regional-Scale Numerical Model | 21 |
| 2.4 Geochemistry | 21 |
| 2.5 Hydrogeologic Parameters | 25 |
| 3. NUMERICAL MODEL DESCRIPTION AND THEORY | 29 |
| 3.1 FRAC3DVS-OPG | 29 |
| 3.1.1 Model Description | 29 |
| 3.1.2 Density-Dependent Flow and Transport | 31 |
| 3.1.3 Equivalent Freshwater Heads and Environmental Heads | 33 |
| 3.1.4 Numerical Implementation | 33 |
| 3.1.5 Implementation of Paleoclimate and Surface Boundary Conditions | 34 |
| 3.2 System Performance Measures | 35 |
| 3.2.1 Sensitivity Coefficients | 36 |
| 3.2.2 Lifetime Expectancy as a Performance Indicator | 37 |
| 3.2.2.1 Age and Lifetime Statistics | 38 |
| 3.2.2.2 Direct Solutions for Mean Age and Life Expectancy | 38 |
| 4. REGIONAL-SCALE CONCEPTUAL MODEL | 40 |
| 4.1 Model Domain | 40 |
| 4.2 Flow Boundary and Initial Conditions | 40 |
| 4.3 Hydraulic and Transport Parameters | 41 |
| 4.3.1 Total Dissolved Solids | 42 |
| 4.4 Alternate Scenarios for the Regional-Scale System | 47 |
| 5. REGIONAL-SCALE GROUNDWATER FLOW AND BRINE MIGRATION ANALYSES | 51 |
| 5.1 Analysis of the Base-Case for the Regional-Scale Domain | 51 |
| 5.2 Characteristics of Estimates of Mean Life Expectancy | 57 |
| 5.3 Regional Scale Simulations: Analysis of Alternate Cases | 63 |

| | | |
|-----------|---|------------|
| 5.3.1 | Summary of Scenario Analyses | 63 |
| 5.3.2 | Analysis of the Surface Boundary Condition | 63 |
| 5.3.3 | Investigation of Geological Framework Model | 65 |
| 5.3.4 | Density-Independent Flow | 65 |
| 5.3.5 | Alternate Hydraulic Conductivity Models for the Ordovician and Silurian Units | 68 |
| 5.3.6 | Analysis of the Lateral Boundary Condition | 70 |
| 5.3.7 | Analyses of the Cambrian | 74 |
| 6. | PALEOCLIMATE ANALYSIS | 76 |
| 6.1 | Long-term Climate Change | 76 |
| 6.2 | Simulation Results | 79 |
| 6.3 | Dissipation of Pressures from Glacial Loading | 86 |
| 7. | SITE-SCALE GROUNDWATER FLOW MODEL | 88 |
| 7.1 | Site-Scale Conceptual Model | 89 |
| 7.2 | Development of the Embedment Approach for Site-Scale Modelling | 91 |
| 7.2.1 | Verification of the Embedment Approach | 91 |
| 7.2.2 | Comparison of the Model-in-Model and Embedment Approaches | 92 |
| 7.3 | Site-Scale Analyses | 92 |
| 7.3.1 | Analysis of Measured Pressure Profile at the Composite DGR-1 and DGR-2 Borehole | 92 |
| 7.3.2 | Analysis of Dewatering at the DGR | 99 |
| 8. | DISCUSSION AND CONCLUSIONS | 102 |
| 8.1 | Overview of the Regional-Scale Groundwater System | 103 |
| 8.2 | Analysis of the Composite DGR-1 and DGR-2 Pressure Profile | 104 |
| 8.3 | Analyses of the Regional-Scale Groundwater System | 105 |
| 8.4 | Mean Life Expectancy | 106 |
| 8.5 | Regional-Scale Paleoclimate Analyses | 108 |
| 8.6 | The Spatial Extent of the Regional-Scale Domain | 108 |
| 8.7 | Geologic Structure | 109 |
| 8.8 | Summary of Key Study Findings | 110 |
| 8.9 | Stakeholder Questions | 110 |
| 9. | REFERENCES | 116 |

LIST OF TABLES

| | Page | |
|----------|---|----|
| Table 1. | Core log, hydraulic test data and geochemical data for DGR-1 and DGR-2. | 13 |
| Table 2. | Three-dimensional geological framework unit thickness compared with DGR site data | 25 |
| Table 3. | Paleozoic hydraulic conductivities from Raven et al. (1992) | 27 |
| Table 4. | Paleozoic hydraulic conductivities from Golder Associates Ltd (2003) | 27 |
| Table 5. | Paleozoic hydraulic conductivities from Novakowski and Lapcevic (1988) | 28 |

| | | |
|-----------|---|-----|
| Table 6. | Paleozoic hydraulic conductivities from Intera Engineering Ltd. (1988) | 28 |
| Table 7. | Material hydraulic properties for base case scenario analysis. | 43 |
| Table 8. | Fluid and rock compressibilities | 43 |
| Table 9. | Transport parameters | 44 |
| Table 10. | Initial TDS and relative concentrations with respect to 300 g/L for base case preliminary and GLL00 geology | 45 |
| Table 11. | Parameters, boundary conditions and initial conditions for regional-scale analyses | 50 |
| Table 12. | Summary of normalized sensitivity coefficients of MLE to hydraulic conductivity of the Ordovician limestone, siltstone and shale units. | 63 |
| Table 13. | Estimated Mean Life Expectancy at the DGR for the scenarios investigated in this study. | 64 |
| Table 14. | The Peclet numbers at the location of the proposed DGR for the base-case scenario and Scenarios 8, 9 and 10 | 69 |
| Table 15. | Key findings from the Scenario analyses of this study | 107 |

LIST OF FIGURES

| | Page | |
|------------|---|----|
| Figure 1. | Location of proposed DGR site. | 1 |
| Figure 2. | Paleozoic stratigraphy of southwestern Ontario from locations in the Michigan Basin, Algonquin Arch and Appalachian Basin (modified from Armstrong and Carter (2006)) | 2 |
| Figure 3. | Spatial extent of the Michigan Basin and locations of the Frontenac Arch, Algonquin Arch, Chatham Sag, Findlay Arch, and Cincinnati Arch. | 4 |
| Figure 4. | Major structural boundaries of southern Ontario and interpreted tectonic block boundaries derived from Landsat imagery by (Sanford et al., 1985). | 5 |
| Figure 5. | Elevation of the Great Lakes | 7 |
| Figure 6. | Regional scale elevations and river courses | 8 |
| Figure 7. | Environmental heads in a composite DGR-1 and DGR-2 borehole based on pressures measured on March 3, 2008. | 14 |
| Figure 8. | Location of OGSR boreholes. | 17 |
| Figure 9. | Map of bedrock subcrop beneath the glacial sediments of southern Ontario | 19 |
| Figure 10. | The spatial extent of the Cambrian in the regional domain. | 22 |
| Figure 11. | The spatial extent of the Niagaran (refer to the Middle Silurian in the legend) in the regional domain. | 22 |
| Figure 12. | The regional domain below the drift. | 23 |
| Figure 13. | The regional domain showing all geological units. | 23 |
| Figure 14. | The regional domain showing all geological units with no vertical exaggeration. | 24 |
| Figure 15. | Fence diagram of the regional domain showing all geological units. | 24 |
| Figure 16. | Conceptualized relationship between density and concentration. | 26 |
| Figure 17. | Base case equivalent freshwater head (m) distribution. | 52 |
| Figure 18. | Fence diagram of the base-case equivalent freshwater head (m) distribution. | 53 |
| Figure 19. | Base-case environmental head (m) distribution. | 54 |
| Figure 20. | Fence diagram of the base-case environmental head (m) distribution. | 54 |
| Figure 21. | Base-case Total Dissolved Solids distribution. | 55 |

| | | |
|------------|--|----|
| Figure 22. | Base-case pore water velocity magnitude (m/a) distribution. | 56 |
| Figure 23. | Fence diagram of base-case ratio of vertical velocity to velocity magnitude. | 56 |
| Figure 24. | Base-case mean life expectancy (years). | 57 |
| Figure 25. | Fence diagram showing base-case mean life expectancy (years). | 58 |
| Figure 26. | Fence diagram showing path of average water particles released from the vicinity of the proposed DGR. | 58 |
| Figure 27. | Mean Life Expectancy at the DGR as a function of pseudo-equilibrium time for the base case parameters. | 60 |
| Figure 28. | Fence diagram showing normalized sensitivity coefficients of MLE to the hydraulic conductivity of the Queenston siltstone and shale for the base case parameters. | 61 |
| Figure 29. | Fence diagram showing normalized sensitivity coefficients of MLE to the hydraulic conductivity of the Georgian Bay/Blue Mountain shale for the base case parameters. | 62 |
| Figure 30. | Fence diagram showing normalized sensitivity coefficients of MLE to the hydraulic conductivity of the Cobourg limestone for the base case parameters. | 62 |
| Figure 31. | Environmental head (m) distribution for base-case parameters and preliminary geological framework model. | 66 |
| Figure 32. | Mean life expectancy (years) for base-case parameters and preliminary geological framework model. | 66 |
| Figure 33. | Fence diagram showing path of average water particles released from the vicinity of the proposed DGR for the case with density-independent flow. | 68 |
| Figure 34. | Environmental head (m) distribution for base case parameters with high permeability zone along domain boundaries (Scenario 16). | 71 |
| Figure 35. | Fence diagram of environmental head (m) distribution for base case parameters with high permeability zone along domain boundaries (Scenario 16). | 71 |
| Figure 36. | Velocity magnitude for base case parameters with high permeability zone along domain boundaries (Scenario 16). | 72 |
| Figure 37. | Fence diagram of ratio of vertical velocity to velocity magnitude for base case parameters with high permeability zone along domain boundaries (Scenario 16). | 72 |
| Figure 38. | Mean Life Expectancy distribution for base case parameters with high permeability zone along domain boundaries (Scenario 16). | 73 |
| Figure 39. | Fence Diagram of Mean Life Expectancy distribution for base case parameters with high permeability zone along domain boundaries (Scenario 16). | 73 |
| Figure 40. | Time series plots of (a) permafrost depth, (b) ice load in equivalent metres of water for climate simulation nn9930, and (c) simulated environmental heads for Scenario 17 in the Guelph Formation of the Niagaran Group, Cobourg and Cambrian for a loading efficiency of zero. | 77 |
| Figure 41. | Triangulated Irregular Network (TIN) used to interpolate properties for the regional-scale spatial domain from grid blocks of the Peltier (2008) nn9930 glacial model. | 78 |
| Figure 42. | Environmental heads at 90,000a bp for Scenario 17 and a loading efficiency of zero. | 80 |
| Figure 43. | Environmental heads at 60,000a bp for Scenario 17 and a loading efficiency of zero. | 81 |
| Figure 44. | Environmental heads at 30,000a bp for Scenario 17 and a loading efficiency of zero. | 81 |

| | | |
|------------|---|-----|
| Figure 45. | Environmental heads at the present for Scenario 17 and a loading efficiency of zero. | 82 |
| Figure 46. | Total dissolved solids distribution at the present for the paleoclimate simulation with the base case parameters and a loading efficiency of zero. | 82 |
| Figure 47. | Block-cut diagram showing pore water velocity magnitude at the present for the base case parameters and a loading efficiency of zero. | 83 |
| Figure 48. | Fence diagram showing the ratio of the vertical pore water velocity to the velocity magnitude at the present for the base case parameters and a loading efficiency of zero. | 83 |
| Figure 49. | Block-cut diagram showing the depth of penetration of a tracer at the present for the base case parameters and a loading efficiency of zero. | 84 |
| Figure 50. | Time series plots of (a) permafrost depth, (b) ice load in equivalent metres of water for climate simulation nn9930, and (c) recharge for a loading efficiency of zero. | 85 |
| Figure 51. | Time series plots of (a) permafrost depth, (b) ice load in equivalent metres of water for climate simulation nn9930, and (c) simulated environmental heads for Scenario 17 in the Guelph Formation of the Niagaran Group, Cobourg and Cambrian for a loading efficiency of one. | 86 |
| Figure 52. | Regional-scale discretization showing location of site-scale spatial domain. . | 89 |
| Figure 53. | Regional-scale discretization showing site-scale discretized spatial domain. | 90 |
| Figure 54. | Regional-scale discretization showing vertical details of site-scale discretized spatial domain. | 90 |
| Figure 55. | Predicted equivalent freshwater head profile at DGR-2 for base case parameters and no pressure support for the Niagaran or Cambrian at various times. | 94 |
| Figure 56. | Predicted environmental head profile at DGR-2 for base case parameters and no pressure support for the Niagaran or Cambrian. at various times | 95 |
| Figure 57. | Predicted equivalent freshwater head profile at DGR-2 for base case parameters; pressure support for the Cambrian and no pressure support for the Niagaran at various times. | 95 |
| Figure 58. | Predicted environmental head profile at DGR-2 for base case parameters; pressure support for the Cambrian and no pressure support for the Niagaran at various times. | 96 |
| Figure 59. | Predicted equivalent freshwater head profile at DGR-2 for base case parameters; pressure support for both the Niagaran and the Cambrian at various times. | 96 |
| Figure 60. | Predicted environmental head profile at DGR-2 for base case parameters; pressure support for both the Niagaran and the Cambrian at various times. . | 97 |
| Figure 61. | Predicted equivalent freshwater head profile at DGR-2 for base case parameters; pressure support for the Niagaran and no pressure support for the Cambrian at various times. | 97 |
| Figure 62. | Predicted environmental head profile at DGR-2 for base case parameters; pressure support for the Niagaran and no pressure support for the Cambrian at various times. | 98 |
| Figure 63. | Environmental heads at 1 million years for dewatering at the location of the proposed DGR. | 99 |
| Figure 64. | TDS concentration distribution at 1 million years for dewatering at the location of the proposed DGR. | 100 |

| | | |
|------------|---|-----|
| Figure 65. | Pore water velocity magnitude at 1 million years for dewatering at the location of the proposed DGR. | 100 |
| Figure 66. | Ratio of vertical velocity to velocity magnitude at 1 million years for dewatering at the location of the proposed DGR. | 101 |

APPENDICES

| | Page |
|---|-------------|
| Appendix A: Tables of Properties for Scenario Analyses | 121 |
| Appendix B: Analysis of Surface Boundary Condition | 129 |
| Appendix C: Impact of Constant Fluid Density | 137 |
| Appendix D: Alternate Hydraulic Conductivity Distributions for the Ordovician Formations | 143 |
| Appendix E: Alternate Hydraulic Conductivity Distributions for the Silurian Formations . | 147 |
| Appendix F: Cambrian Heterogeneity | 157 |
| Appendix G: Paleoclimate Simulations | 175 |
| Appendix H: Dissipation of an Initial High Freshwater Head | 199 |
| Appendix I: Sub-gridding Verification | 209 |
| Appendix J: Analysis of Pressure Distribution at DGR-1/DGR-2 | 227 |

1. INTRODUCTION

A Deep Geologic Repository (DGR) for Low and Intermediate Level (L&IL) radioactive waste has been proposed by Ontario Power Generation (OPG) for the Bruce site on the shore of Lake Huron near Tiverton, Ontario (Figure 1). The DGR is to be excavated at a depth of approximately 680 m within the argillaceous limestone of the Ordovician Cobourg Formation (Figure 2). In order to reasonably assure safety of the radioactive waste at the site and to better understand the geochemistry and hydrogeology of the formations surrounding the proposed DGR, a regional-scale and site-scale numerical modelling study has been completed, as reported herein. This numerical modelling study provides a framework to investigate the groundwater flow system as it relates to and potentially affects the safety and long-term performance of the DGR. The integrity and long-term stability of the sedimentary sequence that isolates the DGR from the biosphere is assessed for timeframes of 1 million years and beyond.

This regional and site-scale hydrogeological modelling study is one of seven studies that comprise the Phase 1 Geosynthesis Program of the DGR (Gartner Lee Limited, 2008a). The other six studies include: Phase 1 Regional Geology Study (Gartner Lee Limited, 2008b), Regional Hydrogeochemistry (Hobbs et al., 2008), Regional Geomechanics, Long-Term Climate Change (Peltier, 2008), and site specific Geomechanical Stability. The regional-scale modelling

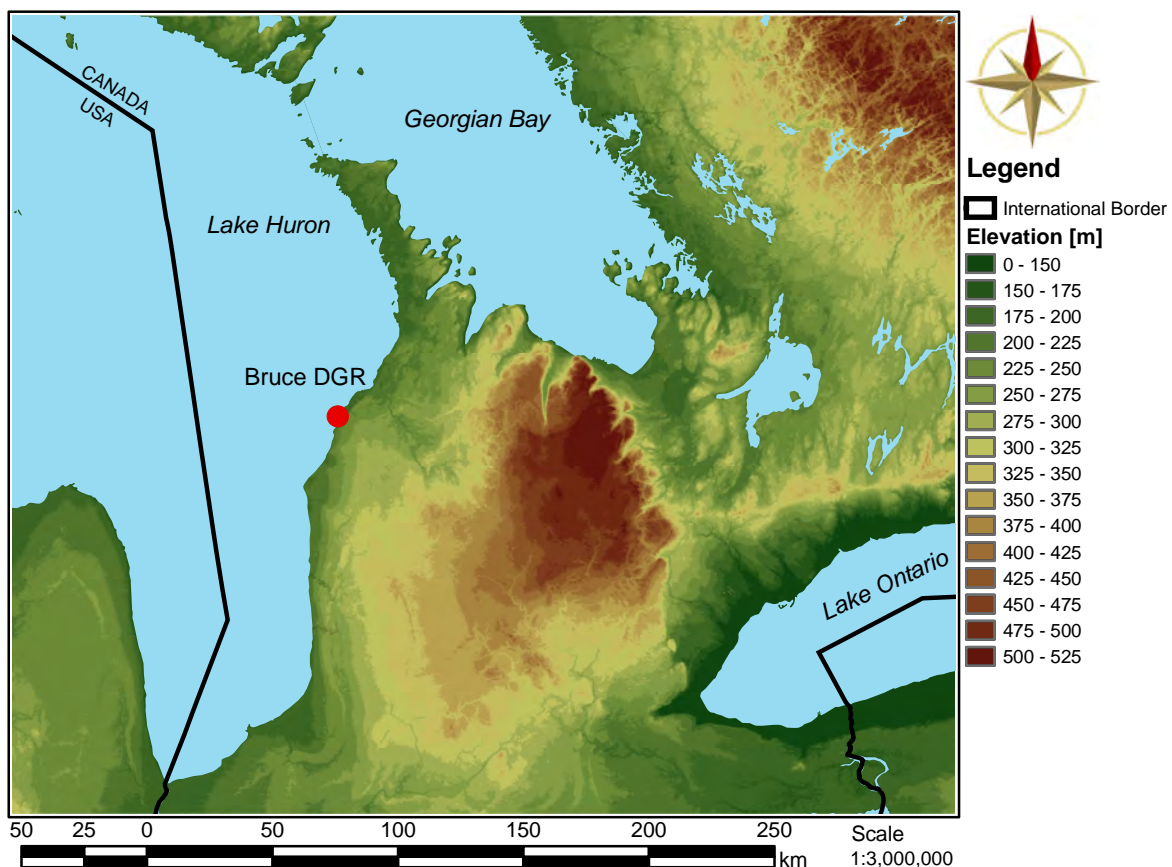


Figure 1: Location of proposed DGR site.

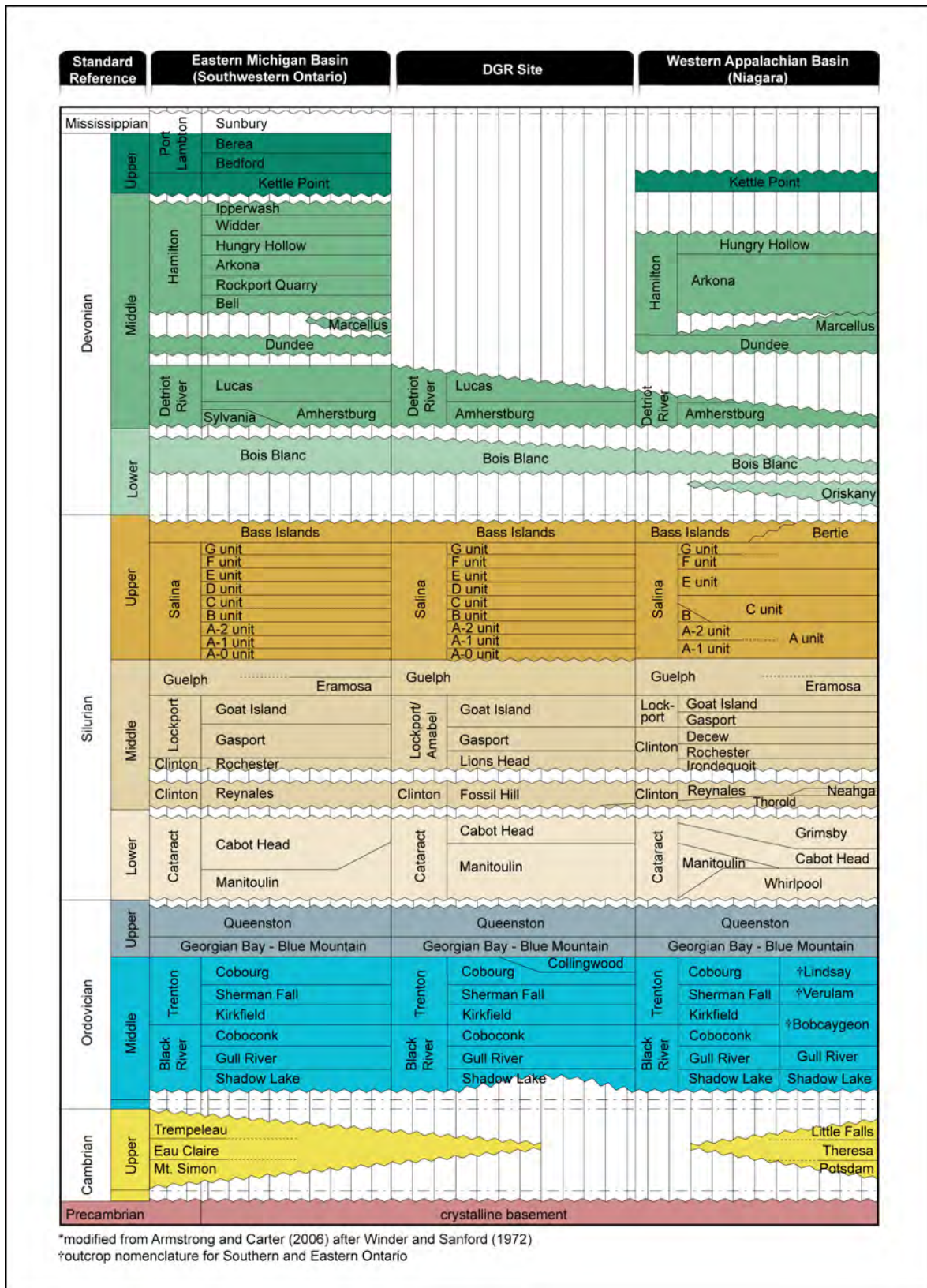


Figure 2: Paleozoic stratigraphy of southwestern Ontario from locations in the Michigan Basin, Algonquin Arch and Appalachian Basin (modified from Armstrong and Carter (2006))

integrates aspects of the other Geosynthesis studies in one framework through the development and analysis of a regional and site-scale geosphere conceptual model. The work product of the Regional Geology Study defines the geologic framework of the conceptual model. The pore water chemistry is defined by the Hydrogeochemistry Study, as well as data from the Phase 1 site characterization. The Long Term Climate Change Study defines the glacial loading and the evolution of the formation properties for paleoclimate analyses.

In order to capture and recreate both the regional and site-scale groundwater system, in both near-surface and deep environments, a groundwater flow model is developed for a fully three-dimensional representation of the bedrock stratigraphy within a portion of south-western Ontario centered on the Bruce DGR site. From a hydrogeologic perspective, the domain at the Bruce site can be subdivided into three horizons: a shallow zone characterized by the dolomite and limestone units of the Devonian that have higher permeability and groundwater composition with a relatively low total dissolved solids content; an intermediate zone comprised of the low permeability shale, salt and evaporite units of the Upper Silurian, the more permeable Niagaran Group (including the Guelph, Goat Island and Gasport in Figure 2) and the Lower Silurian carbonates and shales; and a deep groundwater zone extending to the Precambrian and characterized by the Ordovician shales and carbonate formations and the Cambrian sandstones and dolomites. Pore water in the deeper zone is thought to be stagnant and has high total dissolved solids (TDS) concentrations that can exceed 300 g/L with a corresponding specific gravity of 1.2 for the fluids. In this study, the term stagnant is used to define groundwater in which solute transport is dominated by molecular diffusion. This definition results from the fact that advective velocities calculated using Darcy's law will be zero only if either or both of the energy gradient or the permeability are zero. The measurement of a zero permeability for a porous medium is beyond current field instrumentation methods. A zero gradient is also difficult to either measure or estimate. Thus, stagnant must imply that the advective velocity is low in some sense - in this case relative to transport by molecular diffusion.

The more permeable formations in the deep zone include the Cambrian (Figure 2). The direction of groundwater flow in the shallow zone is strongly influenced by topography while the low-permeability intermediate zone isolates the deep groundwater domain from the influence of local scale topographic changes. Flow in the deep domain, as it may occur, most likely will be controlled by basin wide topography and potential formational facies changes. With the deep fluids having a specific gravity that is greater than the shallow groundwater, fluid density gradients may also influence regional flow. As a consequence, any horizontal gradients that govern flow in the deep domain are expected to be low resulting in diffusion dominated solute transport.

The Phase 1 regional-scale modelling was accomplished using FRAC3DVS-OPG. Developed from FRAC3DVS (Therrien et al., 2004), the model provides a solution of three-dimensional density-dependent groundwater flow and solute transport in porous and discretely-fractured media. Details of the FRAC3DVS-OPG model that are pertinent to this study are described in Chapter 3.

The modelling process requires a large computational effort for this horizontally layered geological sequence. Pre- and post-processors are essential for data interpretation, synthesis, manipulation, management and visualization.

1.1 Geological Framework

The Michigan Basin is a sedimentary geological feature found in the southern peninsula of Michigan, southern Ontario, as well as a few states surrounding Michigan (Figure 3). The northern edge of the Michigan Basin rim is defined as the areas where the depositionally continuous basal Paleozoic sediments come in contact with older rocks of Precambrian age (Stonehouse, 1969). In southern Ontario, the Michigan Basin is bounded to the east by the Algonquin Arch. The Algonquin Arch is a feature in the crystalline basement rock that trends NE-SW (Mazurek, 2004). The Algonquin Arch ranges in elevation from approximately 300 m where it outcrops to –1000 m at the Chatham Sag. South of the Chatham Sag, the Michigan Basin is bounded by the Findlay Arch (Ellis, 1969). The Findlay Arch is the southern continuation of the Algonquin Arch.

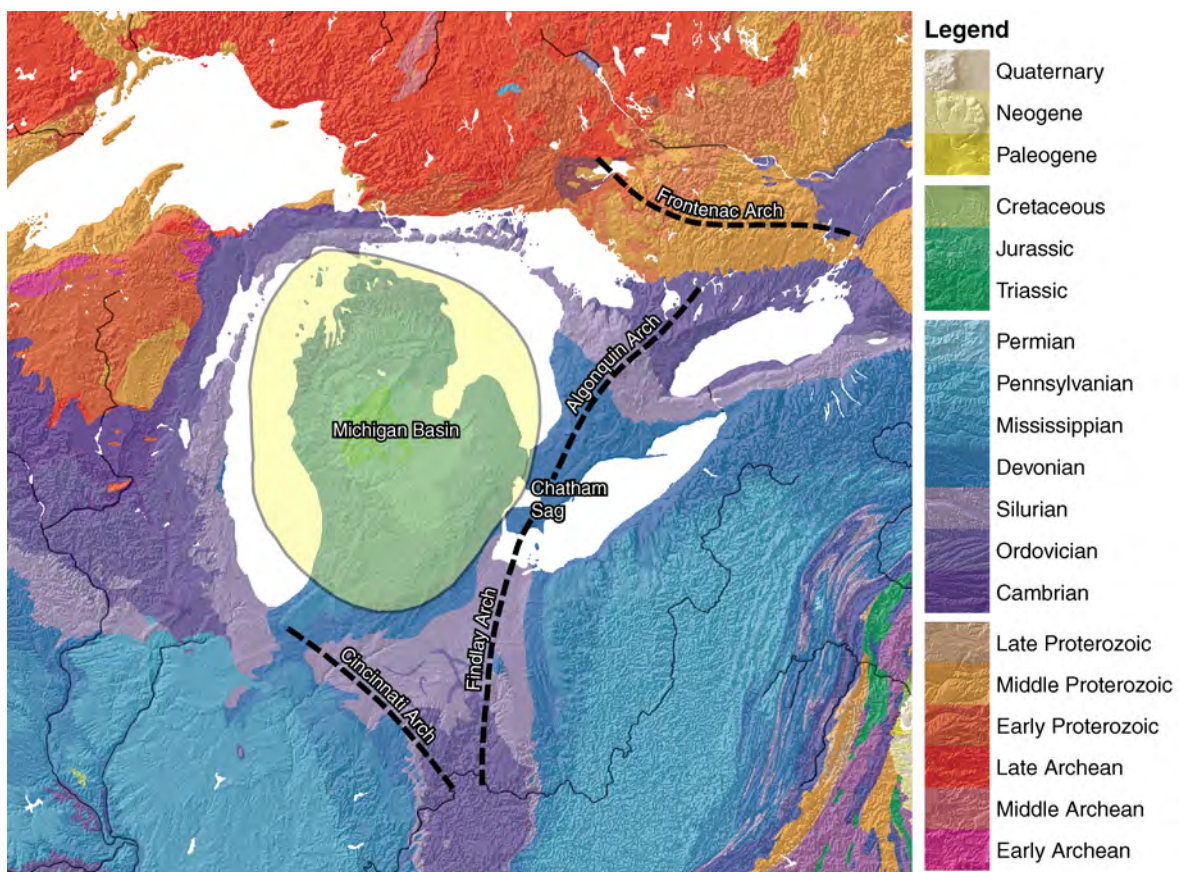


Figure 3: Spatial extent of the Michigan Basin and locations of the Frontenac Arch, Algonquin Arch, Chatham Sag, Findlay Arch, and Cincinnati Arch. Underlying geologic map, modified from Barton et al. (2003), is coloured by geologic period (Quaternary to Cambrian) and geologic era (Proterozoic to Archean).

Southern Ontario has been structurally divided into two megablocks (Sanford et al., 1985). The megablocks, named the Niagara Megablock and the Bruce Megablock, are divided by the Algonquin Arch (Figure 4). The proposed location for the DGR places it in the Bruce Megablock.

Sanford et al. (1985) propose a conceptual fracture distribution for southern Ontario. However, the validity of the fracture model has not been tested or resolved in the literature. Gartner Lee Limited (2008b) review the Sanford et al. (1985) model.

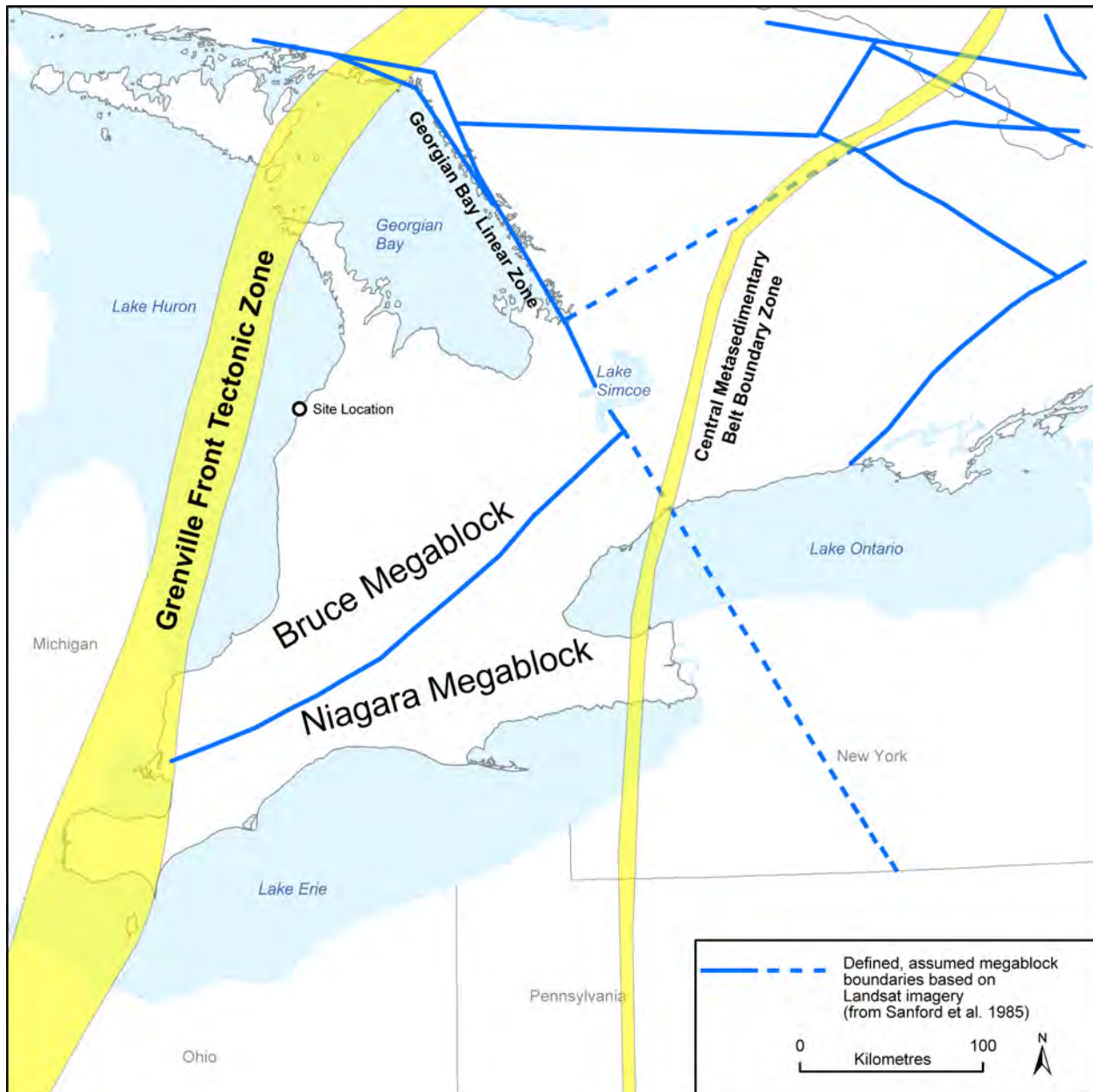


Figure 4: Major structural boundaries of southern Ontario and interpreted tectonic block boundaries derived from Landsat imagery by (Sanford et al., 1985).

The suitability of a sedimentary formation as a horizon for a potential repository depends on many criteria including low or minimal groundwater flow. Other criteria include sufficient depth below surface in a geologic unit with sufficient thickness, lateral contiguity and simple internal

homogeneity and favourable geochemical retardation properties (Mazurek, 2004). For water with varying density, groundwater flow is proportional to the energy gradient with this being the sum of the flow energy or pressure gradient and a potential energy gradient. The potential energy gradient is given in terms of a density gradient and a gravitational gradient. The regional-scale hydrogeologic modelling and analyses will investigate the case that at the proposed repository horizons, there are low energy gradients and that the combination of the low permeabilities and gradients will result in diffusional groundwater systems with favourable retardation properties.

1.2 Regional-Scale Conceptual Model

The regional-scale groundwater model can be described in terms of an upper and lower regime separated by the intermediate regime. The upper regime is restricted to units above the Salina Formation (refer to Figure 2). This is because the low hydraulic conductivity of the Salina Formation restricts near surface groundwater from penetrating to greater depths. The upper regime therefore mimics the topography with groundwater flowing from the highlands of the Niagara Escarpment to Lake Huron and Georgian Bay.

The lower regime is located beneath the Manitoulin dolomites of the Lower Silurian. Based on the conceptual model used in this study, there is little hydraulic connection between the deep geologic formations and the near-surface units at the proposed DGR site. The driving forces causing horizontal flow at depth are related to the energy gradient and they are expected to be very low. The only location for groundwater recharge into the rocks of the lower regime will be where they outcrop because the low permeability units of the intermediate regime, where present, act as an aquiclude, effectively preventing connection to surface recharge.

In order to determine the maximum energy gradient found in the deeper units, the lake elevations (Figure 5) are important. The highest possible elevation gradient throughout the Great Lakes region would be between Lake Superior and Lake Ontario, which have a difference in elevation of approximately 108 m. Although the head difference between these lakes is considerable, the substantial distance between them would result in a negligible potential horizontal energy gradient. When assessing the possible gradient between Lake Michigan and Lake Huron in the deeper units, the identical surface water elevation would eliminate the potential energy driving force due to elevation differences.

The potential energy gradients that occur at depth in the Michigan Basin will be reduced due to the presence of dense saline groundwater found within the formations of the lower regime. Where these formations outcrop at recharge areas, there will be a potential for fresh water to infiltrate the geologic units and displace higher density water until there is a balance between the elevation gradient and the density gradient. At this equilibrium point, the energy gradient will approach zero. With the dense brine, there will be associated higher viscosities which will act to further impede flow. The combination of the negligible horizontal energy gradients with the dense brine and low permeabilities in the lower groundwater regime can lead to a system that is dominated by diffusion.

On the basis of the negligible horizontal energy gradients expected within the lower regime, it is then possible to limit the spatial extent that will be modelled to include a section of the Michigan Basin, as opposed to the basin as a whole. A criteria for determining the extent of the regional

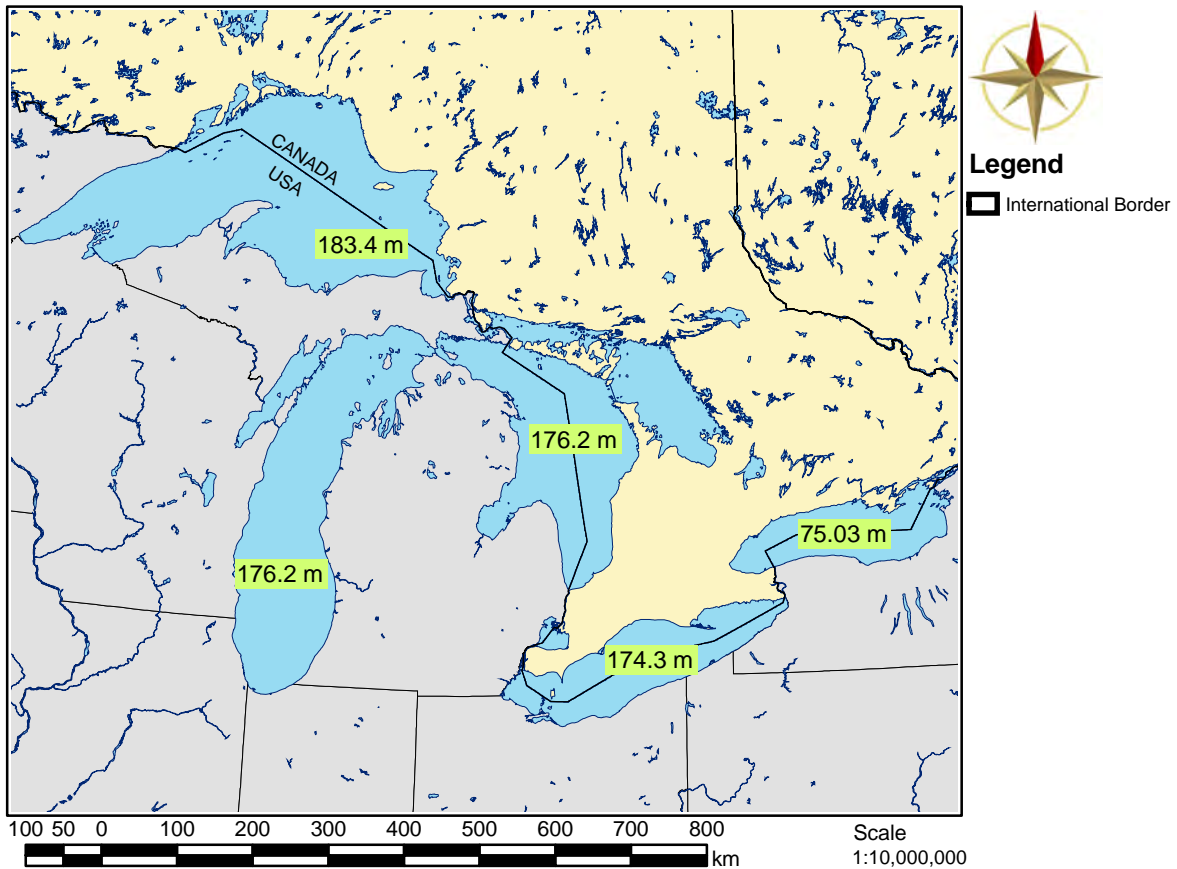


Figure 5: Elevation of the Great Lakes

domain that is a subset of the entire Michigan basin is that the domain should include appropriate recharge/discharge zones for the deeper units that have high total dissolved solids concentrations and that the proximity of these recharge/discharge zones be the closest possible to the location of the proposed DGR. This is accomplished by extending the domain to include the outcrop regions for these units. The gravitational driving force between Lake Michigan and Lake Huron can be replicated by including both Georgian Bay and Lake Huron in the domain. Potential flow paths between these two water bodies are significantly shorter than that between Lake Michigan and Lake Huron.

The boundaries assigned to the model domain (Figure 6) were defined using the following criteria. The south-eastern portion of the conceptual model boundary lies such that it follows the regional surface water divides surrounding the Bruce site. The surface water divide was determined by using a DEM derived from data from NASA's Shuttle Radar Topography Mission (SRTM) and a river map in ArcGIS (Figure 6). With the assumption that the groundwater system is a subdued reflection of topography, the topographic divide boundary conditions would only apply to the shallow groundwater zone and the Niagaran Group of the intermediate groundwater zone. The domain includes the local topographic high in southern Ontario. The model domain extends to the deepest portion of both Lake Huron and Georgian Bay. The National Oceanic and Atmospheric Administration (NOAA) digital bathymetric mapping of Lake Huron and Georgian

Bay was used to define the model boundaries in these areas. The eastern boundary of the domain is west of the Algonquin Arch.

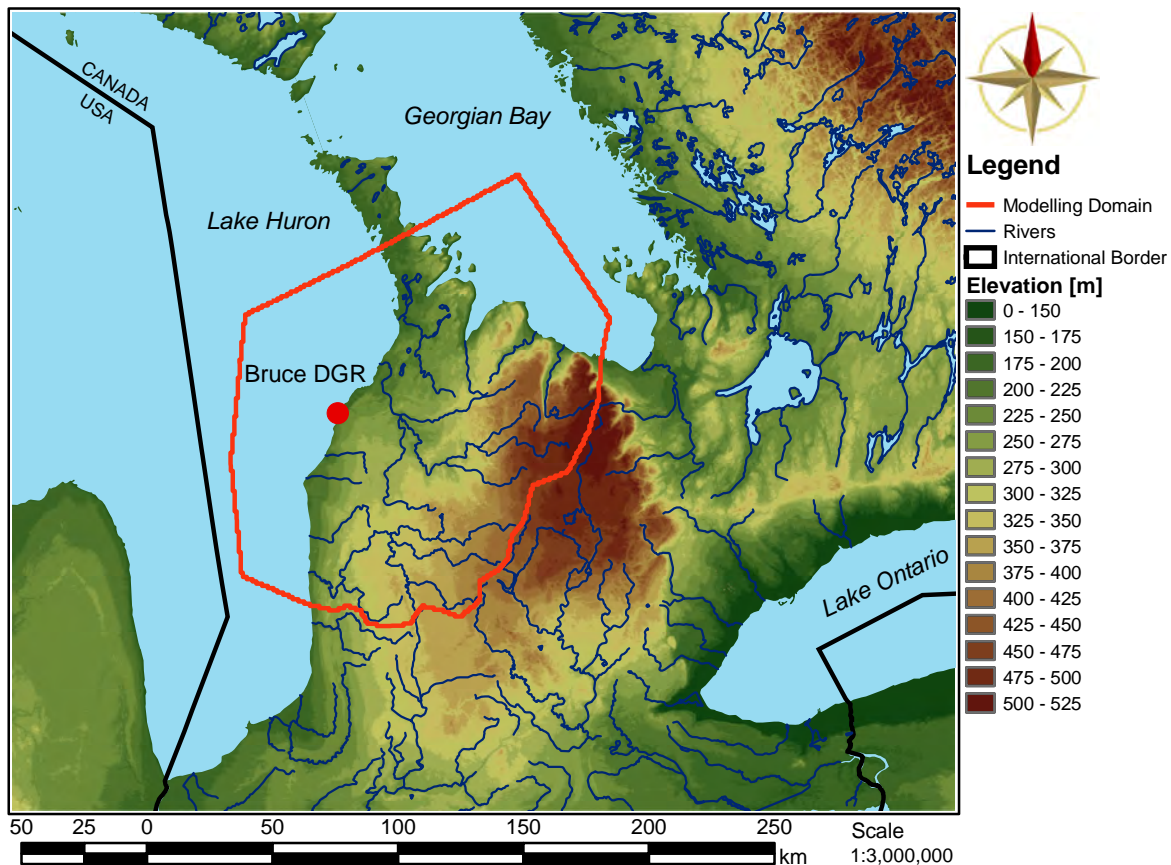


Figure 6: Regional scale elevations and river courses

1.3 Scope and Objectives

The objective of the Phase 1 regional-scale and site-scale groundwater modelling study as part of the geosynthesis program and site characterization is to assist in developing the safety case for the proposed Bruce Deep Geologic Repository. This assistance is provided by characterizing and analyzing the groundwater system in the deep geologic formations by creating a robust numerical groundwater model. In order to properly characterize the flow in the deep geological units, it is especially pertinent to ensure that the basis for the numerical model is developed from sound geologic interpretations and models. This will contribute to a more accurate distribution of unit properties such as permeability for an appropriate realization of the domain geometry. The distribution of permeability is of importance due to the requirement of sufficient thickness and lateral contiguity, and predictability of the geologic units that may be potentially impacted by the proposed repository.

Methods to calibrate or estimate model parameters, such as permeabilities, are well developed in literature. The most common method involves the assumption of an estimator or objective function with the sum of the square of the difference between observed heads and model estimated head values being most common. The goal of calibration is to minimize the objective function subject to constraints such as permeability bounds. The establishment of defensible parameter constraints is an important part of parameter estimation methods as the constraints define the solution space. Gradient based search algorithms are often used to facilitate calibration although ad-hoc or trial-and-error procedures are also commonly used. At the regional scale of this study, data are not sufficient to permit the calibration, in a formal sense, of model parameters such as permeability. However, the predictability of lithology will permit reasonable and defensible extrapolation and upscaling of point estimates and the development of parameter bounds or constraints. The investigation of the impact of parameter constraints is an important aspect of this study. The investigation is achieved through sensitivity analyses in which parameters are perturbed within reasonable and acceptable limits. The impact of the parameter perturbation on the groundwater system and solute transport is then determined. The assessment of the impact, if any, on regional-scale and site-scale flow and solute transport of geologic structure such as the faults postulated by Sanford et al. (1985), is addressed only to a limited extent in this Phase 1 study.

Argillaceous media are being considered by many countries as potential host rocks for radioactive waste. Numerical modelling, whether as part of site-characterization, geosynthesis, performance assessment or safety assessment, provides an important tool in the evaluation of the features, events and processes that may be relevant to the long-term safety of a repository. The modelling requires a sound understanding of the basic physical and chemical processes that govern water and solute transport through the host media. A framework that facilitates the evaluation of the suitability of a proposed repository involves the development and the use of FEPCATs, with this being an acronym for “features, events and processes catalogue” (Mazurek et al., 2003). For a repository system hosted in argillaceous media, there are three separate FEPCATs that are most relevant to this study with these being transport mechanisms, retardation mechanisms and paleohydrogeology. Following Jensen (2007), a further description of these concerns is presented in the following paragraphs.

Transport of a radionuclide within and from a deep geologic repository occurs by a number of possible transport mechanisms, and it is counteracted by a number of retardation mechanisms (Mazurek et al., 2003). Numerical models, laboratory experiments and field experiments are components that are considered in the assessment and resolution of transport and retardation mechanisms. The transport mechanisms and factors or processes that influence it include:

- Stratigraphy/hydrostratigraphy - predictability/homogeneity/bedrock layering (3-D Geometry)
- Hydraulic gradients - gravity, density, anomalous
- Hydraulic conductivities - extremely low; anisotropic, inter-formational/intra-formational
- Hydrogeochemistry - brine viscosity, formation distinct pore fluid compositions (elemental/isotopic), scale dependency (laboratory (cm) vs. field scale (10s of m))
- Diffusivities - Cobourg/Ordovician shales (i.e. pore geometry/connectivity, porosity, pore space, anisotropy)
- Structural geology - geometry of regional/local scale discontinuities
- Colloid transport - principles, process and likelihood

The parameters and features that are relevant in the determination of the retardation mechanisms that modify the rate at which solutes migrate through the groundwater system include:

- Grain size distribution/mineralogy
- Pore water composition (inorganic/organic)
- Dissolution/precipitation of secondary mineral phases
- Matrix diffusion where fracture flow occurs

Numerical modelling at both the regional-scale and the site-scale plays an important role in demonstrating and illustrating the transport and retardation mechanisms. This report will contribute to the assessment of these mechanisms through the use of the model FRAC3DVS-OPG to demonstrate and illustrate:

- Flow, transport or time domain probability estimates of particle residence time in the regional flow system based on estimates of the transport mechanisms of advection, dispersion and diffusion
- Flow system anisotropy at inter-/intra-formational scale
- Influence of variable density flow (i.e. horizontal stratification)
- Influence of basin hydrostratigraphy and geometry on absence of exfiltration zones
- Migration of unretarded/non-decaying environmental isotopes within the subsurface
- Role/implications of sub-vertical transmissive features in a variably dense groundwater flow domain

The evaluation of a feature or process using numerical models can be accomplished using, in part, a sensitivity analysis that estimates the change in a system performance measure to changes in a system parameter. These estimated sensitivity coefficients are local derivatives evaluated in terms of the base case parameters that describe the system. The robustness of the sensitivity coefficients for large changes or perturbations of parameters also can be assessed. The performance measures that can be used to characterize the system can include, but are not restricted to:

- Darcy fluxes and average linear velocities for both steady-state and transient, density-dependent flow
- Salinity and environmental isotope concentrations
- Fluid pressures and energy gradients for both steady-state and transient, density-dependent flow
- Average water particle paths
- Time domain probabilities of fluid particle residence times
- Flow system discharge

Regional-scale modelling can provide the framework for the assessment of paleohydrogeology. Based on the work of Peltier (2002, 2003a), it is clear that to credibly address the long-term safety of a deep geologic repository, long-term climate change and, in particular, a glaciation scenario, needs to be incorporated into geosynthesis modelling activities. In addition, by simulating flow system responses to the last Laurentide (North American) glacial episode, insight is gained into the role of significant past stresses (mechanical, thermal and hydrological) on determining the nature of present flow system conditions, and by extension, the likely impact of similar, future boundary condition changes on long-term flow system stability. The Wisconsinian glacial episode,

that occurred over a 120 000 year time period, included at least three cycles of glacial advance and retreat, with maximum ice thickness over the southern Ontario DGR site reaching more than 2 km. Between glacial episodes were extensive periods of transient, peri-glacial conditions during which permafrost could impact the subsurface, depending on location, to several hundreds of metres. Near the end of a glacial episode, significant basal meltwater production occurred. This study will restrict itself to the development of a model domain and parameters that will provide a framework for the assessment of paleohydrogeology. This assessment includes:

- Evaluating the expected flow system perturbation by glacial events (boreal, peri-glacial or ice sheet)
- Assessing the depth of penetration by glacial meltwaters into Paleozoic formations
- Illustrating numerically the transient influence of glacial event(s) on the DGR site flow system
- Estimating pore fluid residence times during Quaternary glacial events

The Phase 1 regional-scale and site-scale modelling of the DGR site using FRAC3DVS-OPG is restricted to saturated isothermal flow. The extent of the regional domain is defined in Figure 6. Analyses include both steady-state, density-independent flow and transient flow that couples the density-dependent flow equation with the equation that describes the transport of the total dissolved solids within the system domain. The assessment of the impact of parameter perturbations on system performance measures that can include fluid pressure, fluid velocity, groundwater life expectancy and groundwater age will be accomplished using direct parameter sampling and, to a limited extent, a sensitivity derivative framework. The base case parameters that describe the regional domain are dependent on the geological and geochemical framework and the Phase 1 field investigations at the Bruce site with these being described in Chapter 2. The elements of FRAC3DVS-OPG that are relevant to the regional scale modelling are described in Chapter 3. The regional scale groundwater flow conceptual model is detailed in Chapter 4. The analyses of the regional-scale model and the paleoclimate simulations are developed in Chapters 5 and 6, respectively. The site-scale model and analyses are developed in Chapter 7 while conclusions are presented in Chapter 8. Over the course of this study, hundreds of model simulations were undertaken. Selected graphics that illustrate the salient results are presented in the chapters of this report, but predominantly in the Appendices.

2. GEOLOGICAL AND GEOCHEMICAL FRAMEWORK

2.1 DGR Phase 1 Site Investigation

Data for the regional-scale conceptual model was developed from published reports and papers, government and other data bases, and site specific field studies. The Phase 1 field activities at the Bruce site are described in the Geoscientific Site Characterization Plan (Intera Engineering Ltd., 2006). The activities included wireline drilling and core logging of a vertical deep borehole (DGR-1) to the top of the Queenston shale to confirm the stratigraphic sequence and general rock quality of the Silurian and Devonian bedrock sequence. A second adjacent borehole (DGR-2) was developed to the Precambrian bedrock. Rotary drilling with a grout casing was used to the top of the Queenston and wireline drilling with core logging was used for the balance of the borehole. Opportunistic groundwater sampling during drilling was accomplished for both boreholes. Core samples from the boreholes were collected and preserved for geochemical testing, porewater extraction and testing, geomechanical testing, diffusion testing and petrophysical testing. Open-hole straddle packer hydraulic testing was undertaken. Pressure monitoring, groundwater sampling and hydraulic testing for both boreholes were enabled by the installation of Westbay MP multi-level casings.

The thickness and depth below ground surface for the stratigraphic units at DGR-1 and DGR-2 are listed in Table 1. Also shown in the table are the measured horizontal hydraulic conductivities and total dissolved solids concentrations for the units from which the fluid viscosities and densities were estimated. The vertical hydraulic conductivities were not estimated in the Phase 1 study; as a rule-of-thumb, the vertical hydraulic conductivities can be an order-of-magnitude, or more, lower than the horizontal hydraulic conductivities estimated in a field program. The importance of the vertical hydraulic conductivities is evaluated in this model study. In the table, the member units of the Niagaran Group (Lockport/Amabel and Guelph Formations, refer to Figure 2) that are observed in the boreholes are listed. The low permeability of the F-Unit defines the top of the intermediate regime or zone. Above this zone, measured TDS concentrations are low. In and below the intermediate zone, TDS concentrations trend to 300 g/L or higher. Units below the intermediate zone where higher permeabilities have been estimated include the Guelph dolomites and the Cambrian sandstones and carbonates. Between these two units there is approximately 460 m of low permeability shale and limestone that includes the Cobourg, the target horizon for the proposed DGR.

Pressure data from the Westbay MP multi-level casing in the DGR-1 and DGR-2 boreholes have been used to estimate the vertical profile of equivalent freshwater head and the environmental head from the ground surface to the Precambrian at the Bruce site. The definition of freshwater and environmental heads is given in Chapter 3. The environmental heads, which can be used to estimate vertical groundwater gradients, were approximated from the measured pressure (density) profile within the open hole prior to inflation of Westbay casing packers; the density profile data may be refined with the ongoing field testing, sampling and laboratory analyses. The estimated environmental head profile in the composite DGR-1 and DGR-2 borehole from pressure data obtained on March 3, 2008 is presented in Figure 7. The first sampling of the pressures in DGR-2 were undertaken on December 11, 2007. Data from subsequent measurement events indicate that the pressures are slowly shifting, particularly for the low permeability units, toward equilibrium values. As such, the pressures used to develop the data

Table 1: Core log, hydraulic test data and geochemical data for DGR-1 and DGR-2.

| Unit | Thickness [m] | Depth to Top [m] | K_H [m/s] † | TDS [g/L] |
|-------------------|---------------|------------------|-------------------------|------------|
| Drift | 20.0 | 0 | | 0.5 |
| Lucas/Amherstburg | 55.0 | 20.0 | 1.0×10^{-5} | 0.5 |
| Bois Blanc | 49.0 | 75.0 | 1.0×10^{-5} | 1.6 |
| Bass Islands | 54.0 | 124.0 | 1.0×10^{-5} | 1.6 |
| Salina | | | | |
| G Unit | 5.0 | 178.0 | | |
| F Unit | 40.0 | 183.0 | 4.0×10^{-12} P | 310 |
| E Unit | 20.0 | 223.0 | 4.0×10^{-12} P | |
| D Unit | 1.6 | 243.0 | 1.0×10^{-10} | |
| C Unit | 15.7 | 244.6 | 6.0×10^{-12} P | |
| B Unit | 30.9 | 260.3 | 2.0×10^{-12} P | |
| B Anhydrite | 1.9 | 291.2 | | |
| A-2 Carbonate | 26.9 | 293.1 | 1.0×10^{-10} D | |
| A-2 Evaporite | 8.0 | 320.0 | 2.0×10^{-7} S | 340 |
| A-1 Carbonate | 39.0 | 328 | 2.0×10^{-12} P | 300 |
| A-1 Evaporite | 3.5 | 367.0 | | |
| A-0 Unit | 4.0 | 370.5 | 1.0×10^{-8} S | |
| Guelph ‡ | 5.5 | 374.5 | 1.0×10^{-8} S | 300 |
| Goat Island | 20.5 | 380.0 | | |
| Gasport | 3.75 | 400.5 | | |
| Lions Head | 4.05 | 404.25 | 2.0×10^{-11} D | |
| Fossil Hill | 2.7 | 408.3 | 2.0×10^{-11} D | |
| Cabot Head | 20.5 | 411.0 | 2.0×10^{-11} D | 240 |
| Manitoulin | 16.15 | 431.5 | 2.0×10^{-12} P | |
| Queenston | 70.35 | 447.65 | 1.3×10^{-11} P | |
| Georgian Bay | 98.5 | 518.0 | 1.2×10^{-11} P | 180 to 270 |
| Blue Mountain | 35.5 | 616.5 | 1.0×10^{-11} P | |
| Collingwood | 7.5 | 652.0 | 9.6×10^{-12} P | |
| Cobourg | 27.0 | 659.5 | 9.6×10^{-12} P | 210 |
| Sherman Fall | 45.5 | 686.5 | 7.9×10^{-12} P | |
| Kirkfield | 30.0 | 732.0 | 1.0×10^{-11} P | 282 |
| Coboconk | 16.75 | 762.0 | 5.2×10^{-11} P | |
| Gull River | 59.85 | 778.75 | 3.6×10^{-11} P | 304 |
| Shadow Lake | 5.1 | 838.6 | | 295 |
| Cambrian | 17.0 | 843.7 | 3.0×10^{-6} F | 320 |
| Precambrian | | 860.7 | | 288 |

Note: † P = Pulse Test, D = Drill Stem Test, S = Slug Test, F = Flow Test

‡ The Guelph, Goat Island, Gasport and Lions Head comprise the Niagaran Group

shown in Figure 7 are not at their final values. Based on a surface elevation of 185.84 mASL, the environmental head profile in DGR-2 clearly shows that the Cambrian is significantly over-pressured with respect to the ground surface, the Ordovician and Lower Silurian are significantly under-pressured while units in the Niagaran are moderately over-pressured. Groundwater gradients are thus upward from the Cambrian to the Ordovician, and downward from the Niagaran to the Ordovician. The low permeability of the Salina isolates the Niagaran from the more permeable units of the Devonian.

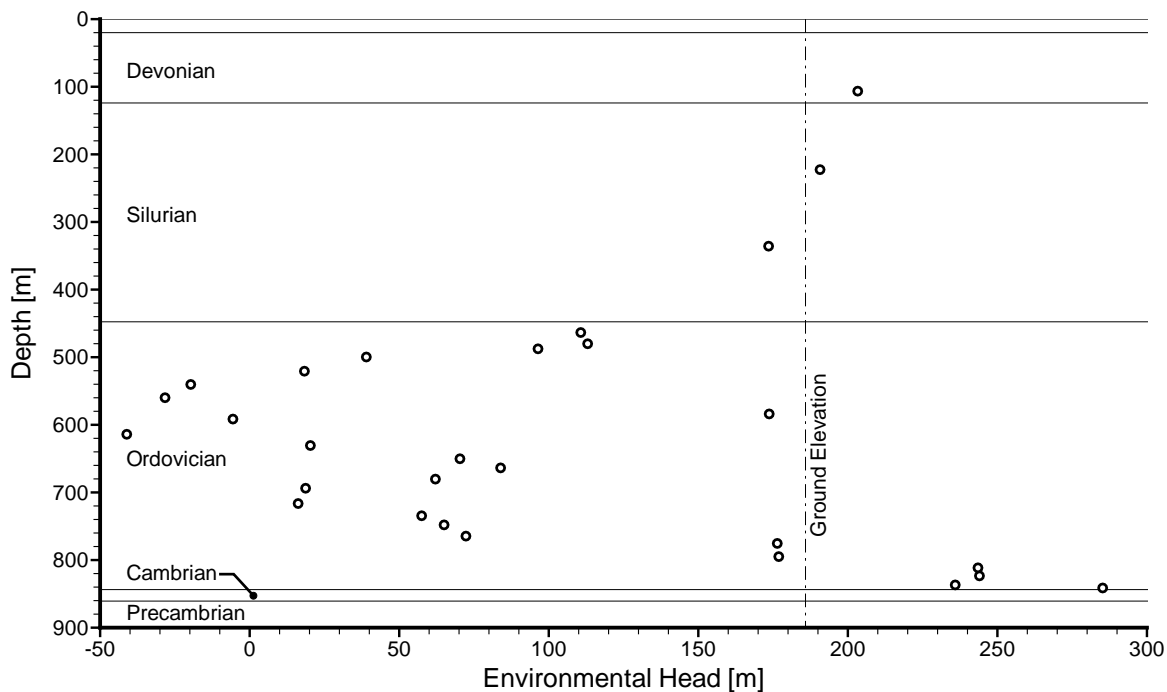


Figure 7: Environmental heads in a composite DGR-1 and DGR-2 borehole based on pressures measured on March 3, 2008.

2.2 Geological Units

The Paleozoic stratigraphic units at the Bruce site (listed in Table 1 and in Figure 2) were deposited on crystalline Precambrian basement rock. The Precambrian rocks underlying southern Ontario are metamorphic rock types ranging from felsic gneisses to mafic metavolcanics to marble (Armstrong and Carter, 2006). The following summary from Armstrong and Carter (2006) describes the Paleozoic rocks encountered within the regional study area.

The Cambrian units of Ontario, deposited over the irregular and weathered Precambrian surface, are composed primarily of quartzose sandstones with dolomitic quartz sandstones and sandy dolostones (Armstrong and Carter, 2006). Cambrian deposits extend from the Appalachian Basin to the Michigan Basin but have largely been eroded over the Algonquin Arch (Bailey Geological Services Ltd. and Cochrane, 1984). Well log records obtained from the Ontario Oil, Gas and Salt Resource (OGSR) Library in London, Ontario indicate that Cambrian deposits are present at

isolated locations over the arch. It is possible that these deposits are remnants of the eroded Cambrian or they represent isolated patches of sandstones of unknown origin/age as described by Bailey Geological Services Ltd. and Cochrane (1984). As a result, the Cambrian sediments are not continuous throughout the regional model domain and as shown in Table 1, its permeability is significantly higher than both of its bounding units. The hydraulic conductivity listed for the Cambrian in Table 1 is an integrated value representing the total thickness of the unit.

The Cambrian sandstones and dolostones are overlain by the low permeability rocks of Middle Ordovician age. When the Cambrian rocks are not present, as is the case at the Algonquin Arch, the Ordovician rocks directly overlay the Precambrian basement rock. The first unit of Ordovician age is the Black River Group. This Group consists of the Shadow Lake, Gull River and Coboconk Formations. The Shadow Lake Formation in southern Ontario is composed of red and green shales, argillaceous sandstones and argillaceous dolostones (Armstrong and Carter, 2006). The second geological formation that comprises the Black River Group is the Gull River Formation. The Gull River Formation consists primarily of very fine grained limestone with minor dolostone and shale interbeds. The Coboconk Formation is the youngest Black River Group unit and consists of fine-medium grained bioclastic limestones (Armstrong and Carter, 2006).

The overlying Trenton Group includes the Kirkfield, Sherman Fall, and the Cobourg Formations. The Kirkfield Formation is composed of fossiliferous limestones, while the overlying Sherman Fall Formation ranges in lithology from argillaceous limestones, found lower in the formation, to bioclastic limestone that characterize the upper portions of the formation (Armstrong and Carter, 2006). The upper (youngest) formation of the Trenton Group is the Cobourg Formation. The Cobourg Formation is the proposed horizon for the DGR (Intera Engineering Ltd., 2006). The Cobourg Formation consists of very fine-coarse grained, fossiliferous limestones and argillaceous limestones. The upper member of the Cobourg Formation is known as the Collingwood Member, which is described by Armstrong and Carter (2006) as dark grey to black, organic-rich, calcareous shales.

Overlying the Cobourg Formation are the Upper Ordovician Georgian Bay and Blue Mountain Formations. These units consist of thick non-calcareous shales with minor limestone, siltstone and sandstone interbeds. The youngest Upper Ordovician unit is the Queenston Formation, which consists of red to maroon, noncalcareous to calcareous shale with minor siltstone, sandstone and limestone interbeds (Armstrong and Carter, 2006).

The Silurian rocks comprise the intermediate groundwater zone or domain. The oldest units forming the intermediate groundwater domain are comprised of the Lower Silurian Manitoulin dolostones and shales of the Cabot Head Formation. The lower hydrostratigraphic regime is isolated from the upper groundwater regime, in part, by the low hydraulic conductivities of units in the intermediate groundwater domain, specifically the horizontally bedded Upper Silurian Salina Formation.

The Middle Silurian at the DGR site consists of dolostones of the Fossil Hill Formations, Lions Head Formation, Gasport Formation, Goat Island Formation and the more permeable dolostones of the Guelph Formation. The Guelph Formation ranges from reef to inter-reef lithologies throughout southern Ontario. At the DGR site, the Guelph Formation is characterized by thin inter-reef dolostones (Intera Engineering Ltd., 2008).

The Upper Silurian Formations are comprised of the Salina Group and the Bass Islands Formations. These units consist of sequences of dolostones/limestones, argillaceous dolostones/limestones, shale, and evaporite (i.e., gypsum, anhydrite, salt). The Salina Group is subdivided into 11 members which are in order of succession A-0, A-1 Evaporite, A-1 Carbonate, A-2 Evaporite, A-2 Carbonate, B Unit, C Unit, D Unit, E Unit, F Unit, and G Unit. The Bass Islands Formation dolostones overly the Salina Group. The evaporite, shale and argillaceous dolostone units in the Salina Formation will form a major barrier impeding the vertical hydraulic connection of deeper geologic formations with shallower formations.

Above the Bass Islands Formation is the Lower Devonian aged Bois Blanc Formation. The Bois Blanc Formation is described as a fossiliferous and cherty dolostone (Armstrong and Carter, 2006). The Bois Blanc Formation is overlain by the Middle Devonian Amherstburg and Lucas formations of the Detroit River Group. These units are characterized by fossiliferous dolostones/limestones to poorly fossiliferous limestones with minor evaporite (Armstrong and Carter, 2006). The Detroit River Group comprises the upper or shallow groundwater zone. In the southern portion of the regional study area (model domain) the limestones and dolostones of the Middle Devonian Dundee Formation overlies the Detroit River Group.

2.3 Geological Reconstruction

A key element of the Phase 1 Geosynthesis project was the creation of a three-dimensional geological framework that will form the basis of both the regional-scale and site-scale numerical groundwater model. The geological framework model consists of a three-dimensional reconstruction of the geology of a portion of southern Ontario within and immediately adjacent to the range of the computational domain (refer to Figure 6). Two approaches were taken in the development of a geological framework: Sykes (2007) developed a preliminary geologic framework model that was used to investigate solution methodologies for the regional-scale analyses; Gartner Lee Limited (2008b) developed the geologic framework model (referred to as model GLL00) that is the basis of the analyses of this Phase 1 report. The importance of the geologic framework model was assessed in the analysis of Section 5.3.3.

2.3.1 Preliminary Geologic Framework Model

The initial approach by Sykes (2007) developed a geologic framework model that was used in the preliminary modelling phase to develop the solution methodology followed in this report. The Sykes (2007) geological framework model was developed using a database that contained more than 50,000 boreholes in southern Ontario that were obtained from the Ontario Oil, Gas and Salt Resource (OGSR) Library in London, Ontario (Figure 8). The borehole data consisted of a series of databases that included geologic formation description, contact depth, ground surface elevation as well as the spatial coordinates for each associated borehole. The OGSR data contained some possible inconsistencies, including: uncertain ground elevations and locations for boreholes, and alternative interpretations of the presence of various geologic units in certain boreholes. In the geological framework developed by Sykes (2007), the raw borehole data were screened and classified. The Microsoft Access relational data base system was used by Sykes (2007) as a tool to facilitate the assessment of the OGSR data. Data from queries were sorted to determine anomalies. The contouring of data using Rockworks facilitated visual inspection. The

correlation structure of data such as unit thickness was determined using the Geopack Kriging program (Yates and Yates, 1989). Due to the large number of boreholes that were to be included within the geologic reconstruction, in the preliminary development of a geological framework, only the 10 boreholes proximal to the proposed Bruce DGR site were analyzed in detail to assess the accuracy of the formation contact depths. It was observed that there were instances where units, such as the Cambrian as an example, may not be present in wells that otherwise penetrate the underlying Precambrian surface. This absence could be attributed to differences in stratigraphic nomenclature conventions used by the technician logging the core. However, the geologic model put forth by Bailey Geological Services Ltd. and Cochrane (1984) indicates that the Cambrian is absent over the Algonquin Arch.

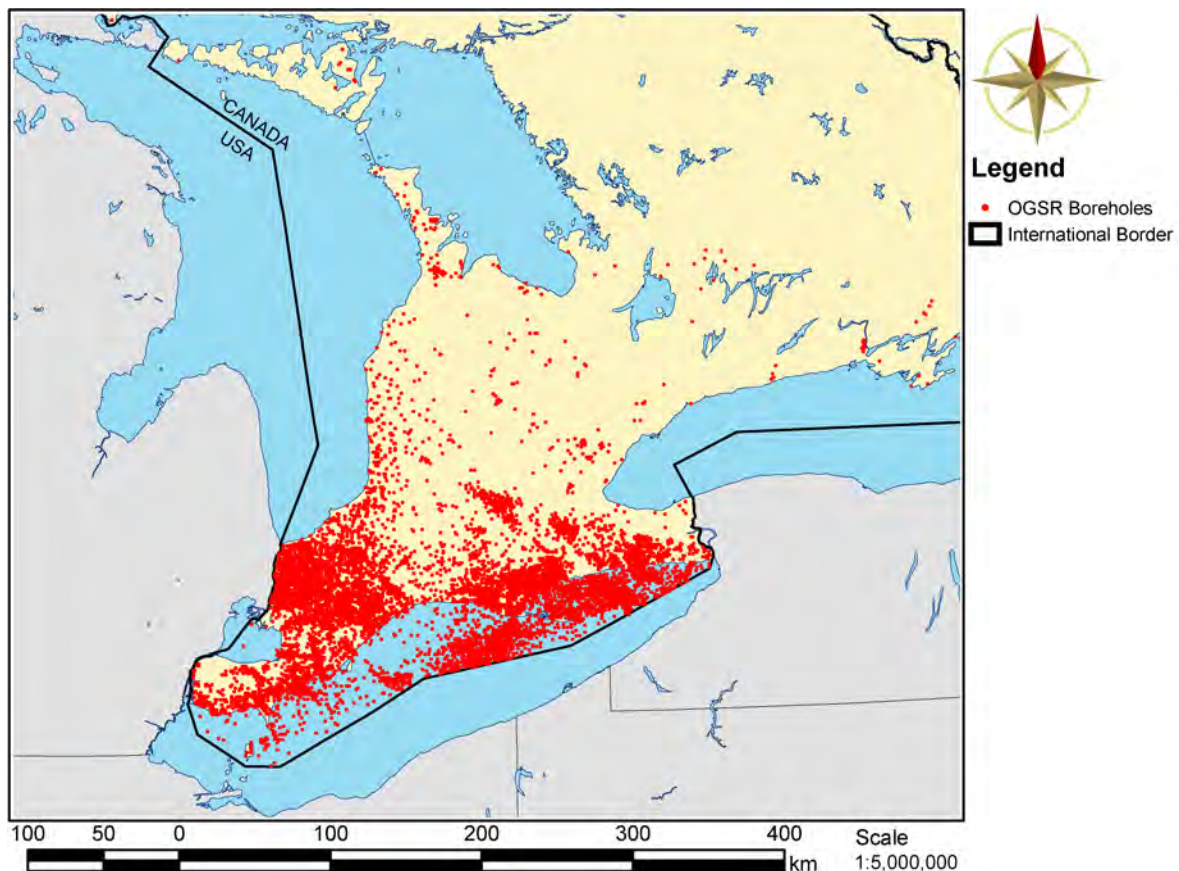


Figure 8: Location of OGSR boreholes.

The approach used by Sykes (2007) for the development of the geological framework investigated inconsistencies in the borehole surface elevation and location. The borehole data contained anomalies in the surface elevations used to reference the boreholes. The dataset provided the stratigraphic elevations both in terms of metres above sea level and depth below ground surface. Within the dataset, there were occurrences of boreholes whose elevations would be on the order of 10s of metres different from neighbouring boreholes. To compensate for the elevation disparities, a Digital Elevation Model (DEM) of southern Ontario was used in conjunction with the depth below ground surface data for the geologic contacts. The use of the

DEM ensured that all of the formation contacts would be referenced to a single and known datum. The Digital Elevation Model (DEM) for the conceptual model domain was developed using the 1:250 000 Natural Resources Canada map. The raster data for the DEM has a 3 arc second resolution on an approximately 60 m east-to-west by 100 m north-to-south grid. The integer elevations on the grid range from approximately 176 m to 539 m above mean sea level.

In addition to possible vertical error, there is the possibility for error from the spatial location of the coordinates. This can be attributed to wells having incorrect longitude and latitude coordinates. This may possibly explain the instances where boreholes with distinct license names and geological records will have the same geographic coordinates. The error from the spatial location of the well will then become further compounded from the elevation. This will occur because wells in an incorrect location will then be assigned an elevation from the DEM that may be higher or lower than what the actual correct field measurement would have been.

In addition to the borehole data, surficial bedrock geologic data were used to supplement and constrain the data set. The surficial geologic contacts were discretized and subsequently added to the dataset. To discretize the map of bedrock subcrops beneath the glacial sediments in southern Ontario (Figure 9), the contacts between geologic units on the map were rendered into a series of points in GIS. Elevation data for the surficial bedrock geology were then extracted from the DEM at these points. The addition of the supplemental data was to ensure that during the spatial interpolation of the borehole data, the geologic units would be forced to intersect an elevation and location in a pattern that is consistent with surface mapping.

To create a three-dimensional geologic model of a portion of southern Ontario, a variety of geostatistical interpolation methods can be used. Sykes (2007) used the program Rockworks to perform the geostatistical interpolation. Three different methods were considered: Kriging, inverse distance squared and a first-order polynomial. The first-order polynomial method was selected to correlate between boreholes because of the high aptitude it has for extrapolation and interpolation between scarce points. The first-order polynomial approach fits a planar surface through the data points. Although this may cause a reduction in geologic competency of some undulating and generally non-linear geologic features, the first-order polynomial increases the plausibility of fit in areas with few data points. The first-order polynomial method is also appropriate to handle the uncertainties that are inherent in the borehole dataset used to generate the three-dimensional geologic model. The uncertainty related to extrapolation is important for the regional geologic reconstruction because the domain extends beyond the shores of Lake Huron and Georgian Bay, where there is a notable absence of borehole data. It was necessary to ensure that the volume created through interpolation and extrapolation corresponds to the known surface elevations and the Lake Huron and Georgian Bay bathymetry. To ensure the topographic and bathymetric control, a script was written using Visual Basic to remove any interpolated volumes that occurred above ground and lake bottom surfaces (Sykes, 2007).

2.3.2 The GLL00 Geologic Framework Model

In the second approach, Gartner Lee Limited (2008b) developed a geological framework model that is used as the basis of the analyses and simulations presented in this study. The model extends from the Precambrian basement to the surface topography, including watershed features (lakes, rivers), and bathymetry. Itasca Consulting Canada Inc. was retained by OPG to work

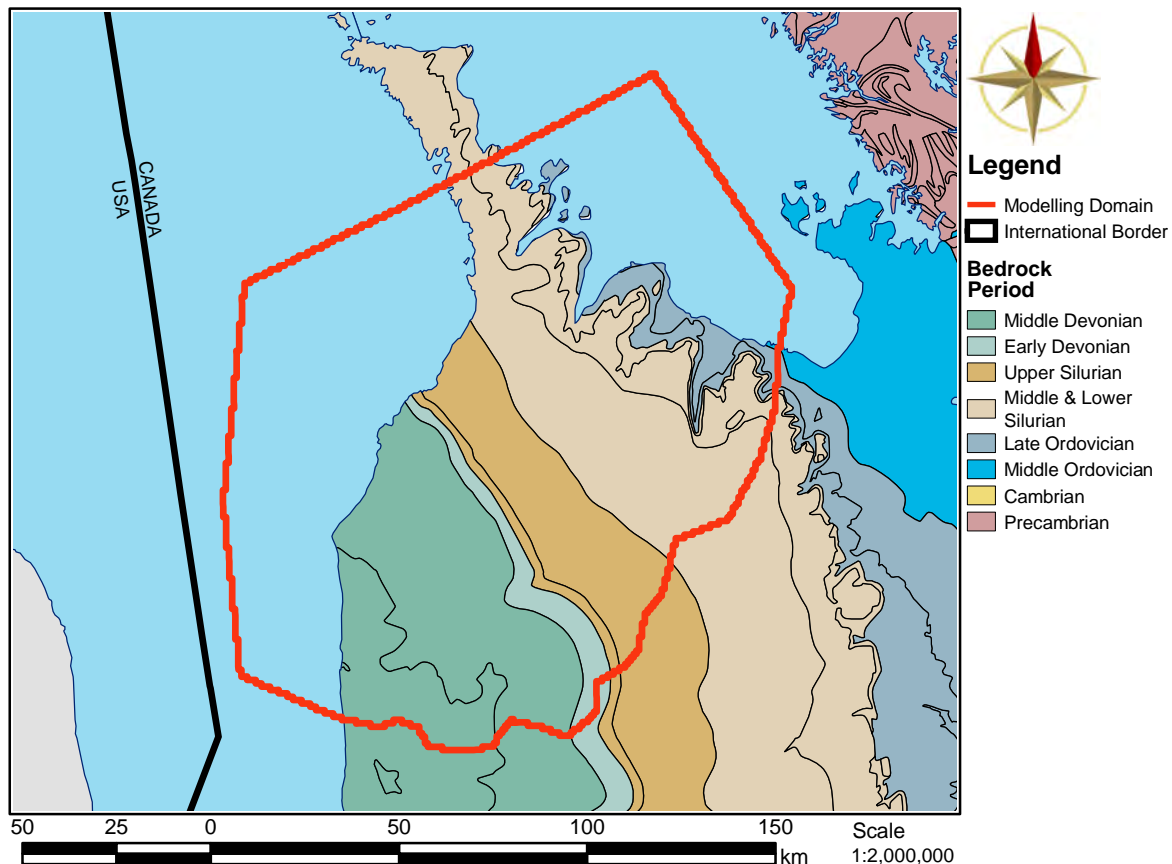


Figure 9: Map of bedrock subcrop beneath the glacial sediments of southern Ontario

closely with the study team of Gartner Lee Limited (2008b) in developing the three-dimensional Geological Framework model (3DGF) used in this Phase 1 report. With Itasca, the framework was designed using the advanced 3D earth modelling and scientific visualization technology Gocad™ software. Interpolation was accomplished by the iterative Discrete Smooth Interpolation (DSI) method. As stated in Section 6.1 and Appendix A.1 of Gartner Lee Limited (2008b), the goal of DSI is to create a smooth result. Unlike Kriging, DSI does not provide a point estimation of the precision of the interpolation. Gartner Lee Limited (2008b) state that DSI should not be used to replace classical methods such as Kriging, but is a complementary tool to get an approximation of values of classical interpolation techniques. Details on the use of DSI are provided in Gartner Lee Limited (2008b).

As with the geologic framework model developed by Sykes (2007), the primary data source for the Gartner Lee Limited (2008b) geologic framework construction was the OGSR Database. As shown in Figure 8, the vast majority of these wells are located in southwestern Ontario along the shore of Lake Erie extending towards Sarnia/Lambton County. The Regional Study Area (RSA) contained a total of 341 wells, which were reduced to 302 wells through the data validation process. The relative lack of petroleum wells in the RSA reflects a general scarcity of petroleum resources in this area. The purpose of the wells can be generally grouped into three main categories:

- i) those wells drilled to prove salt resources near the southern portion of the RSA;
- ii) oil/gas exploration wells drilled into Silurian strata (primarily reefs); and
- iii) oil/gas exploration wells drilled into Ordovician strata.

In addition to the wells within the RSA, a further 57 petroleum Reference Wells (Armstrong and Carter, 2006) and 76 petroleum wells from the Michigan State Geological Survey Digital Well Database located outside of the RSA were used. Other key sources of data also included downhole geophysics (used to verify well contacts/picks), acquired from the OGSR Library for select wells within the RSA, and from Armstrong and Carter (2006), an updated guide to the Paleozoic stratigraphy of southern Ontario. Reference wells were used by (Armstrong and Carter, 2006) to generate a series of representative geological cross-sections through the subsurface of southern Ontario. These same reference wells were used in the 3DGF as a verification tool and to provide consistency with the accepted Ontario geological nomenclature and understanding.

Other important data includes:

- i) 1:50,000 OGS Digital Bedrock Geology of Ontario Seamless Coverage ERLIS Data Set 6;
- ii) Michigan State Geological Survey mapping and Petroleum Well Database;
- iii) OGS Digital Bedrock topography and overburden thickness mapping, southern Ontario (Gao et al., 2006); and
- iv) National Oceanic and Atmospheric Administration (NOAA) digital bathymetry mapping of Lake Huron and Georgian Bay (NOAA, 2007).

For the Gartner Lee Limited (2008b) geologic framework, the bathymetry mapping was used as a tool to correlate scarp faces within Lake Huron with the stratigraphic data extrapolated from the subsurface well data and bedrock maps. Note that no well data exists within Lake Huron, as a result, the State of Michigan geological mapping and selected petroleum well data were used to provide some guidance for extrapolating data beneath Lake Huron.

The remaining data sources were published literature, government reports (i.e., MNR and OGS), and consulting reports. These data sources were useful for confirming the extent and predictability of geological units across the RSA and as guidance for understanding detailed stratigraphic relationships in the subsurface.

The data base from which the geological framework model was developed is continually being updated; data from additional boreholes can be added to the database and used to develop a new spatial model. The marginal benefit of the new data will depend on factors such as the location of a new well and the reliability of the data as compared to that from nearby wells.

The Gartner Lee Limited (2008b) geologic framework model includes only the units/formations/groups that could be reliably interpreted within the study area. Gartner Lee Limited (2008b) state that several units were not consistently logged within the OGSR data base but rather were grouped within other larger units/formations. Referring to Figure 2 and the units logged in the DGR-1 and DGR-2 boreholes (Table 1), the grouping is as follows: the B Unit and the C Unit were combined; the A0 Unit was not identified in the regional domain; the Guelph, Goat Island, Gasport and Lions Head were combined as the Niagaran as the contacts for the individual units were not consistently picked; and, the Georgian Bay, Blue Mountain and

Collingwood were combined as the Collingwood was commonly not individually logged and more likely to have been logged as part of the Blue Mountain Formation shales.

Table 2 summarizes the data used to develop the Gartner Lee Limited (2008b) geologic framework model. Also listed, for comparison, are the thicknesses of the units observed in the DGR-1 and DGR-2 boreholes. In spite of the variability of the data, it should be noted that the presence of the Ordovician shale and limestone units is easily predictable given the data. When the average thicknesses and their corresponding standard deviations are taken into account, it can be concluded that despite the variability in the thicknesses, the data support the conclusion that the Ordovician shale and limestone units are continuous across the regional domain with large observed thicknesses occurring in the vicinity of the proposed Bruce DGR.

2.3.3 Incorporating the GLL00 Model in the Regional-Scale Numerical Model

The geological framework model developed by Gartner Lee Limited (2008b) was used to define the layers of the regional-scale spatial domain that was used as the basis of the analyses presented in this study; details of the framework model are given in their report. Figure 10 shows the extent of the Cambrian in the regional-scale spatial domain. An important attribute of this more permeable unit (refer to Table 1) is that it is present only over the more westerly part of the domain. In comparison, the geologic framework model developed by Sykes (2007) using a first-order polynomial interpolation scheme, resulted in the Cambrian extending over the entire model domain, although the thickness assigned to the more easterly portion of the domain was less than one metre. The impact of this conceptualization on the model results is explored in Section 5.3.3.

The extent of the Niagaran of the Middle Silurian, also with a higher permeability as shown in Table 1, is presented in Figure 11. The zone with a smooth surface corresponds to the portion of the Niagaran that is overlain by the Salina in the Upper Silurian whereas the extensive subcrop of the unit beneath the glacial sediments can be identified in the figure by the portion with a rough textured appearance. Figure 12 shows the three-dimensional geological framework model for all units below the surface drift while the drift is added in Figure 13 which has a vertical exaggeration of 40 to 1, in Figure 14 with no vertical exaggeration and in the fence diagram of Figure 15 (the vertical exaggeration is 40 to 1). The thinness of the regional domain as compared to its spatial extent is readily apparent in Figure 14.

2.4 Geochemistry

Regarding the hydrogeochemistry of the Michigan Basin, the groundwater can be typified as being Na-Ca-Cl or Ca-Na-Cl brines. The brines also exhibit levels of total dissolved solids (TDS) that range from approximately 10 g/L to 400 g/L; the levels associated with the Bruce site sedimentary sequences are listed in Table 1. The low TDS values are attributed to the shallower geologic formations, such as the Dundee and Lucas formations, where there is a strong influence by meteoric water. The groundwater in the deeper formations have much higher TDS levels. The higher TDS levels will cause the groundwater to have a comparatively higher density, as the conceptual relationship of Figure 16 demonstrates. The relationship between dissolved solids concentration and density requires the measurement of the concentration of the various ions

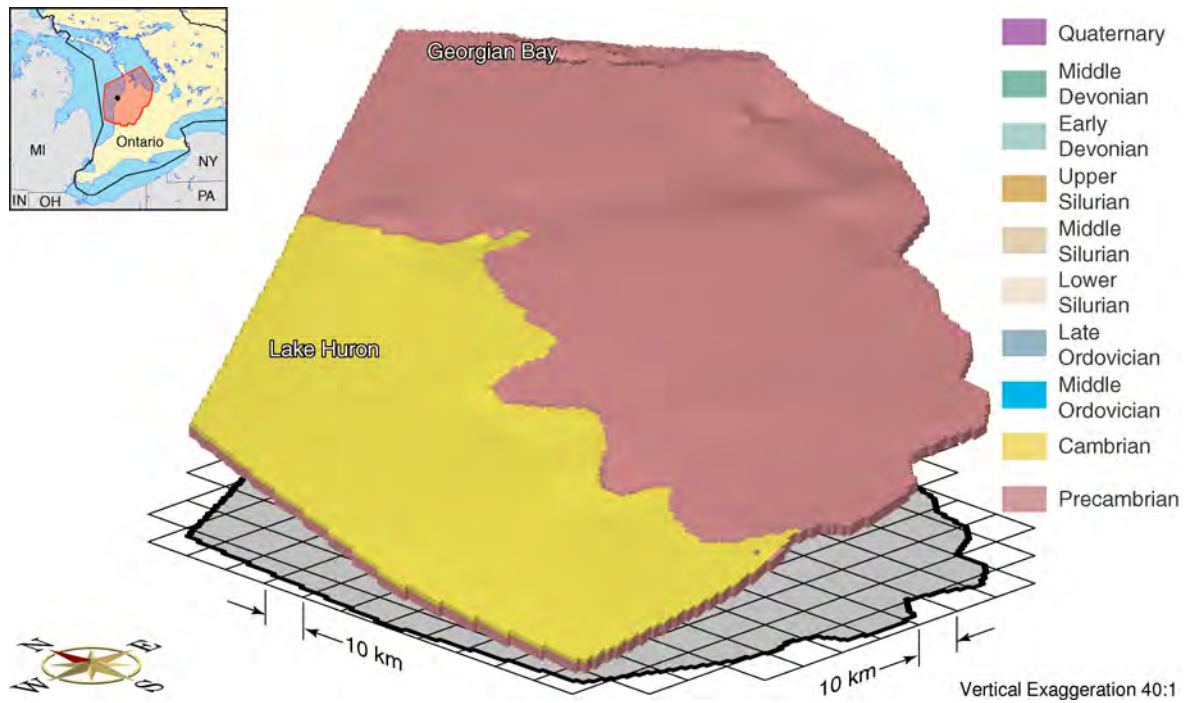


Figure 10: The spatial extent of the Cambrian in the regional domain.

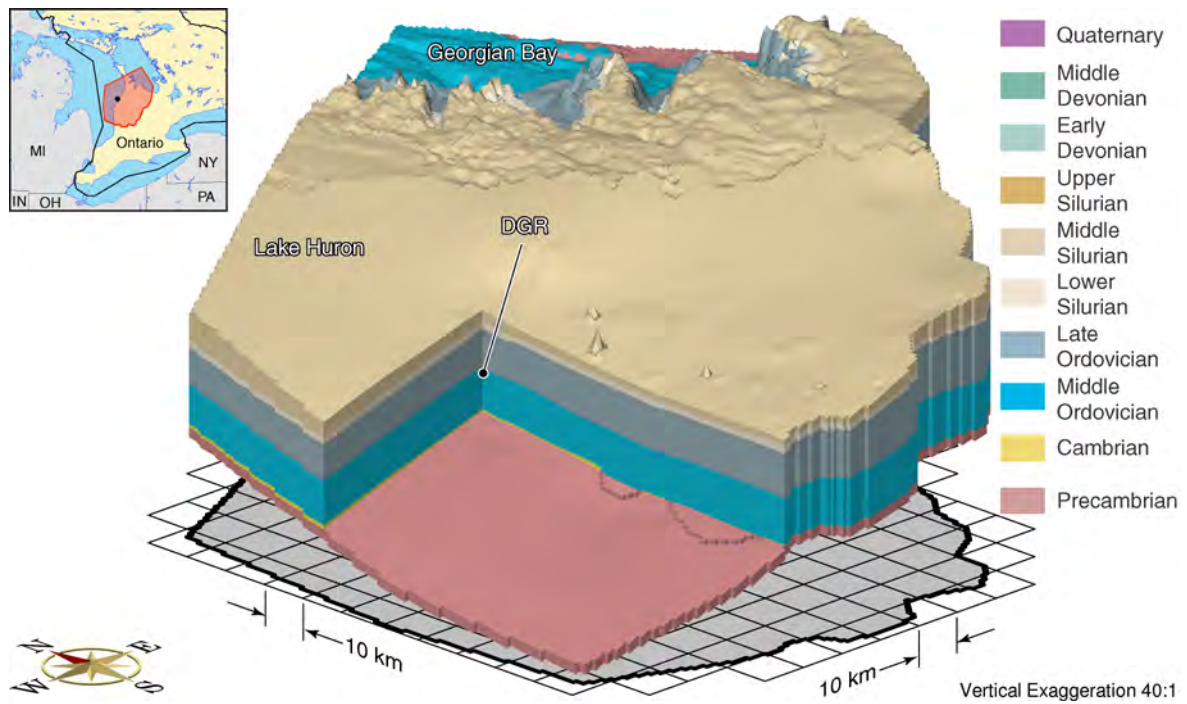


Figure 11: The spatial extent of the Niagaran (refer to the Middle Silurian in the legend) in the regional domain.

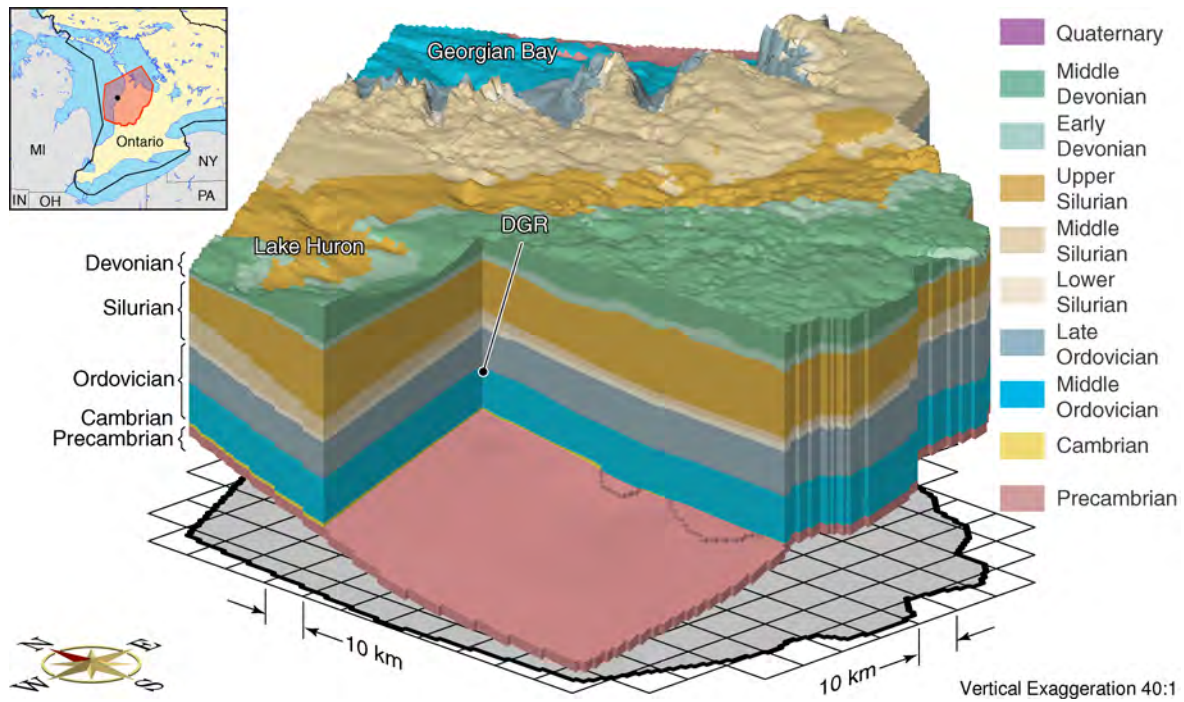


Figure 12: The regional domain below the drift.

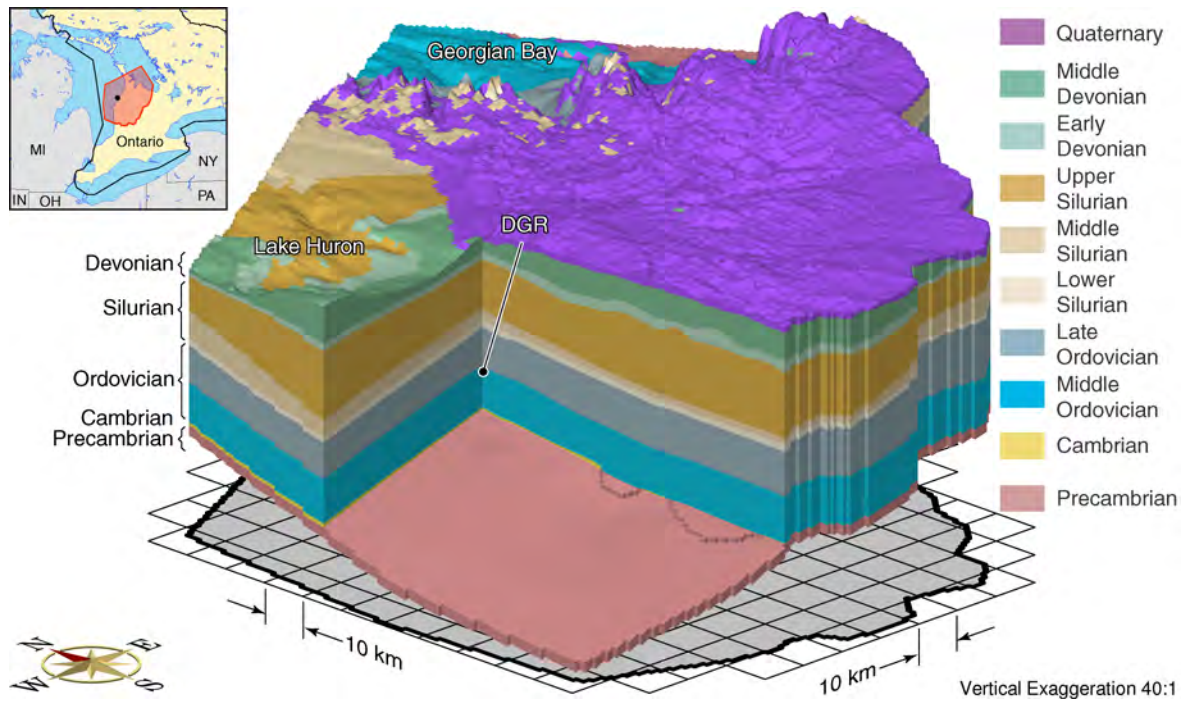


Figure 13: The regional domain showing all geological units.

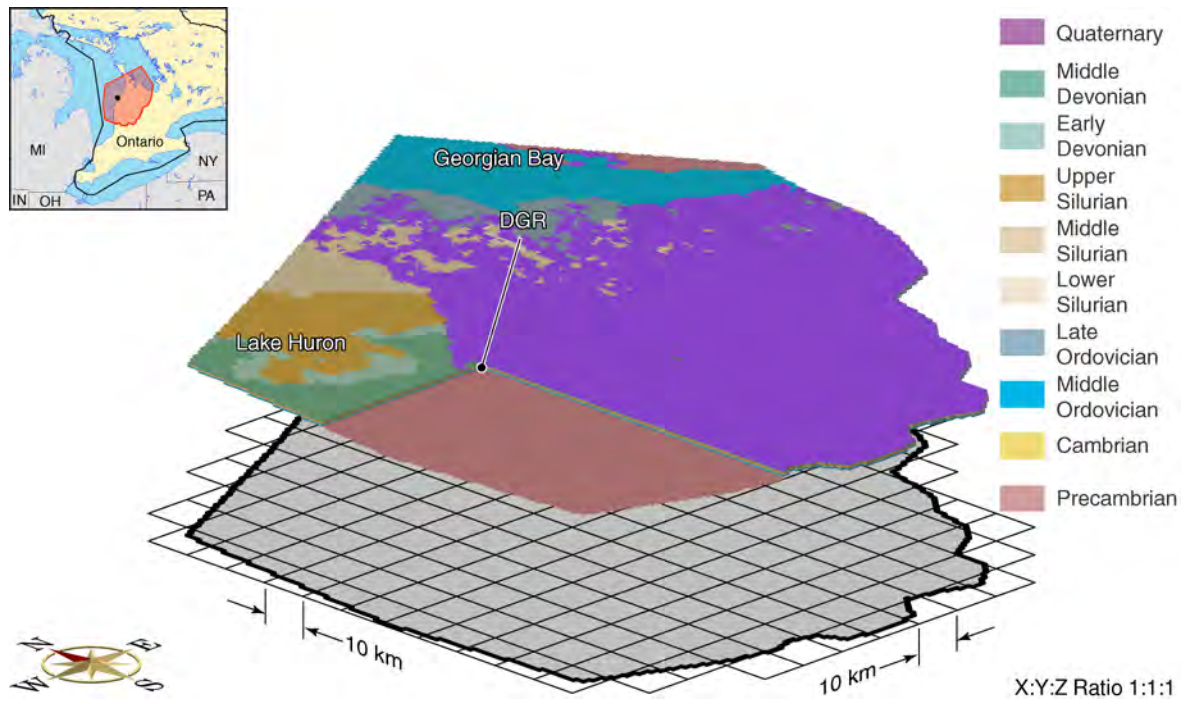


Figure 14: The regional domain showing all geological units with no vertical exaggeration.

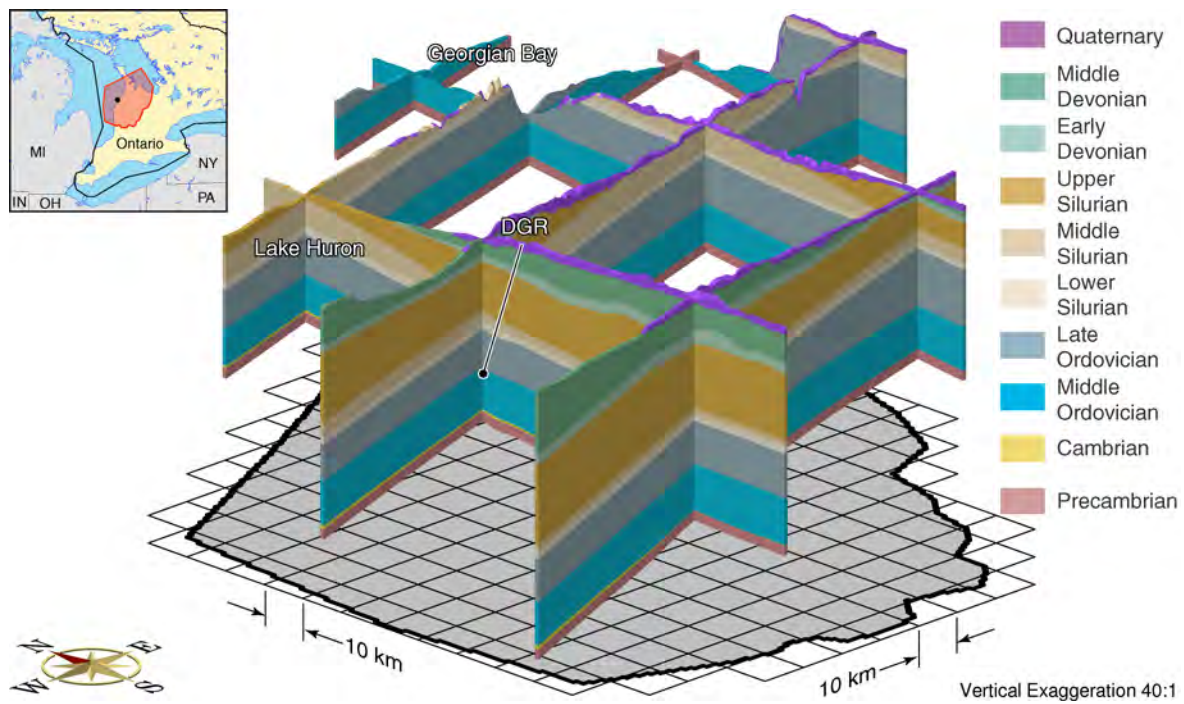


Figure 15: Fence diagram of the regional domain showing all geological units.

Table 2: Three-dimensional geological framework unit thickness compared with DGR site data

| Geological Unit | Samples | Mean Thickness [m] | Standard Deviation of Thickness [m] | Thickness at DGR [m] † |
|------------------------|---------|--------------------|-------------------------------------|------------------------|
| Dundee | 67 | 15 | 8 | * |
| Detroit River | 94 | 103 | 31 | ** |
| Bois Blanc | 93 | 52 | 19 | 49 |
| Bass Islands | 121 | 50 | 17 | 54 |
| G Unit | 90 | 9 | 6 | 5 |
| F Unit | 9 | 46 | 4 | 40 |
| F Salt | 10 | 15 | 6 | * |
| E Unit | 43 | 27 | 7 | 20 |
| D Unit | 44 | 9 | 3 | 2 |
| B and C Units | 88 | 28 | 7 | 47 |
| B-Anhydrite/Salt | 84 | 49 | 31 | 2 |
| A-2 Carbonate | 87 | 33 | 10 | 27 |
| A-2 Anhydrite/Salt | 85 | 13 | 11 | 8 |
| A-1 Carbonate | 82 | 36 | 8 | 39 |
| A-1 Evaporite | 82 | 5 | 4 | 8 |
| Niagaran | 109 | 55 | 39 | 34 |
| Reynales/Fossil Hill | 105 | 7 | 4 | 3 |
| Cabot Head | 71 | 21 | 12 | 21 |
| Manitoulin | 71 | 11 | 4 | 16 |
| Queenston | 72 | 85 | 25 | 70 |
| Georgian Bay/Blue Mtn. | 84 | 135 | 50 | 142 |
| Cobourg | 76 | 48 | 17 | 27 |
| Sherman Fall | 73 | 44 | 13 | 46 |
| Kirkfield | 70 | 39 | 11 | 30 |
| Coboconk | 73 | 13 | 8 | 17 |
| Gull River | 77 | 45 | 16 | 60 |
| Shadow Lake | 26 | 9 | 8 | 5 |
| Cambrian | 20 | 7 | 5 | 17 |

Note: † thickness of units at DGR-1 and DGR-2

* not present at site

** full thickness not present at site

contributing to the dissolved solids. An analysis and discussion of the regional hydrogeochemical data is presented in Hobbs et al. (2008).

2.5 Hydrogeologic Parameters

An important aspect characterizing the regional scale groundwater system will be the assignment of reasonable permeabilities to the hydrostratigraphic units. Careful estimation of permeability values will help increase the accuracy of the geologic model. The estimated horizontal hydraulic

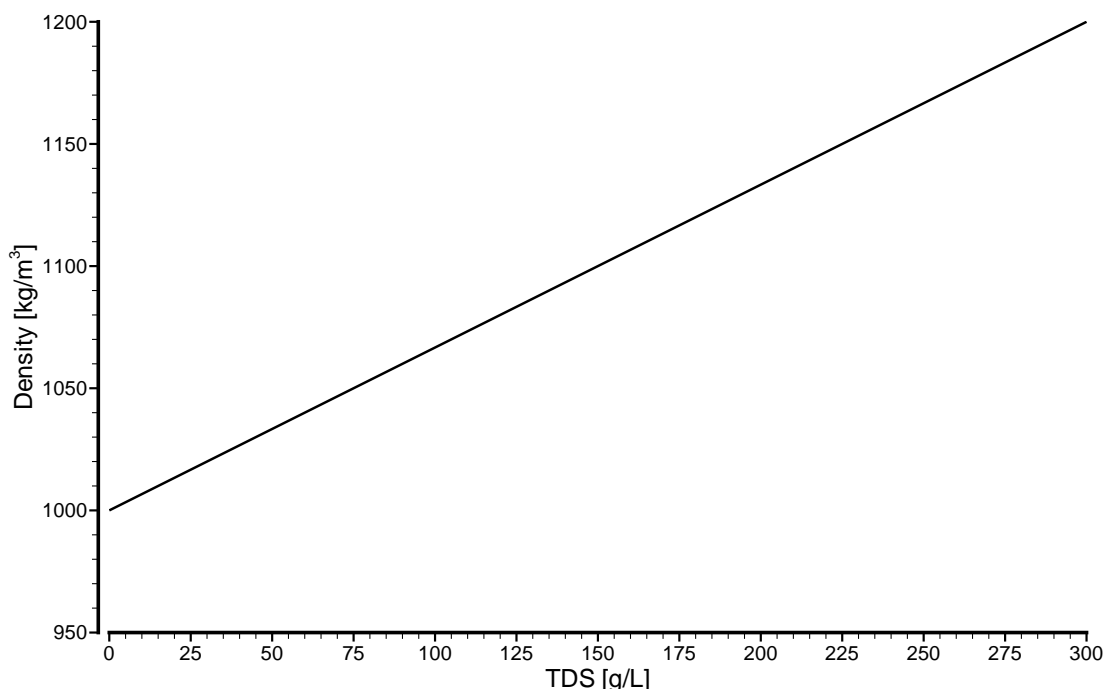


Figure 16: Conceptualized relationship between density and concentration.

conductivities developed from the Phase 1 field investigation at the Bruce site are listed in Table 1. Other reported data from insitu measurements are listed in Table 3, Table 4, Table 5 and Table 6. The minimum and maximum values of hydraulic conductivity that are reported in the tables represent the range of values for a given unit. It should be noted that in many instances, the minimum hydraulic conductivities reported are at the measurement limit of the hydrogeologic testing equipment. The values from testing programs in the 1980s and the 1990s still reflect values that are obtained with current testing practice. Further, the values reported in the tables generally represent point estimates at boreholes with the hydraulic conductivities reflecting a small volume around the borehole wall; that is, they are not up-scaled values that may be more representative of a regional-scale flow domain. Finally, the tables include values for the various units of the Niagaran Group rather than an integrated value for that group.

In each of the tables, the formations with the lowest measured hydraulic conductivities are the Ordovician shales and limestones, with hydraulic conductivities typically in the range of approximately 1×10^{-11} m/s. The low permeability Ordovician and Lower Silurian units are bounded above by the Niagaran Group, which is more permeable with reported horizontal hydraulic conductivities typically estimated at 1×10^{-8} m/s, and bounded below by the Cambrian Formation which, based on field measurements performed on the DGR-2 borehole at the Bruce site, has a horizontal hydraulic conductivity value of 3×10^{-6} m/s. Although the hydraulic conductivity for the Cambrian is much higher than the low permeability Ordovician shales and limestones, it is not believed to be a potential pathway for fluid migration because it is discontinuous (Armstrong and Carter, 2006) and bounded above and below by low permeability formations. Further, based on data from the Phase 1 field program (Table 1 and Figure 7), the Cambrian is significantly over-pressured with respect to the overlying Ordovician units. Present

Table 3: Paleozoic hydraulic conductivities from Raven et al. (1992)

| Formation | Borehole | K_{min} [m/s] | K_{max} [m/s] |
|----------------------|----------------------|-----------------------|-----------------------|
| Dundee | MDMW-1 Sarnia | 4.0×10^{-13} | 1.3×10^{-7} |
| Lucas | MDMW-1 Sarnia | 2.5×10^{-9} | 3.2×10^{-7} |
| Amherstberg | MDMW-1 Sarnia | 3.2×10^{-11} | 7.9×10^{-9} |
| Guelph | USNI-1 Niagara Falls | 1.6×10^{-7} | 1.0×10^{-5} |
| Guelph | NI-1 Niagara Falls | 7.9×10^{-9} | 6.3×10^{-5} |
| Goat Island | USNI-1 Niagara Falls | 3.2×10^{-8} | 1.0×10^{-5} |
| Goat Island | NI-1 Niagara Falls | 3.2×10^{-9} | 2.0×10^{-5} |
| Gasport | USNI-1 Niagara Falls | 1.0×10^{-13} | 1.0×10^{-13} |
| Gasport | NI-1 Niagara Falls | 2.0×10^{-8} | 2.0×10^{-8} |
| Rochester | USNI-1 Niagara Falls | 1.0×10^{-13} | 2.5×10^{-7} |
| Rochester | NI-1 Niagara Falls | 1.3×10^{-9} | 1.3×10^{-7} |
| Reynales/Fossil Hill | USNI-1 Niagara Falls | 1.0×10^{-12} | 2.5×10^{-11} |
| Reynales/Fossil Hill | USNI-1 Niagara Falls | 3.2×10^{-11} | 3.2×10^{-11} |
| Cabot Head | NI-1 Niagara Falls | 6.3×10^{-11} | 6.3×10^{-11} |
| Queenston | USNI-1 Niagara Falls | 2.5×10^{-13} | 2.0×10^{-11} |
| Queenston | USNI-1 Niagara Falls | 4.0×10^{-11} | 1.0×10^{-9} |
| Georgian Bay | OHD-1 Lakeview | 1.0×10^{-13} | 4.0×10^{-12} |
| Collingwood | OHD-1 Lakeview | 1.0×10^{-12} | 1.0×10^{-12} |
| Cobourg | OHD-1 Lakeview | 1.0×10^{-13} | 6.3×10^{-12} |
| Cobourg | UN-2 Darlington | 6.3×10^{-14} | 1.6×10^{-11} |
| Sherman Fall | OHD-1 Lakeview | 2.0×10^{-14} | 1.3×10^{-12} |
| Sherman Fall | UN-2 Darlington | 1.0×10^{-13} | 7.0×10^{-9} |
| Kirkfield | OHD-1 Lakeview | 1.0×10^{-13} | 4.0×10^{-12} |
| Kirkfield | UN-2 Darlington | 1.0×10^{-13} | 4.0×10^{-12} |
| Gull River | OHD-1 Lakeview | 2.5×10^{-14} | 2.5×10^{-11} |
| Gull River | UN-2 Darlington | 1.0×10^{-13} | 1.0×10^{-12} |
| Shadow Lake | OHD-1 Lakeview | 1.0×10^{-13} | 1.0×10^{-09} |
| Shadow Lake | UND-1 Darlington | 1.0×10^{-13} | 1.0×10^{-12} |

Table 4: Paleozoic hydraulic conductivities from Golder Associates Ltd (2003)

| Formation | Borehole | K_{min} [m/s] | K_{max} [m/s] |
|--------------|----------------------|-----------------------|-----------------------|
| Bois Blanc | Bruce | 5.0×10^{-11} | 9.0×10^{-5} |
| Cobourg | DDH01/02 Bowmanville | 1.3×10^{-12} | 4.0×10^{-11} |
| Sherman Fall | DDH01/02 Bowmanville | 5.0×10^{-13} | 2.0×10^{-9} |
| Kirkfield | DDH01/02 Bowmanville | 1.0×10^{-11} | 6.3×10^{-9} |
| Gull River | DDH01/02 Bowmanville | 2.0×10^{-11} | 6.3×10^{-9} |
| Shadow Lake | DDH01/02 Bowmanville | 5.0×10^{-9} | 1.0×10^{-8} |

Table 5: Paleozoic hydraulic conductivities from Novakowski and Lapcevic (1988)

| Formation | Borehole | K_{min} [m/s] | K_{max} [m/s] |
|----------------------|----------|-----------------------|-----------------------|
| Guelph | Niagara | 1.4×10^{-8} | 2.8×10^{-4} |
| Goat Island | Niagara | 7.8×10^{-11} | 5.5×10^{-4} |
| Gasport | Niagara | 1.0×10^{-11} | 1.7×10^{-6} |
| Rochester | Niagara | 1.0×10^{-11} | 1.7×10^{-6} |
| Reynales/Fossil Hill | Niagara | 1.0×10^{-11} | 1.7×10^{-6} |
| Cabot Head | Niagara | 1.0×10^{-11} | 2.0×10^{-7} |
| Queenston | Niagara | 1.0×10^{-11} | 2.4×10^{-10} |

Table 6: Paleozoic hydraulic conductivities from Intera Engineering Ltd. (1988)

| Formation | Borehole | K_{min} [m/s] | K_{max} [m/s] |
|--------------|--------------------|-----------------------|-----------------------|
| Dundee | Sarnia | 5.0×10^{-12} | 1.0×10^{-9} |
| Dundee | Ojibway Mine | 1.0×10^{-7} | 1.0×10^{-6} |
| Lucas | Sarnia | 1.0×10^{-8} | 1.0×10^{-7} |
| Lucas | Goderich Mine | 1.0×10^{-7} | 1.0×10^{-6} |
| Lucas | Ojibway Mine | 1.0×10^{-7} | 1.0×10^{-6} |
| Amherstberg | Sarnia | 1.0×10^{-11} | 1.0×10^{-9} |
| Amherstberg | Goderich Mine | 1.0×10^{-7} | 1.0×10^{-6} |
| Amherstberg | Ojibway Mine | 1.0×10^{-7} | 1.0×10^{-6} |
| Bois Blanc | Nanticoke Tunnel | 1.0×10^{-9} | 1.0×10^{-8} |
| Bass Islands | Goderich Mine | 1.0×10^{-7} | 1.0×10^{-6} |
| Bass Islands | Ojibway Mine | 1.0×10^{-7} | 1.0×10^{-6} |
| Cobourg | Darlington Tunnels | 1.0×10^{-12} | 1.0×10^{-12} |
| Cobourg | Wesleyville | 1.0×10^{-11} | 1.0×10^{-8} |
| Cobourg | Wesleyville | 2.0×10^{-10} | 4.0×10^{-6} |
| Sherman Fall | Wesleyville | 1.0×10^{-11} | 1.0×10^{-8} |

day hydraulic gradients at the Bruce site are upward from the Cambrian to the Ordovician units. Similar to the Cambrian, the Niagaran Group has a much higher permeability than the underlying Lower Silurian and Ordovician formations, and is also bounded immediately above by the Salina Formation and bounded below by low permeability formations such as the Cabot Head shale; the Niagaran Group is also highly continuous.

3. NUMERICAL MODEL DESCRIPTION AND THEORY

3.1 FRAC3DVS-OPG

3.1.1 Model Description

The model FRAC3DVS-OPG v1.0.0-beta3, developed from FRAC3DVS (Therrien et al., 2004), was used for the analyses of this study. It is a numerical model capable of solving three-dimensional variably-saturated density-dependent groundwater flow and solute transport in porous and discretely fractured media. Although the model is capable of handling dual porosity simulations, for the purpose of this regional study, an equivalent porous media approximation was assumed. To solve the density-dependent non-linear flow equation, a Picard iterative solver is utilized.

The assumptions on which FRAC3DVS-OPG is based in order to solve the governing flow equation include: porous media grains are non-deformable; the system being described in the model is under isothermal conditions; and the air phase, where present, is infinitely mobile.

FRAC3DVS-OPG is formulated in terms of Richards' Equation; while only saturated conditions are analyzed in this study, the more complete variably saturated form of the flow equation is presented in the following paragraphs. In order to describe the three-dimensional variably-saturated flow, the following form of Richards' Equation was used:

$$-\nabla \cdot (\omega_m q) + \sum \Gamma_{ex} \pm Q = \omega_m \frac{\partial}{\partial t} (\theta_s S_w) \quad (1)$$

where ω_m [dimensionless] is the volumetric fraction of the total porosity of the porous medium. The volumetric fraction always will be equal to 1.0 for single porosity calculations. In Richards' Equation, the fluid flux [L T⁻¹] is given by:

$$q = -\mathbf{K} k_r \nabla (\psi + z) \quad (2)$$

where $k_r = k_r(S_w)$ represents the relative permeability [dimensionless] of the porous medium with respect to the degree of water saturation (S_w), ψ is the pressure head [L], z is the elevation head [L] and θ_s is the saturated water content [dimensionless]. The saturated water content is assumed to be equal to the porosity. The term Q [L³ L⁻³ T⁻¹] represents the volumetric fluid flux per unit volume. This term is used to represent a source or a sink.

The hydraulic conductivity tensor \mathbf{K} [L T⁻¹] is given by

$$\mathbf{K} = \frac{\rho g}{\mu} \mathbf{k} \quad (3)$$

where g is the gravitational acceleration [L T⁻²], μ is the viscosity of the groundwater [M L⁻¹ T⁻¹], \mathbf{k} is the permeability tensor of the porous medium [L⁻²] and ρ is the density of the groundwater [M L⁻³]. The density of the groundwater can be dependent on a concentration C [M L⁻³] of a given solute such that $\rho = \rho(C)$.

Water saturation is related to the water content θ [dimensionless] by the relationship

$$S_w = \frac{\theta}{\theta_s} \quad (4)$$

In Equation (1), Γ_{ex} represents the volumetric fluid exchange rate [$L^3 L^{-3} T^{-1}$] between the subsurface domain and any applicable model supported domain types. This parameter is expressed as a unit volume of the other domain types. The possible domain types may be surface wells, tile drains, discrete fractures or dual continuum.

In Equation (1), the primary solution variable is the pressure head. To solve for this variable, a constitutive relationship is required to relate the pressure head to other secondary variables such as the saturation and permeability terms. The saturation can be related to the pressure using the Brooks and Corey (1964) relationship:

$$\begin{aligned} S_w &= S_{wr} + (1 - S_{wr})|\alpha\psi|^{-\beta} \text{ for } \psi < -1/\alpha \\ S_w &= 1 \text{ for } \psi \geq -1/\alpha \end{aligned} \quad (5)$$

and the relative permeability is described by:

$$k_r = S_e^{2/\beta + l_p + 2} \quad (6)$$

where α [L^{-1}] is the inverse of the air entry pressure head, β [dimensionless] is the poresize distribution index, l_p is the pore connectivity parameter, which is assumed to be equal to 2.0 in Brooks and Corey (1964) and S_e , the effective saturation. The effective saturation is determined by $S_e = (S_w + S_{wr})/(1 - S_{wr})$, with S_{wr} referring to the residual water saturation [dimensionless].

The following pressure-saturation relationship was described by Van Genuchten (1980):

$$\begin{aligned} S_w &= S_{wr} + (1 - S_{wr}) \left[1 + |\alpha\psi|^\beta \right]^{-\nu} \text{ for } \psi < -1/\alpha \\ S_w &= 1 \text{ for } \psi \geq -1/\alpha \end{aligned} \quad (7)$$

with the permeability being described by:

$$k_r = S_e^{(l_p)} \left[1 - \left(1 - S_e^{1/\nu} \right)^\nu \right]^2 \quad (8)$$

where:

$$\left(\nu = 1 - \frac{1}{\beta} \right), \quad \beta > 1 \quad (9)$$

and where α and β are obtained by fitting Equation (7) and Equation (8) to experimental data.

The description of subsurface flow in the saturated zone is done by expanding the storage term on the right hand side of Equation (1) to relate a change in storage to a change in fluid pressure

through compressibility terms. This requires the assumption that the bulk compressibility of the porous medium is constant for saturated conditions. For unsaturated conditions, it is assumed that the compressibility effects on the storage of water is negligible when compared with the changes in saturation. Following Cooley (1971) and Neumann (1973), the following expression for the storage term is developed:

$$\frac{\partial}{\partial t}(\theta_s S_w) \approx S_w S_s \frac{\partial \psi}{\partial t} + \theta_s \frac{\partial S_w}{\partial t} \quad (10)$$

where S_s is the specific storage coefficient of the porous medium [L^{-1}].

3.1.2 Density-Dependent Flow and Transport

At greater depths within the Michigan Basin, the pore-fluids begin to become more saline and generally have significantly higher total dissolved solids than shallow groundwater. The increased salinity of the fluid will act as an impediment to flow as the less dense surficial waters are unable to displace the more saline, higher density deeper fluids given the relatively low topographic gradients in the Michigan Basin. Considering the impact of both temperature and concentration, the physical properties of groundwater in the regional-scale domain can vary by greater than 25% for density and by one order-of-magnitude for viscosity. Density and viscosity changes may retard or enhance fluid flow or contaminant transport driven by other mechanisms: flow and transport is dependent on fluid density and viscosity, as well as media properties such as permeability, porosity, and dispersivity. Thus, variations in fluid density and viscosity may have significant impacts on the groundwater system with consequences for various relevant processes.

For density-dependent flow and transport, the governing equations include Darcy's Law and the continuity equations for flow and transport. Density-dependent flow in FRAC3DVS-OPG is formulated in terms of equivalent freshwater heads. The equivalent freshwater head at a point i in groundwater of variable density is defined as the water level in a well filled with fresh water from i to a level high enough to balance the existing pore water pressure at i (Luszczynski, 1961).

The saturated, density dependent form of Darcy's Law is given by:

$$q_i = -\frac{k_{ij}}{\mu} \left(\frac{\partial p}{\partial x_j} + \rho g \eta_j \right) \quad (11)$$

where q_i [$L T^{-1}$] is the flux in the i th direction, k_{ij} [L^2] is the permeability tensor, μ is the viscosity [$M L^{-1} T^{-1}$], p [L] is the pressure, ρ [$M L^{-3}$] is the density of groundwater and $\eta = 1$ [L] for the vertical (z) direction, while $\eta = 0$ for the horizontal directions (x and y). When Equation (11) is rewritten in terms of equivalent freshwater heads (which is defined as follows: $h = p/\rho_0 g + z$), it becomes:

$$q_i = -\frac{k_{ij}}{\mu g} \left(\frac{\partial h}{\partial x_j} + \rho_r \eta_j \right) \quad (12)$$

where ρ_r [dimensionless] is the relative density, given by $\rho/\rho_0 - 1$ where ρ_0 is the reference freshwater density. For elastic fluids, the density of a fluid becomes a function of the fluid pressure and solute concentration:

$$\rho = \rho_0 [1 + c_w (p - p_0) + \gamma C] \quad (13)$$

where ρ_0 [M L⁻³] is the freshwater density at a reference pressure p_0 , c_w is the compressibility of water, γ is a constant derived from the maximum density of the fluid, ρ_{max} and is defined as $\gamma = (\rho_{max}/\rho_0 - 1)$ and C is the relative concentration.

Under isothermal conditions, the viscosity μ is a function of the concentration of the fluid. For the viscosity, it is assumed that there is a linear relation between the relative concentration so long as the maximum viscosity change is insignificant in isothermal conditions.

$$\mu = \mu_0 (1 + \gamma_\mu C) \quad (14)$$

where μ_0 is the viscosity of freshwater and $\gamma_\mu = (\mu_{max}/\mu_0 - 1)$. When the equations for the elasticity of the fluid and the viscosity are included in the Darcy's equation, it becomes:

$$q_i = -\frac{k_{ij}}{\mu_0 g} \cdot \frac{1}{1 + \gamma_\mu C} \left(\frac{\partial h}{\partial x_j} + [c_w (p - p_0) + \gamma C] \eta_j \right) \quad (15)$$

The groundwater flow equation can then be derived using Equation (15) and the continuity of energy principle.

$$\frac{\partial}{\partial x_i} \left[K_{ij}^0 \cdot \frac{1}{1 + \gamma_\mu C} \left(\frac{\partial h}{\partial x_j} + [c_w (p - p_0) + \gamma C] \eta_j \right) \right] = S_s \frac{\partial h}{\partial t} \quad (16)$$

where $K_{ij}^0 = k_{ij}/\mu_0 g$ and S_s is the specific storage term.

The solute continuity equation is written in terms of relative concentration as:

$$\frac{\partial}{\partial x_i} \left(\phi D_{ij} \frac{\partial C}{\partial x_j} \right) - \frac{\partial}{\partial x_i} (q_i C) = \phi \frac{\partial C}{\partial t} \quad (17)$$

where the Darcy flux q_i is computed by solving Equation (16), ϕ is the porosity and D_{ij} is the hydrodynamic dispersion tensor (Bear, 1988):

$$\phi D_{ij} = (\alpha_l - \alpha_t) \frac{q_i q_j}{|q|} + \alpha_t |q| \delta_{ij} + \phi \tau D_w \delta_{ij} \quad (18)$$

where α_l and α_t are the longitudinal and transverse dispersivities respectively, $|q|$ is the magnitude of the Darcy flux, τ is the tortuosity, D_w is the free solution diffusion coefficient or simply the diffusion coefficient and δ_{ij} is the Kronecker delta. The pore water diffusion coefficient is obtained by τD_w . In literature, the pore water diffusion coefficient is also referred to as the diffusion coefficient of the porous medium (Bear, 1988).

It should be noted that the equations for density-dependent flow and transport are nonlinear; to solve the flow Equation (16), the relative densities, which are dependent upon the transport Equation (17), which itself requires Darcy fluxes from Equation (16), are required.

For more detail on the implementation of density-dependent flow in FRAC3DVS-OPG, refer to Therrien et al. (2004).

3.1.3 Equivalent Freshwater Heads and Environmental Heads

The governing density-dependent flow equation (refer to Equation (16) in Section 3.1.2) in FRAC3DVS-OPG is formulated in terms of equivalent freshwater heads. The velocity components are calculated in the model using the density-dependent form of Darcy's equation (refer to Equation (15) in Section 3.1.2). In physical terms, the equation shows that there are two components contributing to the gradient: the derivative of head or head gradient and an additional density gradient term or fractional excess density term. As noted by Massman et al. (2006), in the vertical, this density driving force acts in the direction of the gravitational unit vector and is sufficient to drive flow even in the absence of external hydraulic gradients. Lusczynski (1961) showed that incorrect vertical velocities will be calculated using the equivalent freshwater heads in the commonly used constant-density form of Darcy's equation. The interpretation of vertical hydraulic gradients from plots of equivalent freshwater heads is thus complex and conclusions will often be incorrect, particularly in regards to the magnitude and direction of the vertical gradient. To graphically interpret the vertical gradients, Lusczynski (1961) introduced the term environmental water head. The environmental water head at a given point i in groundwater of variable density is defined as the freshwater head reduced by an amount corresponding to the difference between the freshwater density and the average salt dependent pore water density in the environmental water between the point i and the top of the zone of saturation. The environmental head is defined in terms of the equivalent freshwater head at the point i as (Lusczynski, 1961):

$$h_{in} = h_{if} - \left(1 - \frac{\rho_a}{\rho_f}\right) (z_i - z_r) \quad (19)$$

where h_{if} is the equivalent freshwater head at point i , h_{in} is the environmental head at point i , ρ_f is the fresh water density, ρ_a is the average density of water between z_i the elevation of i (measured positively upwards) and z_r the elevation of a reference point from which the average density of water to i is determined and above which water is fresh and is given as:

$$\rho_a = \frac{1}{z_r - z_i} \int_{z_i}^{z_r} \rho dz \quad (20)$$

In practice, z_r is defined at the top of the saturated zone. From Equation (19), the vertical gradient of h_{in} differs from the vertical gradient of h_{if} by a term derived by Lusczynski (1961) as $(\rho_i - \rho_f) / \rho_f$ where ρ_i is the density of water at i . Just as the equivalent freshwater heads cannot be compared along a vertical, the environmental heads cannot be compared along the horizontal in groundwater of variable density.

3.1.4 Numerical Implementation

Equation (17) is identical to the equation for transport in freshwater. Numerical discretization for Equation (17) and solution strategies are detailed in Therrien et al. (2004). Nonlinear flow and transport equations are solved by using Picard iteration in each time step, until the changes in equivalent freshwater head and relative concentration are negligible for convergence.

The dependent variable for flow in FRAC3DVS-OPG is equivalent freshwater head; the model does not calculate environmental heads. For this study, to facilitate the graphical interpretation of

the flow domain, a computer script was written to post-process the model freshwater heads and vertical density distribution estimated using the model total dissolved solids distribution to determine the environmental heads from Equation (19) and Equation (20). Three-dimensional plots of regional-scale and site-scale environmental heads could then be generated. While the plots enable the interpretation of vertical gradients, they should not be used to infer horizontal gradients. Three-dimensional plots of equivalent freshwater heads can be used to infer horizontal gradients, however, they are misleading for the determination of vertical gradients in variably dense groundwater systems.

Hydrostatic equilibrium in the vertical direction can be applied to the domain as an initial condition for density-dependent flow and transport simulations. A vertically hydrostatic equilibrium condition is expressed using the variable-density formulation of Darcy's equation and equivalent freshwater heads as:

$$q_z = -\frac{k_{zz}}{\mu_0 g} \cdot \frac{1}{1 + \gamma_\mu C} \cdot \left(\frac{\partial h}{\partial z} + [c_w(\rho - \rho_0) + \gamma C] \right) = 0 \quad (21)$$

where as in the preceding paragraphs, z represents the vertical direction. By integrating Equation (21) from z_r to z_i , where z_r is the reference elevation at which the equivalent freshwater head $h(z_r)$ is prescribed, the equivalent freshwater head at z_i in an equilibrium condition can be derived:

$$h(z_i) = h(z_r) + \int_{z_i}^{z_r} [c_w(\rho - \rho_0) + \gamma C] dz \quad (22)$$

The post-processor developed for the calculation of environmental heads requires the numerical integration of N vertically aligned nodes in a discretized domain:

$$h_i^{it} = h_{r,N} + \sum_{k=i}^N [c_w(\bar{p}_k^{it-1} - \rho_0) + \gamma \bar{C}_k] \Delta z_k \quad (23)$$

where superscript it represents the nonlinear iteration count and summation is implied over elements between node i and the top reference node N of reference head h_r while \bar{p} and \bar{C} are the average elemental fluid pressure and relative concentration in the element, respectively. The verification of the initial vertically hydrostatic equilibrium condition is presented in Normani et al. (2007).

3.1.5 Implementation of Paleoclimate and Surface Boundary Conditions

The climate and surface boundary conditions are provided by Peltier (2008). Two parameters are used in this study: permafrost depth (d_{PF}), and the normal stress (σ_{ice}) at ground surface due to the presence of ice. Both of these parameters are used, with some assumptions, in FRAC3DVS-OPG. Firstly, the ice load is applied as equivalent freshwater head using a Dirichlet boundary condition across all surface nodes. Assuming purely vertical strain and areally homogeneous loading, the ice stress also is used to modify the pore pressure of the rock as would occur with its compression on loading and dilation on load removal (Neuzil, 2003). Secondly, the permafrost depth modifies the porous media hydraulic conductivity depending on

the depth of permafrost. Both permafrost depth and normal stress vary in time with 500 year time steps. FRAC3DVS-OPG can vary time steps to suit groundwater flow and solute transport maximum change criteria ($\Delta h, \Delta C$).

The equations that describe the impact of glaciation and deglaciation on groundwater pressures and flow can be simplified by assuming that ice loads are areally homogeneous in which case, the lateral strains are zero. The assumption is valid for cases where the speed of advance and retreat of the glacier is fast relative to the horizontal flow velocity in the groundwater system. For this case of purely vertical strain and following the development of Neuzil (2003), the density-dependent flow equation becomes:

$$\frac{\partial}{\partial x_i} \left[K_{ij}^0 \cdot \frac{1}{1 + \gamma_\mu C} \left(\frac{\partial h}{\partial x_j} + [c_w (\rho - \rho_0) + \gamma C] \eta_j \right) \right] = S_s \frac{\partial h}{\partial t} - S_s \zeta \frac{\partial \sigma_{zz}}{\partial t} \quad (24)$$

where σ_{zz} is the vertical stress. The one-dimensional loading efficiency, ζ , is a function of Poisson's ratio for the rock, the drained bulk modulus of the porous medium, the modulus of the solids and the porosity. Values for the loading efficiency vary between zero and one. When ζ equals zero, Equation (24) is equal to Equation (16). The last term in Equation (24) is independent of the equivalent freshwater head h and modifies the pressure throughout the one-dimensional column beneath the surface ice by adding water on loading and extracting water on unloading with the volume of water being defined by the porosity and compressibility terms in the specific storage.

The hydraulic conductivity of frozen porous media is assigned the value of 1.6×10^{-3} m/year (5×10^{-11} m/s) and is assumed to be isotropic (McCauley et al., 2002). For each time step, if the depth of permafrost extends below the top of an element, calculated at the centroid of the top face, that element will be assigned the permafrost permeability.

The normal stress due to the weight of ice on the domain is used to calculate an equivalent freshwater head which is applied at all surface nodes as a Dirichlet boundary condition, h_{ice} according to:

$$h_{ice} = \frac{\sigma_{ice}}{\rho g} + z \quad (25)$$

where ρ is freshwater density, g is the gravitational constant, and z is elevation of the water table, itself located 3 m below ground surface and also specified using a Dirichlet boundary condition for most modelling scenarios. If $\sigma_{ice} = 0$, then the specified head is defined as in the non paleoclimate simulations. A meltwater production rate is not used for the ice-sheet.

3.2 System Performance Measures

The DGR safety case relies, in part, on the ability of the far-field to provide a long-term barrier to solute transport. In trying to robustly characterize the groundwater flow and transport regimes in the deeper basinal formations, it is prudent to determine and quantify what impact, if any, the variability of model parameters will have upon the model results. It is by demonstrating and determining the sensitivity of the model to perturbations in model parameters that a more rigorous understanding of the groundwater system at depth can be achieved.

Common measures of the performance of a groundwater system include the flow state variables of equivalent freshwater head or environmental head and the derived pore water velocity, the solute concentration for a conservative tracer, average water particle paths and travel time, and as developed in Normani et al. (2007), mean lifetime expectancy and groundwater age. Lifetime expectancy can be estimated by determining the time required for a water particle at a spatial position in a groundwater system to reach a potential outflow point. Groundwater age of a water particle at a spatial position can be determined by the time elapsed since the water particle entered the system from a boundary condition. Sensitivity analyses using marginal sensitivity coefficients and normalized sensitivity coefficients also provide information on the groundwater system. Each of these performance measures have their advantages and disadvantages. Sensitivity coefficients are local derivatives and for systems with a large number of spatially and possibly temporally varying parameters, there is considerable computational burden in calculating the sensitivity coefficients for each parameter. While average water particle paths can indicate the discharge point for water from a repository, most algorithms are based on steady-state flow and the associated travel time accounts for advection, but neither dispersion nor diffusion. The travel time can thus significantly overestimate the arrival of a contaminant along a path in which diffusion dominates advection. Mean lifetime expectancy (MLE) correctly replicates the transport processes, but like all numerical solutions developed for a form of the advection dispersion equation, it is subject to the classical problems of numerical instability. As implemented in FRAC3DVS-OPG, where the dispersion model used for total dissolved solids is the same as that used in the equation used to estimate MLE, to achieve a solution, dispersivity coefficients must be carefully selected as a function of grid block size. For a model with large grid blocks and hence a large dispersivity that meets grid or cell Peclet number criteria, MLE may thus underestimate the required time for a constituent to reach a discharge point. The method does not define either the path followed by the constituent or the discharge point. Details of the performance measures are provided in the following sections.

3.2.1 Sensitivity Coefficients

In order to gauge the performance of the groundwater system being characterized in the model, it is prudent to perform some form of sensitivity analysis. These analyses are done to determine the influence a change in parameter will have on the model. The influence of parametric perturbations is then determined by measuring any changes to a state variable or a selected performance measure as a function of a change in parameter:

$$S_{ij} = \frac{\partial P_i(\alpha)}{\partial \alpha_j} \quad (26)$$

where S_{ij} is the sensitivity coefficient, P_i is the state variable or performance measure, which itself is dependent upon α_j , an independent parameter. The sensitivity coefficient S_{ij} can be interpreted as the change in P_i given a unit change in α_j . A negative sensitivity coefficient implies that a positive change in α_j will yield a decrease in P_i . The sensitivity coefficient as expressed by Equation (26) is a local derivative. A normalized sensitivity coefficient can be determined by modifying equation Equation (26) such that:

$$S_{ij} = \frac{\partial P_i}{\partial \alpha_j} \cdot \frac{\alpha_j}{P_i} \quad (27)$$

The normalized sensitivity coefficients S_{ij} are dimensionless and indicate the percent change in P_i for a one percent change in α_j . The normalized sensitivity coefficient for different parameters α_j can be directly compared so as to reveal the system parameter to which P_i is most sensitive.

Possible variables that may be used as an indicator of the system performance include heads, concentrations, groundwater velocity directions and magnitudes, travel time and lifetime expectancy.

3.2.2 Lifetime Expectancy as a Performance Indicator

Groundwater age can be defined as being a relative quantity with respect to a starting location with an assumed age of zero (Cornaton and Perrochet, 2006). For a given spatial position within a domain, the age (denoted as a variable A) of a particle at that position can be determined by the time elapsed since the water particle entered the system at a location where a boundary condition has been applied. The water at an influx boundary condition would have an assumed age of zero. Conversely, the lifetime expectancy (denoted as a variable E) of a particle at the same spatial position can be estimated by determining the time required for a particle from that position to reach a potential outflow point. This definition of lifetime expectancy results in outflow points within the model having a mean lifetime expectancy of zero for the water. The variables for both age and lifetime expectancy are random variables and as such their behaviour can be characterized by that of a probability density function describing the distribution of water particles with respect to time (refer to (Cornaton and Perrochet, 2006)).

For the travel time probability, the amount of time required for a particle to travel from a starting point x_i to a position x is characterized by $g_t(t, x|t_0, x_i)$. In the case of the location probability, the density characterizing the probability of finding a particle at a point x at a time t after the release from a starting point x_i is $g_x(x, t|x_i, t_0)$. Furthermore, if the inlet to a system is correspondent with an inflow source (Γ_-), the travel time will correspond with the groundwater age. Conversely, if the inlet to a system is correspondent with an outflow source (Γ_+), the travel time will correspond with the lifetime expectancy. It is through a solution to the Advection Dispersion Equation (ADE) that the age and lifetime expectancy probability density functions (PDF) can be obtained. These PDFs are determined through applications of specialized boundary conditions.

When the ADE is solved for the case of a unit tracer applied to an inlet (Γ_-), the age PDF for a position x within a domain Ω can be determined. This calculation will result in the probabilistic age distribution. The age PDF is determined by solving the following boundary value problem for a pre-solution of a velocity field:

$$\frac{\partial \phi g}{\partial t} = -\nabla \cdot \mathbf{q}g + \nabla \cdot \phi \mathbf{D} \nabla g + q_i \delta(t) - q_o g \quad \text{in } \Omega \quad (28a)$$

$$g(x, 0) = g(x, \infty) = 0 \quad \text{in } \Omega \quad (28b)$$

$$\mathbf{J}(x, t) \cdot \mathbf{n} = (\mathbf{q} \cdot \mathbf{n} \delta(t)) \quad \text{on } \Gamma_- \quad (28c)$$

$$\mathbf{J}(x, t) \cdot \mathbf{n} = 0 \quad \text{on } \Gamma_0 \quad (28d)$$

where $g(\mathbf{x}, t) = g_A(\mathbf{x}, t)$ represents the transported age PDF [T^{-1}], \mathbf{q} represents the groundwater flux vector [LT^{-1}], q_i and q_o are the fluid source and sink terms [T^{-1}], $\mathbf{J}(x, t)$ represents the total

age mass flux vector $[LT^{-1}]$. \mathbf{D} is the macro-dispersion tensor $[L^2T^{-1}]$, $\mathbf{x} = (x, y, z)$ is the vector of cartesian coordinates $[L]$, t represents time $[T]$, $\phi = \phi(x)$ is either the porosity or the mobile water-content [dimensionless], \mathbf{n} represents a normal outward unit vector and finally, $\delta(t)$ is the time-Dirac delta function $[T^{-1}]$. The purpose of the time-Dirac delta function is to ensure a pure impulse on Γ_- . The total mass age flux vector, $\mathbf{J}(x, t)$, is then defined as being:

$$\mathbf{J}(x, t) = \mathbf{q} g(x, t) - \mathbf{D} \nabla g(x, t) \quad (29)$$

which is the sum of the advective and dispersive fluxes.

The life expectancy probability density function is solved by using the backwards form of the ADE, which acts to reverse time and space, thereby allowing the life expectancy to be determined.

$$\frac{\partial \phi g}{\partial t} = \nabla \cdot \mathbf{q} g + \nabla \cdot \phi \mathbf{D} \nabla g - q_I g \quad \text{in } \Omega \quad (30a)$$

$$g(x, 0) = g(x, \infty) = 0 \quad \text{in } \Omega \quad (30b)$$

$$\mathbf{J}(x, t) \cdot \mathbf{n} = -(\mathbf{q} \cdot \mathbf{n} \delta(t)) \quad \text{on } \Gamma_+ \quad (30c)$$

$$-\mathbf{D} \nabla g(x, t) \cdot \mathbf{n} = 0 \quad \text{on } \Gamma_0 \quad (30d)$$

where $g(\mathbf{x}, t) = g_E(\mathbf{x}, t)$ represents the transported life expectancy PDF $[T^{-1}]$ and the total life expectancy mass flux vector is:

$$\mathbf{J}(x, t) = -\mathbf{q} g(x, t) - \mathbf{D} \nabla g(x, t) \quad (31)$$

3.2.2.1 Age and Lifetime Statistics

From a given age and/or lifetime expectancy probability density function, the mean and standard deviations can be calculated. The case of the mean age or mean life expectancy can be determined by taking the first moment of the PDF solution $g_t(t, x)$:

$$\mu(x) = \int_0^{+\infty} t g_t(t, x) dt \quad (32)$$

The standard deviation for the age and lifetime distributions can be determined using:

$$\sigma(x) = \sqrt{\int_0^{+\infty} t^2 g_t(t, x) dt - \mu^2} \quad (33)$$

3.2.2.2 Direct Solutions for Mean Age and Life Expectancy

It is possible to derive direct solutions for mean age and mean lifetime expectancy by taking the first moments of Equation (28) and Equation (30). The equation for the mean age is the following:

$$-\nabla \cdot \mathbf{q} \langle A \rangle + \nabla \cdot \phi \mathbf{D} \nabla \langle A \rangle - q_O \langle A \rangle + \phi = 0 \quad \text{in } \Omega \quad (34)$$

where $\langle A \rangle$ represents mean age. The equation requires the following boundary conditions:

$$\langle A \rangle(x) = 0 \quad \text{on } \Gamma_- \quad (35a)$$

$$\mathbf{J}(x) \cdot \mathbf{n} = 0 \quad \text{on } \Gamma_0 \quad (35b)$$

Using the same method, the equation for mean life expectancy can be obtained as follows:

$$\nabla \cdot \mathbf{q}\langle E \rangle + \nabla \cdot \phi \mathbf{D} \nabla \langle E \rangle - q_I \langle E \rangle + \phi = 0 \quad \text{in } \Omega \quad (36)$$

$$\langle E \rangle(x) = 0 \quad \text{on } \Gamma_- \quad (37a)$$

$$-\mathbf{D} \nabla \langle E \rangle(x) \cdot \mathbf{n} = 0 \quad \text{on } \Gamma_0 \quad (37b)$$

Using these formulations, mean ages and mean lifetime expectancies will be continuously calculated during groundwater flow. This results because $\phi = \phi(x)$ will act as a source term in equations Equation (34) and Equation (36) and implies that the groundwater will be aging an average of one unit per unit time. At the time of the writing of this report, MLE has been implemented in FRAC3DVS-OPG for steady-state flow only.

4. REGIONAL-SCALE CONCEPTUAL MODEL

4.1 Model Domain

The regional scale domain, shown in Figure 6, occupies an aerial extent of approximately 18 000 km². It has vertical elevations that range from –1000 m at the lowest point in the Precambrian to 539 m at the highest point on the Niagara Escarpment. The regional-scale figures shown in this report have vertical exaggeration of 40 times. The domain was discretized into slices with 27 728 nodes each, which were then used to create quadrilateral elements. Based on an areal discretization with 200 rows and 200 columns, these quadrilateral elements have sides of 762.8 m in the East-West direction by 900.9 m in the North-South direction. Each of the 31 units from the geological reconstruction was assigned a model layer so that the numerical model would closely resemble that of the GLL00 geological framework model. This resulted in 31 layers in the numerical model.

The elevation of the nodes for each slice were determined from the geological framework model described in Gartner Lee Limited (2008b) and Chapter 2.3 of this report. This framework model is referenced as GLL00 in this report. Each geologic interface in the geological framework model, representing the top of a geologic formation or unit, is comprised of a triangulated surface mesh. A computer script was written to interpolate the elevation of the slice nodes from the appropriate layer of the geological framework model. If a given interface from the geological framework model did not exist at a particular slice node, then the elevation of the node was assigned as the elevation of the interface immediately below and the properties for the layer were assigned to be that of the underlying layer. This will result in zero thickness layers. High aspect ratios for grid blocks can lead to computational difficulties; to minimize problems, the minimum thickness for a geologic layer in the model was set to 1.0 m. Geologic layers that had a thickness between 0 and 0.5 m were assigned a thickness of zero and the properties of the layer below. Where the interpolated thickness was between 0.5 and 1.0 m, the thickness was set to be 1.0 m. The methodology results in multiple layers, some with zero thickness, with the same property; the layer thicknesses for such a grouping were then adjusted so that the multiple layers evenly occupy the same thickness as the layer in the geological framework model. Lastly, grid block properties were assigned based on the nodal properties of the thickest corner of the grid block. Although there is a large amount of congruency in the hydraulic and material properties of the 31 layers and the number of layers in the numerical model could be further reduced by grouping lithofacies; the 31 distinct lithofacies were included to facilitate analyses.

4.2 Flow Boundary and Initial Conditions

The boundary conditions of the model were Neumann no-flow boundary conditions for the sides and bottom, and type-one or Dirichlet for the surface of the model. The elevation of the nodes at the top of the model domain are defined by either the DEM or the lake bathymetry. For surface nodes with an elevation greater than 176 m, the assigned prescribed head was set as the elevation minus 3 m but not less than the 176 m Lake Huron water elevation. Areas within the domain that are occupied by either Lake Huron or Georgian Bay have a prescribed equivalent freshwater head for the top slice of the model matching the lake elevation, 176 m. The imposed surface boundary condition permits recharge and discharge to occur as determined by the

surface topography and the hydraulic conductivity of the top model layer. The assigned head represents a water table occurring at an assumed depth of 3 m below ground surface. Because of the resolution of the DEM, stream channels are conceptualized to have a depth to water that is 3 m less than defined by the DEM. The impact of varying the depth to the water table can be investigated in a sensitivity analysis. Alternate conceptualizations of the upper boundary that were investigated in this report (refer to Section 5.3.2) included using prescribed heads for grid blocks that coincided with major rivers and creeks, and recharge elsewhere.

An important issue to be addressed is the selection of a no-flow boundary condition for the sides of the model domain when, in fact, the domain is a subset of the Michigan Basin and horizontal fluid influx and efflux could occur at the lateral boundaries for some units. The selected boundary condition is appropriate for the shallow flow zone occurring above the units of the Salina Formation; as indicated in Section 1.2, flow in this zone is expected to be topographically controlled. The boundary conditions also are appropriate for the low permeability intermediate zone Salina units where, typical of aquitards, flow is expected to be predominantly vertical to overlying and underlying units that have significantly higher permeability. For the intermediate and deep zones, it is possible that lateral flow into and out of the domain could occur in the more permeable units of the Cambrian and Niagaran. However, as indicated by Sanford et al. (1985) the Cambrian is not continuous as a result of fault blocking and as shown in Figure 10 it only occurs on the western portion of the regional spatial domain. The lateral boundary condition for the Cambrian is thus only an issue for the part of the domain boundary that intersects the unit. The Niagaran is conceptualized as being continuous over its spatial extent shown in Figure 11. For the Niagaran, the lateral boundary condition is only an issue for the portion of it that occurs below the Salina in the intermediate zone (refer to Figure 9). However, as shown in Figure 14, the spatial domain is thin relative to its horizontal extent. The impact of the conceptual model for the lateral boundaries on a repository will be greatly reduced by its distance from the boundary. This issue is investigated in a case study (refer to Section 5.3.6).

In the absence of a source that can generate salt and hence total dissolved solids, the simulation of density-dependent flow using coupled flow and transport equations requires a transient analysis. In this Phase 1 study, the initial equivalent freshwater head distribution for the analysis was determined as the steady-state solution of density-independent flow subject to the same flow boundary conditions as that of the transient analysis. Alternate initial head distributions were investigated in the preliminary phase of the model study. The initial head condition discussed in this paragraph was selected based on its superior computational efficiency. The initial TDS distribution is described in a following section.

4.3 Hydraulic and Transport Parameters

The base-case data set for the conceptual model consists of 31 model layers, with each layer corresponding to a unit in the stratigraphic section. Table 7 shows the layers and their associated hydraulic conductivities, porosities and specific storage coefficients. While numbers in the table are reported to two digit accuracy, it is recognized that the second digit may be beyond the accuracy of field measurement techniques. The porosity values were developed from data compiled by Golder Associates Ltd (2003) and revised as appropriate by data from the Bruce site field program. As an example, Golder Associates Ltd (2003) cite a porosity of 0.01 for the Cambrian; however, the value is inconsistent with the appearance of cores. The hydraulic

conductivity values of Table 7 include the field data listed in Table 1 for the units where tests were performed. For the remaining units, the values were derived from the reports and the data listed in Table 3, Table 4, Table 5 and Table 6. The horizontal hydraulic conductivity for the shallow drift layer was assigned a value of 1×10^{-7} m/s.

Following Freeze and Cherry (1979), the specific storage coefficient can be developed as:

$$S_s = \rho g (C_r + \phi C_w) \quad (38)$$

where ρ is the fluid density, g is the gravitational constant, C_w is the compressibility of the fluid, ϕ is the porosity and C_r is the rock compressibility. The specific storage coefficients listed in Table 7 were derived using the fluid densities corresponding to a unit's TDS concentration, the unit's porosity and the appropriate compressibility from Table 8.

The OGSR borehole data define a thin drift at the surface; in many logs it is less than a metre thick. No shallow weathered zone is identified for the most shallow rock horizons. Where the units of the Silurian and Ordovician outcrop, their low permeability would occur at the surface of the regional-scale domain. To simulate the impact that a weathered zone will have on shallow flow, the upper 20 metres of the spatial domain was assumed to be characterized by more permeable rock; the horizontal hydraulic conductivity for the zone was assumed to be 1×10^{-7} m/s. The anisotropy ratios of Table 7 were assumed to be applicable. The impact of this assumed layer and groundwater recharge were investigated as part of the sensitivity analyses.

Table 9 gives the parameters assumed for both the migration of total dissolved solids and for the estimation of mean life expectancy. Using a grid Peclet number constraint, the longitudinal dispersivity coefficient was selected as approximately one half of the maximum length of the side of a regional-scale grid block. The diffusion coefficient is listed in the table; temperature effects were not considered.

4.3.1 Total Dissolved Solids

Salinity plays an important role with regard to fluid flow at the proposed DGR. As discussed in Section 2.4, an increase in the concentration of total dissolved solids (TDS) will result in an increase in the fluid density. The increase in density of the deeper fluids will then act as an inhibitor of active flow at depth. The explanation for this is that as defined in Bernoulli's equation, the potential energy increases for positive elevation changes and positive changes in density. Progressing to depth along a flow path from the freshwater at recharge areas, the density will increase along the flow path while the elevation decreases. It is therefore important to understand the impact that the salinity profile will have on the energy gradient and groundwater system behaviour.

The total dissolved solids distribution in the model can be assigned using different conceptual models. One way to characterize the brine distribution is to use an initial prescribed salinity distribution and allow, in a transient analysis, the density-dependent flow to equilibrate to a new state from the initial prescribed profile. In using this method to synthesize a salinity distribution, the total mass of dissolved solids and its distribution in the model domain is assumed to be known and will be a maximum initially as there are no sources to generate dissolved solids (it is

Table 7: Material hydraulic properties for base case scenario analysis.

| Period | Geology | K_H [m/s] | K_V [m/s] | K_V/K_H | Porosity | Specific Stor. |
|-------------|------------------------|-----------------------|-----------------------|-----------|----------|----------------------|
| Quaternary | Drift | 1.0×10^{-7} | 2.0×10^{-8} | 0.2 | 0.10 | 9.9×10^{-5} |
| Devonian | Traverse Group | 1.0×10^{-7} | 1.0×10^{-8} | 0.1 | 0.10 | 9.9×10^{-5} |
| | Dundee | 1.0×10^{-7} | 1.0×10^{-8} | 0.1 | 0.10 | 9.9×10^{-5} |
| | Detroit River Group | 1.0×10^{-7} | 1.0×10^{-8} | 0.1 | 0.10 | 1.4×10^{-6} |
| | Bois Blanc | 1.0×10^{-7} | 1.0×10^{-8} | 0.1 | 0.10 | 1.4×10^{-6} |
| Silurian | Bass Islands | 1.0×10^{-7} | 1.0×10^{-8} | 0.1 | 0.10 | 1.4×10^{-6} |
| | G-Unit | 1.0×10^{-7} | 1.0×10^{-8} | 0.1 | 0.08 | 1.3×10^{-6} |
| | F-Unit | 4.0×10^{-12} | 4.0×10^{-13} | 0.1 | 0.03 | 1.2×10^{-4} |
| | F-Salt | 1.0×10^{-13} | 1.0×10^{-13} | 1.0 | 0.08 | 1.6×10^{-6} |
| | E-Unit | 4.0×10^{-12} | 4.0×10^{-13} | 0.1 | 0.08 | 1.6×10^{-6} |
| | D-Unit | 1.0×10^{-10} | 1.0×10^{-11} | 0.1 | 0.03 | 1.3×10^{-6} |
| | B&C Units | 4.0×10^{-12} | 4.0×10^{-13} | 0.1 | 0.08 | 1.2×10^{-4} |
| | B Anhydrite-Salt | 1.0×10^{-13} | 1.0×10^{-13} | 1.0 | 0.08 | 1.6×10^{-6} |
| | A2-Carbonate | 1.0×10^{-10} | 1.0×10^{-11} | 0.1 | 0.08 | 1.6×10^{-6} |
| | A2 Anhydrite-Salt | 1.0×10^{-13} | 1.0×10^{-13} | 1.0 | 0.08 | 1.6×10^{-6} |
| | A1-Carbonate | 2.0×10^{-12} | 2.0×10^{-13} | 0.1 | 0.08 | 1.6×10^{-6} |
| | A1-Evaporite | 1.0×10^{-13} | 1.0×10^{-13} | 1.0 | 0.08 | 1.6×10^{-6} |
| | Niagaran | 1.0×10^{-7} | 1.0×10^{-8} | 0.1 | 0.08 | 1.6×10^{-6} |
| | Fossil Hill | 2.0×10^{-11} | 2.0×10^{-12} | 0.1 | 0.08 | 1.6×10^{-6} |
| | Cabot Head | 2.0×10^{-12} | 2.0×10^{-13} | 0.1 | 0.03 | 1.2×10^{-4} |
| | Manitoulin | 1.5×10^{-12} | 1.5×10^{-13} | 0.1 | 0.01 | 1.2×10^{-6} |
| Ordovician | Queenston | 1.3×10^{-11} | 1.3×10^{-12} | 0.1 | 0.11 | 1.2×10^{-4} |
| | Georgian Bay/Blue Mtn. | 9.1×10^{-12} | 9.1×10^{-13} | 0.1 | 0.11 | 1.2×10^{-4} |
| | Cobourg | 9.6×10^{-12} | 9.6×10^{-13} | 0.1 | 0.02 | 1.3×10^{-6} |
| | Sherman Fall | 9.0×10^{-12} | 9.0×10^{-13} | 0.1 | 0.02 | 1.3×10^{-6} |
| | Kirkfield | 1.4×10^{-11} | 1.4×10^{-12} | 0.1 | 0.02 | 1.3×10^{-6} |
| | Coboconk | 5.2×10^{-11} | 5.2×10^{-12} | 0.1 | 0.02 | 1.3×10^{-6} |
| | Gull River | 3.6×10^{-11} | 3.6×10^{-12} | 0.1 | 0.02 | 1.3×10^{-6} |
| | Shadow Lake | 8.0×10^{-12} | 8.0×10^{-13} | 0.1 | 0.01 | 1.2×10^{-6} |
| Cambrian | Cambrian | 3.0×10^{-6} | 3.0×10^{-7} | 0.1 | 0.01 | 1.2×10^{-6} |
| Precambrian | Precambrian | 8.0×10^{-12} | 8.0×10^{-13} | 0.1 | 0.01 | 1.2×10^{-6} |

Table 8: Fluid and rock compressibilities

| Material | Compressibility [Pa^{-1}] |
|-------------|--------------------------------------|
| Fluid | 4.4×10^{-10} |
| Sandstone | 1×10^{-10} |
| Limestone | 1×10^{-10} |
| Dolomite | 1×10^{-10} |
| Shale | 1×10^{-8} |
| Precambrian | 1×10^{-10} |

Table 9: Transport parameters

| Parameter | Value |
|--|--|
| Tortuosity | 1.0 |
| Diffusion Coefficient | $1.2 \times 10^{-10} \text{ m}^2/\text{s}$ |
| Longitudinal Dispersivity | 500 m |
| Transverse Dispersivity/Longitudinal Dispersivity | 0.1 |
| Vertical Transverse Dispersivity/Longitudinal Dispersivity | 0.01 |

further assumed that there are no dissolved solids in the water recharging the domain). With this approach, as time progresses, the dissolved solids will gradually reduce as the groundwater discharges from the system. An alternate conceptualization to represent the presence of the total dissolved solids is to assume a source that generates the fluid composition.

The initial condition for total dissolved solids must specify concentrations that are constant at a given location for a given lithology and independent of the depth of the unit below ground surface. At the time of the analyses of this report, regional-scale data are not available for either the actual distribution in the shallow units or the spatial distribution, particularly, in the deeper units. In the absence of data, a plausible TDS distribution can be generated using the physically-based regional model. For the coupled density-dependent flow and transport system, fresh water can recharge at the surface, reducing the TDS concentration in the shallow zone. However, the time to flush the dissolved solids from a unit is a function of the permeability of the unit and the energy of the displacing fluid as compared to the energy of the fluid being displaced. Fluids with lower total dissolved solids, such as recharging water, will have a lower energy as compared to higher total dissolved solids water with the same elevation and pressure. Therefore, for low-permeability units with a relatively high total dissolved solids concentration, the time to flush the unit or displace the fluids can be very long (millions of years). Complete flushing may only occur as a result of diffusion because energy gradients and/or low permeabilities may yield low fluid fluxes that may not be sufficient for advective displacement to occur.

The spatial distribution of TDS concentration in the units of the Ontario portion of the Michigan Basin have been compiled in studies by Golder Associates Ltd (2003) and Hobbs et al. (2008). The developed TDS concentrations for the DGR-1 and DGR-2 boreholes are listed in Table 1. There is a considerable range in the TDS values with the concentration level depending on several factors including borehole location (for example, whether the location is deep or shallow) and the state of the flow domain at the sample point (for example, whether the point is near a recharge zone or a discharge zone). In the preliminary modelling undertaken for this study (Sykes, 2007), the TDS concentrations from the Golder Associates Ltd (2003) report were used to define an initial TDS distribution to the regional-scale model domain. The values listed in Table 10 represent the average of the minimum and maximum values reported for given units. For the analyses presented in this study using the GLL00 geological framework model, the initial TDS distribution (refer to Table 10) was assigned based on the DGR-1 and DGR-2 values; the concentrations correspond to the higher values reported for a given unit from both the Golder Associates Ltd (2003) and Hobbs et al. (2008). As discussed in the preceding paragraph, these concentrations will be redistributed in a density-dependent flow analysis and in parts of the domain they will be diluted by infiltrating fresh water. The use of the maximum TDS

concentrations for a unit is therefore appropriate as an initial condition. Finally, the geological framework model integrates the various units of the Niagaran Group into a single layer; only a single TDS value is given for that layer in Table 10.

Table 10: Initial TDS and relative concentrations with respect to 300 g/L for base case preliminary and GLL00 geology

| Period | Geology | Preliminary Geology | | GLL00 Geology | |
|-------------|------------------------|---------------------|----------------|---------------|----------------|
| | | TDS [g/L] | Relative Conc. | TDS [g/L] | Relative Conc. |
| Quaternary | Drift | 0.045 | 0.0 | 0.045 | 0.0 |
| Devonian | Traverse Group | 0.045 | 0.0 | 0.045 | 0.0 |
| | Dundee | 2.5 | 0.01 | 3 | 0.01 |
| | Detroit River Group † | 2.5 | 0.01 | 3 | 0.01 |
| | Bois Blanc | 2.5 | 0.01 | 3 | 0.01 |
| Silurian | Bass Islands | 2.5 | 0.01 | 3 | 0.01 |
| | G-Unit | 200 | 0.67 | 3 | 0.01 |
| | F-Unit | 200 | 0.67 | 300 | 1.0 |
| | F-Salt | 200 | 0.67 | 300 | 1.0 |
| | E-Unit | 200 | 0.67 | 300 | 1.0 |
| | D-Unit | 200 | 0.67 | 300 | 1.0 |
| | B&C Units | 200 | 0.67 | 300 | 1.0 |
| | B Anhydrite-Salt | 200 | 0.67 | 300 | 1.0 |
| | A2-Carbonate | 200 | 0.67 | 300 | 1.0 |
| | A2 Anhydrite-Salt | 200 | 0.67 | 300 | 1.0 |
| | A1-Carbonate | 200 | 0.67 | 300 | 1.0 |
| | A1-Evaporite | 200 | 0.67 | 300 | 1.0 |
| | Niagaran ‡ | 200 | 0.67 | 300 | 1.0 |
| | Fossil Hill | 200 | 0.67 | 300 | 1.0 |
| | Cabot Head | 200 | 0.67 | 300 | 1.0 |
| Manitoulin | 200 | 0.67 | 300 | 1.0 | |
| Ordovician | Queenston | 225 | 0.75 | 300 | 1.0 |
| | Georgian Bay/Blue Mtn. | 225 | 0.75 | 300 | 1.0 |
| | Cobourg | 112.5 | 0.38 | 300 | 1.0 |
| | Sherman Fall | 112.5 | 0.38 | 300 | 1.0 |
| | Kirkfield | 112.5 | 0.38 | 300 | 1.0 |
| | Coboconk | 112.5 | 0.38 | 300 | 1.0 |
| | Gull River | 112.5 | 0.38 | 300 | 1.0 |
| | Shadow Lake | 112.5 | 0.38 | 300 | 1.0 |
| Cambrian | Cambrian | 112.5 | 0.38 | 300 | 1.0 |
| Precambrian | Precambrian | 112.5 | 0.38 | 300 | 1.0 |

Note: † Includes the Lucas/Amherstburg listed in Table 1

‡ The Niagaran Group is comprised of the Guelph, Goat Island, Gasport and Lions Head

The sensitivity of the groundwater flow to the conceptual model for the total dissolved solids concentration distribution is discussed in the following paragraphs. For the case with a defined

initial total dissolved solids concentration distribution, the concentration boundary conditions were: the surface of the model was set as a Type 3 boundary condition with recharge having zero concentration, except areas beneath Lake Huron and Georgian Bay, which had a prescribed relative concentration of zero. The prescribed boundary condition for the surface grid blocks beneath the lakes was investigated and selected in the preliminary study (Sykes, 2007); the use of a Type 3 boundary condition in combination with the large longitudinal dispersivity that was required in order to obtain a solution resulted in surface concentrations that were too high in the units that subcrop beneath the lakes. Zero-flux Neumann boundary conditions were used for the sides and bottom of the domain. The salinities used for the initial concentration conditions for each of the geologic units are listed in Table 10. The highest total dissolved solids concentrations are assigned to the units of the intermediate and deep flow zones, while the shallow active groundwater zone of the Devonian units have low dissolved solids concentrations. The initial head condition for the transient, fully-coupled density-dependent flow equation was the steady-state density-independent equivalent freshwater head distribution.

The computational burden for the simulation and analysis of density-dependent flow is significant. The computer time is a function of factors including the number of degrees-of-freedom, the length of time steps for the necessary transient analysis, the spatial discretization and the size of grid blocks, and the assigned tolerance level for convergence at a time step. Of these, the length of time steps is most critical. In FRAC3DVS-OPG, the length of a time step is controlled, in part, by the cell Courant number for the grid blocks with higher velocities. Within the regional domain, the shallow Devonian units have significantly higher velocities than the deeper Ordovician units. To control numerical dispersion and potential instability problems in the higher velocity shallow units, small time steps are required. In numerical experiments, it was found that time steps on the order of days were required in order to obtain results with satisfactory convergence. Thus, there is a balance between the accuracy of a solution, the length of time required for the system to reach a pseudo-equilibrium between energy potential, fluid flux and total dissolved solids distributions, and computer simulation time. In this report, a suitable balance was established by assuming that pseudo-equilibrium would be obtained 1 million years after the imposed initial conditions. The impact of this assumption and cut-off time were investigated in a sensitivity analysis. The state of the system and boundary conditions are constant in time over the duration of the transient analysis used to determine the solution at pseudo-equilibrium time. Changes in state may be more significant than the changes in the velocity and total dissolved solids distribution that may result with the assumption of a different pseudo-equilibrium time.

After 1 million years, the model, having been allowed to reach pseudo-equilibrium, produces salinity profiles that are compatible with the geological framework, boundary conditions and hence the flow domain. In the north-eastern part of the model domain, the brine will be unable to accumulate because of a combination of the absence of the source term and the effect of meteoric recharge near Georgian Bay where the Ordovician formations outcrop. This is contrasted by the western portion of the domain which, because of the absence of a velocity to transport the brine from the system, will maintain a high salinity concentration. The location of the proposed DGR repository is located within this area. At such a location, stagnation of the groundwater is expected due to both the low permeability of the Ordovician units and the effect that density will have on reducing the flow velocity.

An alternate way to characterize the brine distribution in the model is to use a first-order source term in the Silurian salt units to generate the brine. This method will result in the continual

creation of salinity with time, until a maximum relative concentration of 1.0 is reached at the source zones. The surface of the model was set as a Type 3 boundary condition, except in areas beneath Lake Huron and Georgian Bay, which had a prescribed relative concentration of 0.0. The domain is initially free of salinity. At the writing of this report, the origin of the dissolved solids in the deep units at the DGR is unresolved.

After sufficient time has passed, the model will reach a pseudo-steady-state brine distribution. The first-order source term should create a salinity profile that is very similar to the profile created by using prescribed initial concentrations (as discussed in the preceding paragraphs). The north-eastern part of the domain, specifically at the Niagara Escarpment and beneath Georgian Bay will have low concentrations. These low concentrations can be attributed to the freshwater that recharges at the outcrop for the deeper units near Georgian Bay. In regions remote from the escarpment, where there will be markedly less impact from Georgian Bay and recharge, the brine accumulates. As in the case based on the prescribed initial concentrations, the formations found at the target horizon of the DGR will have high salinity levels, which will act to reduce groundwater flow rates.

The two methods for the synthesis of a TDS distribution were explored in the preliminary phase of the model study (Sykes, 2007). One of the major differences between the different conceptualizations for the salinity profile is the computational time required. For large-scale problems such as the one investigated in this report, computational time can be an important criterion. Although there was a large degree of similarity between the case using a prescribed initial condition and the case using a first-order source term in the Silurian salt units, the computational time can be effectively halved by using the prescribed initial concentrations.

4.4 Alternate Scenarios for the Regional-Scale System

The geological framework, flow boundary and initial conditions, TDS boundary and initial conditions and system parameters for the base case conceptual model (Scenario 1) have been defined in the preceding sections of this report. The solution methodology for the simulation of isothermal, density-dependent flow and TDS migration at the regional-scale also has been presented. This section develops alternate cases or scenarios for the conceptual model; the genesis of the scenarios are issues raised in the development of the base case model and the tenets of the geosynthesis program for the DGR. The objectives are: to reveal the attributes of the flow system that are important in the development of a safety case for a deep geologic repository; and, to investigate the sensitivity of the numerical solution to selected parameters. The performance measure for the analyses is MLE (mean life expectancy). The investigation of the attributes of the conceptual model and its parameters, boundary conditions and geological framework can also be approached using user defined performance measures and sensitivity coefficients (refer to Section 3.2.1). With this method, the sensitivity coefficients are local derivatives and in this study, they are derived for the base-case parameters.

Table 11 presents a summary of the regional-scale scenarios developed in this study; additional cases, beyond that listed, also were investigated. The conceptual model parameters for the scenarios are included in Appendix A. The first issue investigated is the magnitude of the longitudinal dispersivity used for both the solution of the equation for TDS migration and the calculation of MLE (Scenarios 2 and 3). Only the magnitude of the longitudinal dispersivity was

perturbed in the analysis with alternate cases being 250 m and 100 m; the base case value is 500 m. All other parameters are that of the base case. The goal of the analysis was the determination of the smallest possible value of the longitudinal dispersivity for which a FRAC3DVS-OPG model solution could be obtained. Smaller values would lead to a reduction in the contribution of dispersion as compared to advection for both TDS concentration transport and MLE equations.

The surface boundary condition for flow is investigated in Scenarios 4 and 5. The former assumes no weathered zone with the base case parameters while the latter investigates a recharge boundary condition. The sensitivity of the flow solution and MLE to an alternate realization of the geological framework model is analyzed with Scenario 6. This analysis is achieved by comparing the flow system using the geological framework model developed in Sykes (2007) with the results obtained using the GLL00 geological framework. An important hypothesis of this study is that the high TDS concentrations and hence fluid densities for the Silurian and deeper units contributes to the development of stagnant flow for those layers as lighter surface waters are unable to displace the deeper fluids. The impact on MLE of assuming density-independent flow is determined with Scenario 7. The base case parameters are used for the analysis.

The low permeability of the Ordovician and Lower Silurian units is an important attribute for the safety case for the DGR. Scenarios 8 through 12 investigate the impact of higher permeabilities for the units on the groundwater domain and the MLE estimates. The hydraulic parameters for the scenarios are given in Table A.2, Table A.3, Table A.4, Table A.5 and Table A.6 in Appendix A. The boundary conditions, initial conditions and solution methodology are the same as that of the base case.

As described in Section 2.1, data from the DGR-2 borehole indicate that the Cambrian is over-pressured with respect to the surface. Over-pressurization of the deep sparsely fractured crystalline rock also has been observed at the Underground Research Laboratory (URL) near Lac du Bonnet Manitoba. It has been postulated that the low permeabilities at depth at the URL slowly release the higher pore pressures that would have occurred during glacial loading. To further the understanding of the possible impact of glacial loading on a deep geologic repository, the time for the dissipation of an initial equivalent freshwater head of 600 m imposed throughout the regional-scale domain is determined for three realizations of the Ordovician hydraulic conductivity (Scenarios 13 to 15). The parameters for the simulations are the same as those of Scenarios 8 to 10.

The conceptual model of scenario 16 is designed to investigate the impact that the no-flow lateral boundary conditions have on the environmental head at the DGR and the estimate of MLE. For the analysis, grid blocks at the lateral edge of the regional-scale domain were assigned a high hydraulic conductivity so that all geologic layers could communicate with the surface topography. The TDS distribution was set as the base-case concentration at 1 million years (Scenario 1) but with transport turned off in FRAC3DVS-OPG. All parameters were that of the base case.

Scenarios 17 through 20 present analyses of the impact of glaciation on the regional-scale temporal flow and the TDS distribution. Scenario 17 uses the base-case parameters while scenarios 18 to 20 use the same parameters as that of scenarios 8 to 10. Chapter 6 presents the paleoclimate analyses.

The Cambrian has a significantly higher hydraulic conductivity than either the overlying Shadow Lake Formation or the underlying Precambrian rock (refer to Table 7). The analyses of Scenarios 1 to 20 assume that the Cambrian is horizontally isotropic. To ascertain the impact of this assumption, alternate models were explored using an anisotropic hydraulic conductivity tensor assigned to the Cambrian. For the principle components of the tensor, the K_1 value was set as the base-case hydraulic conductivity. The K_2 value was reduced using a harmonic mean to account for a possible lower horizontal permeability that would occur in a direction normal to that of the K_1 value. The K_3 value (vertical) was assigned using the base-case anisotropy ratio. Four cases with different orientations were investigated (Scenarios 21 to 24). The other parameters were that of the base case.

Table 11: Parameters, boundary conditions and initial conditions for regional-scale analyses

| Parameters | | Base Case | | MLE Dispersivity | | Surface Boundary Condition | | Geologic Model | Impact of No Density | Ordovician Hydraulic Conductivity | | | Silurian Hydraulic Conductivity | | Cambrian High Pressure | | | Horizontal Boundary Condition | Paleoclimate Simulations | | |
|----------------------------|------------------------|-----------|---|------------------|-------|----------------------------|--------|----------------|----------------------|-----------------------------------|----------|----------|---------------------------------|----------|------------------------|----------|----------|-------------------------------|--------------------------|----------|----------|
| | | 1 | 2 | 250 m | 100 m | Case 1 | Case 2 | | | P-Case 1 | P-Case 2 | P-Case 3 | S-Case 4 | S-Case 5 | P-Case 1 | P-Case 2 | P-Case 3 | | Base Case | P-Case 1 | P-Case 2 |
| Scenario | | 1 | 2 | 3 | 4 | 5 | 6 | 7 | 8 | 9 | 10 | 11 | 12 | 13 | 14 | 15 | 16 | 17 | 18 | 19 | 20 |
| Initial Heads | Steady State 600 m | • | • | • | • | • | • | • | • | • | • | • | • | | • | • | • | • | • | • | • |
| Hydraulic | Base Case | • | • | • | • | • | • | • | • | • | • | • | • | • | • | • | • | • | • | • | • |
| Anisotropy | Base Case Isotropic | • | • | • | • | • | • | • | • | • | • | • | • | • | • | • | • | • | • | • | • |
| Initial TDS | Base Case Zero | • | • | • | • | • | • | • | • | • | • | • | • | • | • | • | • | • | • | • | • |
| MLE | 500 m | • | | | • | • | • | • | • | • | • | • | • | • | • | • | • | • | | | |
| Longitudinal Dispersivity | 250 m | | • | | | | | | | | | | | | | | | | | | |
| | 100 m | | | • | | | | | | | | | | | | | | | | | |
| Ordovician Perturbation | P-Case 1 | | | | | | | | • | | | | | | • | | | | | • | |
| | P-Case 2 | | | | | | | | | • | | | | | | • | | | | | • |
| | P-Case 3 | | | | | | | | | | • | | | | | | • | | | | • |
| Silurian Perturbation | S-Case 4 | | | | | | | | | | | • | | | | | | | | | |
| | S-Case 5 | | | | | | | | | | | | • | | | | | | | | |
| Surface Boundary Condition | Type 1 at 3 m | • | • | • | • | | • | • | • | • | • | • | • | • | • | • | • | | | | |
| | Recharge | | | | | • | | | | | | | | | | | | | | | |
| | Paleoclimate | | | | | | | | | | | | | | | | | • | • | • | • |
| Weathered Zone | 20 m | • | • | • | | • | • | • | • | • | • | • | • | • | • | • | • | • | • | • | • |
| | 0 m | | | | • | | | | | | | | | | | | | | | | |
| MLE | | • | • | • | • | • | • | • | • | • | • | • | • | | | | • | | | | |

5. REGIONAL-SCALE GROUNDWATER FLOW AND BRINE MIGRATION ANALYSES

5.1 Analysis of the Base-Case for the Regional-Scale Domain

The regional-scale conceptual model for the base-case analysis describes the present day state of the groundwater system. The geological framework model, hydraulic parameters, transport parameters, pore water concentrations and boundary conditions are all based on observations, analyses and interpretations of this state. The initial conditions of TDS concentration and equivalent freshwater heads assumed for the conceptual model evolve to a pseudo-equilibrium solution for this state. The objective of the analysis, in part, is to reveal system behaviour and to identify observed attributes that may be the signature of a different state. The purpose of the various cases defined in Section 4.4 is to investigate alternative descriptions and states of the regional-scale domain.

Based on a surface water level for Lake Huron of 176 mASL, the observed under-pressurization of the Ordovician and Lower Silurian units at the DGR-1/DGR-2 borehole (refer to Section 2.1) is a consequence of a different state than that described by the base-case conceptual model. The pressures may be the result of rock dilation, from either glacial unloading or significant removal of mass through erosion, that was at a rate that is greater than that of water influx to these low permeability units from the over and under-lying units with higher pressure; the pressure distribution is still evolving. Alternatively, the low pore fluid pressures may indicate the presence of a trapped non-wetting gas phase. The analysis of the pressure profile at DGR-2 can be approached from two perspectives: an assessment of the cause of the under-pressurization of the Ordovician and Lower Silurian and the over-pressurization of the Cambrian; and the evolution of the pressures from their current state. The former analysis would require either realizations of the previous state of the regional-scale system or the simulation of immiscible, two-phase flow of gas and water. With the exception of the paleoclimate simulations investigated in Chapter 6, these analyses are beyond the scope of this Phase 1 report. The assessment of the evolution of the pressures cannot be undertaken at the regional scale due to a lack of data on the pressures at other locations in the domain; however, the analysis can be developed at the site scale (refer to Section 7.3.1).

The equivalent freshwater head distribution for the base-case simulation after 1 million years (pseudo-equilibrium time) is shown in block-cut form in Figure 17 and as a fence diagram in Figure 18. The environmental head distribution for the base case parameters and boundary conditions is shown in Figure 19 and Figure 20. As explained in Section 3.1.3, plots of equivalent freshwater heads can be used to interpret horizontal flow gradients but not vertical gradients; conversely, the plots of environmental heads can be used to interpret vertical gradients but not horizontal gradients. The shallow flow regime is the region above the Salina. It is dominated by flow that mimics topography. Beneath the shallow groundwater zone, the heads are not controlled to the same extent by the local elevation of the surface. The main control for the horizontal component of the density-dependent energy gradient at depth is the elevation difference between Lake Huron and the topographic high at the Niagara Escarpment. The head signature will be transmitted from the outcrop area and will be dissipated, depending on the energy gradient, across the domain (refer to Figure 18). At a given location, the vertical component of the energy gradient is controlled by the difference in the environmental heads between the more permeable units that are separated by low permeability units (refer to Figure 20). For the regional domain,

the higher permeability Cambrian, where present, and Niagaran Group are separated by the low permeability units of the Ordovician and Lower Silurian. The Niagaran is confined in the south-western part of the domain by the overlying low permeability units of the Salina. Flow in the Niagaran where it is unconfined (refer to Figure 9) is controlled by surface topography.

The high environmental heads observed in the Cambrian at the DGR-2 borehole (Figure 7) are not predicted in the pseudo steady-state analysis with the base-case parameters, initial conditions and boundary conditions. Several causes can be postulated for the elevated Cambrian pressures. They may reflect a pressure distribution from a state of thermal, hydraulic and geomechanical conditions that were significantly different from that simulated by the base-case analysis; this would imply that the pressures are slowly evolving to a distribution that is compatible with the current state and boundary conditions of the groundwater system. The elevated environmental heads also may reflect conditions at the center of the Michigan Basin where the Cambrian is several kilometers deep with a significant column of higher density saline fluids above; this would require continuity of the Cambrian's permeability from the center to the margins of the basin. The pressures also may be the result of the presence of a gas phase that provides pressure support for the unit. Clearly, for the high pressures in the relatively thin permeable Cambrian to be sustained over the period of the analysis (1 million years), both the effective vertical fluid permeability (or mobility) for the overlying Ordovician units must be significantly lower than that used in the base-case simulation, and the Cambrian must be discontinuous in some manner such that the fluids in it are trapped. The over-pressurization of the Cambrian is further investigated in subsequent analyses presented in this report. At the location of the DGR-2 borehole, the model base-case environmental head for the Cambrian is 192.37 m, the Cobourg is 193.80 m and the Niagaran is 197.64 m.

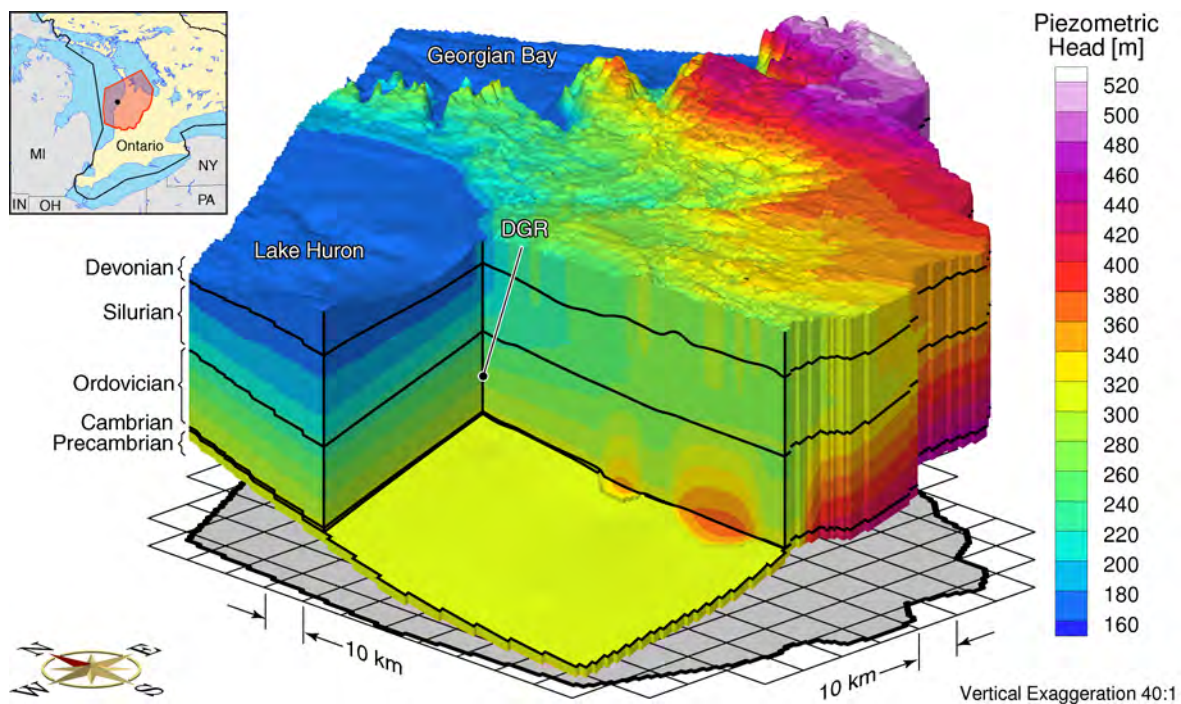


Figure 17: Base case equivalent freshwater head (m) distribution.

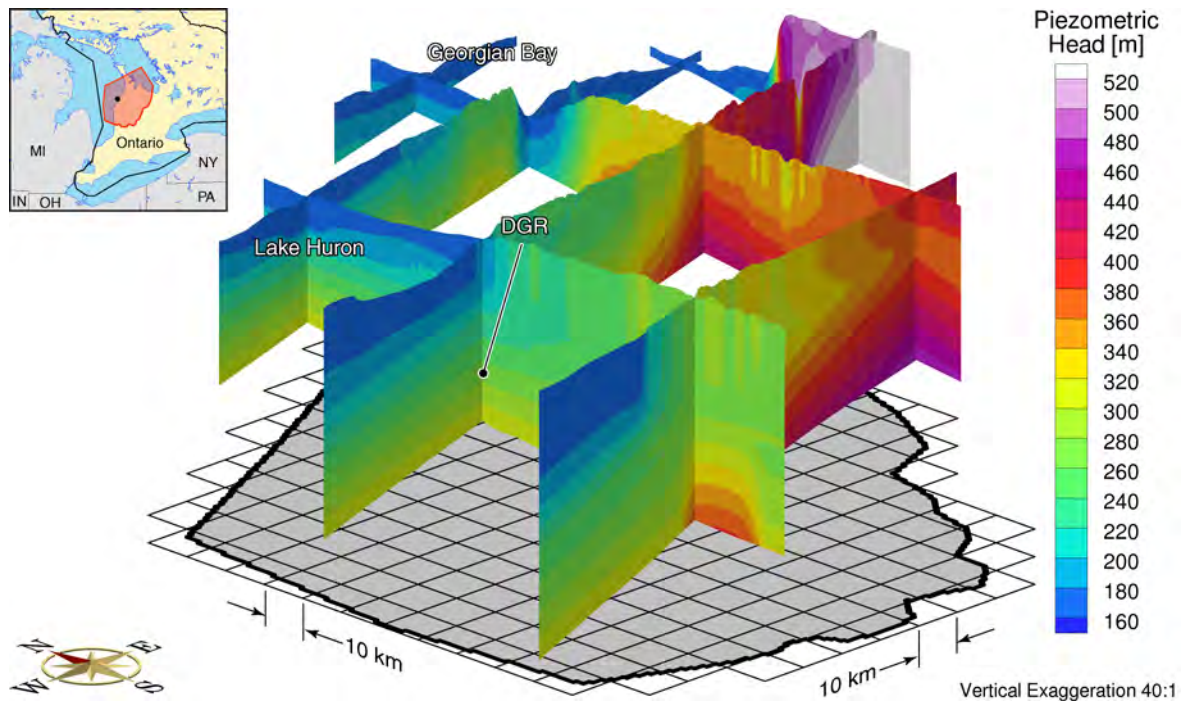


Figure 18: Fence diagram of the base-case equivalent freshwater head (m) distribution.

In addition to the elevation component of the gravitational gradient imposed by the topographic high at the Niagara Escarpment, the density of the brine in the deep groundwater zone will have an impact on the energy gradients. The salinity profile for the base-case at a pseudo-equilibrium time of 1 million years (Figure 21) consists of relatively fresh groundwater for the shallow groundwater zone and an area with much higher TDS concentrations for the intermediate and deep groundwater zone (below the Salina where present). The shallow groundwater zone will remain devoid of salinity because the continual inflow of meteoric water through recharge to the zone will dilute any salinity that diffuses upward through the Silurian or Ordovician. The brine concentrations in the low permeability Ordovician units at the Niagara Escarpment, where the Silurian is absent, will also experience some flushing as well; however, the higher density groundwater found in the deeper zone that has a higher energy than water with low total dissolved solids will prevent any significant penetration of freshwater. The TDS transition zone occurs across the Salina; variations in the upward flow through this unit in combination with the high longitudinal dispersivity result in the spatial oscillations in the salinity that is apparent in the figure (note the interface between the 200 g/L and the 100 g/L contours).

The base-case pore water velocity magnitudes are presented in Figure 22. The highest velocities occur in the more permeable shallow groundwater zone. The lower velocities beneath Lake Huron and Georgian Bay are the result of the absence of a horizontal gradient. The reduction of the velocities in the Salina Group is clearly evident in the figure as are the higher velocities of the Niagaran in the Silurian (these velocities appear as the orange/red band above the Ordovician-Silurian interface). Above the Niagaran, higher velocities are also evident in the D-Unit and the A2-Carbonate of the Silurian. In Figure 22, the A2-Carbonate velocities are the orange to yellow band immediately above the Niagaran while the D-Unit velocities are the higher

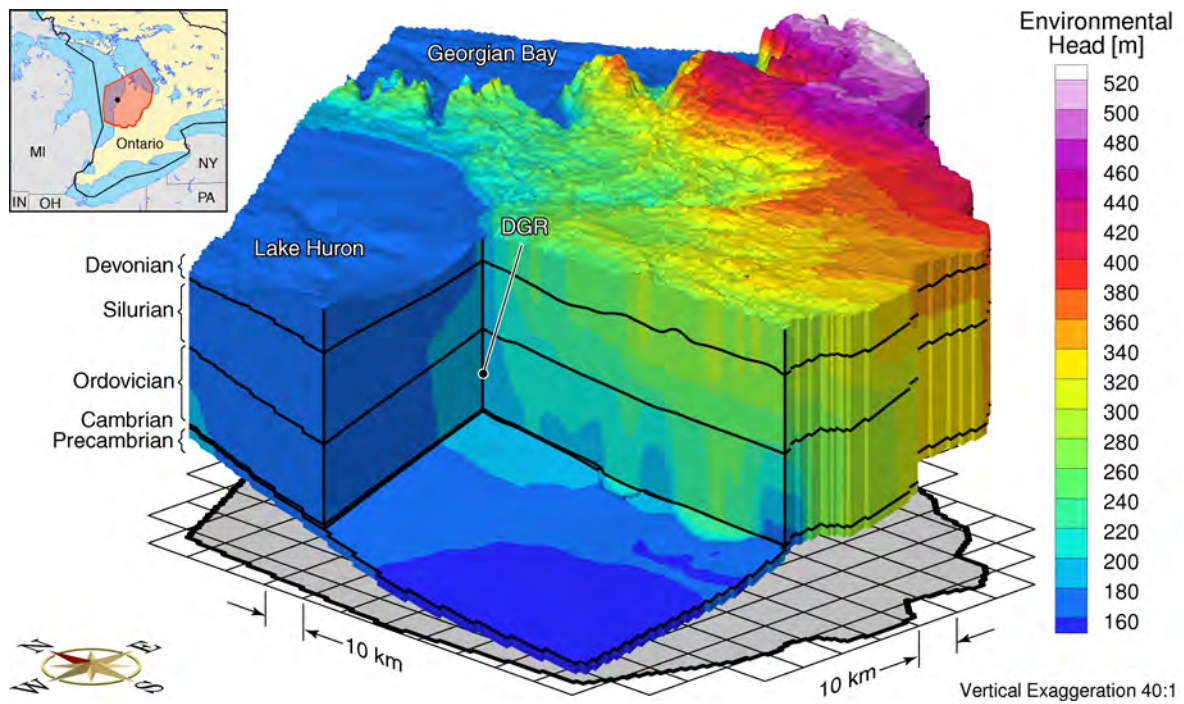


Figure 19: Base-case environmental head (m) distribution.

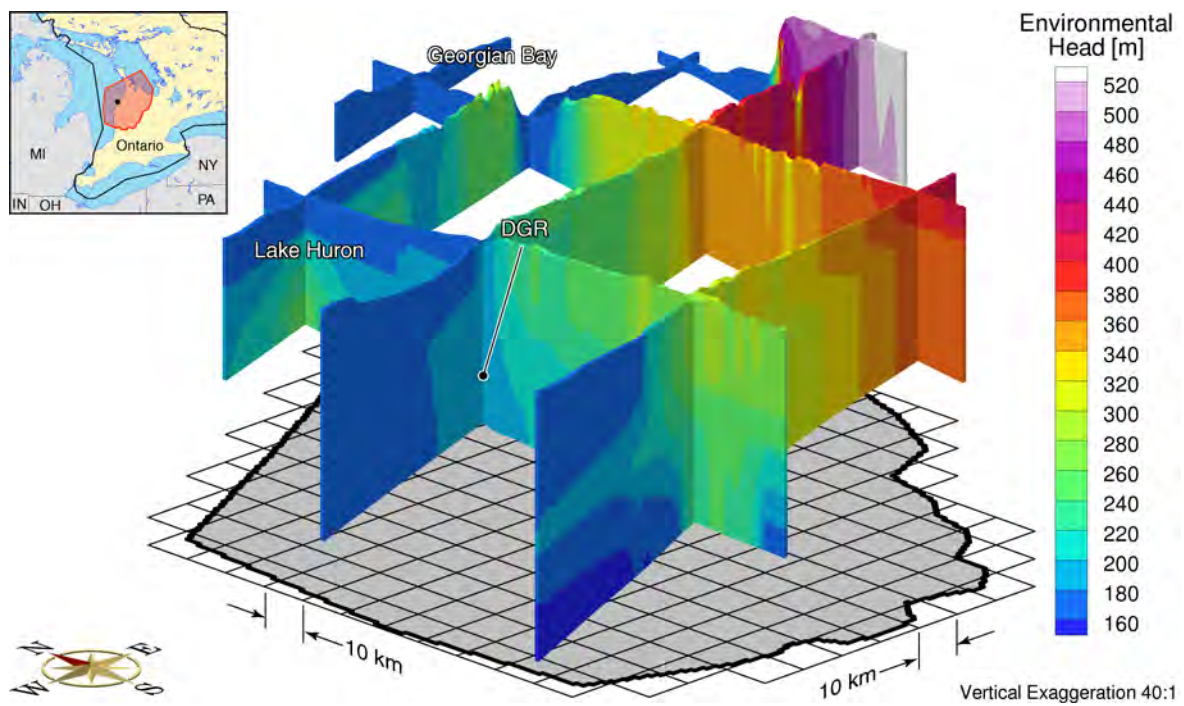


Figure 20: Fence diagram of the base-case environmental head (m) distribution.

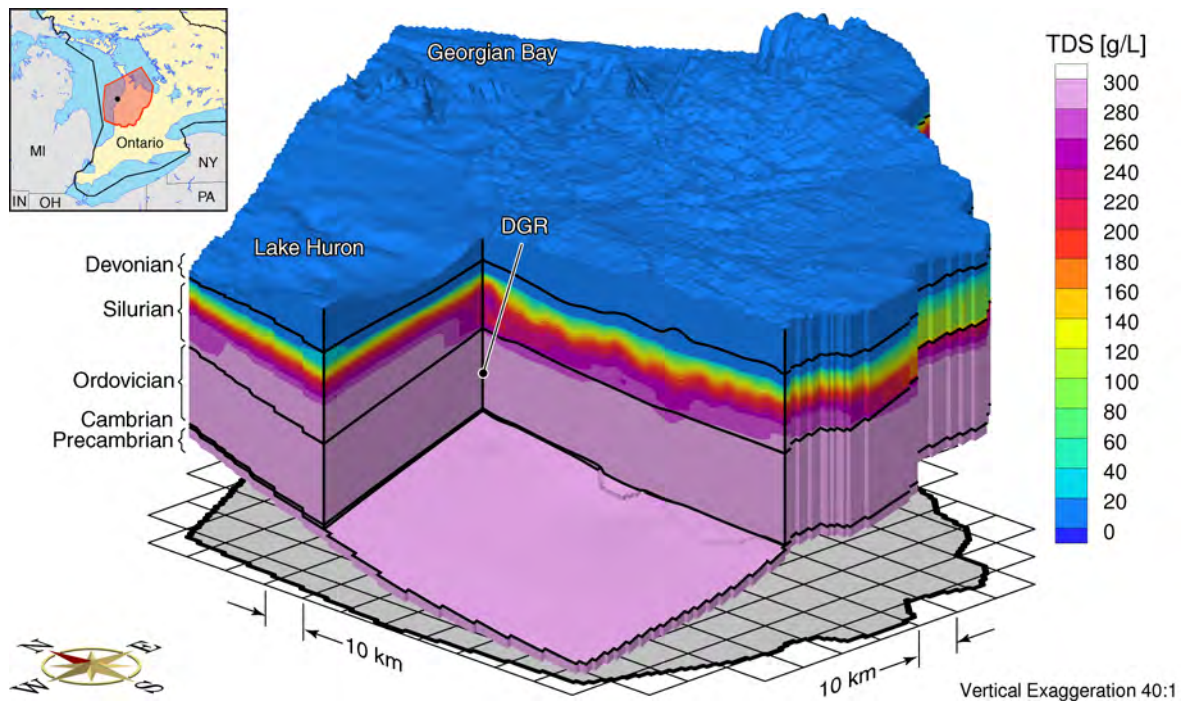


Figure 21: Base-case Total Dissolved Solids distribution.

thinner yellow to orange band. Within the Ordovician in the vicinity of the proposed DGR, the groundwater pore velocities are less than 0.0001 m/year. Higher velocities are predicted for a zone at the bottom of the Ordovician that is upgradient of the eastern extent of the Cambrian. This zone, characterized by the orange at the southern end of the north-south blockcut face in Figure 22, corresponds to the area of higher horizontal gradients that are apparent in Figure 18. Even within this zone, pore water velocities are estimated to be less than 0.001 m/year. Based on the estimated low velocities and relative to a diffusion coefficient of $1.2 \times 10^{-10} \text{ m}^2/\text{s}$, solute transport in the Ordovician will be diffusion dominated.

The ratio of vertical velocity to velocity magnitude is plotted in Figure 23 for the regional-scale domain. In the figure, blue corresponds to vertically downward velocities, white to horizontal velocities and red to vertically upward velocities. Transition zones also are evident in the figure. For the base-case parameters and a pseudo-equilibrium time of 1 million years, flow in the shallow groundwater zone is predominantly horizontal as is the flow in the more permeable units such as the Cambrian, Niagaran, A2 Carbonate and D-Unit. These units can be identified by the horizontal white bands in Figure 23. Flow in the Salina is strongly vertical. The direction of flow in the Ordovician and Lower Silurian is predominantly horizontal where the Cambrian is absent and vertical where it is present (refer to Figure 10). There is a degree of topographic control on the direction of flow; the trend is for upward flow (red) for the portion of the Ordovician below Lake Huron and downward flow (blue) from the Niagaran to the Cambrian for the land areas with the transition occurring at or near the shoreline.

The performance measure selected for the evaluation of the groundwater system is the mean life expectancy (Figure 24). The general trend for the mean life expectancy is similar to that found in the head and velocity distributions. The shallow groundwater zone has significantly shorter life

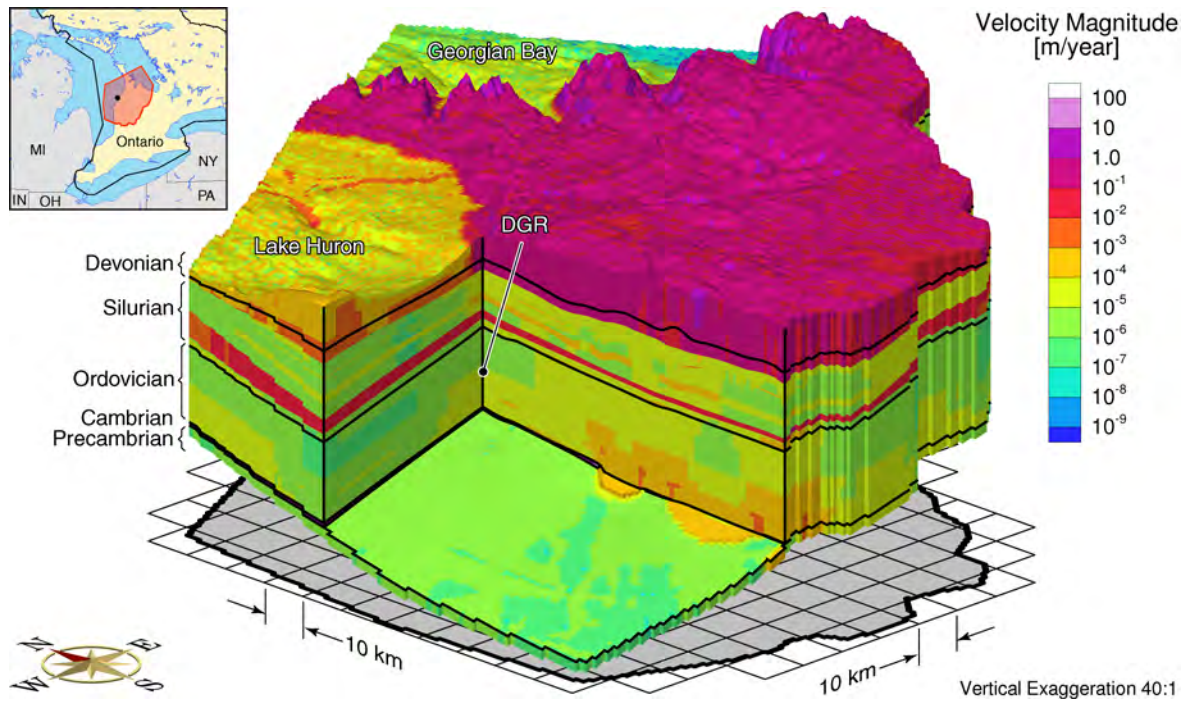


Figure 22: Base-case pore water velocity magnitude (m/a) distribution.

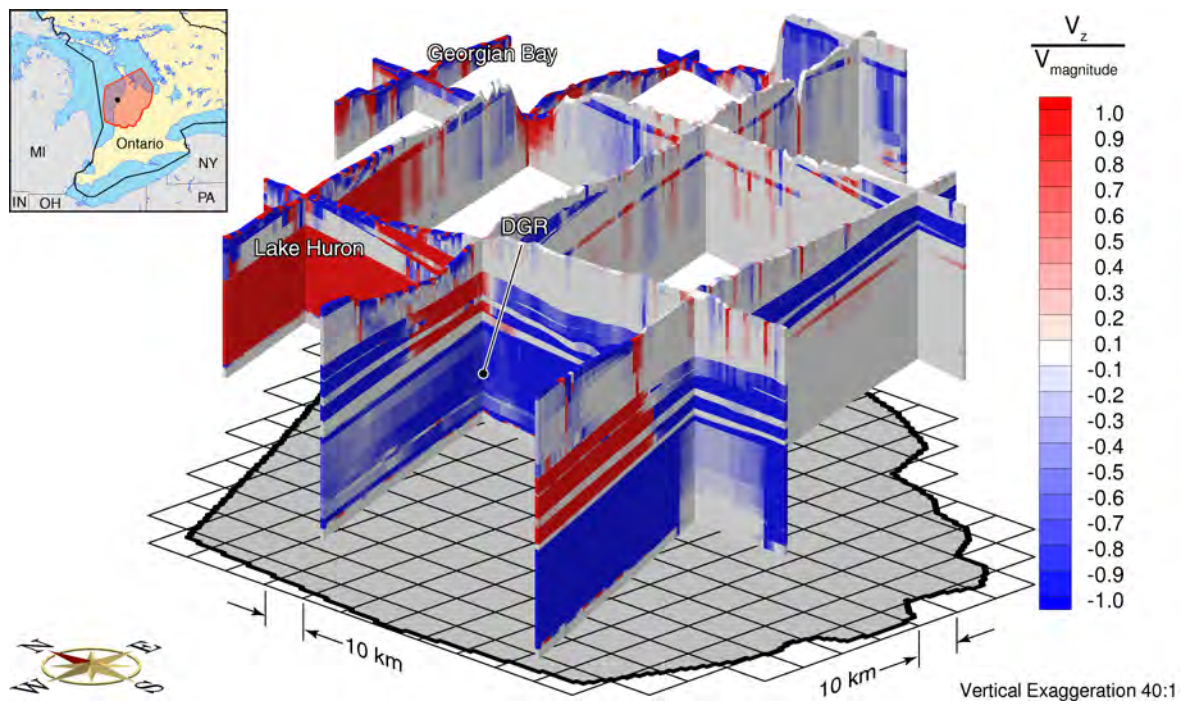


Figure 23: Fence diagram of base-case ratio of vertical velocity to velocity magnitude.

expectancies compared to the deep groundwater zone. The areas of recharge versus discharge can be noted in the figure as the recharge areas have a high MLE while the discharge areas have low MLEs. The groundwater area surrounding the proposed DGR (shown in a fence diagram, Figure 25) is calculated to have a mean life expectancy of approximately 8.9 million years for the base-case conceptual model.

The paths of nine average water particles released from the vicinity of the proposed DGR are shown in Figure 26. For the base-case, the path followed by the particles is downward from their point of release to the Cambrian, then westerly in the Cambrian to the point below the Lake Huron shoreline where upward flow occurs in the Ordovician (red in Figure 23). The upward particle paths continue to the Niagaran and then follow the unit to the point of subcrop in Lake Huron. The preferential path for the particles is horizontal through the higher permeability Niagaran rather than vertically upward through the low permeability Salina. The time of travel, based on advection only, varies for eight of the particles from 168 million years to 607 million years. One particle had a time of travel of 31 million years. Diffusion and mechanical dispersion will reduce this time.

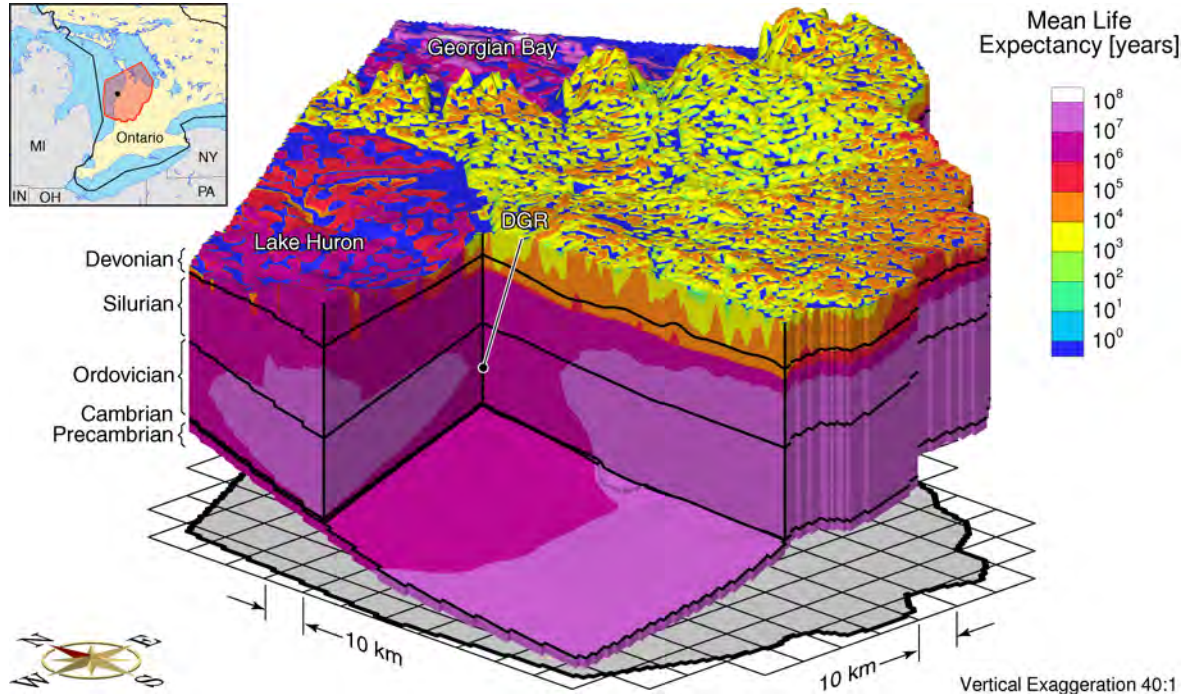


Figure 24: Base-case mean life expectancy (years).

5.2 Characteristics of Estimates of Mean Life Expectancy

This study has developed a conceptual model of regional groundwater flow in the Bruce Megablock of the Michigan Basin and its effect on flow and transport in the vicinity of the proposed Bruce DGR. Of particular importance in the analysis are the characteristics of the Cobourg Ordovician limestone that is the host unit for the proposed repository. The characteristics relevant to this study include estimated energy gradients, estimated groundwater

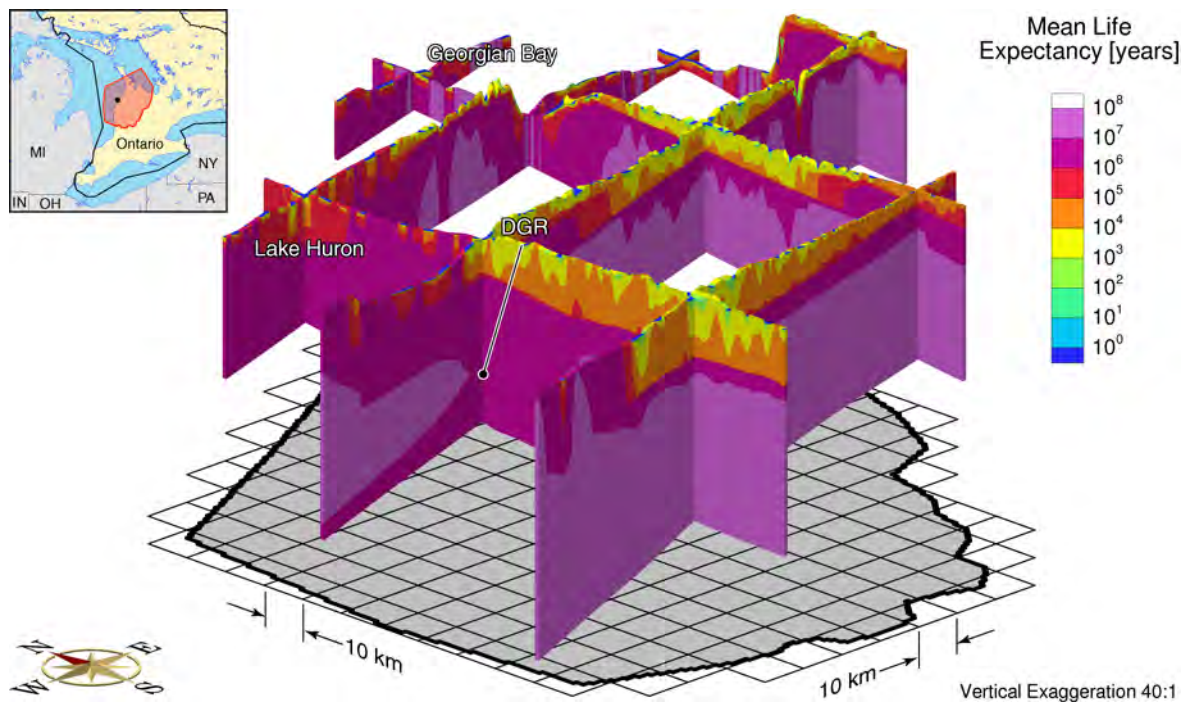


Figure 25: Fence diagram showing base-case mean life expectancy (years).

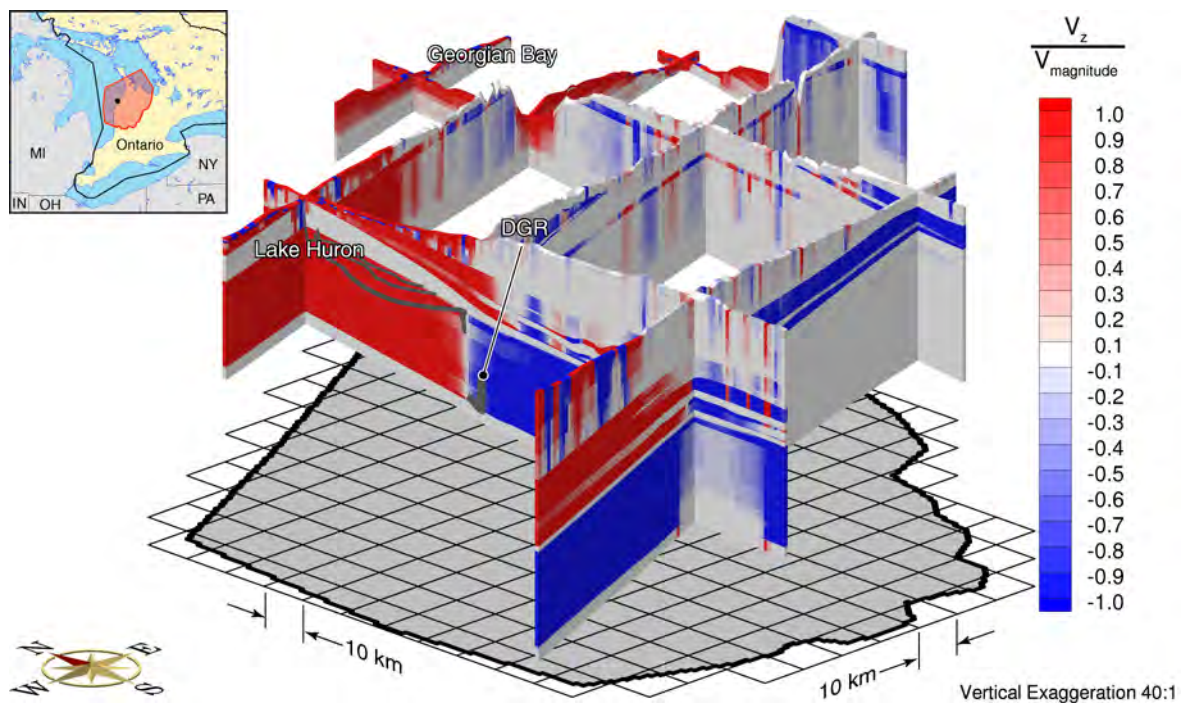


Figure 26: Fence diagram showing path of average water particles released from the vicinity of the proposed DGR.

velocity and calculated pressures at the repository horizon, as well as mean life expectancy (MLE). The MLE is an estimate of the average time that a water particle will take to migrate from a point of interest, such as the DGR repository, to an exit point or biosphere discharge point for the system. It is used in this study as a performance measure to evaluate the impact of alternate parameters and conceptual model attributes on the groundwater system (refer to Section 3.2). As shown in Equation (36), estimates of the MLE are dependent on the spatial distribution of the groundwater velocity vector at pseudo-equilibrium time and the dispersion tensor which, as implemented in FRAC3DVS-OPG, is represented as a function of both a mechanical dispersion component and a diffusion component.

The sensitivity of the estimated MLE to the pseudo-equilibrium time was investigated for the base-case parameters with the results being presented graphically in Figure 27. For a pseudo-equilibrium time of 100 000 years the MLE for the DGR repository horizon was estimated to be 9.8 million years while an MLE of 11.7 million years was estimated for a pseudo-equilibrium time of 100 million years. In the absence of a TDS source and with the continual efflux of mass from the domain, the density-dependent velocities and the TDS distribution will change with pseudo-equilibrium time; the MLE will change correspondingly.

The impact of the longitudinal dispersivity (α_L) was investigated with Scenario 2 and Scenario 3 shown in Table 11. Both cases have smaller dispersivities than that used in the base-case analysis. The large base-case value of α_L equal to 500 m, corresponding to a grid or cell Peclet number of approximately 2, can result in mechanical dispersion being significant even for small pore velocities. It also contributes to the estimation of lower values of MLE than that calculated for smaller values of α_L . Unfortunately, FRAC3DVS-OPG failed to converge for the 2 scenarios so that solutions could not be obtained for the smaller dispersivities and hence larger grid Peclet numbers.

The robustness of estimates of the MLE can be assessed in a sensitivity analysis. This analysis can investigate the sensitivity of the estimate of the MLE to changes in the system parameters. These parameters can include the spatial distribution of permeabilities and porosities, the transport parameters including dispersivity, effective diffusion coefficient, and the boundary conditions and initial conditions used to describe the salinity distribution. The sensitivity analysis can also include an investigation of the sensitivity of MLE to the geologic conceptual model and the extent of the regional spatial domain. This Phase 1 report investigates the sensitivity of the DGR MLE to the permeability of the Ordovician limestone and shale units. The rationale for this subset of parameters is that the primary geologic barrier for the DGR is the Ordovician. Further, the scale of the regional model and the developed discretization is not appropriate for the evaluation of the importance of diffusion processes. This can be more readily accomplished in a site-scale analysis that has multiple model layers for the units such as the Cobourg limestone. Finally, in this report, the sensitivity analysis is investigated by calculating the normalized sensitivity coefficients that express the percent change in the MLE that will result from a one percent change in the parameter of interest. These sensitivity coefficients are local derivatives. The range of validity of these derivatives over larger parameter perturbations can be investigated in subsequent analyses. The sensitivity coefficients can also depend on the size of the perturbation of the parameter of interest. While it is common to perturb parameters by several percent in a sensitivity analysis, because of the very large range in the permeabilities for the geologic units included in this study, parameters were perturbed by 10% in order to minimize the effect, if any, of computer errors related to significant digits. The following paragraphs investigate

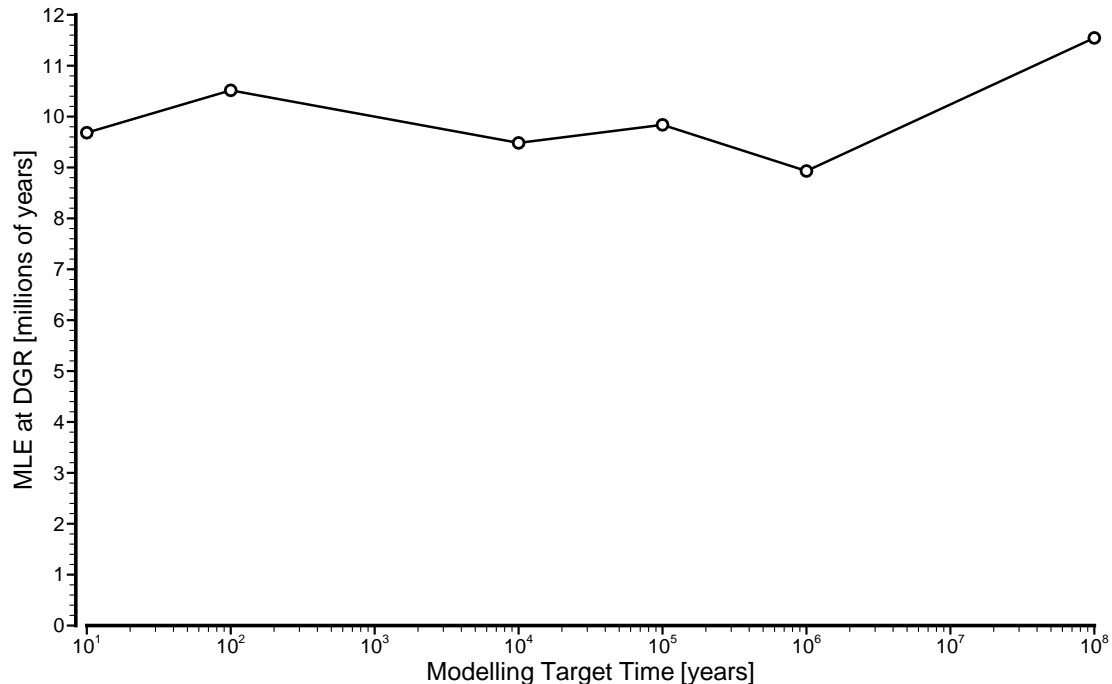


Figure 27: Mean Life Expectancy at the DGR as a function of pseudo-equilibrium time for the base case parameters.

the sensitivity of the MLE at all grid blocks in the spatial domain to the permeability for the Ordovician units.

The sensitivity of the MLE to perturbations of the hydraulic conductivity for the Queenston, Georgian Bay/Blue Mountain and Cobourg Formations was investigated. Following the sensitivity method described in Section 3.2.1, the base-case hydraulic conductivity for a given formation was perturbed by 10% with all other parameters being the base-case values. Figure 28 presents a fence diagram of the normalized sensitivity coefficients for the MLE to perturbations of the Queenston siltstone and shale hydraulic conductivity. In the figure, red indicates that increases in hydraulic conductivity result in increases in the MLE while blue indicates an inverse relationship. White corresponds to a decreased sensitivity of MLE to the Queenston hydraulic conductivity. The largest absolute values of the normalized sensitivity coefficients occur in the areas where either the flow in the Queenston is vertical (refer to Figure 23) or areas where the unit outcrops and the Cambrian is absent (refer to Figure 9 and Figure 10, respectively). In areas where the flow is vertically upward from the Queenston, an increase in the hydraulic conductivity for the unit will decrease the MLE for areas beneath while for the regions where the flow is downward, increasing the hydraulic conductivity will result in an increase in the MLE for areas underlying the unit. The magnitude of the values is accentuated by the large longitudinal dispersivity value that when multiplied by the pore velocity in the estimation of mechanical dispersion, masks the diffusive transport component in the calculation of the MLE. At the location of the proposed DGR, a normalized sensitivity coefficient of 0.0067 is estimated indicating that at that location, the MLE is insensitive to the hydraulic conductivity of the Queenston Formation.

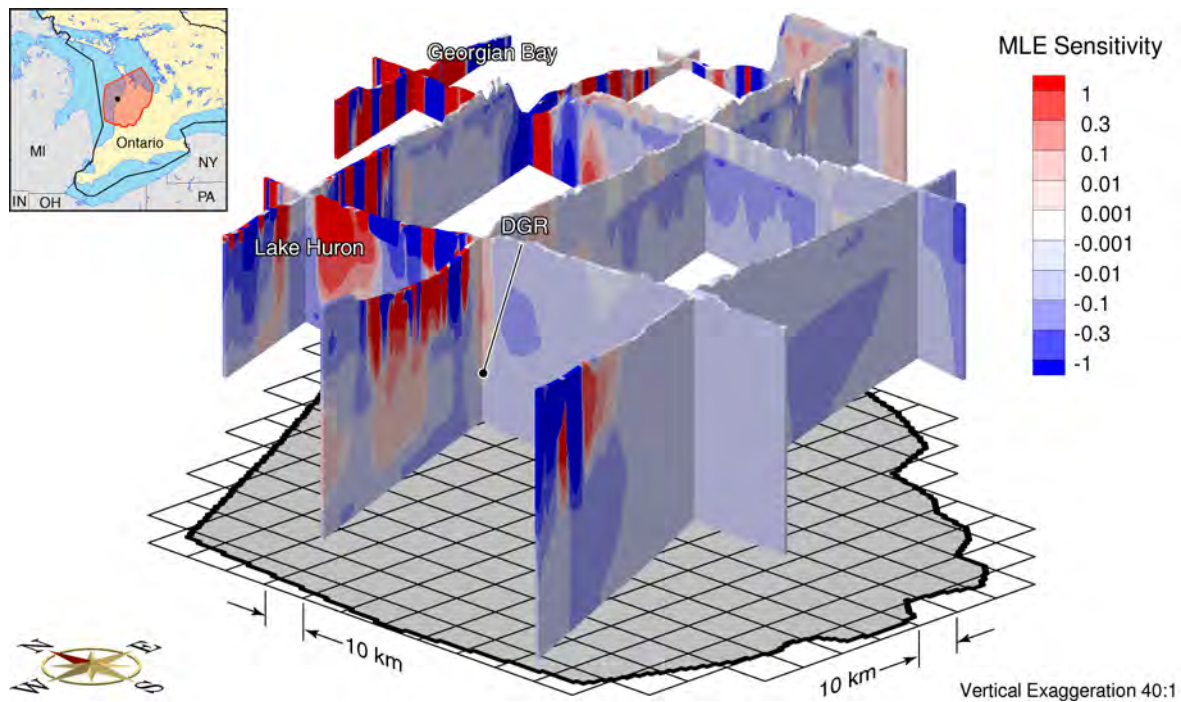


Figure 28: Fence diagram showing normalized sensitivity coefficients of MLE to the hydraulic conductivity of the Queenston siltstone and shale for the base case parameters.

The normalized sensitivity coefficients for the MLE to perturbations of the hydraulic conductivity for the Georgian Bay/Blue Mountain shale are presented in Figure 29. The pattern is similar to that of the Queenston Formation shown in Figure 28. At the location of the proposed DGR, a normalized sensitivity coefficient of -0.135 is estimated indicating a moderate sensitivity. Increases in the formation's hydraulic conductivity will result in a decreased MLE. The increased sensitivity value, as compared to that for the Queenston, reflects both the greater thickness of the Georgian Bay/Blue Mountain Formations at the DGR (refer to Table 1) and the impact of the large longitudinal dispersivity coefficient.

The proposed DGR is to be located in the Cobourg Formation. Figure 30 shows the calculated normalized sensitivity coefficients of the MLE to perturbations of the hydraulic conductivity for the Cobourg Formation. The trend of the sensitivity coefficients is similar to that of the two preceding analyses. At the DGR location, the estimated normalized sensitivity coefficient is 0.052 . The low value indicates a relative insensitivity of the MLE at the repository to the hydraulic conductivity; the value supports the assessment that contaminant transport is dominated by factors other than velocity. The positive coefficient can be explained by the fact that flow at the DGR for the base-case parameters and boundary conditions is downward from the Cobourg Formation to the underlying Cambrian. Increasing the hydraulic conductivity for the Cobourg will increase this downward flow and reduce the upward mechanical dispersion from the unit. The effect will be a longer transport path. Again, the mechanical dispersion is magnified by the large longitudinal dispersivity required for convergence of FRAC3DVS-OPG.

The normalized sensitivity coefficients of the MLE at the DGR to perturbations of the Ordovician hydraulic conductivity are summarized in Table 12. As shown in this study, the estimated MLE

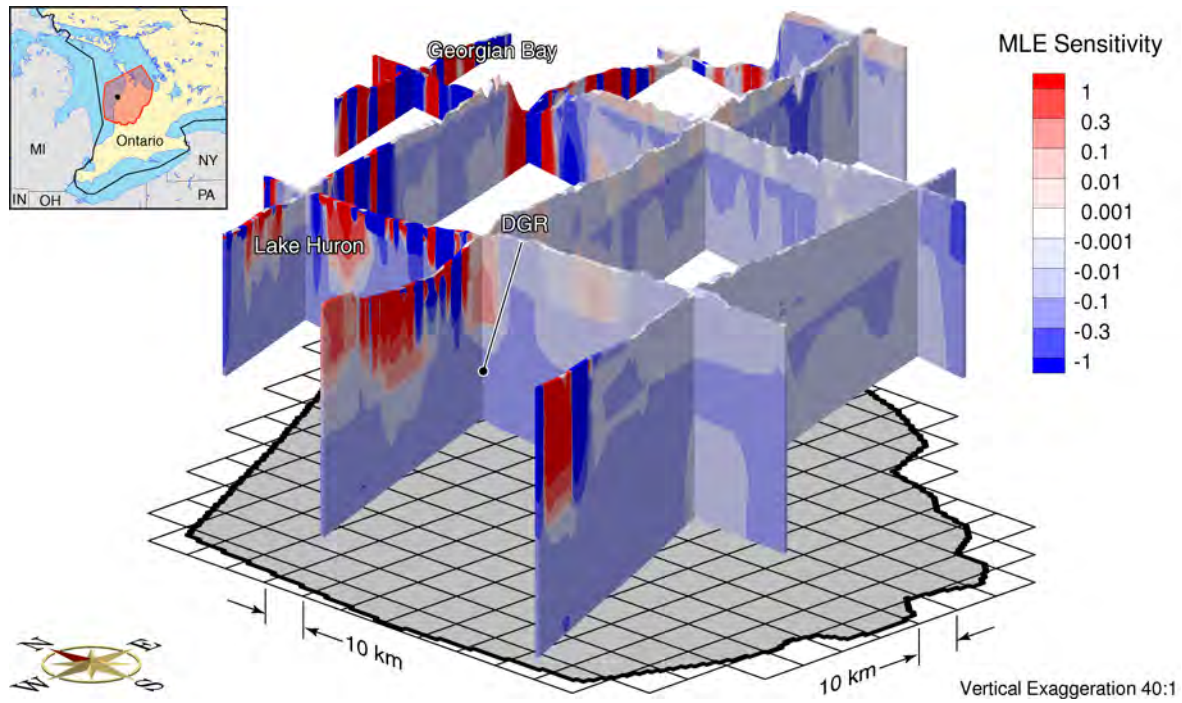


Figure 29: Fence diagram showing normalized sensitivity coefficients of MLE to the hydraulic conductivity of the Georgian Bay/Blue Mountain shale for the base case parameters.

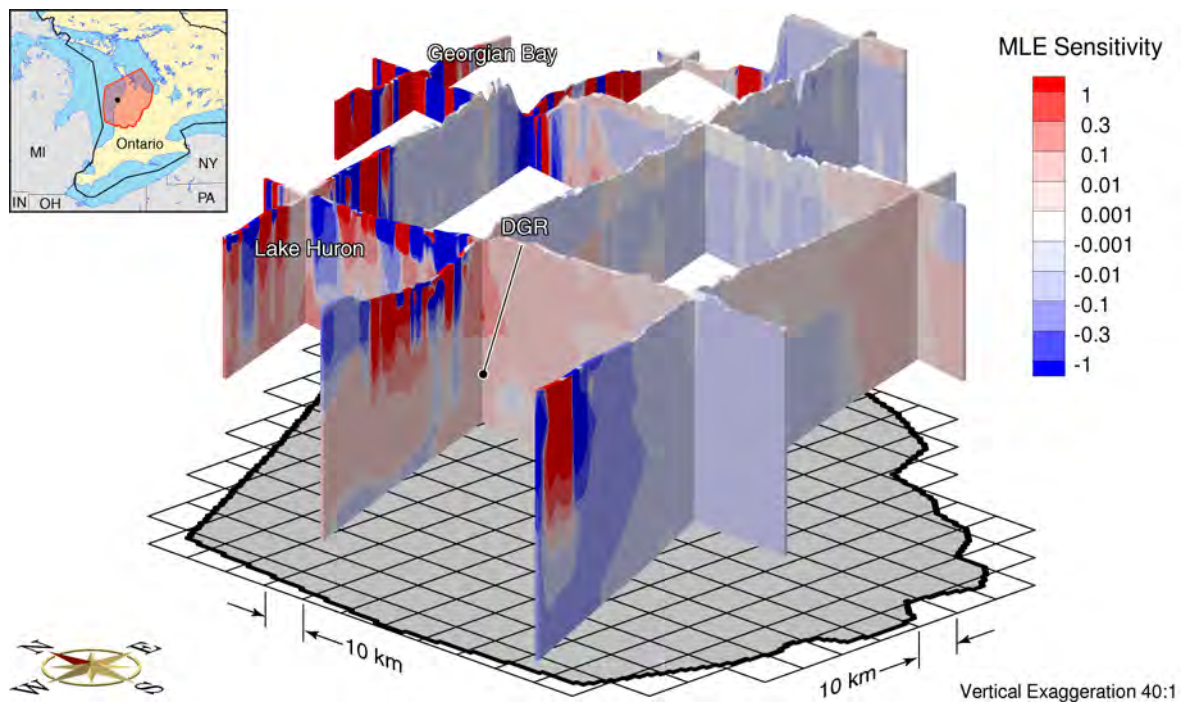


Figure 30: Fence diagram showing normalized sensitivity coefficients of MLE to the hydraulic conductivity of the Cobourg limestone for the base case parameters.

values will be influenced by several factors that include the assumed state, the pseudo-equilibrium time and the magnitude of the longitudinal dispersivity. Larger values of longitudinal dispersivity will tend to decrease the MLE while smaller values will generally result in an increase in the MLE. In the limit, as the longitudinal dispersivity is reduced to zero, the MLE will approach a value that is characterized by the advection and diffusion. Because of the large longitudinal dispersivity value used in this study, MLE estimates calculated using the regional-scale model are conservative.

Table 12: Summary of normalized sensitivity coefficients of MLE to hydraulic conductivity of the Ordovician limestone, siltstone and shale units.

| Unit | Normalized Sensitivity Coefficient |
|------------------------|------------------------------------|
| Queenston | 0.0067 |
| Georgian Bay/Blue Mtn. | -0.14 |
| Cobourg | 0.052 |

5.3 Regional Scale Simulations: Analysis of Alternate Cases

5.3.1 Summary of Scenario Analyses

Table 13 summarizes the mean life expectancies (MLE) at the location of the proposed DGR for the various scenarios (refer to Table 11) presented in the following sections. The lowest calculated MLE from all of the analyses was greater than 1 million years. However, the values are conservative as a result of the use of a large longitudinal dispersivity.

5.3.2 Analysis of the Surface Boundary Condition

A Dirichlet boundary condition defining either the regional water table or the elevation of Lake Huron is used for the surface of the base-case regional-scale model. The influx and efflux of water across the surface is controlled, in part, by the hydraulic conductivity of the top layer of the model as well as topographic gradients. It is assumed that, on average, the water table is located 3 m below the ground surface and that, to reflect weathering, the upper 20 m has a higher hydraulic conductivity than the underlying units. Alternate conceptualizations of the surface boundary condition were investigated with Scenarios 4 and 5 (refer to Table 11). The figures for the analysis of the two scenarios are included in Appendix B.

The impact on groundwater flow of the assumed 20 m weathered zone at the surface of the regional-scale domain was investigated in Scenario 4. The scenario uses a prescribed water table as implemented in the base-case analysis with no weathered zone. The hydraulic conductivities for the upper 20 m of the domain are defined by the lithology of the geological framework model and the parameters of Table 7. All other parameters are the same as the base-case simulation of Scenario 1. The results for the analysis are presented in Figure B.1 to Figure B.7. By comparing the figures to those of the base-case analysis presented in Section 5.1, it can be concluded that the model results are insensitive to the inclusion of a weathered zone in

Table 13: Estimated Mean Life Expectancy at the DGR for the scenarios investigated in this study.

| Scenario | Description | Mean Life Expectancy [millions of years] |
|----------|-------------------------------|---|
| 1 | Base Case | 8.9 |
| 4 | Surface Boundary Condition | 8.9 |
| 5 | Surface Boundary Condition | 7.0 |
| 6 | Geologic Model | 1.6 |
| 7 | Density-Independent Flow | 11.2 |
| 8 | Ordovician K Model (P-Case 1) | 14.9 |
| 9 | Ordovician K Model (P-Case 2) | 38.6 |
| 10 | Ordovician K Model (P-Case 3) | 44.38 |
| 11 | Silurian K Model (S-Case 4) | 38.6 |
| 12 | Silurian K Model (S-Case 5) | 39.1 |
| 16 | Horizontal Boundary Condition | 6.2 |
| Camb-1 | Cambrian Anisotropy | 7.8 |
| Camb-2 | Cambrian Anisotropy | 22.7 |
| Camb-3 | Cambrian Anisotropy | 18.4 |

the model. The estimated MLE at the location of the proposed DGR for Scenario 4 is 8.9 million years - the same as that estimated for the base case analysis.

Scenario 5 investigates the use of an areally constant net recharge flux boundary condition in conjunction with prescribed equivalent freshwater heads at the major rivers of the regional-scale spatial domain. In this study, net recharge is defined as the amount of water that contributes to the base flow of the rivers defined by prescribed equivalent freshwater heads. As shown in Figure 6, the network of rivers at the regional-scale excludes many of the small rills, gullies, ditches, creeks, brooks and streams that are important in the surface flow system. For grid blocks that are 900.9 m by 762.8 m, a large fraction of the recharge that occurs at a point will be interflow that contributes to the base flow of these smaller scale features. Thus, the impact of upscaling of point recharge in a model that includes only regional-scale rivers is to significantly reduce the net recharge. The parameters for the base-case conceptual model were used for the analysis of Scenario 5. Through a sensitivity analysis, the upscaled, areal average, net recharge for Scenario 5 was determined to be 0.27 mm/year. The constraint used in the estimation of the value was the location of the model-determined water table relative to the elevation of the ground surface of the spatial domain. The low value is a reflection of the fact that most point groundwater recharge will discharge to the surface at a scale that is considerably smaller than that of a regional-scale grid block. The results for the analysis are given in Figure B.8 to Figure B.14 of Appendix B. As compared to the base-case analysis (refer to Section 5.1), the model results with a prescribed recharge present a smoother shallow groundwater system. The difference is most obvious with a comparison of the MLE of Figure B.13 and Figure 24. For the case with recharge, the higher MLE at surface water divides (red in Figure B.13) and lower values at rivers (blue and yellow) are clearly apparent. The regional-scale rivers are obvious in the figure. The base-case analysis is considerably more complex as water that recharges at one block can discharge at an immediately adjacent block. However, the impact of the different conceptualizations of the surface

boundary condition is dampened significantly by the low permeability of the Salina. At the location of the proposed DGR, a MLE of 7.0 million years was estimated for a pseudo-equilibrium time of 1 million years. In this study, the use of a prescribed water table rather than a recharge boundary condition was selected for the base-case due to its reduced computational time.

5.3.3 Investigation of Geological Framework Model

Scenario 6 in Table 11 was designed to investigate the sensitivity of the groundwater flow system to the geological framework model (refer to Section 2.3). Two models have been developed in this study; the GLL00 geological framework developed by Gartner Lee Limited (2008b) improved the preliminary approach of Sykes (2007), in part, by data screening and augmenting the OGSR data base with information from 57 petroleum Reference Wells (Armstrong and Carter, 2006) and 76 petroleum wells outside of the study area from the Michigan State Geological Survey Digital Well Database. The most notable difference between the models is the characterization of the Cambrian. Because the Cambrian has a relatively high hydraulic conductivity, the characterization of its spatial extent is important. Based on their screening of well records, database augmentation and interpretive methods, the Cambrian in the GLL00 model has lesser extent in the west to east direction (refer to Figure 10) than that of the Sykes (2007) model. The distribution of the thicknesses of the various units in the models also differ because of differences in the methods used to interpolate and extrapolate the structural contours of the units in the model. The environmental heads and MLE for the base-case results with the GLL00 model are presented in Figure 19 and Figure 24, respectively. For the base-case parameters, boundary conditions and the preliminary Sykes (2007) geological framework model, the regional-scale environmental heads and MLE estimates are given in Figure 31 and Figure 32, respectively. A comparison of the distributions of environmental head indicate that higher vertically upward gradients are predicted west of the DGR site beneath Lake Huron for the preliminary model than those predicted for the GLL00 model. The cause of the higher gradients is related to the higher environmental heads in the Cambrian predicted for the preliminary model as compared to those estimated for the GLL00 model. With an increased eastern extent for the Cambrian in the preliminary model, the higher heads are associated with increased topographic elevation. The Cambrian was assumed to be homogeneous in both analyses. The MLE at the location of the proposed DGR for the preliminary model was 1.6 million years. The results of the analysis emphasize the importance of the geological framework model and the characterization of the hydraulic conductivity distribution for the Cambrian. Alternate characterizations of the Cambrian hydraulic conductivity are presented in Section 5.3.7.

5.3.4 Density-Independent Flow

The TDS distribution varies over a considerable range at the DGR-1 and DGR-2 boreholes. The shallow groundwater zone above the Salina is characterized by low, near freshwater TDS concentrations while the intermediate and deep groundwater zones have TDS concentrations that can be up to 300 g/L. To reflect the TDS distribution, the regional-scale base-case analysis simulates density-dependent flow. Scenario 7 investigates the impact of assuming that groundwater flow is independent of density. The base-case parameters and boundary conditions are used for the analysis. The solution methodology, however, is considerably simplified as flow is determined from a steady-state solution with the TDS concentration set to zero throughout the

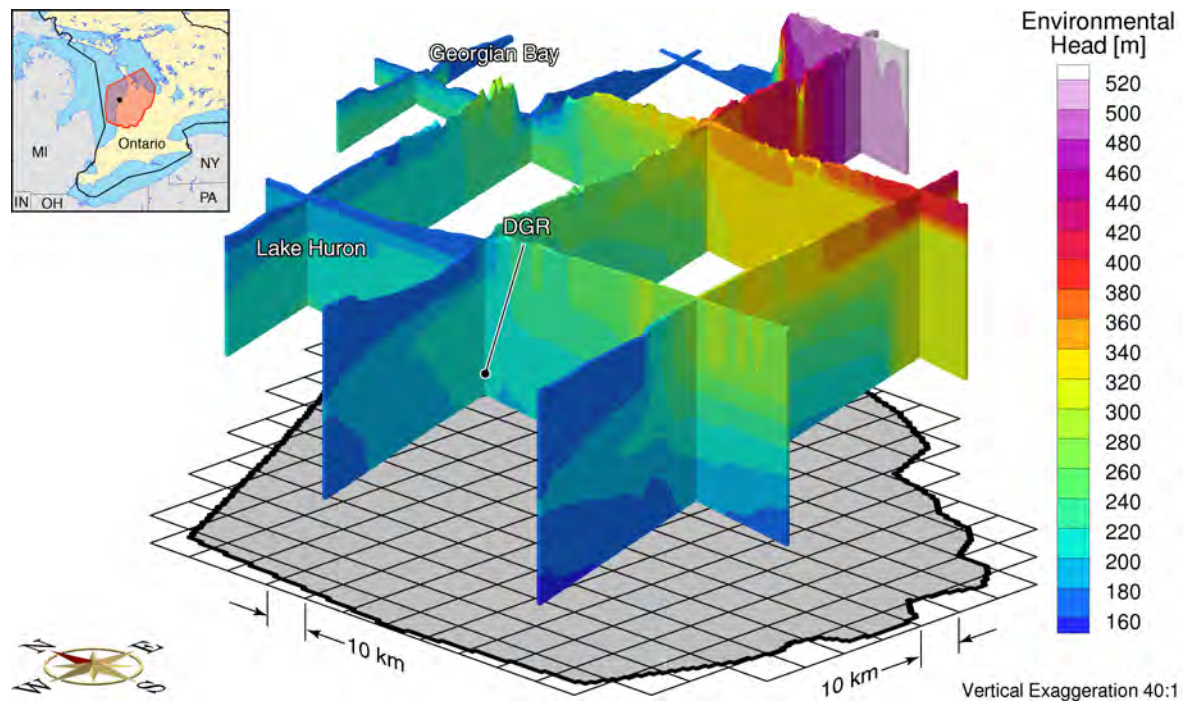


Figure 31: Environmental head (m) distribution for base-case parameters and preliminary geological framework model.

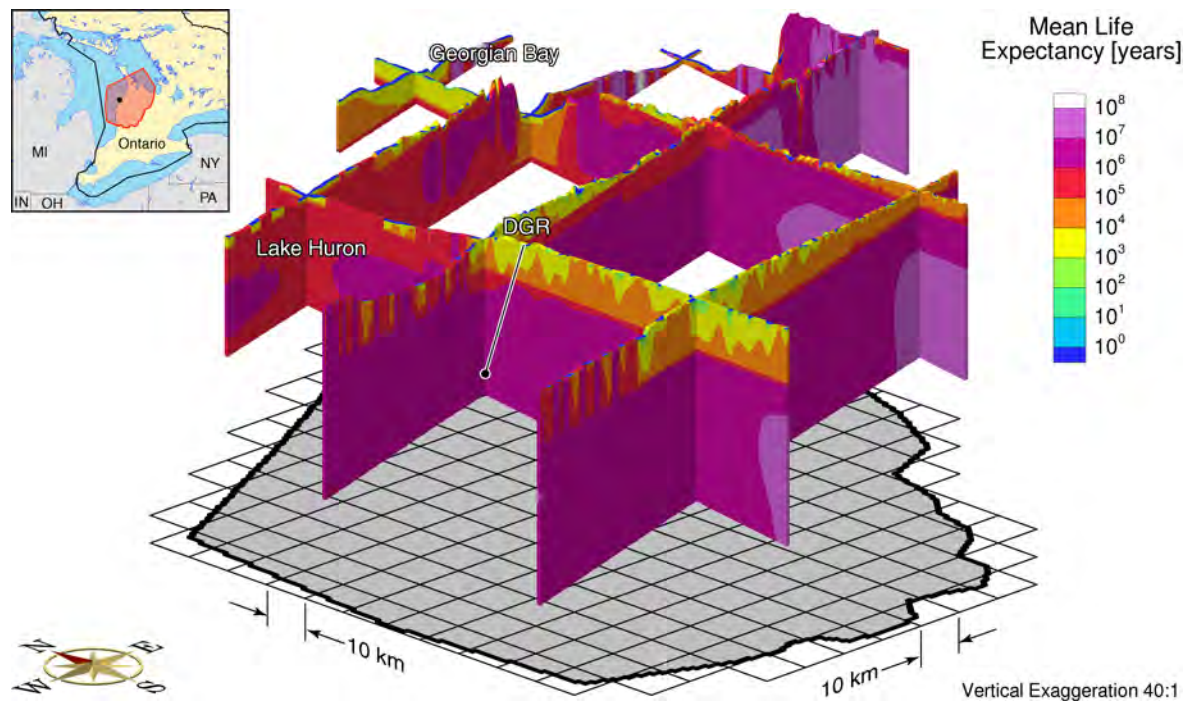


Figure 32: Mean life expectancy (years) for base-case parameters and preliminary geological framework model.

domain. The MLE analysis also is simplified as it is based on the steady-state velocities rather than a solution that changes with the pseudo-equilibrium time as occurs in the analysis of density-dependent flow. The Scenario 7 analysis of density-independent flow is presented in Figure C.1 to Figure C.7 of Appendix C. In comparing the figures to those of the density-dependent base-case analysis, the most notable difference is in the estimated vertical gradients. The difference is evident beneath Lake Huron in a comparison of the piezometric heads of Figure C.2 with the environmental heads of Figure 20 and a comparison of the ratio of vertical velocity to the velocity magnitude of Figure C.5 and Figure 23. For density-independent flow, the velocities in the Ordovician and Lower Silurian are strongly vertical and uniform with fewer zones of sub-horizontal flow. The velocities are indicative of diffusion dominant transport. The pattern of vertical gradients for the case of density-dependent flow is more complex.

The paths of nine average water particles released from the vicinity of the proposed DGR for the case with density-independent flow are plotted in Figure 33. The path followed by the particles for the imposed boundary conditions and present state is downward from the point of release to the Cambrian, then northward through the Cambrian to the domain boundary to a point where the Silurian is absent and then upward through the Ordovician to the surface. The upward path at the domain boundary is a result of the use of a no-flow lateral boundary condition. In comparison, the particle paths for the case with density-dependent flow followed the Niagaran (refer to Figure 26). The time of travel for the nine particles varied from 34 million years to 70 million years for the density-independent analysis. Based on the analysis, the important impact of variable fluid density is that particle paths originating from the vicinity of the proposed DGR in the Ordovician are dominated by flow through the shallower Niagaran Group. In the absence of density-dependent flow, paths can follow the deeper Cambrian units rather than the Niagaran Group. For both cases, the Salina units are a significant barrier to vertical migration. Also of importance is that no horizontal migration occurred through the low permeability units such as the Ordovician, Lower Silurian or Salina. Horizontal flow only occurred in the more permeable units.

At the location of the proposed DGR, a MLE of 11.2 million years was estimated for the case of density-independent flow. As discussed in the preceding paragraph, the path followed by average water particles released from the vicinity of the proposed DGR differ for the case from that determined for density-dependent flow for which the MLE at the location of the proposed DGR was calculated to be 11.7 million years for the base-case velocity field at a pseudo-equilibrium time of 100 million years. Lower MLE values were also calculated for different pseudo-equilibrium times (refer to Section 5.2). The difference in the MLE for the two cases is less than the range in the MLE that results when different pseudo-equilibrium times are used for the estimation of the density-dependent value. It also appears that MLE may not be a reliable metric to assess the impact of varying fluid density on the flow domain, particularly for a system in which transport is dominated by diffusion; the use of average water particle paths may be a more reliable means of assessing the importance of fluid density (refer to the preceding paragraph). The fluid density modifies the energy gradient term in the calculation of Darcy velocities. As was shown in Section 5.2, the MLE is relatively insensitive to perturbations of the velocity for the low permeability units. For a system dominated by low permeability units, the MLE may have a greater sensitivity to the geological framework model, unit properties, boundary conditions and model constrained dispersion coefficients.

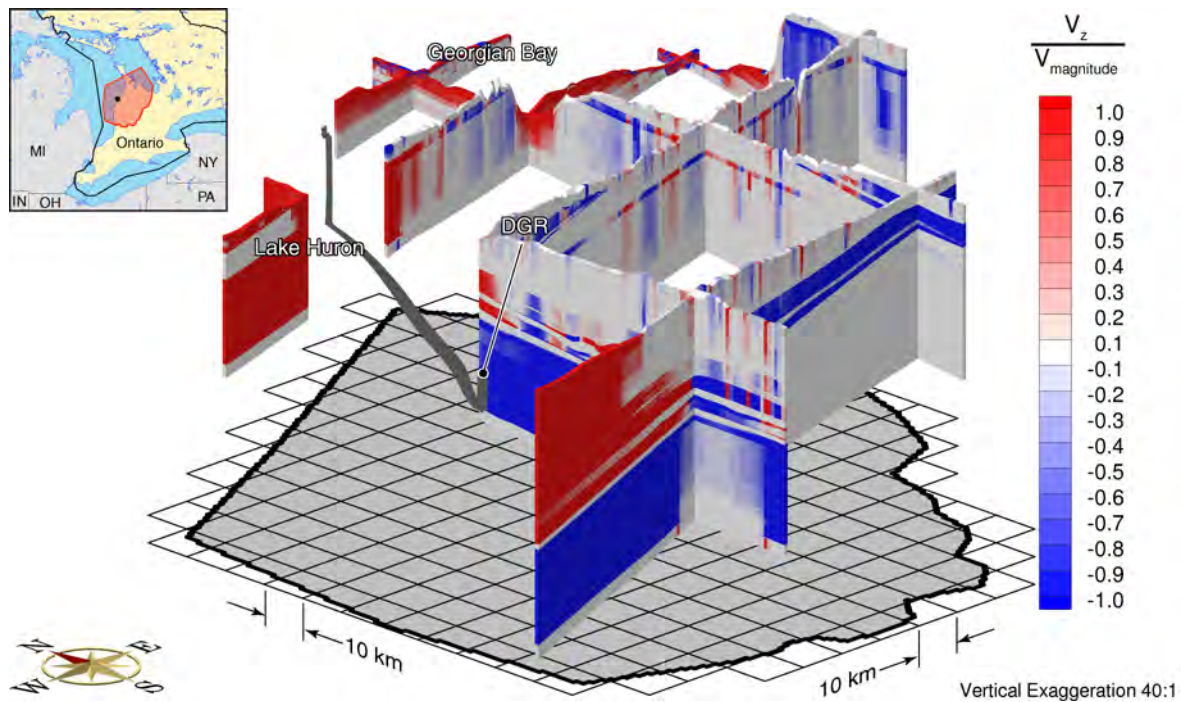


Figure 33: Fence diagram showing path of average water particles released from the vicinity of the proposed DGR for the case with density-independent flow.

5.3.5 Alternate Hydraulic Conductivity Models for the Ordovician and Silurian Units

Section 5.2 investigated the impact on MLE of small changes (10%) in the hydraulic conductivity of the Ordovician units as the calculated normalized sensitivity coefficients are local derivatives. In this section, the impact on the regional-scale flow domain and estimates of MLE is investigated for large changes (orders-of-magnitude) of the hydraulic conductivity for the Ordovician and Silurian Formations.

Scenarios 8, 9 and 10 investigate large changes in the hydraulic conductivity distribution for the Ordovician units. The properties for the three scenarios are given in Table A.2, Table A.3 and Table A.4 respectively of Appendix A. In comparison, the base-case horizontal conductivity for the Ordovician units varied from 8.0×10^{-13} m/s to 9.1×10^{-12} m/s. For Scenario 8, the Ordovician units were assumed to be homogeneous with a horizontal conductivity of 1.0×10^{-11} m/s and a horizontal to vertical anisotropy ratio of 10:1. Scenario 9 and Scenario 10 assumed homogeneous values of 1.0×10^{-13} m/s and 1.0×10^{-15} m/s, respectively, for the Ordovician units. The boundary conditions for the analyses are the same as those of the base-case. The MLE results of the simulations are presented in Figure D.1 to Figure D.6 of Appendix D.

For all cases, the MLE at the location of the proposed DGR in the Ordovician units is estimated to be greater than 10 million years. At the location of the proposed DGR, the MLE for Scenarios 8, 9 and 10 were estimated to be 14.9 million years, 38.6 million years and 44.3 million years, respectively. The sensitivity of the MLE to the large changes in the hydraulic conductivity can be explained by the impact the change has on the mechanical dispersion term of the MLE equation. While the large longitudinal dispersivity of the term cannot be reduced because of computational

considerations, the reduction of the hydraulic conductivity can significantly reduce the velocities in the term with no computational consequences. This can be further explained using the Peclet number in which the characteristic length of the numerator is the longitudinal dispersivity and the denominator is the molecular diffusion. The Peclet number, as defined, is thus the ratio of mechanical dispersion to diffusion: $Pe = \alpha_L v / D^*$. Based on a diffusion coefficient of the porous medium of $D^* = 0.0038 \text{ m}^2/\text{yr}$ and a longitudinal dispersivity $\alpha_L = 500 \text{ m}$, the Peclet number in the Ordovician at the location of the proposed DGR was calculated for the base-case scenario and the Ordovician hydraulic conductivity Scenarios 8, 9 and 10 (Table 14). The Peclet numbers show that mechanical dispersion is greater than molecular diffusion for Scenario 1. With low velocities, the magnitude of the Peclet number is due to the large value of longitudinal dispersivity required to obtain a solution. The contribution of mechanical dispersion to transport is significantly less for Scenarios 8, 9 and 10; the result is an increase in the MLE.

Table 14: The Peclet numbers at the location of the proposed DGR for the base-case scenario and Scenarios 8, 9 and 10

| Scenario | Pseudo-Equilibrium Time [millions of years] | Mean Life Expectancy [millions of years] | Linear Velocity [m/year] | Peclet Number |
|----------|--|---|-----------------------------|------------------------|
| 1 | 1 | 8.9 | 1.90×10^{-5} | 2.50 |
| 1 | 100 | 11.65 | 1.19×10^{-5} | 1.57 |
| 8 | 1 | 14.9 | 3.37×10^{-6} | 0.444 |
| 9 | 1 | 38.6 | 3.61×10^{-8} | 0.474×10^{-2} |
| 10 | 1 | 44.3 | 4.40×10^{-9} | 0.578×10^{-3} |

The Salina units of the Silurian in the vicinity of the proposed DGR are a significant barrier to flow between the overlying, shallow groundwater system of the Devonian and the underlying, more permeable Niagaran. The sensitivity of MLE to the hydraulic conductivity distribution of the Salina units was investigated in Scenarios 11 and 12; the hydraulic properties for the two scenarios are listed in Table A.5 and Table A.6 of Appendix A. The boundary conditions for the analysis are the same as those used in the base-case Scenario 1. For Scenario 11, the horizontal hydraulic conductivity from the B&C Unit to the A1-Evaporite was assigned an arbitrarily large value of $1 \times 10^{-8} \text{ m/s}$. The salt and evaporite units were assumed to be isotropic while the carbonate units were assigned a horizontal to vertical anisotropy ratio of 10:1. The horizontal hydraulic conductivity for the Ordovician units was assigned a value of $1.0 \times 10^{-13} \text{ m/s}$ with an anisotropy ratio of 10:1; the values are similar to those used in Scenario 9 but, most importantly, lower than those used for the Ordovician in the base-case analysis. The results for the simulation are presented in Figure E.1 to Figure E.8 of Appendix E. As shown in the figures, the increase in the hydraulic conductivity for the Salina results in the extension of the surface dominated groundwater system to the top of the Queenston Formation. Evidence for this is the reduction of the TDS concentrations in the Silurian units, the increase in the velocity magnitude for the units, the occurrence of horizontal flow in the units with a similar pattern to that of the Devonian units, and a significant reduction of the MLE as compared to that of the base-case analysis. However, the Ordovician remains as a significant barrier with a MLE of 38.6 million years at the location of the proposed DGR for a target time or pseudo-equilibrium time of 1 million years. The MLE estimate is similar to that estimated for Scenario 9. The principle pathway for transport, as in the base-case simulation, is horizontally through the Niagaran rather than vertically upward through

the less permeable (by an order-of-magnitude), overlying and confining Salina units. The results of Scenarios 11 and 12 indicate that large increases in the model permeability of the Salina do not have a significant impact on MLE or travel paths from the location of the proposed DGR. The results reaffirm those of Scenarios 8, 9 and 10 - the reduction of the permeability of the Ordovician units increases the estimated MLE.

The horizontal hydraulic conductivity and anisotropy ratio of the Salina units for Scenario 12 is similar to that of Scenario 11 except that the A2 Anhydrite Salt unit was assigned an isotropic hydraulic conductivity of 1×10^{-13} m/s. The results for the analysis are shown in Figure E.9 to Figure E.16 of Appendix E. The results are similar to that of Scenario 11 with the exception that the A2 Anhydrite Salt acts as a confining layer for the other more permeable units of the Salina. The estimated MLE at the location of the proposed DGR is 39.1 million years.

5.3.6 Analysis of the Lateral Boundary Condition

The regional-scale spatial domain is a subset of the Michigan Basin. For the more permeable units of the intermediate and deep groundwater zones such as the Niagaran and the Cambrian, it is possible that the use of a no-flow boundary condition for the lateral edges of the domain could have an impact on the flow in the units and on the estimate of MLE at the location of the proposed DGR. The objective of Scenario 16 is to relax the constraint on lateral flow imposed by the no-flow boundary condition. This was achieved by assigning an isotropic hydraulic conductivity of 1×10^{-7} m/s from the surface to the Precambrian at the perimeter of the domain. The width of the zone was 3 grid blocks. The upper boundary condition was identical to that of the base-case analysis. Thus, the zone allows communication at the domain edges between all of the deeper units and the surface where the equivalent freshwater heads were assigned based on surface topography. The hydraulic parameters for the analysis were the same as those of the base-case analysis. However, the solution methodology had to be altered as the high permeability perimeter zone allowed freshwater to penetrate to depth flushing TDS from units such as the Cambrian. To overcome this problem, the TDS concentration distribution of the base-case analysis at a pseudo-equilibrium time of 1 million years was assigned to all grid blocks of the regional-scale domain and the transport solution turned off in FRAC3DVS-OPG. The resulting flow equation would thus include the impact of density as determined by the TDS concentration distribution but would not be able to alter the concentration as flow occurred.

The environmental head distribution for Scenario 16 is shown in Figure 34 and Figure 35, the velocity magnitude is shown in Figure 36 while the ratio of vertical velocity to the velocity magnitude is given in Figure 37. Finally, the calculated MLE for the scenario is given in Figure 38 and Figure 39. The impact of the communication zone at the domain perimeter on velocities is evident in Figure 37 with high velocities apparent in the zone. The zone also results in small vertical environmental head gradients at the domain boundary such that flow in units such as the Niagaran and Cambrian is horizontal and topographically driven (refer to Figure 37). As expected, the MLE in the perimeter communication zone is low; however, the MLE values for the Ordovician units in the internal part of the domain are greater than 1 million years. At the location of the proposed DGR, the MLE was estimated to be 6.2 million years. The path either downward through the Ordovician to the Cambrian or upwards to the Niagaran Group and then to the domain boundary is long.

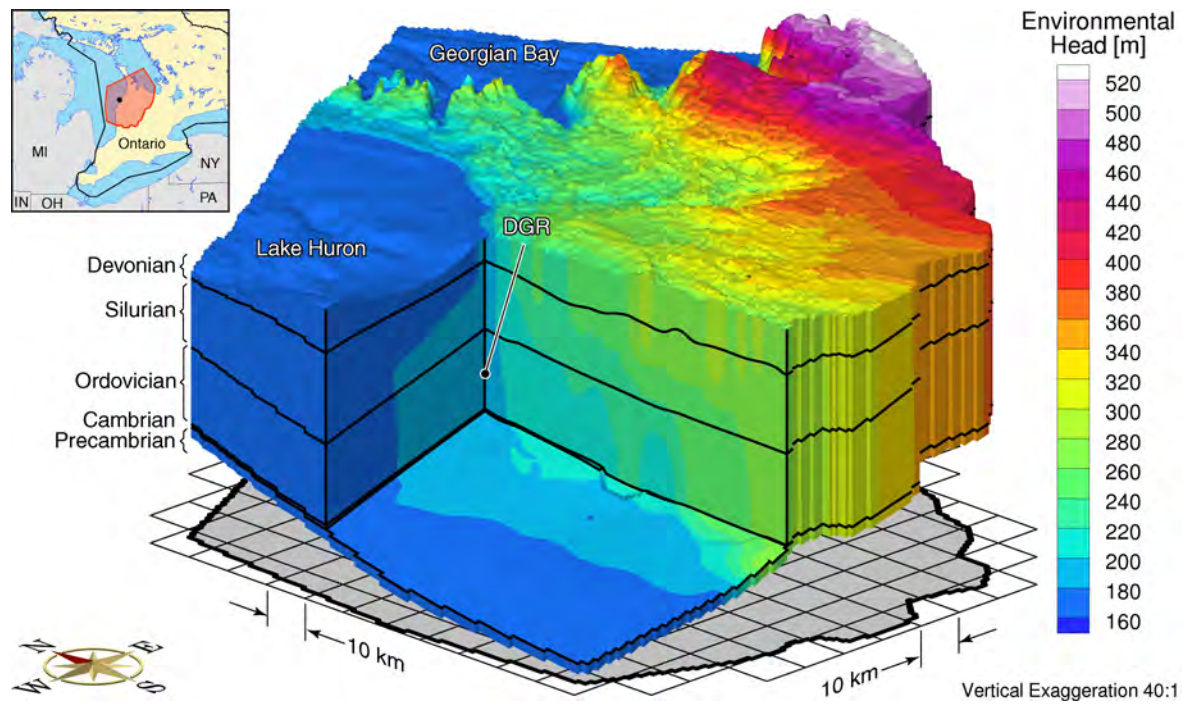


Figure 34: Environmental head (m) distribution for base case parameters with high permeability zone along domain boundaries (Scenario 16).

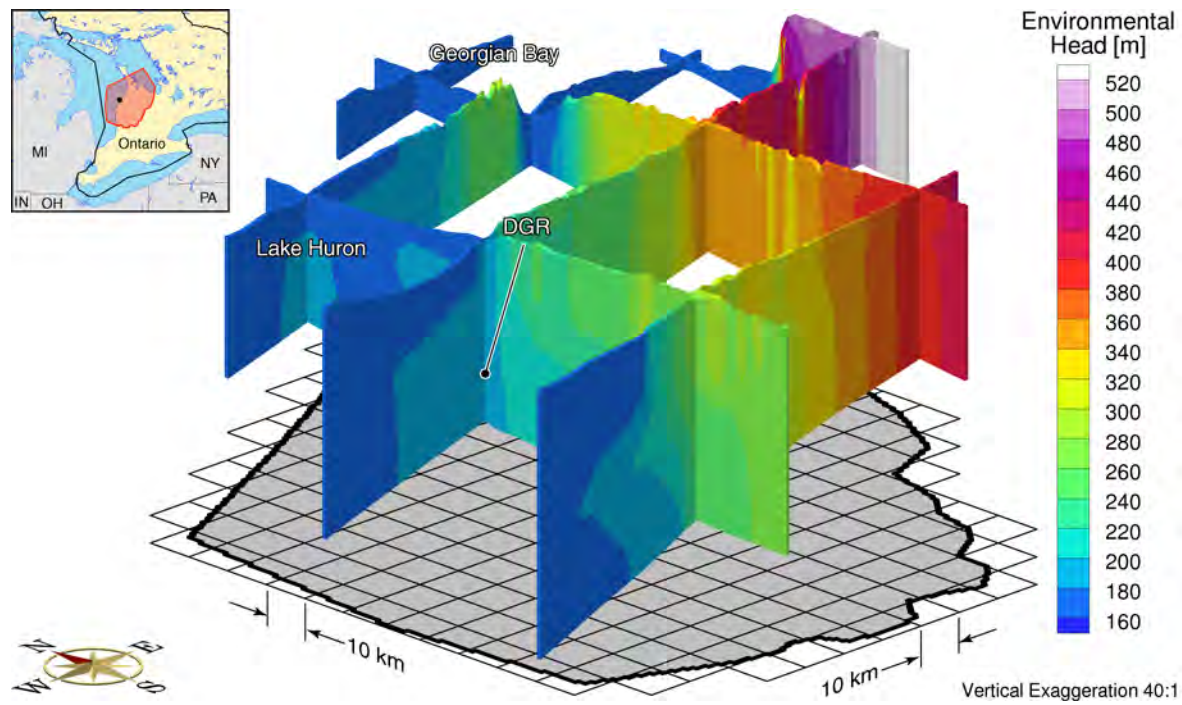


Figure 35: Fence diagram of environmental head (m) distribution for base case parameters with high permeability zone along domain boundaries (Scenario 16).

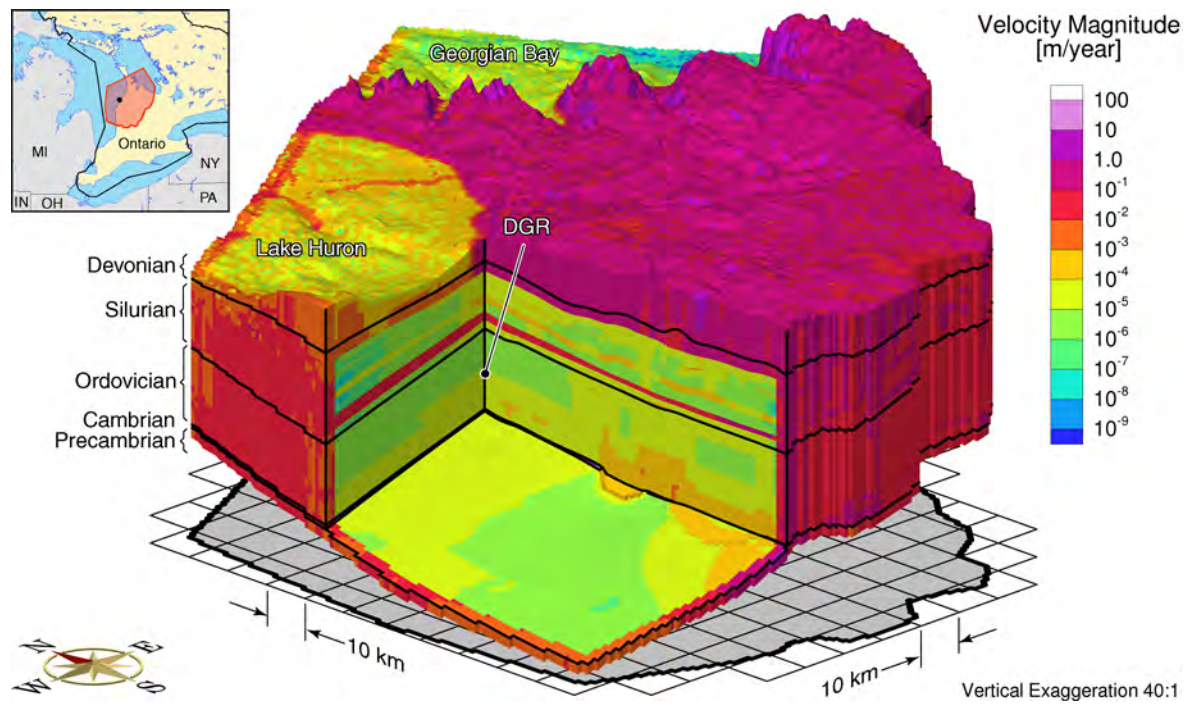


Figure 36: Velocity magnitude for base case parameters with high permeability zone along domain boundaries (Scenario 16).

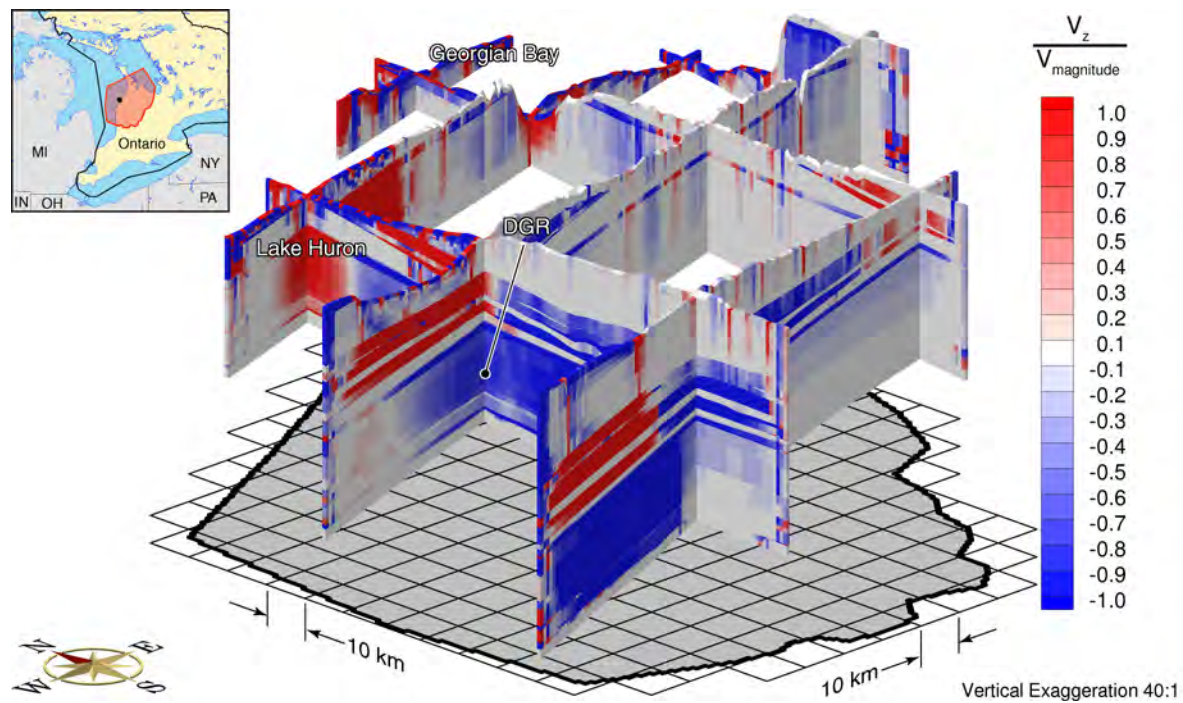


Figure 37: Fence diagram of ratio of vertical velocity to velocity magnitude for base case parameters with high permeability zone along domain boundaries (Scenario 16).

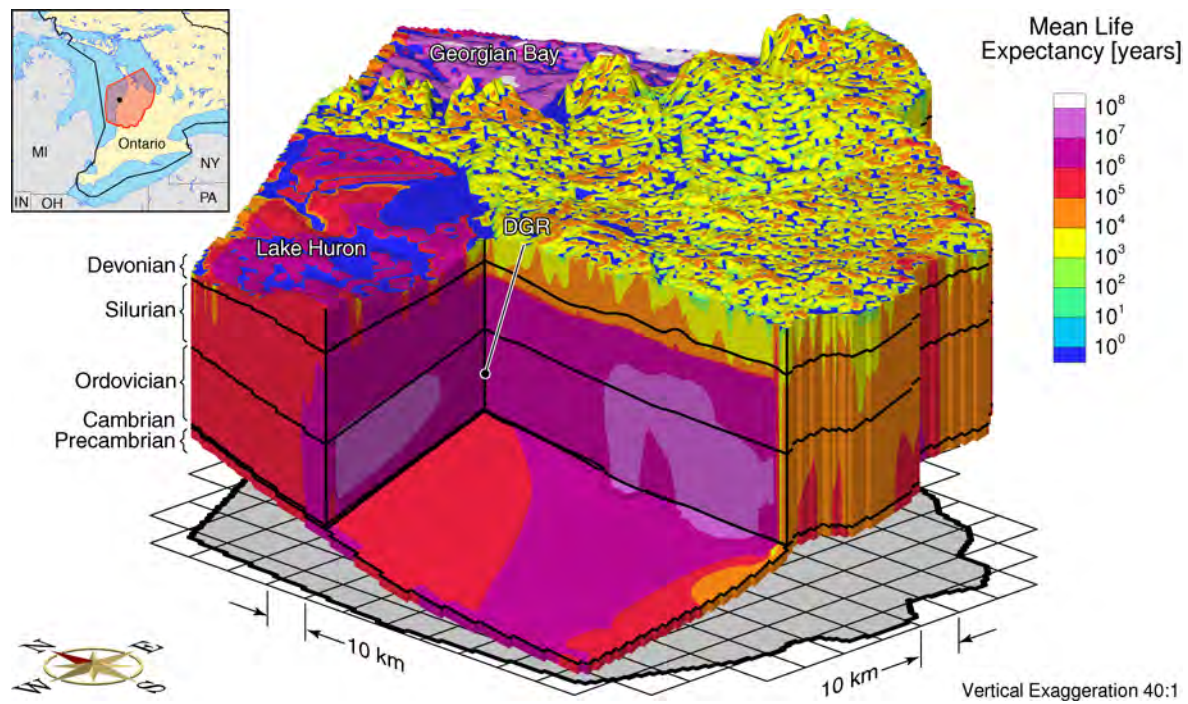


Figure 38: Mean Life Expectancy distribution for base case parameters with high permeability zone along domain boundaries (Scenario 16).

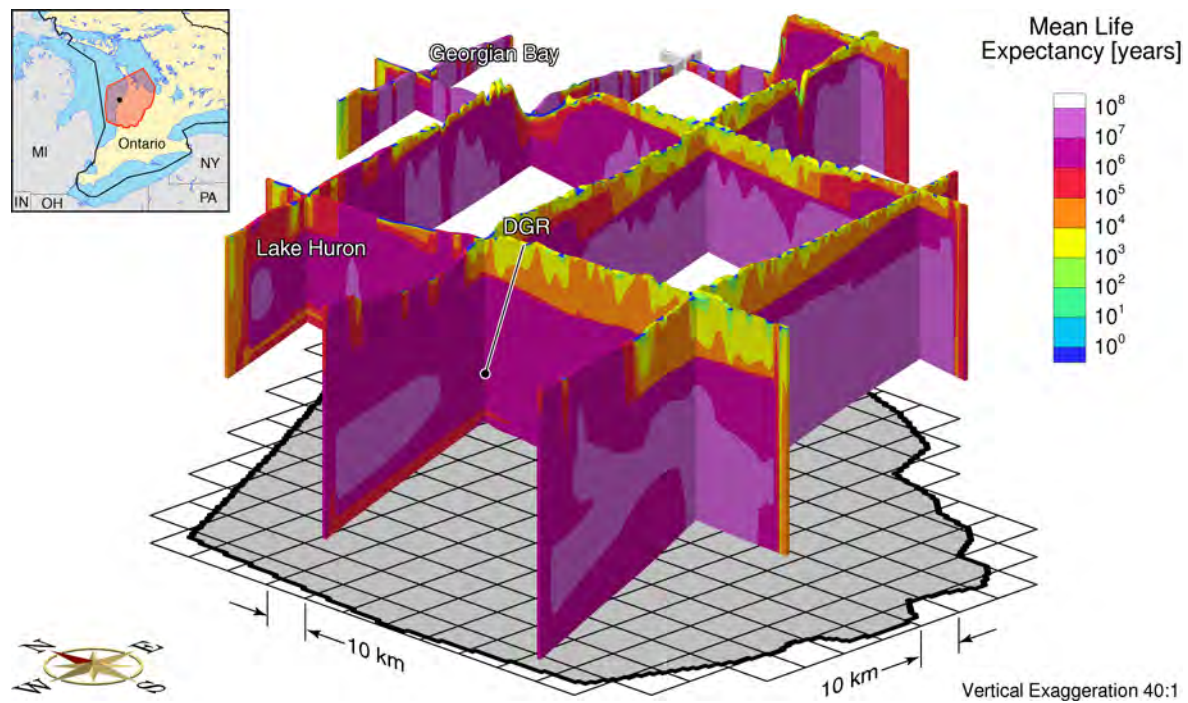


Figure 39: Fence Diagram of Mean Life Expectancy distribution for base case parameters with high permeability zone along domain boundaries (Scenario 16).

5.3.7 Analyses of the Cambrian

The analyses of the preceding sections support the finding that the pathway that a solute would follow from the location of the proposed DGR to the accessible biosphere is sensitive to the conceptualization of the Cambrian and the parameters used for its characterization. The measured pressure data for the composite DGR-1 and DGR-2 borehole and TDS concentration distribution for the units intersected by the borehole yields an estimate of the environmental head for the Cambrian that is greater than the environmental head at the water table (refer to Figure 7). The Cambrian pressures are also considerably greater than those of the Ordovician units; the environmental head profile at the DGR-1/DGR-2 borehole indicates that the energy gradient is upward from the Cambrian to the overlying Ordovician units. A hypothesis of this study is that the present state of the regional-scale flow system as characterized by the present boundary conditions, parameters and geological framework model would not generate the observed pressure profile at the DGR-1/DGR-2 borehole. However, a theme of this study is the investigation of the attributes that are important in the assessment of groundwater flow for the present state of the system. The groundwater flow for this state is described by the base-case analysis of Scenario 1; it represents the equilibrium system to which the groundwater would evolve as it transits from the conditions of a prior state to those of the present state. The attribute investigated in this section is the hydraulic conductivity model used for the Cambrian and its impact on the groundwater system described by the present state.

The Cambrian is a relatively thin, permeable unit in which flow could be impacted by the presence of faults at which offset has occurred. With the overlying Shadow Lake Formation and the underlying Precambrian having low permeability, flow in the direction normal to the fault could be restricted. This section investigates flow in the Cambrian using a homogeneous anisotropic hydraulic conductivity model in which the principal directions of the hydraulic conductivity tensor are oriented in the direction of hypothetical parallel faults. The K_1 component for the Cambrian is oriented parallel to the hypothetical faults and has a value of 3×10^{-6} m/s with this being the same as the horizontal hydraulic conductivity used in the base-case analysis. The K_2 component is oriented normal to the faults and was assigned a value of 8×10^{-11} m/s using harmonic averaging of the base-case hydraulic conductivities for the Cambrian and the Precambrian and appropriate distances between faults. The K_3 component of the hydraulic conductivity tensor has a principal direction that is vertical; the base-case value was used. For this study, the orientation of the hypothetical faults was assumed to be uncertain. Four cases with different directions of the principal components of the hydraulic conductivity tensor were considered. Based on angles in a counter clockwise rotation from a west-to-east axis, the directions are: Camb-1 at 90 degrees, Camb-2 at 0 degrees, Camb-3 at 45 degrees and Camb-4 at 135 degrees. The parameters for the other units and the boundary conditions are the same as that of the base-case analysis. The results of the four simulations, presented in Appendix F, are similar to that of the base-case analysis with the exception of the direction of the horizontal gradients in the Cambrian and underlying Precambrian. These can be noted by a comparison of the plots of equivalent freshwater heads. The MLE values at the location of the proposed DGR are: Camb-1 = 7.8 million years, Camb-2 = 22.7 million years, and Camb-3 = 18.4 million years. The MLE for the Camb-4 scenario could not be estimated due to unresolved computational errors that are evident in Figure F.31. As in the base-case, the path for an average water particle from the proposed DGR includes the Cambrian. The orientation of K_1 in a north to south direction (Camb-1) has an MLE that is similar to that of the base-case analysis. When the low K_2 value is oriented in a north

to south direction (Camb-2), the MLE increases significantly. The MLE is thus sensitive to the hydraulic conductivity model for the Cambrian. It is likely that the rate of possible dissipation of the elevated pressures in the Cambrian, as may occur with a well that produces water from the unit, will also be sensitive to the hydraulic conductivity model and the nature of the possible discontinuities of the Cambrian.

6. PALEOCLIMATE ANALYSIS

6.1 Long-term Climate Change

Based on the work of Peltier (2002, 2003a, 2008), it is clear that to credibly address the long-term safety of a deep geologic repository, long-term climate change and in particular a glaciation scenario, must be incorporated into performance assessment modelling activities. In addition, by simulating flow system responses to the last Laurentide (North American) glacial episode, insight is gained into the role of significant past stresses (mechanical, thermal and hydrological) on determining the nature of present flow system conditions, and by extension, the likely impact of similar, future boundary condition changes on long-term flow system stability. The last Laurentide glacial episode was characterized by the following:

- occurred over a 120 000 year time period,
- included at least three cycles of glacial advance and retreat, with maximum ice thickness over a typical northern Ontario site reaching nearly 3 km,
- included extensive periods of transient, peri-glacial conditions during which permafrost could impact the subsurface, depending on location, to several hundreds of metres, and
- was accompanied by significant basal meltwater production near the end of the glacial episode.

The effects of long-term climate change (e.g., permafrost) on the groundwater flow system are investigated by modifying the permeability of rock within the permafrost zone, by changing the surface boundary conditions to reflect a glacial scenario, and depending on the loading efficiency (refer to Equation (24)), by the inclusion of a pressure modifying term in the flow equation using the methodology described in Section 3.1.5.

The methodology used by Peltier (2008) to construct probabilistically accurate models of the evolution of the North American ice-sheet complex and its surrounding and sub-glacial permafrost follows a Bayesian approach. Using the deterministic University of Toronto Glacial Systems Model (GSM) of continental ice-sheet evolution (Peltier, 2003b), an ensemble of on the order of 1000 solutions are determined by randomly selecting values of the model parameters from within the a-priori specified range of each. The ensemble of solutions is then used to "train" a neural network, a procedure that results in the equivalent of a million or more individual emulations of solutions for the GSM. The final step in the iterative procedure is to use a Markov Chain Monte Carlo method to place error bars on the parameters of the GSM which lead to successful fits to the observational constraints for the model. The result is the generation of an ensemble of successful models that may differ from one another because of "trade-offs" that are allowed between various parameters of the model. Refer to Peltier (2008) for details of the solution methodology. Peltier (2008) focuses on eight of the models of the ensemble that span the apparent range of model characteristics that provide acceptable fits to the totality of the observational constraints. Two of the best models based on aggregate misfit and the use of the highest resolution treatment of permafrost development are nn9921 and nn9930 (Peltier, 2008). Of the two models, nn9930 had less permafrost and this should permit the deepest penetration of basal meltwater. It was chosen for the paleoclimate analysis of this report.

A plot of permafrost depth and ice load, expressed as equivalent metres of water, is shown in Figure 40 for the nn9930 glaciation scenario and the location of the proposed DGR. Two glaciation events were predicted to occur over the regional-scale domain with the first event spanning a period from approximately -62.5 kyr to -56 kyr and the most recent event occurring in the period from approximately -24 kyr to -13 kyr. Permafrost occurs approximately 12 kyr to 14 kyr prior to the onset of glaciation and is fully absent approximately 1 kyr after onset. While Peltier (2008) provides estimates from the nn9930 glaciation scenario of the basal meltwater production and the lake depth at the location of the proposed DGR, these data are not used in the simulations of this study.

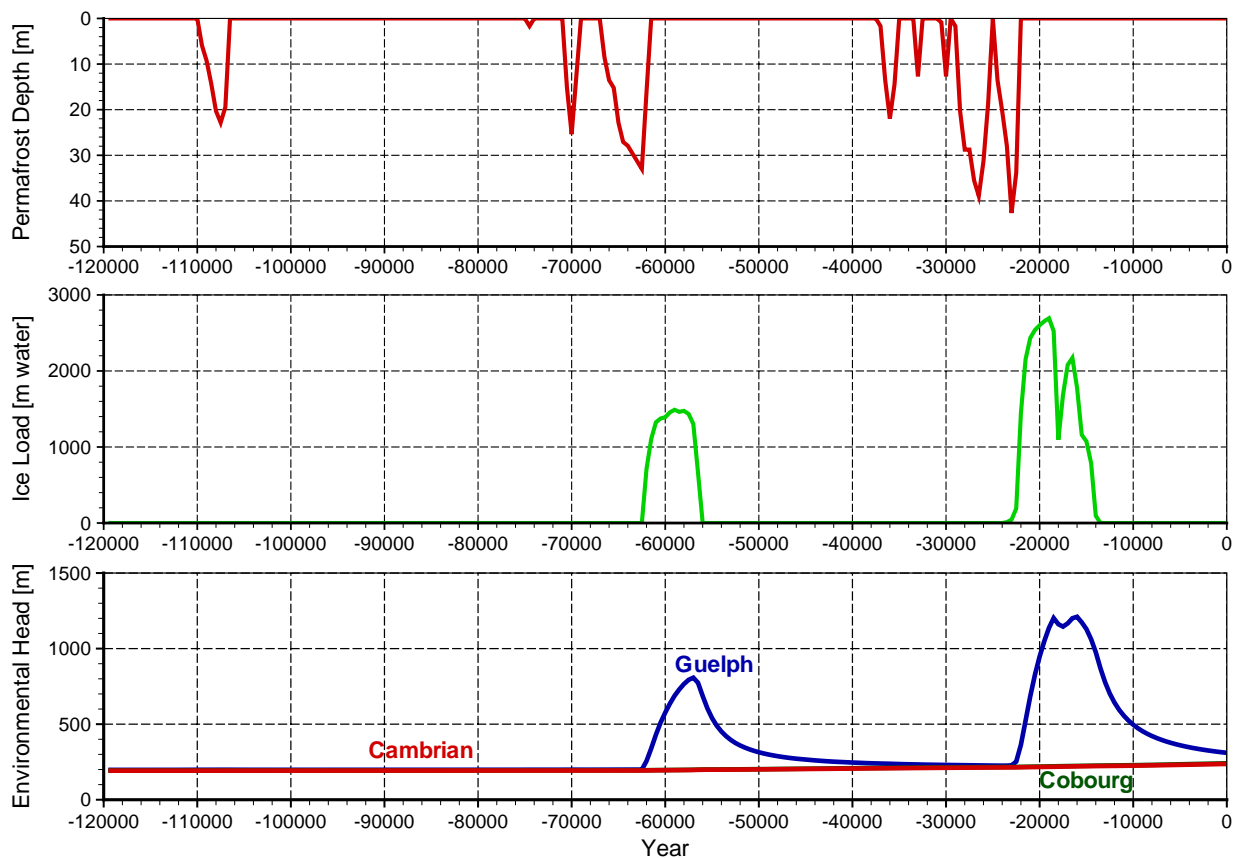


Figure 40: Time series plots of (a) permafrost depth, (b) ice load in equivalent metres of water for climate simulation nn9930, and (c) simulated environmental heads for Scenario 17 in the Guelph Formation of the Niagaran Group, Cobourg and Cambrian for a loading efficiency of zero.

The spatial domain for GSM encompasses the ice covered portion of the North American continent. The 20 GSM grid blocks used to estimate the temporal change of permafrost depth and ice stress at the grid block nodes of this study are superimposed on the regional-scale domain in Figure 41. The GSM grid blocks are approximately 80 km in the west-to-east direction and 60 km in the south-to-north direction; linear interpolation was used for estimation.

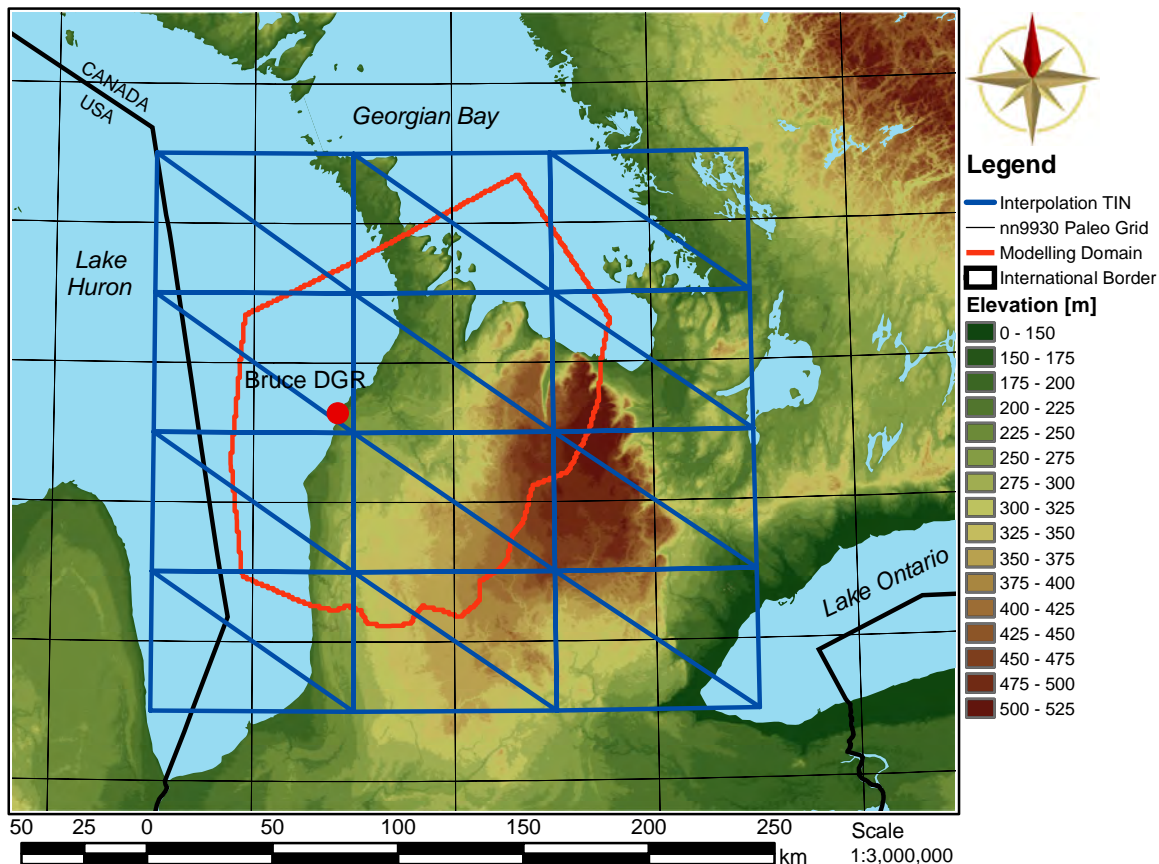


Figure 41: Triangulated Irregular Network (TIN) used to interpolate properties for the regional-scale spatial domain from grid blocks of the Peltier (2008) nn9930 glacial model.

The base-case hydraulic and transport parameters were used for the paleoclimate simulation of Scenario 17. Zero flux Neumann boundary conditions were used for the lateral and bottom surfaces of the model domain. A Dirichlet boundary condition was applied to the upper surface as described in Section 3.1.5. The ice loading was assumed to be applied as an equivalent freshwater head equal to the normal stress imposed by the ice sheet upon the domain. It was also incorporated as a pressure modifying term throughout the domain that, with the assumption of vertical strain and homogeneous loading, approximates the impact of the applied load on the rock. As described in Equation (24), this term includes a loading efficiency ζ ; for Scenarios 17 to 20 a loading efficiency of zero ($\zeta = 0$) was assumed. Scenario 17 also was repeated with a loading efficiency of one. Although FRAC3DVS-OPG does not rigorously account for hydro-mechanical effects, this analysis does demonstrate the behaviour of deep groundwater flow systems subjected to permafrost conditions and glacial loading events and provides a basis to qualitatively understand the magnitude and time rate-of-change of flow in response to ice-sheet advance and retreat.

The initial condition used for the density-dependent simulation is the base-case Scenario 1 TDS concentration distribution and the equivalent freshwater head distribution at a pseudo-equilibrium time of 10^6 years. This implies that the boundary conditions at the onset of the last glacial episode are the same as those observed today. This state precludes both an over-pressurization

of the Cambrian and the under-pressurization of the Ordovician units. It also assumes the rocks of the regional-scale domain are water saturated. The time step length for a paleoclimate simulation is 500 years.

Scenarios 18, 19 and 20 investigate the impact of glaciation for large changes in the hydraulic conductivity distribution for the Ordovician units. The properties for the three scenarios are given in Table A.2, Table A.3 and Table A.4, respectively, of Appendix A. For Scenario 18, the Ordovician units were assumed to be homogeneous with a horizontal conductivity of 1.0×10^{-11} m/s and a horizontal to vertical anisotropy ratio of 10:1. Scenario 19 and Scenario 20 assumed homogeneous values of 1.0×10^{-13} m/s and 1.0×10^{-15} m/s, respectively, for the Ordovician units. The boundary conditions are the same as that used for Scenario 17. A loading efficiency of zero was assumed for the three cases.

Basal meltwater and pro-glacial lakes could result in the penetration of oxygenated recharge waters to depth during and following a glaciation event. To analyze this situation, a unit load of concentration was applied at the surface nodes of the regional-scale numerical model. Recharge occurring during the 120 000 year simulation is thereby tagged with a tracer of unit concentration. Mean life expectancy could not be used since it is only applicable to steady-state simulations. Plotting an iso-surface representing 5% recharge water (a concentration of 0.05) can provide an indication of the depth to which recharge waters can migrate. Alternatively, plots of the tracer concentration distribution in the regional-scale domain can be used to reveal the impact of glaciation.

The pressure data for the composite DGR-1 and DGR-2 borehole indicate that the Ordovician units are significantly under-pressured with respect to the ground surface. Vinard (1998) and Vinard et al. (1993) report that a 900 m marl-shale aquitard at the Wellenberg site in Switzerland is under-pressured. They hypothesize that the under-pressures could be related to stress relief due to deglaciation, extensive erosion or tectonic-thrusting scenarios that results in the dilation of the rock. They also state that the under-pressurization could result from the presence of a gas-phase in the aquitard. They investigated their preferred scenario of the deglaciation process using a geomechanical model. However, they did not investigate the pore pressure distribution during the stress loading stage of glaciation. The argument that the pressure profile in the Ordovician units is based on a glaciation scenario must be based on the evolution of pressures during both the rock compression stage of glaciation and the rock dilation stage of deglaciation. For the paleoclimate Scenario nn9930 of Peltier (2008), this is critical since the glaciation time is shorter than the deglaciation stage. Section 6.3 investigates the evolution of an initial high equivalent freshwater head distribution that was imposed on the regional-scale domain. The objective of the analysis is the assessment of the rate at which the high pressures are dissipated.

6.2 Simulation Results

The paleoclimate scenario nn9930 for the location of the proposed DGR is shown in Figure 40. The environmental heads at -90 kyr, -60 kyr, -30 kyr and the present for Scenario 17 are shown in Figure 42, Figure 43, Figure 44 and Figure 45, respectively. The total dissolved solids concentration distribution at the present for the paleoclimate simulation with the base case parameters is shown in Figure G.22. A block-cut diagram of the velocity magnitude at the present is shown in Figure 47, while a fence diagram of the ratio of vertical velocity to velocity magnitude

at the present is given in Figure 48. The tracer concentration distribution in the regional-scale domain at the present is shown in Figure 49. Other results for the Scenario 17 simulation are given in Figure G.1 to Figure G.13 of Appendix G.

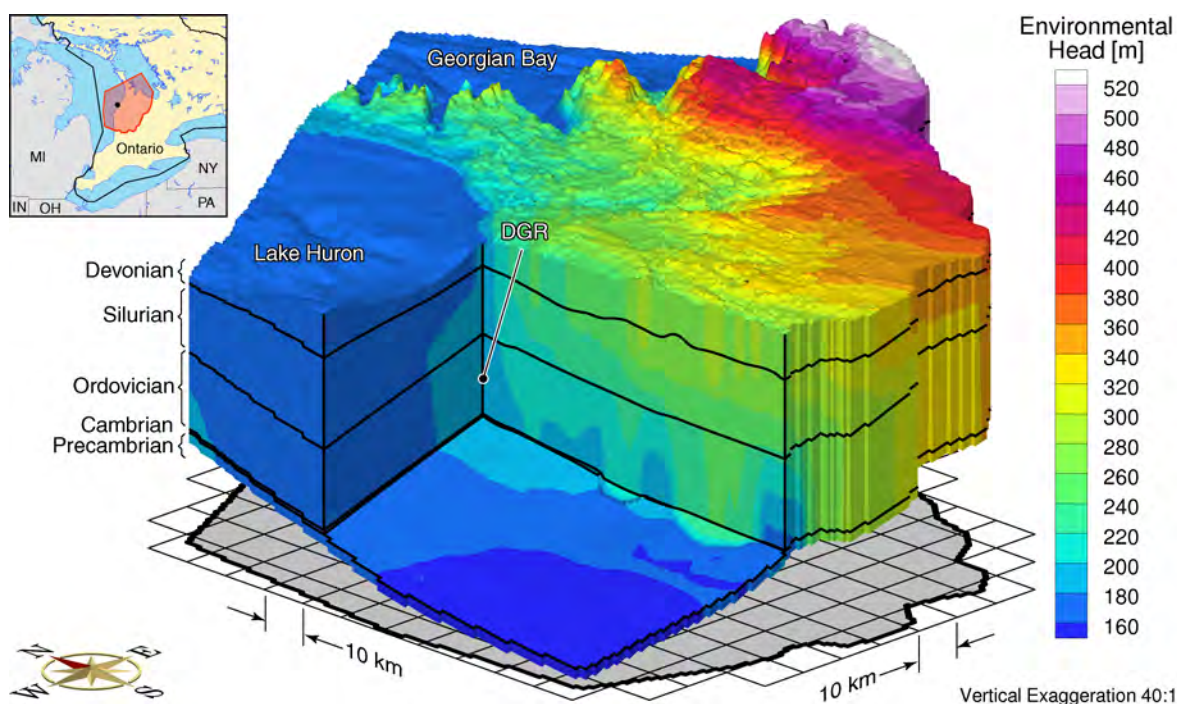


Figure 42: Environmental heads at 90,000a bp for Scenario 17 and a loading efficiency of zero.

The loading efficiency for Scenario 17 (base-case parameters) is zero. As a result, there is no impact on the pore pressure at depth from the compression of the rock under ice loading. The ice load is assumed to impact only the surface pore pressure. This increased surface pressure propagates into the domain at a rate depending on the temporal loading, permafrost depth and properties, fluid compressibility, rock compressibility and the hydraulic conductivity distribution. The resulting energy gradient into the domain is maximum for a loading efficiency of zero ($\zeta = 0$). A higher loading efficiency will result in increased pore pressures throughout the rock column as the rock is compressed, the impact is to reduce the vertically downward energy gradient. On de-glaciation, the pore pressure at the domain surface is reduced and the pore pressure throughout the rock column is correspondingly relieved by the ice stress term in Equation (24). A consequence of a maximum pore pressure energy gradient is maximum penetration of basal meltwater into the domain. The tracer concentration distribution at the end of the 120 kyr simulation is shown in Figure 49. At the location of the DGR, glacial meltwater has not penetrated through the low permeability units of the Salina. The TDS concentration distribution also shows the importance of the Salina: throughout Scenario 17, meteoric and basal meltwater infiltration to the Devonian results in low TDS concentrations; higher concentrations near 300 g/L remain in the units below the Salina.

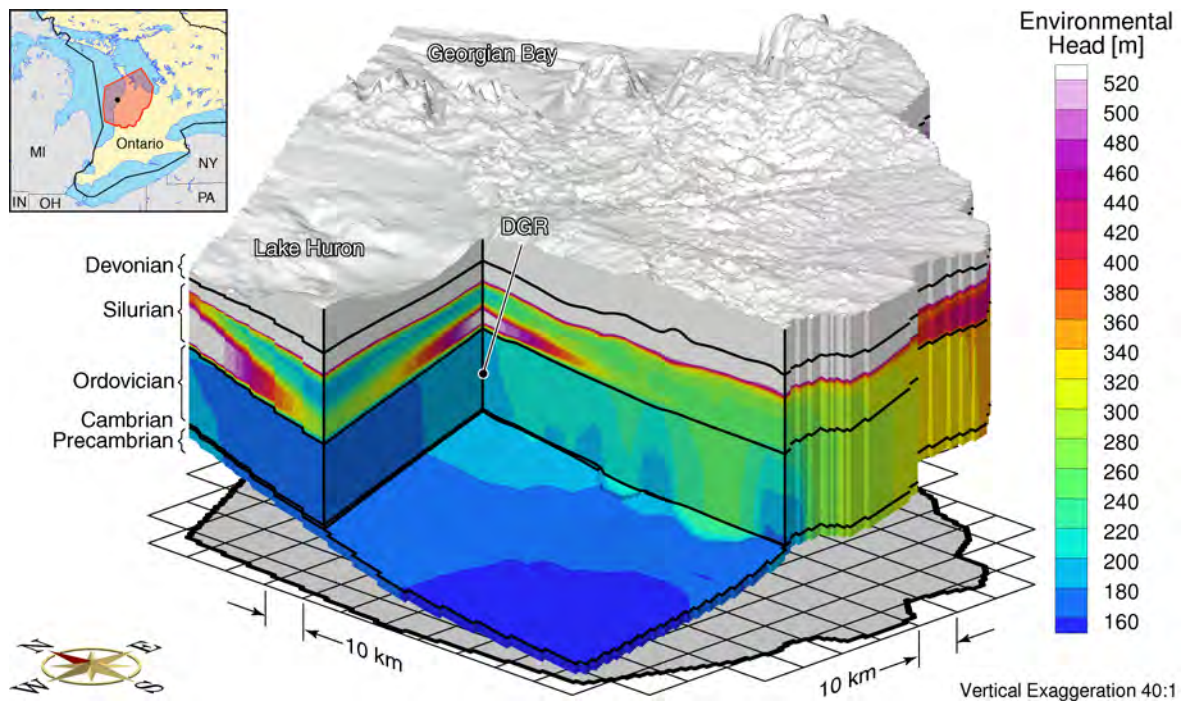


Figure 43: Environmental heads at 60,000a bp for Scenario 17 and a loading efficiency of zero.

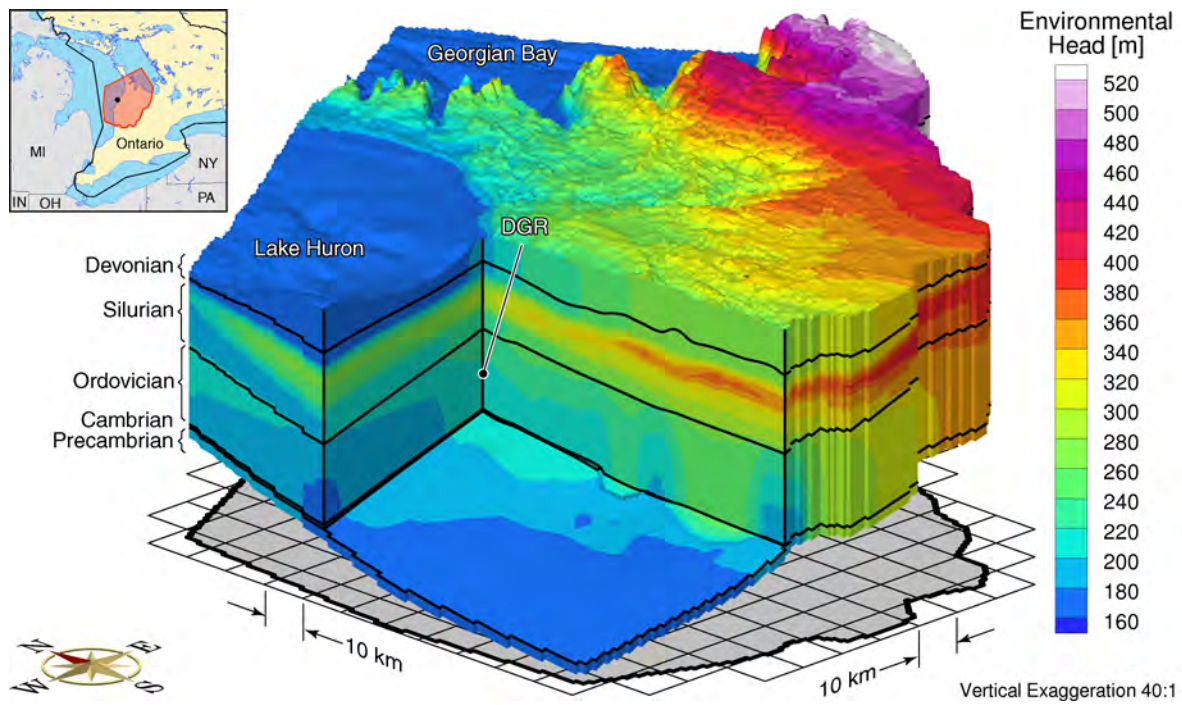


Figure 44: Environmental heads at 30,000a bp for Scenario 17 and a loading efficiency of zero.

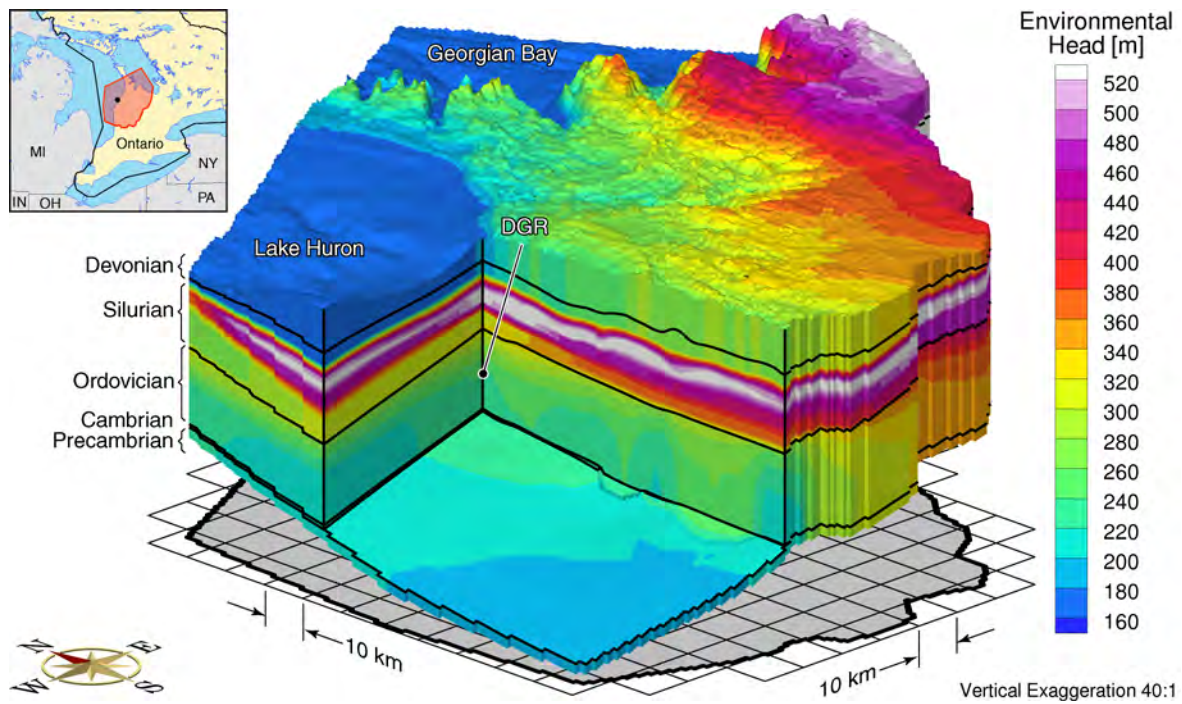


Figure 45: Environmental heads at the present for Scenario 17 and a loading efficiency of zero.

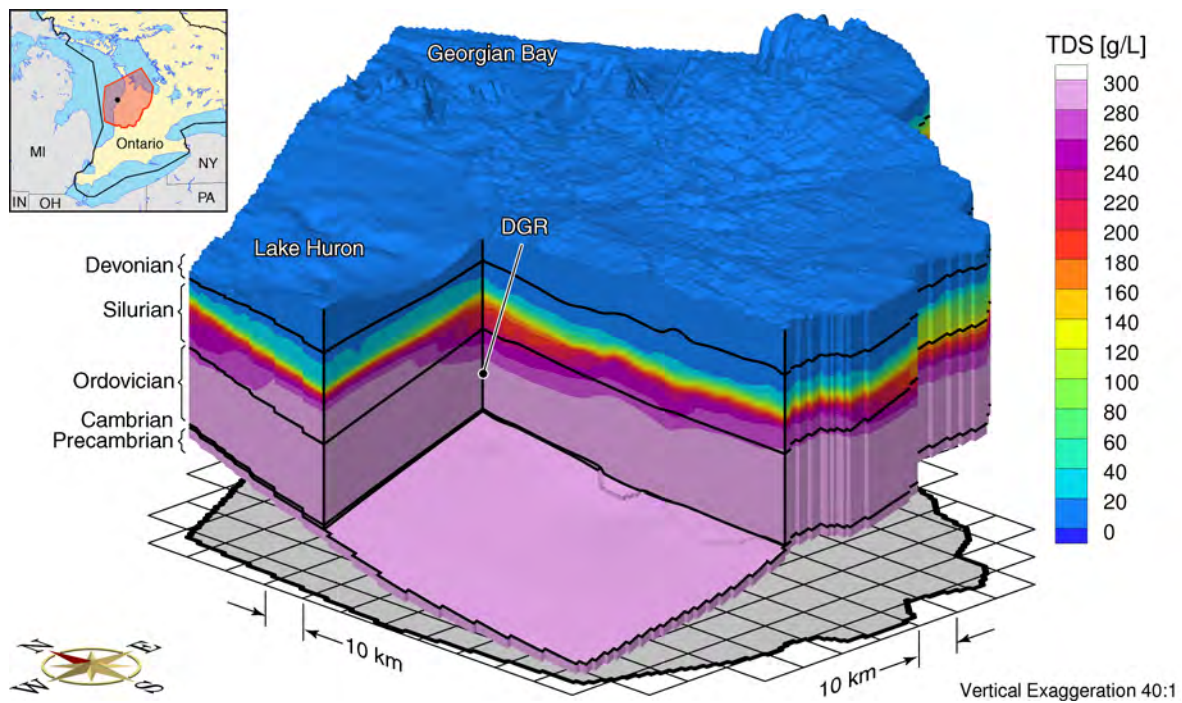


Figure 46: Total dissolved solids distribution at the present for the paleoclimate simulation with the base case parameters and a loading efficiency of zero.

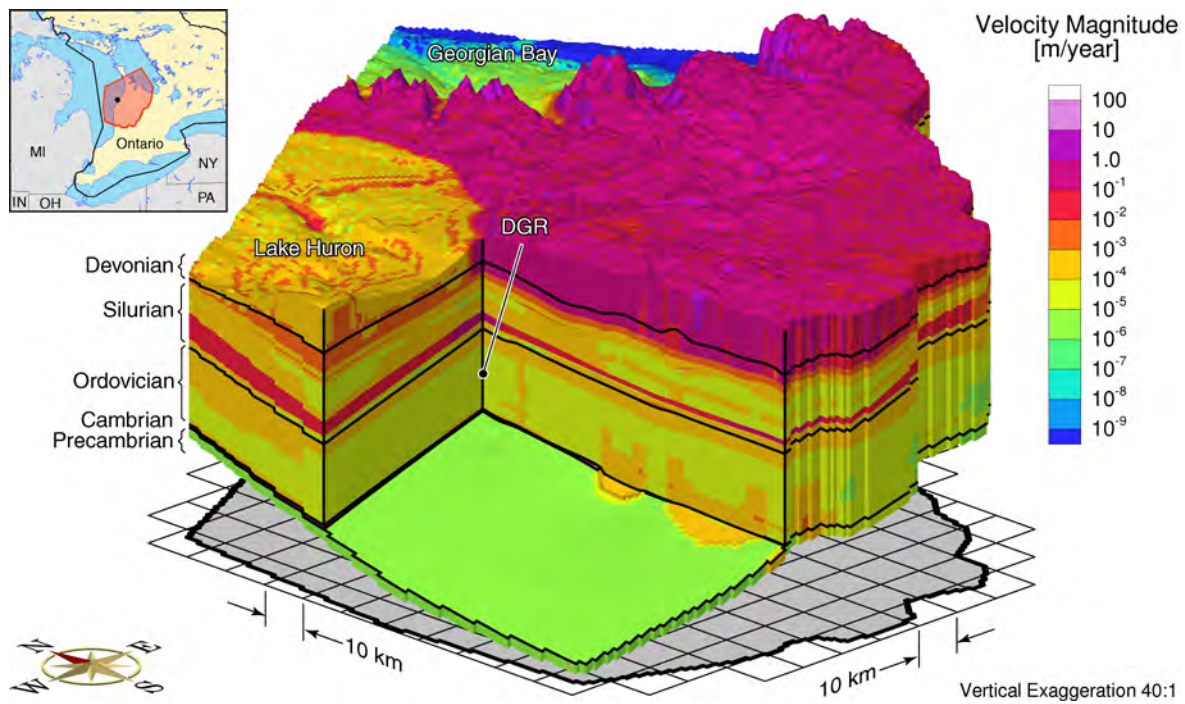


Figure 47: Block-cut diagram showing pore water velocity magnitude at the present for the base case parameters and a loading efficiency of zero.

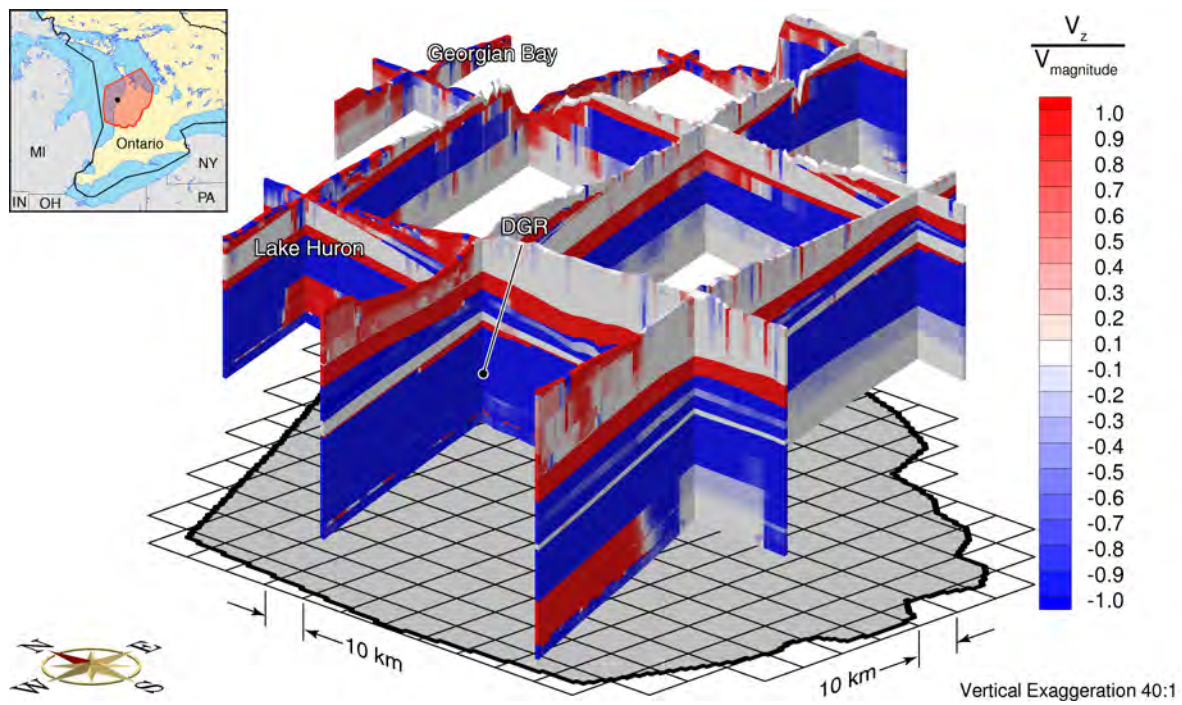


Figure 48: Fence diagram showing the ratio of the vertical pore water velocity to the velocity magnitude at the present for the base case parameters and a loading efficiency of zero.

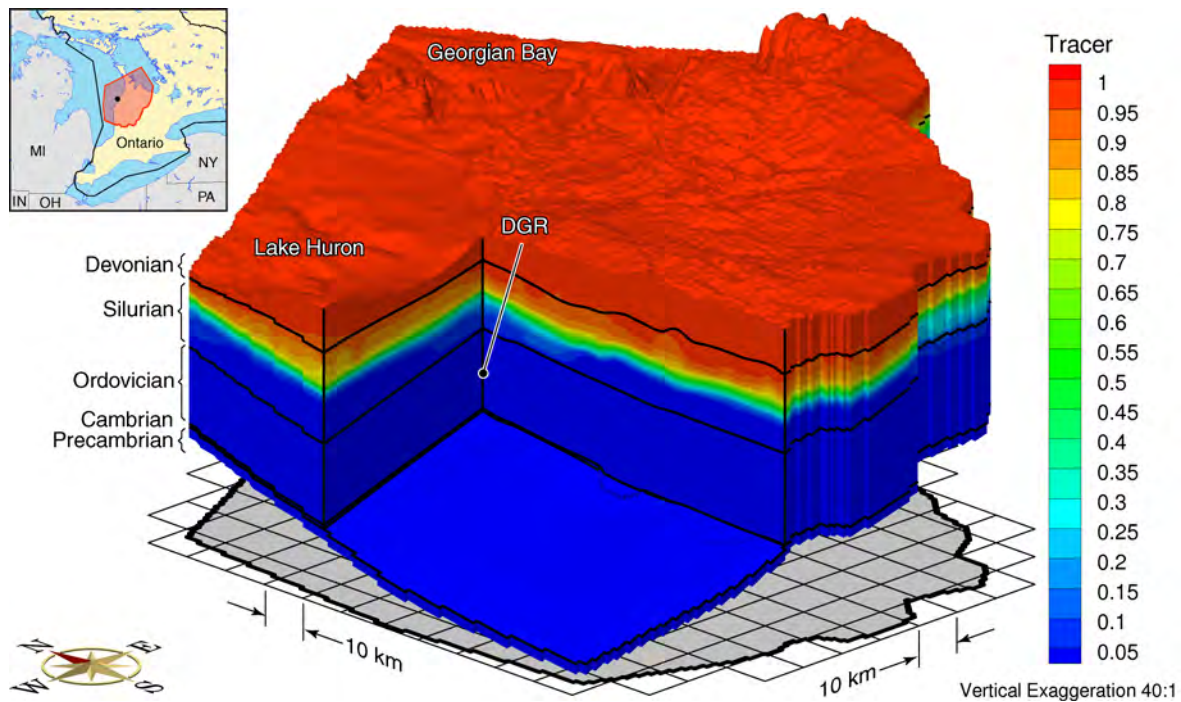


Figure 49: Block-cut diagram showing the depth of penetration of a tracer at the present for the base case parameters and a loading efficiency of zero.

A review of the temporal and spatial distributions of the environmental head reveals that the higher permeability Niagaran is an important pathway for the propagation of the glaciation surface pressures to depth. With a loading efficiency of zero, higher pressures in the unit occur where it outcrops; lower pressures are at depth. The high pressures are transmitted down dip through the unit to the areas overlain by the confining Salina units. These higher pressures in the Niagaran are evident in Figure 43 as the white to red environmental heads in the Silurian at the location of the proposed DGR. The result is that the low permeability Salina receives a high pressure pulse from the Devonian units above and from the underlying Niagaran. These higher pressures propagate vertically into the Salina resulting in it becoming over-pressured with respect to the surface elevation. The residual signature of these higher pressures is evident in Figure 45 as the white to red environmental heads at the midpoint of the Silurian. The temporal change in the environmental heads in the Niagaran Formation, Cobourg Formation and Cambrian Formation at the location of the proposed DGR are shown in Figure 40. It is evident in both this plot and those of Figure 42 to Figure 45 that for a loading efficiency of zero, the low permeability of the Lower Silurian and Ordovician units, the specific storage coefficients for the units and the duration of the glacial loading, that the higher pressures in the Niagaran and Devonian cannot propagate to depth. As shown in Figure 40 there is a large vertically downward gradient between the Niagaran and the lower units. The length of glaciation and de-glaciation for scenario nn9930 is not long enough for the tracer to migrate down dip in the Niagaran to the location of the proposed DGR. Throughout the simulation, the linear velocities in the Ordovician remain below 0.0001 m/year (refer to the velocity magnitude plots in Figure G.5 to Figure G.7 of Appendix G). The areally averaged recharge to the regional-scale domain versus time for Scenario 17 is plotted in Figure 50. The average considers only grid blocks in which recharge occurs. The rate of recharge reflects the presence of permafrost for approximately the first

1000 years of each glaciation event, the shallow hydraulic conductivity distribution and the vertically downward energy gradients that can develop.

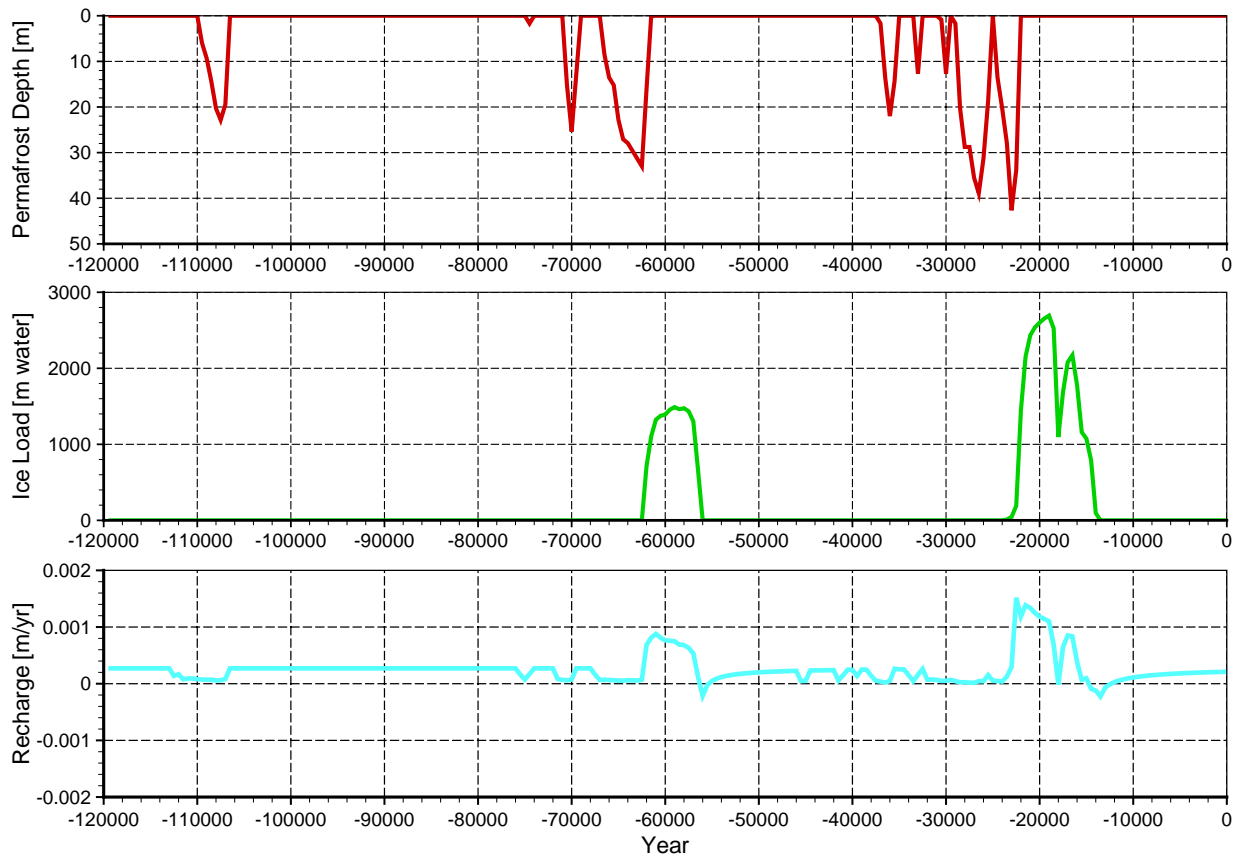


Figure 50: Time series plots of (a) permafrost depth, (b) ice load in equivalent metres of water for climate simulation nn9930, and (c) recharge for a loading efficiency of zero.

The temporal change in the environmental heads in the Niagaran, Cobourg and Cambrian at the location of the proposed DGR is shown in Figure 51 (note that the Niagaran is referred to as the Guelph in the figure) for the Scenario 17 parameters, initial conditions and boundary conditions and a loading efficiency of one ($\zeta = 1$) in Equation (24). As shown in the figure, the impact of the stress term with a loading efficiency of one is an increase in pore pressure with rock compression during glaciation and a decrease in the rock pore pressure as the rock dilates during de-glaciation. The vertical energy gradient is significantly reduced compared to that of the case with a loading efficiency of zero (refer to Figure 40). At the peak loading of the second glaciation event at -19.5 kyr, the environmental heads in the Cambrian and Niagaran (Guelph in the figure) were estimated to be 2905 m and 2837 m respectively. The small upward gradient with $\zeta = 1$ compares to a large downward gradient being predicted at the same time for the case with $\zeta = 0$. Also of note in the figure is the fact that Equation (24) with ($\zeta = 1$) results in no latency in the dissipation of the elevated pressures after complete de-glaciation. The results of Figure 40 and Figure 51 provide the bounding cases for the formulation of Equation (24).

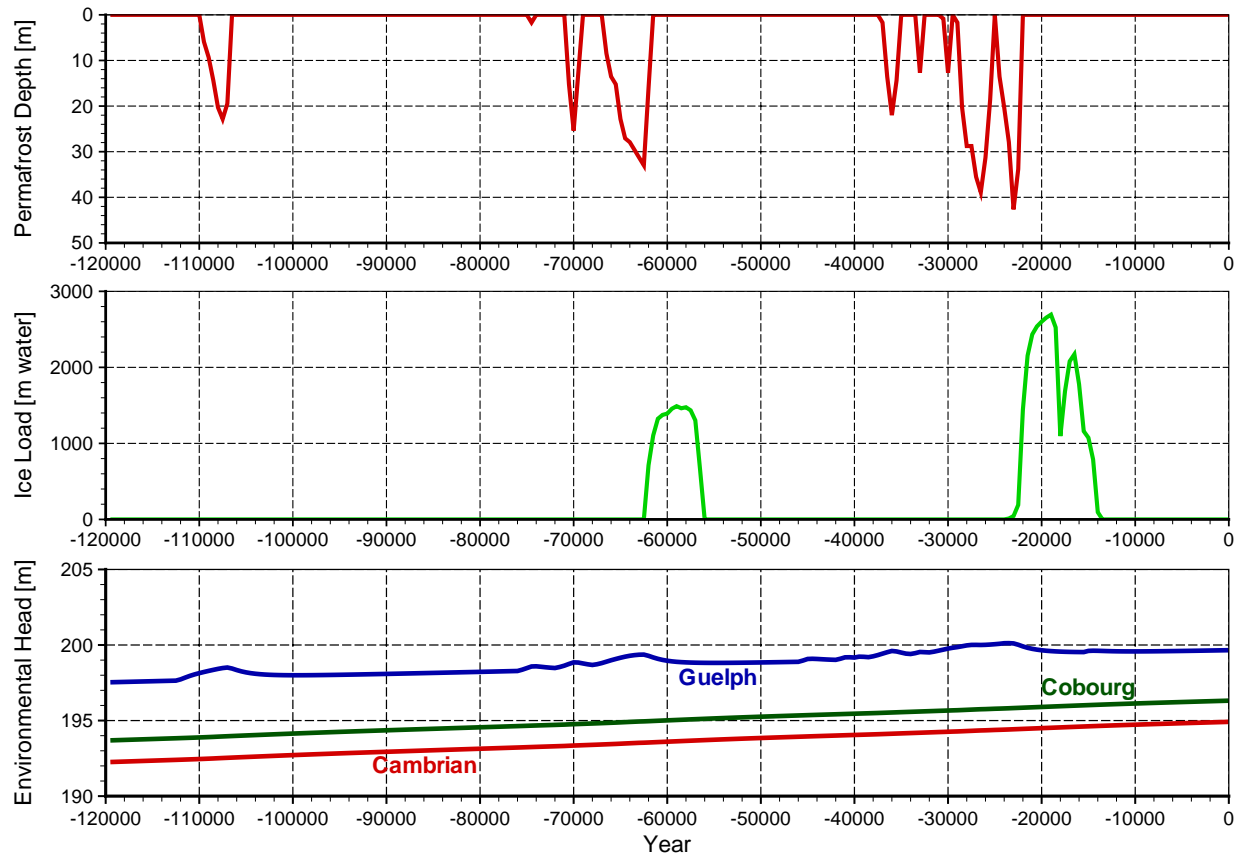


Figure 51: Time series plots of (a) permafrost depth, (b) ice load in equivalent metres of water for climate simulation nn9930, and (c) simulated environmental heads for Scenario 17 in the Guelph Formation of the Niagaran Group, Cobourg and Cambrian for a loading efficiency of one.

The results for the paleoclimate simulations of Scenarios 18, 19 and 20 are given in Figure G.14 to Figure G.43 of Appendix G. The results show that the paleoclimate simulations are relatively insensitive to the reduction of the hydraulic conductivity for the Ordovician units.

6.3 Dissipation of Pressures from Glacial Loading

The time for the dissipation of an initial equivalent freshwater head of 600 m imposed throughout the regional-scale domain was determined for three realizations (Scenarios 13 to 15) of the Ordovician hydraulic conductivity as given in Table A.2, Table A.3 and Table A.4 in Appendix A. The analyses of this section did not explicitly include glacial loading, rather, they investigate only the impact of the loading in creating a hypothetical pressure throughout the regional-scale domain. The boundary conditions and solution methodology are the same as that of the base-case Scenario 1. The initial TDS concentration distribution is that of Scenario 1 at a pseudo-equilibrium time of 1 million years. The results for the transient analyses are given in Figure H.1 to Figure H.18 of Appendix H. The plots of environmental heads are given at

10 000 years and 20 000 years after the imposition of the initial equivalent freshwater head, all other figures are at 20 000 years.

For Scenario 13 (parameters from Table A.2), the Ordovician units were assumed to be homogeneous with a horizontal conductivity of 1.0×10^{-11} m/s and a horizontal to vertical anisotropy ratio of 10:1. Figure H.1 and Figure H.3 show that the Ordovician units remain significantly over-pressured for the duration of the analysis. The heads in the Salina also remain elevated while those of the more permeable Niagaran Group have been significantly reduced. The heads in the shallow groundwater system quickly came into equilibrium with the surface topography. The vertically downward gradient in the lower Ordovician is a result of the conversion of the imposed freshwater head to an environmental head. The importance of the results is that despite a large vertically upward gradient from the Ordovician to the surface and a vertically downward gradient to the Cambrian (refer to Figure H.6), the Ordovician remains over-pressured after 20 000 years. The low permeability of the units retards the dissipation of the pressure. The duration of the analysis should be compared to the duration of the glaciation periods in the paleoclimate scenario nn9930. For the scenario, the time in the last glaciation period to reach glacial maximum from the time of the first onset of ice loading takes approximately 3500 years after which deglaciation begins to occur. The rock would be expected to be in compression during glaciation and begin to dilate as the ice load is reduced. It can be concluded that based on the Scenario 13 analysis, the relatively short period of glaciation combined with the low permeability of the Ordovician units would result in the pressures in the units still being significantly elevated at the onset of deglaciation; that is, the time period to glacial maximum is too short for significant pressure dissipation to occur given the low permeability of the Ordovician units. The dilation of the rock would then return the elevated pressures to their normal level; it would not result in the development of the low Ordovician pressures as evidenced in borehole DGR-2. Thus, for deglaciation to be the cause of the under-pressures as postulated by Vinard et al. (1993), it must be preceded by a glaciation loading period of sufficient length during which elevated pressures are dissipated. Subject to unit permeabilities, dilation of the rock during deglaciation could then result in development of still lower pore pressures. For the DGR site, the pressure dissipation only can reasonably occur in an upward direction; compression of the relatively thin Cambrian and the Precambrian rock and the resulting pore fluid elevation in these units would also occur during ice loading. The low permeability of the Lower Silurian and Salina units will significantly retard the upward dissipation. It also should be noted that the vertical gradients of this analysis are greater than those that would be calculated with a geomechanical model. Also of note is that throughout the analysis the pore velocities in the Ordovician units are low and indicate that solute migration would be dominated by diffusion (refer to Figure H.5).

The results for Scenarios 14 and 15 reflect the impact of a reduction of the hydraulic conductivity for the Ordovician to assumed homogeneous values of 1×10^{-13} m/s and 1.0×10^{-15} m/s respectively. While pressure dissipation has occurred in the shallow groundwater zone and the Niagaran Group, the pressure remains unchanged in the Ordovician units throughout the 20 000 years of the analysis. The results reinforce the conclusion of the preceding paragraph that sufficient depressurization could not occur during glaciation for load relief during deglaciation to be the cause of the observed low Ordovician pressures at the DGR-2 borehole. The results support the argument that the more plausible explanation for the low pressures is either load relief from erosion or the presence of a gas phase in the Ordovician.

7. SITE-SCALE GROUNDWATER FLOW MODEL

The objective of the site-scale hydrogeologic modelling of the proposed DGR is to provide a refined spatial discretization that will allow the simulation of features, events and processes that cannot be appropriately investigated with the regional-scale model. The use of a refined mesh over the entire regional-scale domain would be computationally intensive, particularly for the solution of density-dependent flow. Mehl and Hill (2002) indicate that such discretizations can lead to intractable solutions. The need for a locally refined mesh generally is due to three practical requirements (Mehl and Hill, 2002):

- To capture accurately steep hydraulic gradients near pumping, injecting wells and the features of facilities such as the DGR
- To capture accurately sharp fronts in contaminant transport, and
- To represent local-scale hydrogeologic features (e.g., fractures, stratigraphy, pinnacle reefs) as accurately as practicable.

There are three general approaches used in local mesh refinement: variably spaced meshes, model-in-model and direct embedment. Variably spaced meshes, as commonly used with discretizations of the finite difference method, can lead to grid blocks with large aspect ratios and refinement in areas where such detail is not needed. A model-in-model approach used by Ward et al. (1987) (also referred to as a telescopic mesh refinement) entailed the use of three successively smaller-scale models: regional, local, and site models. In this case the approach for inter-scale information transfer has involved linear interpolation from the coarser scale to the finer scale with this being associated with several disadvantages. Firstly, coupling between two model meshes occurs only in one direction: from the large mesh to the small mesh. Because there is no feedback from the small mesh to the large mesh, non-linear analyses based on iterative solution techniques are not possible, and significant discrepancies can occur in fluxes or state variables (whichever are not used to couple the meshes) at the model interface. Secondly, the interpolation methods may not conserve mass with the result that short-circuiting, where there is fluid influx and efflux at adjacent boundary grid blocks, can occur at the boundaries of the smaller-scale system. The local mesh refinement or spatial sub-discretization approach developed for FRAC3DVS-OPG is based on the direct embedment approach (Guvanasen, 2007). The spatial sub-discretization (sub-gridding) methodology that has been developed allows analysts to refine or coarsen an existing three-dimensional FRAC3DVS-OPG finite-element mesh in an efficient manner. Using a non-adaptive sub-discretization approach all the information for the sub-discretized elements is generated externally. The method is applicable to solid and plate elements only. An existing line element can be simply subdivided into several line elements by introducing additional nodes between the existing two nodes. Each new line element is treated exactly the same as the pre-sub-discretized element in FRAC3DVS-OPG; the solid and plate elements are treated differently at the transition zones between the densely and sparsely discretized areas (Guvanasen, 2007).

In this study, both the direct embedment and the model-in-model approaches are developed for site-scale analyses. The site-scale conceptual model is described in Section 7.1. The embedment approach is verified by comparison with the base-case Scenario 1 results in Section 7.2.1. The results of the two approaches are compared and evaluated in Section 7.2.2.

Finally, the site-scale model is used to investigate the measured pressure profile in the composite DGR-1 and DGR-2 borehole in Section 7.3.1.

7.1 Site-Scale Conceptual Model

The site-scale spatial domain relative to that of the regional-scale domain is depicted in Figure 52 (red zone in the figure). The domain has a spatial extent of 19.078 km in the west-to-east direction and 18.918 km in the south-to-north direction centered on borehole DGR-2. The site-scale domain was discretized by using 6 columns (west-to-east sub-gridding) for each regional-scale column and 8 rows (south-to-north sub-gridding) for each regional-scale row. The resulting site-scale domain has 150 columns and 168 rows with each grid block being 127 m in the west-to-east direction and 112.6 m in the south-to-north direction. The areal discretization is shown in Figure 53. Sub-gridding was also used to refine the discretization of the Cobourg Formation with three layers being used in the site-scale model to represent the single regional-scale layer. As shown in Figure 54, the overlying Collingwood/Blue Mountain and Queenston Formations were each subdivided into two layers. Also evident in Figure 54 are the transition elements between the larger regional-scale elements and the smaller elements of the site-scale mesh.

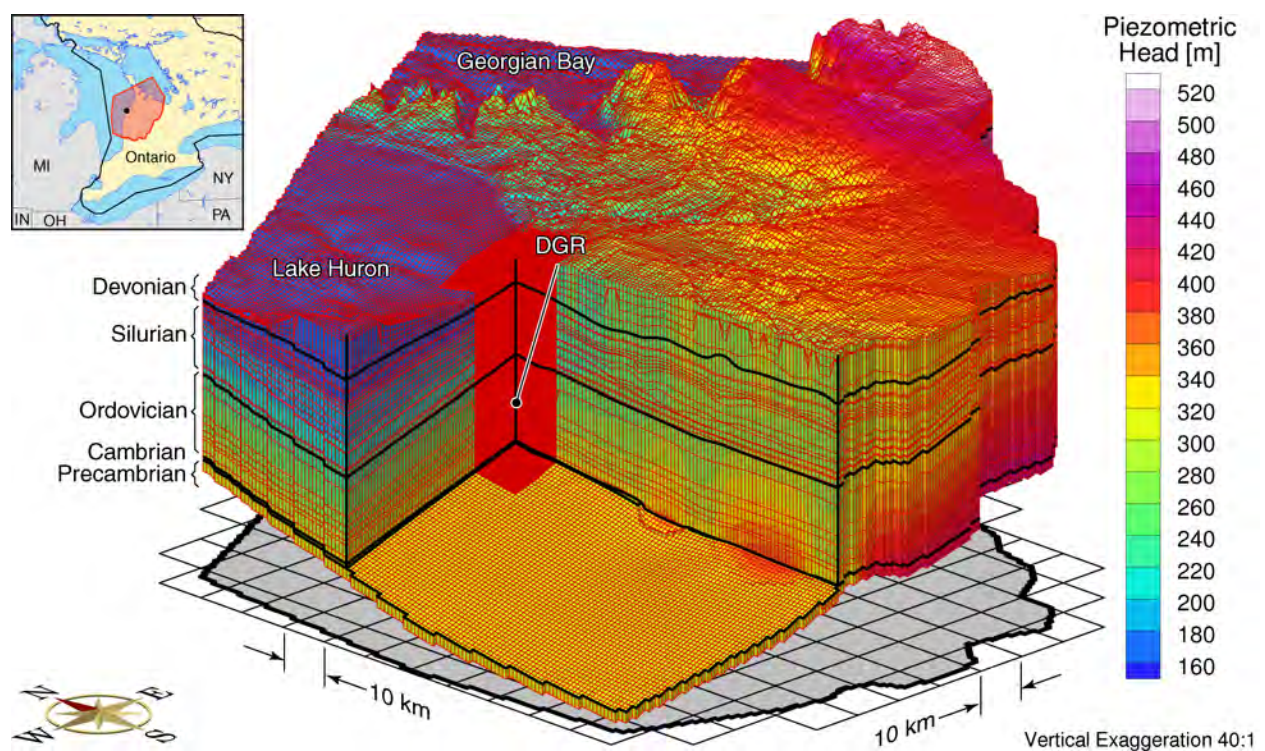


Figure 52: Regional-scale discretization showing location of site-scale spatial domain.

The hydraulic and transport properties used for the base-case site-scale analyses and the verification of the embedment approach are the same as those of the base-case regional-scale

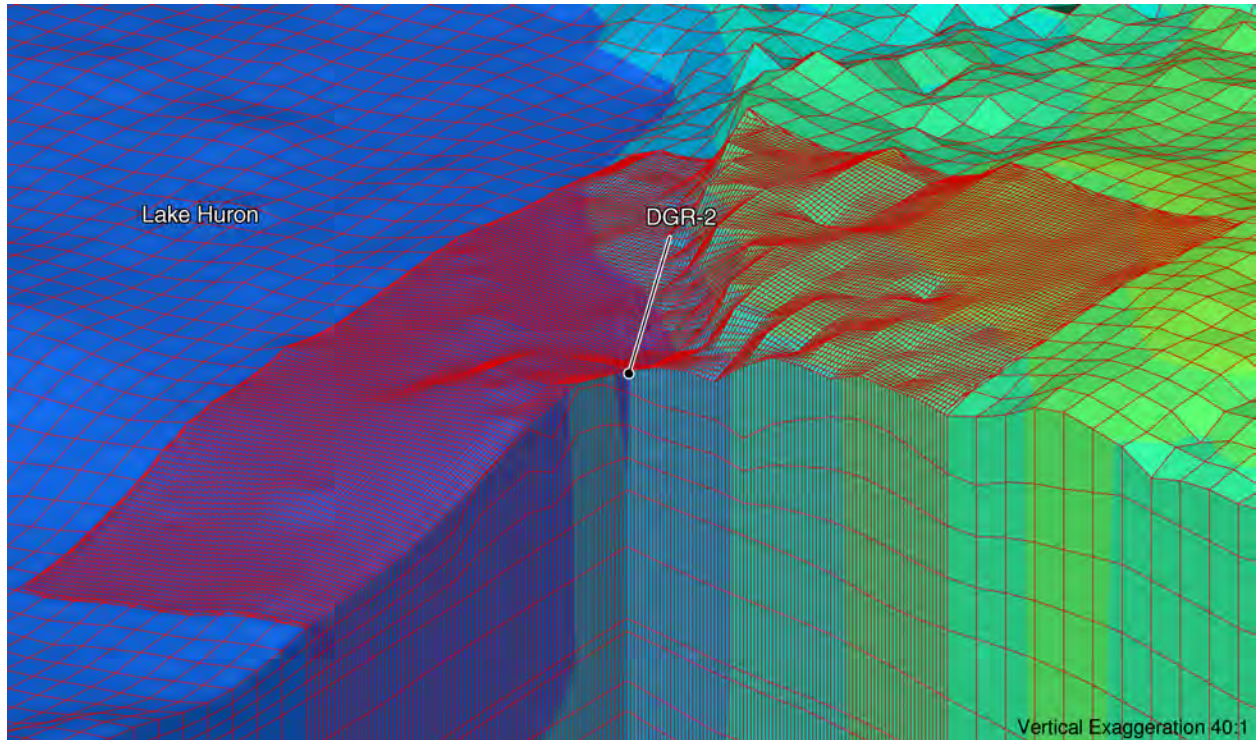


Figure 53: Regional-scale discretization showing site-scale discretized spatial domain.

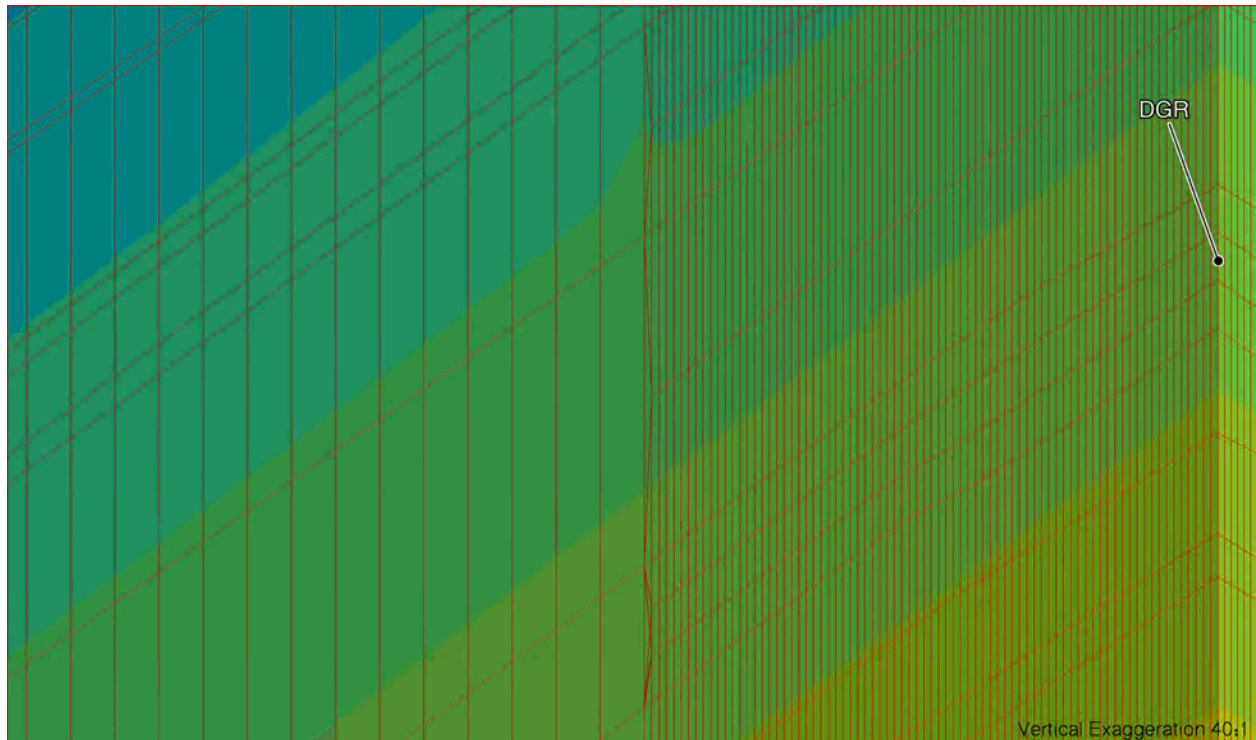


Figure 54: Regional-scale discretization showing vertical details of site-scale discretized spatial domain.

analysis of Scenario 1. As a caveat to the embedment approach in its current formulation in FRAC3DVS-OPG is that the selected longitudinal dispersivities used in the solute transport equation (refer to Equation (17) and Equation (18)) must satisfy the grid or cell Peclet and Courant constraints imposed by the coarser regional-scale elements or grid blocks. Thus, the embedment approach cannot take advantage of the finer site-scale discretization and use smaller values of the longitudinal dispersivity. As a consequence, the contribution to solute migration of mechanical dispersion may be overestimated. The boundary conditions for the embedment approach are those imposed on the regional-scale domain; the solution methodology is the same as that followed in the regional-scale analyses.

For the model-in-model approach, a four-step analysis is performed with the first step being the development of a solution for density-dependent flow for the regional-scale domain at a selected pseudo-equilibrium or target time. The analyses of the preceding chapters have been based on a pseudo-equilibrium time of 10^6 years. The second step is the linear interpolation of the equivalent freshwater heads and TDS concentration at the lateral boundary nodes of the site-scale domain using the calculated values at the appropriate matching nodes from the coarser regional-scale solution. The linear interpolation, as applied in this study, is not mass conservative; short circuiting at the domain boundaries may occur. The implementation procedure for the surface boundary condition for the site-scale domain is the same as that used for the regional-scale analyses. The third step is the development of a steady-state solution for the equivalent freshwater head distribution of density-independent flow in the site-scale domain for the applied boundary conditions of step two. In the fourth and final step, the steady-state solution of the equivalent freshwater heads of step three and an assigned TDS concentration distribution are used as an initial condition for the determination of a site-scale density-dependent solution of the flow-transport system at a selected pseudo-equilibrium time. The boundary conditions for the analysis of step four are the interpolated values from step two. For some site-scale analyses, it may be possible to calculate a model-in-model steady-state density-dependent solution for the interpolated boundary conditions directly after step two. In this study, the model-in-model approach uses the same site-scale refined mesh as that used in the embedment approach.

7.2 Development of the Embedment Approach for Site-Scale Modelling

7.2.1 Verification of the Embedment Approach

As shown in Section 7.1, the site-scale grid is included explicitly as a refined discretization in the regional-scale domain. The embedment approach for site-scale modelling was verified by comparing its results at a pseudo-equilibrium time of 10^6 years with those obtained for the regional-scale analysis of Scenario 1. The results for the comparison are shown in Figure I.1 to Figure I.14 of Appendix I. A visual comparison of the results for environmental head, TDS concentration, pore water velocity magnitude, ratio of vertical velocity to velocity magnitude and MLE shows that the embedment approach has been implemented correctly. The finer mesh at the site-scale for the embedment approach does provide more detail than that afforded by the coarser grid of the regional-scale domain. The impact can be observed in a comparison of the pore water velocity magnitude plots of Figure I.7 and Figure I.8 where differences are evident in the block-cut face south of the DGR-2 borehole location. The results for the regional-scale analysis are somewhat smoother than those provided in the latter figure for the refined embedment discretization.

7.2.2 Comparison of the Model-in-Model and Embedment Approaches

The site-scale results for the model-in-model (nesting) approach are compared to those obtained using the embedment (sub-gridding) approach in Figure I.15 to Figure I.30 of Appendix I. There are subtle differences in the results for the two methods. A comparison of the velocity magnitude plots of Figure I.19 and Figure I.20 indicates that the difference is greatest in the shallow groundwater zone beneath Lake Huron while the velocities in the deep groundwater zone are similar. A comparison of the plots of the ratio of vertical velocity to the velocity magnitude (Figure I.21 and Figure I.22) also reveals differences. The differences in the results for the two site-scale methods can be attributed to the scheme in which pseudo-equilibrium solutions are obtained. The embedment approach determines the solution in the same manner as that used in the regional-scale analyses whereas the multi-step model-in-model approach first requires a regional-scale solution at pseudo-equilibrium time and then a second pseudo-equilibrium solution is obtained for the site-scale domain using boundary conditions determined from the regional-scale solution. Differences would also occur between an embedment solution at a pseudo-equilibrium time of 1 million years and a solution at 2 million years.

A comparison of the estimates of MLE for the two approaches (Figure I.27 and Figure I.28) also reveals a difference in the results. Obtaining a MLE solution for the model-in-model or nested approach can be problematic as a result of the determination of equivalent freshwater head estimates at the site-scale lateral boundaries using interpolation. Gradients can occur between adjacent nodes as a result of the interpolation. The result is a short-circuit of flow with a high MLE being predicted for blocks at which influx occurs and a low value where fluid efflux occurs. The MLE figure for the model-in-model approach excludes the results for the outer band of grid blocks.

Based on the results of this and the preceding section, it is concluded that the embedment approach has been implemented correctly. Subject to the requirement of a large longitudinal dispersivity to meet regional-scale constraints, the embedment approach is preferred to that of the model-in-model approach.

7.3 Site-Scale Analyses

7.3.1 Analysis of Measured Pressure Profile at the Composite DGR-1 and DGR-2 Borehole

The environmental head distribution versus depth for the composite DGR-1 and DGR-2 borehole has been plotted in Figure 7. The data in the figure are based on the March 3, 2008 pressure measurements and the measured TDS concentration distribution in the borehole. Relative to the ground surface at 185.84 mASL, the profile indicates that the Cambrian is over-pressured while units in the upper Ordovician are significantly under-pressured thus reflecting a water deficit relative to the amount of water that would be in the pores for pressures that are hydrostatic relative to the elevation of the ground surface. The evolution of these pressures as they equilibrate to the present day boundary conditions can be investigated using the site-scale model. The modelling methodology undertook transient saturated site-scale analyses of coupled flow and brine transport with the measured pressure profile at the composite DGR-1 and DGR-2 borehole as the initial condition. Boundary conditions for the analyses are based on the present day state. The issues investigated in this study are the vertical hydraulic conductivity for the

Ordovician units and the impact of pressure support in the units that have been observed to be over-pressured with respect to the ground surface. The transient analyses assume saturated flow with the base-case parameters. In addition to the base-case vertical over horizontal hydraulic conductivity anisotropy ratio of 0.1 for the Ordovician units, anisotropy ratios of 0.01 and 0.001 also were investigated; thus, the horizontal hydraulic conductivities for the Ordovician units were constant for all analyses while the vertical hydraulic conductivities were determined from the horizontal values using the given factors. The vertical hydraulic conductivities for the Ordovician units for the three parameter sets are thus approximately 1.0×10^{-12} m/s, 1.0×10^{-13} m/s and 1.0×10^{-14} m/s respectively. The initial condition for the site-scale analyses represents the measured pressure profile using equivalent freshwater heads: the Precambrian and Cambrian were assigned an initial freshwater head of 445 mASL; the Shadow Lake to Fossil Hill an initial freshwater head of 125 mASL; while from the Niagaran Group to the surface, the initial freshwater heads were 235 mASL. The initial TDS concentration distribution for the site-scale model was the results from Scenario 1 at a pseudo-equilibrium time of 1 million years. Zero flux Neumann boundary conditions were used for the freshwater heads for the site-scale domain sides and bottom. As in Scenario 1, a Dirichlet boundary condition related to surface topography was used to represent the water table at the top of the domain. For brine transport, a TDS Dirichlet boundary condition of 300 g/L was assigned to the Precambrian while a zero flux Neumann boundary condition was used for the site-scale domain sides.

The more permeable units below the Salina at the site-scale are the Cambrian and the Niagaran Group. Sanford et al. (1985) states that the Cambrian is discontinuous in southern Ontario while evidence indicates that the Niagaran Group is continuous. The environmental head profile of Figure 7 indicates an upward gradient from the Cambrian to the Ordovician and a downward gradient from the Niagaran to the Ordovician. It is hypothesized that the water deficit in the Ordovician will be met from either the Cambrian or the Niagaran or from both. Based on the analyses of the preceding sections of this report, it is reasonable to assume that flow in the Niagaran is topographically controlled with this providing pressure support for the unit. The Cambrian at the DGR-2 borehole has a thickness of 17 m while the overlying Ordovician is 396 m thick. Based on the storage coefficient of the Cambrian relative to that of the Ordovician, there is insufficient water per unit area in the Cambrian to meet the deficit in the Ordovician. Limited pressure support for the Cambrian, if any, can come from the underlying Precambrian.

Based on the assessment of the preceding paragraph, four cases were considered for each of the three anisotropy ratios with these being: no pressure support for either the Cambrian or the Niagaran; pressure support for the Cambrian but not the Niagaran; pressure support for both the Cambrian and the Niagaran; and, no pressure support for the Cambrian and pressure support for the Niagaran. Pressure support was provided in the site-scale modelling using Dirichlet boundary conditions at the perimeter of a unit with the Cambrian being assigned an equivalent freshwater head of 445 mASL and the Niagaran a freshwater head of 235 mASL.

The results for the four cases and an anisotropy ratio of 0.1 are plotted in Figure 55 to Figure 62. The results for the case where there is no pressure support for either the Cambrian or the Niagaran (Figure 56) indicates that by 1000 years, the elevated pressure in the Cambrian has been dissipated and the water deficit in the Ordovician can only be met from the Devonian above the Salina. Downward gradients are predicted to occur for more than the cutoff time of the analysis (10^5 years). For the second case where it is assumed that there is pressure support for the Cambrian but not the Niagaran Group, the environmental head profiles of Figure 58 show that

at 10^5 years there is still a downward gradient to the Ordovician from the shallow groundwater system. For the third case where there is pressure support for both the Cambrian and the Niagaran Group (Figure 60), the pressure and related water deficit in the Ordovician has been met by approximately 10^5 years and as shown at 10^6 years an upward gradient develops from the Cambrian to the surface. In the fourth case where there is no pressure support for the Cambrian and pressure support for the Niagaran Group, the environmental head profiles of Figure 62 indicate that the over-pressurization of the Cambrian has been dissipated by 10^4 years but that the pressures slowly increase as the domain fills from the Niagaran. At 10^6 years water is still moving downward from the Niagaran Group.

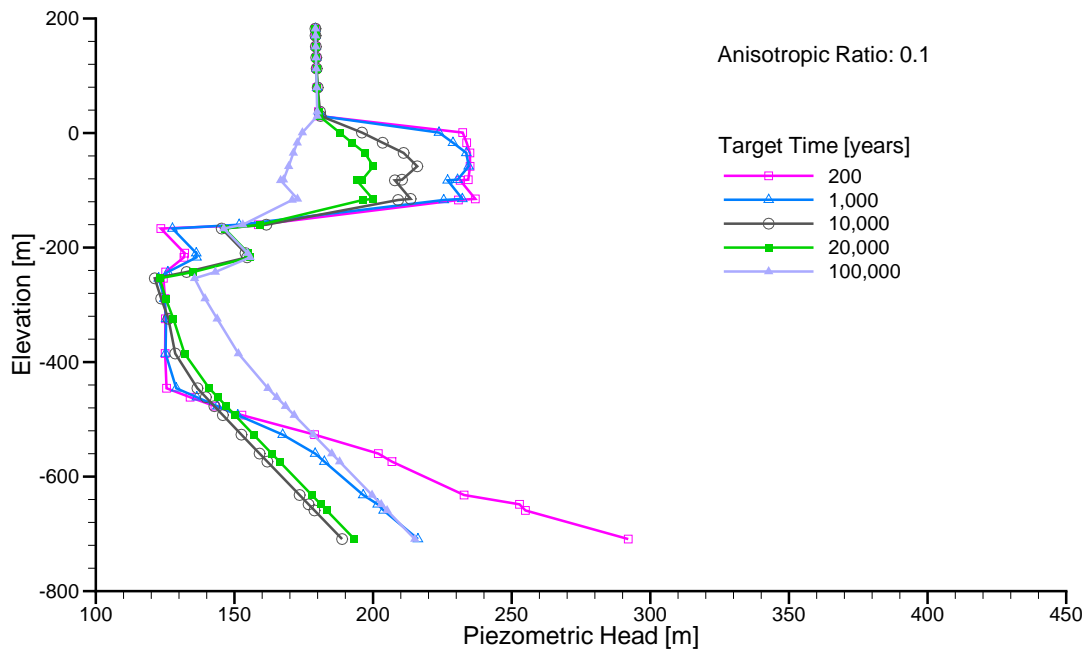


Figure 55: Predicted equivalent freshwater head profile at DGR-2 for base case parameters and no pressure support for the Niagaran or Cambrian at various times.

The analyses with an anisotropy ratio of 0.1 for the Ordovician units indicate that the low pressures in the Ordovician cannot be maintained for times greater than 10^6 years. Similarly, in the absence of pressure support, the high pressure in the Cambrian cannot be maintained. The analyses with anisotropy ratios of 0.01 and 0.001 investigate the sensitivity of the environmental head profiles for the four cases to the vertical hydraulic conductivity for the Ordovician units. The results for the simulations are presented in Appendix J. The impact of lowering the vertical hydraulic conductivity by an order-of-magnitude from that of the analyses described in the preceding paragraph is to delay the dissipation of the pressures in the Cambrian for the cases in which there is no pressure support for the unit or the Niagaran. Whereas for an anisotropy ratio of 0.1 dissipation was accomplished in approximately 1000 years, with an anisotropy ratio of 0.01 for the Ordovician hydraulic conductivity, complete dissipation of the Cambrian pressure occurred by approximately 10 000 years (refer to Figure J.2). For the case with an anisotropy ratio of 0.001, approximately 100 000 years were required for the dissipation of the Cambrian pressure (refer to Figure J.10). With both an anisotropy of 0.01 and 0.001 the Ordovician units remained

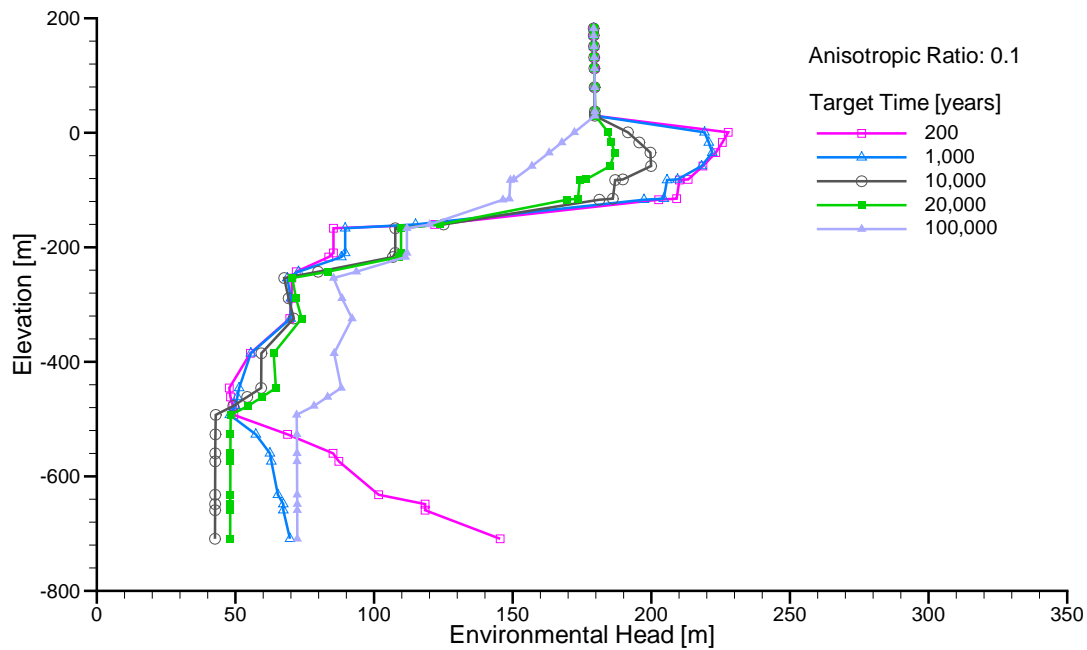


Figure 56: Predicted environmental head profile at DGR-2 for base case parameters and no pressure support for the Niagaran or Cambrian. at various times

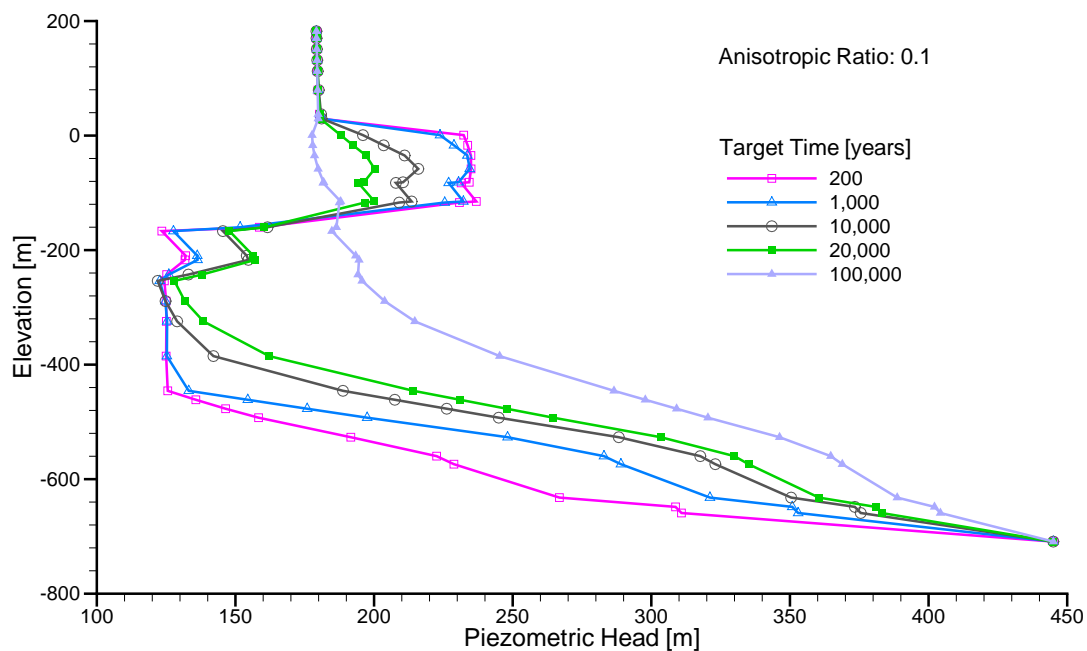


Figure 57: Predicted equivalent freshwater head profile at DGR-2 for base case parameters; pressure support for the Cambrian and no pressure support for the Niagaran at various times.

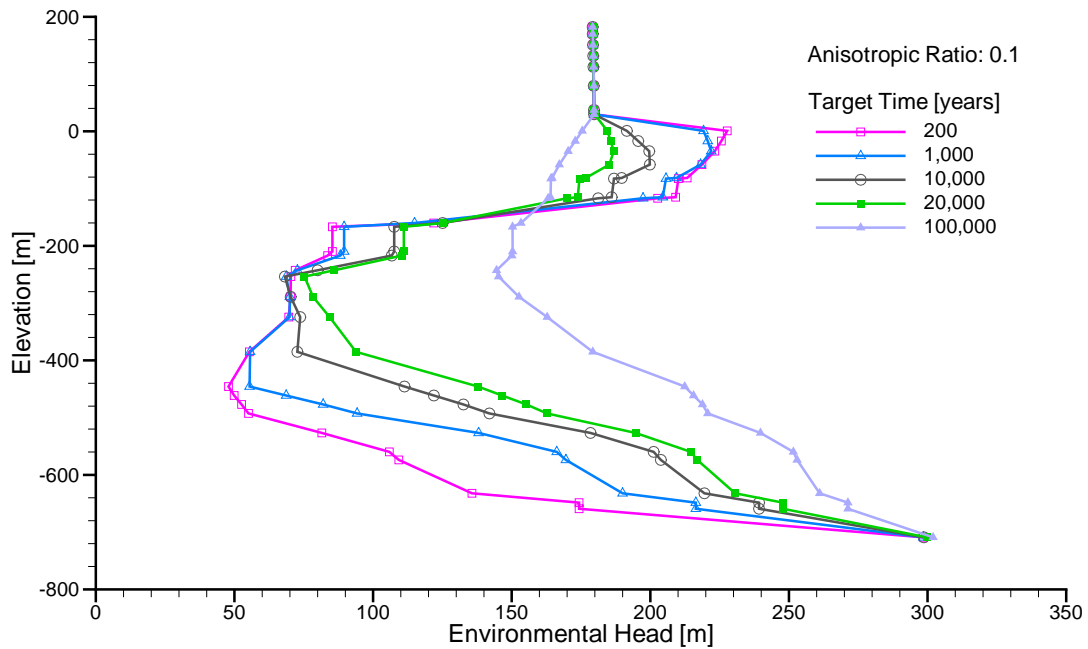


Figure 58: Predicted environmental head profile at DGR-2 for base case parameters; pressure support for the Cambrian and no pressure support for the Niagara at various times.

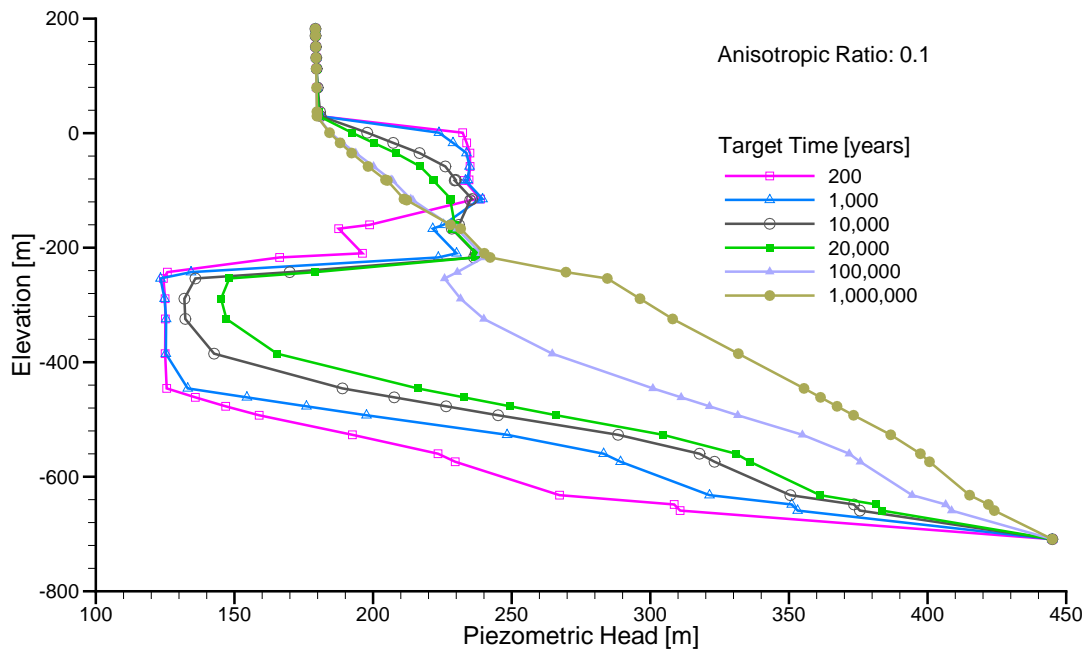


Figure 59: Predicted equivalent freshwater head profile at DGR-2 for base case parameters; pressure support for both the Niagara and the Cambrian at various times.

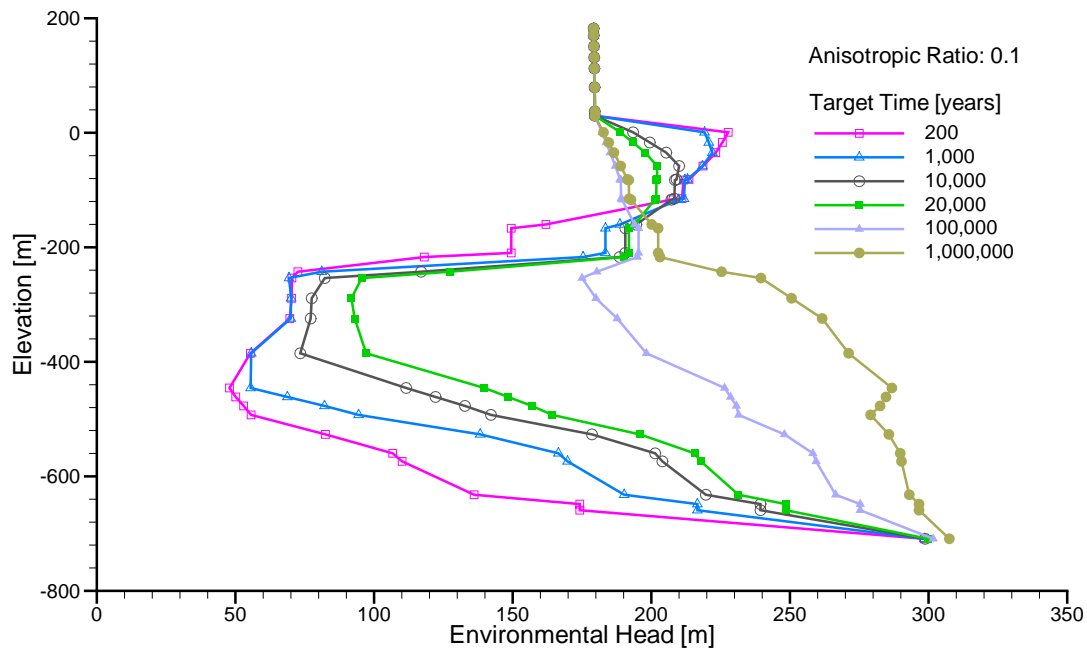


Figure 60: Predicted environmental head profile at DGR-2 for base case parameters; pressure support for both the Niagaran and the Cambrian at various times.

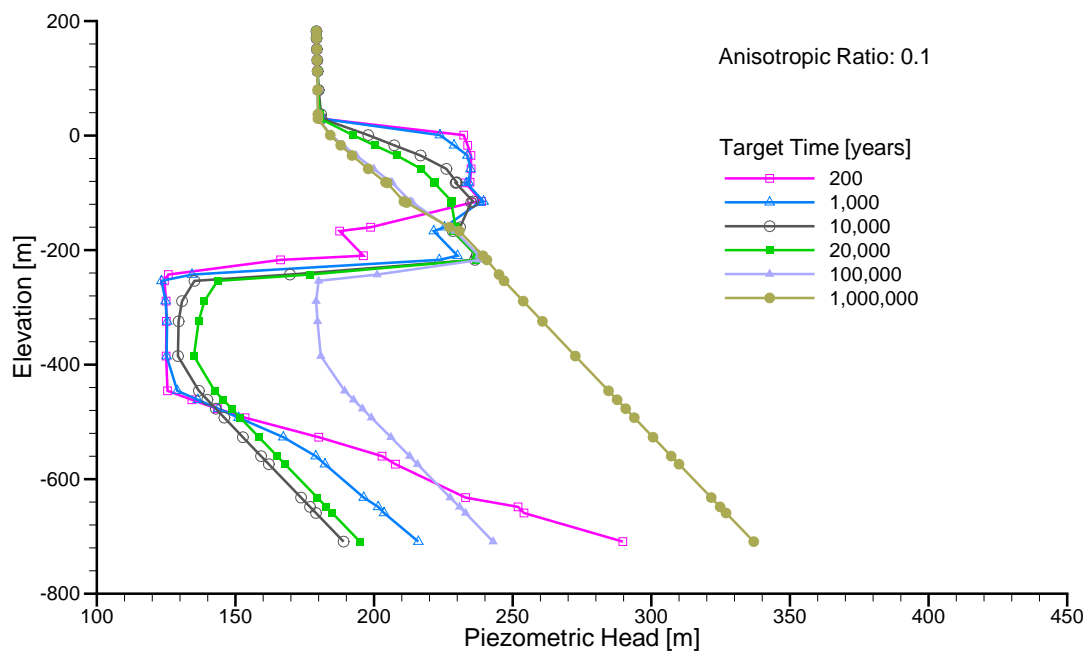


Figure 61: Predicted equivalent freshwater head profile at DGR-2 for base case parameters; pressure support for the Niagaran and no pressure support for the Cambrian at various times.

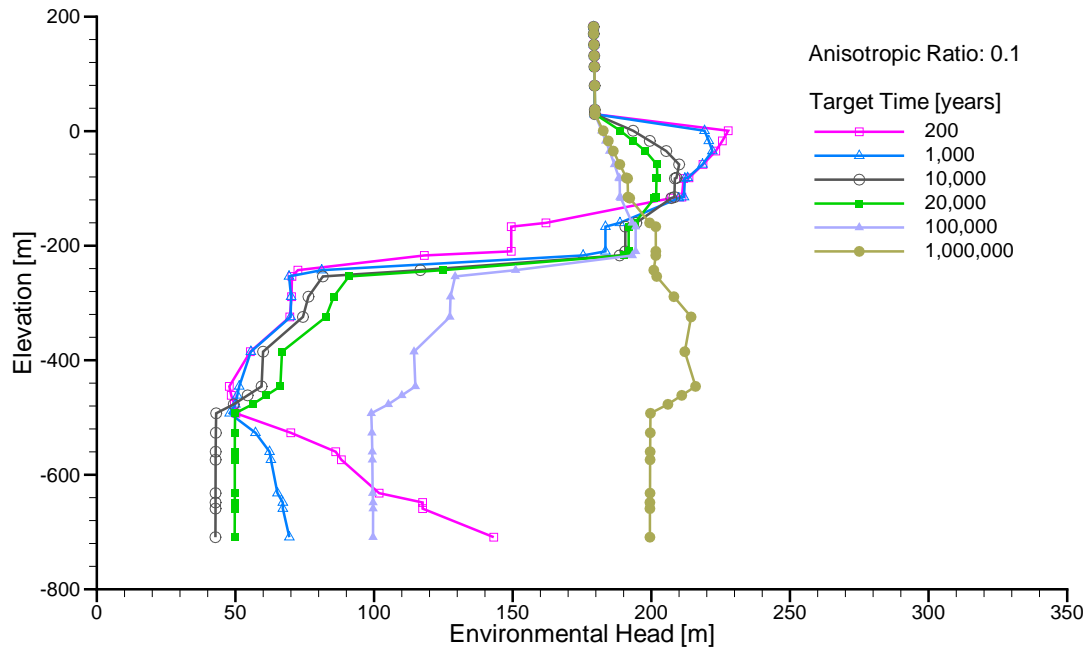


Figure 62: Predicted environmental head profile at DGR-2 for base case parameters; pressure support for the Niagaran and no pressure support for the Cambrian at various times.

significantly under-pressured at the end of the simulation (1 million years); downward gradients from the shallow groundwater system were predicted throughout the analysis. The results for the case with no pressure support in the Cambrian but pressure support in the Niagaran with Ordovician hydraulic conductivity anisotropy ratios of 0.01 and 0.001 are similar: pressure dissipation for the Cambrian takes approximately 10 000 years and 100 000 years respectively; gradients are downward from the Niagaran throughout the simulation time of 1 million years; and, the Ordovician units remain significantly under-pressured (refer to Figure J.8 and Figure J.16 respectively). When there is pressure support for the Cambrian, the Ordovician units remain under-pressured for more than 100 000 years when the anisotropy ratio is 0.01 and for more than 1 million years for an anisotropy ratio of 0.001 (refer to Figure J.6 and Figure J.14).

The analyses of this section support the conclusion that the vertical hydraulic conductivity required to maintain the elevated pressures in the Cambrian and to prevent the re-pressurization of the Ordovician for a period of time greater than 1 million years are significantly lower than that used for the base-case analysis. The presence of a gas phase in the Ordovician and the impact of a relative hydraulic conductivity that is a function of the water saturation would lower the effective vertical hydraulic conductivity or water mobility. Depending on the saturation of a trapped or residual gas phase, if present, the water mobility effectively could become zero resulting in a stagnant water phase in the Ordovician and an inability of the elevated pressures in the Cambrian to be dissipated.

7.3.2 Analysis of Dewatering at the DGR

The impact of the proposed DGR will cause converging flow to occur as a result of dewatering. Assuming saturated flow conditions, dewatering was simulated using FRAC3DVS-OPG and the model-in-model approach with the site-scale spatial domain. The base-case Scenario 1 parameters, boundary conditions and initial conditions were used for this Phase 1 illustrative analysis. The eight nodes for a grid block at the location of the proposed DGR in the Cobourg Formation were assigned equivalent freshwater heads that correspond to the presence of atmospheric pressure at that depth. The results of the simulation after 10^6 years are presented in Figure 63 to Figure 66. The environmental head plot of Figure 63 indicates that heads in the Silurian remain unaffected although the dewatering draws water from the Silurian as shown by the TDS concentration distribution of Figure 64 and the increased velocities that are evident in the upper Ordovician (refer to Figure 65). The plot of the ratio of vertical velocity to velocity magnitude (Figure 66) clearly shows the zone of influence of the dewatering. The results of the simulation indicate that even if atmospheric pressure could be maintained in the DGR for 1 million years, the impact of dewatering in a saturated flow analysis is restricted to the Ordovician units. A reduction of the period of time during which atmospheric pressure in the DGR is maintained would result in a reduction in the volume of the Ordovician that is dewatered.

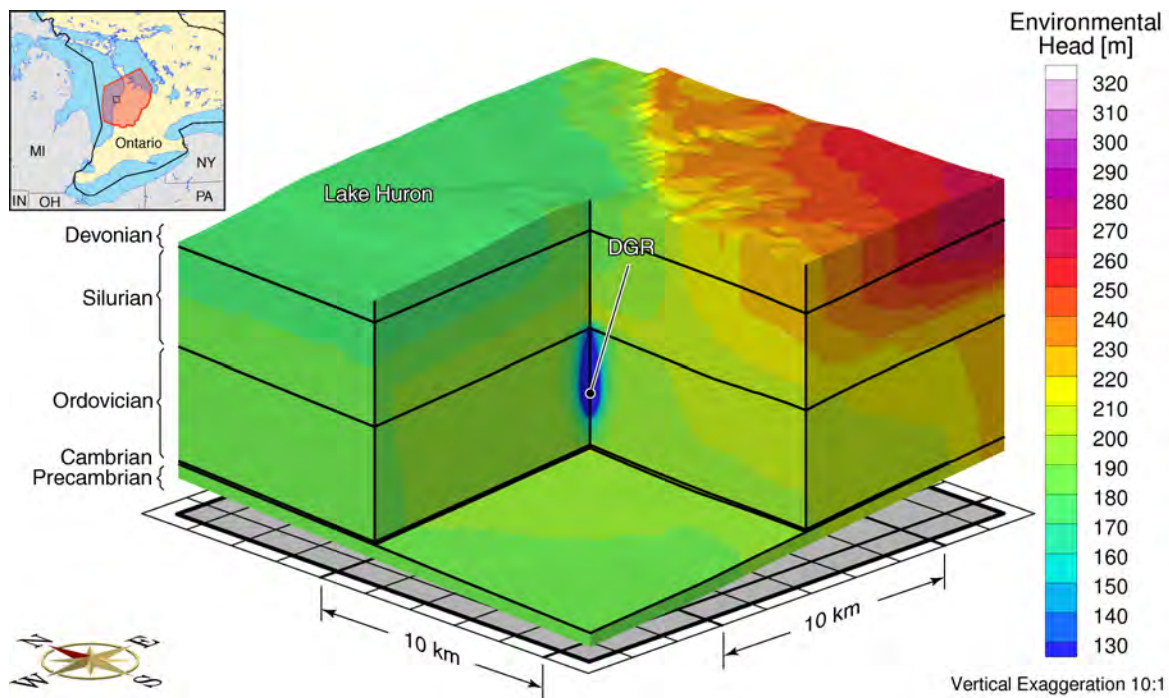


Figure 63: Environmental heads at 1 million years for dewatering at the location of the proposed DGR.

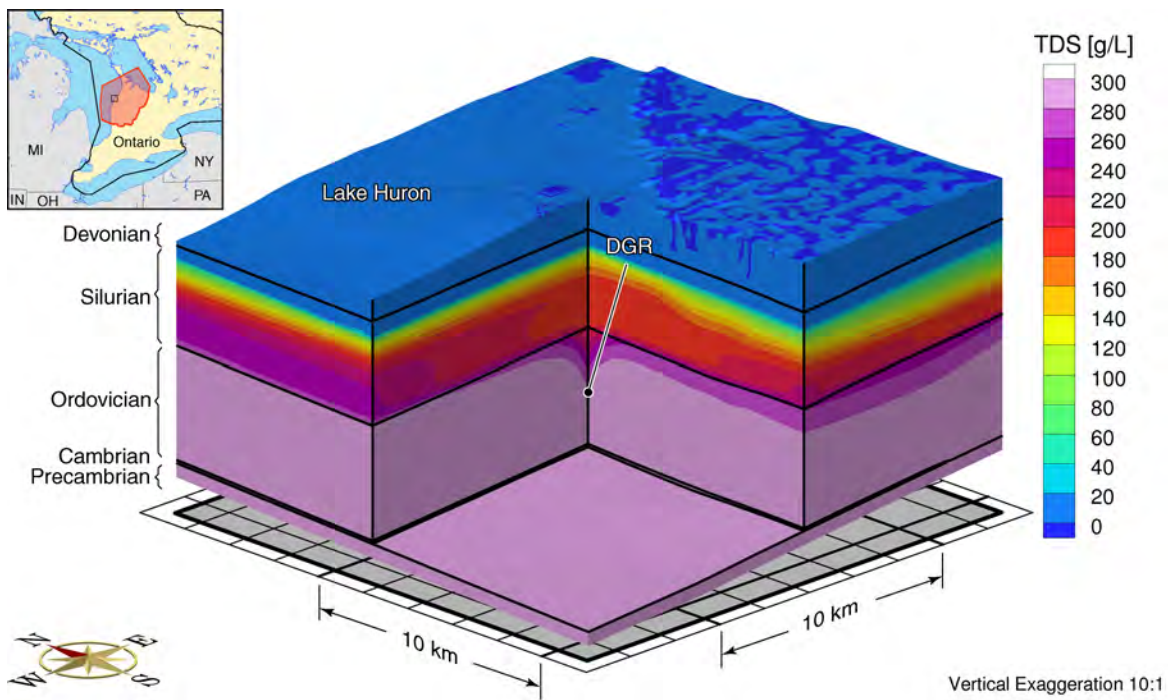


Figure 64: TDS concentration distribution at 1 million years for dewatering at the location of the proposed DGR.

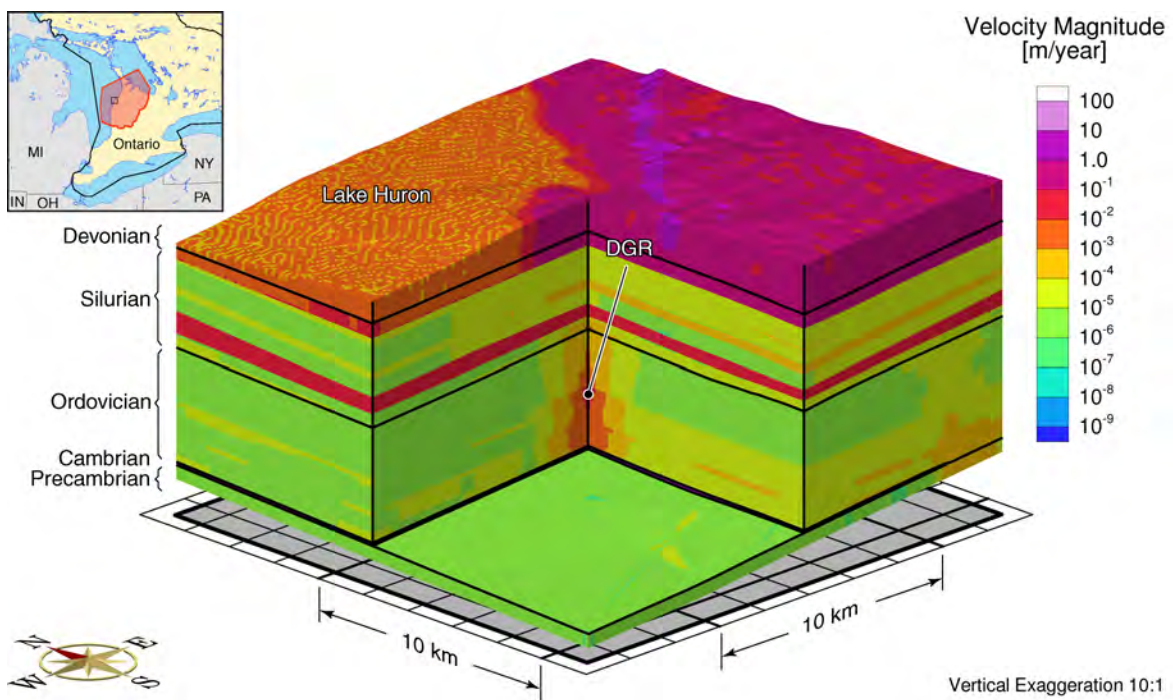


Figure 65: Pore water velocity magnitude at 1 million years for dewatering at the location of the proposed DGR.

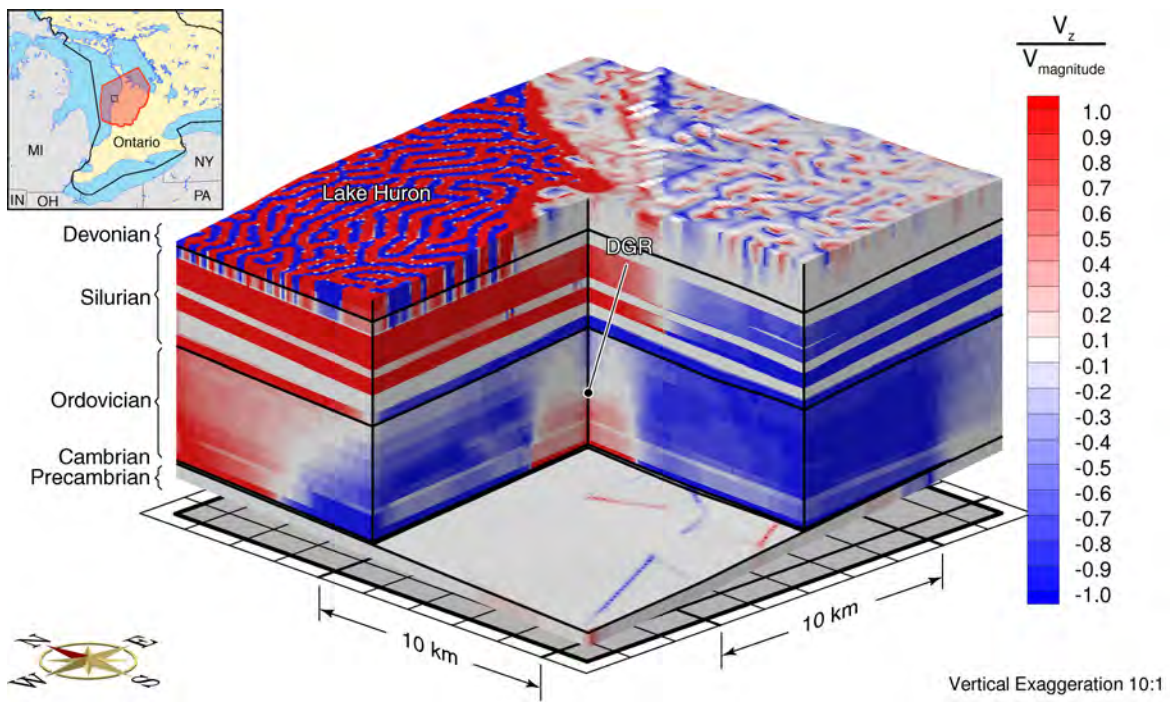


Figure 66: Ratio of vertical velocity to velocity magnitude at 1 million years for dewatering at the location of the proposed DGR.

8. DISCUSSION AND CONCLUSIONS

The regional and site-scale hydrogeological modelling study is one of seven studies that comprise the Phase 1 Geosynthesis Program of the DGR (Gartner Lee Limited, 2008a). The analyses of this study, performed using the three-dimensional model FRAC3DVS-OPG, were designed to gain insight on regional-scale and site-scale groundwater system hydrodynamics and evolution relevant to an understanding of groundwater pathways and solute migration from the location of the proposed DGR in the Cobourg Formation. FRAC3DVS-OPG follows a quality assurance protocol. The regional-scale extent is approximately 18 000 km² while the site-scale extent is approximately 400 km². The boundary conditions for the site-scale analysis were developed using both the traditional model-in-model approach (refer to Section 7) and an innovative embedment approach that better enables the treatment of transient simulations. The approach adopted for all of the analyses is intent on remaining as faithful as possible to the site geometry and boundary conditions with direct linkages to the geological framework model (Gartner Lee Limited, 2008b), hydrogeochemistry (Hobbs et al., 2008) and glacial simulations of long-term climate change (Peltier, 2008). The modelling permits an assessment of the influence of hydrostratigraphy, variable salinity, parameter uncertainty and boundary conditions on the processes and mechanisms governing groundwater flow and solute migration.

The discussion and conclusions of this report are presented in the following sections:

- Section 8.1 presents an overview of the regional-scale groundwater system,
- Section 8.2 discusses the implications of the observed pressure profile in the composite DGR-1 and DGR-2 boreholes on the estimation of permeability of the Ordovician units and on the far-field state of the groundwater system,
- Section 8.3 discusses and develops the salient conclusions of the numerous Scenarios or parameter case studies that were investigated in the work of this report,
- Section 8.4 discusses the caveats of mean life expectancy (MLE) and the development of the conclusion that it is a conservative performance measure,
- Section 8.5 presents a brief discussion of the paleoclimate simulations undertaken in this study,
- Section 8.6 discusses the analyses of this study relevant to the selection of a regional-scale spatial extent that is a subset of the Michigan Basin and the sensitivity of the DGR performance measure, mean life expectancy, and the sensitivity of predicted pathways from the location of the proposed DGR in the Cobourg Formation to the regional-scale boundary conditions,
- Section 8.7 comments on issues relating to geologic structure,
- Section 8.8 summarizes some of the key conclusions from the analyses of this Phase 1 study,
- Section 8.9 presents answers to possible stakeholder questions citing the findings and analyses of this report.

An important aspect of this Phase 1 study is that it explores the solution space for the regional-scale domain centered on the proposed DGR by varying parameters over their feasible range. This approach honours both the geologic framework and the lithology of the groundwater system and it enables the development of robust conclusions relevant to the DGR.

8.1 Overview of the Regional-Scale Groundwater System

The preliminary geological framework model for the Phase 1 regional-scale analysis of the proposed Deep Geologic Repository (DGR) at the Bruce site near Tiverton, Ontario was first developed by Sykes (2007) and then expanded upon and refined by Gartner Lee Limited (2008b). The model of Gartner Lee Limited (2008b) includes 31 layers that could be reliably interpreted within the study area (refer to Section 2.3). The models are significant in that they are the first regional-scale three-dimensional depictions of the stratigraphic units of southern Ontario. The geology in the regional domain was modelled using geostatistical and other interpolation methods to develop the correlation structure of the data and to facilitate interpolation of unit thicknesses and structural contours between boreholes. To ensure that the top of the model conformed to known surface elevations and lake bathymetries, additional data were added to the geologic model from DEMs and bathymetry maps of Lake Huron and Georgian Bay. The geologic model, with corrections for proper topography and bathymetry, was used as the basis for the regional-scale numerical model. The hydrologic parameters of the model are informed, in part, by estimates obtained from the DGR-1 and DGR-2 boreholes.

The regional scale domain, with an area of approximately 18 000 km², can be divided into three major zones at the DGR site: the shallow zone with a thickness of 178 m, the intermediate zone with a thickness of 270 m and the deep zone with a thickness of 413 m. The shallow groundwater zone at the DGR site is characterized by layers with higher permeability and a groundwater composition with a relatively low total dissolved solids concentration (Table 1). It includes the horizons above the base of the Bass Islands Formation (Figure 2) and the dolomite and limestone units of the Devonian formations. The glacially deposited sediments also are part of the shallow zone. The direction of groundwater flow in the shallow zone is strongly influenced by topography and has much shorter Mean Lifetime Expectancies (MLE) than the deeper groundwater zone (the base-case Scenario 1 results are given in Figure 25). With low total dissolved solids, the higher groundwater velocities in the shallow zone (Figure 22) are dependent on energy gradients that are relatively independent of fluid density. Solute transport in the shallow groundwater zone is dominated by advection and the related mechanical dispersion. From a regional-scale flow perspective and the estimation of a mean life expectancy for the horizon of the proposed repository in the Cobourg Formation, the glacially deposited sediments of the shallow zone are unimportant.

Separating the shallow and deep groundwater zones are the layers of the intermediate groundwater zone which extends from the base of the Bass Islands Formation to the bottom of the Manitoulin Formation. Within this zone, the low permeability of aquitard units within the Salina Formation, where present, isolate the topographically driven shallow flow system from that of the underlying Ordovician shale and limestone formations. The Niagaran Group is the most permeable layer in the intermediate zone.

The deep groundwater zone comprises the layers beneath the Manitoulin of the Lower Silurian and includes the Ordovician limestones and shales, as well as the Cambrian sandstones and the crystalline Precambrian basement. Groundwater in the deeper zone can be characterized as being stagnant and has high total dissolved solids (TDS) concentrations that can exceed 300 g/L with a corresponding specific gravity of approximately 1.2. In this study, the term stagnant is used to define groundwater in which solute transport is dominated by molecular diffusion. The deep

groundwater zone has much lower velocities and high Mean Lifetime Expectancies (Figure 22 and Figure 25, respectively). Since the deep groundwater zone is isolated from any local topographic effects by the very low hydraulic conductivities of both the Salina Formation and the Lower Silurian carbonates and shales, the horizontal energy gradients in this zone will be very low and are strongly influenced by density gradients. The only place within the domain for a significant gravitational gradient will be at the Niagara Escarpment where some of the formations in the deep groundwater zone subcrop or outcrop. The most permeable formation in the deep zone is the Cambrian; however, evidence indicates that this relatively thin layer (17 m at the DGR site) is not continuous.

8.2 Analysis of the Composite DGR-1 and DGR-2 Pressure Profile

The environmental head profile from the measured TDS concentrations and pressures at the composite DGR-1 and DGR-2 borehole (Figure 7) indicates that the Cambrian is over-pressured relative to the elevation of the ground surface while the Ordovician shale and limestone units are significantly under-pressured. The Cambrian pinches out east of the DGR site (Figure 10); it is absent at the Algonquin Arch. An essential requirement of the abnormal high pressures of the Cambrian and their slow dissipation is overlying, extensive, low vertical hydraulic conductivity strata. The low pressures in the Ordovician may be the result of stress relief as a result of significant removal of mass through erosion, that was at a rate that is greater than that of water influx to these low permeability units from the over and under-lying units with higher pressure; the pressure distribution is still evolving. Alternatively, the low pore fluid pressures may indicate the presence of a trapped non-wetting gas phase.

The investigation of the evolution of the observed pressure profile was undertaken using the site-scale model with 4 different configurations for the boundary conditions and with 3 different anisotropy ratios for the permeability of the Ordovician units. The analyses of this study indicate that the effective vertical hydraulic conductivity for the Ordovician units required to preserve the observed pressure distribution is most likely on the order of 1×10^{-14} m/s or possibly lower (refer to Figure 7.3.1). The simulations of Chapter 6 support the conclusion that it is unlikely that the environmental head profile at the composite DGR-1 and DGR-2 borehole is related to stress loading during glaciation and stress relief during deglaciation. This conclusion is based, in part, on the paleoclimate scenario investigated where the time for loading is shorter than the period of load relief. It also is concluded that the profile is related to a state that is different from that investigated in the base-case analysis (Scenario 1) of this study. In either an equilibrium or a disequilibrium model (Neuzil, 1995), the profile is a result of past boundary conditions and stresses that are different from those observed today and used in the base-case analysis. Regardless of whether a gas phase is present, in the equilibrium model the pressures in the Cambrian and Ordovician are static and the pore waters stagnant. In the disequilibrium model, the pressures are slowly evolving, in a geologic time sense, to a distribution that is compatible with the boundary conditions and stresses of the currently observed state; flow will be converging on the Ordovician from the overlying Niagaran and the underlying Cambrian. Depending on the effective vertical hydraulic conductivity of the Ordovician units, this process may take millions of years.

An outcome of the analysis of the environmental head profile at the composite DGR-1 and DGR-2 borehole is that the base-case analyses of this study, that are based on a conceptual model that

the groundwater domain is saturated, represents a state to which the current pressure distribution in the Ordovician and Cambrian will evolve. Thus there are two components in the estimation of solute transport from the location in the Ordovician of the proposed DGR: the first is the solute transport during the period that the observed pressure distribution evolves to an equilibrium state corresponding to the present day boundary conditions, flow during this period will be converging on the Ordovician; the second component is the solute transport represented by the base-case and related simulations of this study. From a solute transport perspective, regardless of state, the analyses of this study indicate that solute migration in the Ordovician units is diffusion dominant. Thus, the analyses of different states will have a greater impact on the description of groundwater flow in the more permeable Niagaran Group and the Cambrian than it will on the estimation of velocities and their impact on solute transport in the Ordovician formations.

8.3 Analyses of the Regional-Scale Groundwater System

The analysis of the base case (Scenario 1) represents the groundwater system, or state, that is predicted to develop after the elevated pressure in the Cambrian has dissipated and the water deficit (under-pressure) in the Ordovician formations has been eliminated. Depending upon values assigned to the hydrogeologic parameters for the Ordovician units, and the assumed boundary conditions, calculations suggest that it may take 1 million years or more for this state to be established. Until the currently observed disequilibrium pressures dissipate, groundwater will flow extremely slowly into the Ordovician formations; regardless of state, solute migration in the Ordovician will be diffusion dominant. While the parameters of the developed regional-scale model have not been calibrated in a formal sense (refer to Section 1.3 for a discussion of parameter calibration), the analyses of this study support conclusions relevant to the flow and transport regime at the site of the proposed DGR. Solute transport in the Ordovician limestones and shales of the deep groundwater zone, because of the low velocities, will be diffusion dominated. The model estimated velocities in the Ordovician shale and limestone are less than 0.0001 m/year with Peclet numbers less than 0.01 for the units. The direction of the velocity is generally upward or downward (Figure 23); significant horizontal velocity components were not calculated for the Ordovician formations enclosing the DGR location. This result supports the selection of a regional-scale domain that is a subset of the Michigan Basin as horizontal boundaries are less important in a groundwater system that is dominated by vertical gradients (refer to Section 8.6 for further discussion of this issue). The domain has topography that ranges from 176 m at Lake Huron and Georgian Bay to more than 500 m at the Niagara Escarpment. Through sensitivity analyses using the regional-scale model (refer to Section 5.3 and Table 13), the boundary conditions and extent of the domain were determined to be sufficient to allow the development of horizontal flow components in the deeper Ordovician Formations at the proposed DGR site. However, the estimated velocities are more sensitive to the very low permeability of the units and the dampening impact of density on the energy gradients than they are to either the extent of the regional domain or the boundary conditions of the conceptual model.

The assessment of groundwater system behaviour involved more than 24 Scenarios or parameter case studies. Twenty of these simulations are summarized in Table 15. Also given are the key study findings that when combined indicate a groundwater system in the Ordovician that is stagnant in the sense that it remained diffusion dominant for all simulations that respect field observations.

8.4 Mean Life Expectancy

The performance measure used in the analysis of the regional-scale groundwater model is Mean Lifetime Expectancy (MLE) which is an estimate of the time required for a water particle at a spatial position in a groundwater system to reach a potential outflow point considering the advective and dispersive transport processes. The independent variables for this probabilistic measure are the spatial distribution of the velocities and for the second-order term the dispersivity components and diffusion. The velocities are density-dependent and hence a fully coupled transient flow and brine transport analysis is required for their estimation. A pseudo-equilibrium solution was determined at 1 million years after the imposition of an initial total dissolved solids distribution in the regional domain. The boundary conditions for the analysis were time invariant. For the base-case analysis, the MLE in the Cobourg Formation in the vicinity of the proposed repository was conservatively estimated to be more than 8.9 million years. The sensitivity of the calculated MLE to the assigned permeabilities for the Ordovician shale and limestone formations is related to the occurrence of divide points in the Ordovician units that separate zones of upward flow from downward flow. The shift of the divide point could alter the flow path and the estimate of the time for migration of fluid to a domain boundary; however, solute transport in the Ordovician units is diffusion dominant and insensitive to the advective velocities. The occurrence of the divide points in the Ordovician is related to regional changes in the topography and the height and density of the fluid column above the point. Regardless, MLEs were estimated to be millions of years for all scenarios.

The MLE is sensitive to the fluid density gradient. A density-independent analysis that used the base-case parameters and the same boundary conditions as the density-dependent analyses was undertaken. Whereas the path of average water particles released in the vicinity of the proposed DGR followed the Niagaran Group for the density-dependent base-case scenario (Figure 26), the path in the density-independent analysis followed the Cambrian (Figure 33). The impact of including variable density is thus to minimize deep basin flow. The horizontal permeabilities used in the base-case analysis are based on the estimated values from the DGR-1 and DGR-2 borehole tests. It is likely that the permeabilities used in this study have been overestimated. As a result, the estimated Mean Life Expectancies are likely lower bound estimates. Most important, however, is that a reduction of the dispersivities used in the estimation of the MLE, not possible in this study because of computational constraints, will result in longer MLEs for the deeper formations. Thus, the analyses of this study indicate that the MLE performance measure is conservative and results in the underestimation of the time that a solute would take to reach an outflow point.

Table 15: Key findings from the Scenario analyses of this study

| Scenario | Description | Key Study Findings |
|--|--|---|
| Base Case | permeabilities from Table 1 present day boundary conditions GL001 geological framework | shallow groundwater system topographically driven fluids in low permeability intermediate and deep zone layers are stagnant meteoric recharge is not occurring to units below the Salina Formation indicates extremely low vertical velocities at repository horizon no horizontal velocities at repository horizon |
| Surface Boundary Condition | compare Type I and Type II b.c. base case parameters | groundwater pathways from DGR unchanged |
| Geologic Model | base case parameters | definition of the Cambrian important |
| Density-Independent Flow | base case parameters | density gradients influence groundwater pathways solute transport at DGR horizon remains diffusion dominant density-dependent flow required for prediction of defendable pathways |
| Ordovician Permeability | order-of-magnitude changes | solute transport at DGR horizon remains diffusion dominant |
| Silurian Permeability | perturb Salina permability order-of-magnitude changes | solute transport at DGR horizon remains diffusion dominant |
| Horizontal Boundary Condition | base case parameters high permeability perimeter | solute transport at DGR horizon remains diffusion dominant extremely low vertical velocities at repository horizon |
| Paleoclimate Simulations | base case parameters Sensitivity analysis bounding analyses of glacial loading simplified hydro-mechanical coupling | no glacial meltwater penetration below Salina glacial perturbation not cause of abnormal pressures at DGR boreholes |
| Abnormal Pressures at DGR Boreholes | base case parameters perturbed parameters | Cambrian is discontinuous indicates extremely low permeability in the Ordovician layers no evidence of vertical permeable faults permeable faults would dissipate the abnormal pressures abnormal pressures likely have persisted for more than 1 million years solute transport at DGR horizon remains diffusion dominant |

8.5 Regional-Scale Paleoclimate Analyses

The impact of glaciation and deglaciation on the groundwater system was investigated in a paleoclimate scenario (Chapter 6). The results of the analysis indicate that basal meltwater is unlikely to penetrate below the units of the Salina at the DGR site. The most significant consequence of glacial loading is the generation of higher pressures throughout the rock column, with the level dependent on the one-dimensional loading efficiency of the rock mass. The estimation of the pressures during glaciation were undertaken assuming saturated flow conditions; the presence of a gas phase in the Ordovician would result in a different pressure distribution. The paleoclimate analyses will be refined in a Phase 2 study.

8.6 The Spatial Extent of the Regional-Scale Domain

The regional-scale domain occupies an area of approximately 18 000 km²; as shown in Figure 14, the domain is thin relative to its spatial extent. The approximate western and northern boundaries coincide with the deepest points in Lake Huron and the deepest points in Georgian Bay. The southern and eastern boundaries are set to coincide with the regional divides for the surface water system. The selected domain has a sufficient spatial extent for the appropriate characterization of groundwater flow in the shallow zone above the base of the Bass Islands Formation and flow in the sub- or outcrop portions of the Niagaran Group aquifer in the intermediate zone. The domain includes the outcrop for the Ordovician layers (refer to Figure 9). The analyses of the many regional-scale and site-scale scenarios undertaken in this study combined with the data from the DGR-1 and DGR-2 boreholes enable the assessment of the adequacy of the regional-scale spatial extent for the simulation of flow in the units beneath the Silurian Salina Formation. The factors that contribute to the assessment of adequacy are characterized by the following points.

- Park et al. (2008) show that for increasing TDS concentrations with depth there can be a static brine region because the surface driving forces cannot lift the brine located at depth. Over the entire Michigan Basin, the gravitational driving force imposed by topography is minimal; the gradients attributed to the gravitational driving force are larger in the regional-scale domain as determined by the elevation difference between the Niagara Escarpment and Lake Huron than they are across the Michigan Basin (Lake Michigan and Lake Huron have the same elevation).
- The predicted flow in the low permeability units such as those of the Ordovician layers is low such that solute transport is diffusion dominant; the conclusion that the transport is diffusion dominant is insensitive to the extent of the regional-scale domain.
- The direction of the low flow in the low permeability units in the vicinity of the proposed DGR is strongly vertical with horizontal flow not being predicted for any of the scenarios investigated in this study. The direction of flow, where it is predicted to occur, is either upward from the Ordovician units to the more permeable Niagaran Group or downward from the Ordovician units to the more permeable Cambrian. The direction of flow in the Ordovician units is insensitive to the extent of the regional-scale domain (compare, for example, the base-case analysis of Figure 23 with the results for Scenario 16 shown in Figure 37 where the lateral boundary condition is investigated).

- The path followed by water particles in the base-case Scenario is vertical from the Ordovician to the more permeable units of either the shallower Niagaran Group for the density-dependent case (refer to Figure 26) or the deeper Cambrian sandstones and carbonates for the density-independent case (refer to Figure 33). The total dissolved solids concentration distribution throughout the regional-scale domain do not support the validity of analyses of density-independent fluid flow - while the analyses are informative, they cannot be used to determine the path that average water particles and solute would follow.
- The shallow Niagaran Group has been characterized sufficiently such that the sub- and outcrop portions of the units are included in the regional-scale domain (refer to Figure 9 and to Figure 11).
- The conceptual model postulated by Sanford et al. (1985) and Carter et al. (1996) indicates that the Cambrian is discontinuous. The abnormal pressures for the Cambrian sandstones and carbonates measured in the DGR-2 borehole (refer to Figure 7) support this conceptual model that the Cambrian is discontinuous in that while the preservation of the high pressures requires the presence of extensive low-permeability bounding strata (Neuzil, 1995) such as those of the Ordovician formations, the Cambrian itself cannot have an upscaled permeability that would allow the pressures to dissipate. Therefore, the Cambrian, in spite of the relatively high permeability estimated at the DGR-2 borehole (refer to Table 1), cannot be a significant pathway for solutes from the location of the proposed DGR in the Cobourg Formation.
- The Cambrian sandstones and carbonates are absent over the Algonquin Arch while the unit deepens both to the west and to the south; the Cambrian outcrop is north of the regional-scale domain. A MLE of 6.2 million years was predicted in the assessment of the lateral boundary condition (refer to Section 5.3.6). The extension of the regional-scale domain to include the Cambrian outcrop would result in a longer flow path and hence a longer MLE; the Scenario 16 MLE, that includes permeable pathways to the biosphere for both the Niagaran Group and the Cambrian, is thus very conservative.

In summary, the regional-scale spatial domain is of sufficient extent since it fully includes the potential solute transport pathway through the Niagaran Group from the location of the proposed DGR. The Cambrian does not provide a transport pathway as it is discontinuous (Sanford et al., 1985; Carter et al., 1996), the abnormal elevated pressures in the Cambrian in the DGR-2 borehole support the conclusion that it is discontinuous. Further, for density-dependent flow, the tendency is for the movement of water, if it occurs at all, to shallower permeable aquifers rather than deeper aquifers.

8.7 Geologic Structure

The geological framework model developed by Gartner Lee Limited (2008b) presents an accurate three-dimensional description of the various units/formations/groups of the regional-scale domain. It formed the basis of the conceptual model investigated in this study. Sanford et al. (1985) postulates that faults may occur within this framework (refer to Figure 4) and that these faults explain the development of oil and gas traps, particularly in the Niagara Megablock. While this report cites the hypothesis of Sanford et al. (1985) and Carter et al. (1996), at the time of the writing of the report, there are no data from the Phase 1 Bruce DGR field program to indicate that vertical permeable faults are present in the Ordovician formations within the vicinity of the proposed site (Jensen, 2008). The abnormal pressures measured in the composite DGR-1 and DGR-2 boreholes are inconsistent with the presence of a permeable faults

in the deep zone at the site. Such permeable faults would enable the dissipation of both the elevated pressures in the Cambrian and the under-pressures of the Ordovician units; the abnormal pressures could not exist in the presence of permeable faults that enable flow through the Ordovician. In spite of the lack of evidence for the existence of faults, the analyses of the Cambrian of Section 5.3.7 were undertaken. Consistent with the conclusion that the Cambrian is not a significant pathway for solute migration from the vicinity of the proposed DGR in the Cobourg Formation, the results indicate that the orientation of faults has only a marginal impact on the conservative estimates of MLE at the DGR site. Additional analyses of hypothetical faults will be undertaken in a Phase 2 study.

8.8 Summary of Key Study Findings

Some of the key findings of the work, analyses and interpretations of this Phase 1 study are summarized in the following points:

- The deep groundwater system is isolated; it is resilient to surface perturbations.
- The permeability of the Ordovician sediments is extremely low. This is a necessary requirement for the existence of the abnormal pressures and high gradients observed in the composite DGR-1 and DGR-2 boreholes.
- The analyses support the hypothesis that the Cambrian is discontinuous with this being a necessary condition for the existence of the abnormal (elevated) pressures in the layer.
- The sedimentary sequence at the DGR site provides multiple barriers in both the deep and intermediate zones; for simulations that honour the site data, solute transport in the Ordovician layers is diffusion dominant as is transport in the Silurian Salina Formation.
- The calculated fluid velocities in the Ordovician layers are extremely low and vertical; no horizontal velocities were predicted to occur at the DGR site.
- The analysis of density-dependent flow is required for the determination of groundwater pathways and the assessment of potential solute migration from the horizon of the proposed DGR to the biosphere.
- There is no evidence to support the existence of permeable connected pathways through the sedimentary sequence of the deep groundwater zone; the presence of permeable pathways is inconsistent with the abnormal pressures measured in the DGR boreholes.
- A solute released from the horizon of the proposed DGR in the Cobourg Formation would migrate by diffusion through the Ordovician sediments to the overlying Niagaran Group and to the thin underlying Cambrian layer. The extremely low fluid velocities in the Ordovician will have little impact on this diffusion dominated transport. Transport through the lower Cambrian will be limited and diffusion dominant as evidence indicates that the unit is discontinuous. Both advective and dispersive transport can occur in the Niagaran Group, however the pathway to the accessible biosphere is long resulting in estimated mean life expectancies that are likely considerably greater than 10 million years.

8.9 Stakeholder Questions

The fundamental tenets of the safety case for the DGR site are (Gartner Lee Limited, 2008a):

- (a) Predictable: horizontally layered, undeformed sedimentary shale and limestone formations of large lateral extent;
- (b) Multiple Natural Barriers: multiple low permeability bedrock formations enclose and overlie the DGR;
- (c) Contaminant Transport is Diffusion Dominated: deep groundwater regime is ancient showing no evidence of glacial perturbation or cross-formational flow;
- (d) Seismically Quiet: comparable to stable Canadian Shield setting;
- (e) Natural Resource Potential is Low: commercially viable oil and gas reserves are not present;
- (f) Shallow Groundwater Resources are Isolated: near surface groundwater aquifers isolated; and
- (g) Geomechanically Stable: selected DGR limestone formation will provide stable, virtually dry openings.

The analyses of this study support tenets (a), (b), (c) and (f). The basis of this support is summarized in the preceding paragraphs. It also is provided in the responses to the issues itemized in the text that follows. The analyses of this study do not address tenets (d), (e) and (g).

A list of possible stakeholder and regulatory questions related to hydrogeology have been developed as part of the Geosynthesis Program for the DGR (Jensen, 2008). The regional-scale and site-scale numerical modelling analyses and results that have been presented in this study can be used to address these questions. The questions and responses are:

1) *Where would water from the repository horizon discharge?*

The pressure profile at the composite DGR-1 and DGR-2 borehole (Figure 7) and the analyses of Section 7.3.1 indicate that water is currently converging in the Ordovician units from the Niagaran above and from the Cambrian below. For this state, there will be no water discharge from the proposed repository horizon until the pressure and water deficit in the Ordovician has been met. The analyses indicate, that assuming saturated flow conditions and depending on the vertical hydraulic conductivity for the Ordovician units, this may take up to 10^6 years or more. If a gas phase is present in the Ordovician and depending on the gas saturation, the water in the Ordovician may be stagnant (refer to Section 7.3.1). The analysis of the base-case Scenario 1 represents the state that would develop after the elevated pressures of the Cambrian have been dissipated and the water deficit of the Ordovician units overcome. The pore water velocities in the Ordovician units for the state that would evolve are less than 0.0001 m/year (refer to Figure 22 of Section 5.1). The flux of water through the unit is correspondingly low while solute transport in the units is diffusion dominated. Average water particles released in the vicinity of the proposed location of the DGR follow a path to the Niagaran where it subcrops in Lake Huron (refer to Figure 26). The time of travel for the water to Lake Huron was estimated to be tens of millions of years.

2) *When would contaminants at the repository depths be released to the lake?*

The time of migration of a conservative, non-decaying contaminant from the location of the proposed DGR to the biosphere is a function of the advective velocity, mechanical dispersion, diffusion as well as the path followed. The estimates of Mean Life Expectancy used in this study include these processes. However, as shown in Section 5.2, estimates of MLE overestimate mechanical dispersion as a result of the necessity to use a large longitudinal dispersivity coefficient in order to satisfy numerical constraints. MLE results for

the location of the proposed DGR are thus conservative and underestimate the expected time of arrival at the biosphere. The MLE values for all scenarios are summarized in Table 13. For the base-case Scenario 1 the MLE, representing the time for solute transport rather than the time of travel for an average water particle, was estimated to be 8.9 million years.

3) *How might undetected fractures in the Site Characterization program affect repository performance?*

At the DGR site, the presence of a permeable fracture zone in the Ordovician that transmits water is inconsistent with the pressure profile that has been measured at the composite DGR-1 and DGR-2 borehole (Figure 7). If such a fracture intersected either the over-pressured Cambrian or the Niagaran, it would allow water inflow to the Ordovician to overcome its water deficit. Data do not support this occurrence. Further, the DGR has multiple barriers with these including the long travel paths to the biosphere (Figure 26), the low permeability of the Lower Silurian and the low permeability of the carbonate, shale and evaporites in the Salina (refer to Table 1). These barriers have isolated the DGR horizon from the influx of both meteoric water and glacial basal meltwater. The geochemistry profile at the site supports this conclusion.

4) *What evidence do you have that vertical fracturing through the Ordovician cap rocks will not jeopardize repository performance in the long-term?*

The analyses of this report indicate the presence of multiple barriers. These barriers include: the under-pressurization of the Ordovician units (Figure 7) that indicate either the presence of stagnant fluids or the occurrence of very slowly converging flow (Section 7.3.1); the low permeability of the Ordovician units (Table 1) and resulting low estimates of pore water velocity for the base-case Scenario 1 (Figure 22); the low permeability of the Lower Silurian units (Table 1); the low permeability of the Salina units (Table 1) and possible over-pressurization of the units (Figure 45) that will significantly retard upward migration; and, the long travel path in the Niagaran (Figure 26). Such a multiple barrier system should provide a considerable margin of safety.

5) *Could permafrost affect the performance of a repository?*

This study investigated glacial scenario nn9930 developed by Peltier (2008). For this scenario, permafrost depth did not exceed 45 m (Figure 40). The analyses of Chapter 6 indicate that basal meltwater would not penetrate through the Salina (Figure 49) and that for a one-dimensional loading efficiency of zero in Equation (24) the environmental heads in the Cobourg Formation would be only marginally perturbed (Figure 40). Transport in the Cobourg Formation remained diffusion dominant.

6) *What caused the over-pressure groundwater conditions in the Cambrian sandstone formation beneath the repository?*

The data for the DGR-2 borehole indicate that the Cambrian is over-pressured with-respect-to the elevation of the ground surface (Figure 7). This abnormal pressure state may be a relic feature preserved by a virtual absence of fluid flow over geologic time (Neuzil, 1995). From a hydrodynamic perspective, flow can also play an important role in the development of abnormal pressures with the flow regime being either equilibrated or disequilibrated. Equilibrated-type pressures generally develop from topographically-driven flow but may also occur as a result of fluid density contrasts. The disequilibrium-type abnormal pressures are caused by natural geologic processes such as compaction,

diagenesis, and deformation. Both types require the presence of extensive low-permeability strata (Neuzil, 1995) such as those of the Ordovician formations and Precambrian (Table 1). The analyses of Section 7.3.1 indicate that the vertical hydraulic conductivity for the Ordovician units must be of the order of 1.0×10^{-14} m/s or lower to preserve the high pressures of the Cambrian for more than 10^6 years.

7) *How does groundwater salinity affect contaminant migration?*

The salinity of groundwater affects both the fluid density and the hydraulic conductivity terms in Darcy's equation (Equation (11)). The energy gradient in the equation is the sum of a pressure gradient and a potential energy gradient with the fluid density directly affecting the latter. The hydraulic conductivity is a function of both the properties of the porous medium and the properties of the fluid such as density and viscosity with both of these properties being a function of the total dissolved solids concentration as well as temperature. However, isothermal conditions have been assumed for the analyses reported in this Phase 1 study. The hydraulic conductivity is proportional to density and inversely proportional to viscosity. Solutions of the flow equation, Equation (16), which includes Darcy's equation, show that for increasing TDS concentrations with depth there can be a static brine region because the surface driving forces cannot lift the brine located at depth (Park et al., 2008). The upward vertical velocity can be significantly reduced by the dense brine. Both the regional-scale and the site-scale analyses included the impact of fluid density and groundwater salinity. The path that average water particles follow from the location of the proposed DGR to the biosphere was estimated for both the density-dependent base-case Scenario 1 (refer to Figure 26 of Section 5.1) and for the same parameters assuming density-independent flow (refer to Figure 33 of Section 5.3.4). The paths for the former, reflecting the presence of deep higher density fluids and a static brine region, followed the Niagaran Group while those of the latter followed the much deeper Cambrian.

8) *How do you know that the bedrock permeabilities are representative and low having drilled only 2 boreholes and 6 planned?*

A tenet of the DGR program is that the sediments are well understood and their attributes are predictable and can be extrapolated over large distances. The data analyses used in the reconstruction of the geological framework model in Section 2.3 show that the geometric properties of the various lithologies at the DGR site are predictable. The statistics for selected Ordovician units are presented in Table 2. The physical hydrogeologic properties for the lithofacies, including hydraulic conductivity, have been measured at the DGR-1 and DGR-2 boreholes (Table 1). Other reported data from insitu measurements elsewhere in southern Ontario are listed in Table 3, Table 4 and Table 5. It should be noted that in many instances, the minimum hydraulic conductivities reported are at the measurement limit of the hydrogeologic testing equipment. A review of the data in these tables supports the conclusion that the low Ordovician permeabilities, as measured at the DGR-1 and DGR-2 boreholes, are representative of the values reported in the tables.

9) *How do you know that contaminant transport in the Ordovician sediments is diffusion dominated?*

Diffusion dominated transport is indicated when the Peclet number of molecular diffusion, the ratio of transport by advection to the transport by diffusion, is less than 0.4 (Bear, 1988). The results for the base-case Scenario 1 simulation (refer to Section 5.1) yield pore velocities for the Ordovician sediments in the vicinity of the proposed DGR site that are less than

0.0001 m/year. Based on the estimated low velocities and relative to a pore water diffusion coefficient of $0.0038 \text{ m}^2/\text{year}$ (Table 9), solute transport in the Ordovician will be diffusion dominated with an estimated Peclet number of molecular diffusion for the unit being much less than 0.4. The analyses in Section 5.3.5 and Section 7.3.1 indicate that the velocities estimated for the Ordovician units in the base-case Scenario 1 and other scenarios are conservative.

10) *Can contaminants migrate away from the DGR through the Cambrian sandstone formation?*

The measured pressure profile at the composite DGR-1 and DGR-2 borehole (Figure 7) indicate that the Cambrian is over-pressured with respect to the overlying Ordovician units. The vertical energy gradients that are estimated using the environmental heads (refer to Section 3.1.3), are upward. This gradient would oppose diffusive transport to the Cambrian from the location of the proposed DGR. When the TDS concentration distribution is considered as in Scenario 1, the path that water follows is predominantly through the Niagaran and not the Cambrian (refer to Figure 26). However, with diffusion dominated solute transport in the Ordovician, it may be possible for a solute to reach the Cambrian from the proposed DGR solely by diffusive transport. However, such transport would occur over very long time periods and the mass transported would be extremely small.

11) *What is the influence of glaciation and the post-glacial lakes that occurred in this area on DGR performance?*

The analyses of Chapter 6 indicate that basal meltwaters would not penetrate below the Salina at the DGR site. However, assuming that the Ordovician sediments are water saturated and depending on the one-dimensional loading efficiency (Equation (24)), the influence of glaciation would be to increase the pore water pressure at the repository horizon (refer to Figure 51). The pore water velocities in the Ordovician units would remain low and indicative of diffusion dominated transport. The pore water velocity magnitudes for the conservative case with a loading efficiency of 1 are plotted in Figure 47.

12) *What does anisotropic mean? Are bedrock properties anisotropic? How does this affect repository performance?*

A medium is said to be isotropic with respect to a certain property if that property is independent of direction within the medium. If at a point within the medium a property of the medium, e.g., hydraulic conductivity or diffusivity, varies with direction, the medium is said to be anisotropic at the considered point with respect to that property (Bear, 1988). As indicated by the data of Table 1, the hydraulic conductivity estimates for the various lithologies are assumed to be vertically anisotropic with, depending on the unit, a horizontal to vertical ratio of 10 to 1. Alternate horizontal anisotropy ratios for the Cambrian were investigated in Section 5.3.7 while the analyses of Section 7.3.1 investigated horizontal to vertical anisotropy ratios for the Ordovician hydraulic conductivity of 10:1, 100:1 and 1000:1. Given that the contaminant transport in the Ordovician sediments is diffusion dominant, the repository performance, as indicated in this study by mean life expectancy, is insensitive to the pore water velocity and the anisotropy ratio for the hydraulic conductivity (refer to Figure 28 to Figure 30 and to the MLE estimates in Table 13). However, the estimated time for the pressure and water deficit in the Ordovician units to equilibrate with the boundary conditions for the presently observed state at the DGR site is inversely dependent on the vertical hydraulic conductivity assumed for the Ordovician units (refer to Section 7.3.1).

- 13) *How deep have glacial melt waters penetrated into the sub-surface? Could they affect DGR performance?*

The analyses of Chapter 6 indicate that basal melt waters will not penetrate below the Salina at the DGR site. The low permeability of the Lower Silurian and Ordovician units (Table 1) also will isolate the DGR from glacial melt waters.

- 14) *What does the distribution of groundwater pressures tell you about the site hydrogeology?*

The pressure profile at the composite DGR-1 and DGR-2 borehole (Figure 7) and the analyses of Section 7.3.1 indicate that an essential requirement for maintaining the abnormal pressures in the permeable Cambrian is an effective vertical hydraulic conductivity for the Ordovician units that is on the order of 1×10^{-14} m/s or possibly lower. The analyses of the impact of glaciation (Chapter 6) strongly support the argument that the low pressures in the Ordovician units are not caused by stress loading during glaciation and stress relief during deglaciation.

9. REFERENCES

- Armstrong, D.K. and T.R. Carter. 2006. An updated guide to the subsurface paleozoic stratigraphy of southern Ontario. Ontario Geological Survey, Technical Report Open File Report 6191, 214p.
- Bailey Geological Services Ltd. and R. Cochrane. 1984. Evaluation of the conventional and potential oil and gas reserves of the cambrian of ontario. Ontario Geological Survey, Technical Report Open File Report 5499, 72p.
- Barton, K.E., D.G. Howell, J.F. Vigil, J.C. Reed, and J.O. Wheeler. 2003. The North America tapestry of time and terrain. United States Geological Survey. Geologic Investigations Series I-2781, Version 1.0.
- Bear, J. 1988. Dynamics of Fluids in Porous Media. Dover edition. Dover Publications Inc.
- Brooks, R.J. and A.T. Corey. 1964. Hydraulic properties of porous media: Hydro Paper 3. Colorado State University, Technical report.
- Carter, T., R. Trevail, and R. Easton. 1996. Basement controls on some hydrocarbon traps in southern Ontario, Canada. Geological Society of America, Special Paper 308 , 95–107.
- Cooley, R.L. 1971. A finite difference method for unsteady flow in variably saturated porous media: application to a single pumping well. Water Resources Research 7(6), 1607–1625.
- Cornaton, F. and P. Perrochet. 2006. Groundwater age, life expectancy and transit time distributions in advective–dispersive systems: 1. Generalized reservoir theory. Advances in Water Resources 29(9), 1267–1291.
- Ellis, G.D. 1969. Architecture of the Michigan Basin. In Studies of the Precambrian of the Michigan Basin, Michigan Basin Geological Society Annual Field Excursion Guidebook. 60–80.
- Freeze, R.A. and J. Cherry. 1979. Groundwater. Prentice Hall.
- Gao, C., J. Shirota, R. Kelly, F. Brunton, and S. van Haaften. 2006. Project Unit 05-013; bedrock topography and overburden thickness mapping, southern Ontario. Technical Report Open file report - Ontario Geological Survey, Report 6192, p. 34.1-34.10.
- Gartner Lee Limited. 2008a. Phase 1 geosynthesis. prepared for Ontario Power Generation, Toronto Ontario, Technical Report GLL 61-123 and OPG 00216-REP-01300-00010-R00.
- Gartner Lee Limited. 2008b. Phase 1 Regional Geology, Southern Ontario. prepared for Ontario Power Generation, Toronto Ontario, Technical Report GLL 61-123 OPG 00216-REP-01300-00007-R00.
- Golder Associates Ltd. 2003. LLW geotechnical feasibility study, western waste management facility, Bruce Site, Tiverton, Ontario. report to Municipality of Kincardine and Ontario Power Generation. Golder Associates Ltd, Technical Report 021-1570.
- Guvanasen, V. 2007. FRAC3DVS-OPG enhancements: subgridding, hydromechanical deformation and anisotropic molecular diffusion. prepared for Nuclear Waste Management Organization, Toronto Ontario, Technical Report TR-2007-05.

- Hobbs, M.Y., S.K. Frappe, O. Shouakar-Stash, and L.R. Kennell. 2008. Phase I Regional Hydrogeochemistry, Southern Ontario. Ontario Power Generation and the Department of Earth and Environmental Science, University of Waterloo, Technical Report OPG 00216-REP-01300-00006-R00.
- Intera Engineering Ltd. 1988. Inventory and assessment of hydrogeologic conditions of underground openings in sedimentary rocks. report to Ontario Hydro, Technical report.
- Intera Engineering Ltd. 2006. Geoscientific Site Characterization Plan, OPG's deep repository for low and intermediate level radioactive waste. prepared for Ontario Power Generation, Technical Report OPG 00216-PLAN-00120-00002-R00.
- Intera Engineering Ltd. 2008. Technical report: Bedrock formations in dgr-1 and dgr-2. Technical Report TR-07-05, Revision 1.
- Jensen, M. 2007. Personal communication.
- Jensen, M. 2008. Personal communication.
- Luszczynski, N.J. 1961. Head and flow of groundwater of variable density. *Journal of Geophysical Research* 66 (12), 4247–4256.
- Massman, G., C. Simmons, A. Love, J. Ward, and J. James-Smith. 2006. On variable dense surface water-groundwater interaction: A theoretical analysis of mixed convection in a stably-stratified fresh surface water - saline groundwater discharge zone. *Journal of Hydrology* 329, 390–402.
- Mazurek, M. 2004. Long-term used nuclear fuel waste management: Geoscientific review of the sedimentary sequence in southern Ontario. Institute of Geological Sciences, University of Bern, Switzerland, Technical report.
- Mazurek, M., F.J. Pearson, G. Volckaert, and H. Bock. 2003. FEPCAT project: Features, events and processes evaluation catalogue for argillaceous media. OECD/NEA, Technical report.
- McCauley, C.A., D.M. White, M.R. Lilly, and D.M. Nyman. 2002. A comparison of hydraulic conductivities, permeabilities and infiltration rates in frozen and unfrozen soils. *Cold Regions Science and Technology* 34(2), 117–125.
- Mehl, S. and M. Hill. 2002. Development and evaluation of a local grid refinement method for block-centered finite-difference groundwater models using shared nodes. *Advances in Water Resources* 25, 497–511.
- Neumann, S.P. 1973. Saturated-unsaturated seepage by finite elements. *ASCE J. Hydraul. Div.* 99(HY12), 2233–2251.
- Neuzil, C. 1995. Abnormal pressures as hydrodynamic phenomena. *American Journal of Science* 295, 742–786.
- Neuzil, C.E. 2003. Hydromechanical coupling in geologic processes. *Hydrogeology Journal* 11(1), 41–83.
- NOAA. 2007. Great Lakes Bathymetry Gridding Project. Technical report.

- Normani, S.D., Y.J. Park, J.F. Sykes, and E.A. Sudicky. 2007. Sub-regional modelling case study 2005-2006 status report. NWMO TR-2007-07, Technical report.
- Novakowski, K. and P. Lapcevic. 1988. Regional hydrogeology of the Silurian and Ordovician sedimentary rocks underlying Niagara Falls, Ontario Canada. *Journal of Hydrogeology* 104, 211–236.
- Park, Y., E. Sudicky, and J. Sykes. 2008. Effects of shield brine on the safe disposal of waste in deep geologic environments. submitted to *Geophysical Research Letters* , 1–5.
- Peltier, W.R. 2002. A design basis glacier scenario. Ontario Power Generation, Nuclear Waste Management Division, Technical Report 06819-REP-01200-10069-R00. Toronto, Canada.
- Peltier, W.R. 2003a. Long-term climate change – glaciation. Ontario Power Generation, Nuclear Waste Management Division, Technical Report 06189-REP-01200-10113-R00. Toronto, Canada.
- Peltier, W.R. 2003b. Personal communication.
- Peltier, W.R. 2008. Phase I Glaciation Scenario, Bruce Site. University of Toronto. prepared for Ontario Power Generation, Toronto Ontario, Technical Report OPG 00216-REP-01300-00004-R00.
- Raven, K., K. Novakowski, R. Yager, and R. Heystee. 1992. Supernormal fluid pressures in sedimentary rocks of Southern Ontario - Western New York State. *Canadian Geotechnical Journal* 29, 80–93.
- Sanford, B.V., F.J. Thompson, and G.H. McFall. 1985. Plate tectonics - a possible controlling mechanism in the development of hydrocarbon traps in southwestern Ontario. *Bulletin of Canadian Petroleum Geology* 33(1), 52–71.
- Stonehouse, H. 1969. The Precambrian Around and Under the Michigan Basin, In *Studies of the Precambrian of the Michigan Basin*. Michigan Basin Geologic Society Annual Field Excursion Guidebook , 60–80.
- Sykes, E.A. 2007. Hydro Modelling in Support of OPG's Proposed Deep Geologic Repository, Tiverton Ontario. Master's thesis, University of Waterloo.
- Therrien, R., E.A. Sudicky, and R.G. McLaren. 2004. FRAC3DVS: An Efficient Simulator for Three-dimensional, Saturated-Unsaturated Groundwater Flow and Density-dependent, Chain-Decay Solute Transport in Porous, Discretely-Fractured Porous or Dual-porosity Formations. User's Guide. Groundwater Simulations Group, University of Waterloo, Waterloo, Ontario, Canada.
- Van Genuchten, M.T. 1980. A closed form equation for predicting the hydraulic conductivity of unsaturated soils. *Soil Science Society of America Journal* 44, 892–898.
- Vinard, P., B. Bluming, J. McCord, and G. Aristonenas. 1993. Evaluation of Hydraulic Underpressures at Wellenberg, Sweden. *Int. J. Rock Mechanics and Mining Science* 30/7, 1143–1150.
- Vinard, P.H. 1998. Generation and evolution of hydraulic underpressures in a marl-shale aquitard at Wellenberg, Central Sweden. Ph.D. thesis, Universite de Neuchatel, Sweden.

- Ward, D., D. Buss, J. Mercer, and S. Hughes. 1987. Evaluation of a groundwater corrective action at the chem-dyne hazardous waste site using a telescopic mesh refinement modelling approach. *Water Resources Research* 23(4), 603–617.
- Yates, S. and M. Yates. 1989. *Geostatistics for waste management: A User's manual for the GEOPACK Geostatistical Software System*. USDA Salinity Lab, Riverside, CA.

APPENDIX A – TABLES OF PROPERTIES FOR SCENARIO ANALYSES**LIST OF TABLES**

| | Page |
|--|-------------|
| Table A.1. Material properties for base case scenario analysis | 122 |
| Table A.2. Material properties for parameter P-case 1 scenario analysis | 123 |
| Table A.3. Material properties for parameter P-case 2 scenario analysis | 124 |
| Table A.4. Material properties for parameter P-case 3 scenario analysis | 125 |
| Table A.5. Material properties for parameter S-case 4 scenario analysis | 126 |
| Table A.6. Material properties for parameter S-case 5 scenario analysis | 127 |
| Table A.7. Initial TDS and relative concentrations with respect to 300 g/L | 128 |

Table A.1: Material properties for base case scenario analysis

| Period | Geology | K_H [m/s] | K_V [m/s] | K_V/K_H | Porosity | Specific Stor. |
|-------------|------------------------|-----------------------|-----------------------|-----------|----------------------|----------------------|
| Quaternary | Drift | 1.0×10^{-7} | 2.0×10^{-8} | 0.2 | 0.10 | 9.9×10^{-5} |
| Devonian | Traverse Group | 1.0×10^{-7} | 1.0×10^{-8} | 0.1 | 0.10 | 9.9×10^{-5} |
| | Dundee | 1.0×10^{-7} | 1.0×10^{-8} | 0.1 | 0.10 | 9.9×10^{-5} |
| | Detroit River Group | 1.0×10^{-7} | 1.0×10^{-8} | 0.1 | 0.10 | 1.4×10^{-6} |
| | Bois Blanc | 1.0×10^{-7} | 1.0×10^{-8} | 0.1 | 0.10 | 1.4×10^{-6} |
| Silurian | Bass Islands | 1.0×10^{-7} | 1.0×10^{-8} | 0.1 | 0.10 | 1.4×10^{-6} |
| | G-Unit | 1.0×10^{-7} | 1.0×10^{-8} | 0.1 | 0.08 | 1.3×10^{-6} |
| | F-Unit | 4.0×10^{-12} | 4.0×10^{-13} | 0.1 | 0.03 | 1.2×10^{-4} |
| | F-Salt | 1.0×10^{-13} | 1.0×10^{-13} | 1.0 | 0.08 | 1.6×10^{-6} |
| | E-Unit | 4.0×10^{-12} | 4.0×10^{-13} | 0.1 | 0.08 | 1.6×10^{-6} |
| | D-Unit | 1.0×10^{-10} | 1.0×10^{-11} | 0.1 | 0.03 | 1.3×10^{-6} |
| | B&C Units | 4.0×10^{-12} | 4.0×10^{-13} | 0.1 | 0.08 | 1.2×10^{-4} |
| | B Anhydrite-Salt | 1.0×10^{-13} | 1.0×10^{-13} | 1.0 | 0.08 | 1.6×10^{-6} |
| | A2-Carbonate | 1.0×10^{-10} | 1.0×10^{-11} | 0.1 | 0.08 | 1.6×10^{-6} |
| | A2 Anhydrite-Salt | 1.0×10^{-13} | 1.0×10^{-13} | 1.0 | 0.08 | 1.6×10^{-6} |
| | A1-Carbonate | 2.0×10^{-12} | 2.0×10^{-13} | 0.1 | 0.08 | 1.6×10^{-6} |
| | A1-Evaporite | 1.0×10^{-13} | 1.0×10^{-13} | 1.0 | 0.08 | 1.6×10^{-6} |
| | Niagaran | 1.0×10^{-7} | 1.0×10^{-8} | 0.1 | 0.08 | 1.6×10^{-6} |
| | Fossil Hill | 2.0×10^{-11} | 2.0×10^{-12} | 0.1 | 0.08 | 1.6×10^{-6} |
| | Cabot Head | 2.0×10^{-12} | 2.0×10^{-13} | 0.1 | 0.03 | 1.2×10^{-4} |
| Manitoulin | 1.5×10^{-12} | 1.5×10^{-13} | 0.1 | 0.01 | 1.2×10^{-6} | |
| Ordovician | Queenston | 1.3×10^{-11} | 1.3×10^{-12} | 0.1 | 0.11 | 1.2×10^{-4} |
| | Georgian Bay/Blue Mtn. | 9.1×10^{-12} | 9.1×10^{-13} | 0.1 | 0.11 | 1.2×10^{-4} |
| | Cobourg | 9.6×10^{-12} | 9.6×10^{-13} | 0.1 | 0.02 | 1.3×10^{-6} |
| | Sherman Fall | 9.0×10^{-12} | 9.0×10^{-13} | 0.1 | 0.02 | 1.3×10^{-6} |
| | Kirkfield | 1.4×10^{-11} | 1.4×10^{-12} | 0.1 | 0.02 | 1.3×10^{-6} |
| | Coboconk | 5.2×10^{-11} | 5.2×10^{-12} | 0.1 | 0.02 | 1.3×10^{-6} |
| | Gull River | 3.6×10^{-11} | 3.6×10^{-12} | 0.1 | 0.02 | 1.3×10^{-6} |
| | Shadow Lake | 8.0×10^{-12} | 8.0×10^{-13} | 0.1 | 0.01 | 1.2×10^{-6} |
| Cambrian | Cambrian | 3.0×10^{-6} | 3.0×10^{-7} | 0.1 | 0.01 | 1.2×10^{-6} |
| Precambrian | Precambrian | 8.0×10^{-12} | 8.0×10^{-13} | 0.1 | 0.01 | 1.2×10^{-6} |

Table A.2: Material properties for parameter P-case 1 scenario analysis

| Period | Geology | K_H [m/s] | K_V [m/s] | K_V/K_H | Porosity | Specific Stor. |
|-------------|------------------------|-----------------------|-----------------------|-----------|----------------------|----------------------|
| Quaternary | Drift | 1.0×10^{-7} | 2.0×10^{-8} | 0.2 | 0.10 | 9.9×10^{-5} |
| Devonian | Traverse Group | 1.0×10^{-7} | 1.0×10^{-8} | 0.1 | 0.10 | 9.9×10^{-5} |
| | Dundee | 1.0×10^{-7} | 1.0×10^{-8} | 0.1 | 0.10 | 9.9×10^{-5} |
| | Detroit River Group | 1.0×10^{-7} | 1.0×10^{-8} | 0.1 | 0.10 | 1.4×10^{-6} |
| | Bois Blanc | 1.0×10^{-7} | 1.0×10^{-8} | 0.1 | 0.10 | 1.4×10^{-6} |
| Silurian | Bass Islands | 1.0×10^{-7} | 1.0×10^{-8} | 0.1 | 0.10 | 1.4×10^{-6} |
| | G-Unit | 1.0×10^{-7} | 1.0×10^{-8} | 0.1 | 0.08 | 1.3×10^{-6} |
| | F-Unit | 4.0×10^{-12} | 4.0×10^{-13} | 0.1 | 0.03 | 1.2×10^{-4} |
| | F-Salt | 1.0×10^{-13} | 1.0×10^{-13} | 1.0 | 0.08 | 1.6×10^{-6} |
| | E-Unit | 4.0×10^{-12} | 4.0×10^{-13} | 0.1 | 0.08 | 1.6×10^{-6} |
| | D-Unit | 1.0×10^{-10} | 1.0×10^{-11} | 0.1 | 0.03 | 1.3×10^{-6} |
| | B&C Units | 4.0×10^{-12} | 4.0×10^{-13} | 0.1 | 0.08 | 1.2×10^{-4} |
| | B Anhydrite-Salt | 1.0×10^{-13} | 1.0×10^{-13} | 1.0 | 0.08 | 1.6×10^{-6} |
| | A2-Carbonate | 1.0×10^{-10} | 1.0×10^{-11} | 0.1 | 0.08 | 1.6×10^{-6} |
| | A2 Anhydrite-Salt | 1.0×10^{-13} | 1.0×10^{-13} | 1.0 | 0.08 | 1.6×10^{-6} |
| | A1-Carbonate | 2.0×10^{-12} | 2.0×10^{-13} | 0.1 | 0.08 | 1.6×10^{-6} |
| | A1-Evaporite | 1.0×10^{-13} | 1.0×10^{-13} | 1.0 | 0.08 | 1.6×10^{-6} |
| | Niagaran | 1.0×10^{-7} | 1.0×10^{-8} | 0.1 | 0.08 | 1.6×10^{-6} |
| | Fossil Hill | 2.0×10^{-11} | 2.0×10^{-12} | 0.1 | 0.08 | 1.6×10^{-6} |
| | Cabot Head | 2.0×10^{-12} | 2.0×10^{-13} | 0.1 | 0.03 | 1.2×10^{-4} |
| Manitoulin | 1.5×10^{-12} | 1.5×10^{-13} | 0.1 | 0.01 | 1.2×10^{-6} | |
| Ordovician | Queenston | 1.0×10^{-11} | 1.0×10^{-12} | 0.1 | 0.11 | 1.2×10^{-4} |
| | Georgian Bay/Blue Mtn. | 1.0×10^{-11} | 1.0×10^{-12} | 0.1 | 0.11 | 1.2×10^{-4} |
| | Cobourg | 1.0×10^{-11} | 1.0×10^{-12} | 0.1 | 0.11 | 1.3×10^{-6} |
| | Sherman Fall | 1.0×10^{-11} | 1.0×10^{-12} | 0.1 | 0.11 | 1.3×10^{-6} |
| | Kirkfield | 1.0×10^{-11} | 1.0×10^{-12} | 0.1 | 0.11 | 1.3×10^{-6} |
| | Coboconk | 1.0×10^{-11} | 1.0×10^{-12} | 0.1 | 0.11 | 1.3×10^{-6} |
| | Gull River | 1.0×10^{-11} | 1.0×10^{-12} | 0.1 | 0.11 | 1.3×10^{-6} |
| | Shadow Lake | 1.0×10^{-11} | 1.0×10^{-12} | 0.1 | 0.11 | 1.2×10^{-6} |
| Cambrian | Cambrian | 3.0×10^{-6} | 3.0×10^{-7} | 0.1 | 0.01 | 1.2×10^{-6} |
| Precambrian | Precambrian | 8.0×10^{-12} | 8.0×10^{-13} | 0.1 | 0.01 | 1.2×10^{-6} |

Table A.3: Material properties for parameter P-case 2 scenario analysis

| Period | Geology | K_H [m/s] | K_V [m/s] | K_V/K_H | Porosity | Specific Stor. |
|-------------|------------------------|-----------------------|-----------------------|-----------|----------------------|----------------------|
| Quaternary | Drift | 1.0×10^{-7} | 2.0×10^{-8} | 0.2 | 0.10 | 9.9×10^{-5} |
| Devonian | Traverse Group | 1.0×10^{-7} | 1.0×10^{-8} | 0.1 | 0.10 | 9.9×10^{-5} |
| | Dundee | 1.0×10^{-7} | 1.0×10^{-8} | 0.1 | 0.10 | 9.9×10^{-5} |
| | Detroit River Group | 1.0×10^{-7} | 1.0×10^{-8} | 0.1 | 0.10 | 1.4×10^{-6} |
| | Bois Blanc | 1.0×10^{-7} | 1.0×10^{-8} | 0.1 | 0.10 | 1.4×10^{-6} |
| Silurian | Bass Islands | 1.0×10^{-7} | 1.0×10^{-8} | 0.1 | 0.10 | 1.4×10^{-6} |
| | G-Unit | 1.0×10^{-7} | 1.0×10^{-8} | 0.1 | 0.08 | 1.3×10^{-6} |
| | F-Unit | 4.0×10^{-12} | 4.0×10^{-13} | 0.1 | 0.03 | 1.2×10^{-4} |
| | F-Salt | 1.0×10^{-13} | 1.0×10^{-13} | 1.0 | 0.08 | 1.6×10^{-6} |
| | E-Unit | 4.0×10^{-12} | 4.0×10^{-13} | 0.1 | 0.08 | 1.6×10^{-6} |
| | D-Unit | 1.0×10^{-10} | 1.0×10^{-11} | 0.1 | 0.03 | 1.3×10^{-6} |
| | B&C Units | 4.0×10^{-12} | 4.0×10^{-13} | 0.1 | 0.08 | 1.2×10^{-4} |
| | B Anhydrite-Salt | 1.0×10^{-13} | 1.0×10^{-13} | 1.0 | 0.08 | 1.6×10^{-6} |
| | A2-Carbonate | 1.0×10^{-10} | 1.0×10^{-11} | 0.1 | 0.08 | 1.6×10^{-6} |
| | A2 Anhydrite-Salt | 1.0×10^{-13} | 1.0×10^{-13} | 1.0 | 0.08 | 1.6×10^{-6} |
| | A1-Carbonate | 2.0×10^{-12} | 2.0×10^{-13} | 0.1 | 0.08 | 1.6×10^{-6} |
| | A1-Evaporite | 1.0×10^{-13} | 1.0×10^{-13} | 1.0 | 0.08 | 1.6×10^{-6} |
| | Niagaran | 1.0×10^{-7} | 1.0×10^{-8} | 0.1 | 0.08 | 1.6×10^{-6} |
| | Fossil Hill | 2.0×10^{-11} | 2.0×10^{-12} | 0.1 | 0.08 | 1.6×10^{-6} |
| | Cabot Head | 2.0×10^{-12} | 2.0×10^{-13} | 0.1 | 0.03 | 1.2×10^{-4} |
| Manitoulin | 1.5×10^{-12} | 1.5×10^{-13} | 0.1 | 0.01 | 1.2×10^{-6} | |
| Ordovician | Queenston | 1.0×10^{-13} | 1.0×10^{-14} | 0.1 | 0.11 | 1.2×10^{-4} |
| | Georgian Bay/Blue Mtn. | 1.0×10^{-13} | 1.0×10^{-14} | 0.1 | 0.11 | 1.2×10^{-4} |
| | Cobourg | 1.0×10^{-13} | 1.0×10^{-14} | 0.1 | 0.11 | 1.3×10^{-6} |
| | Sherman Fall | 1.0×10^{-13} | 1.0×10^{-14} | 0.1 | 0.11 | 1.3×10^{-6} |
| | Kirkfield | 1.0×10^{-13} | 1.0×10^{-14} | 0.1 | 0.11 | 1.3×10^{-6} |
| | Coboconk | 1.0×10^{-13} | 1.0×10^{-14} | 0.1 | 0.11 | 1.3×10^{-6} |
| | Gull River | 1.0×10^{-13} | 1.0×10^{-14} | 0.1 | 0.11 | 1.3×10^{-6} |
| | Shadow Lake | 1.0×10^{-13} | 1.0×10^{-14} | 0.1 | 0.11 | 1.2×10^{-6} |
| Cambrian | Cambrian | 3.0×10^{-6} | 3.0×10^{-7} | 0.1 | 0.01 | 1.2×10^{-6} |
| Precambrian | Precambrian | 8.0×10^{-12} | 8.0×10^{-13} | 0.1 | 0.01 | 1.2×10^{-6} |

Table A.4: Material properties for parameter P-case 3 scenario analysis

| Period | Geology | K_H [m/s] | K_V [m/s] | K_V/K_H | Porosity | Specific Stor. |
|-------------|------------------------|-----------------------|-----------------------|-----------|----------------------|----------------------|
| Quaternary | Drift | 1.0×10^{-7} | 2.0×10^{-8} | 0.2 | 0.10 | 9.9×10^{-5} |
| Devonian | Traverse Group | 1.0×10^{-7} | 1.0×10^{-8} | 0.1 | 0.10 | 9.9×10^{-5} |
| | Dundee | 1.0×10^{-7} | 1.0×10^{-8} | 0.1 | 0.10 | 9.9×10^{-5} |
| | Detroit River Group | 1.0×10^{-7} | 1.0×10^{-8} | 0.1 | 0.10 | 1.4×10^{-6} |
| | Bois Blanc | 1.0×10^{-7} | 1.0×10^{-8} | 0.1 | 0.10 | 1.4×10^{-6} |
| Silurian | Bass Islands | 1.0×10^{-7} | 1.0×10^{-8} | 0.1 | 0.10 | 1.4×10^{-6} |
| | G-Unit | 1.0×10^{-7} | 1.0×10^{-8} | 0.1 | 0.08 | 1.3×10^{-6} |
| | F-Unit | 4.0×10^{-12} | 4.0×10^{-13} | 0.1 | 0.03 | 1.2×10^{-4} |
| | F-Salt | 1.0×10^{-13} | 1.0×10^{-13} | 1.0 | 0.08 | 1.6×10^{-6} |
| | E-Unit | 4.0×10^{-12} | 4.0×10^{-13} | 0.1 | 0.08 | 1.6×10^{-6} |
| | D-Unit | 1.0×10^{-10} | 1.0×10^{-11} | 0.1 | 0.03 | 1.3×10^{-6} |
| | B&C Units | 4.0×10^{-12} | 4.0×10^{-13} | 0.1 | 0.08 | 1.2×10^{-4} |
| | B Anhydrite-Salt | 1.0×10^{-13} | 1.0×10^{-13} | 1.0 | 0.08 | 1.6×10^{-6} |
| | A2-Carbonate | 1.0×10^{-10} | 1.0×10^{-11} | 0.1 | 0.08 | 1.6×10^{-6} |
| | A2 Anhydrite-Salt | 1.0×10^{-13} | 1.0×10^{-13} | 1.0 | 0.08 | 1.6×10^{-6} |
| | A1-Carbonate | 2.0×10^{-12} | 2.0×10^{-13} | 0.1 | 0.08 | 1.6×10^{-6} |
| | A1-Evaporite | 1.0×10^{-13} | 1.0×10^{-13} | 1.0 | 0.08 | 1.6×10^{-6} |
| | Niagaran | 1.0×10^{-7} | 1.0×10^{-8} | 0.1 | 0.08 | 1.6×10^{-6} |
| | Fossil Hill | 2.0×10^{-11} | 2.0×10^{-12} | 0.1 | 0.08 | 1.6×10^{-6} |
| | Cabot Head | 2.0×10^{-12} | 2.0×10^{-13} | 0.1 | 0.03 | 1.2×10^{-4} |
| Manitoulin | 1.5×10^{-12} | 1.5×10^{-13} | 0.1 | 0.01 | 1.2×10^{-6} | |
| Ordovician | Queenston | 1.0×10^{-15} | 1.0×10^{-16} | 0.1 | 0.11 | 1.2×10^{-4} |
| | Georgian Bay/Blue Mtn. | 1.0×10^{-15} | 1.0×10^{-16} | 0.1 | 0.11 | 1.2×10^{-4} |
| | Cobourg | 1.0×10^{-15} | 1.0×10^{-16} | 0.1 | 0.11 | 1.3×10^{-6} |
| | Sherman Fall | 1.0×10^{-15} | 1.0×10^{-16} | 0.1 | 0.11 | 1.3×10^{-6} |
| | Kirkfield | 1.0×10^{-15} | 1.0×10^{-16} | 0.1 | 0.11 | 1.3×10^{-6} |
| | Coboconk | 1.0×10^{-15} | 1.0×10^{-16} | 0.1 | 0.11 | 1.3×10^{-6} |
| | Gull River | 1.0×10^{-15} | 1.0×10^{-16} | 0.1 | 0.11 | 1.3×10^{-6} |
| | Shadow Lake | 1.0×10^{-15} | 1.0×10^{-16} | 0.1 | 0.11 | 1.2×10^{-6} |
| Cambrian | Cambrian | 3.0×10^{-6} | 3.0×10^{-7} | 0.1 | 0.01 | 1.2×10^{-6} |
| Precambrian | Precambrian | 8.0×10^{-12} | 8.0×10^{-13} | 0.1 | 0.01 | 1.2×10^{-6} |

Table A.5: Material properties for parameter S-case 4 scenario analysis

| Period | Geology | K_H [m/s] | K_V [m/s] | K_V/K_H | Porosity | Specific Stor. |
|-------------|------------------------|-----------------------|-----------------------|-----------|----------------------|----------------------|
| Quaternary | Drift | 1.0×10^{-7} | 2.0×10^{-8} | 0.2 | 0.10 | 9.9×10^{-5} |
| Devonian | Traverse Group | 1.0×10^{-7} | 1.0×10^{-8} | 0.1 | 0.10 | 9.9×10^{-5} |
| | Dundee | 1.0×10^{-7} | 1.0×10^{-8} | 0.1 | 0.10 | 9.9×10^{-5} |
| | Detroit River Group | 1.0×10^{-7} | 1.0×10^{-8} | 0.1 | 0.10 | 1.4×10^{-6} |
| | Bois Blanc | 1.0×10^{-7} | 1.0×10^{-8} | 0.1 | 0.10 | 1.4×10^{-6} |
| Silurian | Bass Islands | 1.0×10^{-7} | 1.0×10^{-8} | 0.1 | 0.10 | 1.4×10^{-6} |
| | G-Unit | 1.0×10^{-7} | 1.0×10^{-8} | 0.1 | 0.08 | 1.3×10^{-6} |
| | F-Unit | 1.0×10^{-8} | 1.0×10^{-9} | 0.1 | 0.03 | 1.2×10^{-4} |
| | F-Salt | 1.0×10^{-8} | 1.0×10^{-8} | 1.0 | 0.08 | 1.6×10^{-6} |
| | E-Unit | 1.0×10^{-8} | 1.0×10^{-9} | 0.1 | 0.03 | 1.6×10^{-6} |
| | D-Unit | 1.0×10^{-10} | 1.0×10^{-11} | 0.1 | 0.03 | 1.3×10^{-6} |
| | B&C Units | 1.0×10^{-8} | 1.0×10^{-9} | 0.1 | 0.08 | 1.2×10^{-4} |
| | B Anhydrite-Salt | 1.0×10^{-8} | 1.0×10^{-8} | 1.0 | 0.08 | 1.6×10^{-6} |
| | A2-Carbonate | 1.0×10^{-8} | 1.0×10^{-9} | 0.1 | 0.08 | 1.6×10^{-6} |
| | A2 Anhydrite-Salt | 1.0×10^{-8} | 1.0×10^{-8} | 1.0 | 0.08 | 1.6×10^{-6} |
| | A1-Carbonate | 1.0×10^{-8} | 1.0×10^{-9} | 0.1 | 0.08 | 1.6×10^{-6} |
| | A1-Evaporite | 1.0×10^{-8} | 1.0×10^{-8} | 1.0 | 0.08 | 1.6×10^{-6} |
| | Niagaran | 1.0×10^{-7} | 1.0×10^{-8} | 0.1 | 0.08 | 1.6×10^{-6} |
| | Fossil Hill | 2.0×10^{-11} | 2.0×10^{-12} | 0.1 | 0.08 | 1.6×10^{-6} |
| | Cabot Head | 2.0×10^{-12} | 2.0×10^{-13} | 0.1 | 0.03 | 1.2×10^{-4} |
| Manitoulin | 1.5×10^{-12} | 1.5×10^{-13} | 0.1 | 0.01 | 1.2×10^{-6} | |
| Ordovician | Queenston | 1.0×10^{-13} | 1.0×10^{-14} | 0.1 | 0.11 | 1.2×10^{-4} |
| | Georgian Bay/Blue Mtn. | 1.0×10^{-13} | 1.0×10^{-14} | 0.1 | 0.11 | 1.2×10^{-4} |
| | Cobourg | 1.0×10^{-13} | 1.0×10^{-14} | 0.1 | 0.11 | 1.3×10^{-6} |
| | Sherman Fall | 1.0×10^{-13} | 1.0×10^{-14} | 0.1 | 0.11 | 1.3×10^{-6} |
| | Kirkfield | 1.0×10^{-13} | 1.0×10^{-14} | 0.1 | 0.11 | 1.3×10^{-6} |
| | Coboconk | 1.0×10^{-13} | 1.0×10^{-14} | 0.1 | 0.11 | 1.3×10^{-6} |
| | Gull River | 1.0×10^{-13} | 1.0×10^{-14} | 0.1 | 0.11 | 1.3×10^{-6} |
| | Shadow Lake | 1.0×10^{-13} | 1.0×10^{-14} | 0.1 | 0.11 | 1.2×10^{-6} |
| Cambrian | Cambrian | 3.0×10^{-6} | 3.0×10^{-7} | 0.1 | 0.01 | 1.2×10^{-6} |
| Precambrian | Precambrian | 8.0×10^{-12} | 8.0×10^{-13} | 0.1 | 0.01 | 1.2×10^{-6} |

Table A.6: Material properties for parameter S-case 5 scenario analysis

| Period | Geology | K_H [m/s] | K_V [m/s] | K_V/K_H | Porosity | Specific Stor. |
|-------------|------------------------|---|---|-----------|----------------------|----------------------|
| Quaternary | Drift | 1.0×10^{-7} | 2.0×10^{-8} | 0.2 | 0.10 | 9.9×10^{-5} |
| Devonian | Traverse Group | 1.0×10^{-7} | 1.0×10^{-8} | 0.1 | 0.10 | 9.9×10^{-5} |
| | Dundee | 1.0×10^{-7} | 1.0×10^{-8} | 0.1 | 0.10 | 9.9×10^{-5} |
| | Detroit River Group | 1.0×10^{-7} | 1.0×10^{-8} | 0.1 | 0.10 | 1.4×10^{-6} |
| | Bois Blanc | 1.0×10^{-7} | 1.0×10^{-8} | 0.1 | 0.10 | 1.4×10^{-6} |
| Silurian | Bass Islands | 1.0×10^{-7} | 1.0×10^{-8} | 0.1 | 0.10 | 1.4×10^{-6} |
| | G-Unit | 1.0×10^{-7} | 1.0×10^{-8} | 0.1 | 0.08 | 1.3×10^{-6} |
| | F-Unit | 1.0×10^{-8} | 1.0×10^{-9} | 0.1 | 0.03 | 1.2×10^{-4} |
| | F-Salt | 1.0×10^{-8} | 1.0×10^{-8} | 1.0 | 0.08 | 1.6×10^{-6} |
| | E-Unit | 1.0×10^{-8} | 1.0×10^{-9} | 0.1 | 0.03 | 1.6×10^{-6} |
| | D-Unit | 1.0×10^{-10} | 1.0×10^{-11} | 0.1 | 0.03 | 1.3×10^{-6} |
| | B&C Units | 1.0×10^{-8} | 1.0×10^{-9} | 0.1 | 0.08 | 1.2×10^{-4} |
| | B Anhydrite-Salt | 1.0×10^{-8} | 1.0×10^{-8} | 1.0 | 0.08 | 1.6×10^{-6} |
| | A2-Carbonate | 1.0×10^{-8} | 1.0×10^{-9} | 0.1 | 0.08 | 1.6×10^{-6} |
| | A2 Anhydrite-Salt | 1.0×10^{-13} | 1.0×10^{-13} | 1.0 | 0.08 | 1.6×10^{-6} |
| | A1-Carbonate | 1.0×10^{-8} | 1.0×10^{-9} | 0.1 | 0.08 | 1.6×10^{-6} |
| | A1-Evaporite | 1.0×10^{-8} | 1.0×10^{-8} | 1.0 | 0.08 | 1.6×10^{-6} |
| | Niagaran | 1.0×10^{-7} | 1.0×10^{-8} | 0.1 | 0.08 | 1.6×10^{-6} |
| | Fossil Hill | 2.0×10^{-11} | 2.0×10^{-12} | 0.1 | 0.08 | 1.6×10^{-6} |
| | Cabot Head | 2.0×10^{-12} | 2.0×10^{-13} | 0.1 | 0.03 | 1.2×10^{-4} |
| Manitoulin | 1.5×10^{-12} | 1.5×10^{-13} | 0.1 | 0.01 | 1.2×10^{-6} | |
| Ordovician | Queenston | 1.0×10^{-13} | 1.0×10^{-14} | 0.1 | 0.11 | 1.2×10^{-4} |
| | Georgian Bay/Blue Mtn. | 1.0×10^{-13} | 1.0×10^{-14} | 0.1 | 0.11 | 1.2×10^{-4} |
| | Cobourg | 1.0×10^{-13} | 1.0×10^{-14} | 0.1 | 0.11 | 1.3×10^{-6} |
| | Sherman Fall | 1.0×10^{-13} | 1.0×10^{-14} | 0.1 | 0.11 | 1.3×10^{-6} |
| | Kirkfield | 1.0×10^{-13} | 1.0×10^{-14} | 0.1 | 0.11 | 1.3×10^{-6} |
| | Coboconk | 1.0×10^{-13} | 1.0×10^{-14} | 0.1 | 0.11 | 1.3×10^{-6} |
| | Gull River | 1.0×10^{-13} | 1.0×10^{-14} | 0.1 | 0.11 | 1.3×10^{-6} |
| | Shadow Lake | 1.0×10^{-13} | 1.0×10^{-14} | 0.1 | 0.11 | 1.2×10^{-6} |
| Cambrian | Cambrian | 3.0×10^{-6} | 3.0×10^{-7} | 0.1 | 0.01 | 1.2×10^{-6} |
| Precambrian | Precambrian | 8.0×10^{-12} | 8.0×10^{-13} | 0.1 | 0.01 | 1.2×10^{-6} |

Table A.7: Initial TDS and relative concentrations with respect to 300 g/L

| Period | Geology | Preliminary Geology | | GLL00 Geology | |
|-------------|------------------------|---------------------|----------------|---------------|----------------|
| | | TDS [g/L] | Relative Conc. | TDS [g/L] | Relative Conc. |
| Quaternary | Drift | 0.045 | 0.0 | 0.045 | 0.0 |
| Devonian | Traverse Group | 0.045 | 0.0 | 0.045 | 0.0 |
| | Dundee | 2.5 | 0.01 | 3 | 0.01 |
| | Detroit River Group † | 2.5 | 0.01 | 3 | 0.01 |
| | Bois Blanc | 2.5 | 0.01 | 3 | 0.01 |
| Silurian | Bass Islands | 2.5 | 0.01 | 3 | 0.01 |
| | G-Unit | 200 | 0.67 | 3 | 0.01 |
| | F-Unit | 200 | 0.67 | 300 | 1.0 |
| | F-Salt | 200 | 0.67 | 300 | 1.0 |
| | E-Unit | 200 | 0.67 | 300 | 1.0 |
| | D-Unit | 200 | 0.67 | 300 | 1.0 |
| | B&C Units | 200 | 0.67 | 300 | 1.0 |
| | B Anhydrite-Salt | 200 | 0.67 | 300 | 1.0 |
| | A2-Carbonate | 200 | 0.67 | 300 | 1.0 |
| | A2 Anhydrite-Salt | 200 | 0.67 | 300 | 1.0 |
| | A1-Carbonate | 200 | 0.67 | 300 | 1.0 |
| | A1-Evaporite | 200 | 0.67 | 300 | 1.0 |
| | Niagaran ‡ | 200 | 0.67 | 300 | 1.0 |
| | Fossil Hill | 200 | 0.67 | 300 | 1.0 |
| | Cabot Head | 200 | 0.67 | 300 | 1.0 |
| Manitoulin | 200 | 0.67 | 300 | 1.0 | |
| Ordovician | Queenston | 225 | 0.75 | 300 | 1.0 |
| | Georgian Bay/Blue Mtn. | 225 | 0.75 | 300 | 1.0 |
| | Cobourg | 112.5 | 0.38 | 300 | 1.0 |
| | Sherman Fall | 112.5 | 0.38 | 300 | 1.0 |
| | Kirkfield | 112.5 | 0.38 | 300 | 1.0 |
| | Coboconk | 112.5 | 0.38 | 300 | 1.0 |
| | Gull River | 112.5 | 0.38 | 300 | 1.0 |
| | Shadow Lake | 112.5 | 0.38 | 300 | 1.0 |
| Cambrian | Cambrian | 112.5 | 0.38 | 300 | 1.0 |
| Precambrian | Precambrian | 112.5 | 0.38 | 300 | 1.0 |

Note: † Includes the Lucas/Amherstburg listed in Table 1

‡ The Niagaran Group is comprised of the Guelph, Goat Island, Gasport and Lions Head

APPENDIX B – ANALYSIS OF SURFACE BOUNDARY CONDITION

LIST OF FIGURES

| | Page |
|--|-------------|
| Figure B.1. Environmental heads for the base case parameters, no weathered zone at the surface and a prescribed water table | 130 |
| Figure B.2. Fence diagram of environmental heads for the base case parameters, no weathered zone at the surface and a prescribed water table. | 130 |
| Figure B.3. Pore water velocity magnitude for the base case parameters, no weathered zone at the surface and a prescribed water table. | 131 |
| Figure B.4. Ratio of vertical velocity to the velocity magnitude for the base case parameters, no weathered zone at the surface and a prescribed water table. | 131 |
| Figure B.5. Fence diagram of the ratio of vertical velocity to the velocity magnitude for the base case parameters, no weathered zone at the surface and a prescribed water table. | 132 |
| Figure B.6. Mean life expectancies for the base case parameters, no weathered zone at the surface and a prescribed water table. | 132 |
| Figure B.7. Fence diagram showing the mean life expectancies for the base case parameters, no weathered zone at the surface and a prescribed water table. | 133 |
| Figure B.8. Environmental heads for the base case parameters, 20 m weathered zone at the surface and a prescribed net recharge of 0.27 mm/yr. | 133 |
| Figure B.9. Fence diagram of environmental heads for the base case parameters, 20 m weathered zone at the surface and a prescribed net recharge of 0.27 mm/yr. | 134 |
| Figure B.10. Pore water velocity magnitude for the base case parameters, 20 m weathered zone at the surface and a prescribed net recharge of 0.27 mm/yr. | 134 |
| Figure B.11. Ratio of vertical velocity to the velocity magnitude for the base case parameters, 20 m weathered zone at the surface and a prescribed net recharge of 0.27 mm/yr. | 135 |
| Figure B.12. Fence diagram of the ratio of vertical velocity to the velocity magnitude for the base case parameters, 20 m weathered zone at the surface and a prescribed net recharge of 0.27 mm/yr. | 135 |
| Figure B.13. Mean life expectancies for the base case parameters, 20 m weathered zone at the surface and a prescribed net recharge of 0.27 mm/yr. | 136 |
| Figure B.14. Fence diagram showing the mean life expectancies for the base case parameters, 20 m weathered zone at the surface and a prescribed net recharge of 0.27 mm/yr. | 136 |

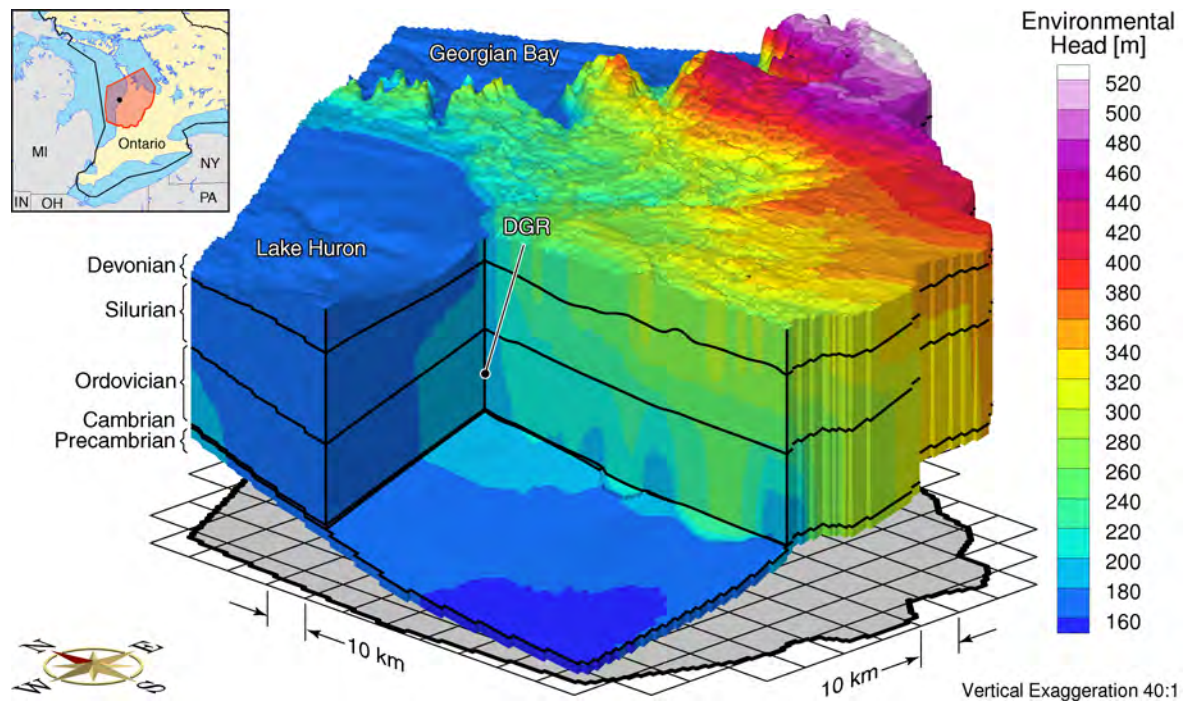


Figure B.1: Environmental heads for the base case parameters, no weathered zone at the surface and a prescribed water table

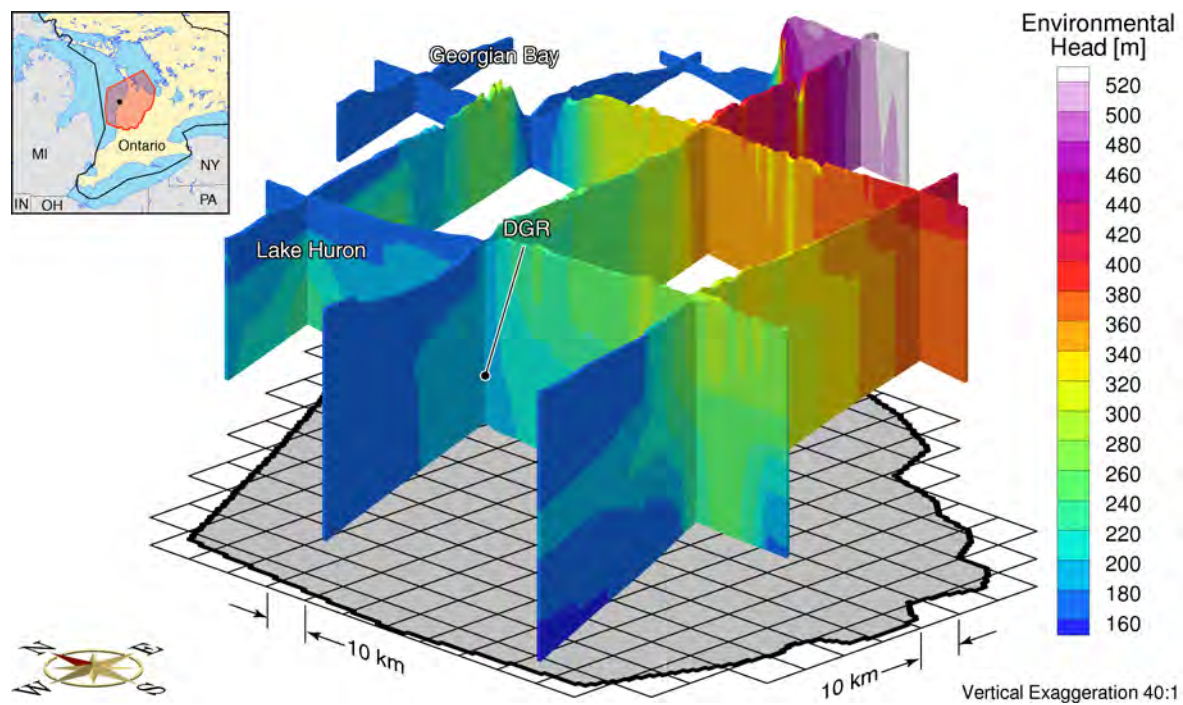


Figure B.2: Fence diagram of environmental heads for the base case parameters, no weathered zone at the surface and a prescribed water table.

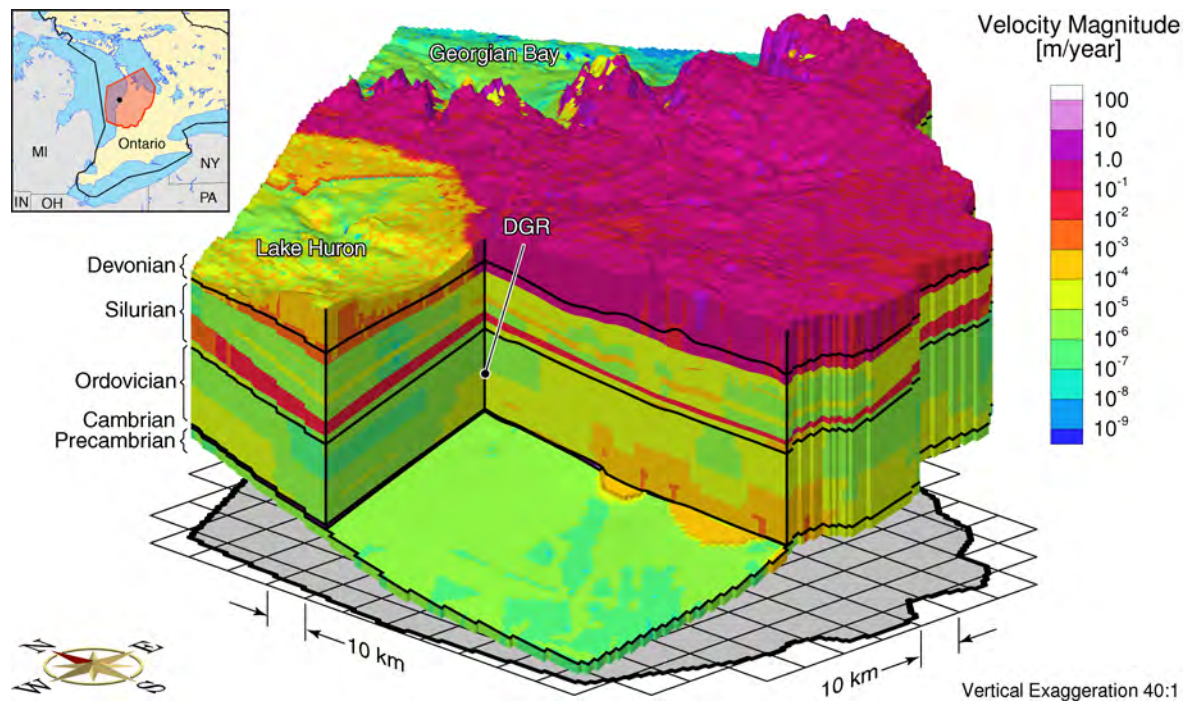


Figure B.3: Pore water velocity magnitude for the base case parameters, no weathered zone at the surface and a prescribed water table.

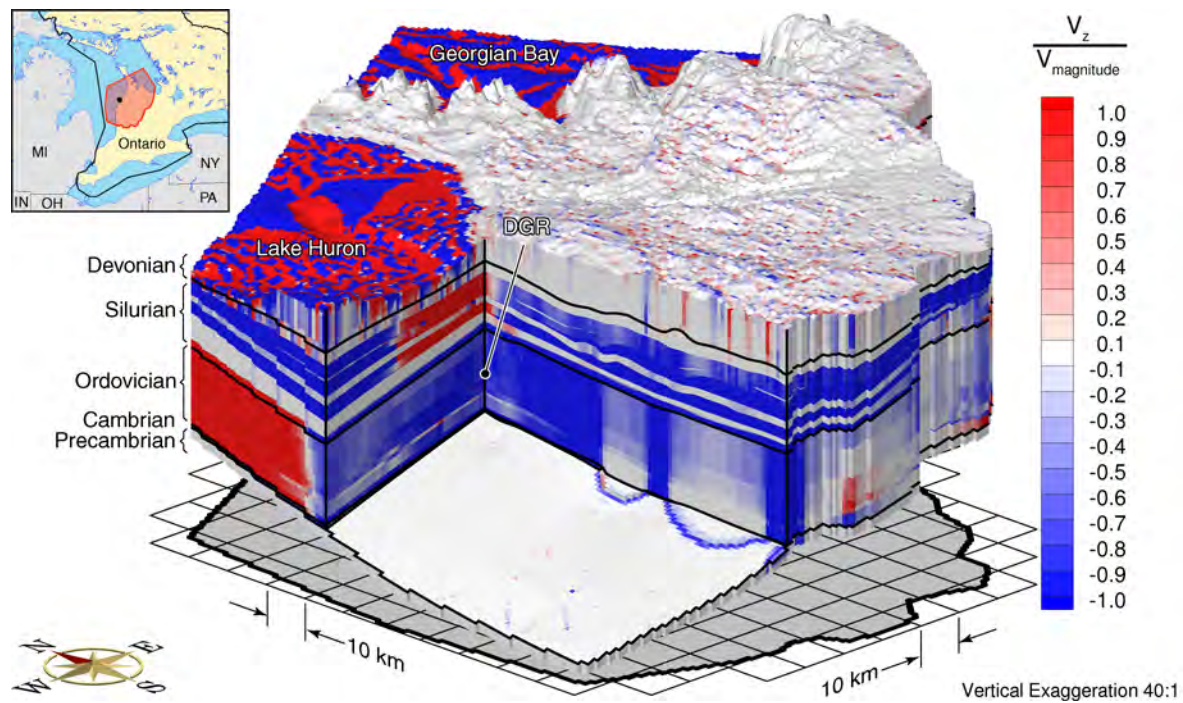


Figure B.4: Ratio of vertical velocity to the velocity magnitude for the base case parameters, no weathered zone at the surface and a prescribed water table.

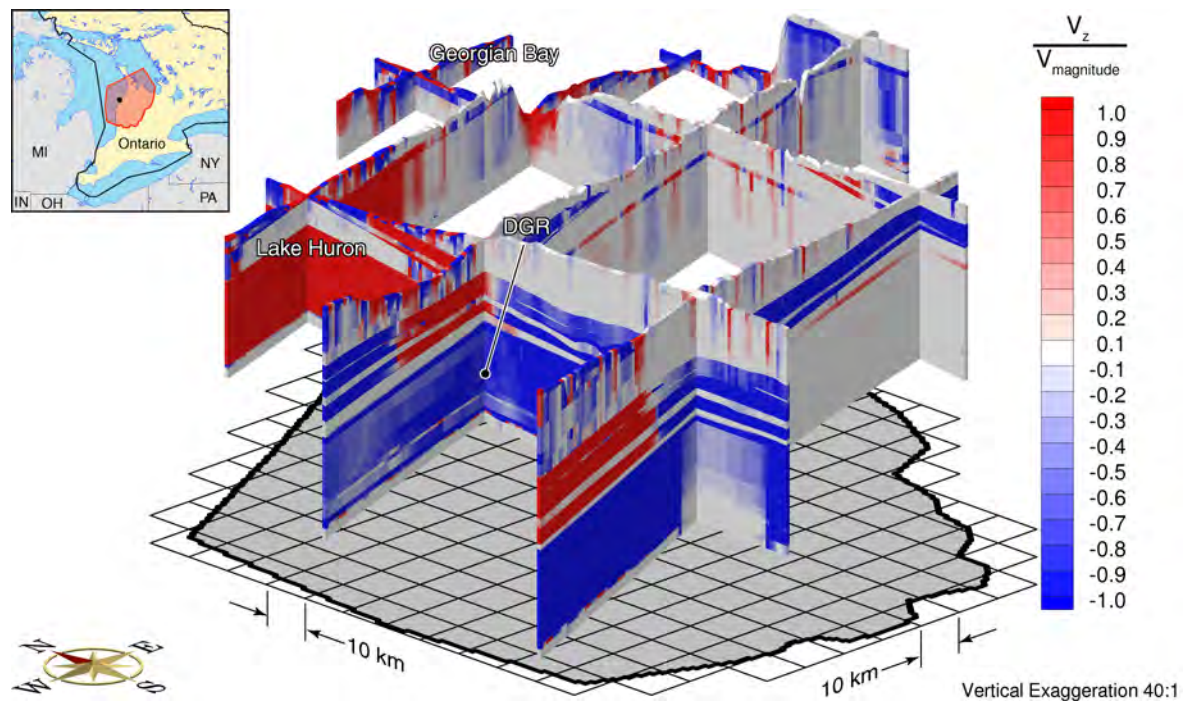


Figure B.5: Fence diagram of the ratio of vertical velocity to the velocity magnitude for the base case parameters, no weathered zone at the surface and a prescribed water table.

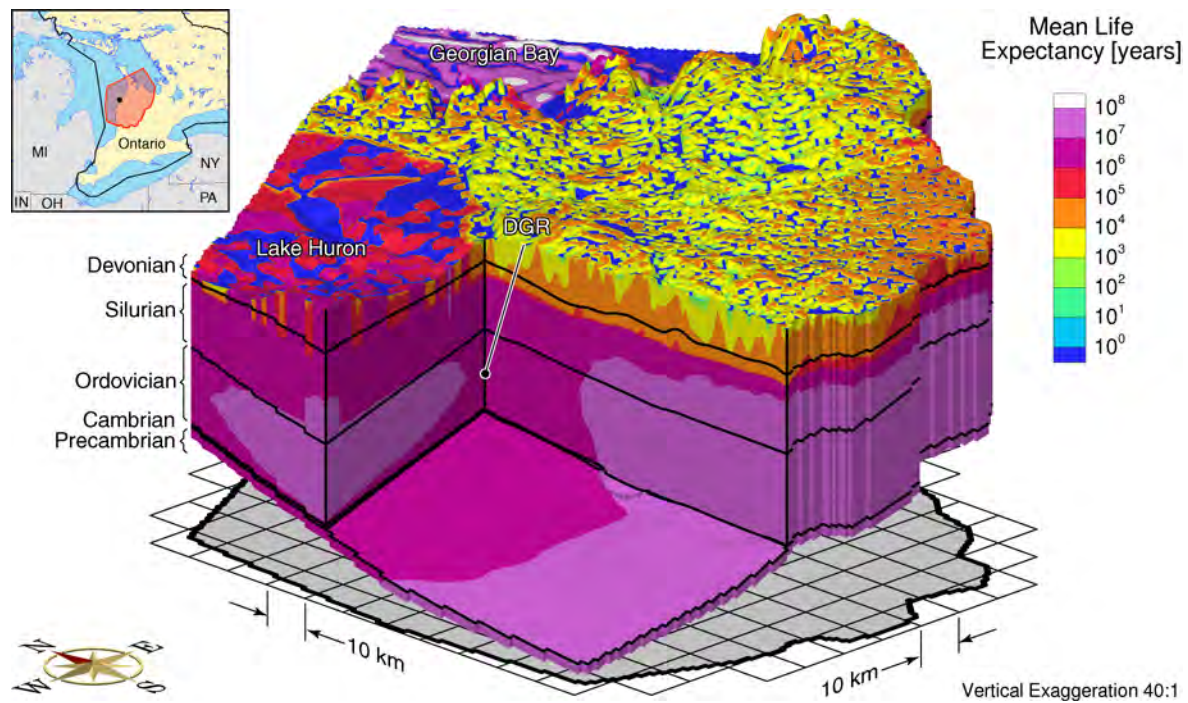


Figure B.6: Mean life expectancies for the base case parameters, no weathered zone at the surface and a prescribed water table.

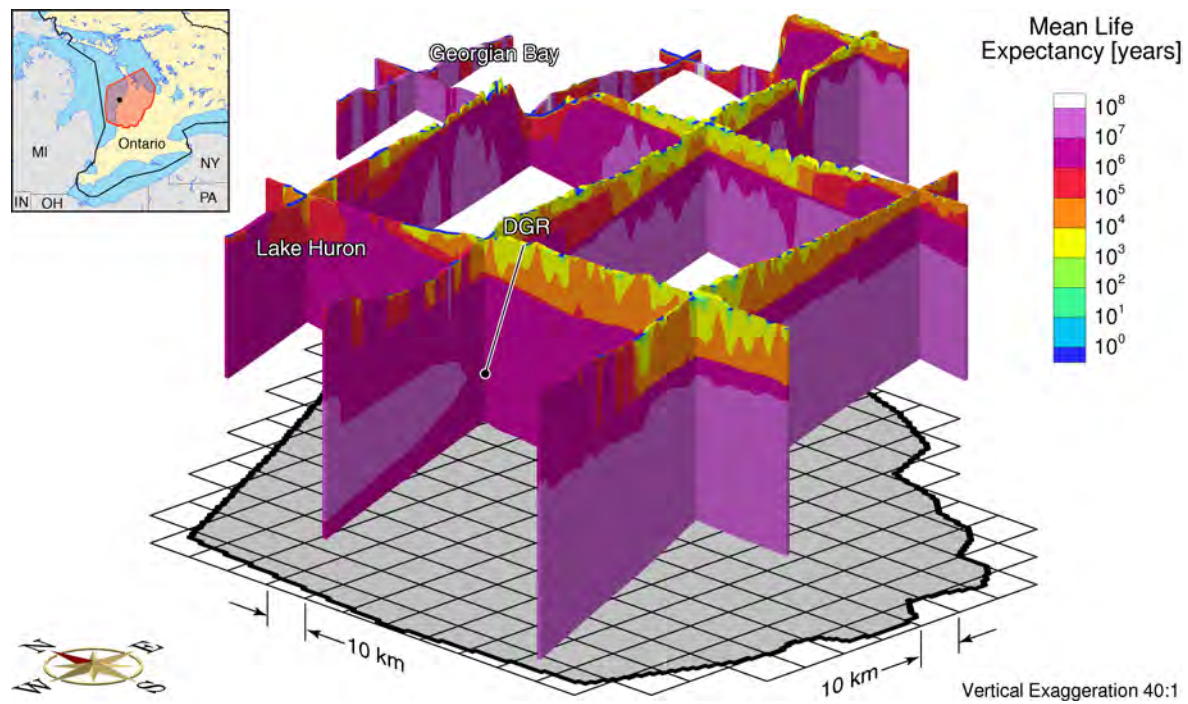


Figure B.7: Fence diagram showing the mean life expectancies for the base case parameters, no weathered zone at the surface and a prescribed water table.

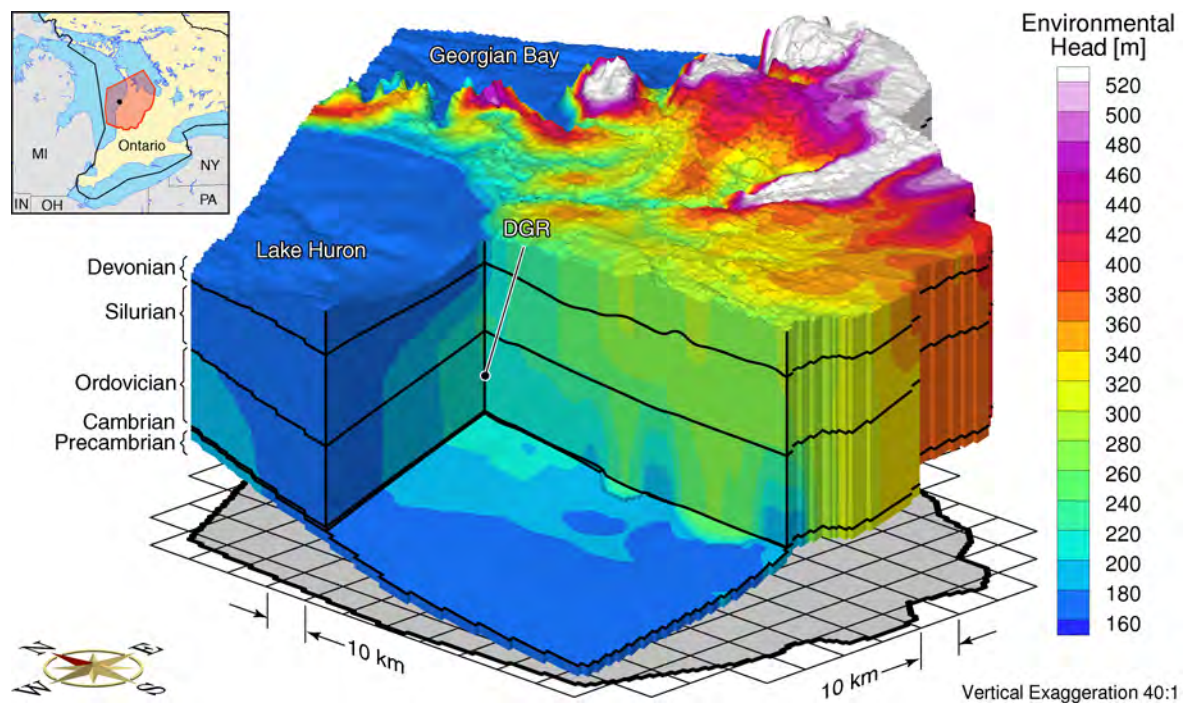


Figure B.8: Environmental heads for the base case parameters, 20 m weathered zone at the surface and a prescribed net recharge of 0.27 mm/yr.

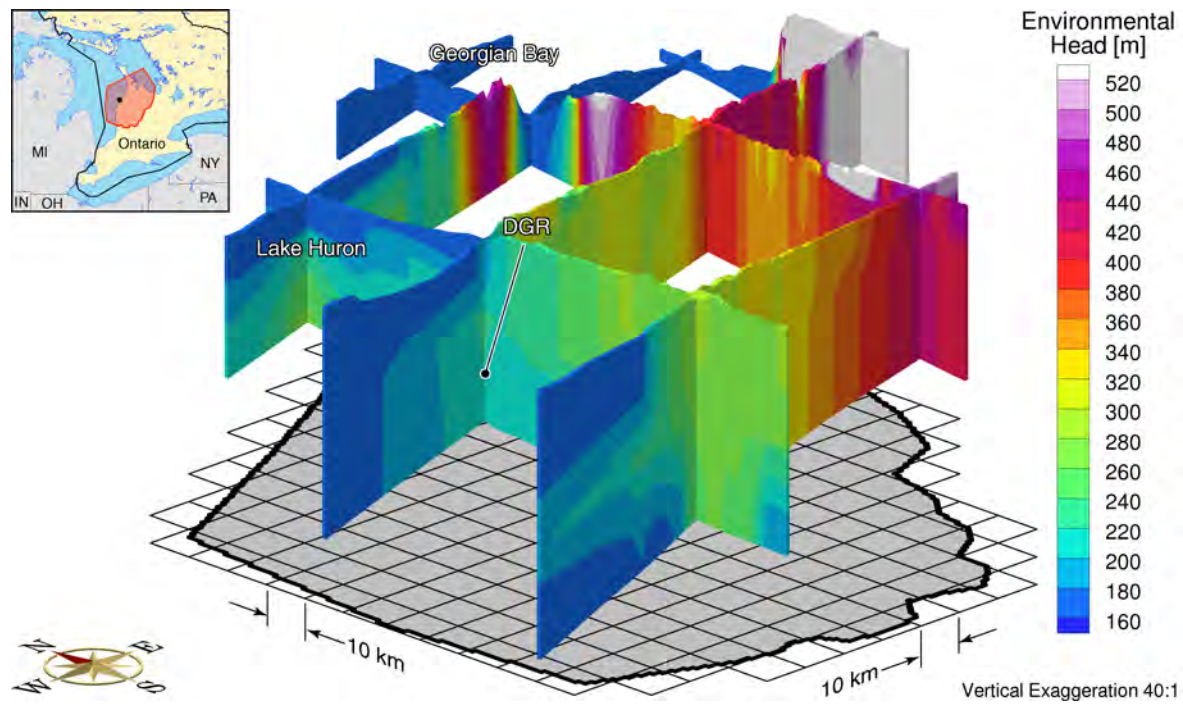


Figure B.9: Fence diagram of environmental heads for the base case parameters, 20 m weathered zone at the surface and a prescribed net recharge of 0.27 mm/yr.

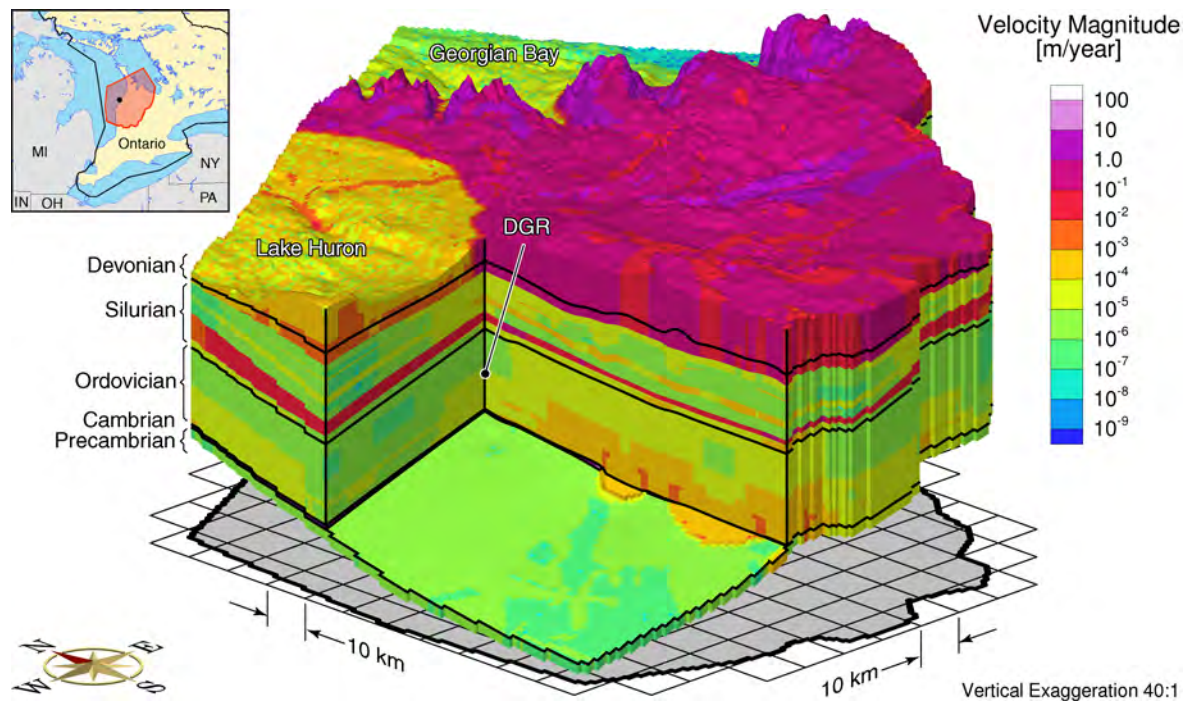


Figure B.10: Pore water velocity magnitude for the base case parameters, 20 m weathered zone at the surface and a prescribed net recharge of 0.27 mm/yr.

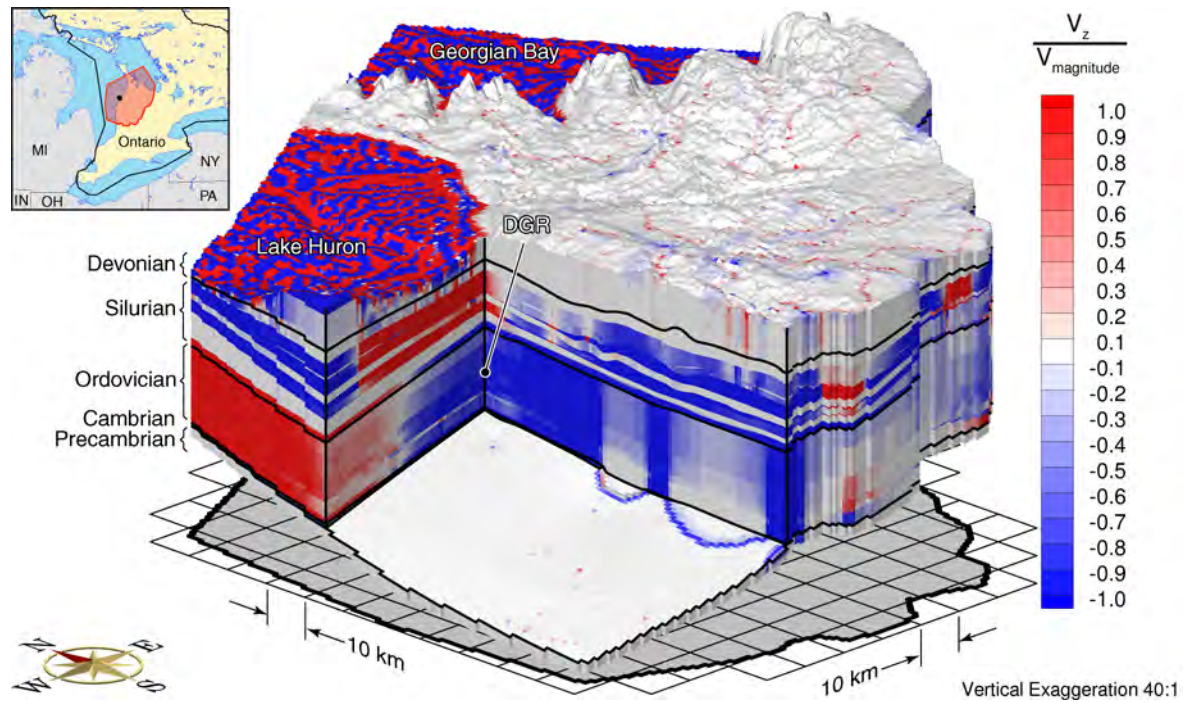


Figure B.11: Ratio of vertical velocity to the velocity magnitude for the base case parameters, 20 m weathered zone at the surface and a prescribed net recharge of 0.27 mm/yr.

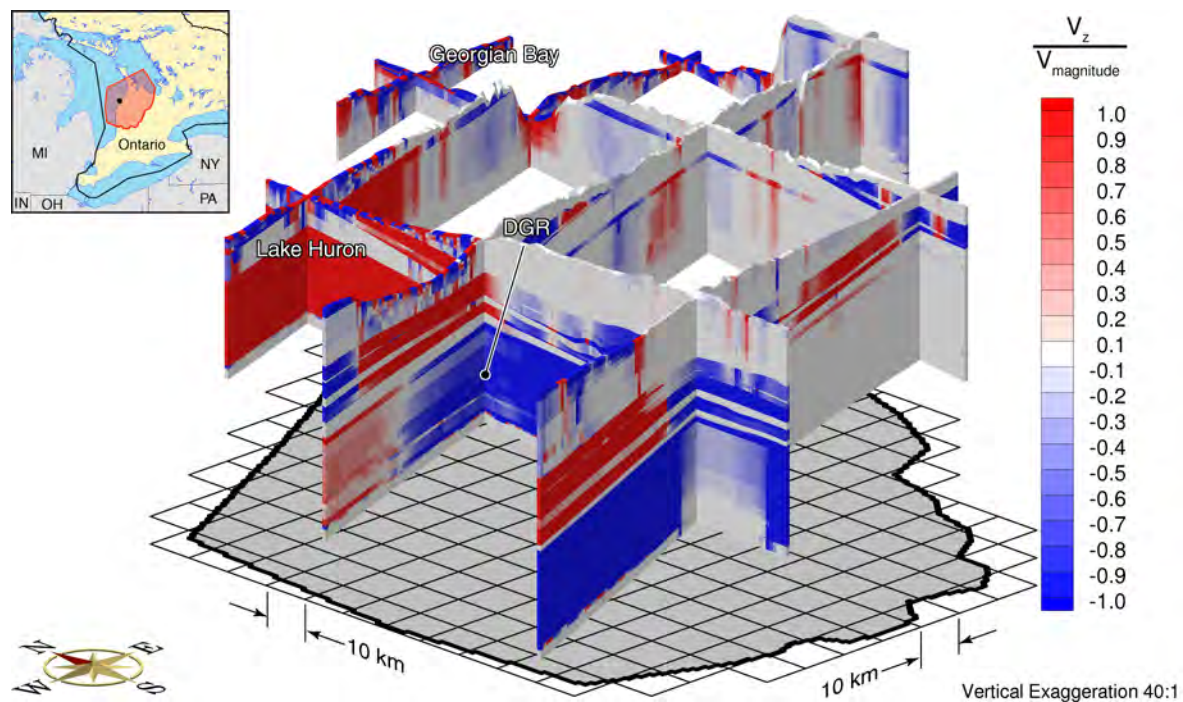


Figure B.12: Fence diagram of the ratio of vertical velocity to the velocity magnitude for the base case parameters, 20 m weathered zone at the surface and a prescribed net recharge of 0.27 mm/yr.

APPENDIX C – IMPACT OF CONSTANT FLUID DENSITY**LIST OF FIGURES**

| | Page |
|---|-------------|
| Figure C.1. Piezometric heads for the base case parameters and constant freshwater fluid density. | 138 |
| Figure C.2. Fence diagram of piezometric heads for the base case parameters and constant freshwater fluid density. | 138 |
| Figure C.3. Pore water velocity magnitude for the base case parameters and constant freshwater fluid density. | 139 |
| Figure C.4. Ratio of vertical velocity to the velocity magnitude for the base case parameters and constant freshwater fluid density. | 139 |
| Figure C.5. Fence diagram of the ratio of vertical velocity to the velocity magnitude for the base case parameters and constant freshwater fluid density. | 140 |
| Figure C.6. Mean life expectancies for the base case parameters and constant freshwater fluid density. | 140 |
| Figure C.7. Fence diagram showing the mean life expectancies for the base case parameters and constant freshwater fluid density. | 141 |

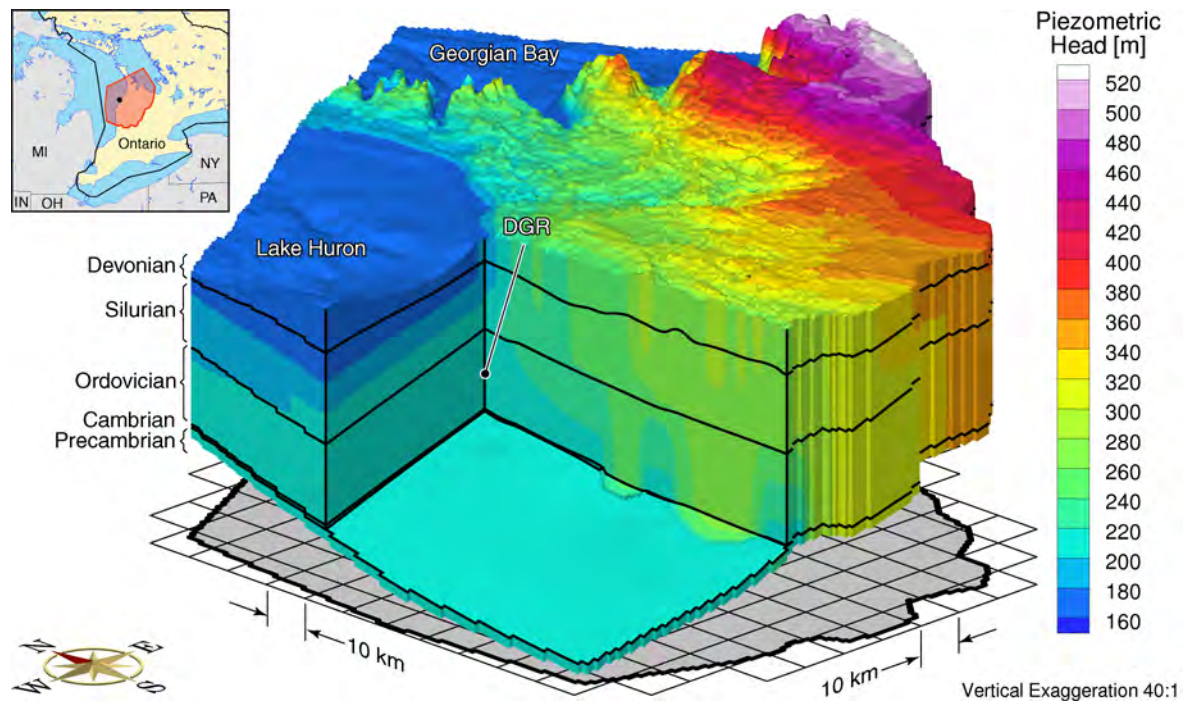


Figure C.1: Piezometric heads for the base case parameters and constant freshwater fluid density.

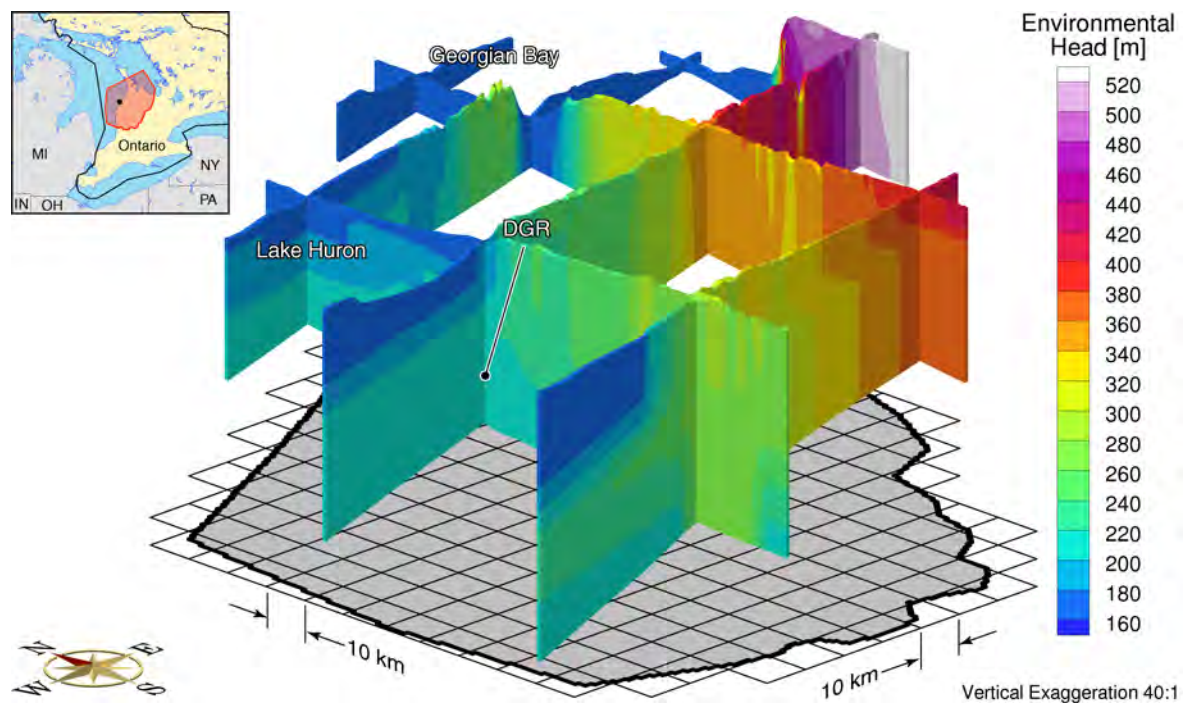


Figure C.2: Fence diagram of piezometric heads for the base case parameters and constant freshwater fluid density.

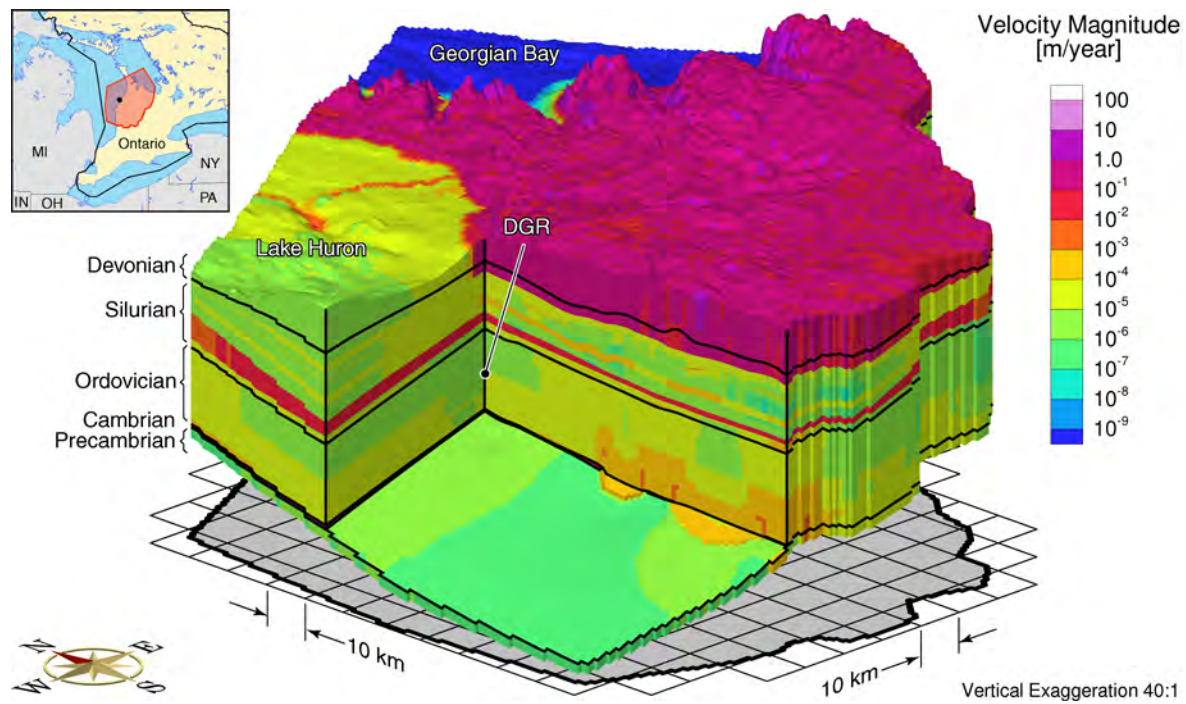


Figure C.3: Pore water velocity magnitude for the base case parameters and constant fresh-water fluid density.

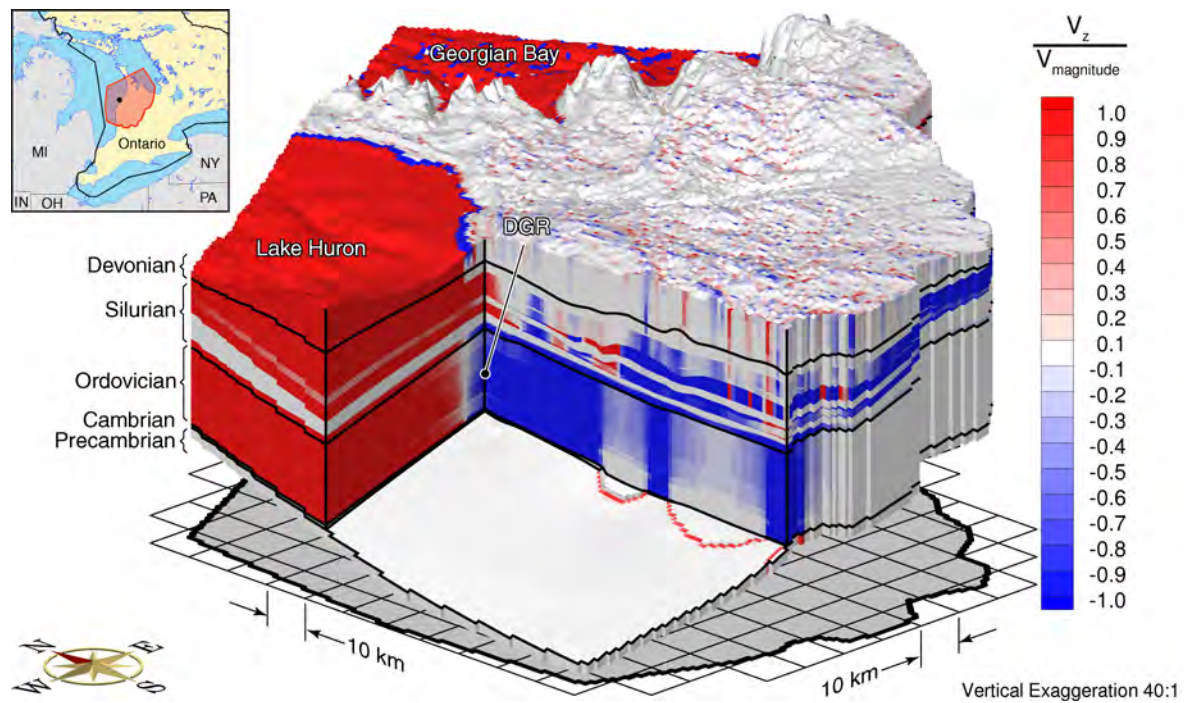


Figure C.4: Ratio of vertical velocity to the velocity magnitude for the base case parameters and constant freshwater fluid density.

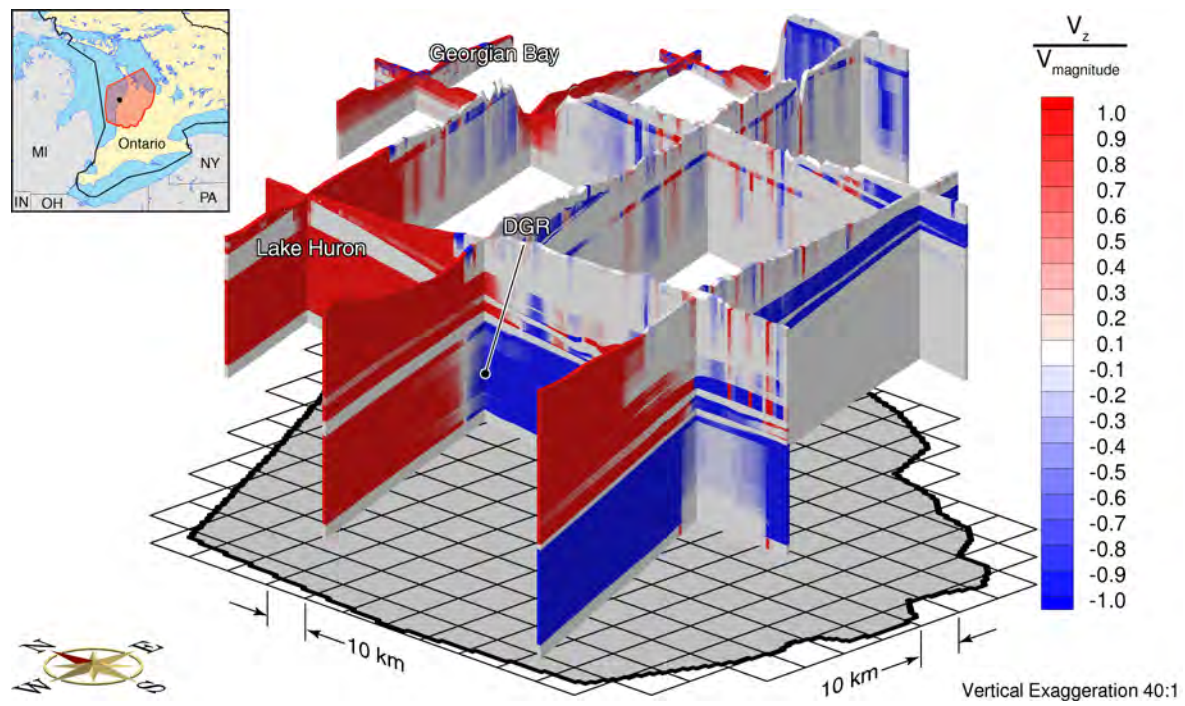


Figure C.5: Fence diagram of the ratio of vertical velocity to the velocity magnitude for the base case parameters and constant freshwater fluid density.

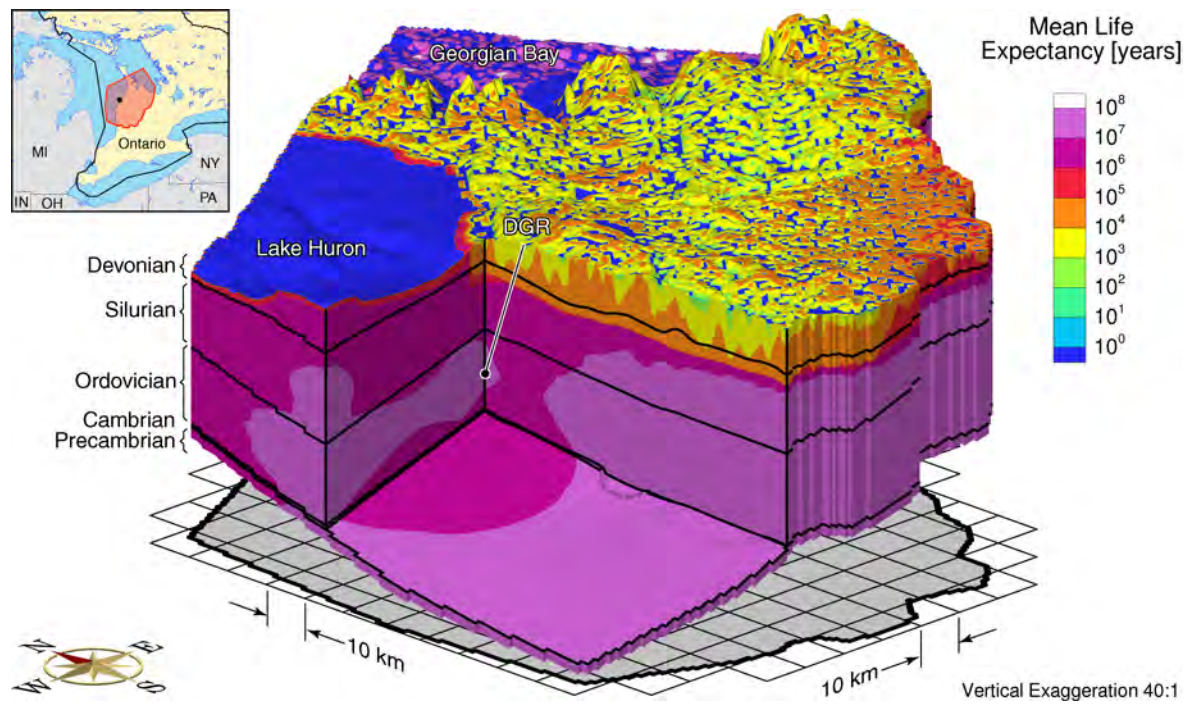


Figure C.6: Mean life expectancies for the base case parameters and constant freshwater fluid density.

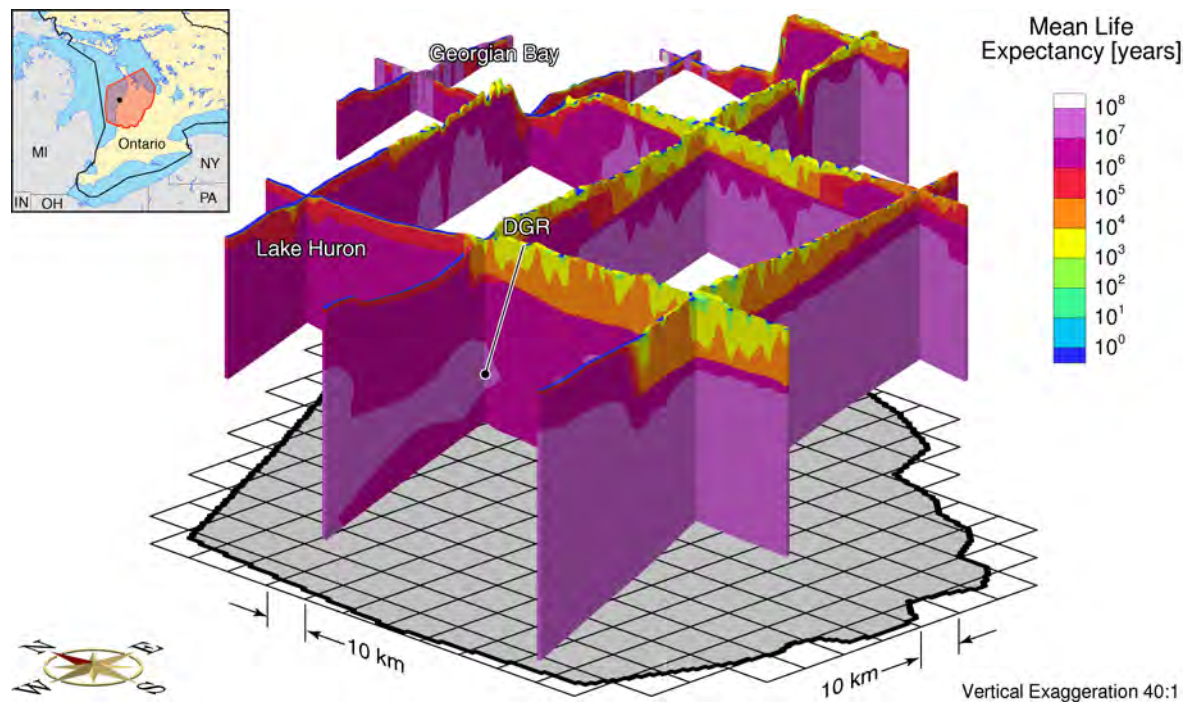


Figure C.7: Fence diagram showing the mean life expectancies for the base case parameters and constant freshwater fluid density.

APPENDIX D – ALTERNATE HYDRAULIC CONDUCTIVITY DISTRIBUTIONS FOR THE ORDOVICIAN FORMATIONS

LIST OF FIGURES

| | Page |
|--|-------------|
| Figure D.1. Mean life expectancies for the parameter P-case 1. | 144 |
| Figure D.2. Fence diagram showing the mean life expectancies for the parameter P-case 1. | 144 |
| Figure D.3. Mean life expectancies for the parameter P-case 2. | 145 |
| Figure D.4. Fence diagram showing the mean life expectancies for the parameter P-case 2. | 145 |
| Figure D.5. Mean life expectancies for the parameter P-case 3. | 146 |
| Figure D.6. Fence diagram showing the mean life expectancies for the parameter P-case 3. | 146 |

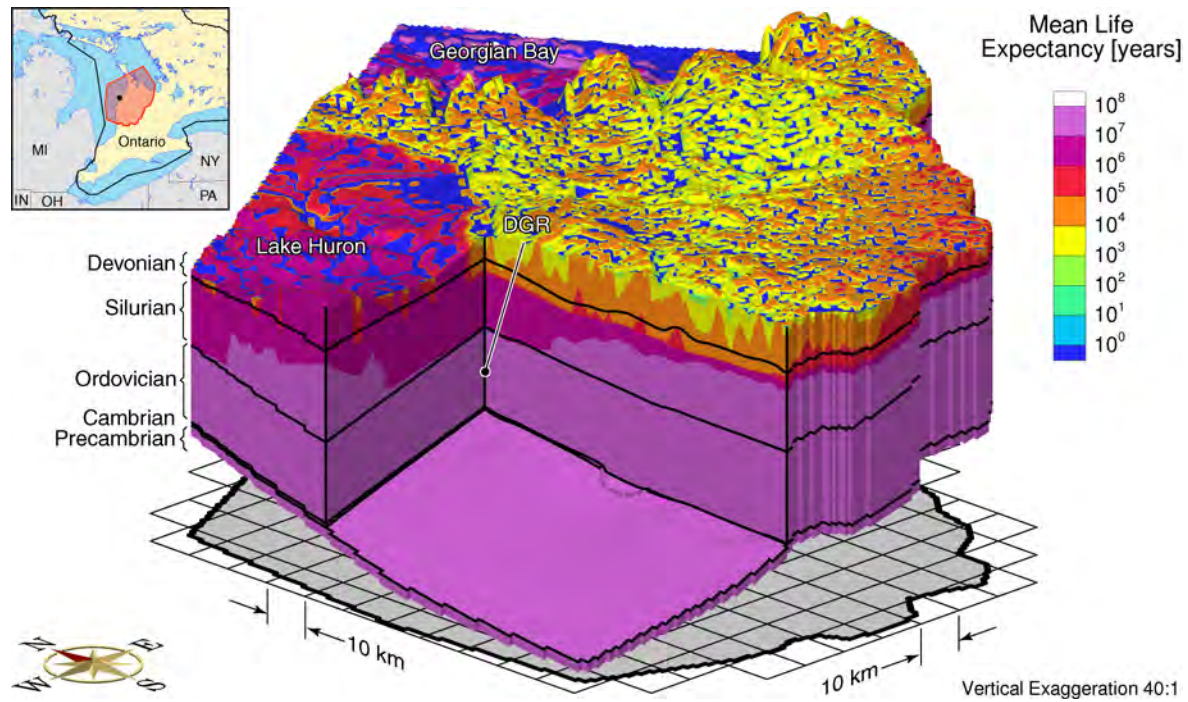


Figure D.1: Mean life expectancies for the parameter P-case 1.

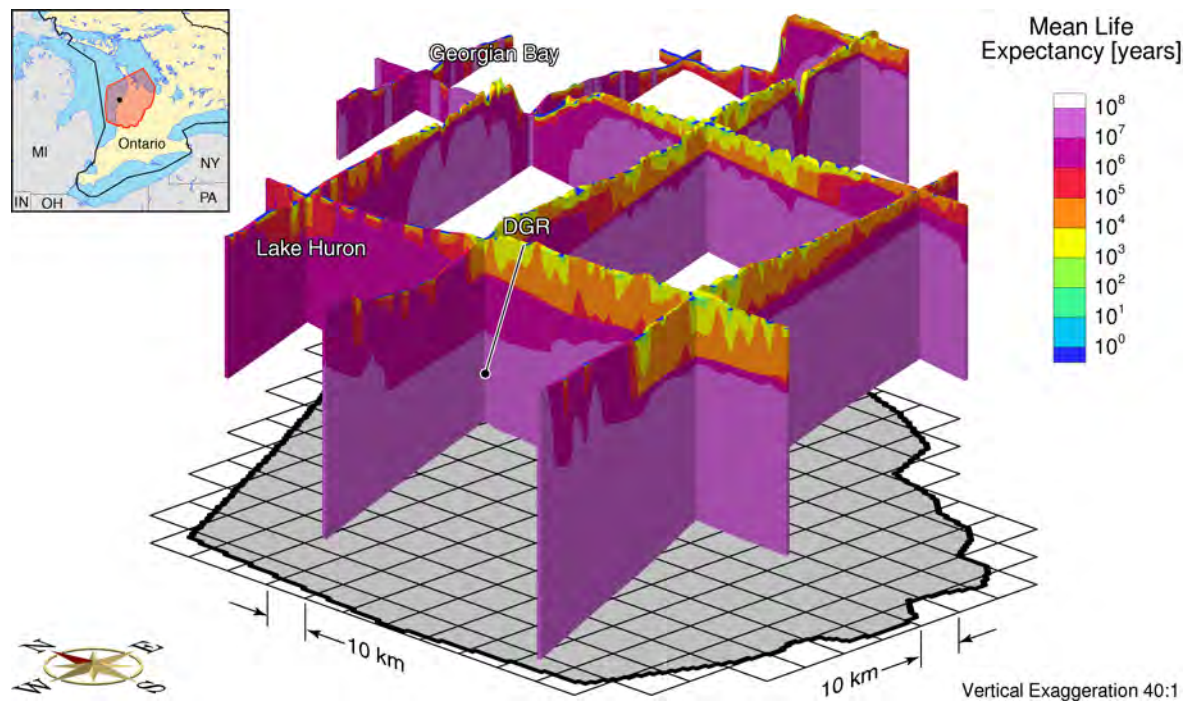


Figure D.2: Fence diagram showing the mean life expectancies for the parameter P-case 1.

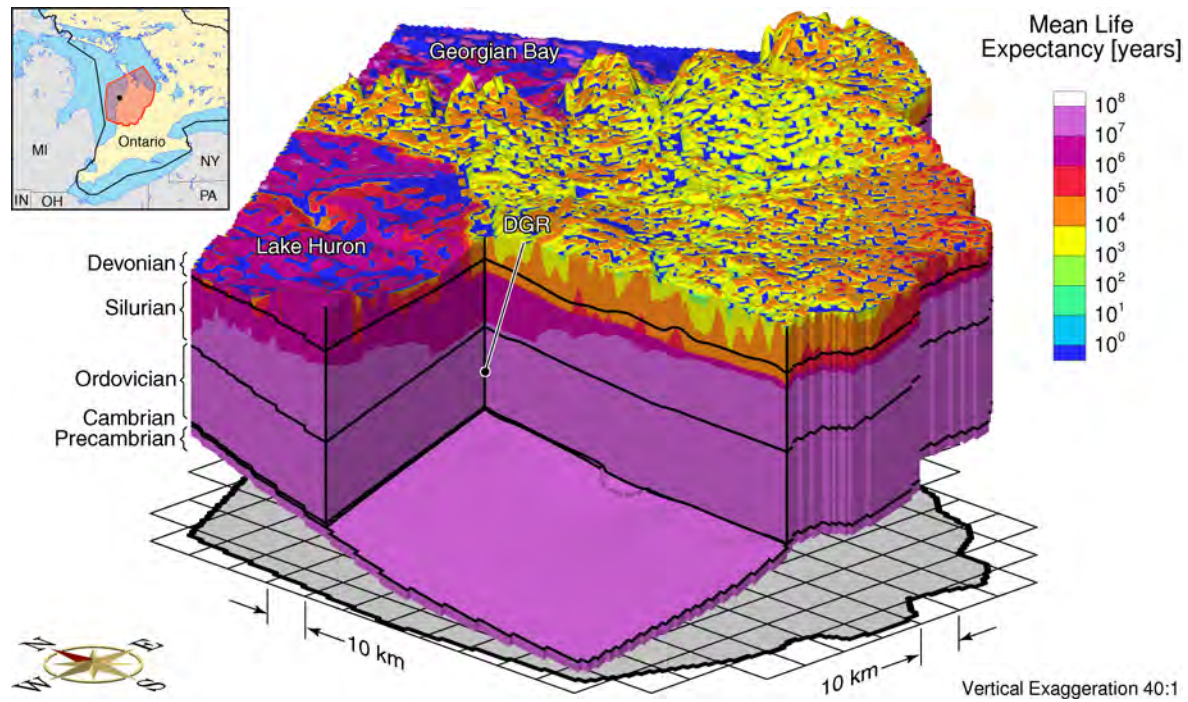


Figure D.3: Mean life expectancies for the parameter P-case 2.

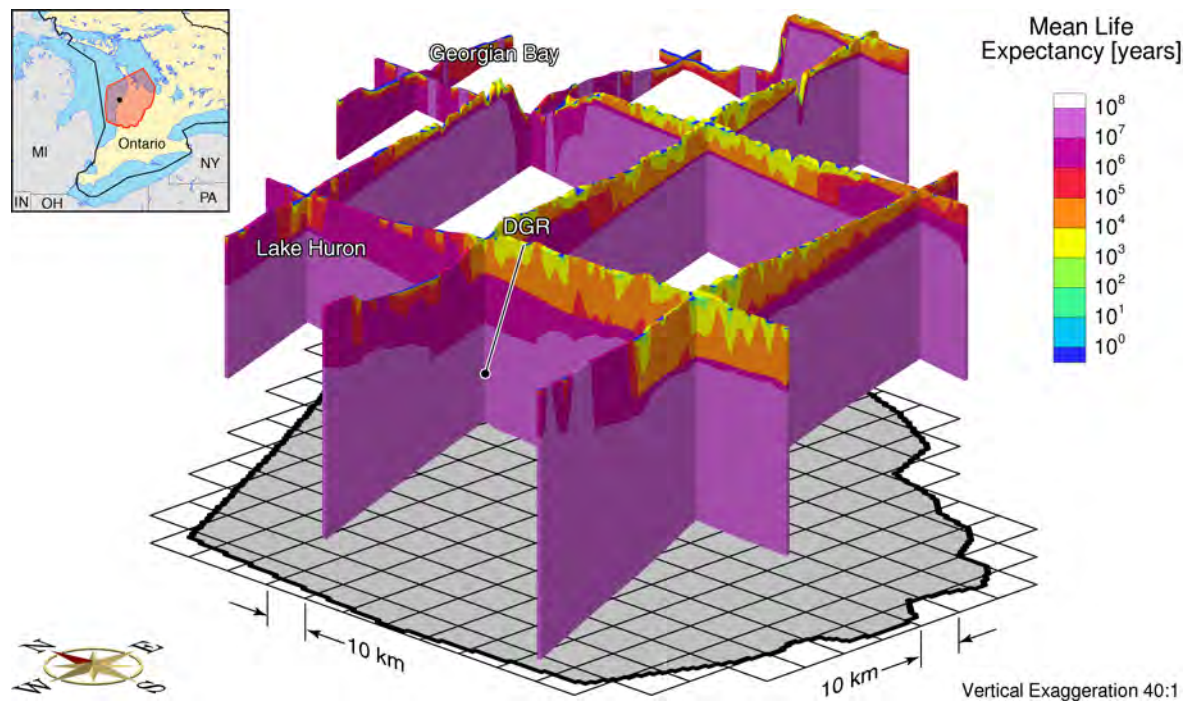


Figure D.4: Fence diagram showing the mean life expectancies for the parameter P-case 2.

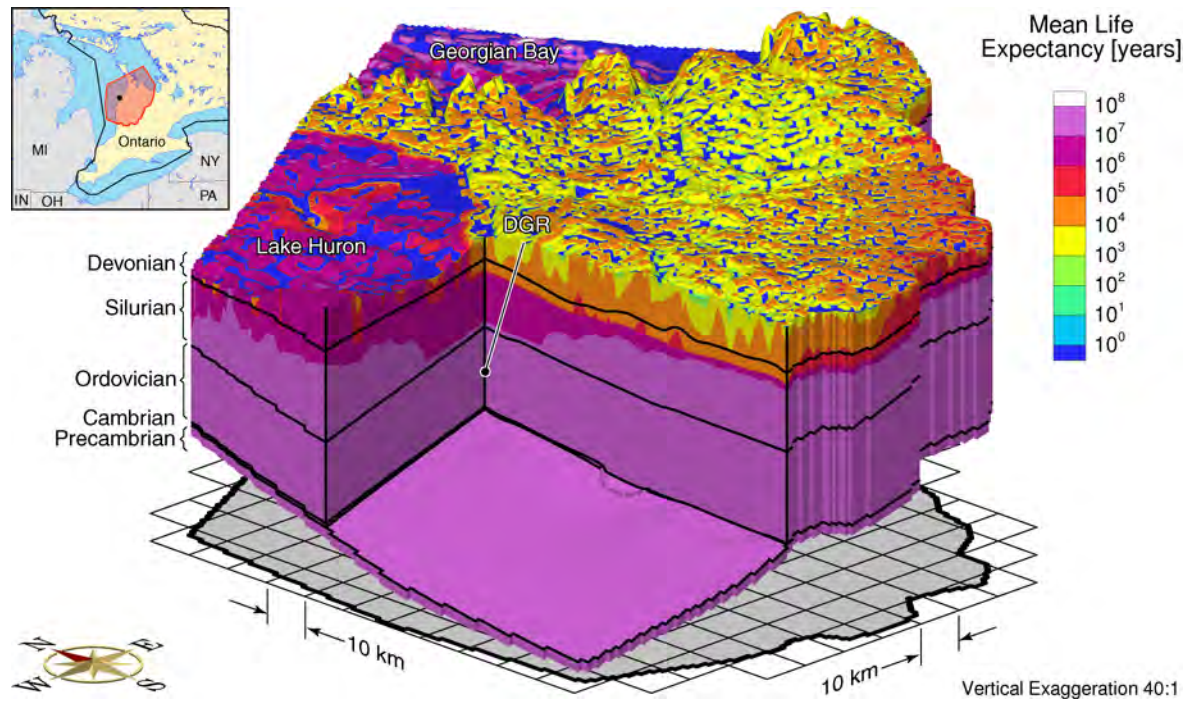


Figure D.5: Mean life expectancies for the parameter P-case 3.

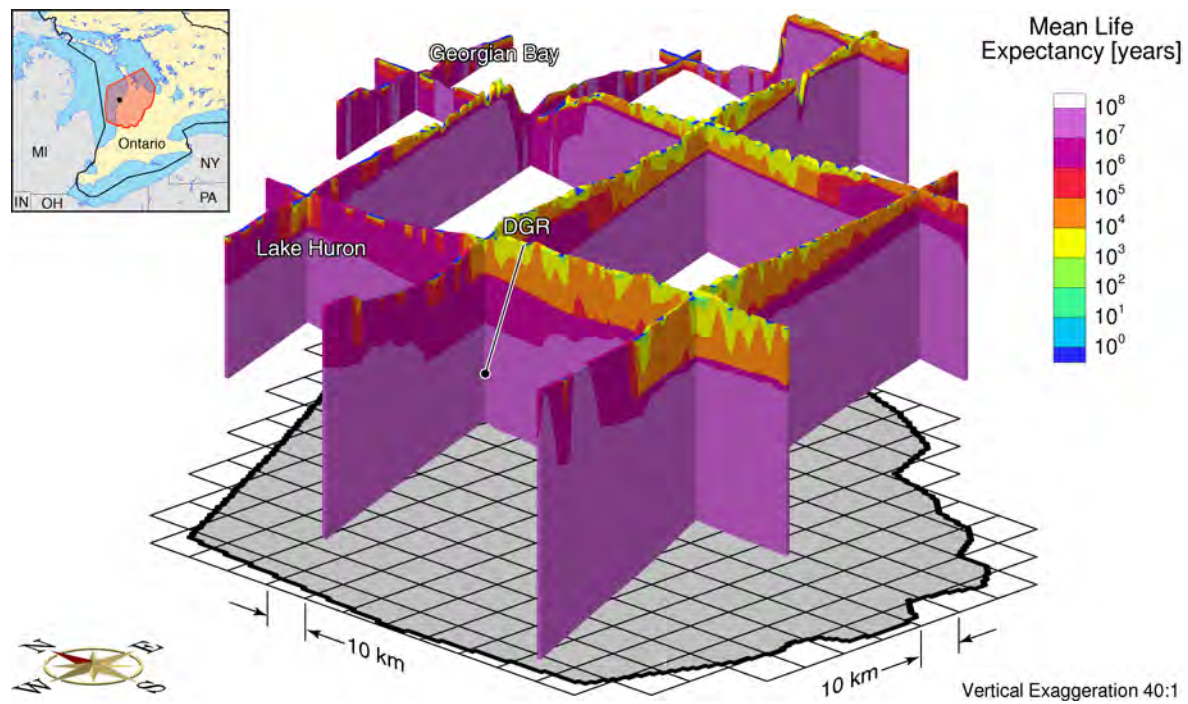


Figure D.6: Fence diagram showing the mean life expectancies for the parameter P-case 3.

APPENDIX E – ALTERNATE HYDRAULIC CONDUCTIVITY DISTRIBUTIONS FOR THE SILURIAN FORMATIONS

LIST OF FIGURES

| | | Page |
|--------------|---|-------------|
| Figure E.1. | Environmental heads for the parameter case S-1. | 148 |
| Figure E.2. | Fence diagram of environmental heads for the parameter case S-1. | 148 |
| Figure E.3. | Ratio of vertical velocity to the velocity magnitude for the parameter case S-1. | 149 |
| Figure E.4. | Fence diagram of the ratio of vertical velocity to the velocity magnitude for the parameter case S-1. | 149 |
| Figure E.5. | Pore water velocity magnitude for the parameter case S-1. | 150 |
| Figure E.6. | Total dissolved solids concentration for the parameter case S-1. | 150 |
| Figure E.7. | Mean life expectancies for the parameter case S-1. | 151 |
| Figure E.8. | Fence diagram showing the mean life expectancies for the parameter case S-1. | 151 |
| Figure E.9. | Environmental heads for the parameter case S-2. | 152 |
| Figure E.10. | Fence diagram of environmental heads for the parameter case S-2. | 152 |
| Figure E.11. | Ratio of vertical velocity to the velocity magnitude for the parameter case S-2. | 153 |
| Figure E.12. | Fence diagram of the ratio of vertical velocity to the velocity magnitude for the parameter case S-2. | 153 |
| Figure E.13. | Pore water velocity magnitude for the parameter case S-2. | 154 |
| Figure E.14. | Total dissolved solids concentration for the parameter case S-2. | 154 |
| Figure E.15. | Mean life expectancies for the parameter case S-2. | 155 |
| Figure E.16. | Fence diagram showing the mean life expectancies for the parameter case S-2. | 155 |

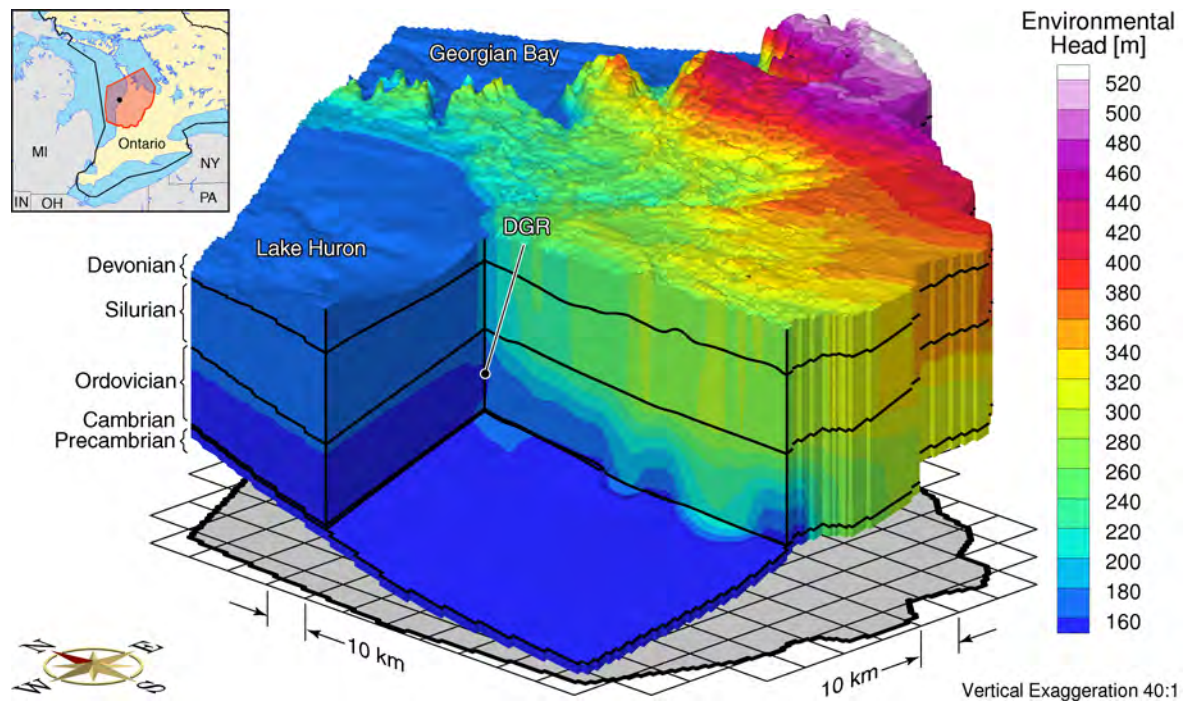


Figure E.1: Environmental heads for the parameter case S-1.

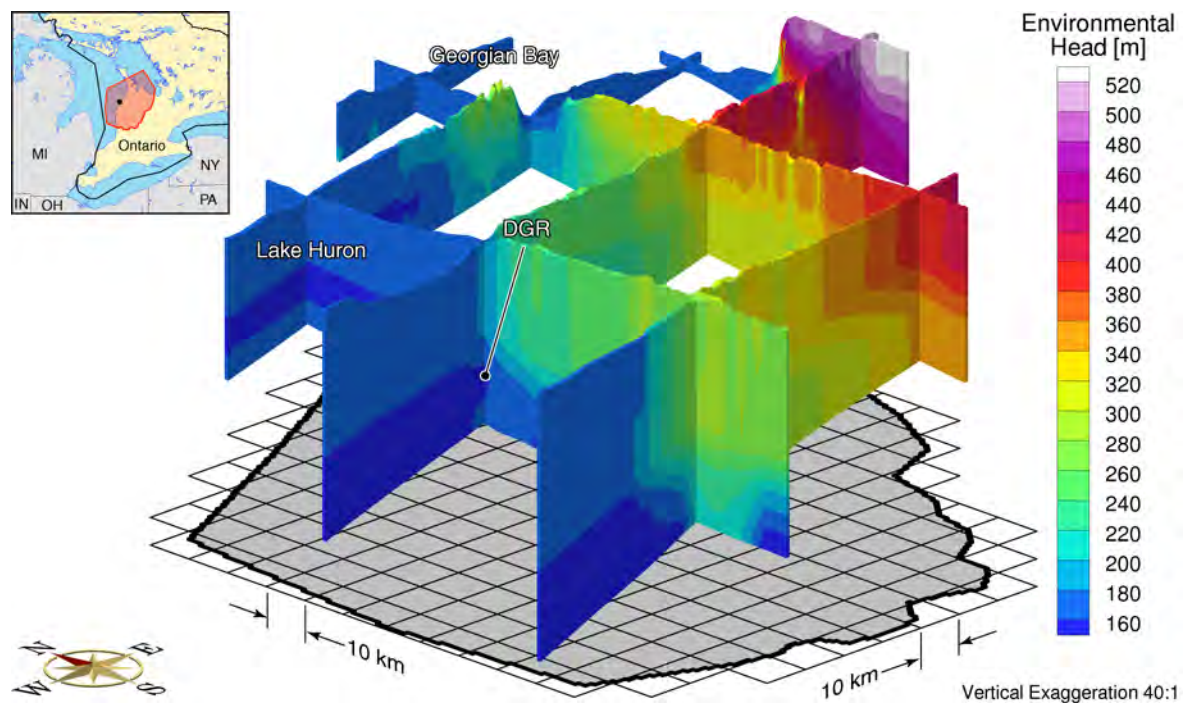


Figure E.2: Fence diagram of environmental heads for the parameter case S-1.

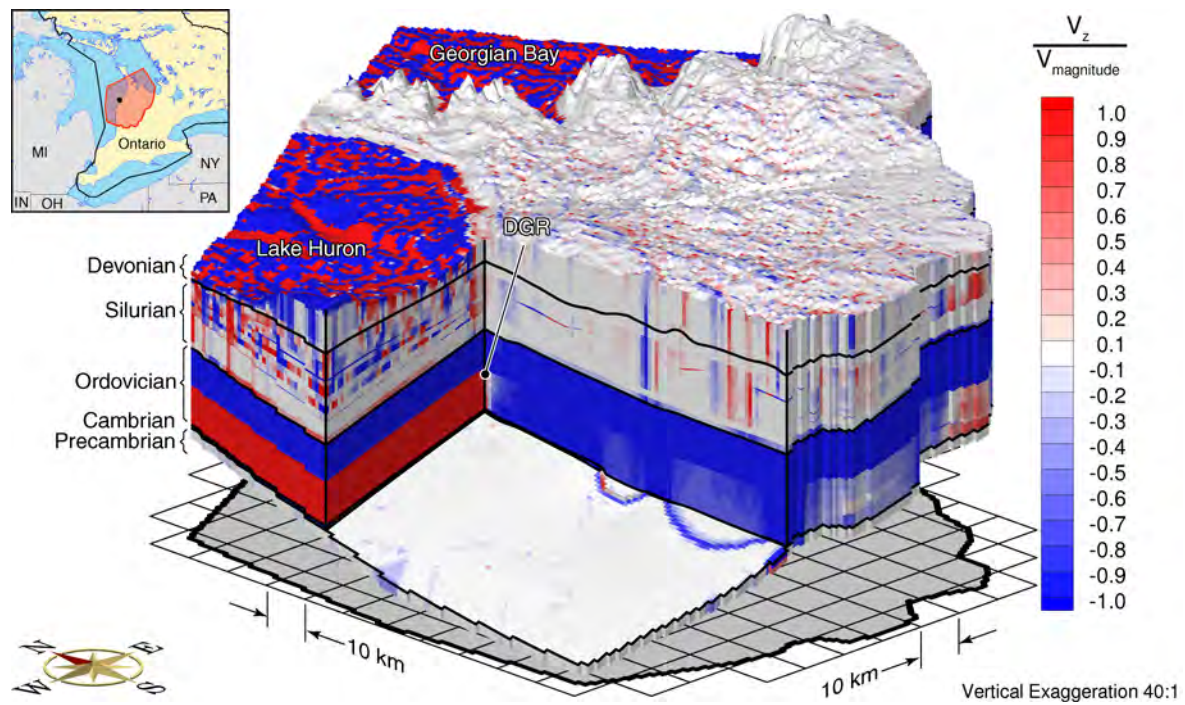


Figure E.3: Ratio of vertical velocity to the velocity magnitude for the parameter case S-1.

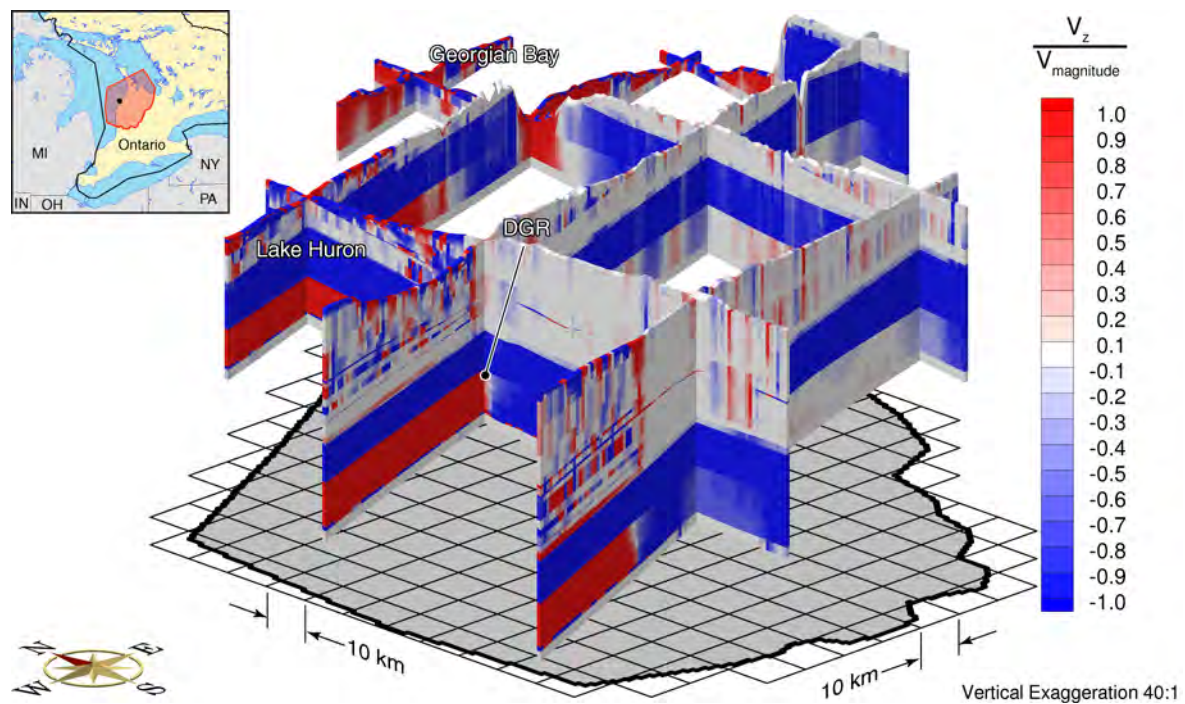


Figure E.4: Fence diagram of the ratio of vertical velocity to the velocity magnitude for the parameter case S-1.

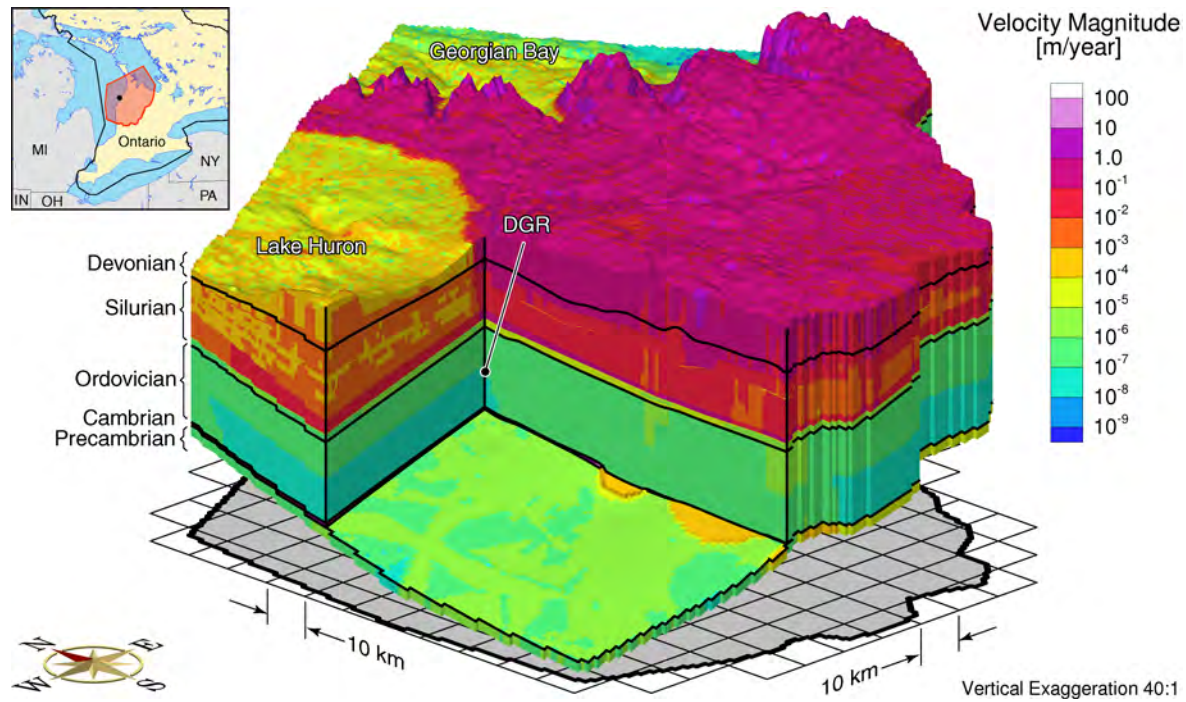


Figure E.5: Pore water velocity magnitude for the parameter case S-1.

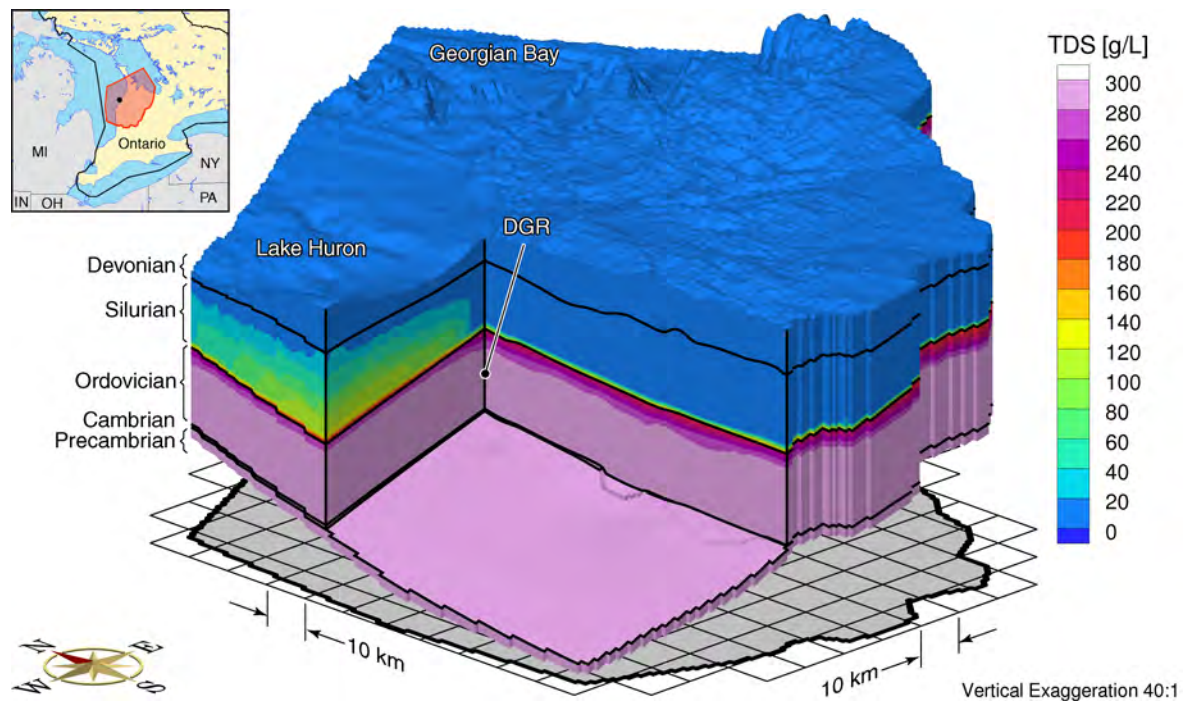


Figure E.6: Total dissolved solids concentration for the parameter case S-1.

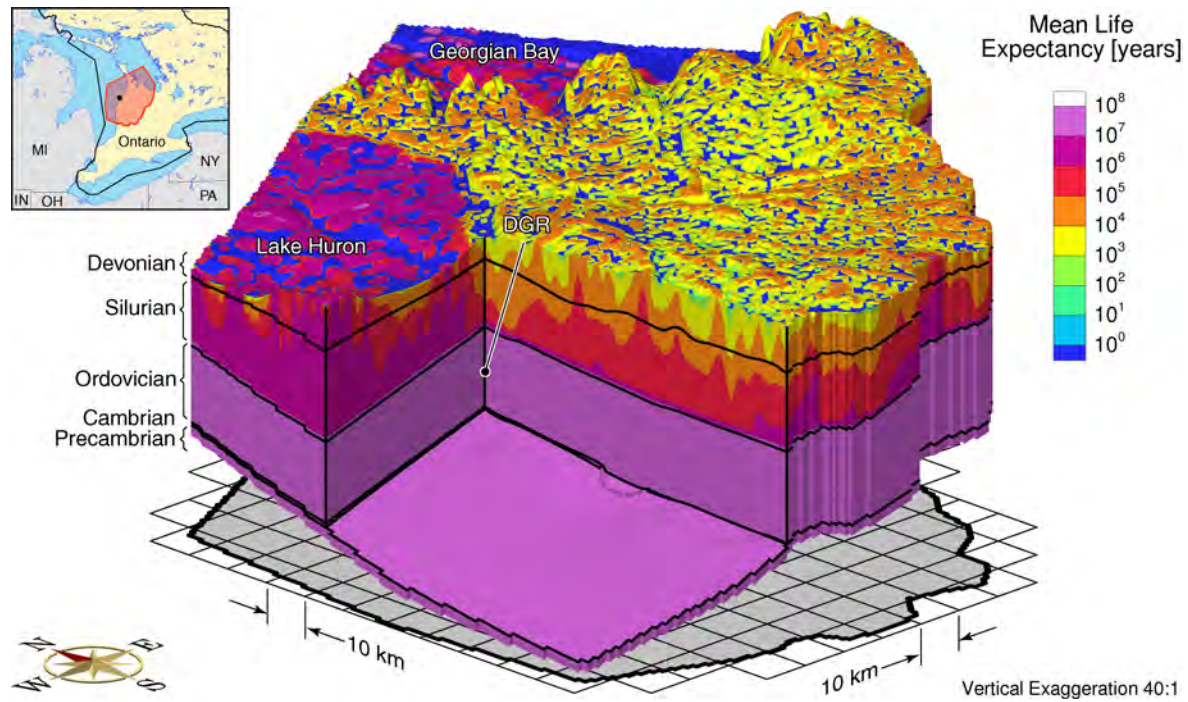


Figure E.7: Mean life expectancies for the parameter case S-1.

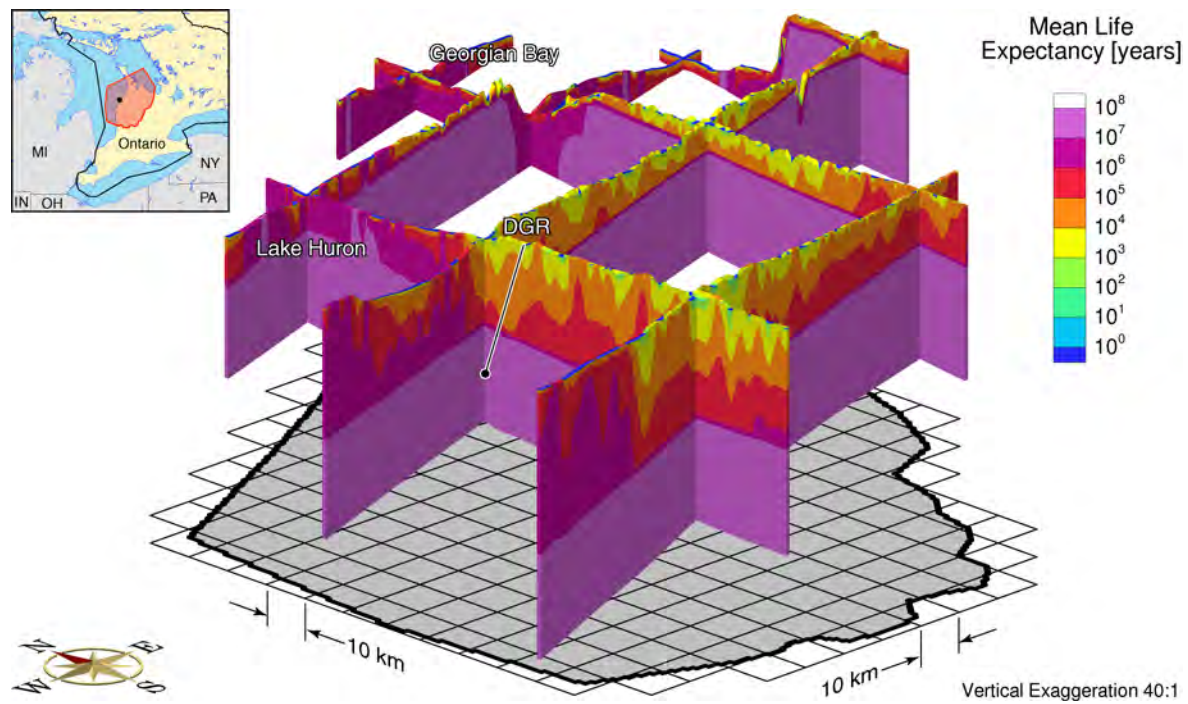


Figure E.8: Fence diagram showing the mean life expectancies for the parameter case S-1.

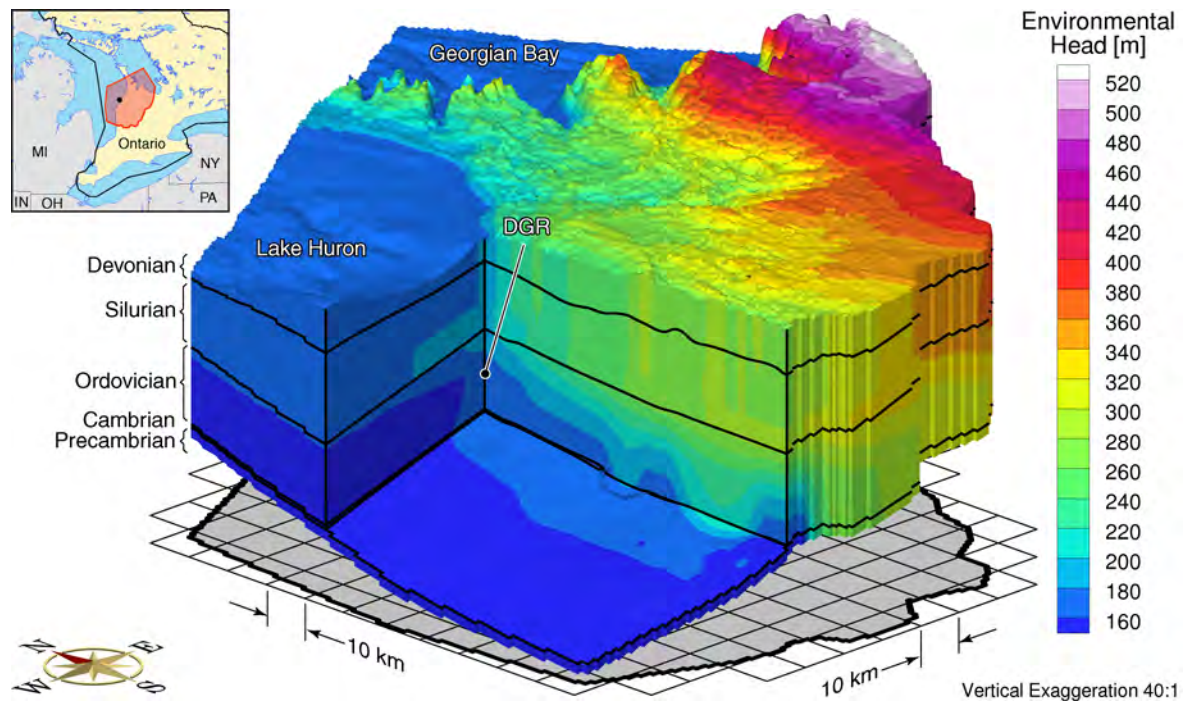


Figure E.9: Environmental heads for the parameter case S-2.

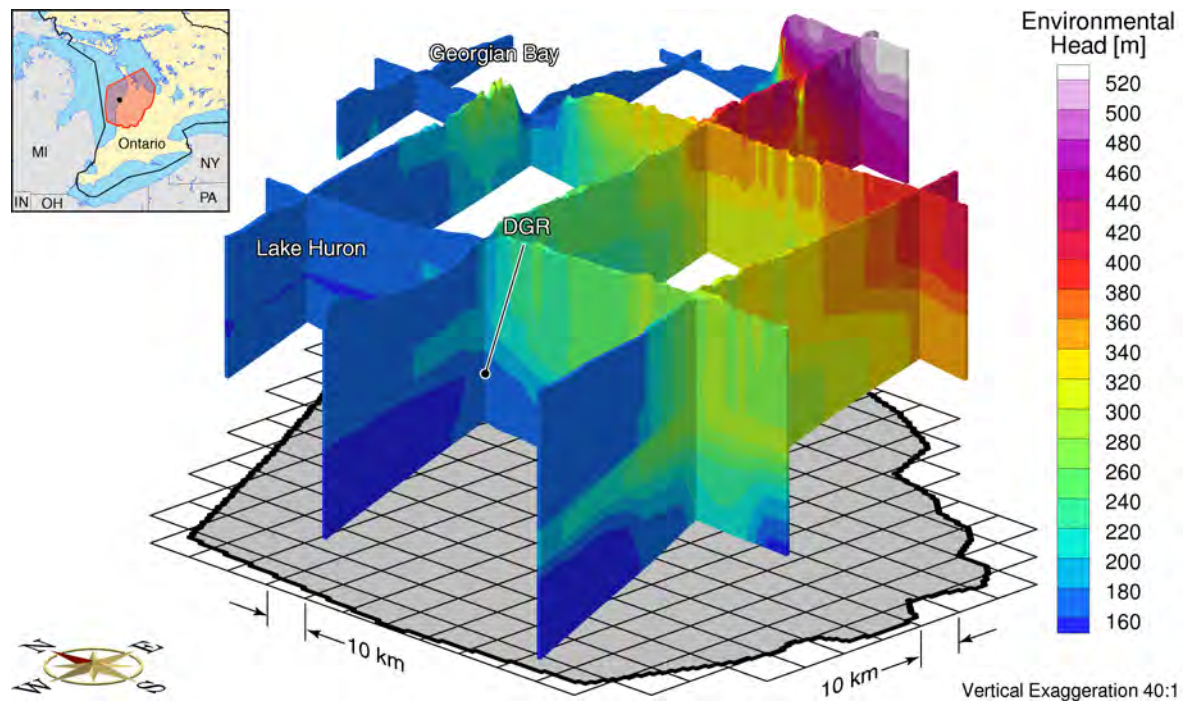


Figure E.10: Fence diagram of environmental heads for the parameter case S-2.

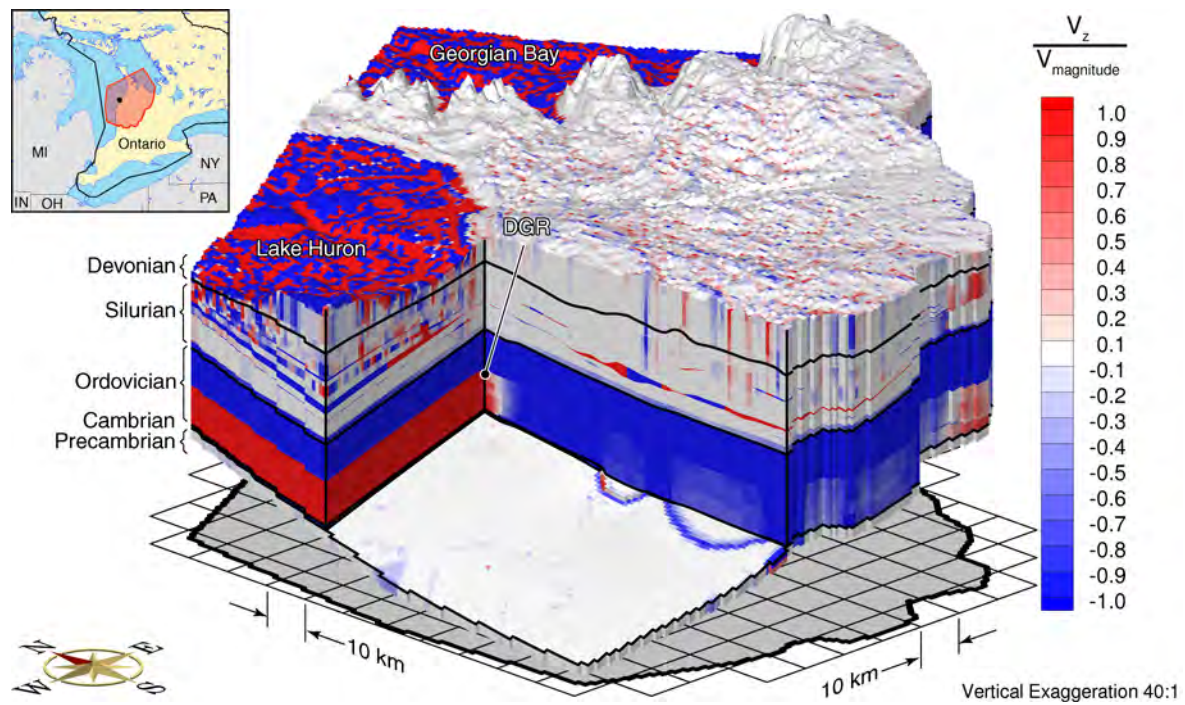


Figure E.11: Ratio of vertical velocity to the velocity magnitude for the parameter case S-2.

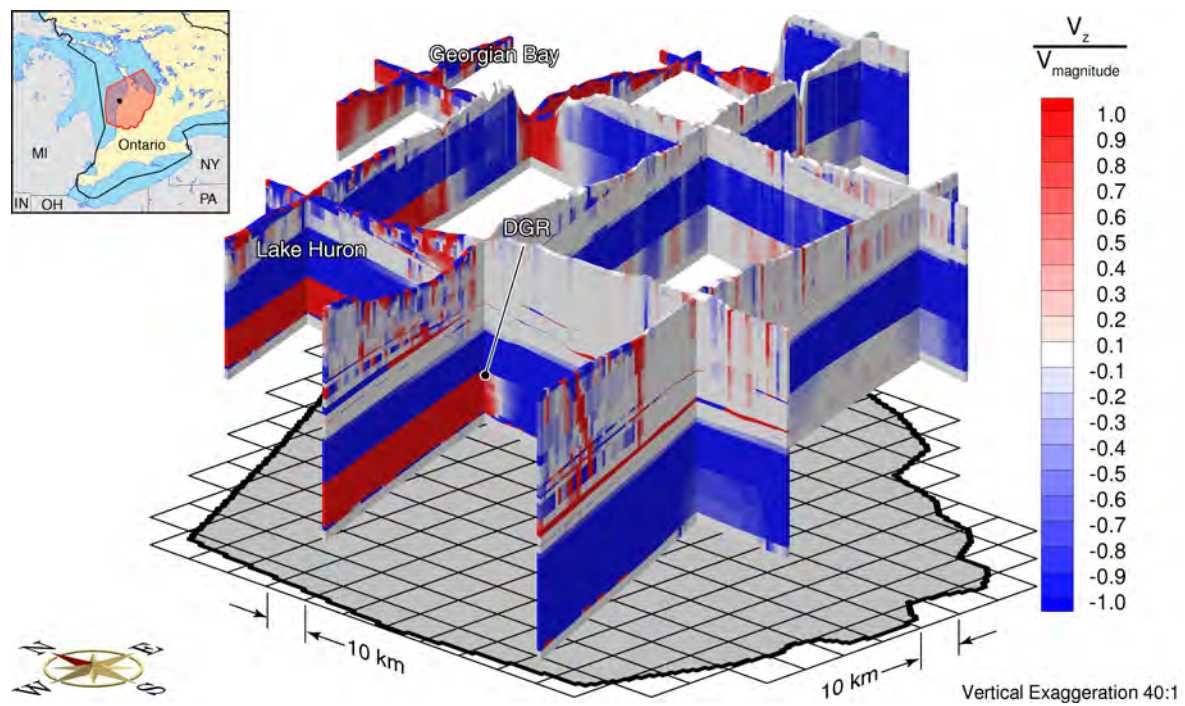


Figure E.12: Fence diagram of the ratio of vertical velocity to the velocity magnitude for the parameter case S-2.

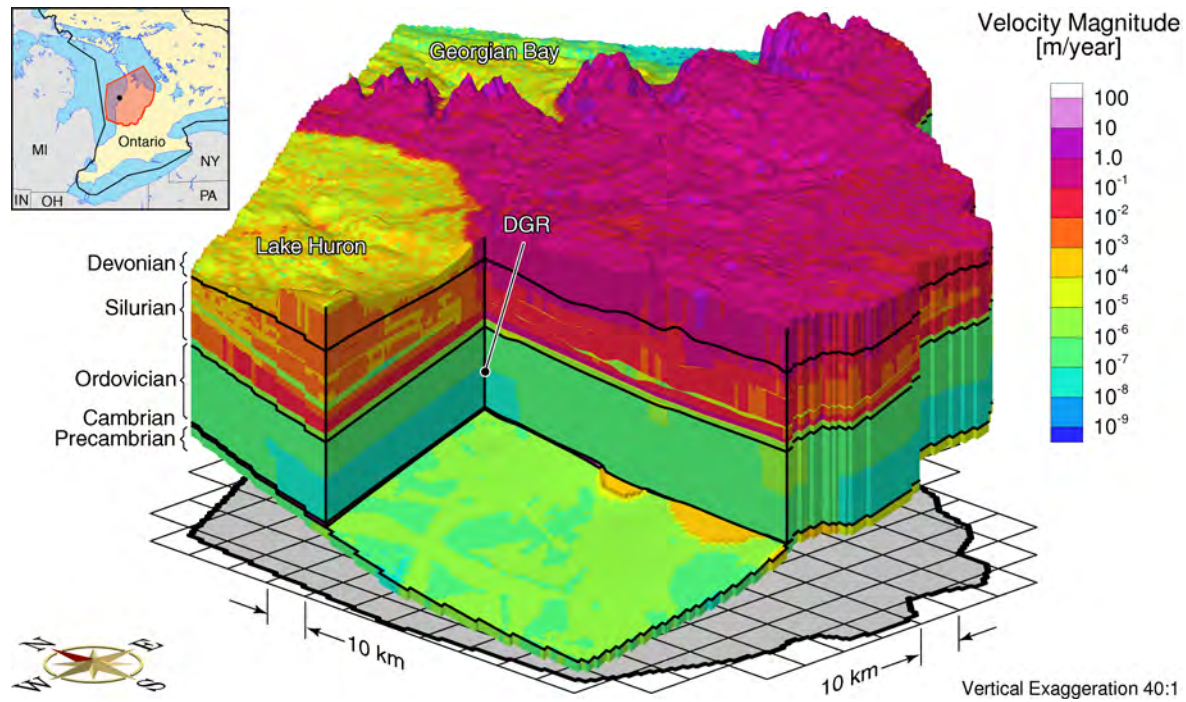


Figure E.13: Pore water velocity magnitude for the parameter case S-2.

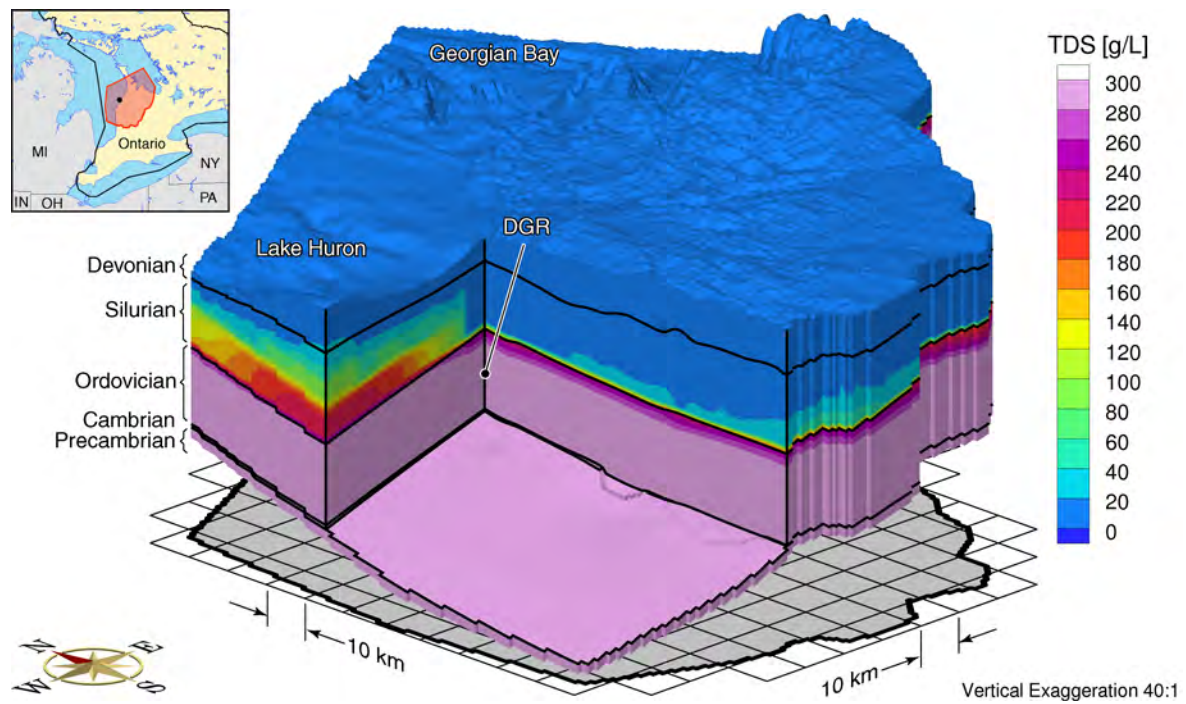


Figure E.14: Total dissolved solids concentration for the parameter case S-2.

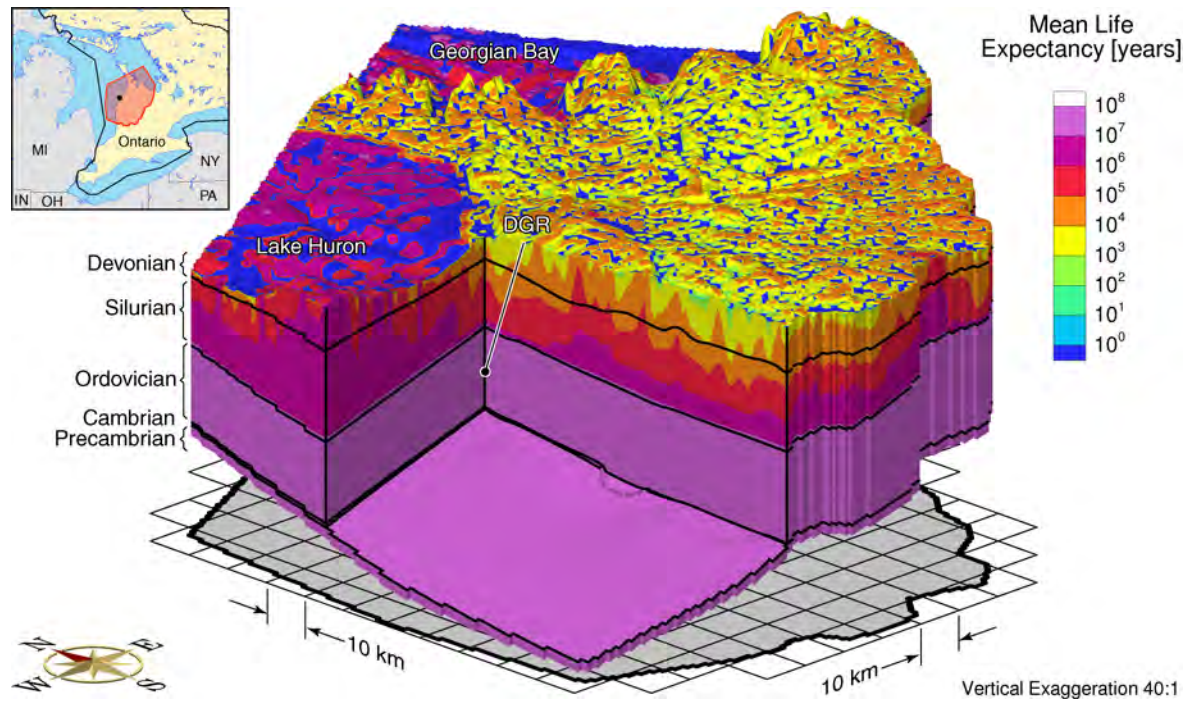


Figure E.15: Mean life expectancies for the parameter case S-2.

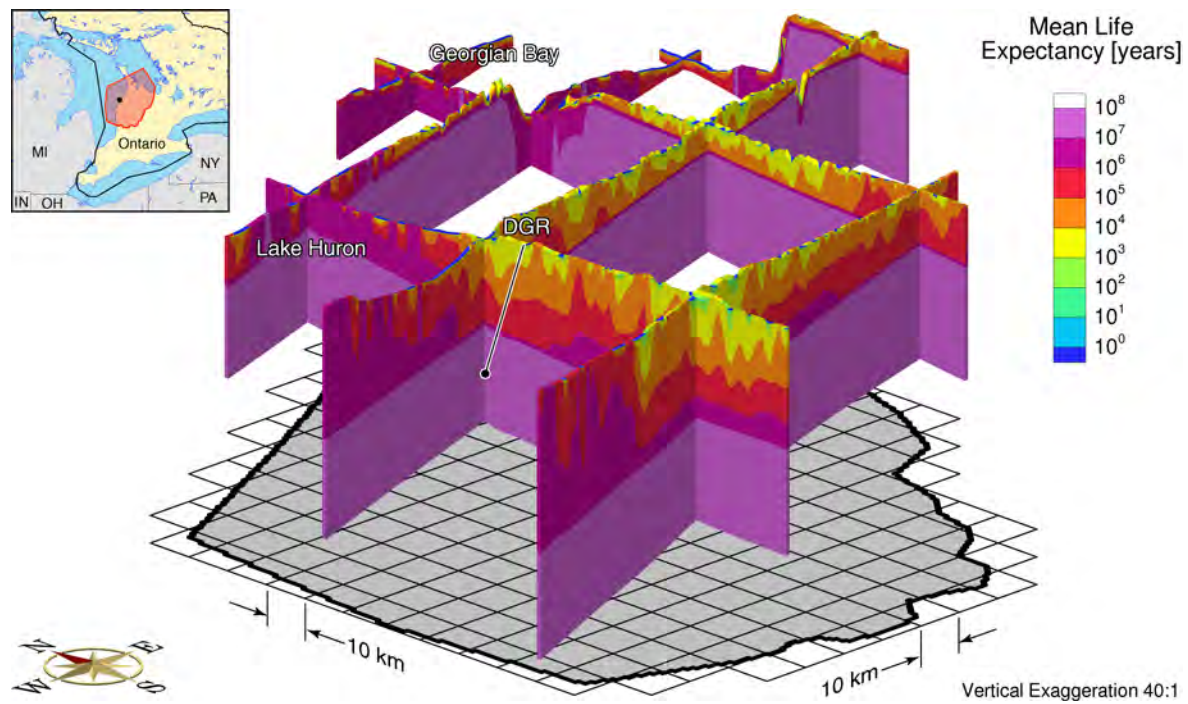


Figure E.16: Fence diagram showing the mean life expectancies for the parameter case S-2.

APPENDIX F – CAMBRIAN HETEROGENEITY

LIST OF FIGURES

| | | Page |
|--------------|--|-------------|
| Figure F.1. | Equivalent freshwater heads for the base case parameters and the Cambrian anisotropy Camb-1. | 159 |
| Figure F.2. | Fence diagram of equivalent freshwater heads for the base case parameters and the Cambrian anisotropy Camb-1. | 159 |
| Figure F.3. | Ratio of vertical velocity to the velocity magnitude for the base case parameters and the Cambrian anisotropy Camb-1. | 160 |
| Figure F.4. | Fence diagram of the ratio of vertical velocity to the velocity magnitude for the base case parameters and the Cambrian anisotropy Camb-1. | 160 |
| Figure F.5. | Pore water velocity magnitude for the base case parameters and the Cambrian anisotropy Camb-1. | 161 |
| Figure F.6. | Total dissolved solids concentration for the base case parameters and the Cambrian anisotropy Camb-1. | 161 |
| Figure F.7. | Mean life expectancies for the base case parameters and the Cambrian anisotropy Camb-1. | 162 |
| Figure F.8. | Fence diagram showing the mean life expectancies for the base case parameters and the Cambrian anisotropy Camb-1. | 162 |
| Figure F.9. | Equivalent freshwater heads for the base case parameters and the Cambrian anisotropy Camb-2. | 163 |
| Figure F.10. | Fence diagram of equivalent freshwater heads for the base case parameters and the Cambrian anisotropy Camb-2. | 163 |
| Figure F.11. | Ratio of vertical velocity to the velocity magnitude for the base case parameters and the Cambrian anisotropy Camb-2. | 164 |
| Figure F.12. | Fence diagram of the ratio of vertical velocity to the velocity magnitude for the base case parameters and the Cambrian anisotropy Camb-2. | 164 |
| Figure F.13. | Pore water velocity magnitude for the base case parameters and the Cambrian anisotropy Camb-2. | 165 |
| Figure F.14. | Total dissolved solids concentration for the base case parameters and the Cambrian anisotropy Camb-2. | 165 |
| Figure F.15. | Mean life expectancies for the base case parameters and the Cambrian anisotropy Camb-2. | 166 |
| Figure F.16. | Fence diagram showing the mean life expectancies for the base case parameters and the Cambrian anisotropy Camb-2. | 166 |
| Figure F.17. | Equivalent freshwater heads for the base case parameters and the Cambrian anisotropy Camb-3. | 167 |
| Figure F.18. | Fence diagram of equivalent freshwater heads for the base case parameters and the Cambrian anisotropy Camb-3. | 167 |
| Figure F.19. | Ratio of vertical velocity to the velocity magnitude for the base case parameters and the Cambrian anisotropy Camb-3. | 168 |
| Figure F.20. | Fence diagram of the ratio of vertical velocity to the velocity magnitude for the base case parameters and the Cambrian anisotropy Camb-3. | 168 |

| | | |
|--------------|--|-----|
| Figure F.21. | Pore water velocity magnitude for the base case parameters and the Cambrian anisotropy Camb-3. | 169 |
| Figure F.22. | Total dissolved solids concentration for the base case parameters and the Cambrian anisotropy Camb-3. | 169 |
| Figure F.23. | Mean life expectancies for the base case parameters and the Cambrian anisotropy Camb-3. | 170 |
| Figure F.24. | Fence diagram showing the mean life expectancies for the base case parameters and the Cambrian anisotropy Camb-3. | 170 |
| Figure F.25. | Equivalent freshwater heads for the base case parameters and the Cambrian anisotropy Camb-4. | 171 |
| Figure F.26. | Fence diagram of equivalent freshwater heads for the base case parameters and the Cambrian anisotropy Camb-4. | 171 |
| Figure F.27. | Ratio of vertical velocity to the velocity magnitude for the base case parameters and the Cambrian anisotropy Camb-4. | 172 |
| Figure F.28. | Fence diagram of the ratio of vertical velocity to the velocity magnitude for the base case parameters and the Cambrian anisotropy Camb-4. | 172 |
| Figure F.29. | Pore water velocity magnitude for the base case parameters and the Cambrian anisotropy Camb-4. | 173 |
| Figure F.30. | Total dissolved solids concentration for the base case parameters and the Cambrian anisotropy Camb-4. | 173 |
| Figure F.31. | Mean life expectancies for the base case parameters and the Cambrian anisotropy Camb-4. | 174 |
| Figure F.32. | Fence diagram showing the mean life expectancies for the base case parameters and the Cambrian anisotropy Camb-4. | 174 |

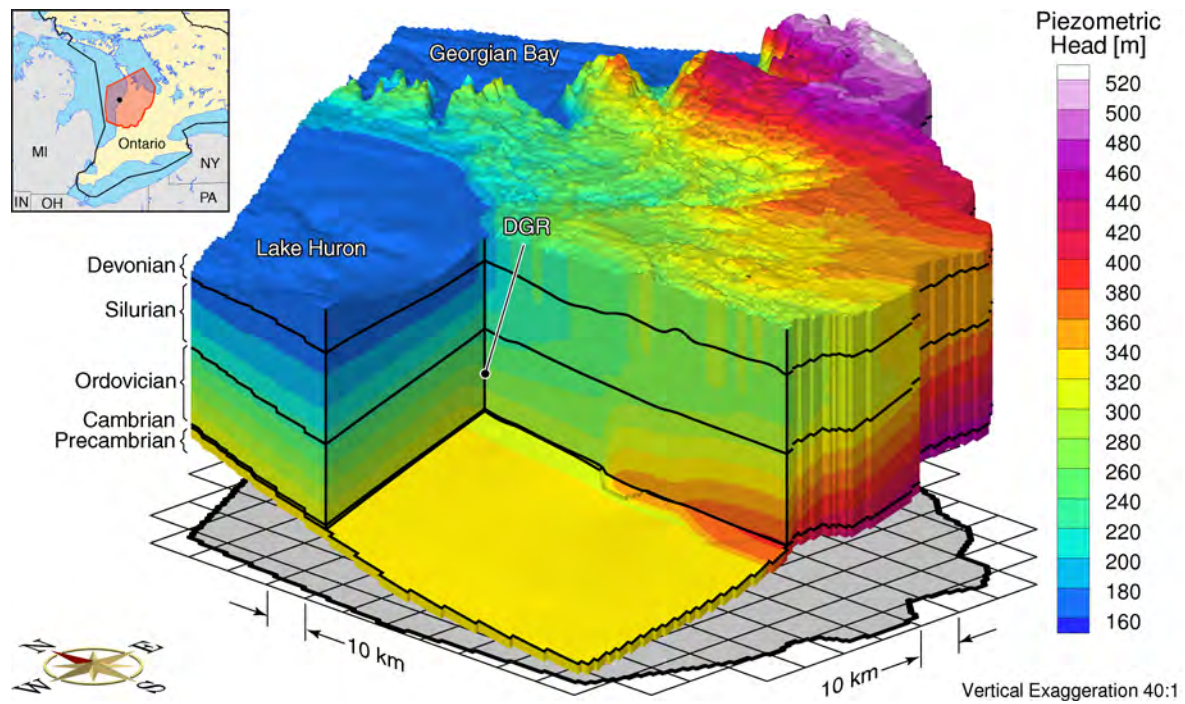


Figure F.1: Equivalent freshwater heads for the base case parameters and the Cambrian anisotropy Camb-1.

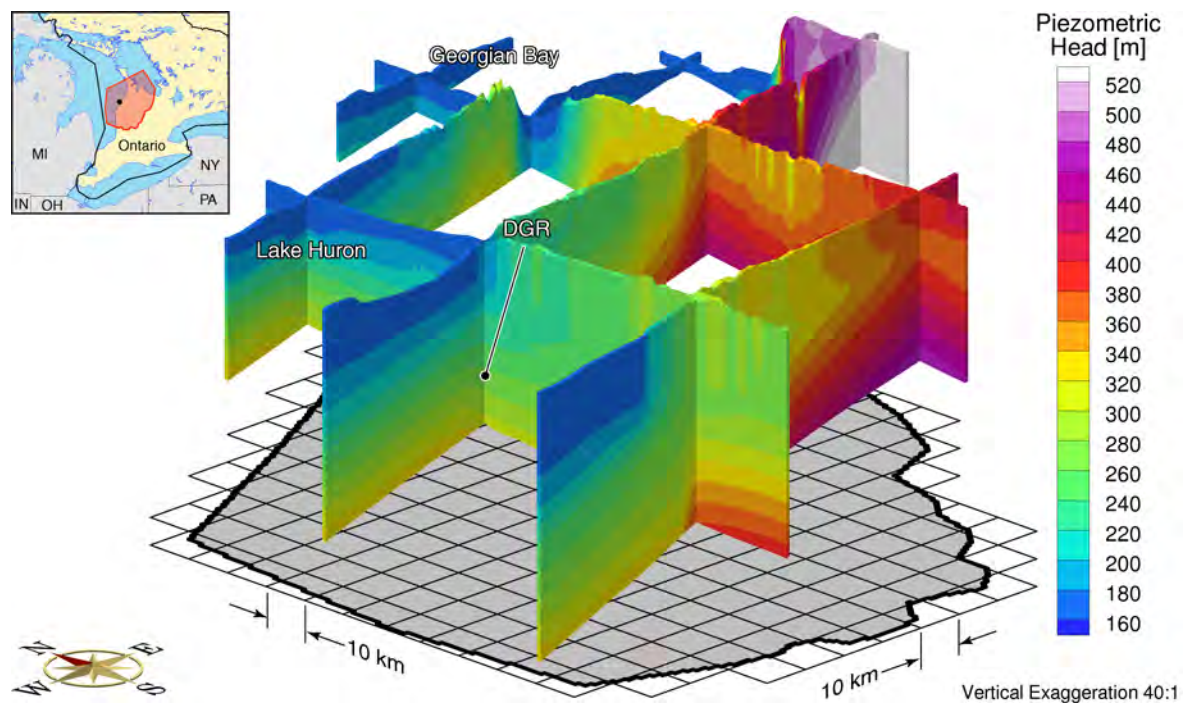


Figure F.2: Fence diagram of equivalent freshwater heads for the base case parameters and the Cambrian anisotropy Camb-1.

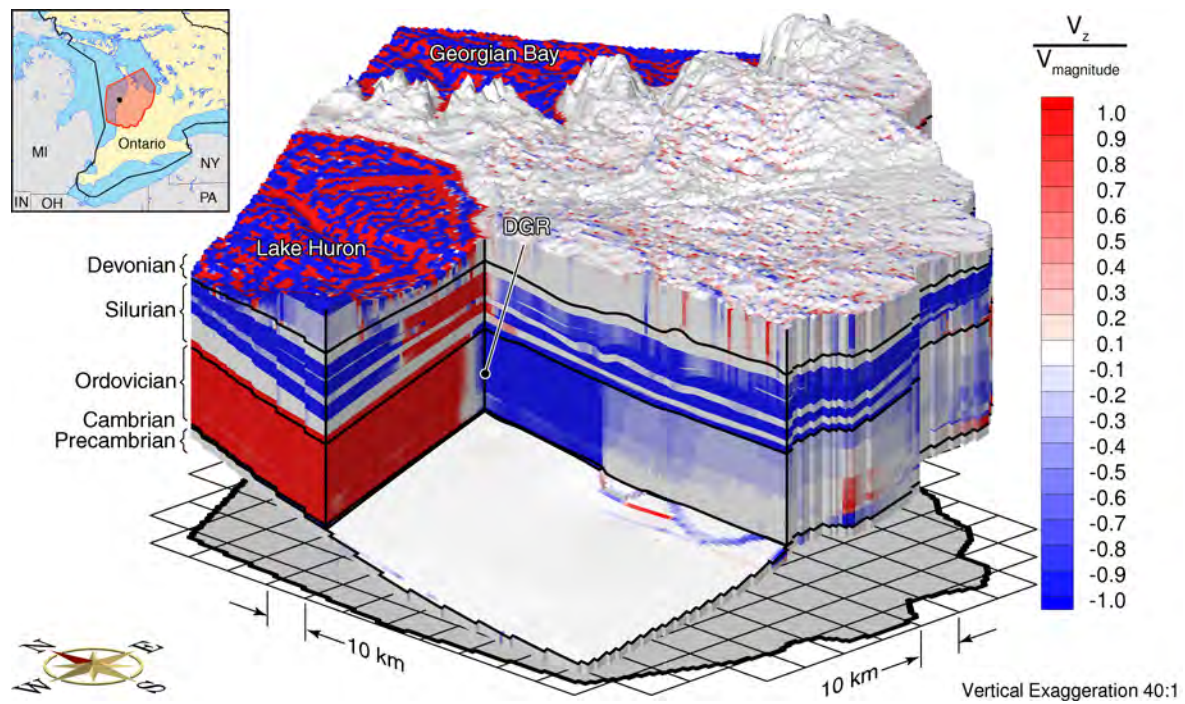


Figure F.3: Ratio of vertical velocity to the velocity magnitude for the base case parameters and the Cambrian anisotropy Camb-1.

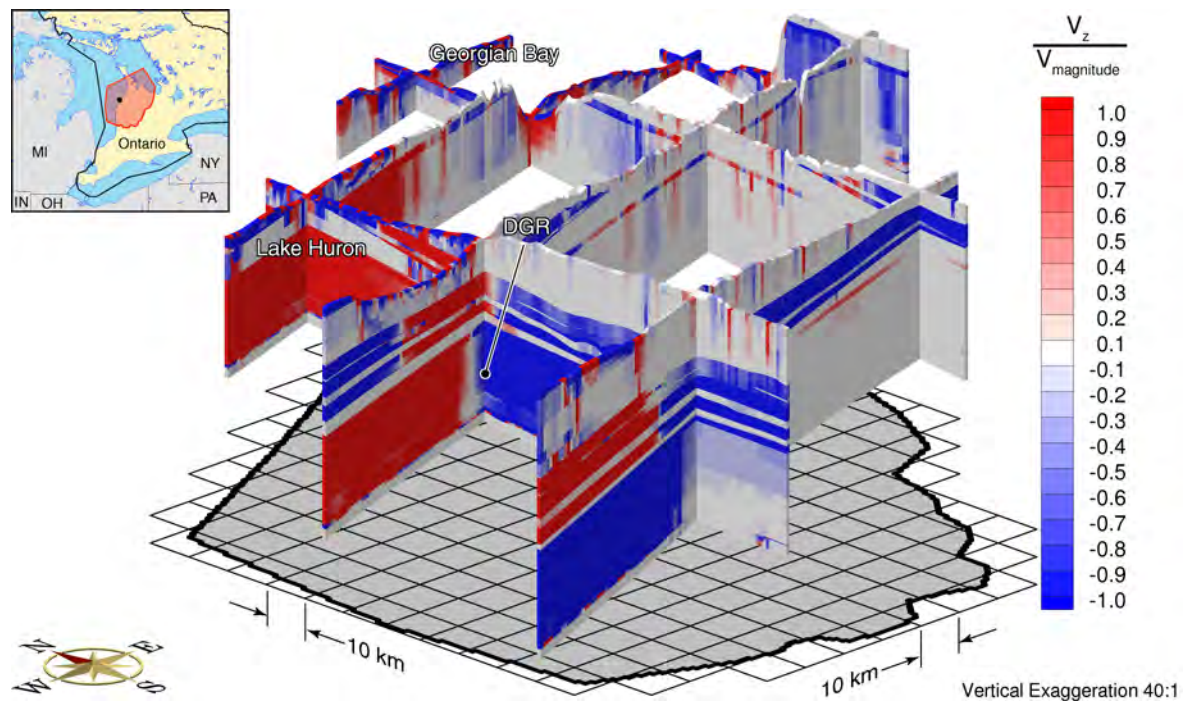


Figure F.4: Fence diagram of the ratio of vertical velocity to the velocity magnitude for the base case parameters and the Cambrian anisotropy Camb-1.

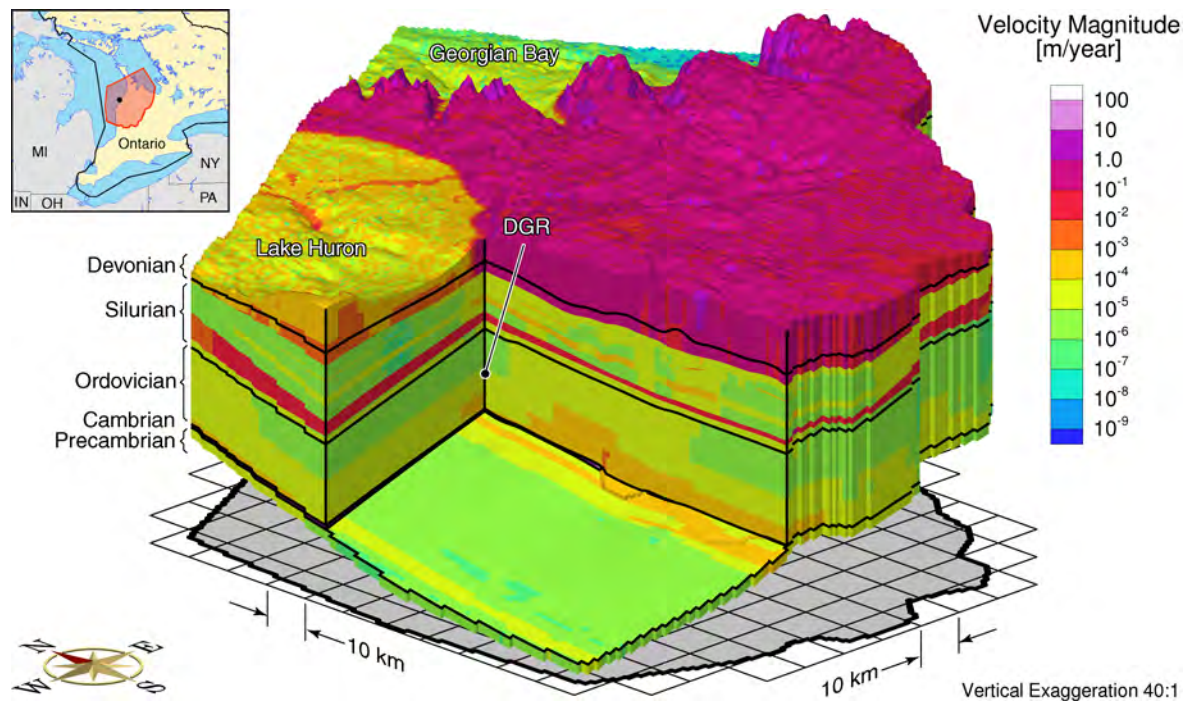


Figure F.5: Pore water velocity magnitude for the base case parameters and the Cambrian anisotropy Camb-1.

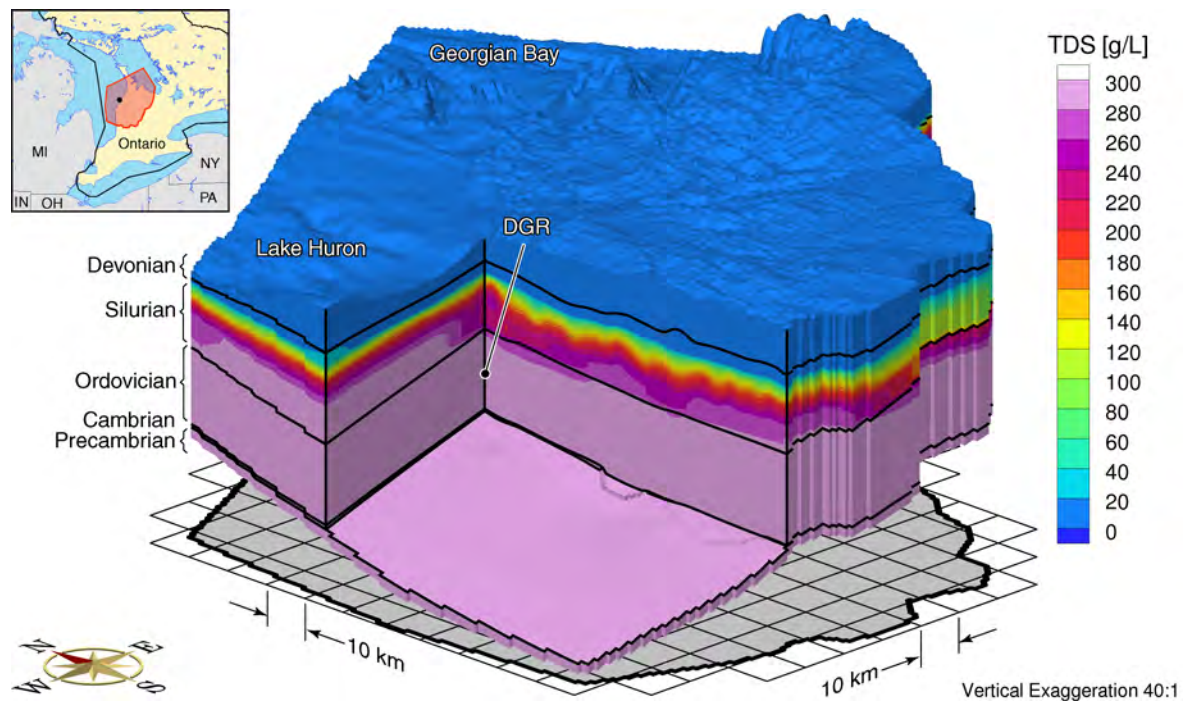


Figure F.6: Total dissolved solids concentration for the base case parameters and the Cambrian anisotropy Camb-1.

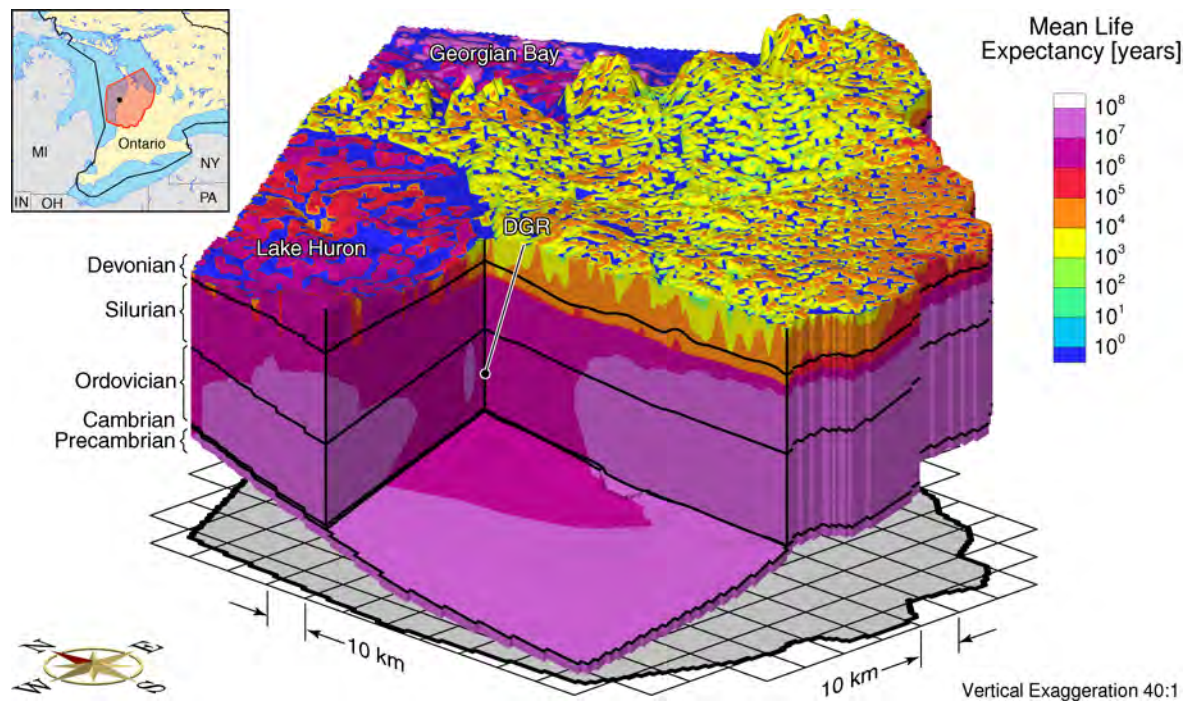


Figure F.7: Mean life expectancies for the base case parameters and the Cambrian anisotropy Camb-1.

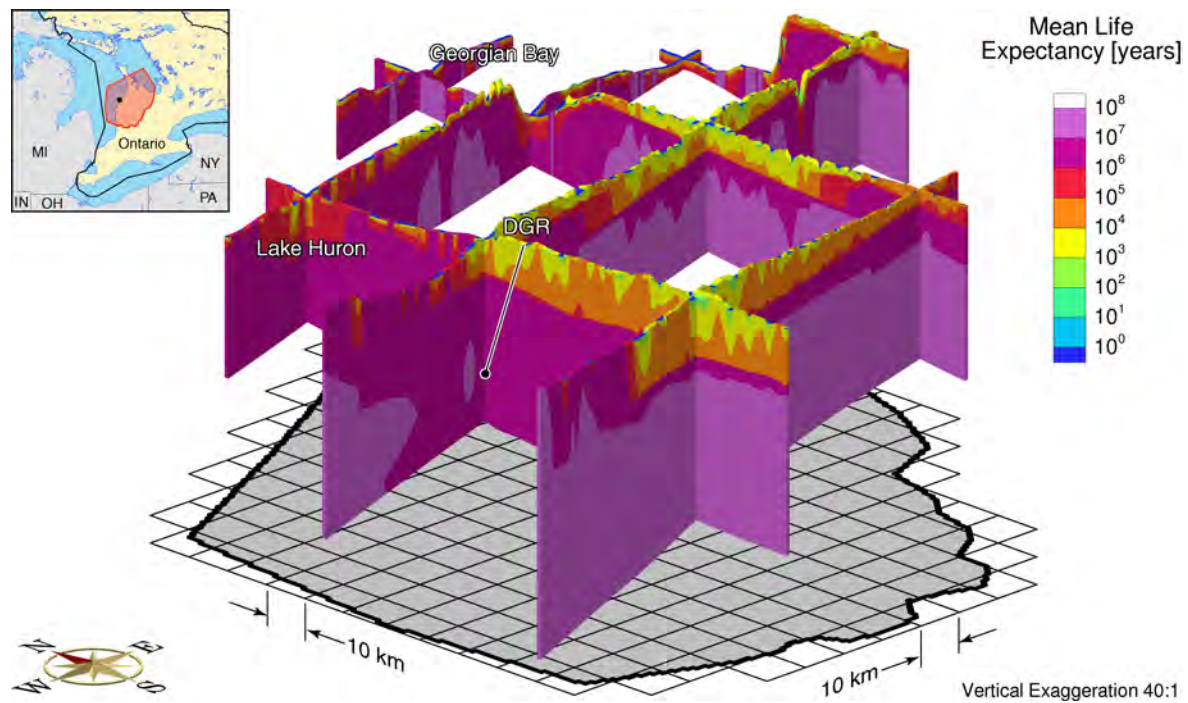


Figure F.8: Fence diagram showing the mean life expectancies for the base case parameters and the Cambrian anisotropy Camb-1.

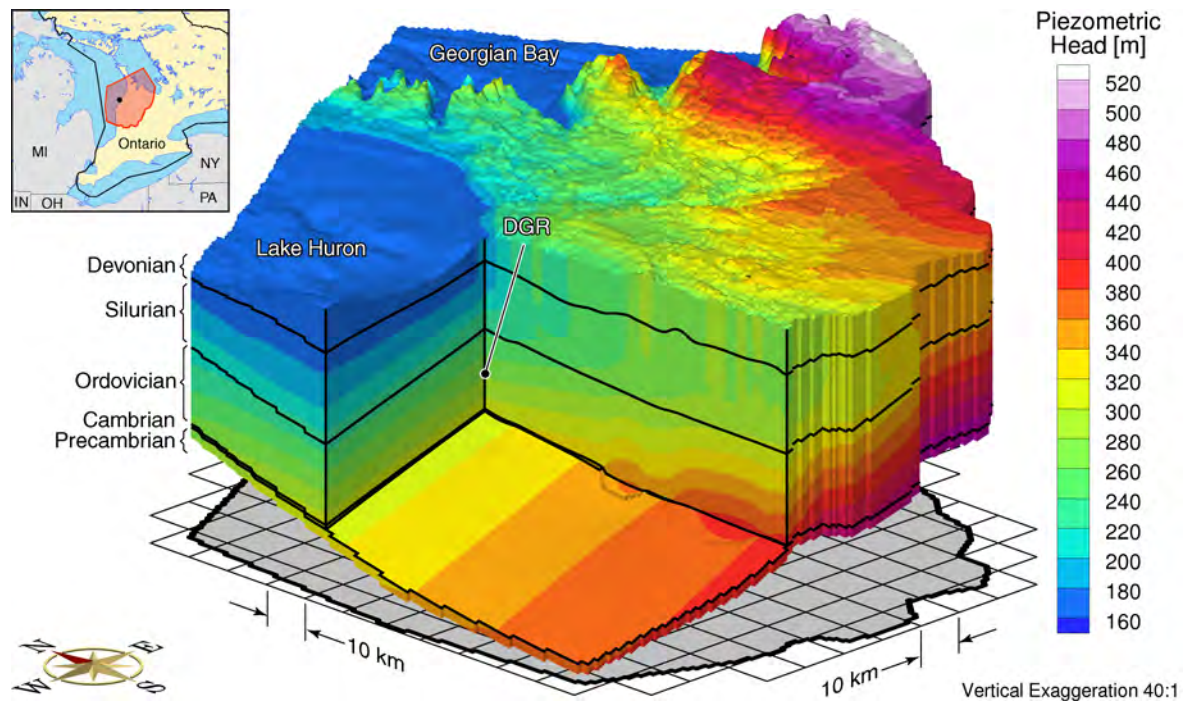


Figure F.9: Equivalent freshwater heads for the base case parameters and the Cambrian anisotropy Camb-2.

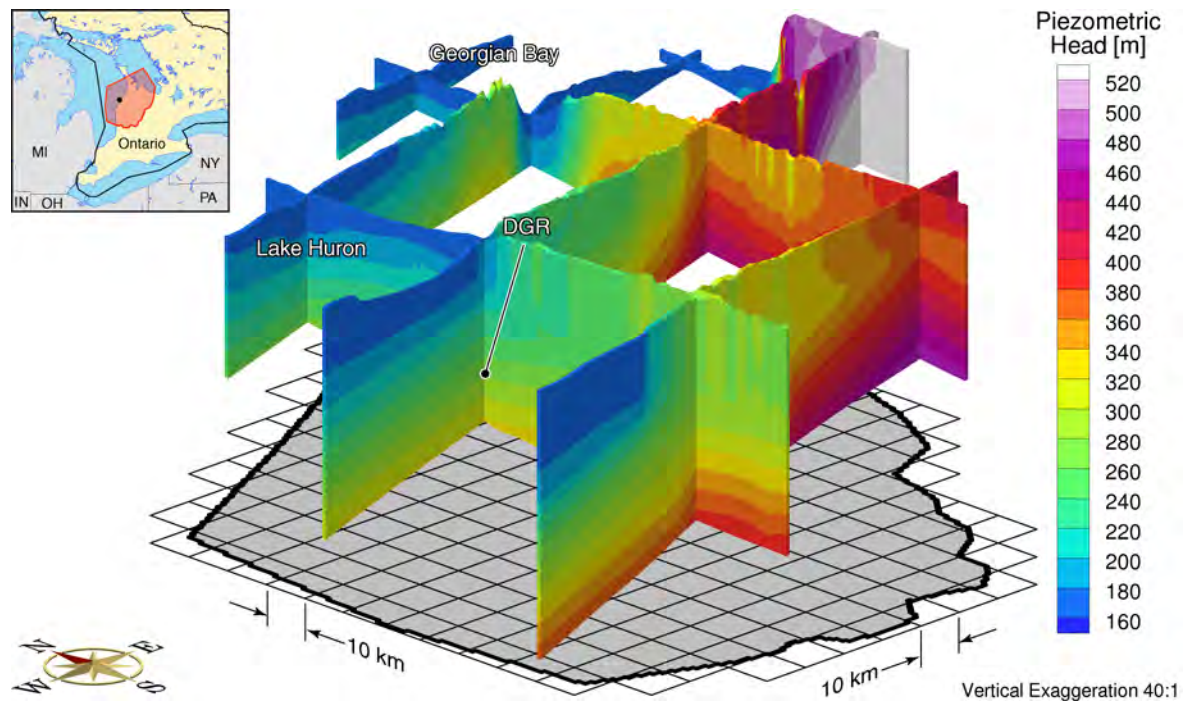


Figure F.10: Fence diagram of equivalent freshwater heads for the base case parameters and the Cambrian anisotropy Camb-2.

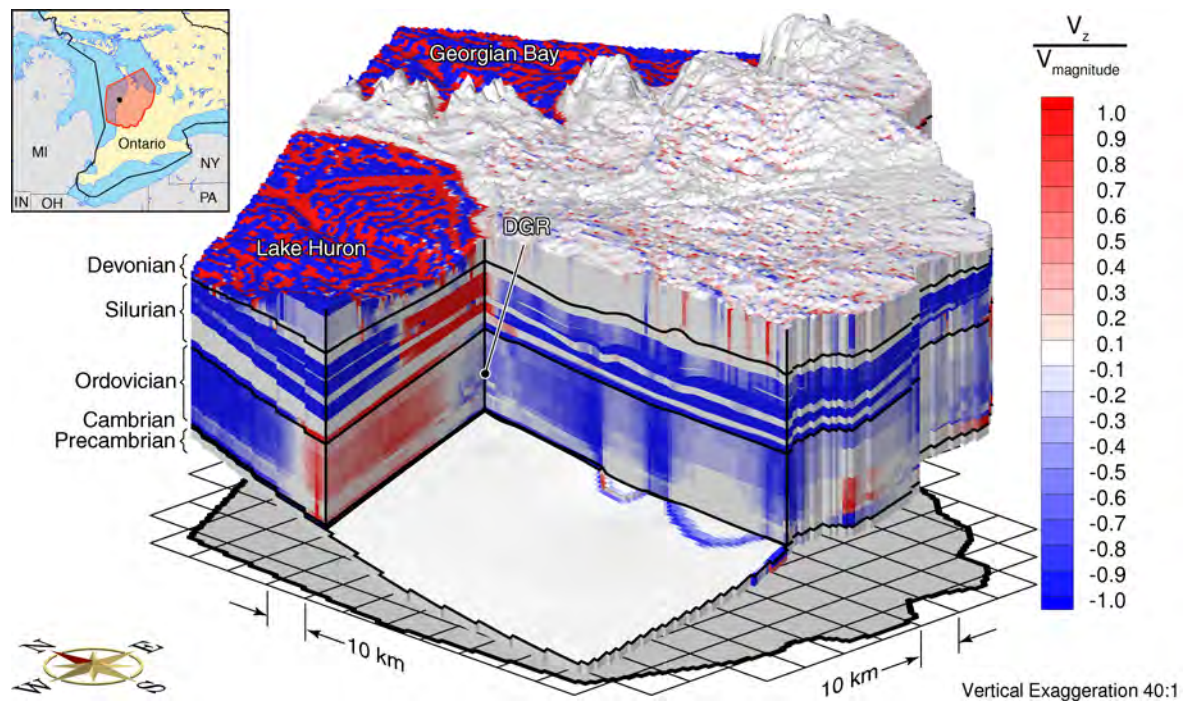


Figure F.11: Ratio of vertical velocity to the velocity magnitude for the base case parameters and the Cambrian anisotropy Camb-2.

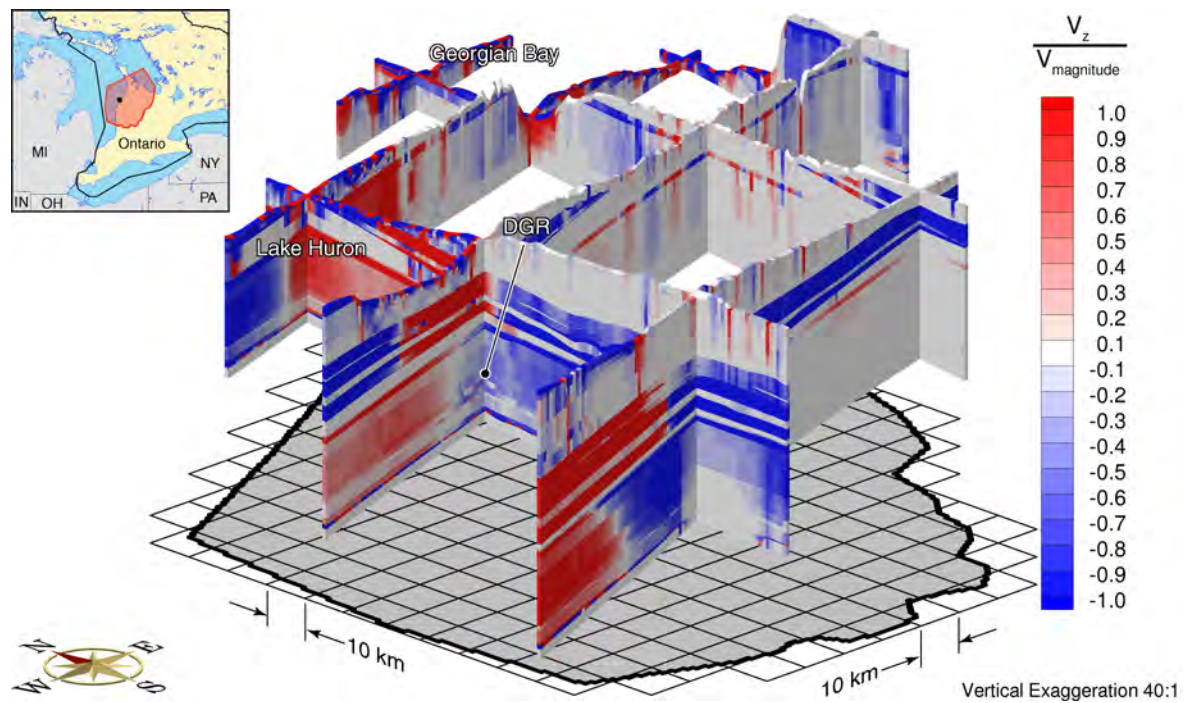


Figure F.12: Fence diagram of the ratio of vertical velocity to the velocity magnitude for the base case parameters and the Cambrian anisotropy Camb-2.

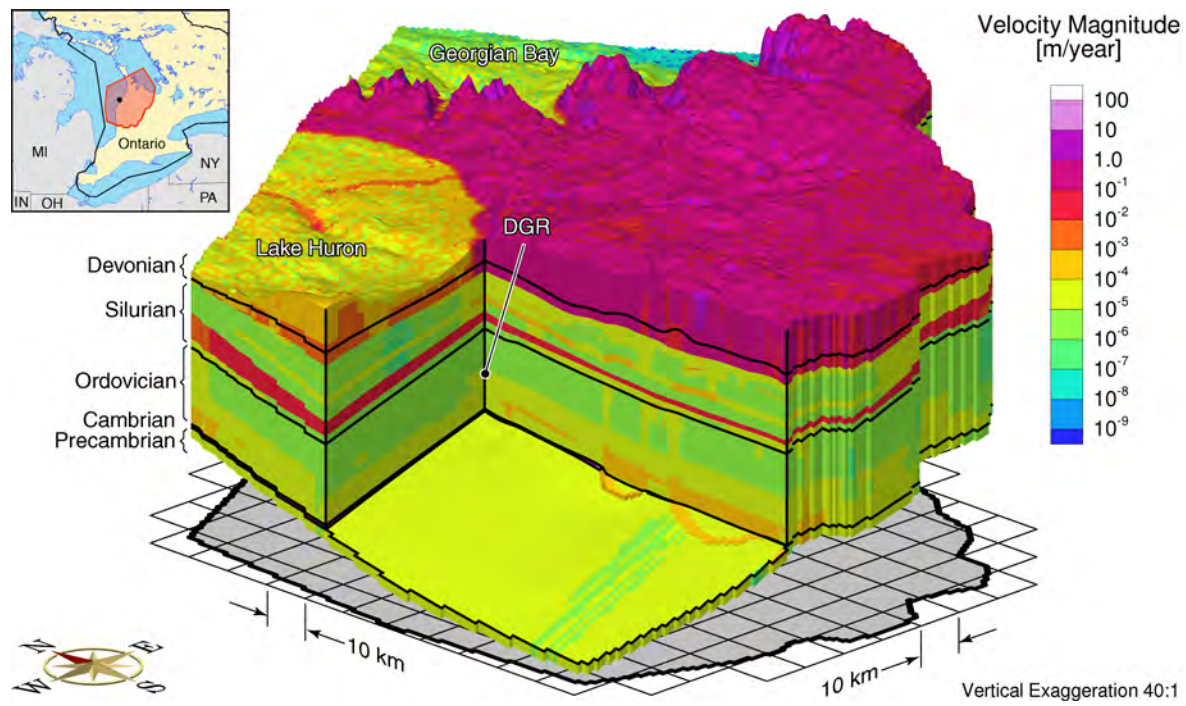


Figure F.13: Pore water velocity magnitude for the base case parameters and the Cambrian anisotropy Camb-2.

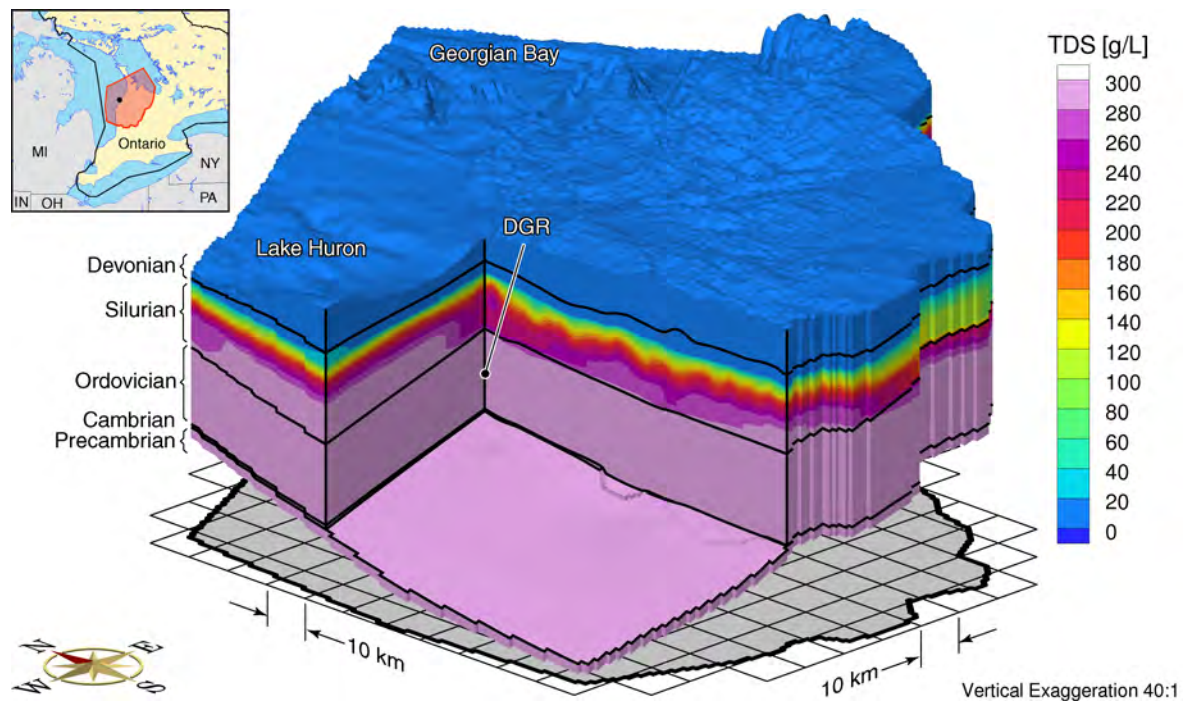


Figure F.14: Total dissolved solids concentration for the base case parameters and the Cambrian anisotropy Camb-2.

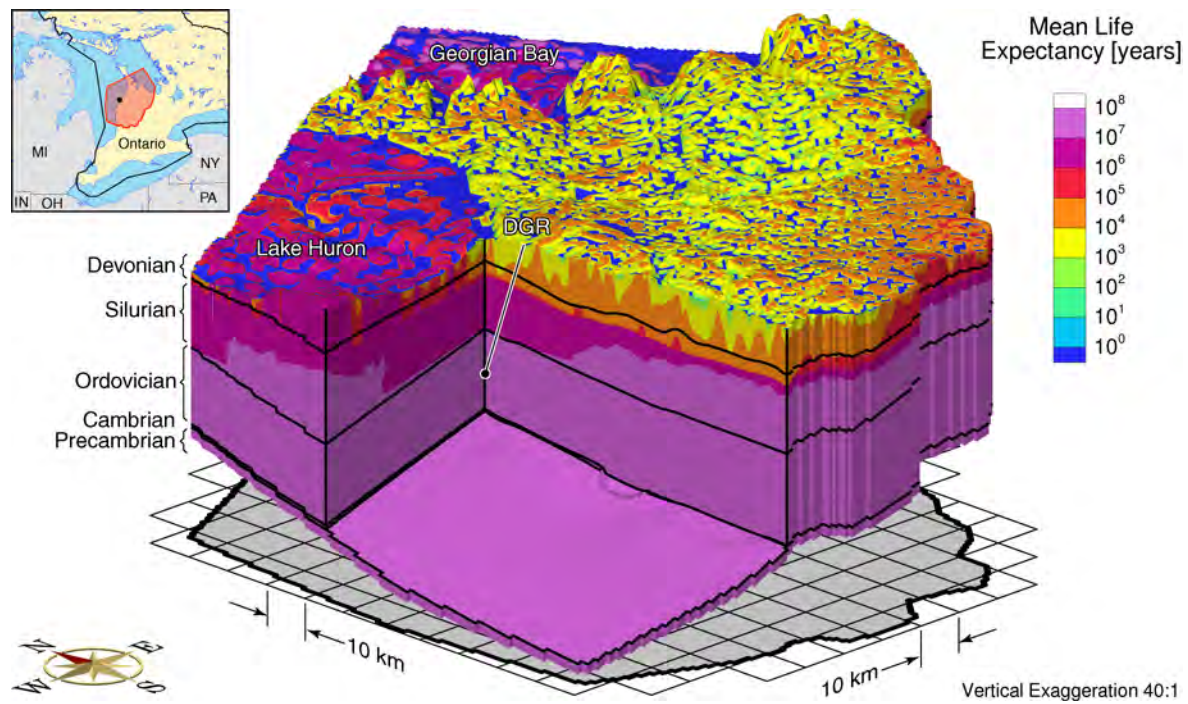


Figure F.15: Mean life expectancies for the base case parameters and the Cambrian anisotropy Camb-2.

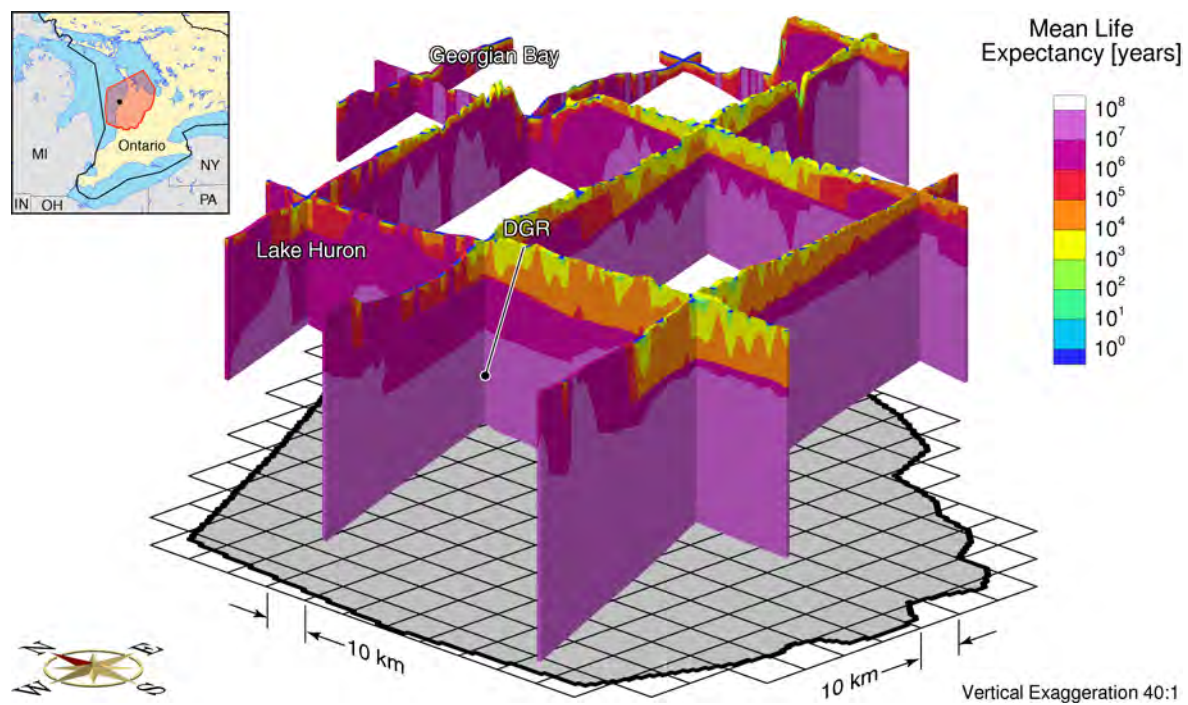


Figure F.16: Fence diagram showing the mean life expectancies for the base case parameters and the Cambrian anisotropy Camb-2.

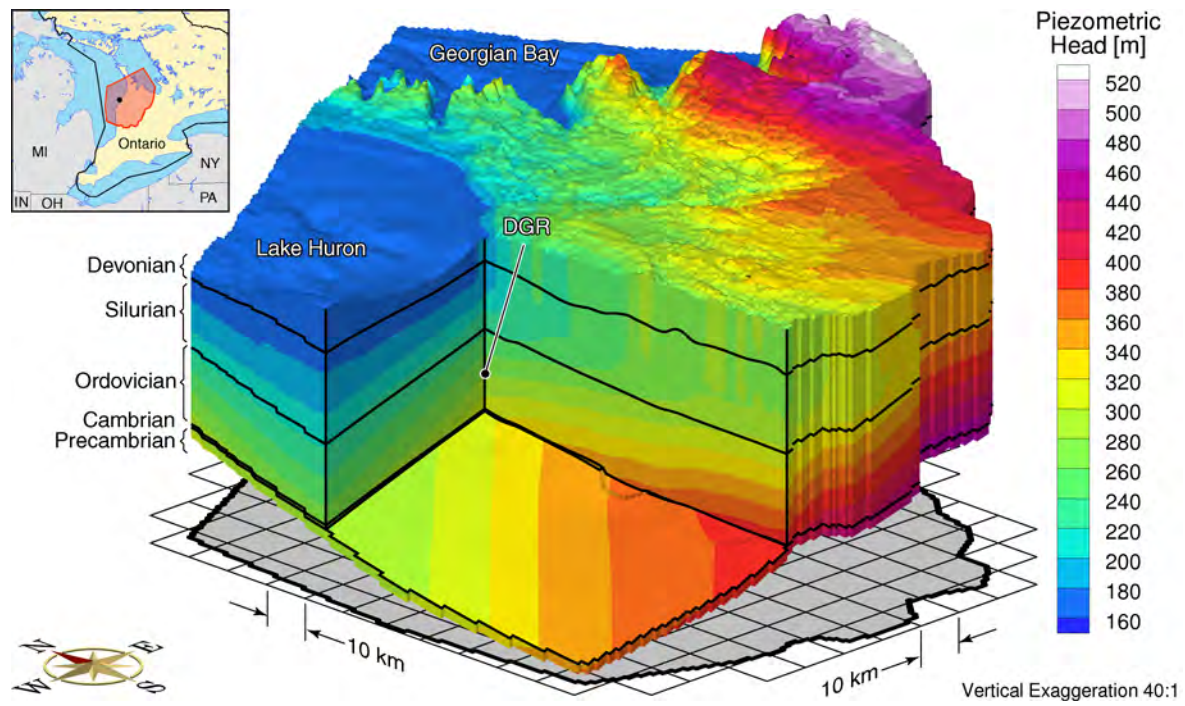


Figure F.17: Equivalent freshwater heads for the base case parameters and the Cambrian anisotropy Camb-3.

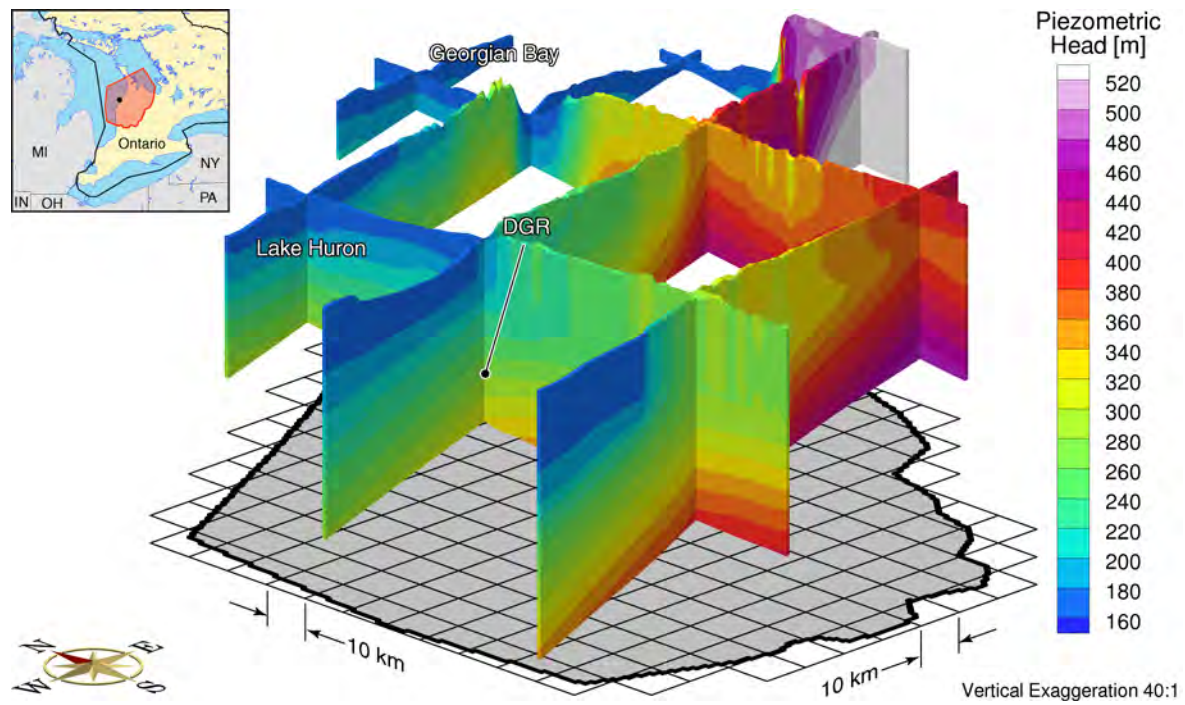


Figure F.18: Fence diagram of equivalent freshwater heads for the base case parameters and the Cambrian anisotropy Camb-3.

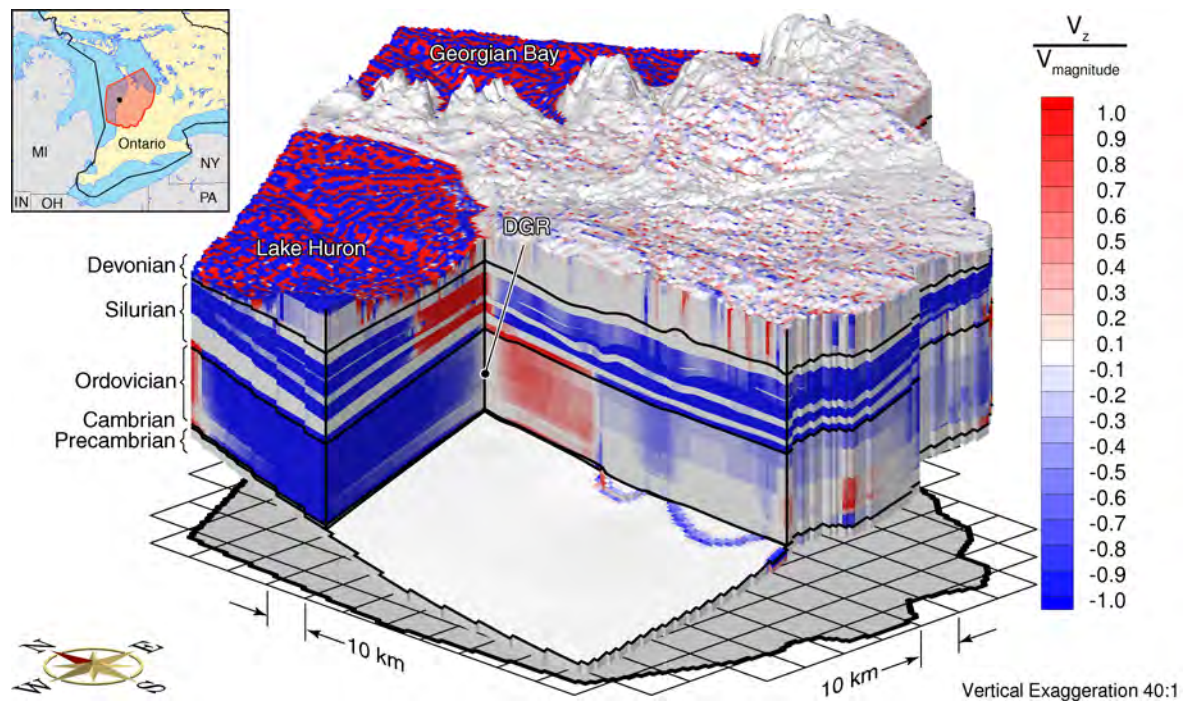


Figure F.19: Ratio of vertical velocity to the velocity magnitude for the base case parameters and the Cambrian anisotropy Camb-3.

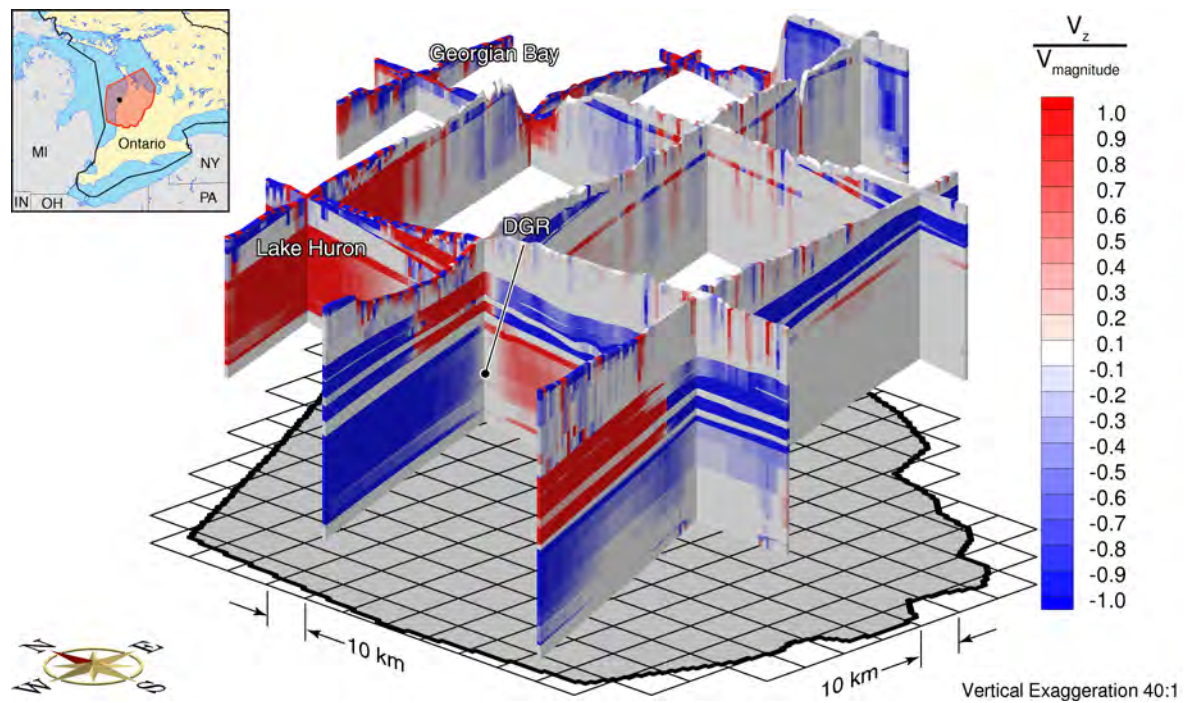


Figure F.20: Fence diagram of the ratio of vertical velocity to the velocity magnitude for the base case parameters and the Cambrian anisotropy Camb-3.

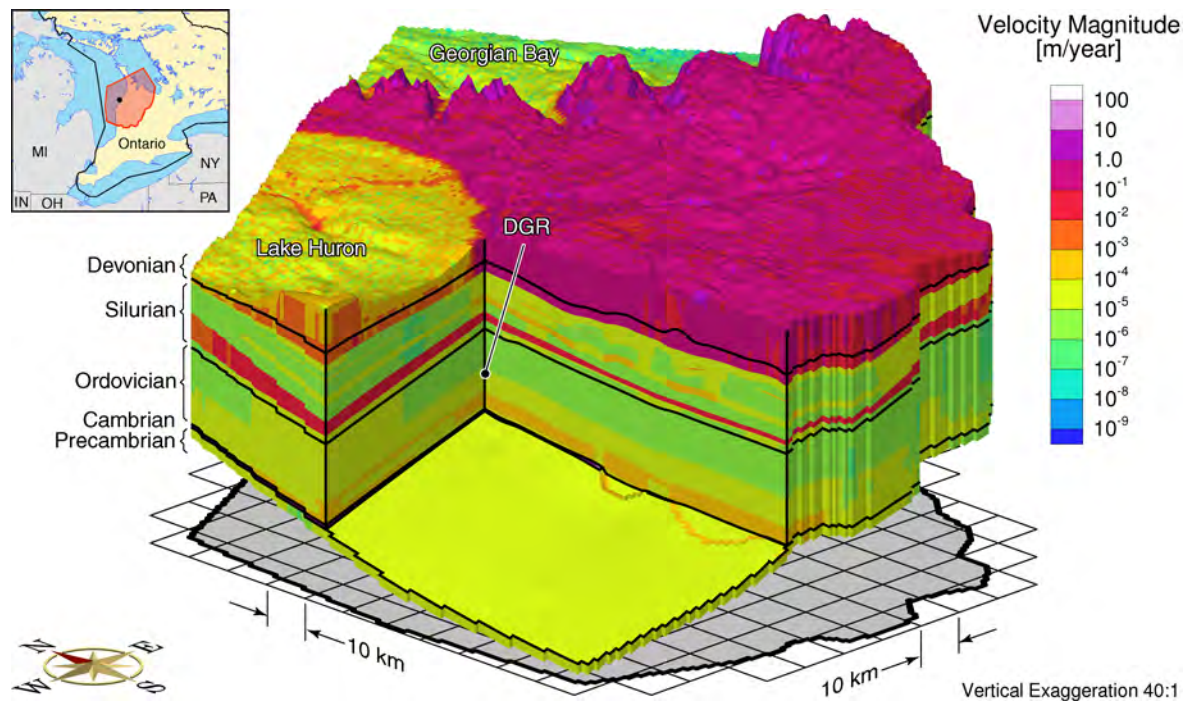


Figure F.21: Pore water velocity magnitude for the base case parameters and the Cambrian anisotropy Camb-3.

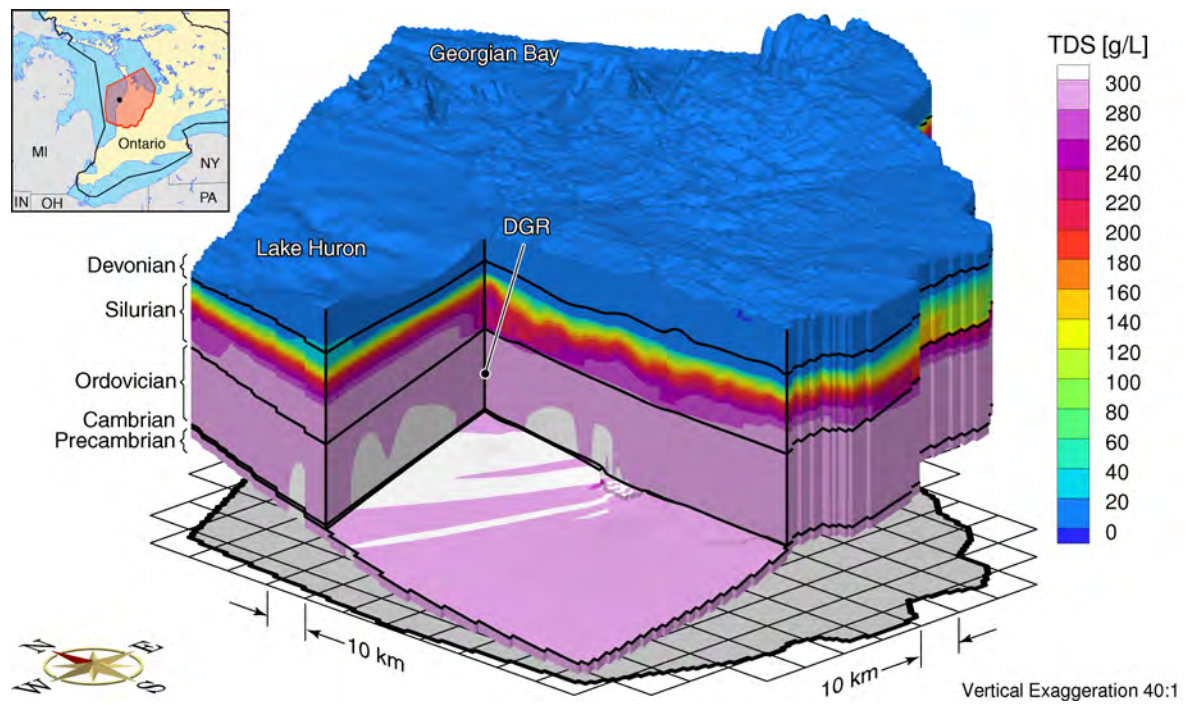


Figure F.22: Total dissolved solids concentration for the base case parameters and the Cambrian anisotropy Camb-3.

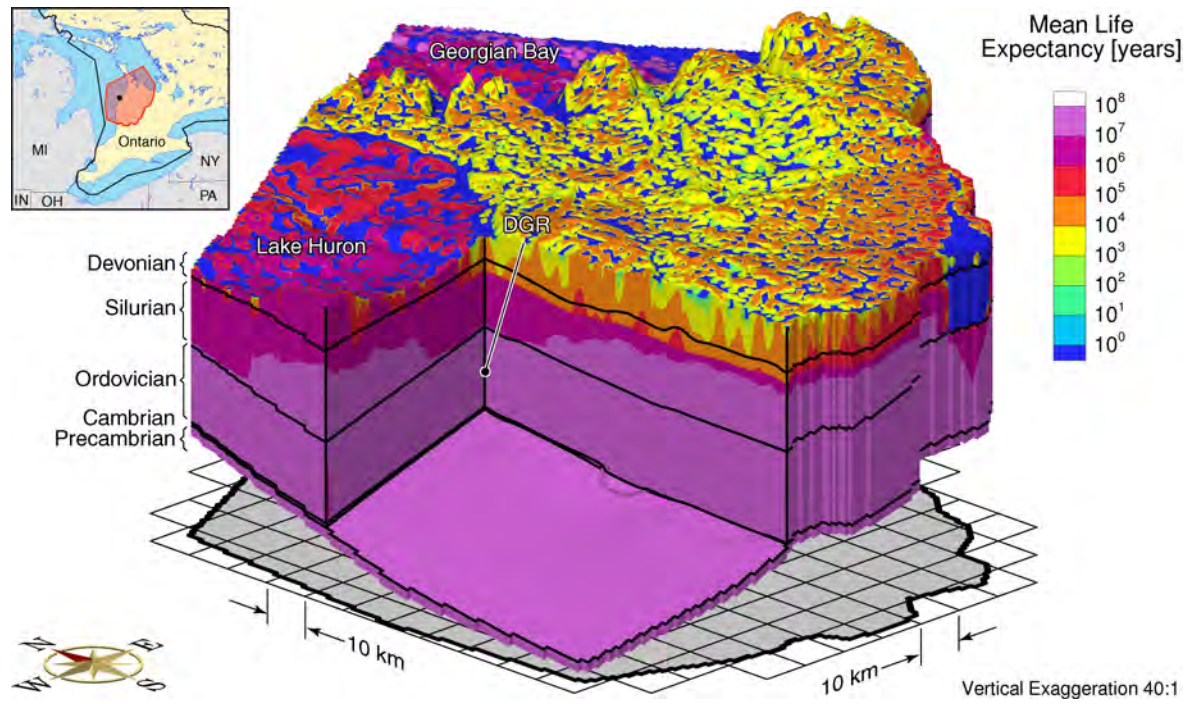


Figure F.23: Mean life expectancies for the base case parameters and the Cambrian anisotropy Camb-3.

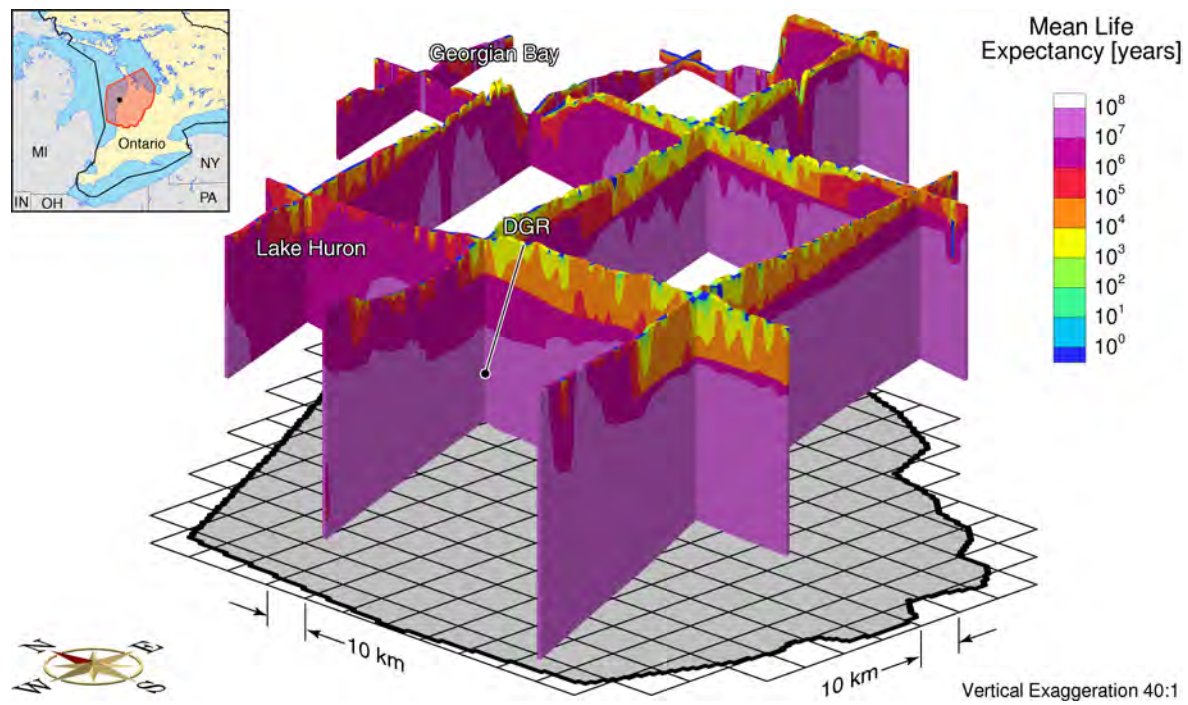


Figure F.24: Fence diagram showing the mean life expectancies for the base case parameters and the Cambrian anisotropy Camb-3.

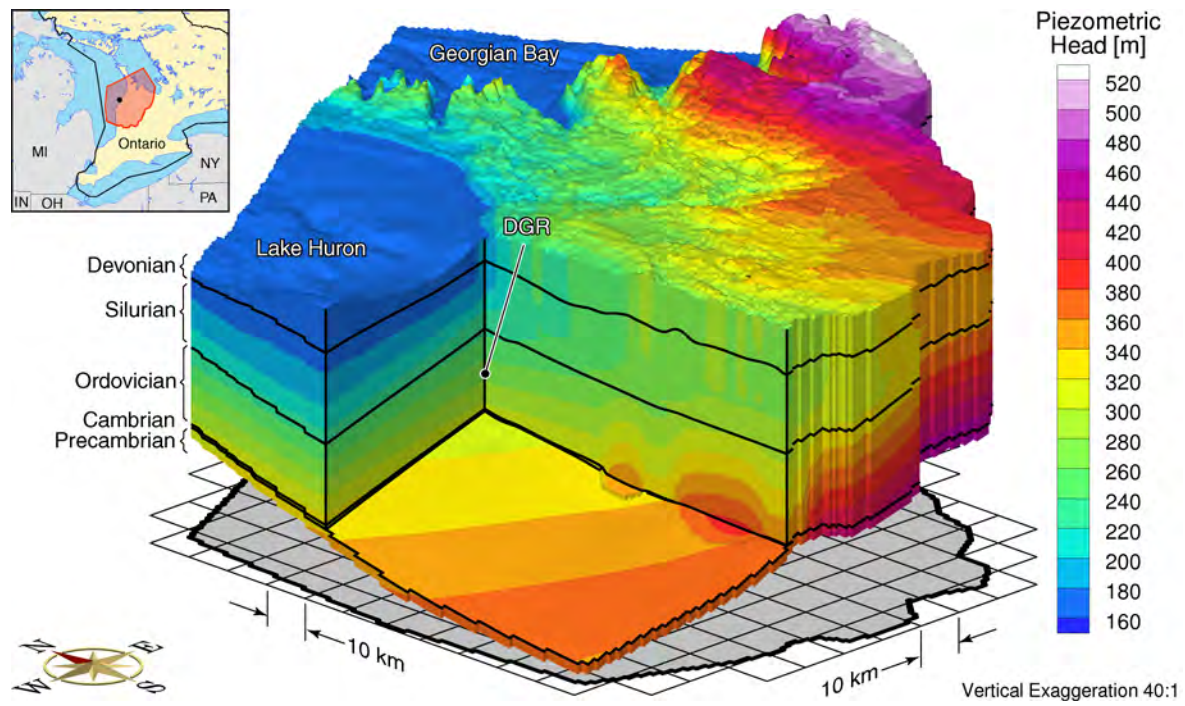


Figure F.25: Equivalent freshwater heads for the base case parameters and the Cambrian anisotropy Camb-4.

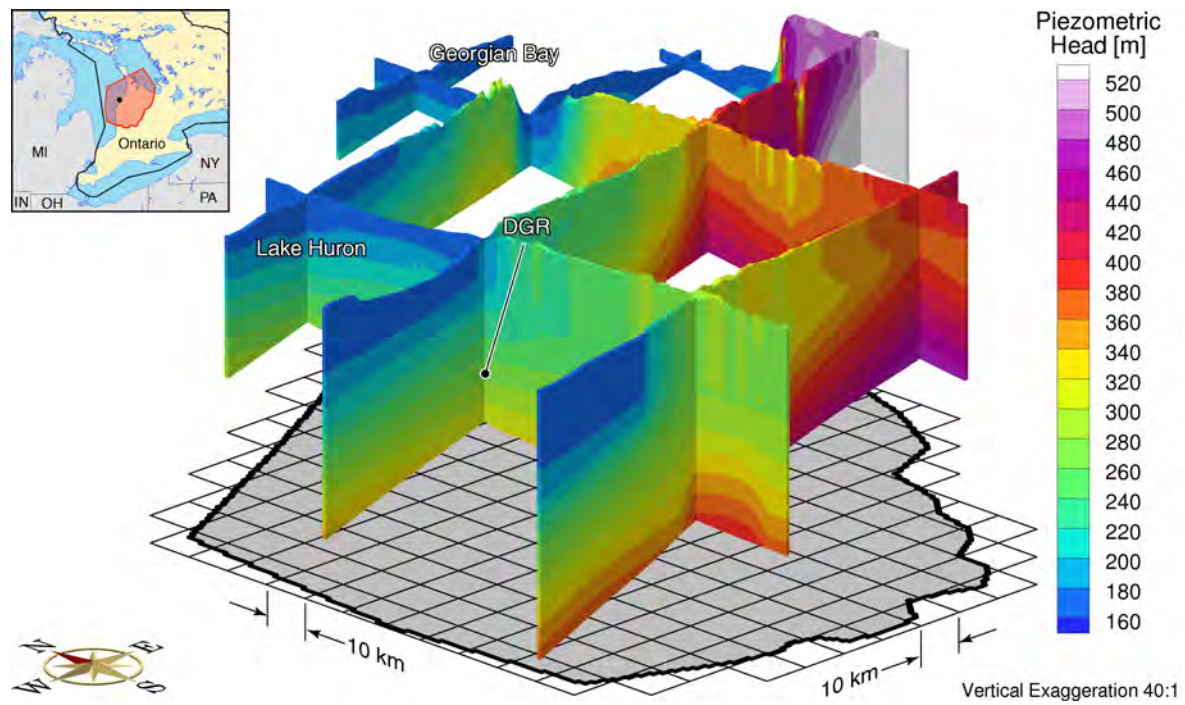


Figure F.26: Fence diagram of equivalent freshwater heads for the base case parameters and the Cambrian anisotropy Camb-4.

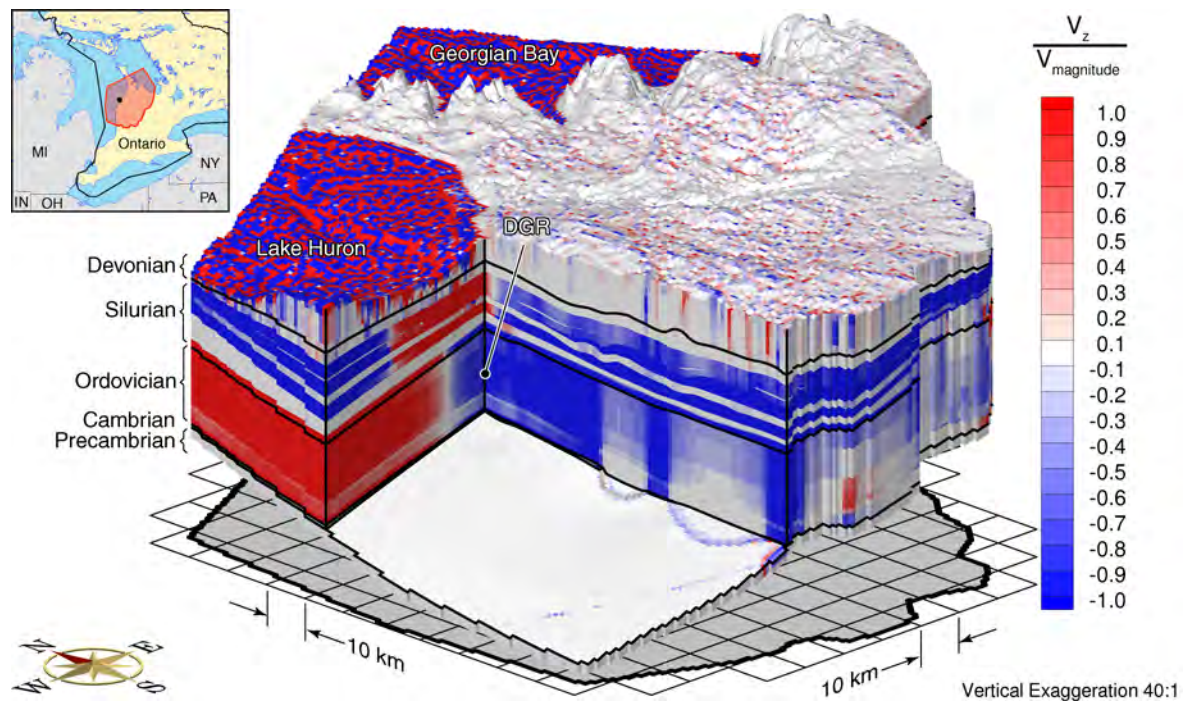


Figure F.27: Ratio of vertical velocity to the velocity magnitude for the base case parameters and the Cambrian anisotropy Camb-4.

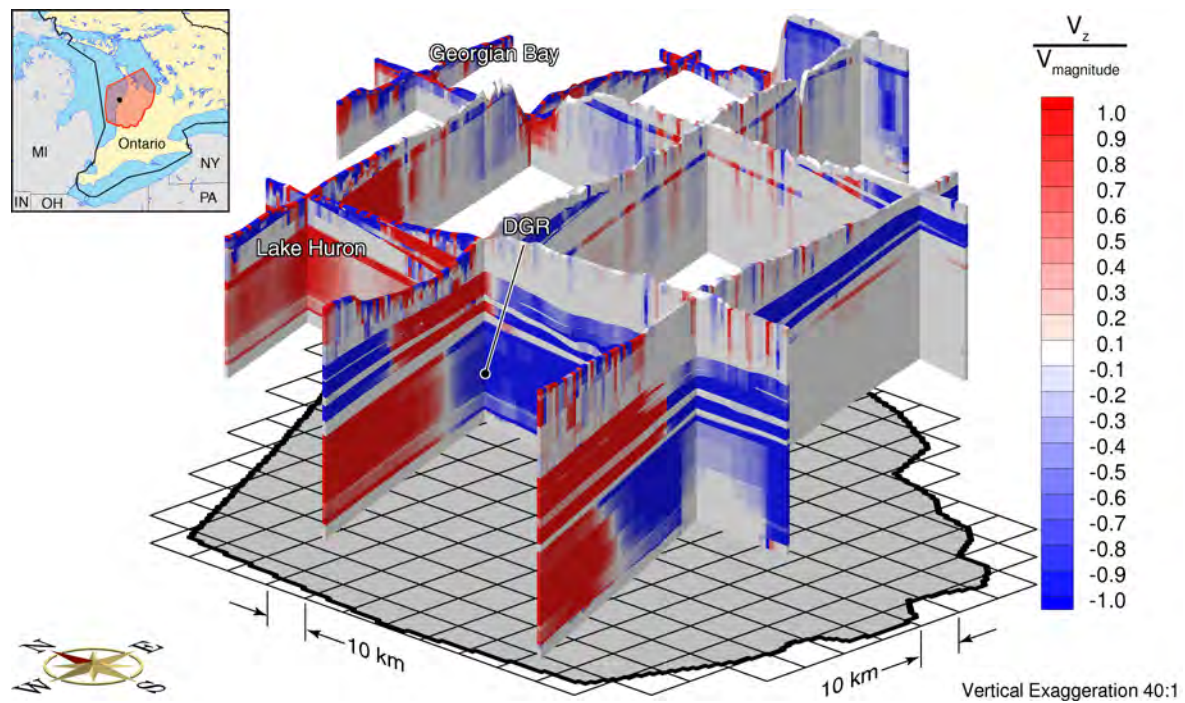


Figure F.28: Fence diagram of the ratio of vertical velocity to the velocity magnitude for the base case parameters and the Cambrian anisotropy Camb-4.

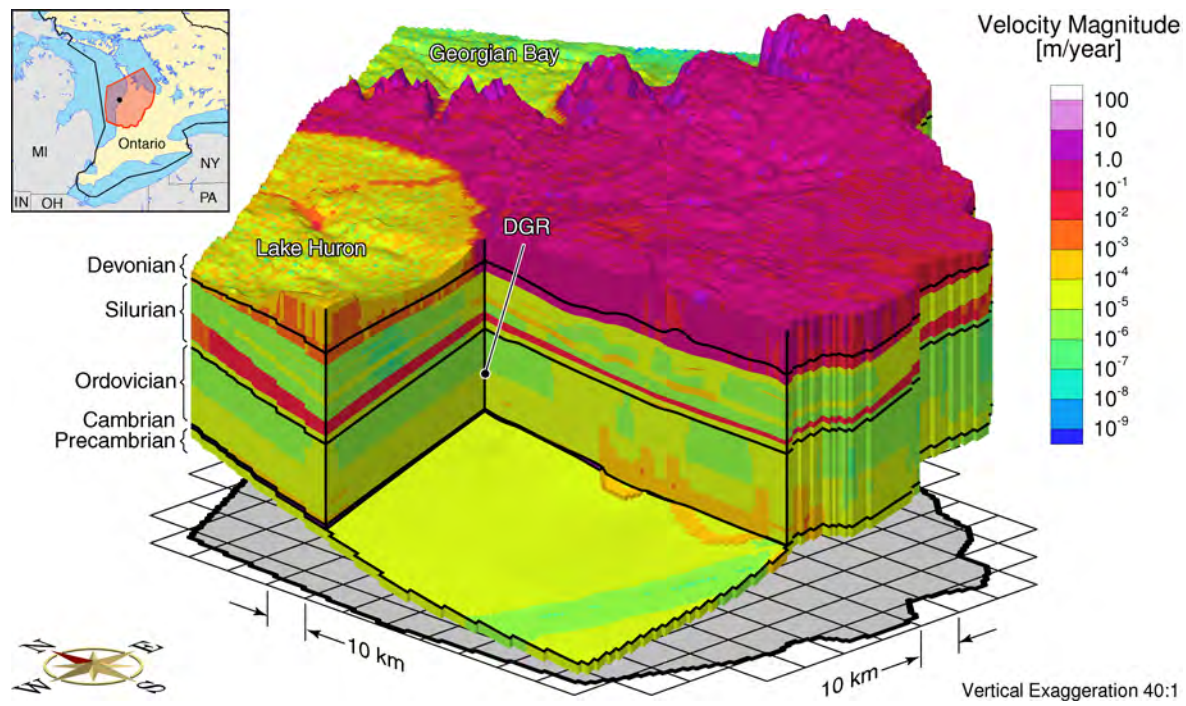


Figure F.29: Pore water velocity magnitude for the base case parameters and the Cambrian anisotropy Camb-4.

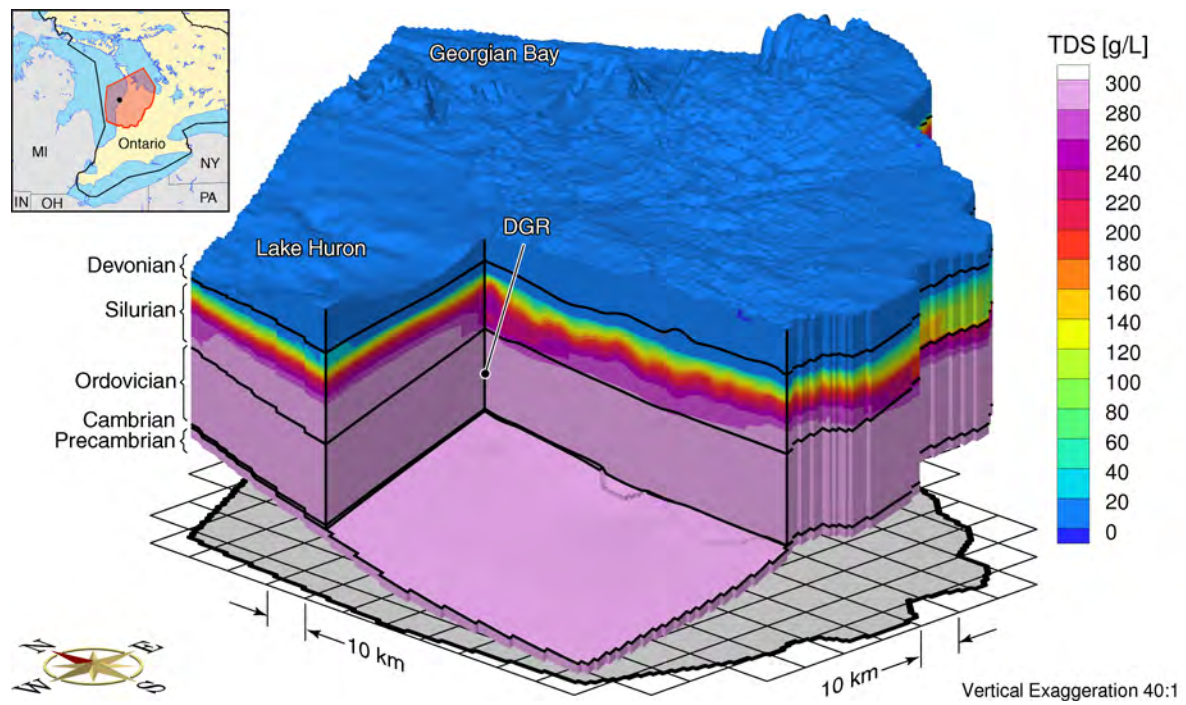


Figure F.30: Total dissolved solids concentration for the base case parameters and the Cambrian anisotropy Camb-4.

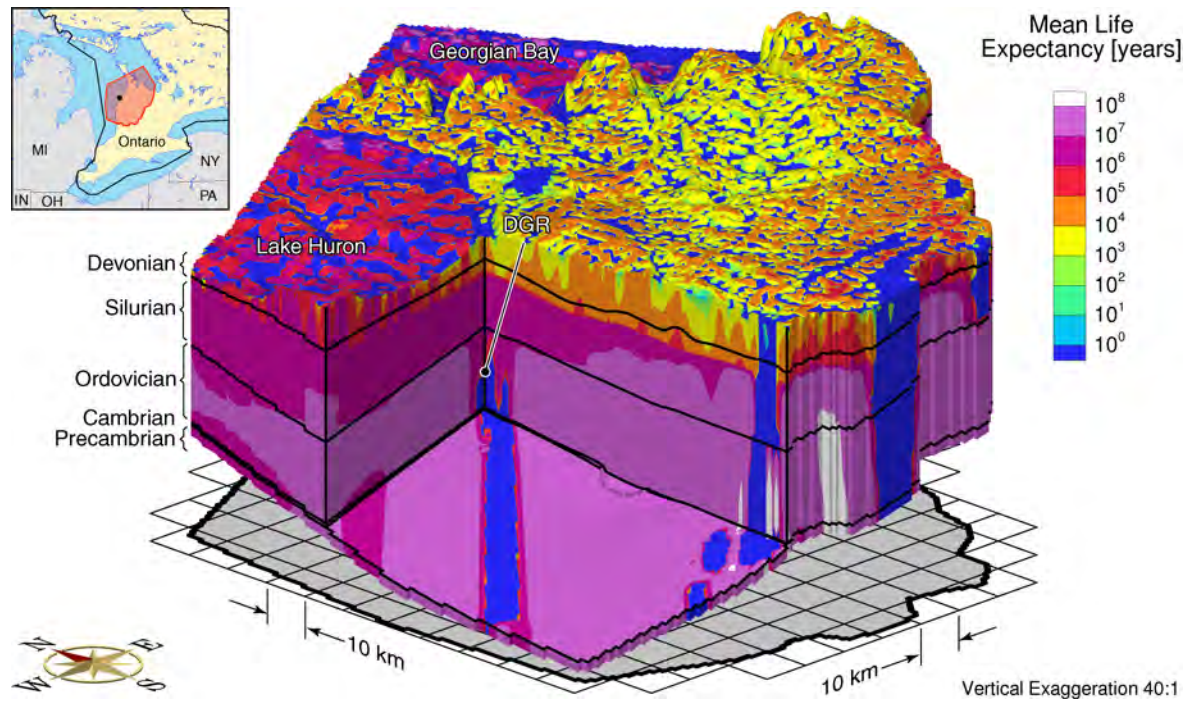


Figure F.31: Mean life expectancies for the base case parameters and the Cambrian anisotropy Camb-4.

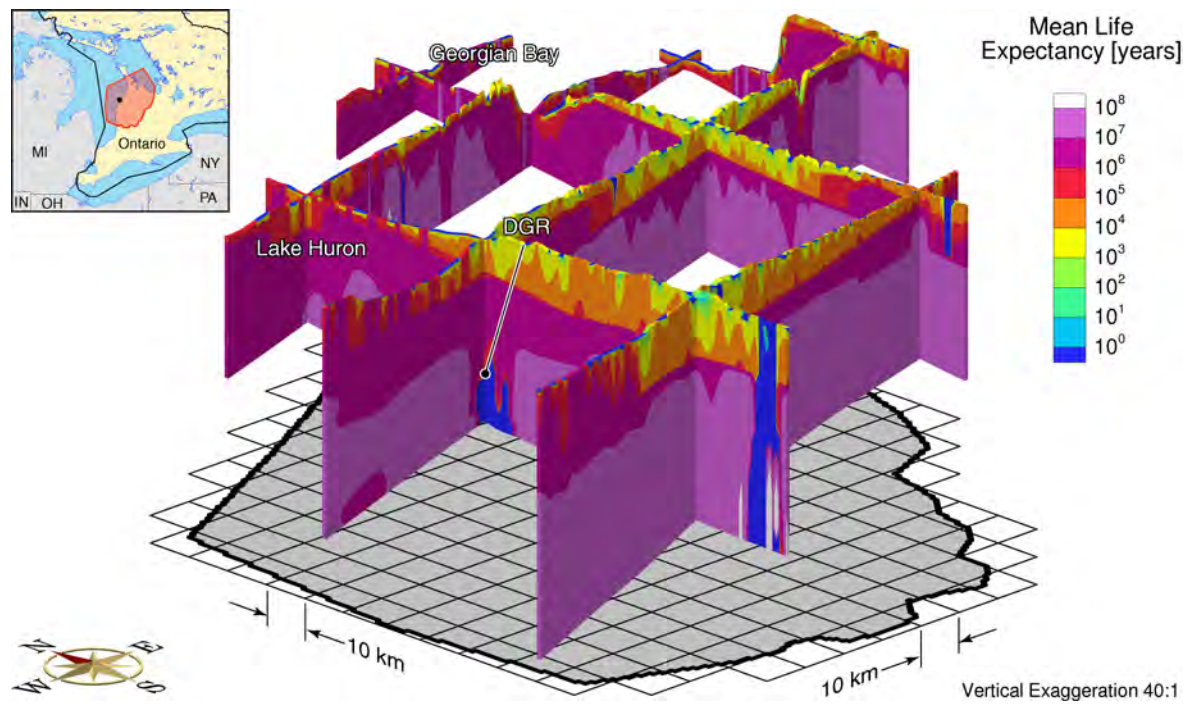


Figure F.32: Fence diagram showing the mean life expectancies for the base case parameters and the Cambrian anisotropy Camb-4.

APPENDIX G – PALEOCLIMATE SIMULATIONS

LIST OF FIGURES

| | | Page |
|--------------|--|-------------|
| Figure G.1. | Fence diagram of environmental heads at 90 000 years before present for the base case parameters. | 177 |
| Figure G.2. | Fence diagram of environmental heads at 60 000 years before present for the base case parameters. | 177 |
| Figure G.3. | Fence diagram of environmental heads at 30 000 years before present for the base case parameters. | 178 |
| Figure G.4. | Fence diagram of environmental heads at the present for the base case parameters. | 178 |
| Figure G.5. | Pore water velocity magnitude at 90 000 years before present for the base case parameters. | 179 |
| Figure G.6. | Pore water velocity magnitude at 60 000 years before present for the base case parameters. | 179 |
| Figure G.7. | Pore water velocity magnitude at 30 000 years before present for the base case parameters. | 180 |
| Figure G.8. | Fence diagram showing the ratio of the vertical pore water velocity to the velocity magnitude at 90 000 years before present for the base case parameters. | 180 |
| Figure G.9. | Fence diagram showing the ratio of the vertical pore water velocity to the velocity magnitude at 60 000 years before present for the base case parameters. | 181 |
| Figure G.10. | Fence diagram showing the ratio of the vertical pore water velocity to the velocity magnitude at 30 000 years before present for the base case parameters. | 181 |
| Figure G.11. | Block-cut diagram showing the depth of penetration of a tracer at 90 000 years before present for the base case parameters. | 182 |
| Figure G.12. | Block-cut diagram showing the depth of penetration of a tracer at 60 000 years before present for the base case parameters. | 182 |
| Figure G.13. | Block-cut diagram showing the depth of penetration of a tracer at 30 000 years before present for the base case parameters. | 183 |
| Figure G.14. | Environmental heads at 90 000 years before present for parameter P-case 1. | 183 |
| Figure G.15. | Environmental heads at 60 000 years before present for parameter P-case 1. | 184 |
| Figure G.16. | Environmental heads at 30 000 years before present for parameter P-case 1. | 184 |
| Figure G.17. | Environmental heads at the present for parameter P-case 1. | 185 |
| Figure G.18. | Fence diagram of environmental heads at 60 000 years before present for parameter P-case 1. | 185 |
| Figure G.19. | Fence diagram of environmental heads at the present for parameter P-case 1. | 186 |
| Figure G.20. | Pore water velocity magnitude at the present for parameter P-case 1. | 186 |
| Figure G.21. | Fence diagram showing the ratio of the vertical pore water velocity to the velocity magnitude at the present for parameter P-case 1. | 187 |
| Figure G.22. | Total dissolved solids distribution at the present for the paleoclimate simulation and parameter P-case 1. | 187 |
| Figure G.23. | Block-cut diagram showing the depth of penetration of a tracer at the present for parameter P-case 1. | 188 |
| Figure G.24. | Environmental heads at 90 000 years before present for parameter P-case 2. | 188 |

| | | |
|--------------|--|-----|
| Figure G.25. | Environmental heads at 60 000 years before present for parameter P-case 2. | 189 |
| Figure G.26. | Environmental heads at 30 000 years before present for parameter P-case 2. | 189 |
| Figure G.27. | Environmental heads at the present for parameter P-case 2. | 190 |
| Figure G.28. | Fence diagram of environmental heads at 60 000 years before present for parameter P-case 2. | 190 |
| Figure G.29. | Fence diagram of environmental heads at the present for parameter P-case 2. | 191 |
| Figure G.30. | Pore water velocity magnitude at the present for parameter P-case 2. | 191 |
| Figure G.31. | Fence diagram showing the ratio of the vertical pore water velocity to the velocity magnitude at the present for parameter P-case 2. | 192 |
| Figure G.32. | Total dissolved solids distribution at the present for the paleoclimate simulation parameter P-case 2. | 192 |
| Figure G.33. | Block-cut diagram showing the depth of penetration of a tracer at the present parameter P-case 2. | 193 |
| Figure G.34. | Environmental heads at 90 000 years before present for parameter P-case 3. | 193 |
| Figure G.35. | Environmental heads at 60 000 years before present for parameter P-case 3. | 194 |
| Figure G.36. | Environmental heads at 30 000 years before present for parameter P-case 3. | 194 |
| Figure G.37. | Environmental heads at the present for parameter P-case 3. | 195 |
| Figure G.38. | Fence diagram of environmental heads at 60 000 years before present for parameter P-case 3. | 195 |
| Figure G.39. | Fence diagram of environmental heads at the present for parameter P-case 3. | 196 |
| Figure G.40. | Pore water velocity magnitude at the present for parameter P-case 3. | 196 |
| Figure G.41. | Fence diagram showing the ratio of the vertical pore water velocity to the velocity magnitude at the present for parameter P-case 3. | 197 |
| Figure G.42. | Total dissolved solids distribution at the present for the paleoclimate simulation parameter P-case 3. | 197 |
| Figure G.43. | Block-cut diagram showing the depth of penetration of a tracer at the present parameter P-case 3. | 198 |

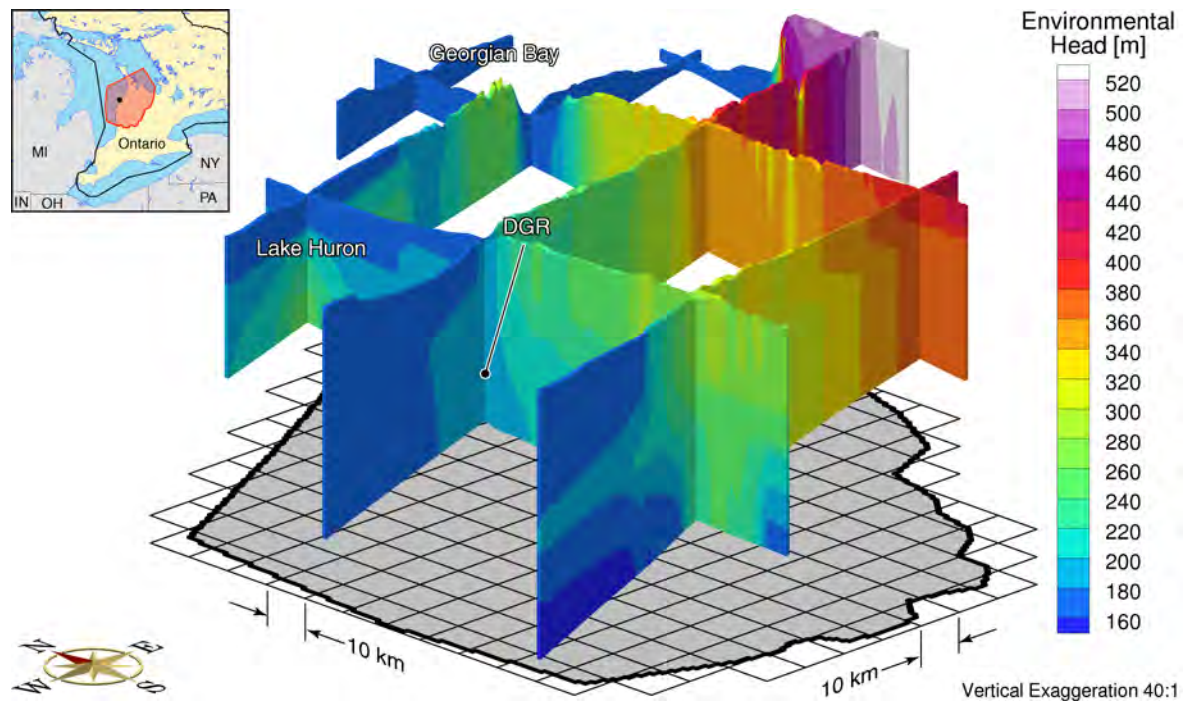


Figure G.1: Fence diagram of environmental heads at 90 000 years before present for the base case parameters.

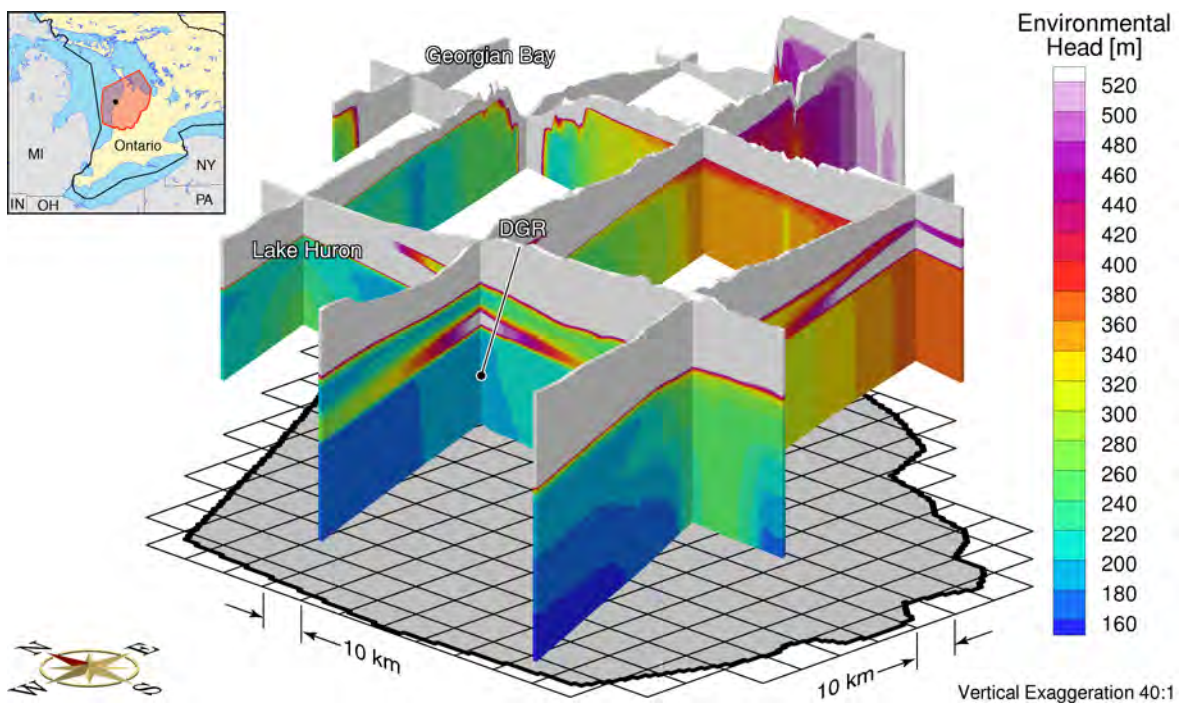


Figure G.2: Fence diagram of environmental heads at 60 000 years before present for the base case parameters.

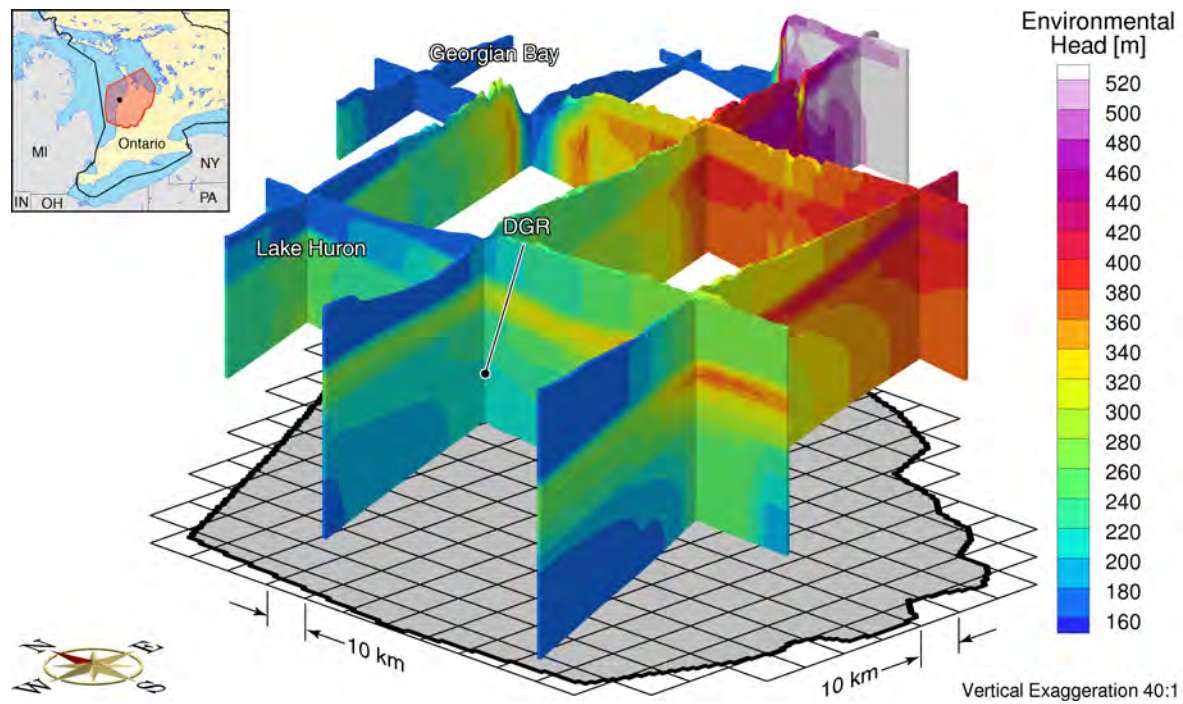


Figure G.3: Fence diagram of environmental heads at 30 000 years before present for the base case parameters.

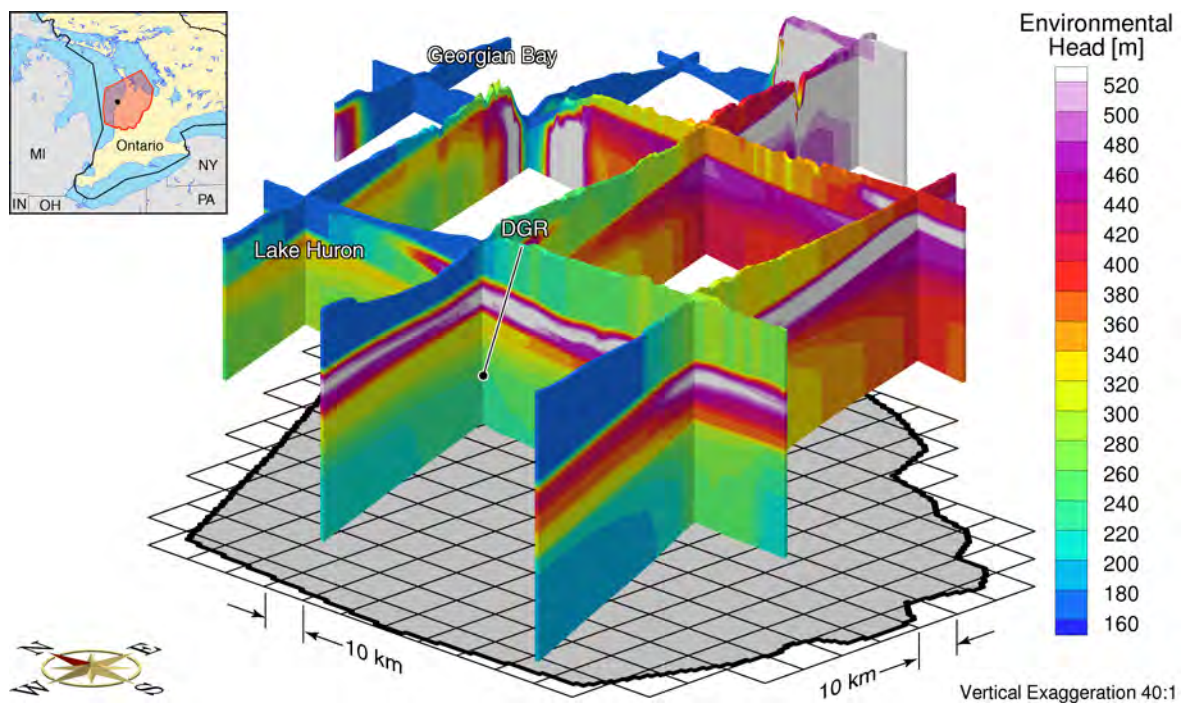


Figure G.4: Fence diagram of environmental heads at the present for the base case parameters.

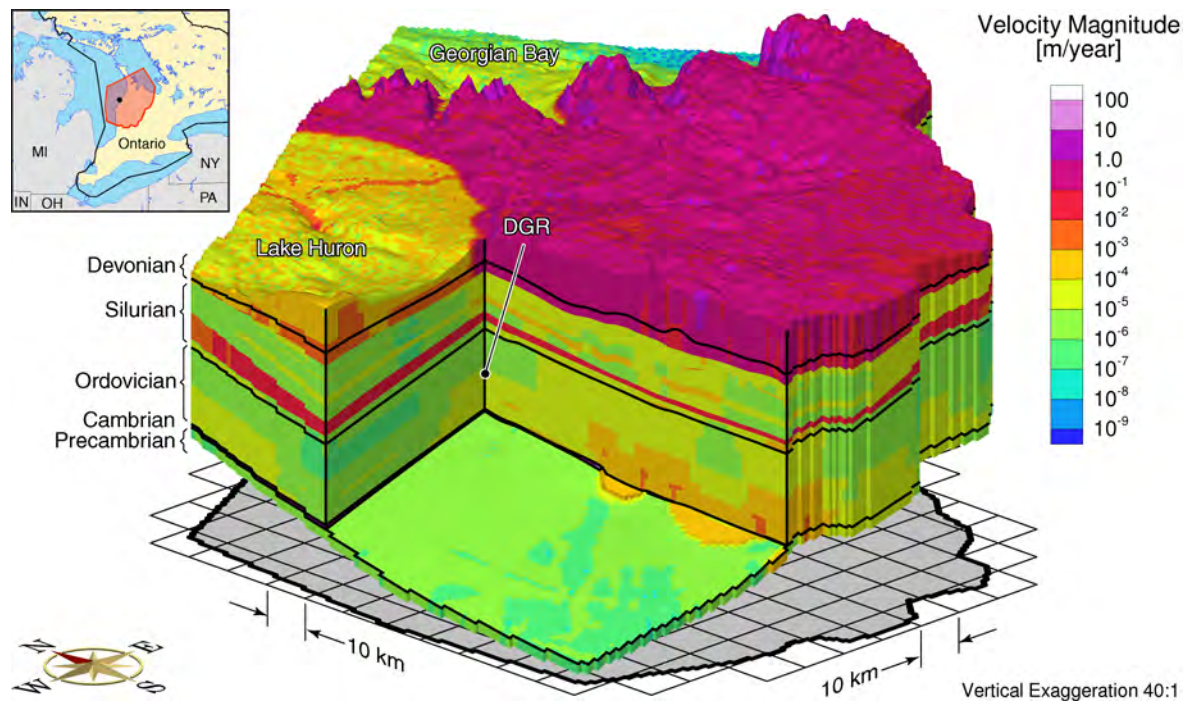


Figure G.5: Pore water velocity magnitude at 90 000 years before present for the base case parameters.

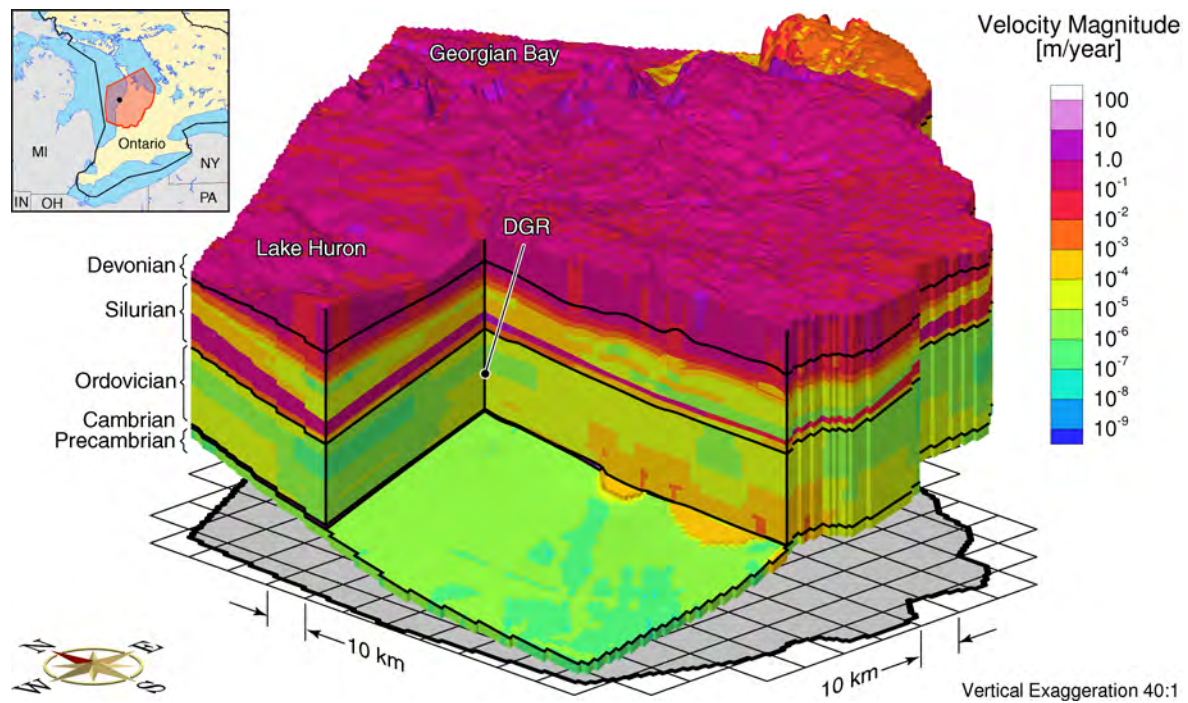


Figure G.6: Pore water velocity magnitude at 60 000 years before present for the base case parameters.

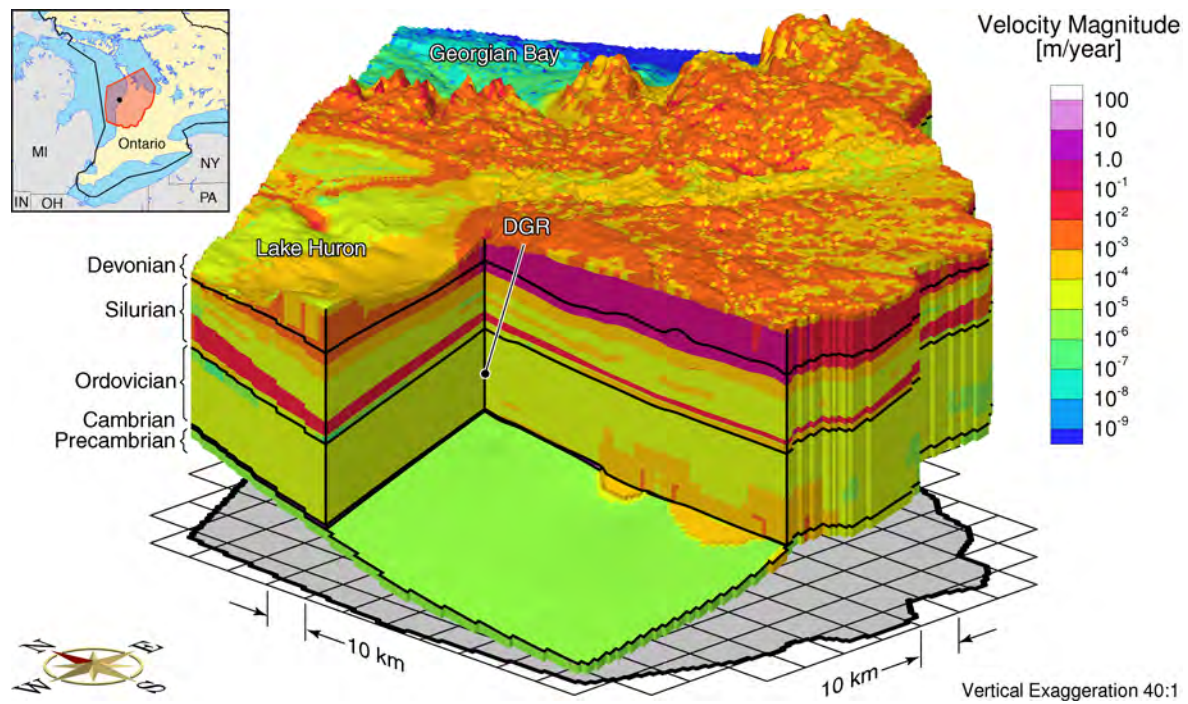


Figure G.7: Pore water velocity magnitude at 30 000 years before present for the base case parameters.

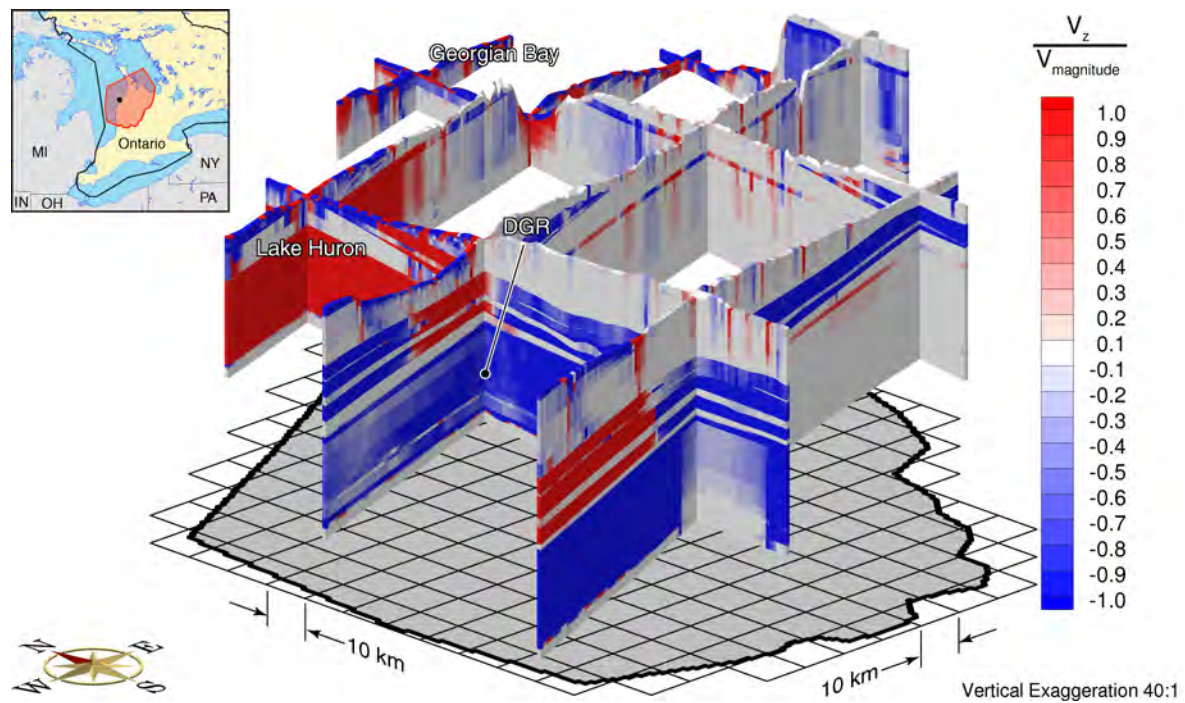


Figure G.8: Fence diagram showing the ratio of the vertical pore water velocity to the velocity magnitude at 90 000 years before present for the base case parameters.

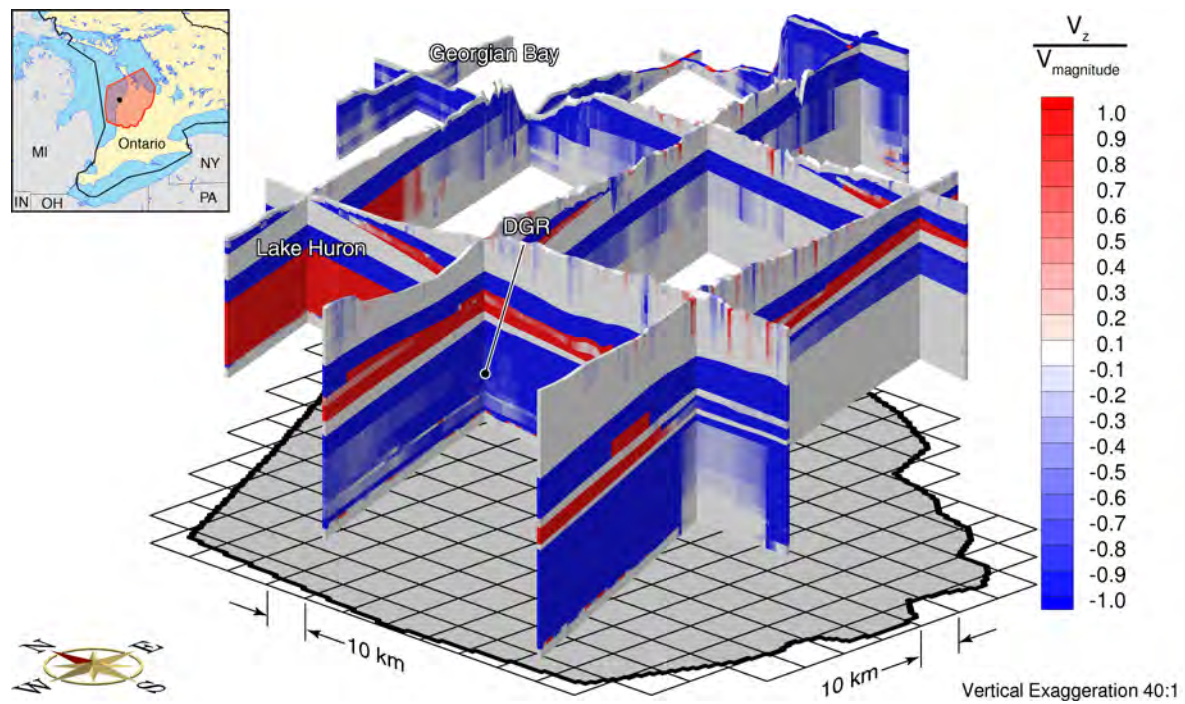


Figure G.9: Fence diagram showing the ratio of the vertical pore water velocity to the velocity magnitude at 60 000 years before present for the base case parameters.

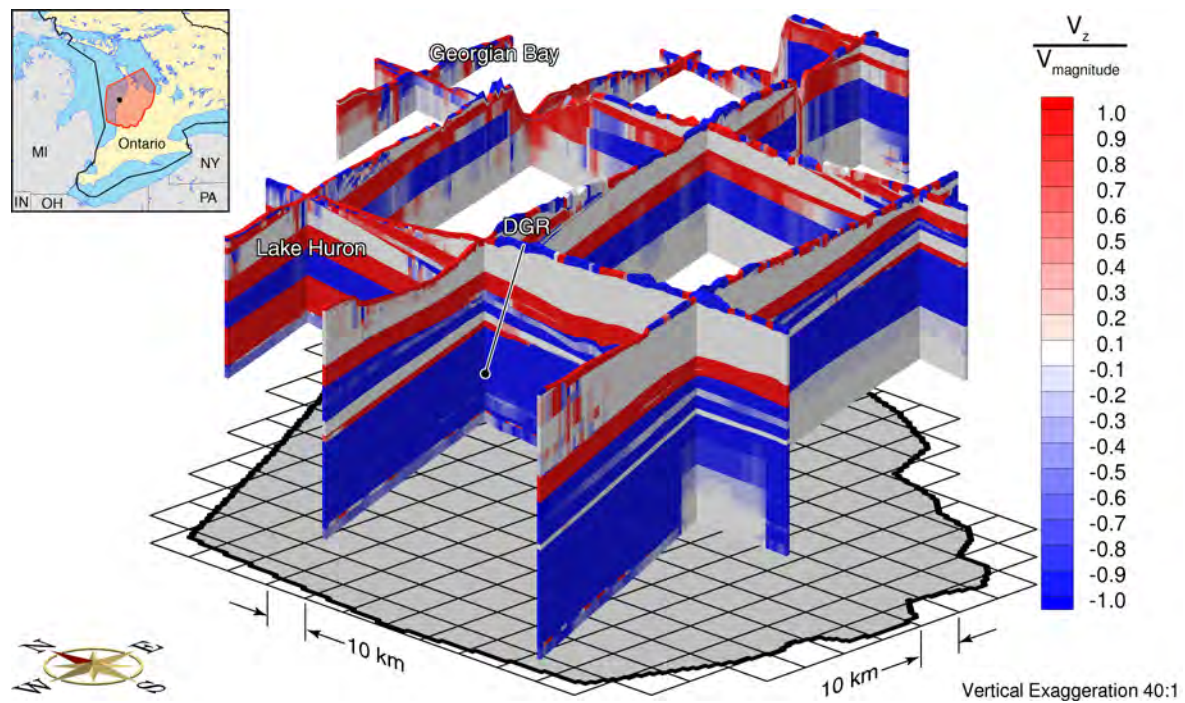


Figure G.10: Fence diagram showing the ratio of the vertical pore water velocity to the velocity magnitude at 30 000 years before present for the base case parameters.

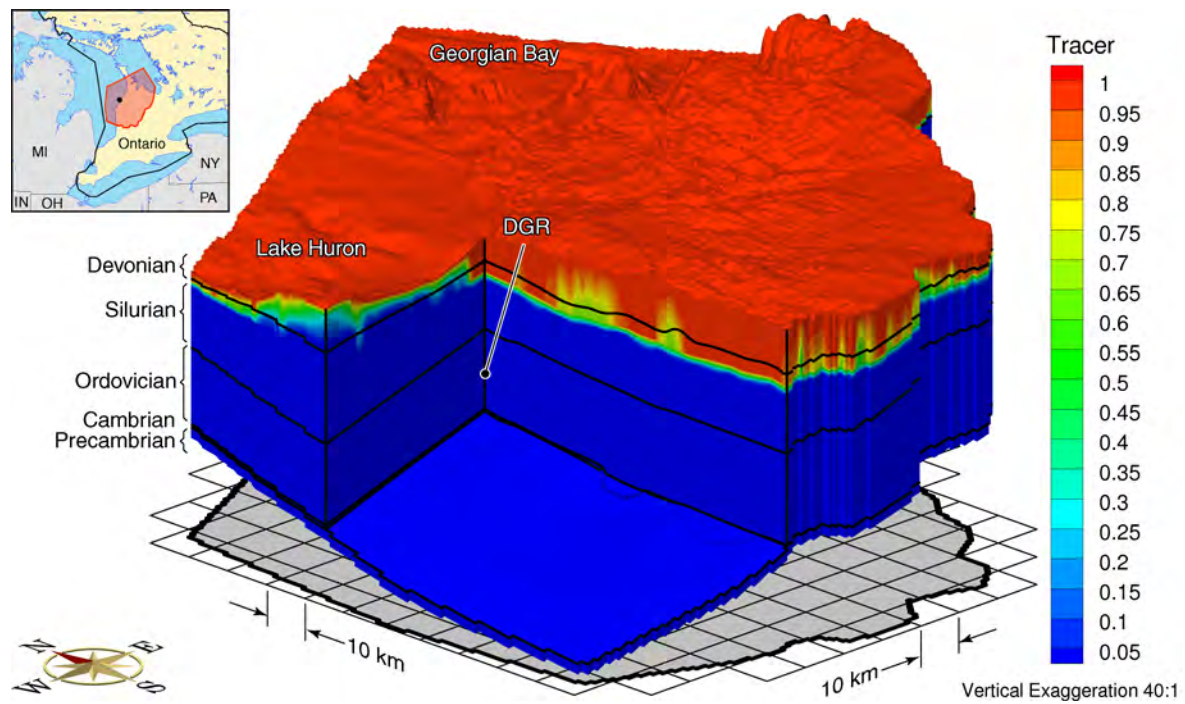


Figure G.11: Block-cut diagram showing the depth of penetration of a tracer at 90 000 years before present for the base case parameters.

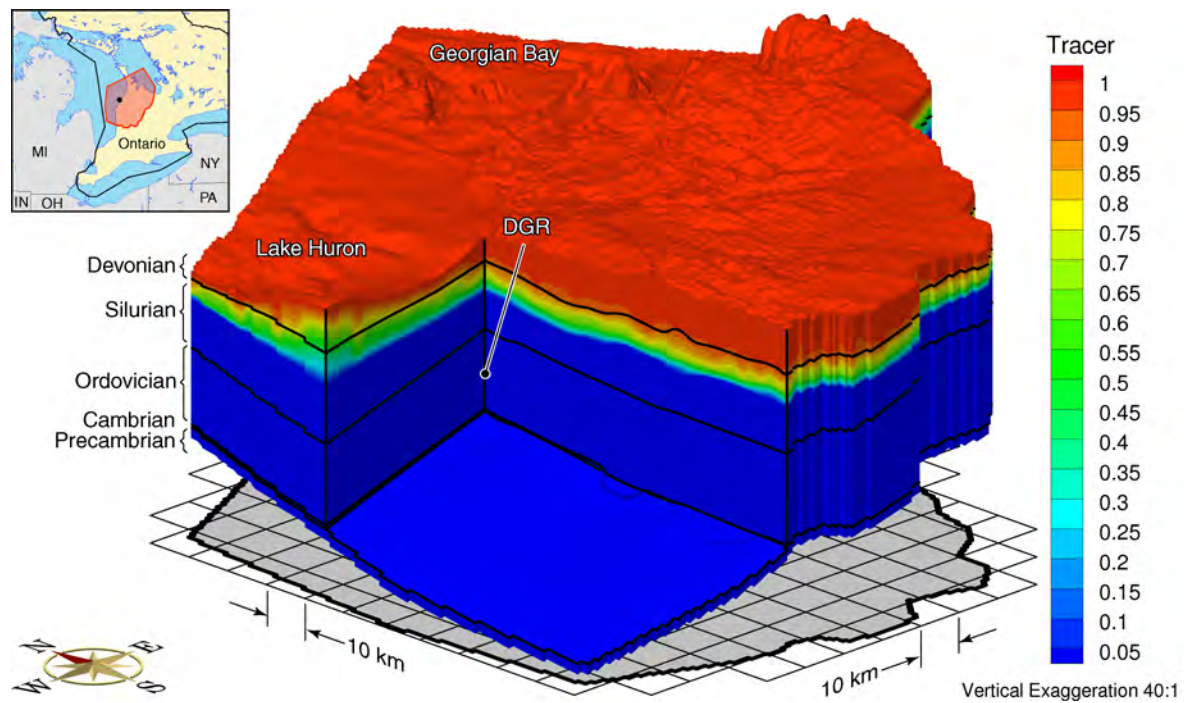


Figure G.12: Block-cut diagram showing the depth of penetration of a tracer at 60 000 years before present for the base case parameters.

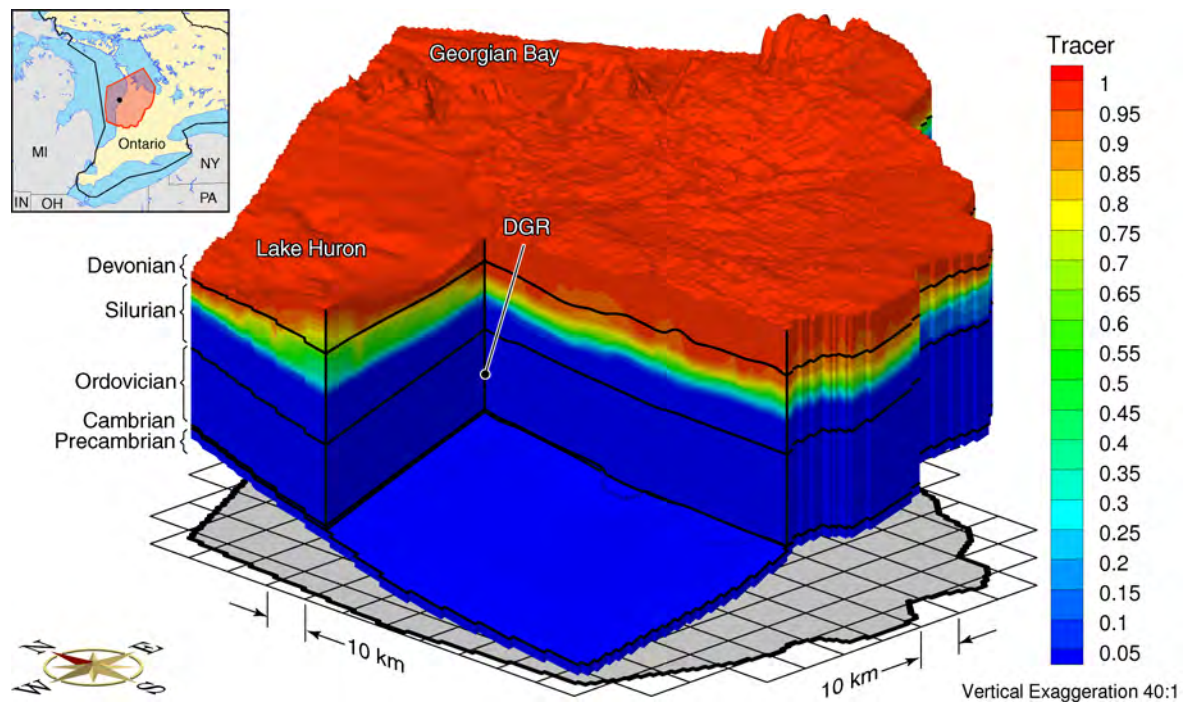


Figure G.13: Block-cut diagram showing the depth of penetration of a tracer at 30 000 years before present for the base case parameters.

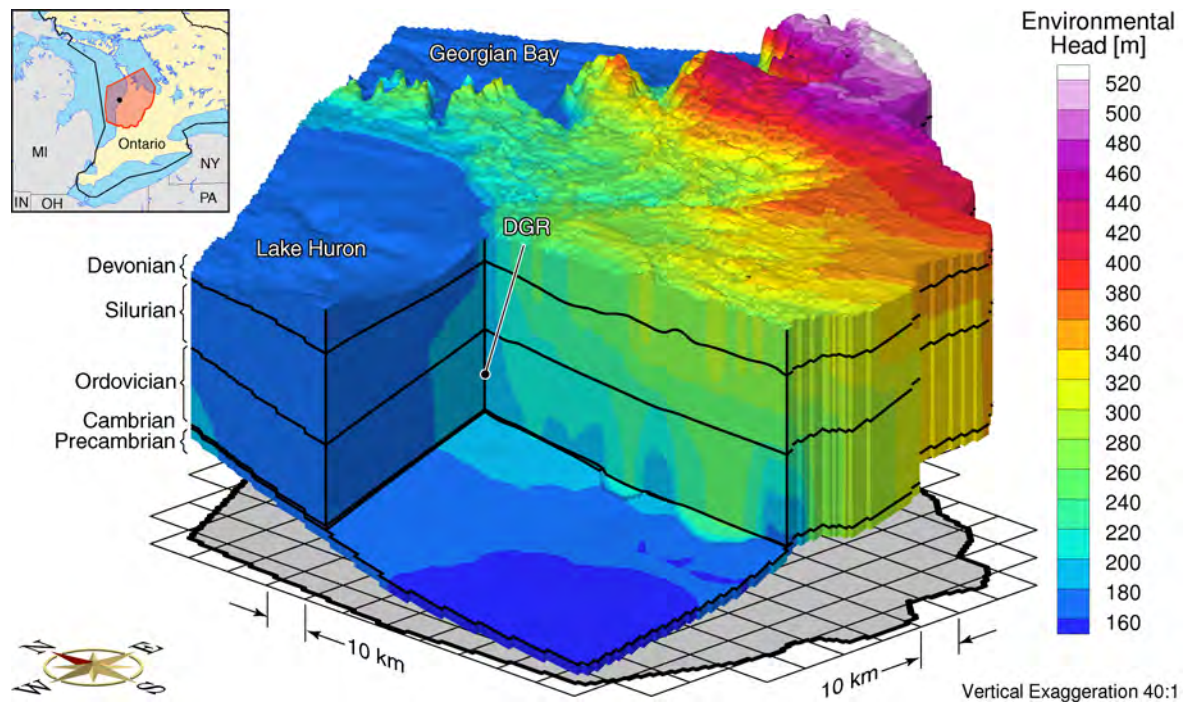


Figure G.14: Environmental heads at 90 000 years before present for parameter P-case 1.

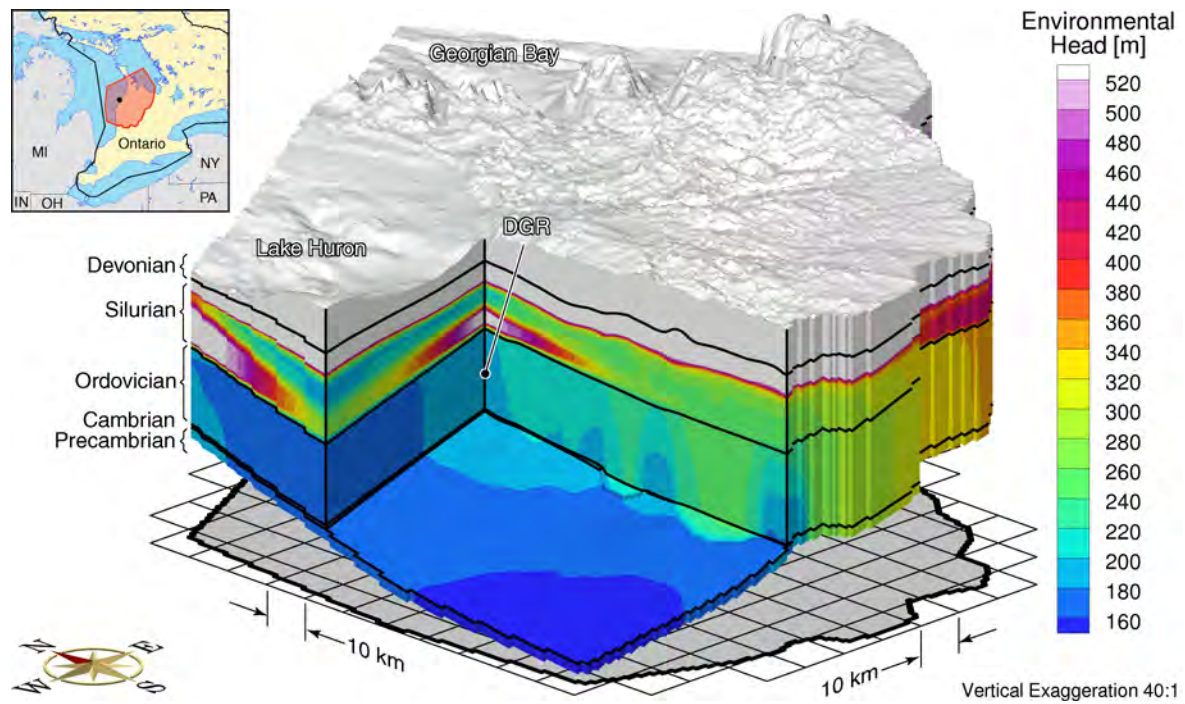


Figure G.15: Environmental heads at 60 000 years before present for parameter P-case 1.

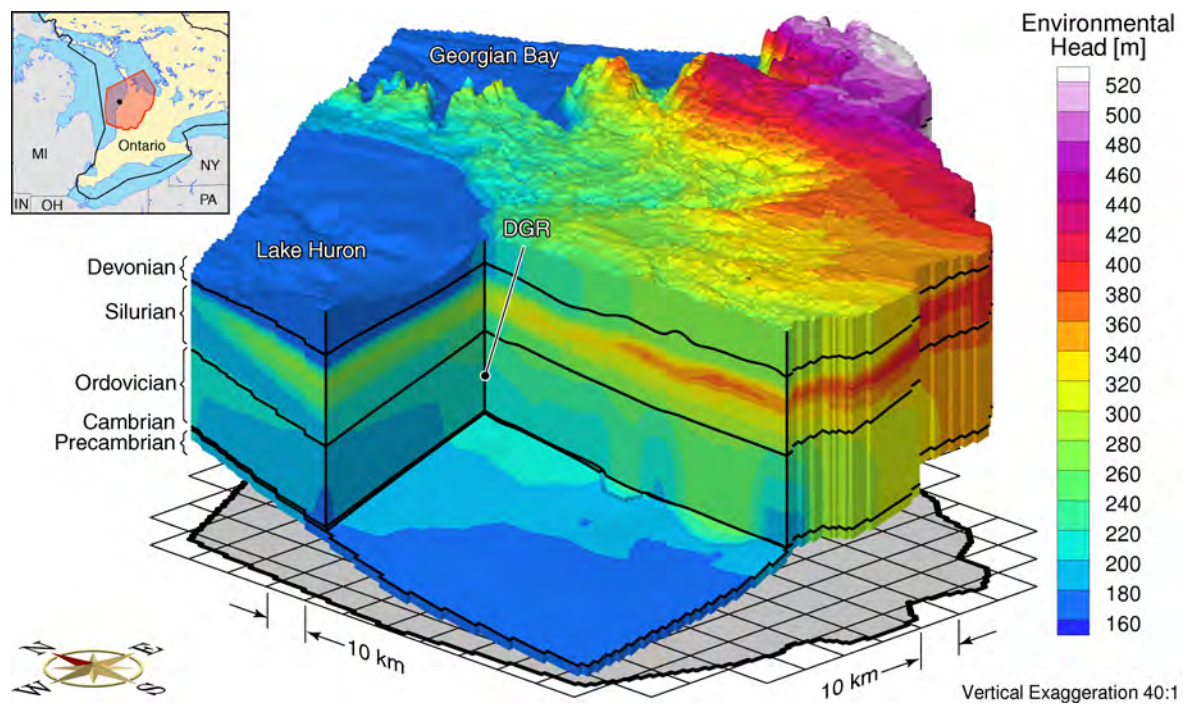


Figure G.16: Environmental heads at 30 000 years before present for parameter P-case 1.

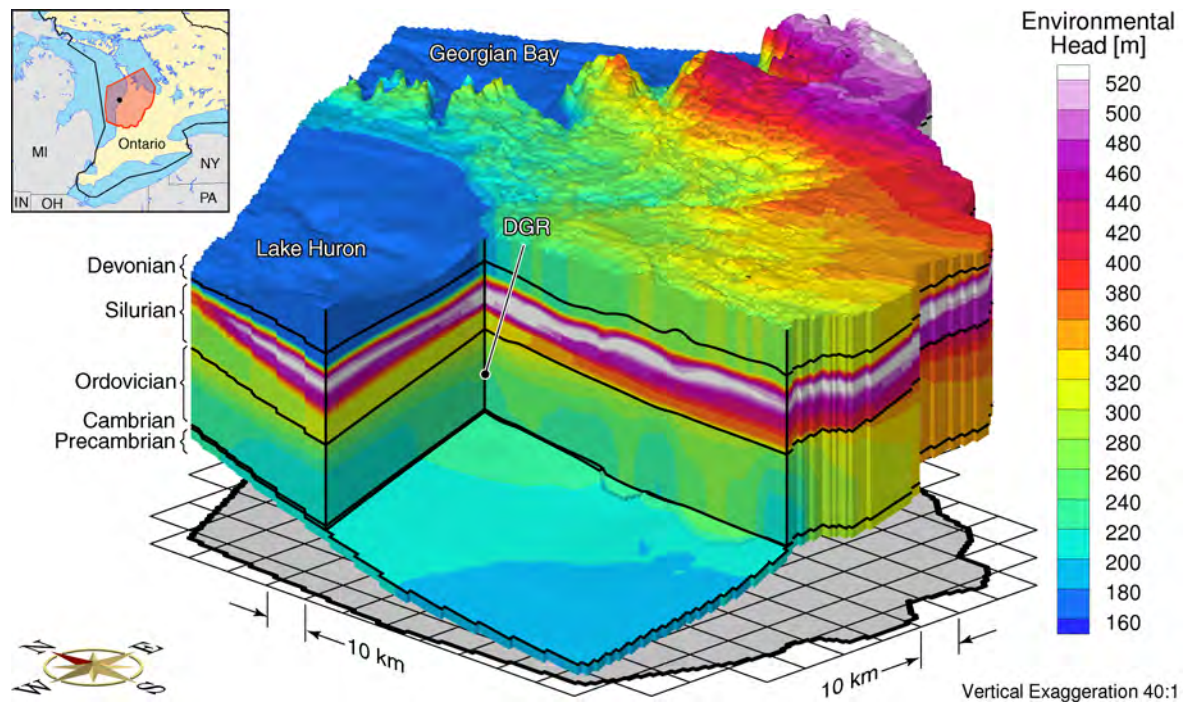


Figure G.17: Environmental heads at the present for parameter P-case 1.

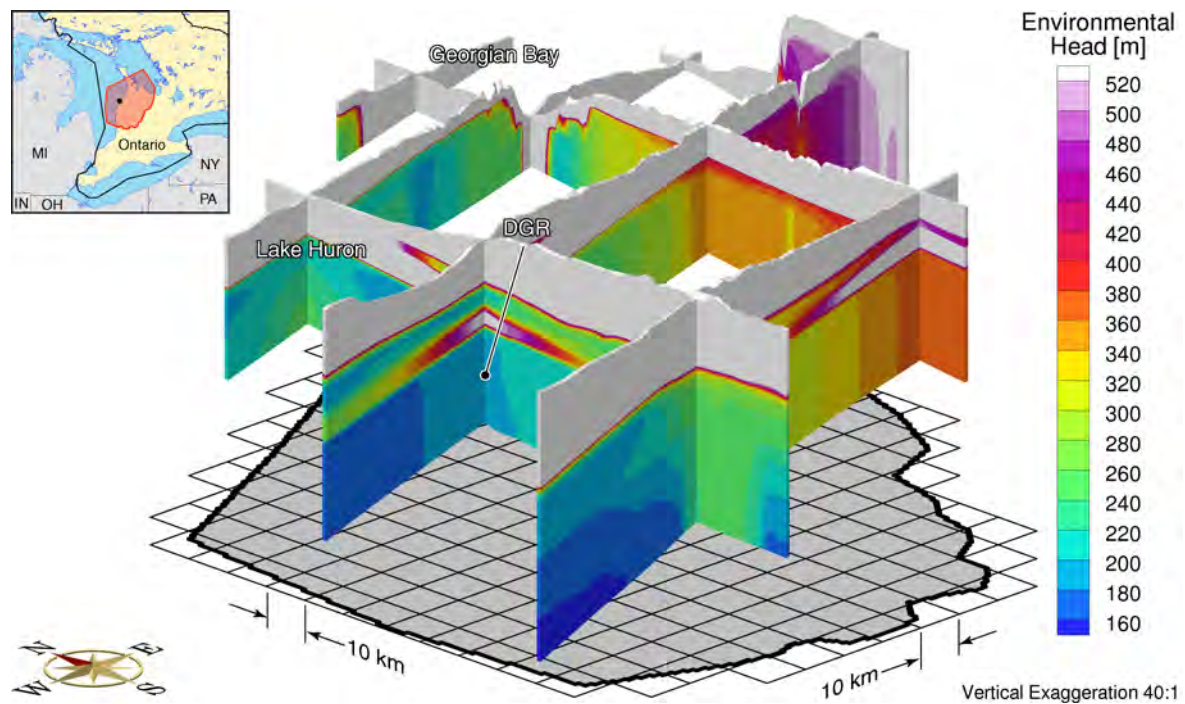


Figure G.18: Fence diagram of environmental heads at 60 000 years before present for parameter P-case 1.

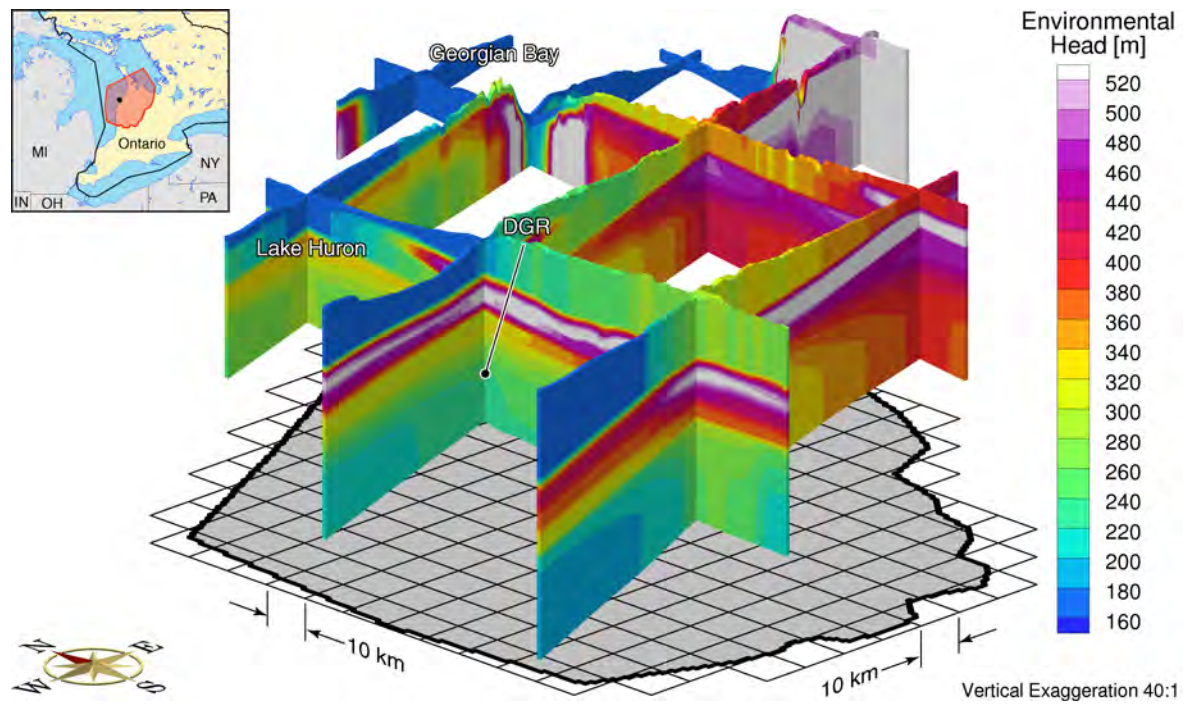


Figure G.19: Fence diagram of environmental heads at the present for parameter P-case 1.

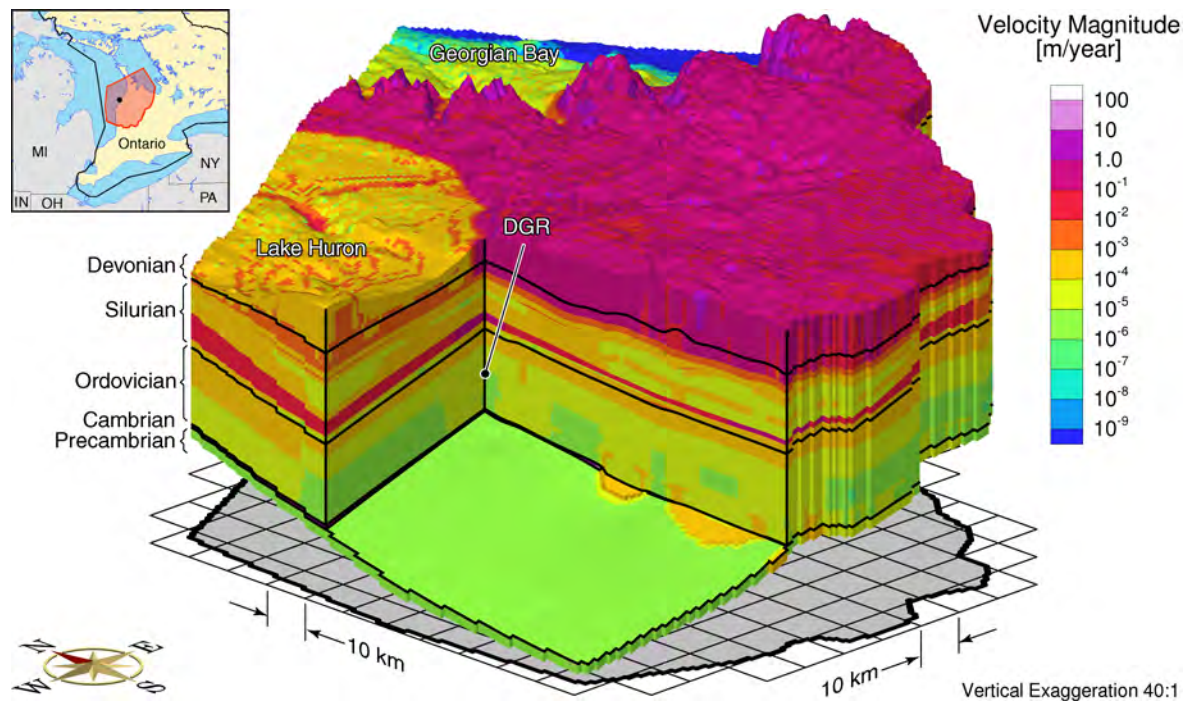


Figure G.20: Pore water velocity magnitude at the present for parameter P-case 1.

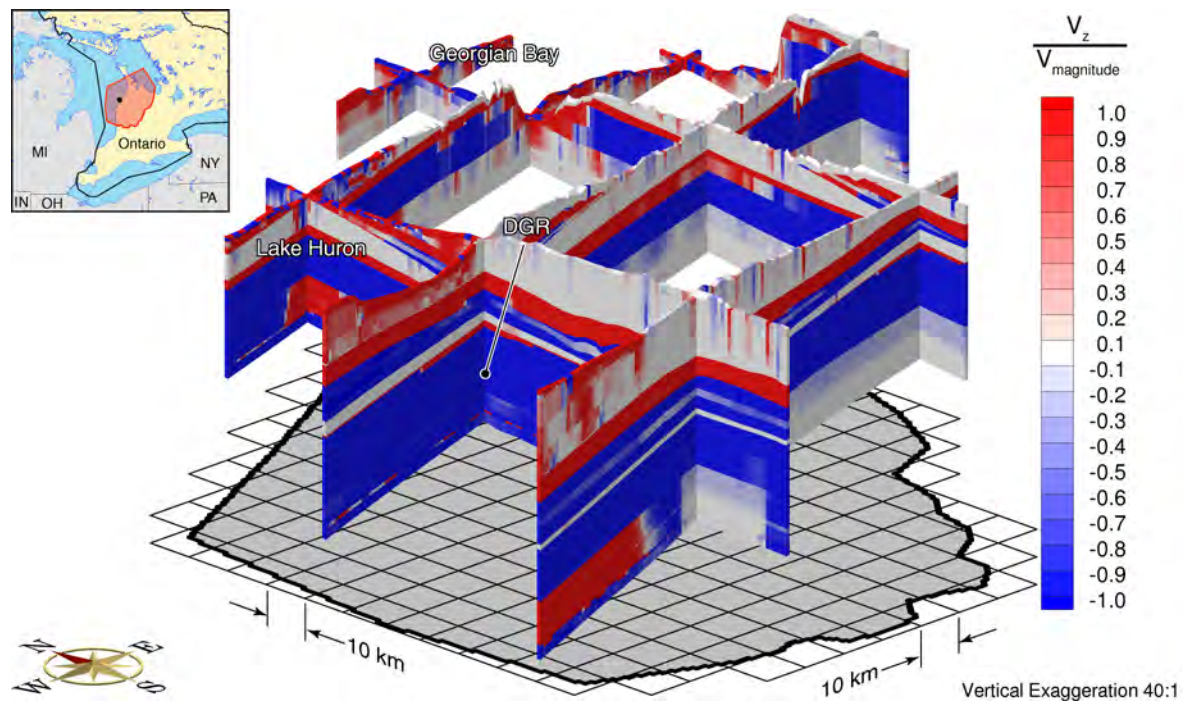


Figure G.21: Fence diagram showing the ratio of the vertical pore water velocity to the velocity magnitude at the present for parameter P-case 1.

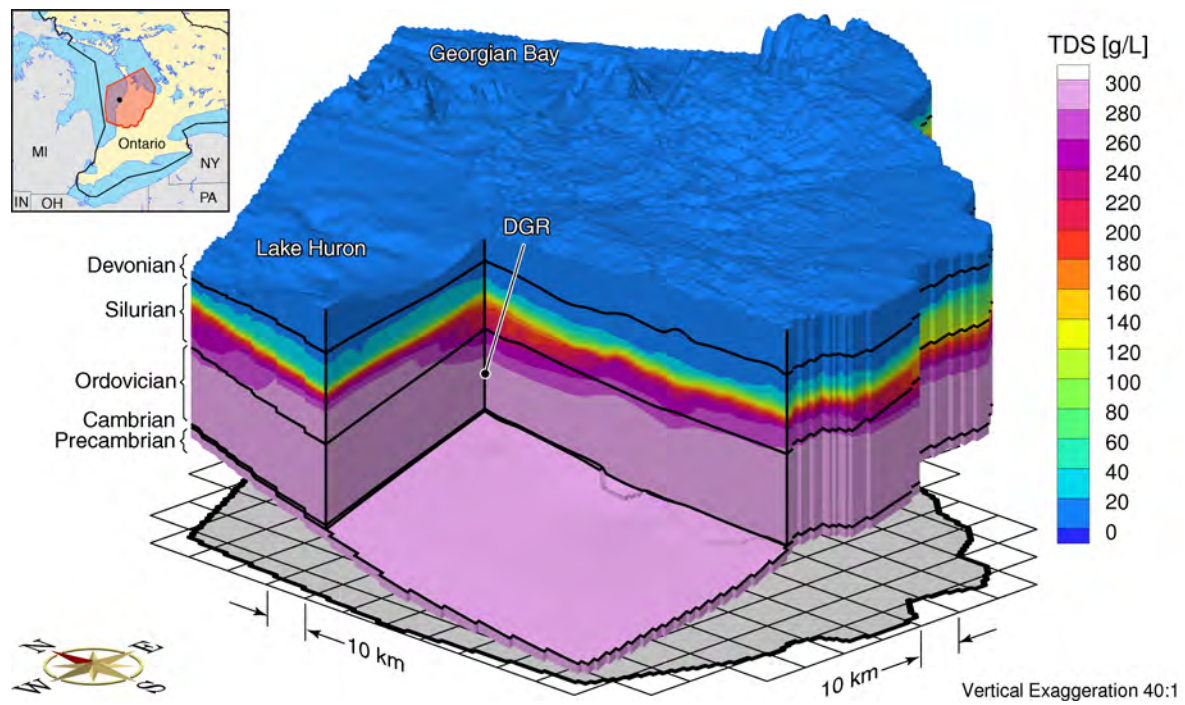


Figure G.22: Total dissolved solids distribution at the present for the paleoclimate simulation and parameter P-case 1.

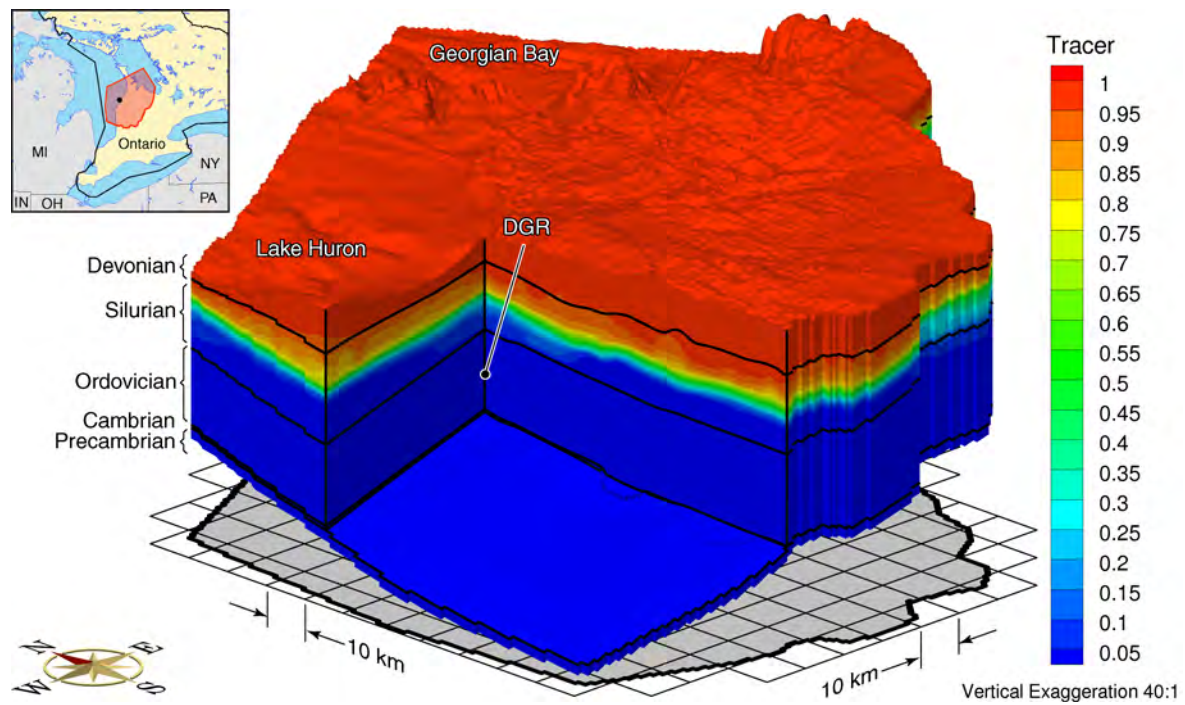


Figure G.23: Block-cut diagram showing the depth of penetration of a tracer at the present for parameter P-case 1.

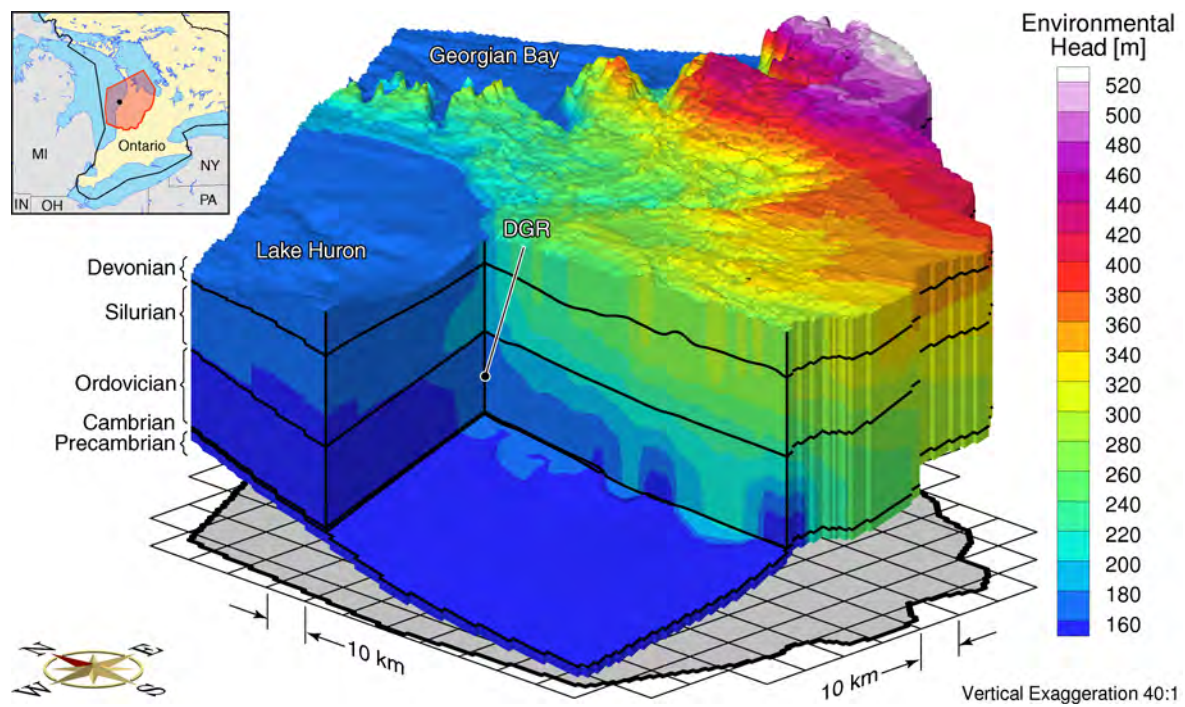


Figure G.24: Environmental heads at 90 000 years before present for parameter P-case 2.

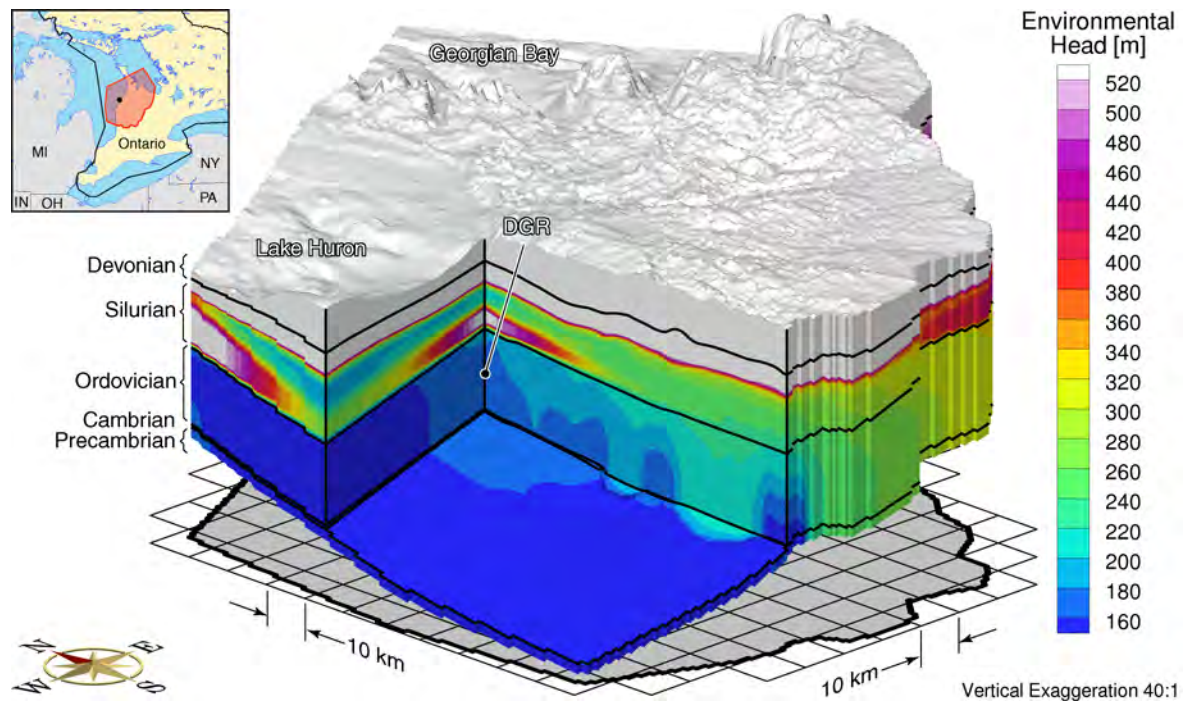


Figure G.25: Environmental heads at 60 000 years before present for parameter P-case 2.

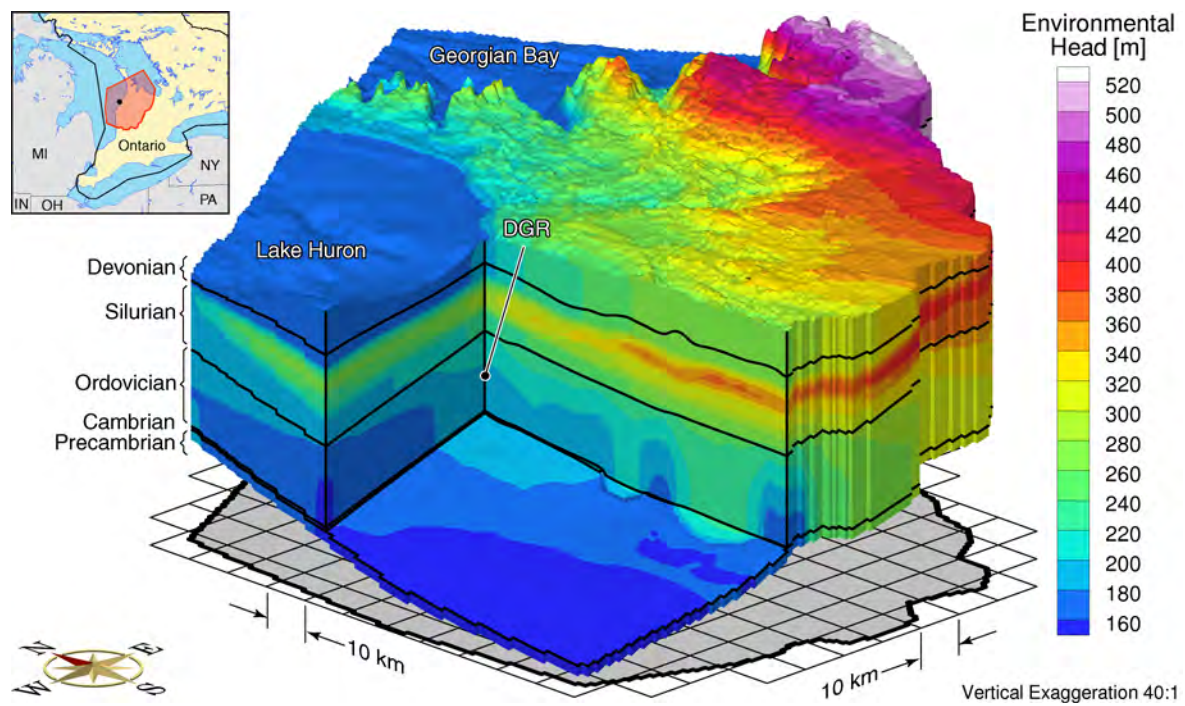


Figure G.26: Environmental heads at 30 000 years before present for parameter P-case 2.

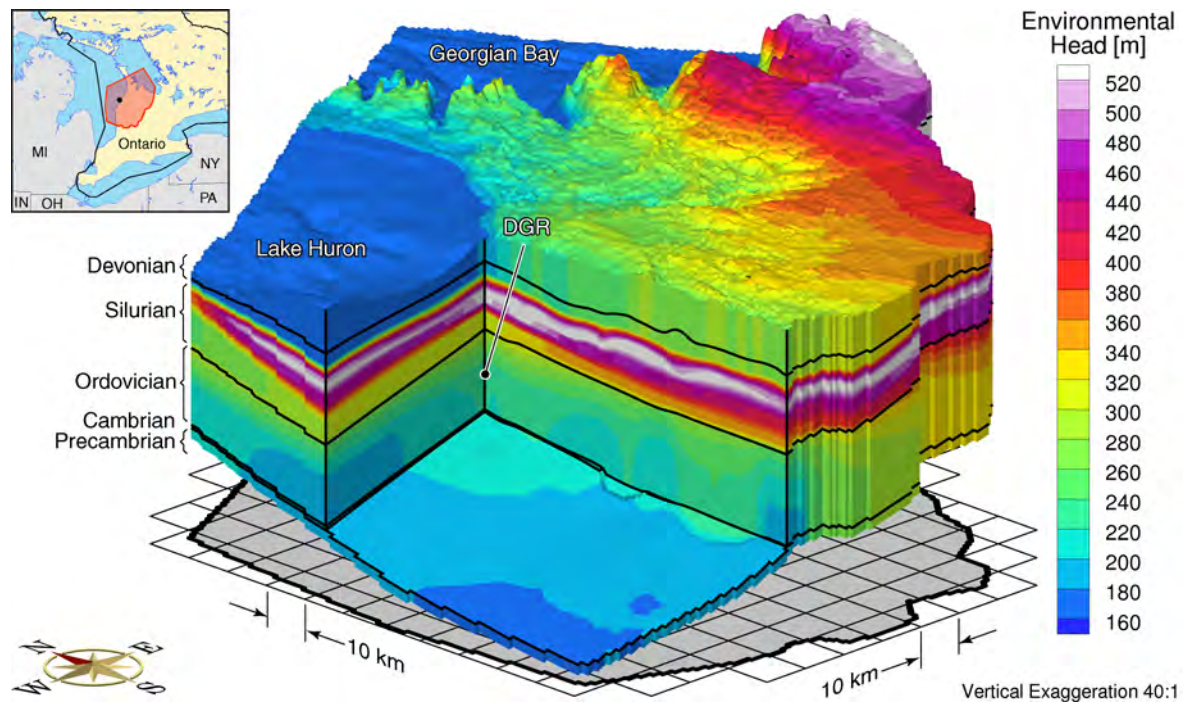


Figure G.27: Environmental heads at the present for parameter P-case 2.

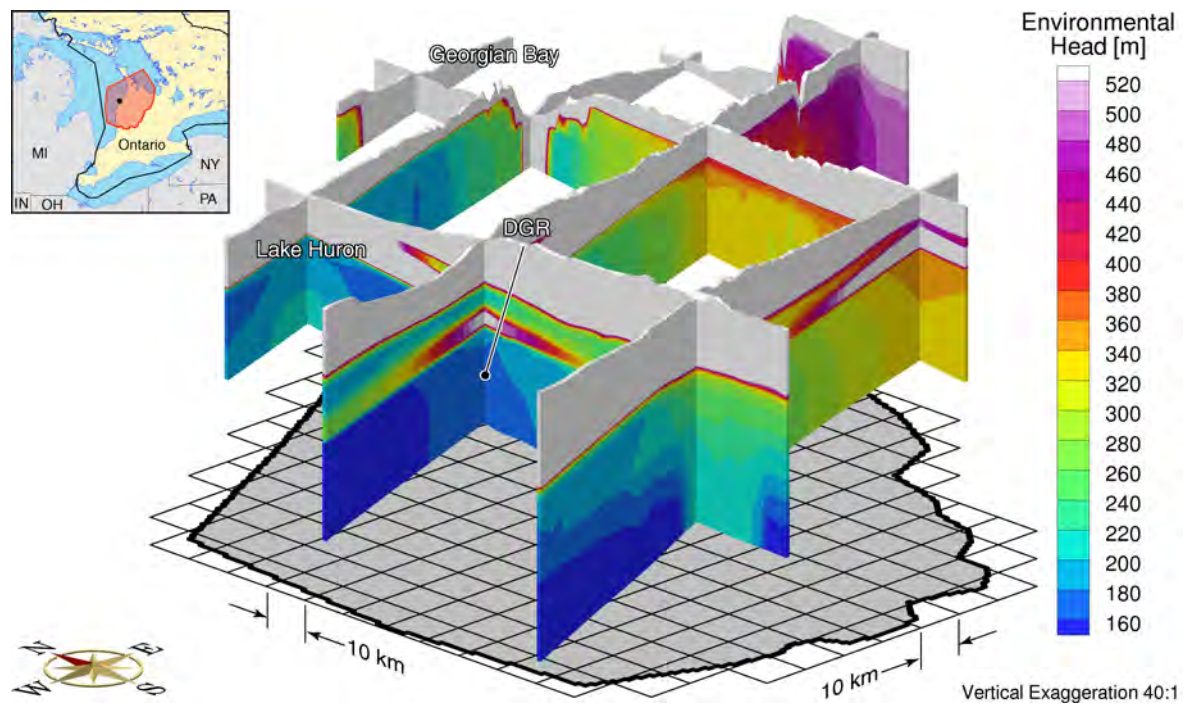


Figure G.28: Fence diagram of environmental heads at 60 000 years before present for parameter P-case 2.

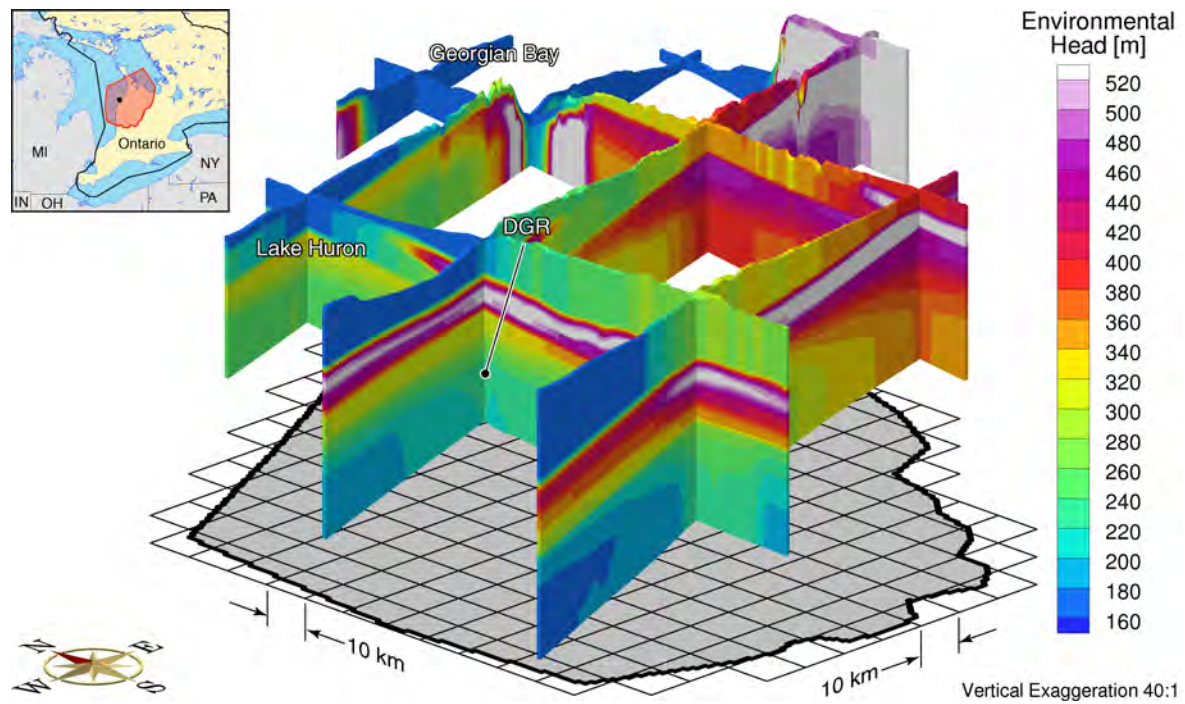


Figure G.29: Fence diagram of environmental heads at the present for parameter P-case 2.

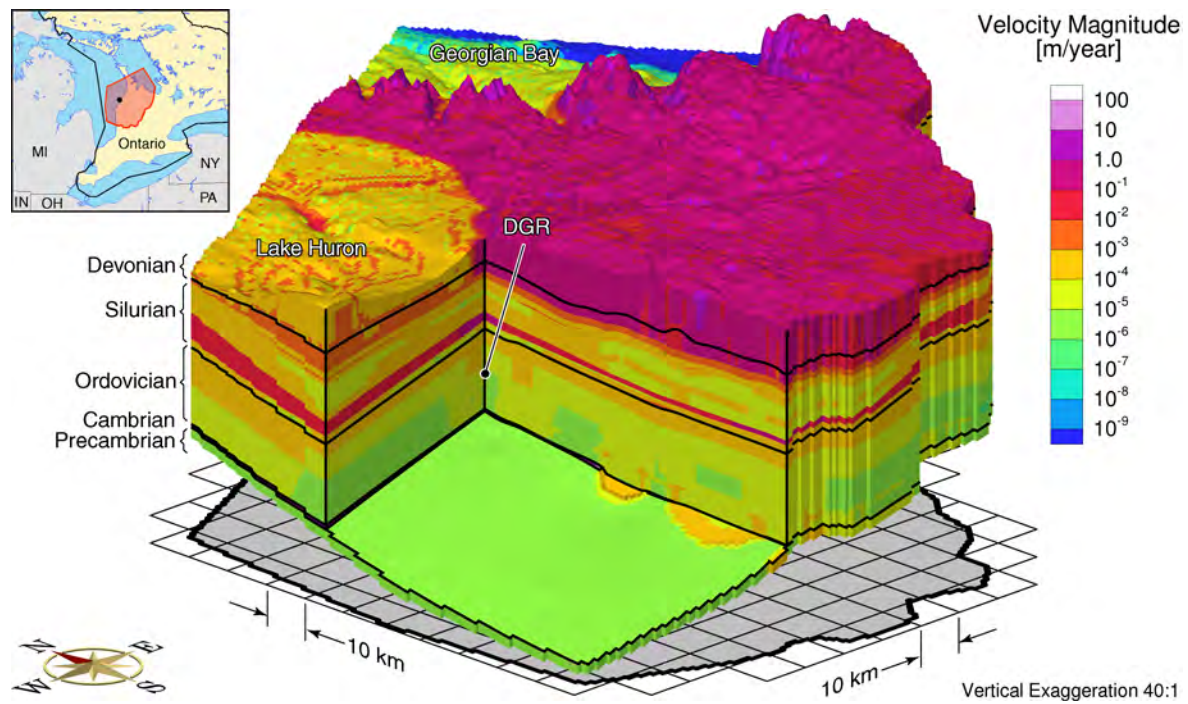


Figure G.30: Pore water velocity magnitude at the present for parameter P-case 2.

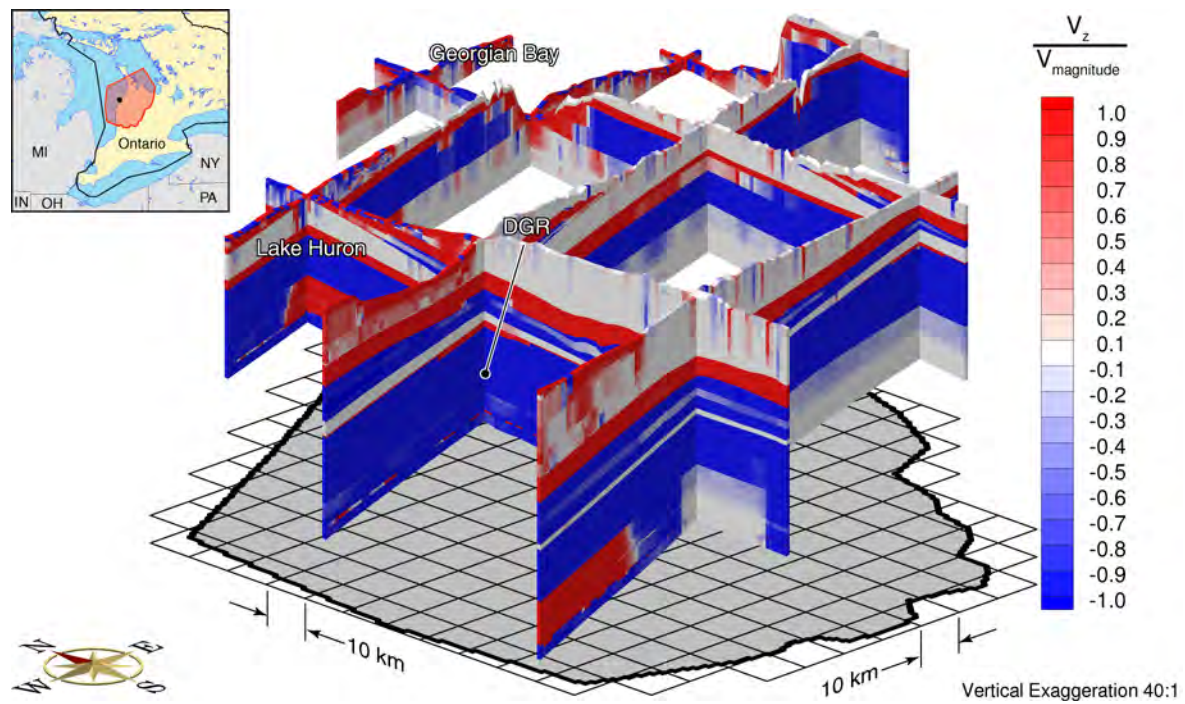


Figure G.31: Fence diagram showing the ratio of the vertical pore water velocity to the velocity magnitude at the present for parameter P-case 2.

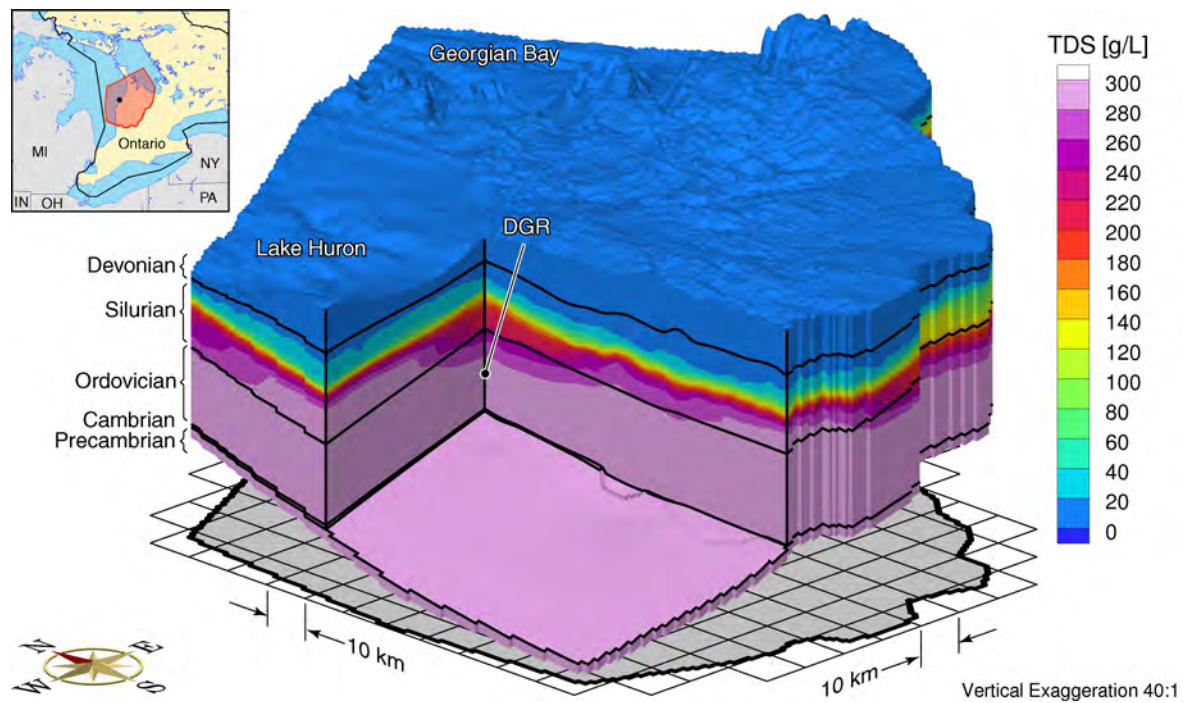


Figure G.32: Total dissolved solids distribution at the present for the paleoclimate simulation parameter P-case 2.

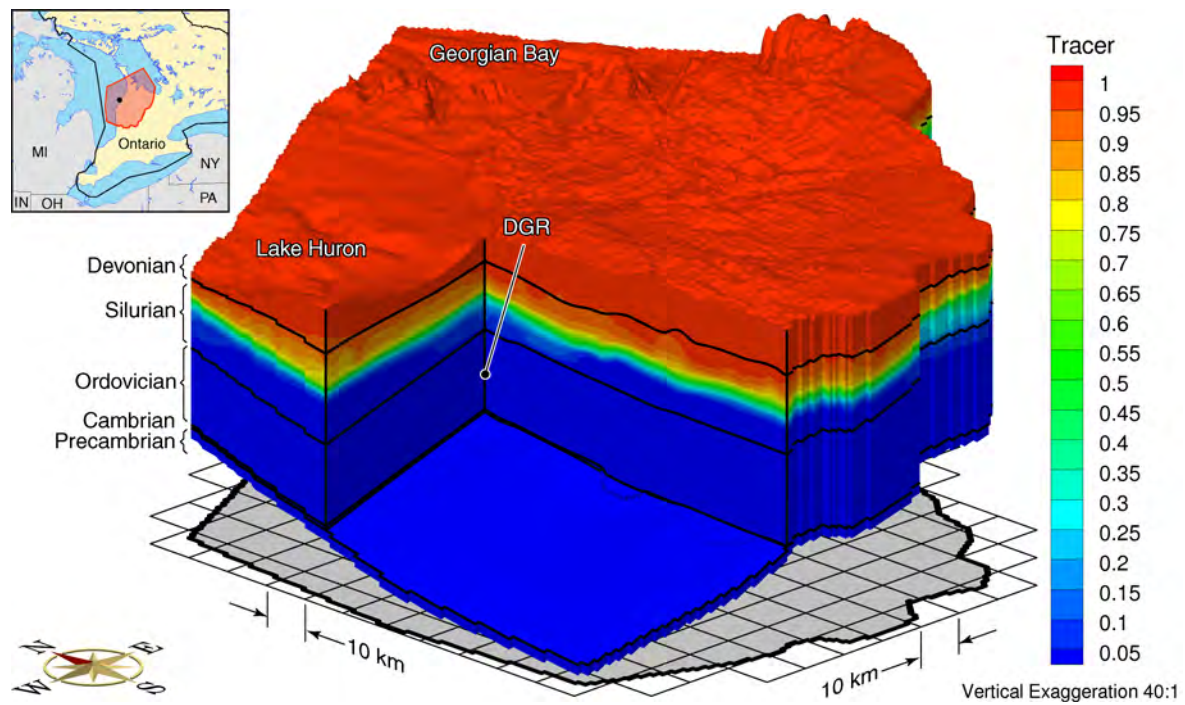


Figure G.33: Block-cut diagram showing the depth of penetration of a tracer at the present parameter P-case 2.

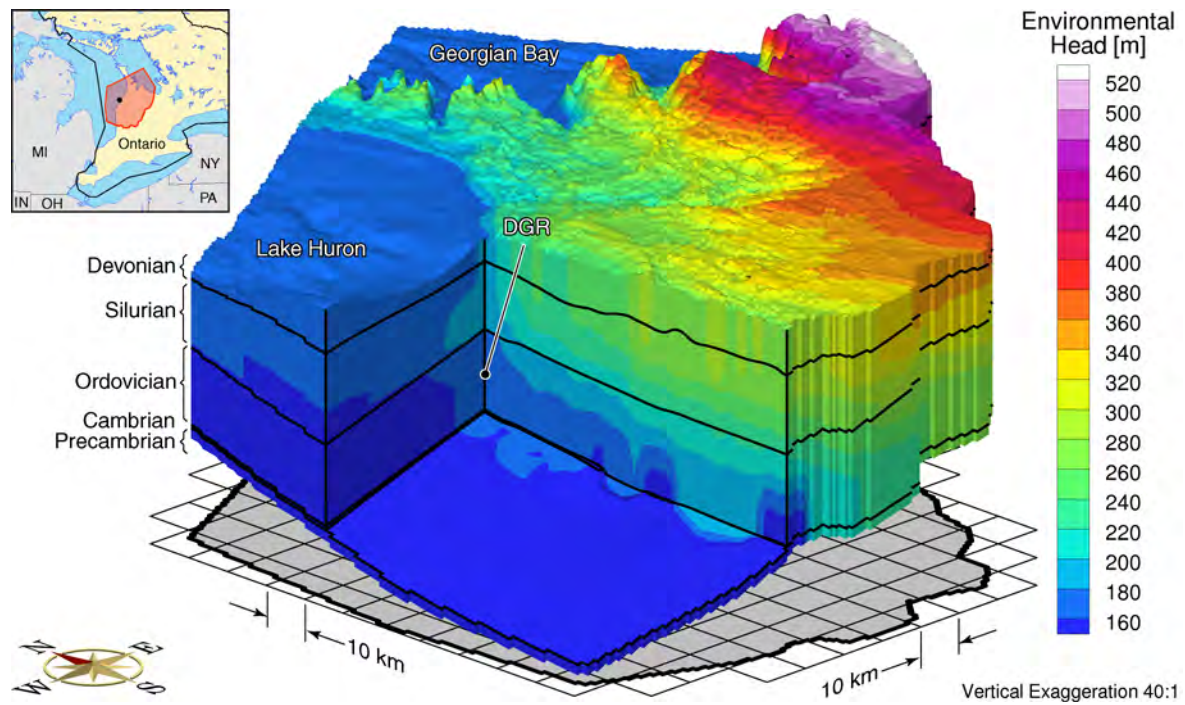


Figure G.34: Environmental heads at 90 000 years before present for parameter P-case 3.

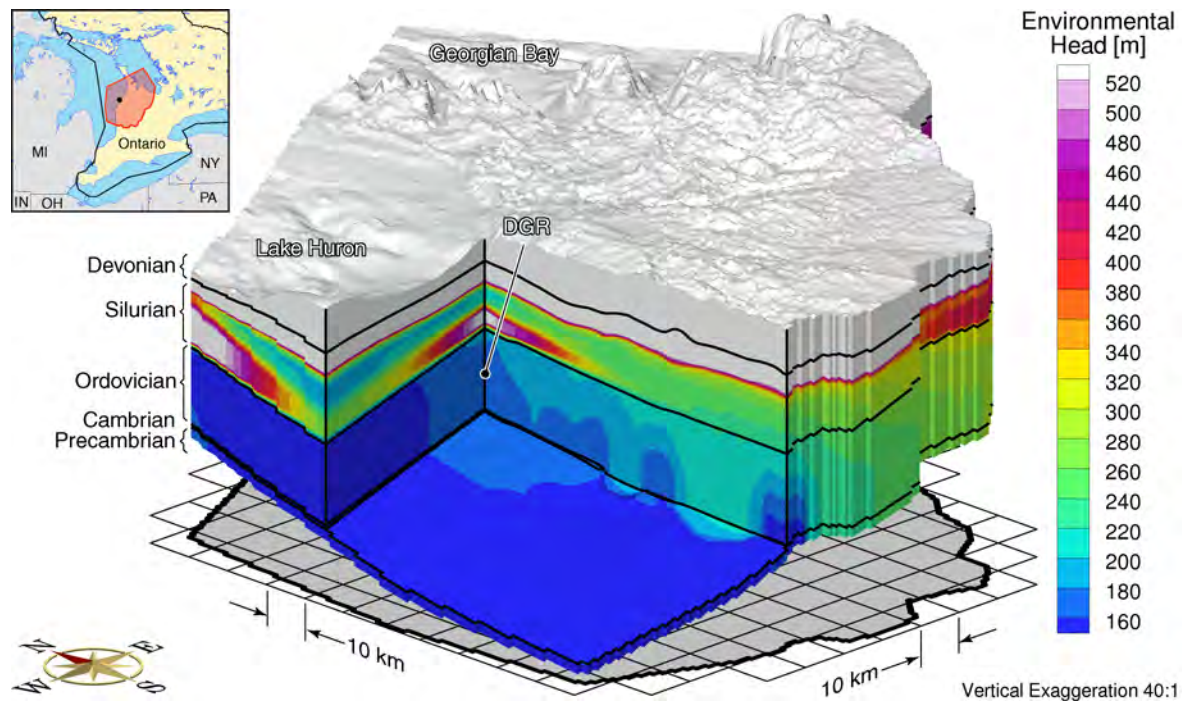


Figure G.35: Environmental heads at 60 000 years before present for parameter P-case 3.

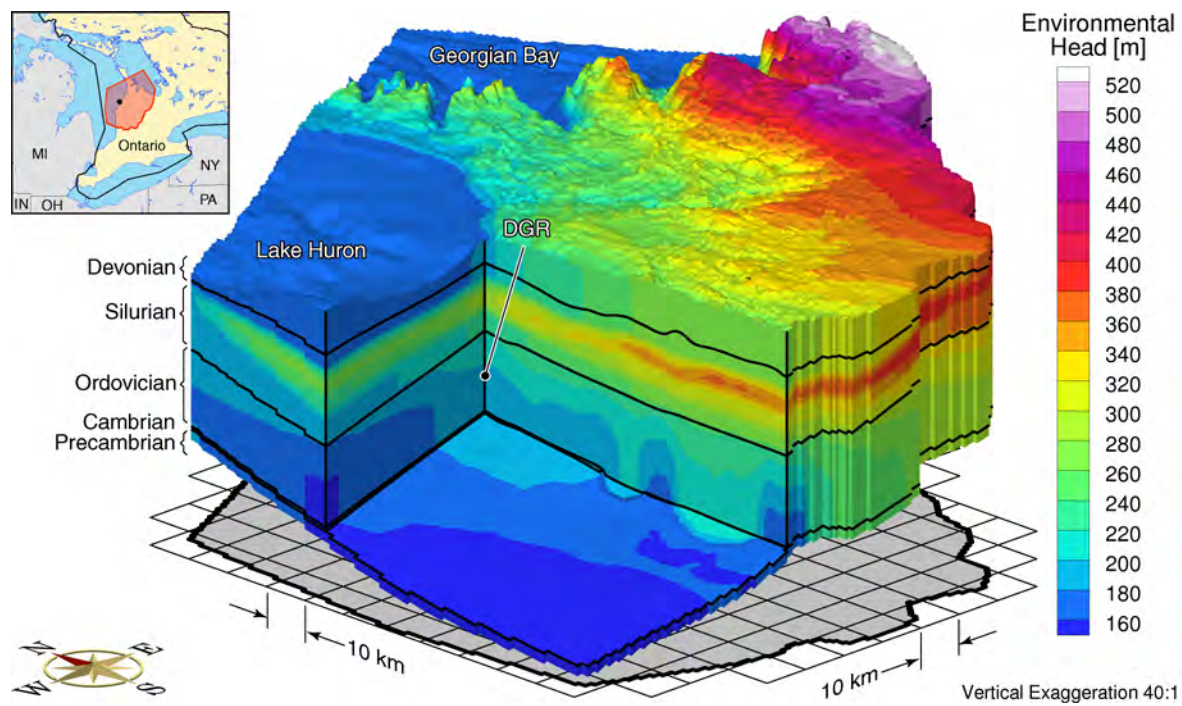


Figure G.36: Environmental heads at 30 000 years before present for parameter P-case 3.

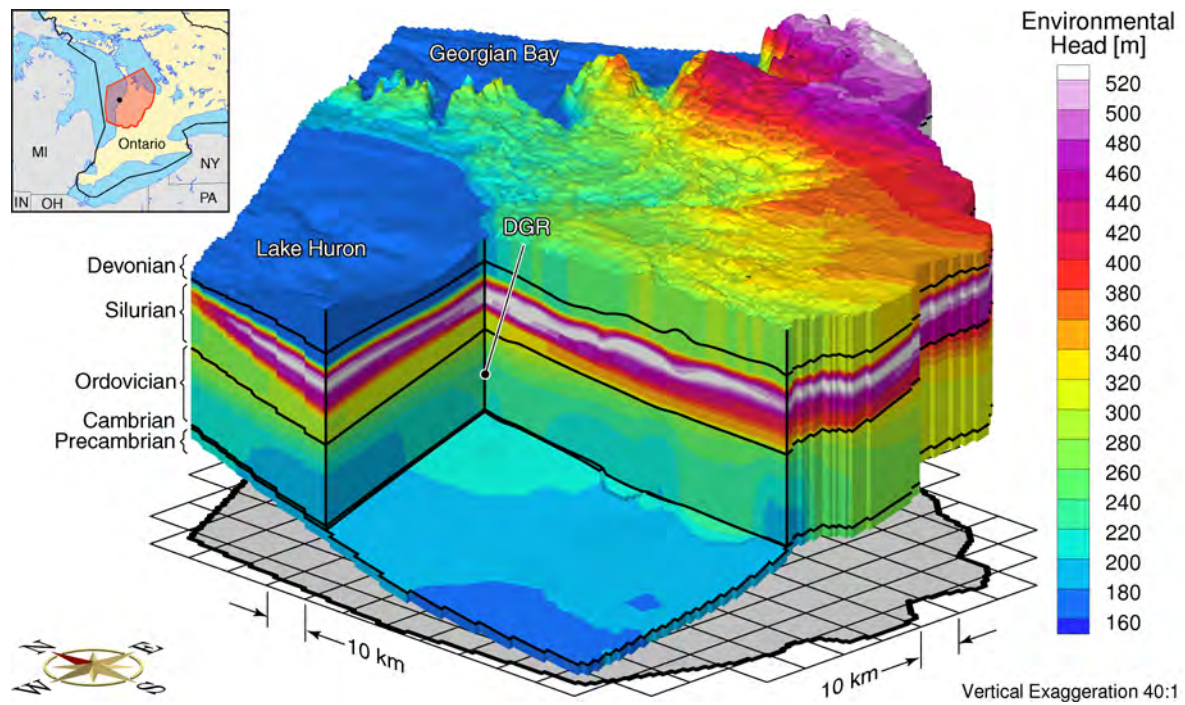


Figure G.37: Environmental heads at the present for parameter P-case 3.

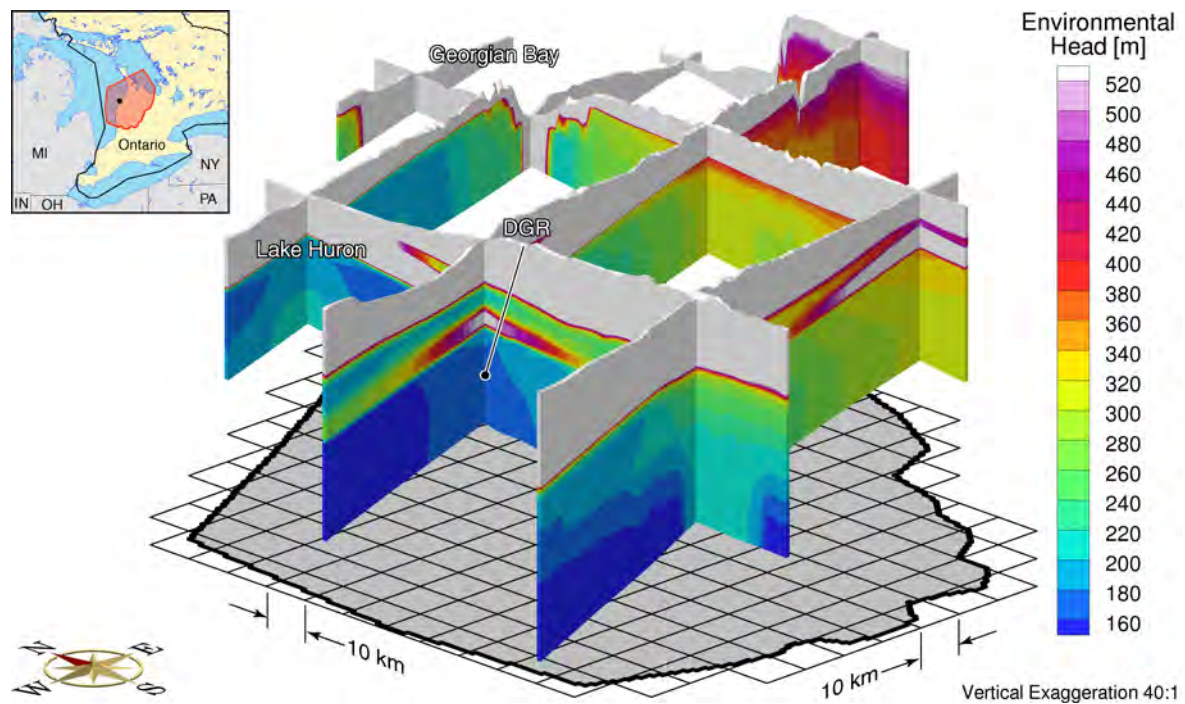


Figure G.38: Fence diagram of environmental heads at 60 000 years before present for parameter P-case 3.

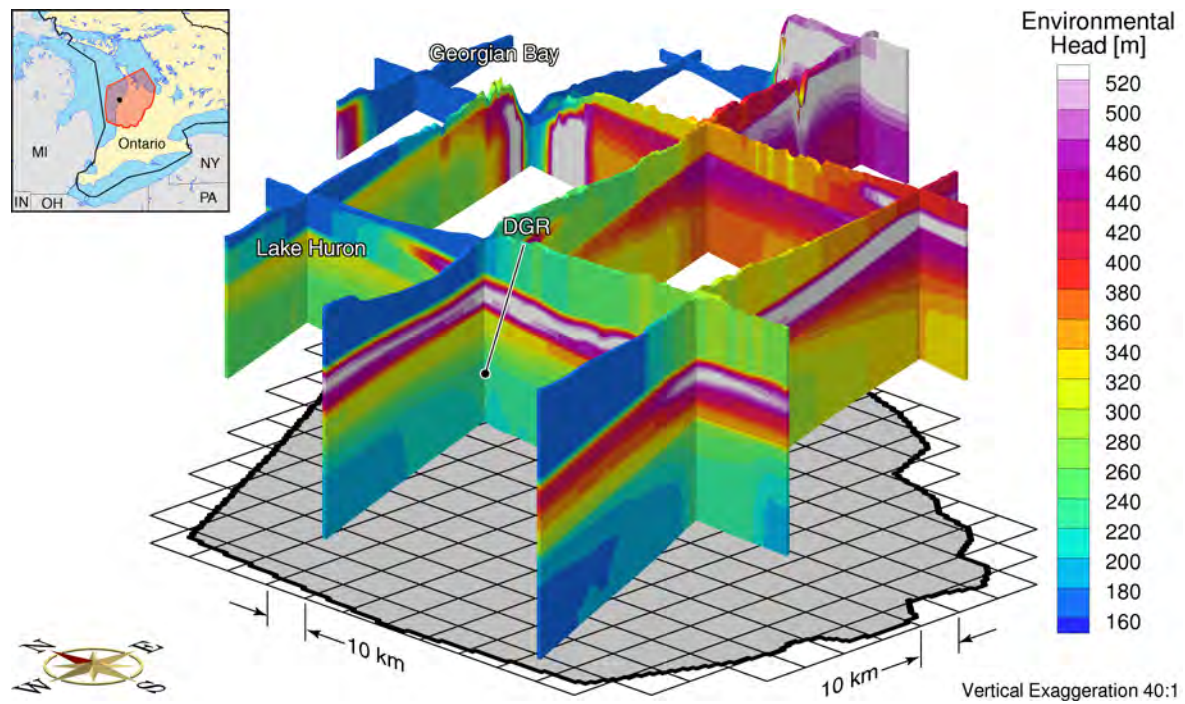


Figure G.39: Fence diagram of environmental heads at the present for parameter P-case 3.

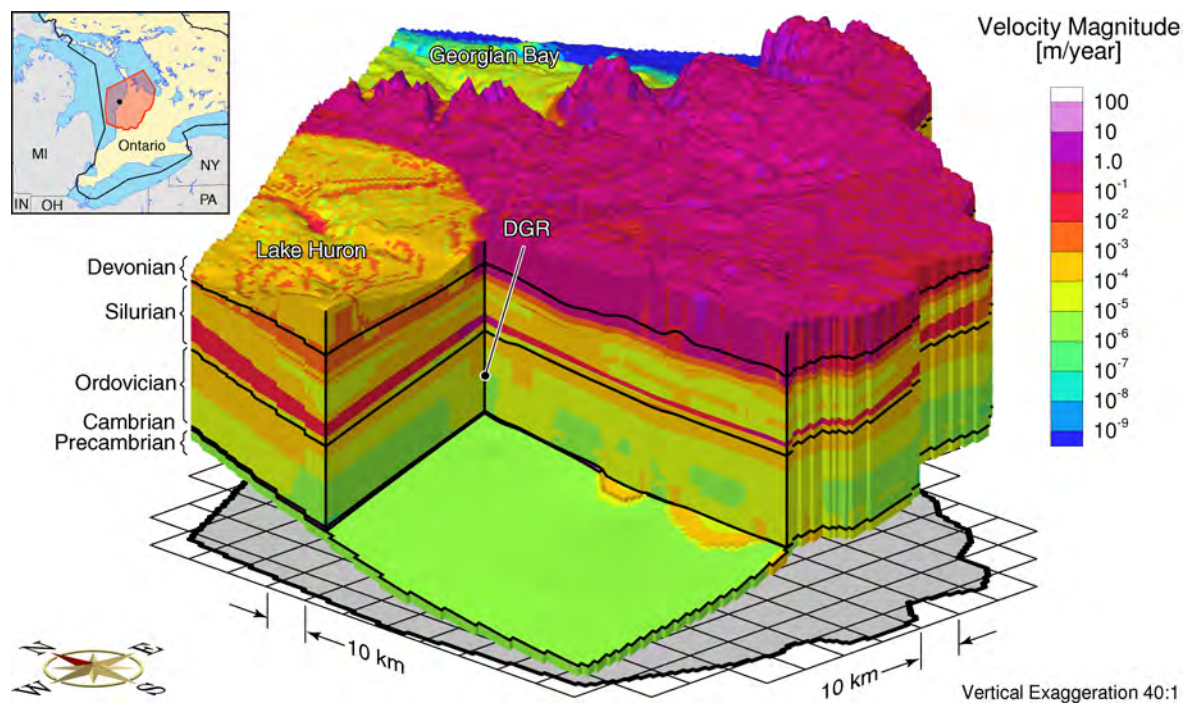


Figure G.40: Pore water velocity magnitude at the present for parameter P-case 3.

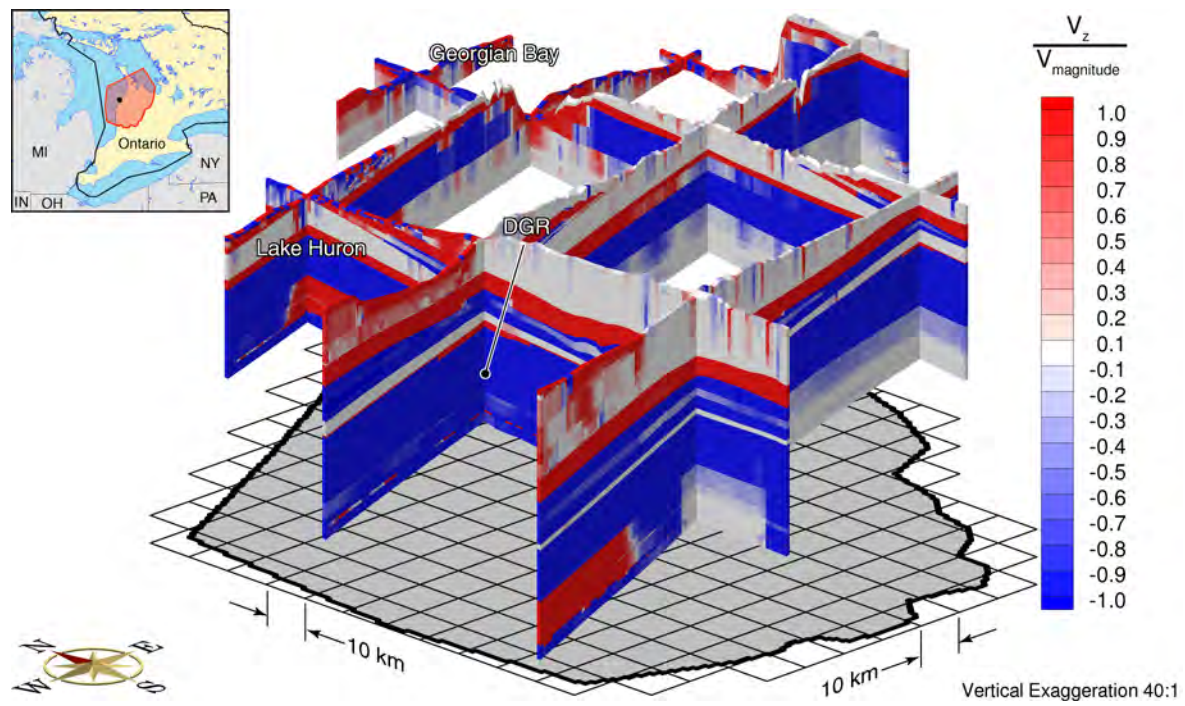


Figure G.41: Fence diagram showing the ratio of the vertical pore water velocity to the velocity magnitude at the present for parameter P-case 3.

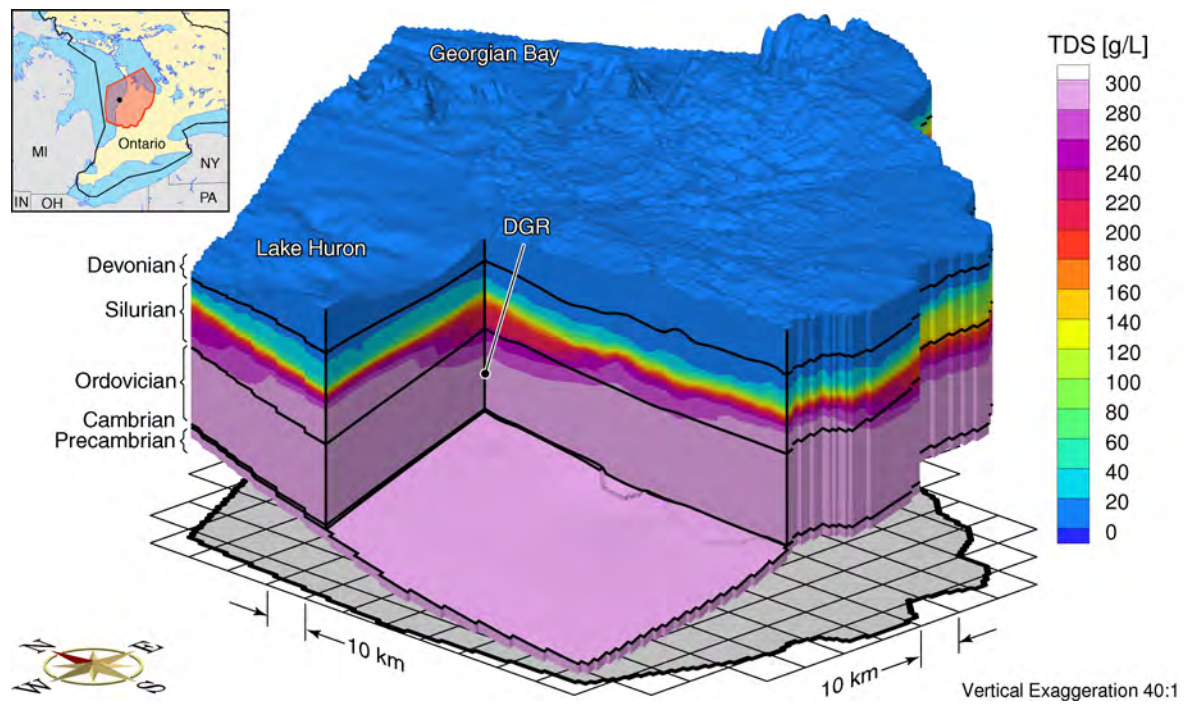


Figure G.42: Total dissolved solids distribution at the present for the paleoclimate simulation parameter P-case 3.

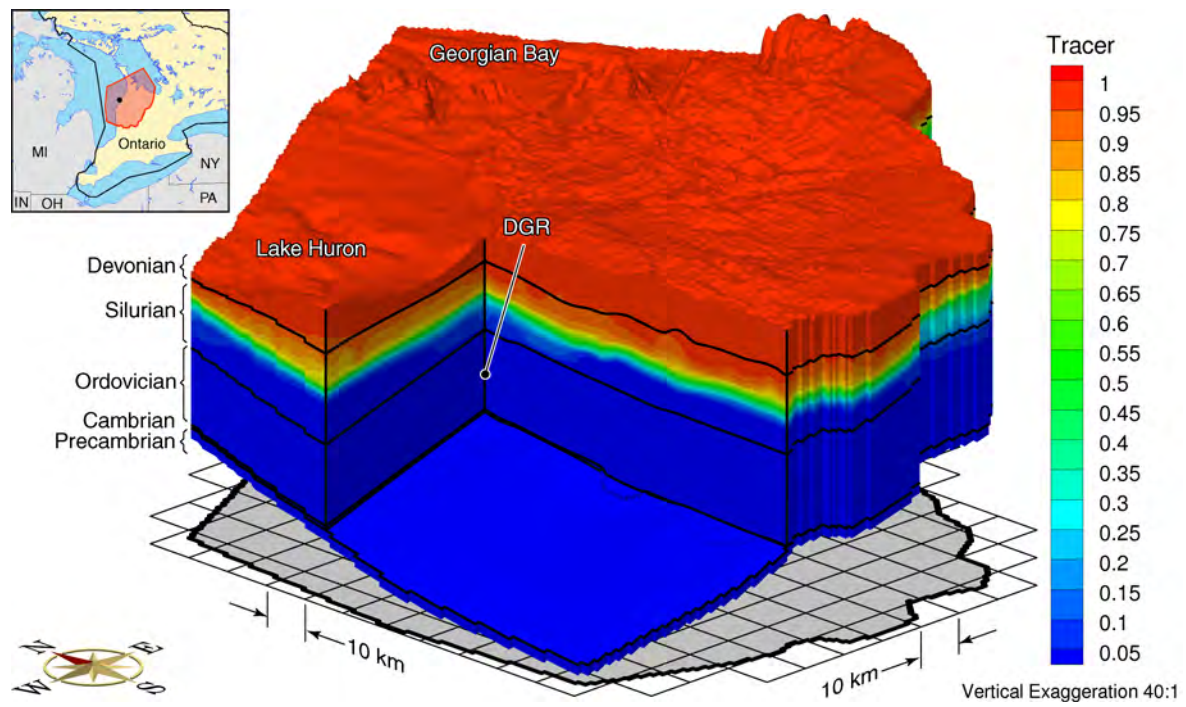


Figure G.43: Block-cut diagram showing the depth of penetration of a tracer at the present parameter P-case 3.

APPENDIX H – DISSIPATION OF AN INITIAL HIGH FRESHWATER HEAD

LIST OF FIGURES

| | Page |
|---|-------------|
| Figure H.1. Environmental heads 10 000 years after an initial freshwater head of 600 m throughout the domain for the parameter P-case 1. | 200 |
| Figure H.2. Fence diagram of environmental heads 10 000 years after an initial freshwater head of 600 m throughout the domain for the parameter P-case 1. | 200 |
| Figure H.3. Environmental heads 20 000 years after an initial freshwater head of 600 m throughout the domain for the parameter P-case 1. | 201 |
| Figure H.4. Fence diagram of environmental heads 20 000 years after an initial freshwater head of 600 m throughout the domain for the parameter P-case 1. | 201 |
| Figure H.5. Pore water velocity magnitude 20 000 years after an initial freshwater head of 600 m throughout the domain for the parameter P-case 1. | 202 |
| Figure H.6. Fence diagram of the ratio of vertical velocity to the velocity magnitude 20 000 years after an initial freshwater head of 600 m throughout the domain for the parameter P-case 1. | 202 |
| Figure H.7. Environmental heads 10 000 years after an initial freshwater head of 600 m throughout the domain for the parameter P-case 2. | 203 |
| Figure H.8. Fence diagram of environmental heads 10 000 years after an initial freshwater head of 600 m throughout the domain for the parameter P-case 2. | 203 |
| Figure H.9. Environmental heads 20 000 years after an initial freshwater head of 600 m throughout the domain for the parameter P-case 2. | 204 |
| Figure H.10. Fence diagram of environmental heads 20 000 years after an initial freshwater head of 600 m throughout the domain for the parameter P-case 2. | 204 |
| Figure H.11. Pore water velocity magnitude 20 000 years after an initial freshwater head of 600 m throughout the domain for the parameter P-case 2. | 205 |
| Figure H.12. Fence diagram of the ratio of vertical velocity to the velocity magnitude 20 000 years after an initial freshwater head of 600 m throughout the domain for the parameter P-case 2. | 205 |
| Figure H.13. Environmental heads 10 000 years after an initial freshwater head of 600 m throughout the domain for the parameter P-case 3. | 206 |
| Figure H.14. Fence diagram of environmental heads 10 000 years after an initial freshwater head of 600 m throughout the domain for the parameter P-case 3. | 206 |
| Figure H.15. Environmental heads 20 000 years after an initial freshwater head of 600 m throughout the domain for the parameter P-case 3. | 207 |
| Figure H.16. Fence diagram of environmental heads 20 000 years after an initial freshwater head of 600 m throughout the domain for the parameter P-case 3. | 207 |
| Figure H.17. Pore water velocity magnitude 20 000 years after an initial freshwater head of 600 m throughout the domain for the parameter P-case 3. | 208 |
| Figure H.18. Fence diagram of the ratio of vertical velocity to the velocity magnitude 20 000 years after an initial freshwater head of 600 m throughout the domain for the parameter P-case 3. | 208 |

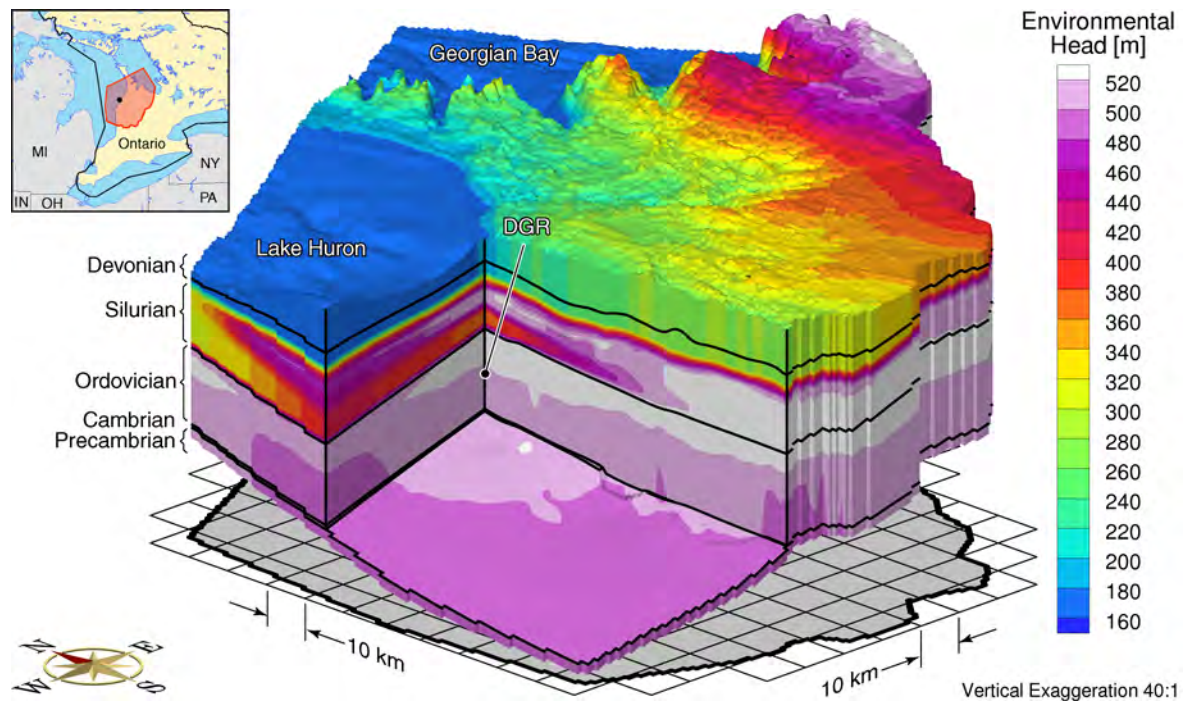


Figure H.1: Environmental heads 10 000 years after an initial freshwater head of 600 m throughout the domain for the parameter P-case 1.

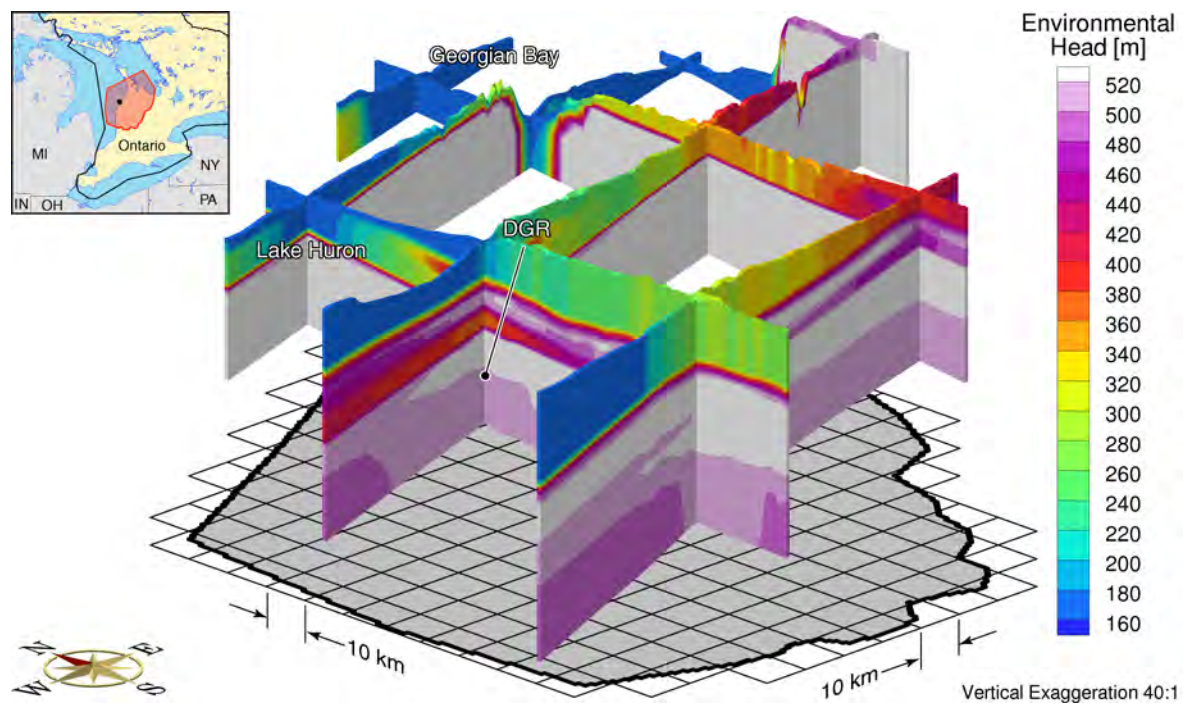


Figure H.2: Fence diagram of environmental heads 10 000 years after an initial freshwater head of 600 m throughout the domain for the parameter P-case 1.

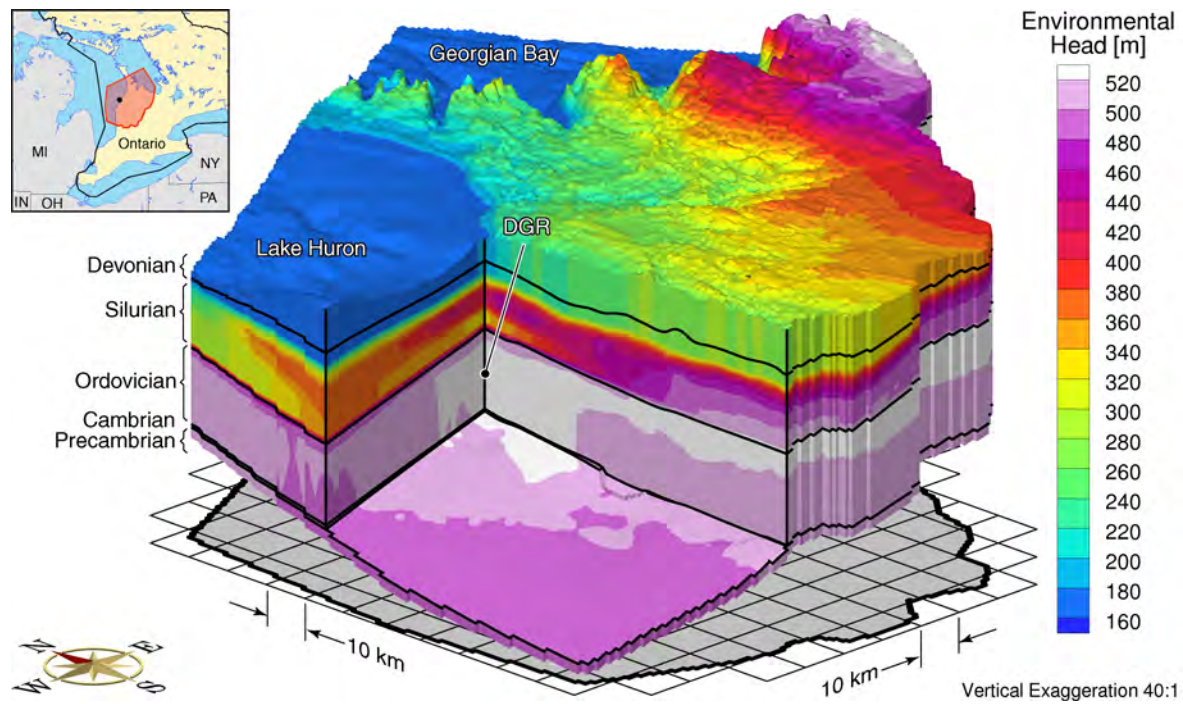


Figure H.3: Environmental heads 20 000 years after an initial freshwater head of 600 m throughout the domain for the parameter P-case 1.

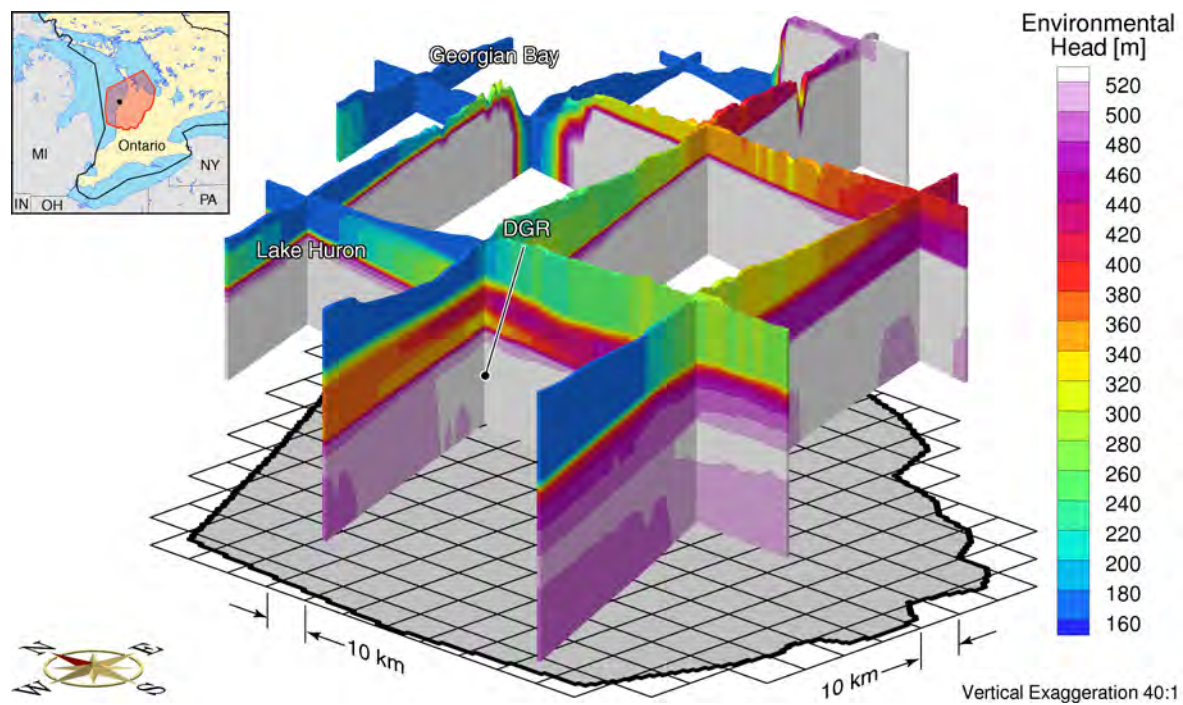


Figure H.4: Fence diagram of environmental heads 20 000 years after an initial freshwater head of 600 m throughout the domain for the parameter P-case 1.

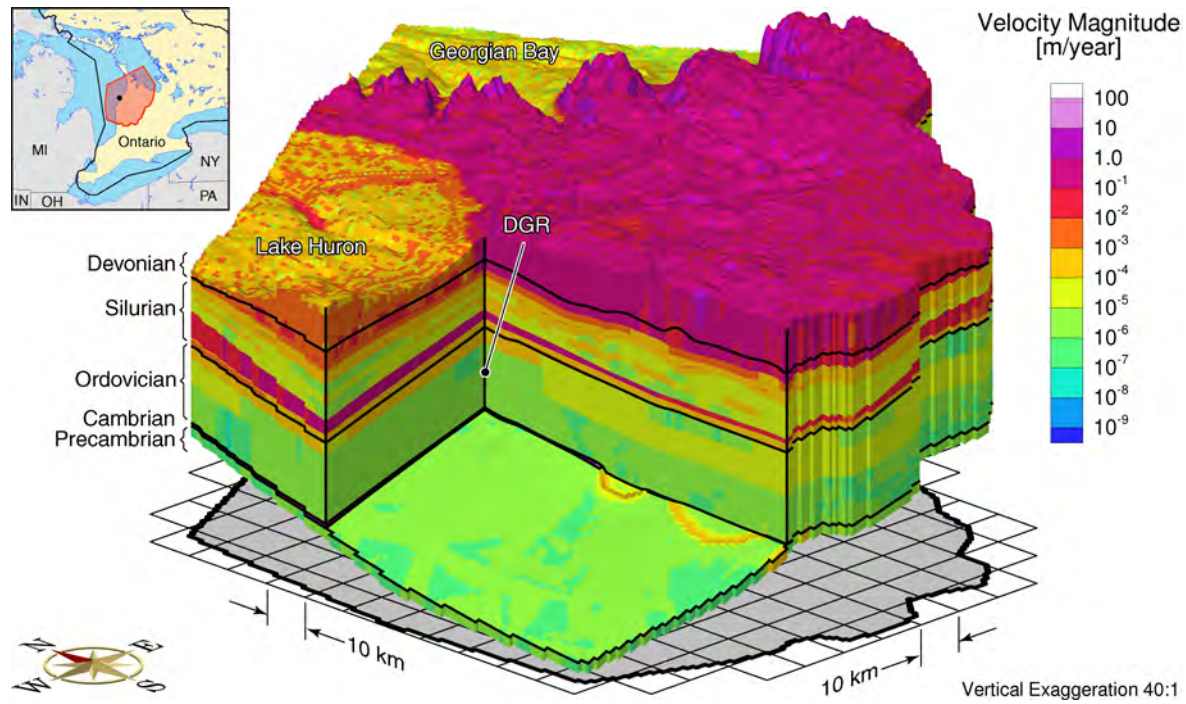


Figure H.5: Pore water velocity magnitude 20 000 years after an initial freshwater head of 600 m throughout the domain for the parameter P-case 1.

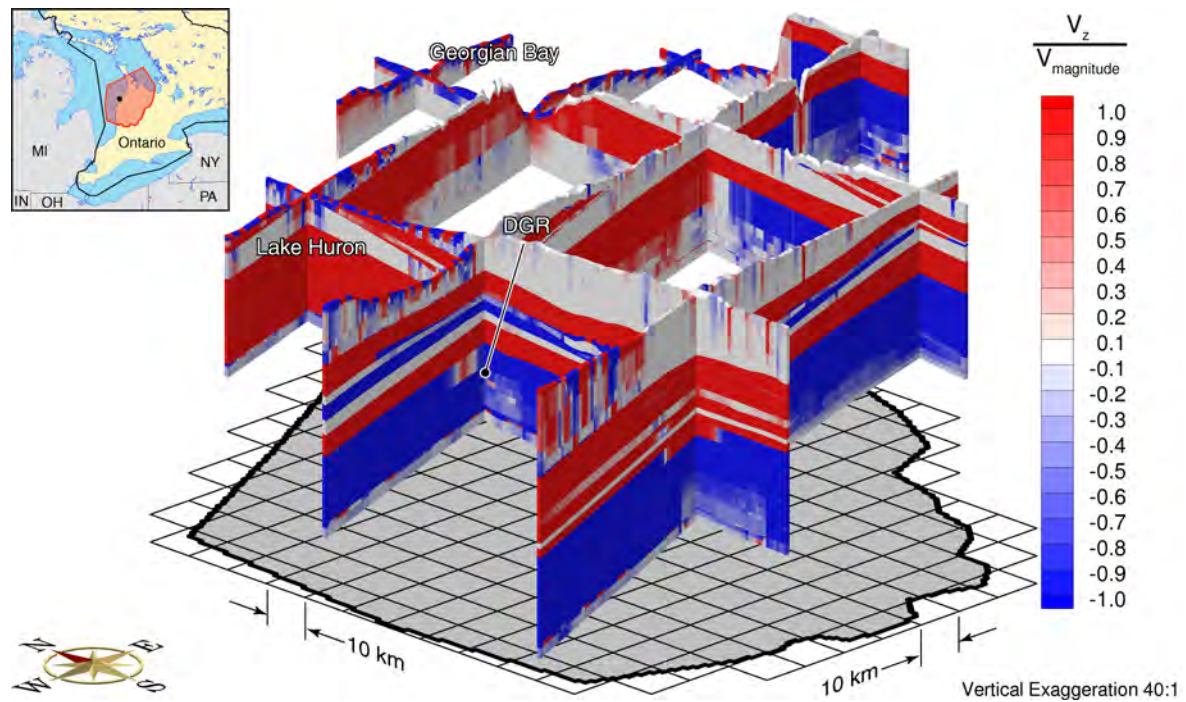


Figure H.6: Fence diagram of the ratio of vertical velocity to the velocity magnitude 20 000 years after an initial freshwater head of 600 m throughout the domain for the parameter P-case 1.

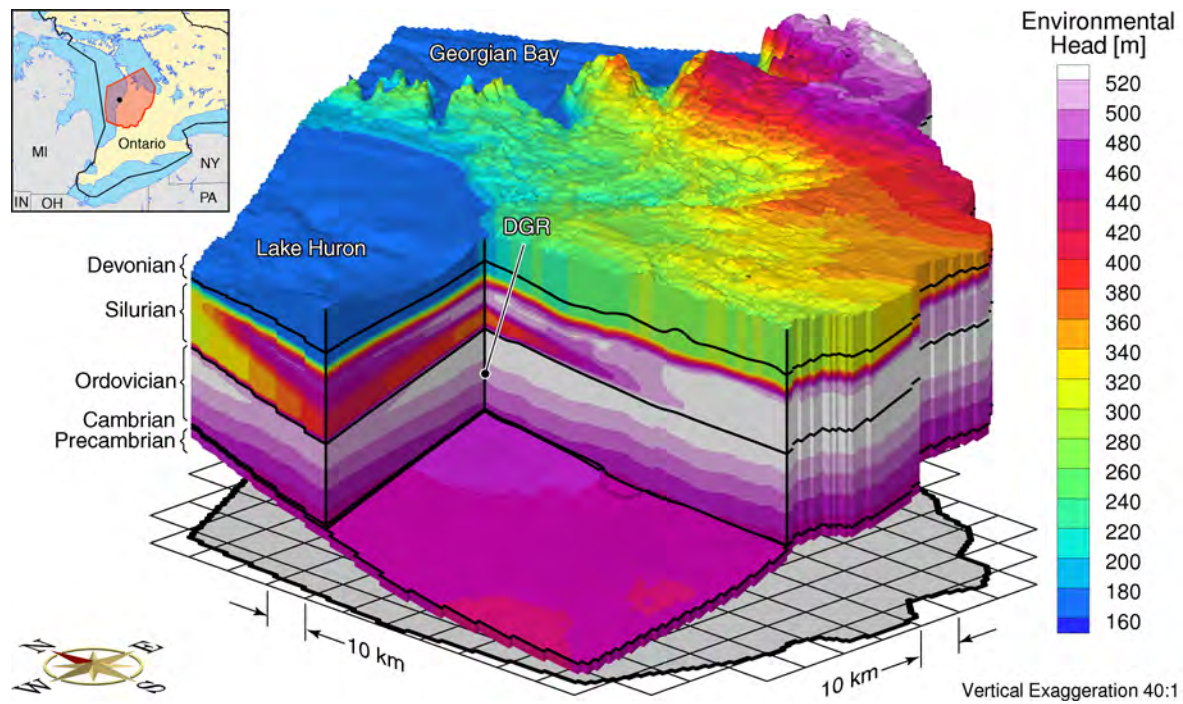


Figure H.7: Environmental heads 10 000 years after an initial freshwater head of 600 m throughout the domain for the parameter P-case 2.

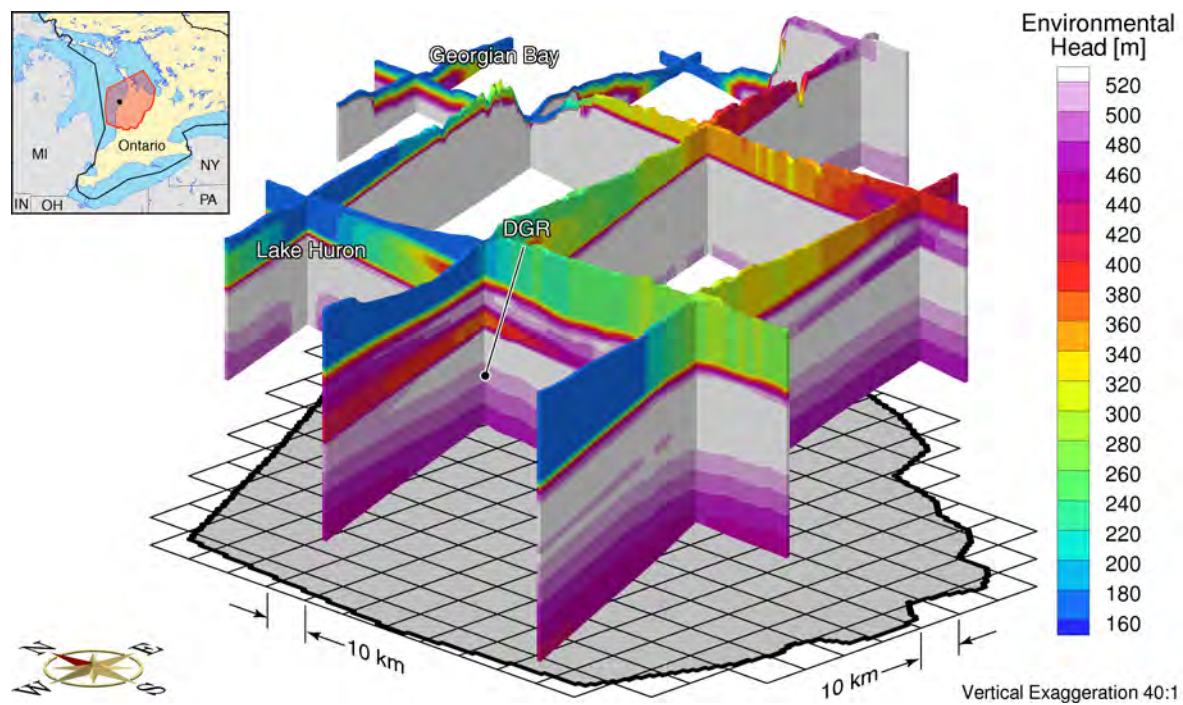


Figure H.8: Fence diagram of environmental heads 10 000 years after an initial freshwater head of 600 m throughout the domain for the parameter P-case 2.

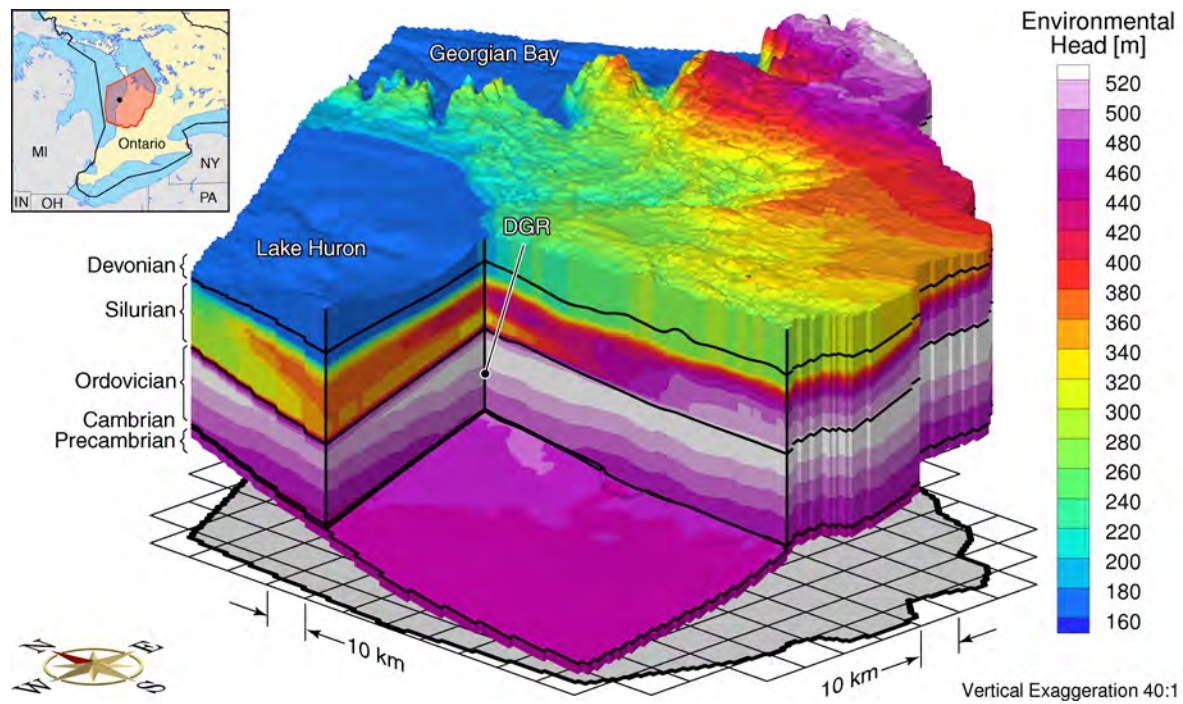


Figure H.9: Environmental heads 20 000 years after an initial freshwater head of 600 m throughout the domain for the parameter P-case 2.

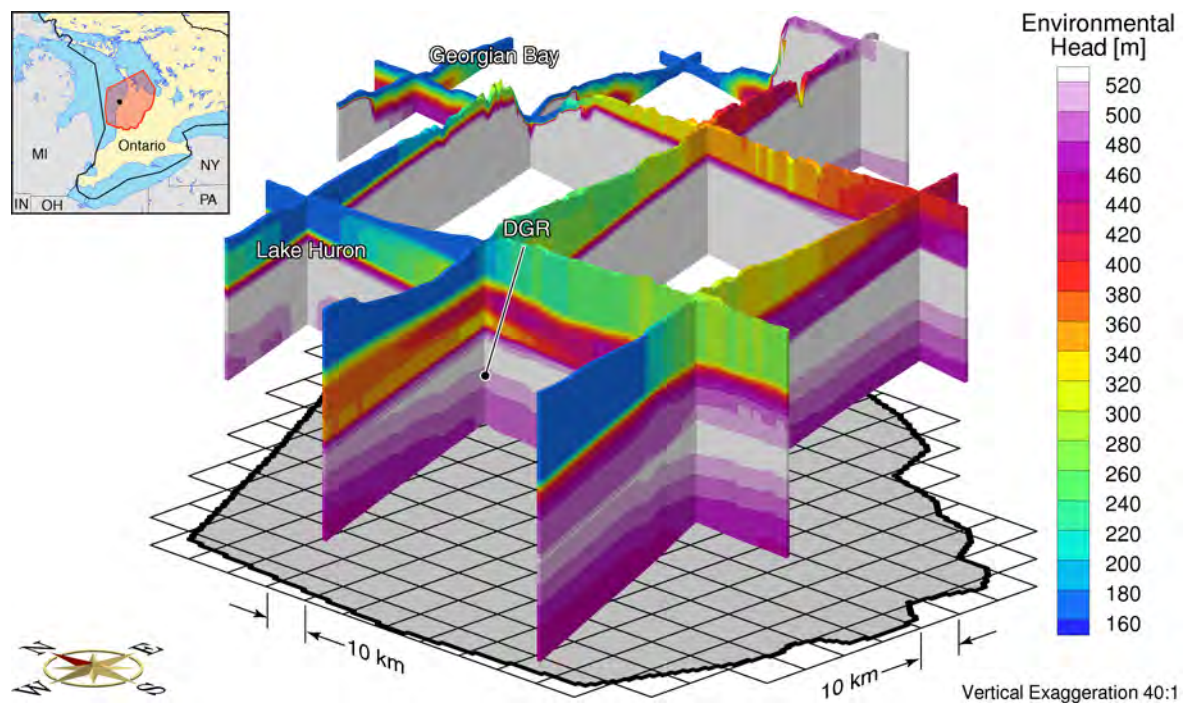


Figure H.10: Fence diagram of environmental heads 20 000 years after an initial freshwater head of 600 m throughout the domain for the parameter P-case 2.

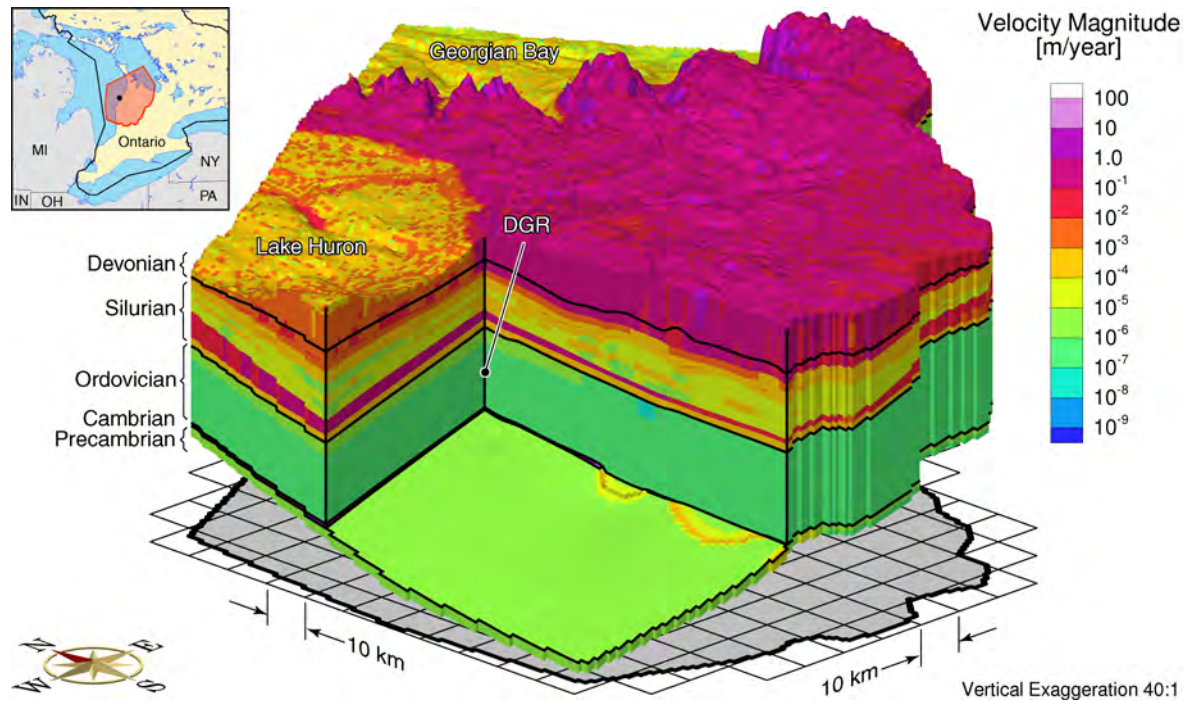


Figure H.11: Pore water velocity magnitude 20 000 years after an initial freshwater head of 600 m throughout the domain for the parameter P-case 2.

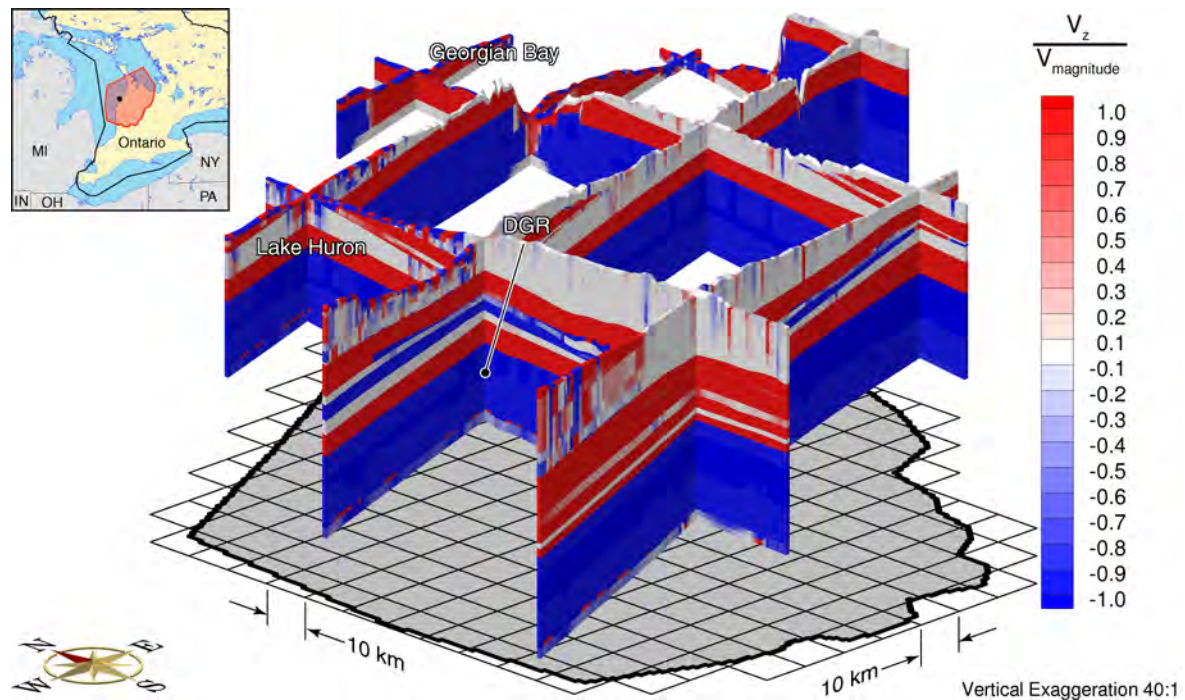


Figure H.12: Fence diagram of the ratio of vertical velocity to the velocity magnitude 20 000 years after an initial freshwater head of 600 m throughout the domain for the parameter P-case 2.

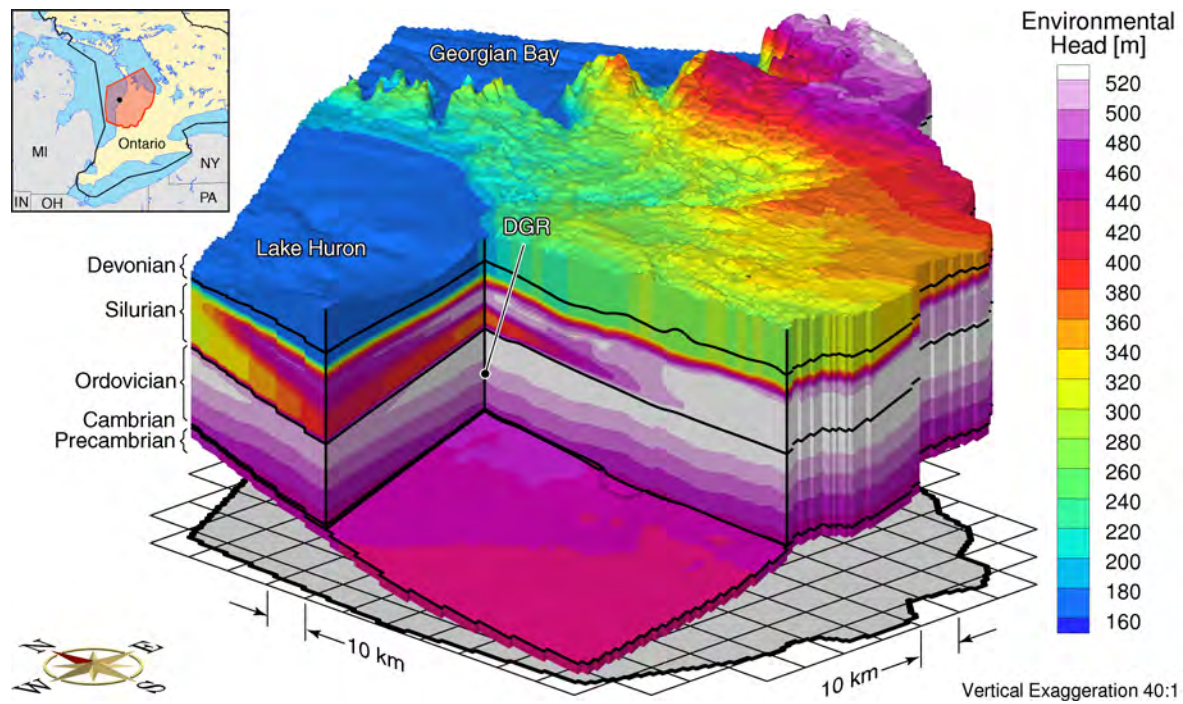


Figure H.13: Environmental heads 10 000 years after an initial freshwater head of 600 m throughout the domain for the parameter P-case 3.

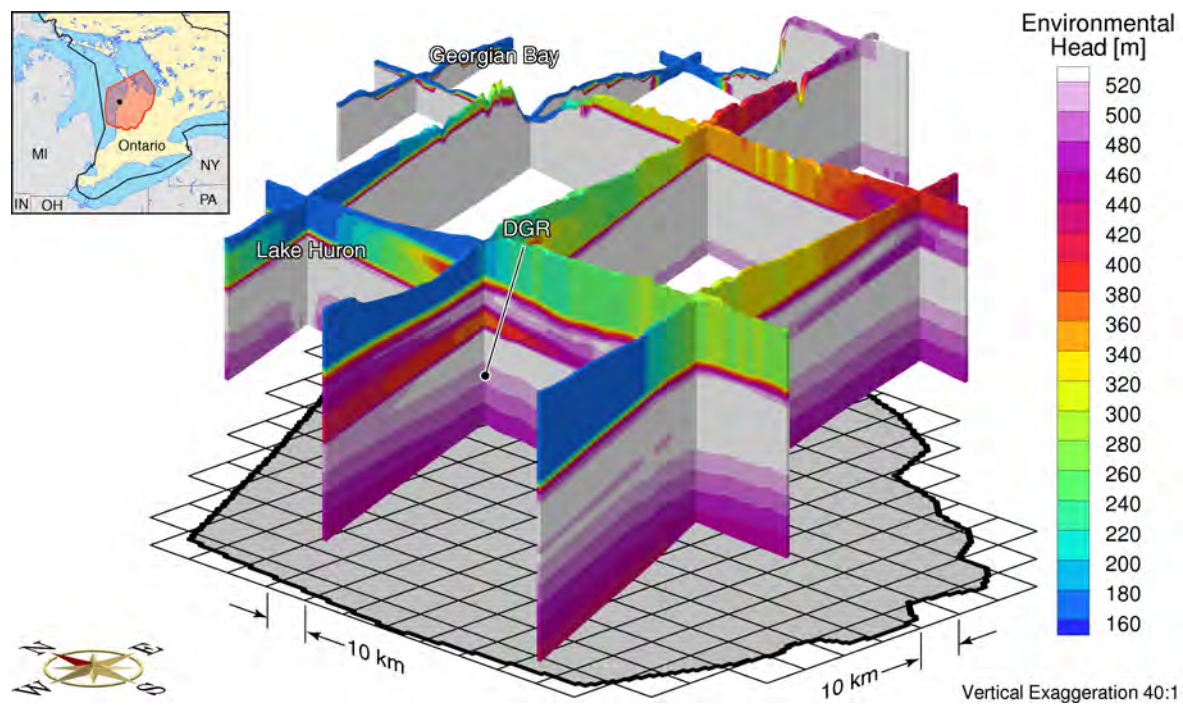


Figure H.14: Fence diagram of environmental heads 10 000 years after an initial freshwater head of 600 m throughout the domain for the parameter P-case 3.

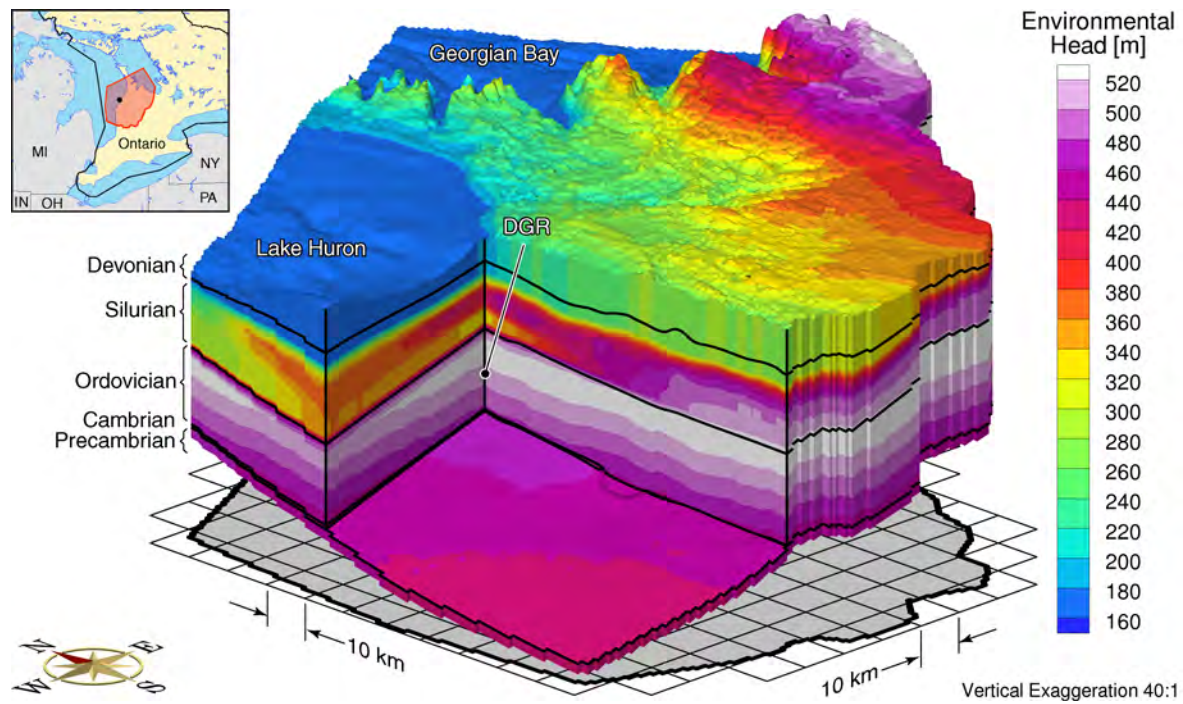


Figure H.15: Environmental heads 20 000 years after an initial freshwater head of 600 m throughout the domain for the parameter P-case 3.

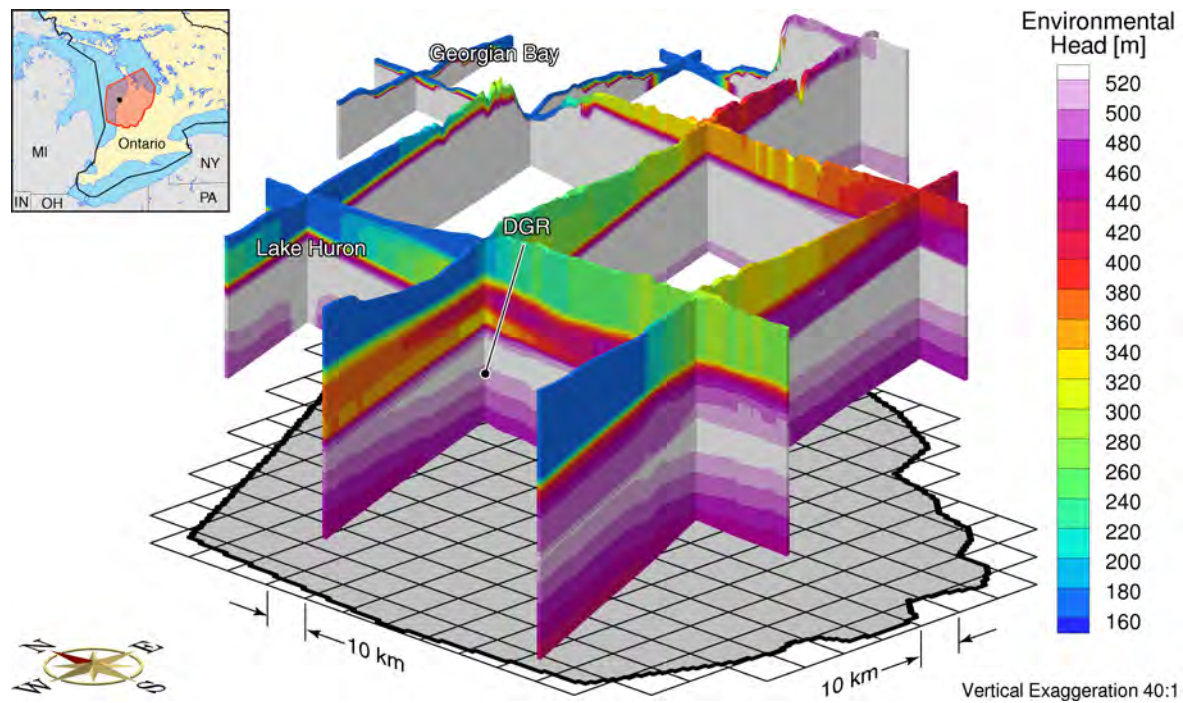


Figure H.16: Fence diagram of environmental heads 20 000 years after an initial freshwater head of 600 m throughout the domain for the parameter P-case 3.

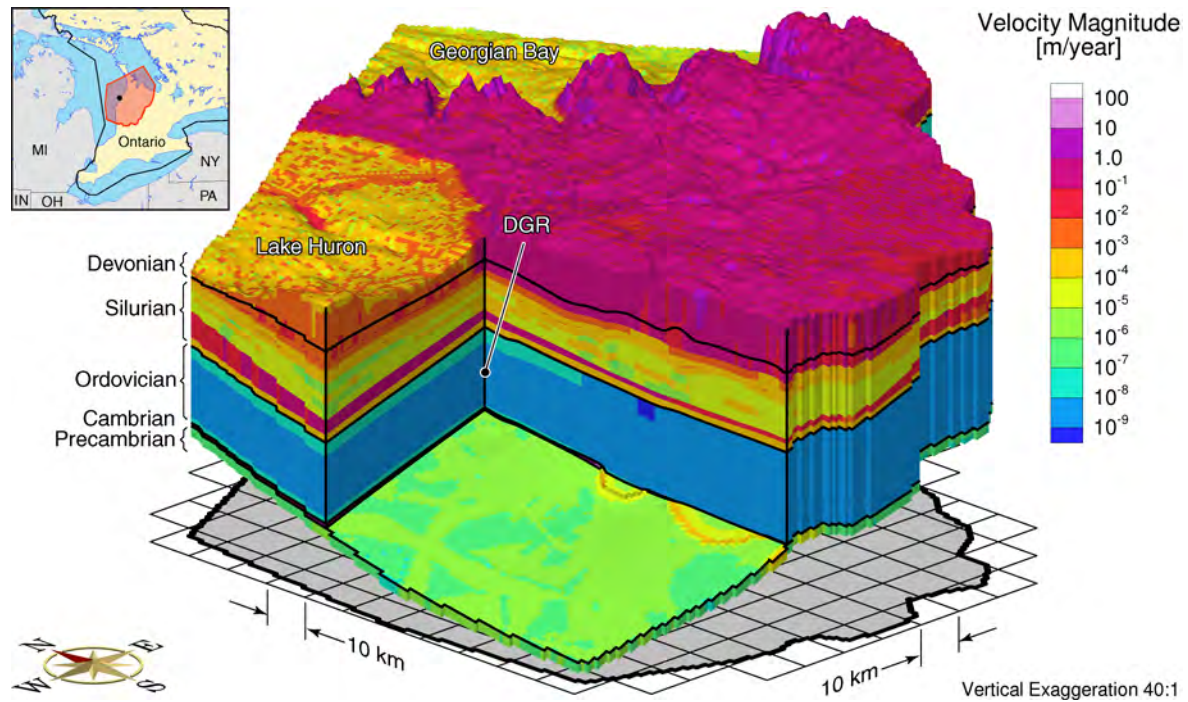


Figure H.17: Pore water velocity magnitude 20 000 years after an initial freshwater head of 600 m throughout the domain for the parameter P-case 3.

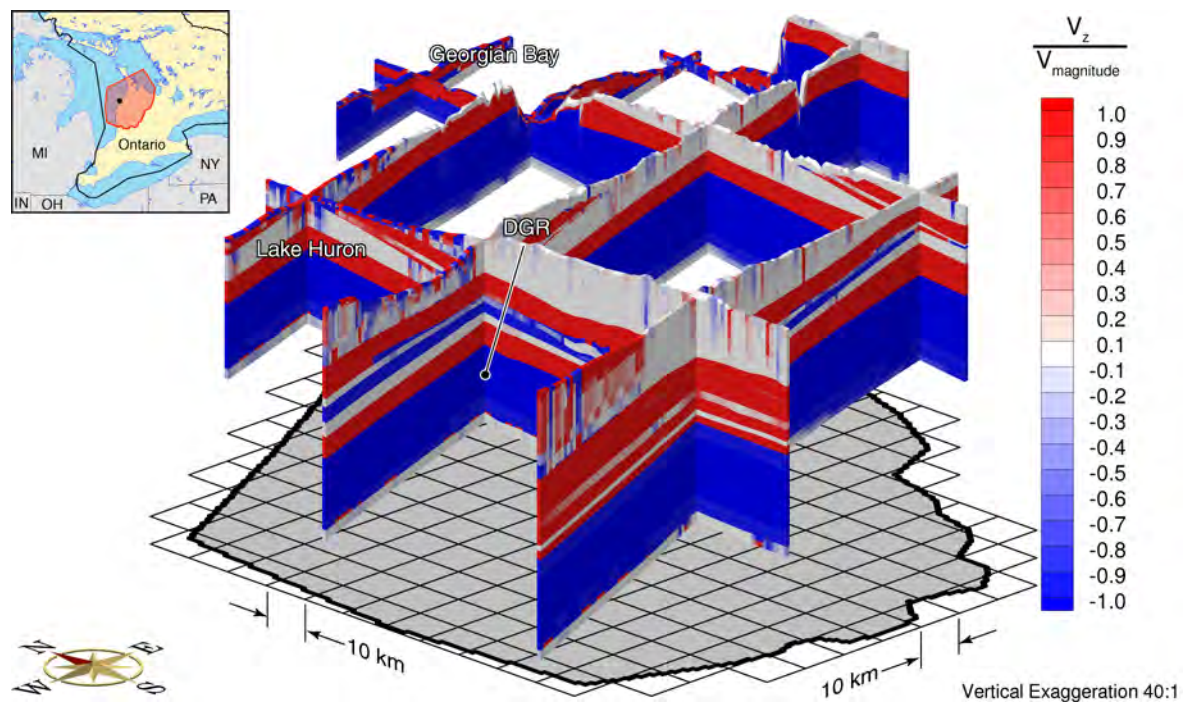


Figure H.18: Fence diagram of the ratio of vertical velocity to the velocity magnitude 20 000 years after an initial freshwater head of 600 m throughout the domain for the parameter P-case 3.

APPENDIX I – SUB-GRIDDING VERIFICATION

LIST OF FIGURES

| | | Page |
|--------------|---|-------------|
| Figure I.1. | Environmental head distribution for base case parameters and domain. . . . | 211 |
| Figure I.2. | Environmental head distribution for base case parameters and site-scale sub-gridding. | 211 |
| Figure I.3. | Fence diagram of environmental head distribution for base case parameters and domain. | 212 |
| Figure I.4. | Fence diagram of environmental head distribution for base case parameters and site-scale sub-gridding. | 212 |
| Figure I.5. | Total Dissolved Solids distribution for base case parameters and domain. . . | 213 |
| Figure I.6. | Total Dissolved Solids distribution for base case parameters and site-scale sub-gridding. | 213 |
| Figure I.7. | Pore water velocity magnitude distribution for base case parameters and domain. | 214 |
| Figure I.8. | Pore water velocity magnitude distribution for base case parameters and site-scale sub-gridding. | 214 |
| Figure I.9. | Fence diagram of ratio of vertical velocity to velocity magnitude for base case parameters and domain. | 215 |
| Figure I.10. | Fence diagram of ratio of vertical velocity to velocity magnitude for base case parameters and site-scale sub-gridding. | 215 |
| Figure I.11. | Mean life expectancies for base case parameters and domain. | 216 |
| Figure I.12. | Mean life expectancies for base case parameters and site-scale sub-gridding. | 216 |
| Figure I.13. | Fence diagram showing mean life expectancies for base case parameters and domain. | 217 |
| Figure I.14. | Fence diagram showing life expectancies for base case parameters and site-scale sub-gridding. | 217 |
| Figure I.15. | Equivalent freshwater heads for the nested site-scale model and the base case parameters. | 218 |
| Figure I.16. | Equivalent freshwater heads at the sub-gridded site-scale for the base case parameters. | 218 |
| Figure I.17. | Fence diagram of equivalent freshwater heads for the nested site-scale model and the base case parameters. | 219 |
| Figure I.18. | Fence diagram of equivalent freshwater heads at the sub-gridded site-scale for the base case parameters. | 219 |
| Figure I.19. | Pore water velocity magnitude for the nested site-scale model and the base case parameters. | 220 |
| Figure I.20. | Pore water velocity magnitude at the sub-gridded site-scale for the base case parameters. | 220 |
| Figure I.21. | Ratio of vertical velocity to the velocity magnitude for the nested site-scale model and the base case parameters. | 221 |
| Figure I.22. | Ratio of vertical velocity to the velocity magnitude at the sub-gridded site-scale for the base case parameters. | 221 |

| | | |
|--------------|---|-----|
| Figure I.23. | Fence diagram of the ratio of vertical velocity to the velocity magnitude for the nested site-scale model and the base case parameters. | 222 |
| Figure I.24. | Fence diagram of the ratio of vertical velocity to the velocity magnitude at the sub-gridded site-scale for the base case parameters. | 222 |
| Figure I.25. | Total dissolved solids concentration for the nested site-scale model and the base case parameters. | 223 |
| Figure I.26. | Total dissolved solids concentration at the sub-gridded site-scale for the base case parameters. | 223 |
| Figure I.27. | Mean life expectancies for the nested site-scale model and the base case parameters. | 224 |
| Figure I.28. | Mean life expectancies for the sub-gridded site-scale model and the base case parameters. | 224 |
| Figure I.29. | Fence diagram showing the mean life expectancies for the nested site-scale model and the base case parameters. | 225 |
| Figure I.30. | Fence diagram showing the mean life expectancies for the sub-gridded site-scale model and the base case parameters. | 225 |

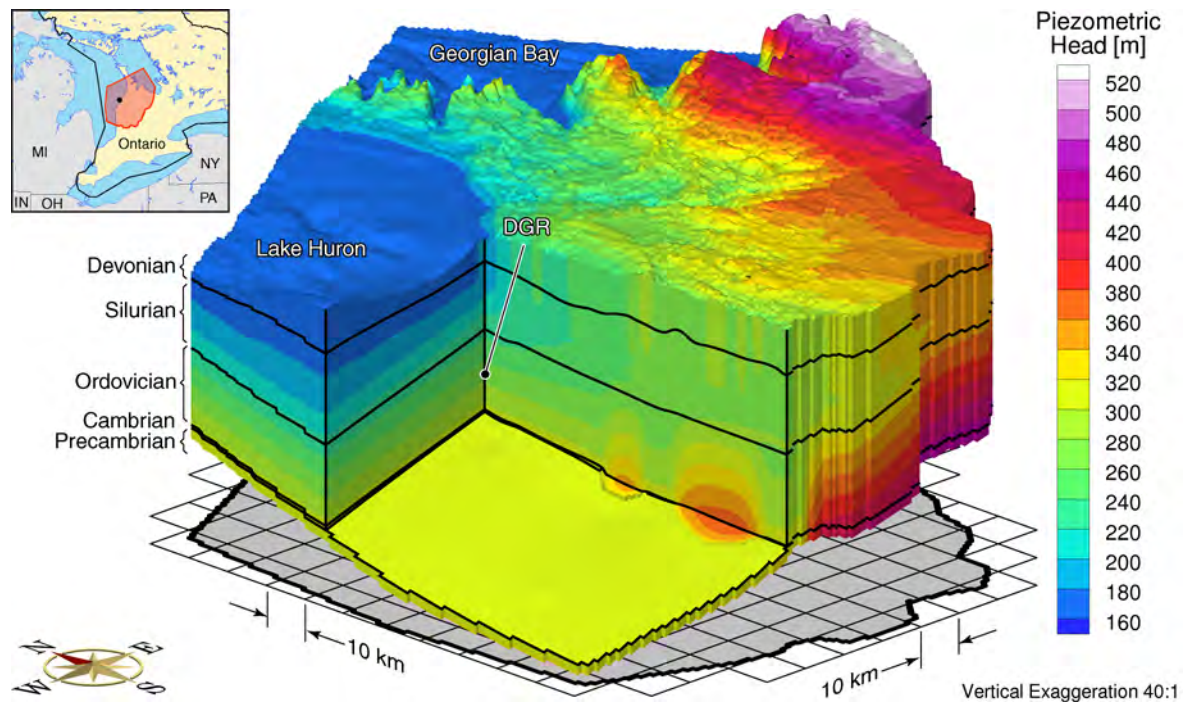


Figure I.1: Environmental head distribution for base case parameters and domain.

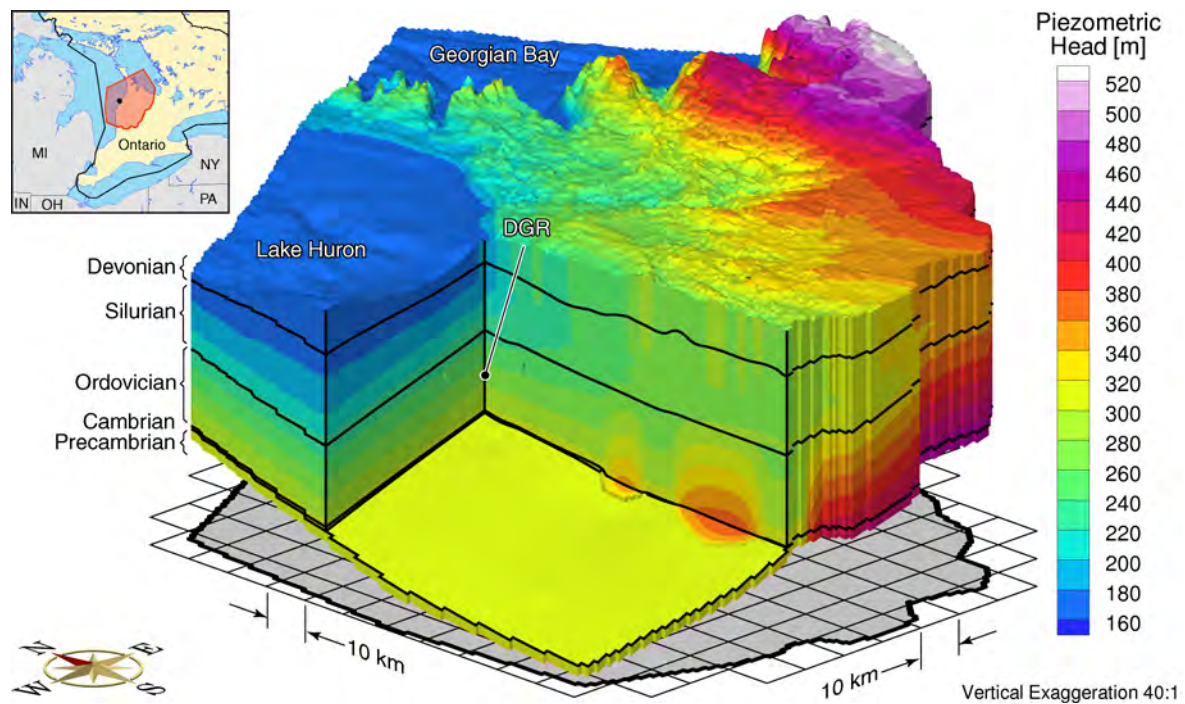


Figure I.2: Environmental head distribution for base case parameters and site-scale sub-gridding.

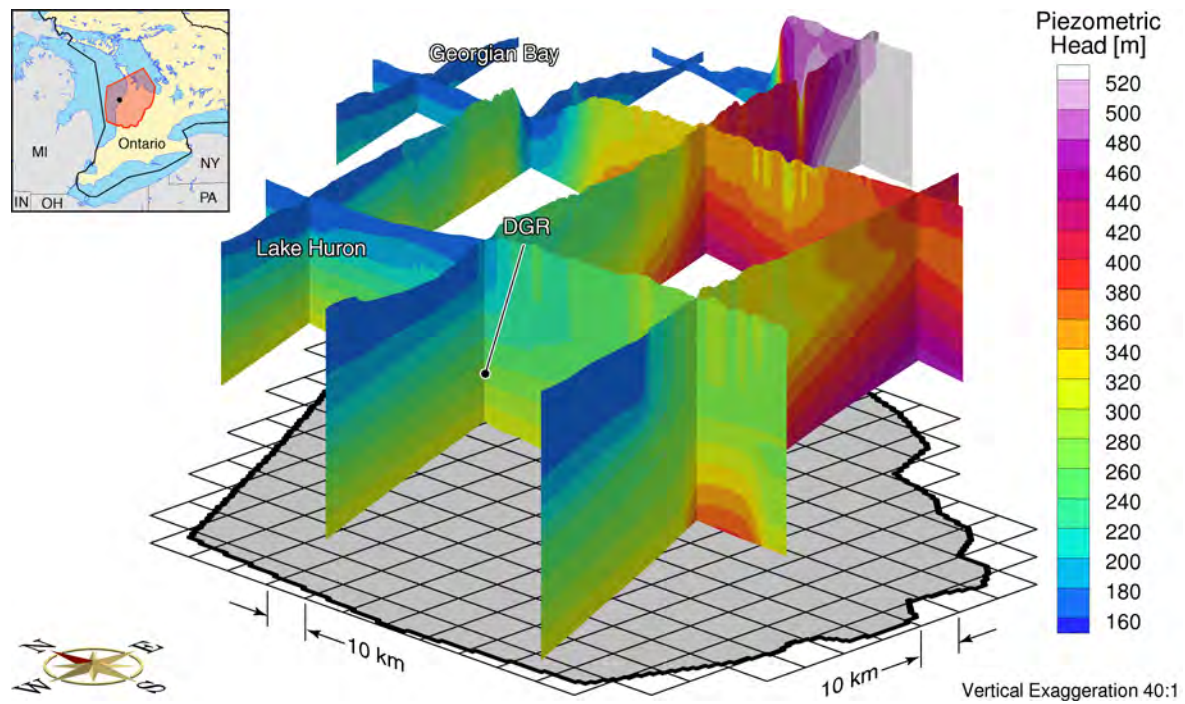


Figure I.3: Fence diagram of environmental head distribution for base case parameters and domain.

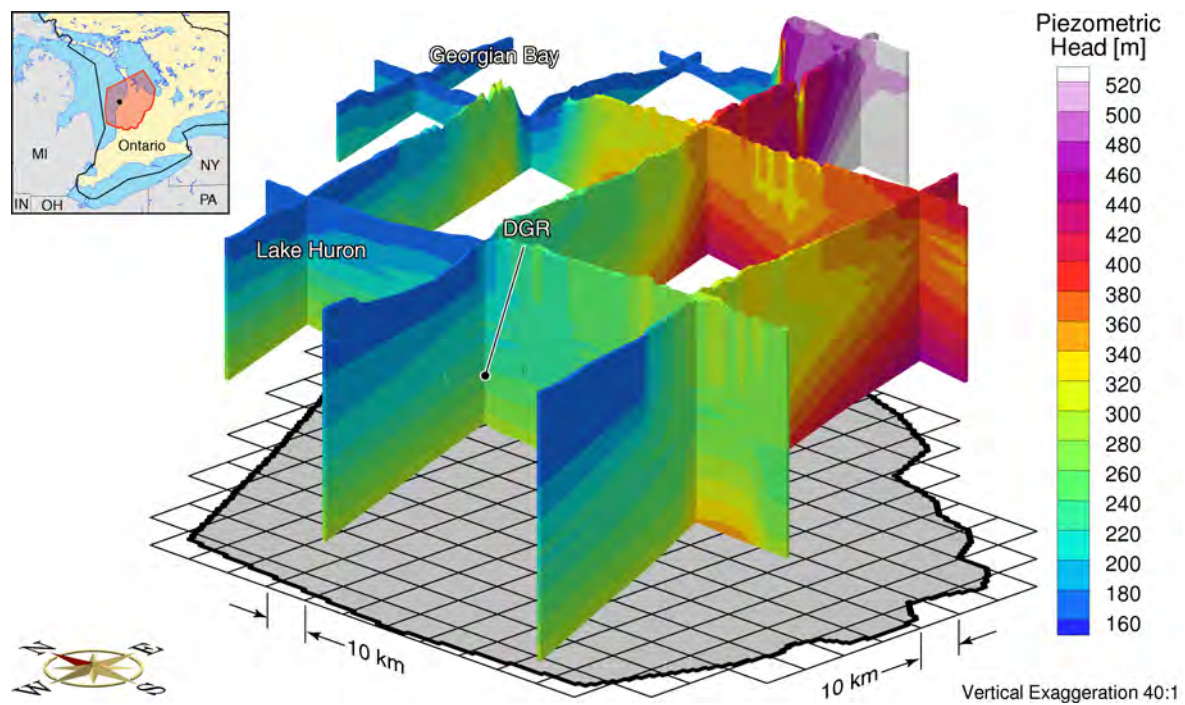


Figure I.4: Fence diagram of environmental head distribution for base case parameters and site-scale sub-gridding.

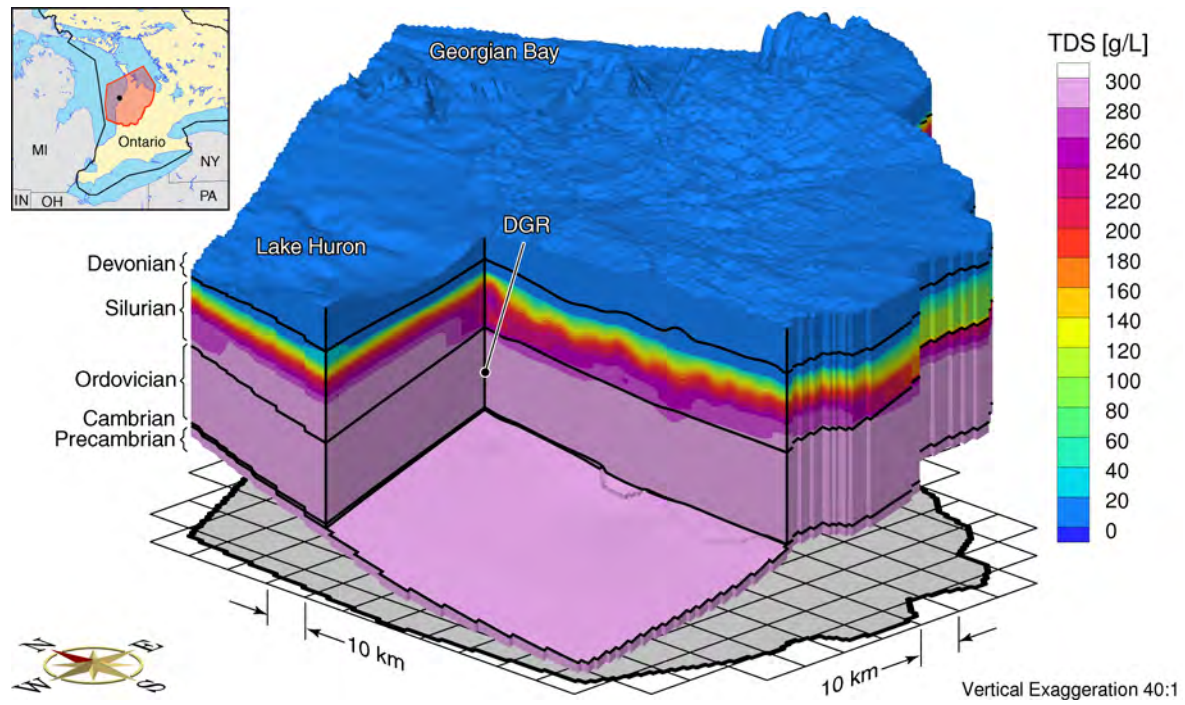


Figure I.5: Total Dissolved Solids distribution for base case parameters and domain.

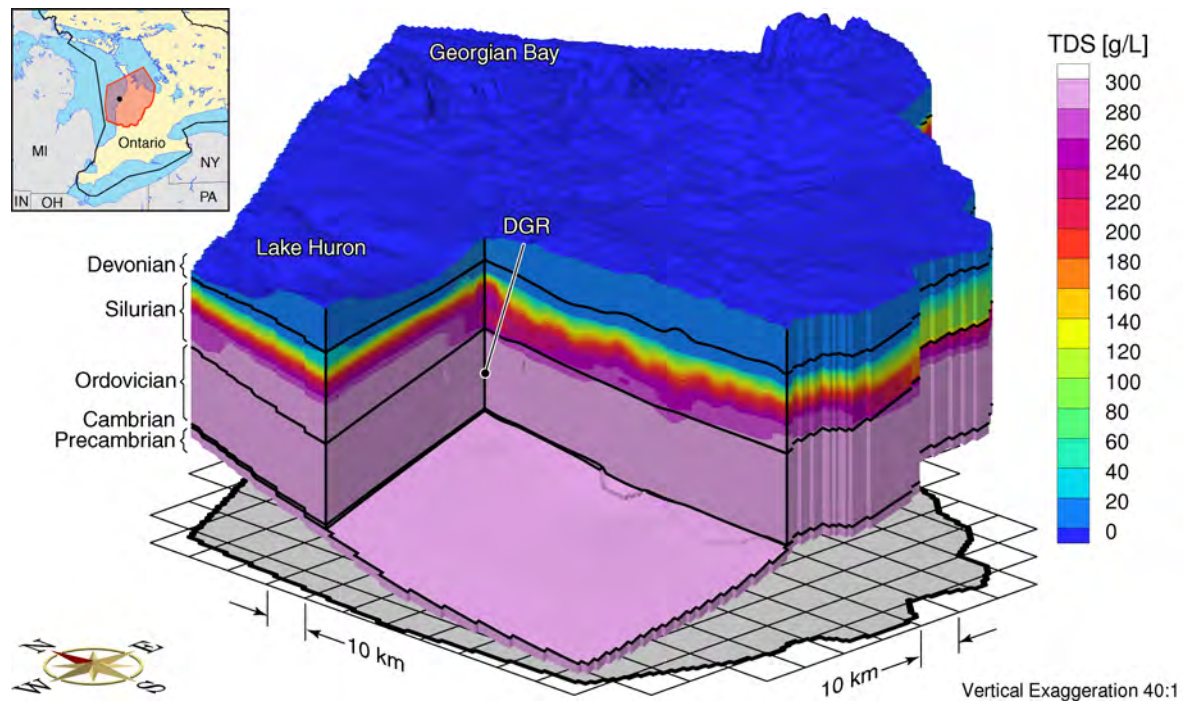


Figure I.6: Total Dissolved Solids distribution for base case parameters and site-scale sub-gridding.

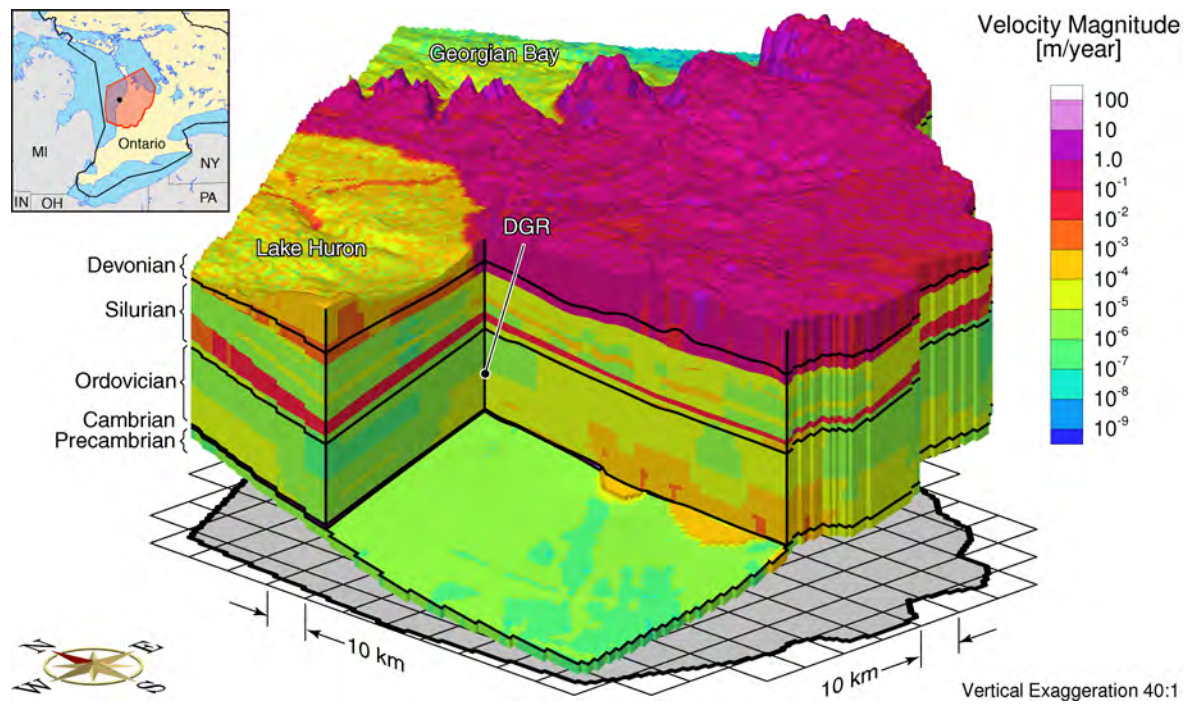


Figure I.7: Pore water velocity magnitude distribution for base case parameters and domain.

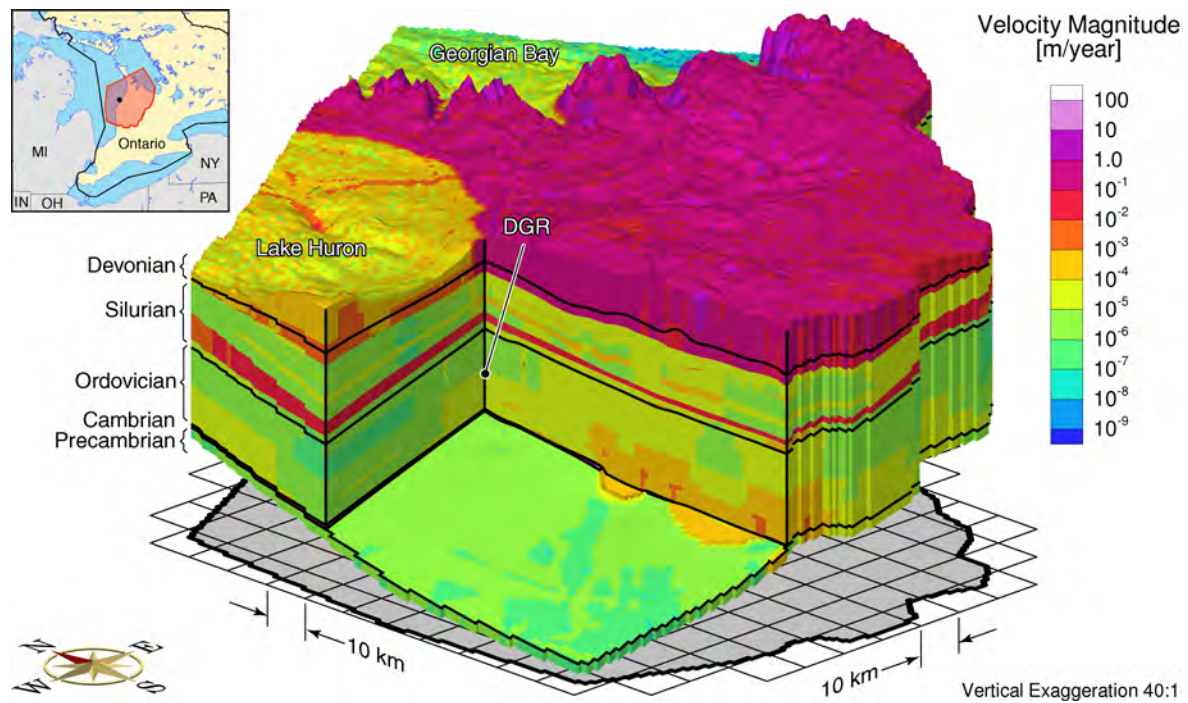


Figure I.8: Pore water velocity magnitude distribution for base case parameters and site-scale sub-gridding.

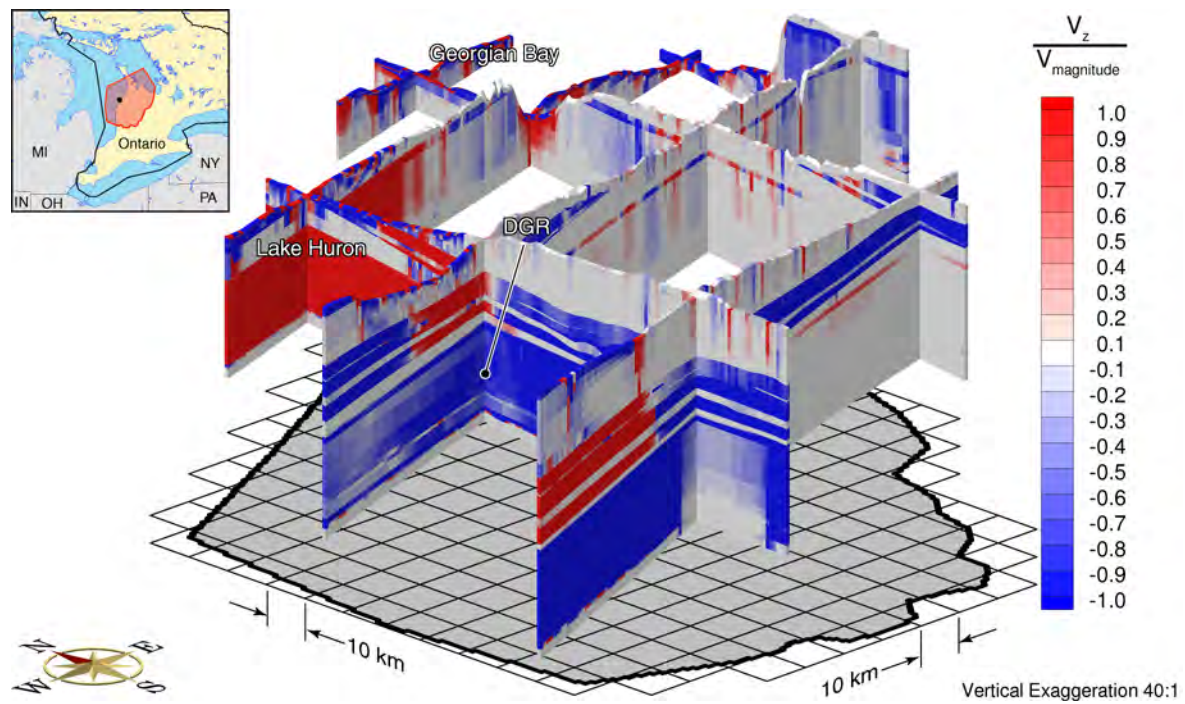


Figure I.9: Fence diagram of ratio of vertical velocity to velocity magnitude for base case parameters and domain.

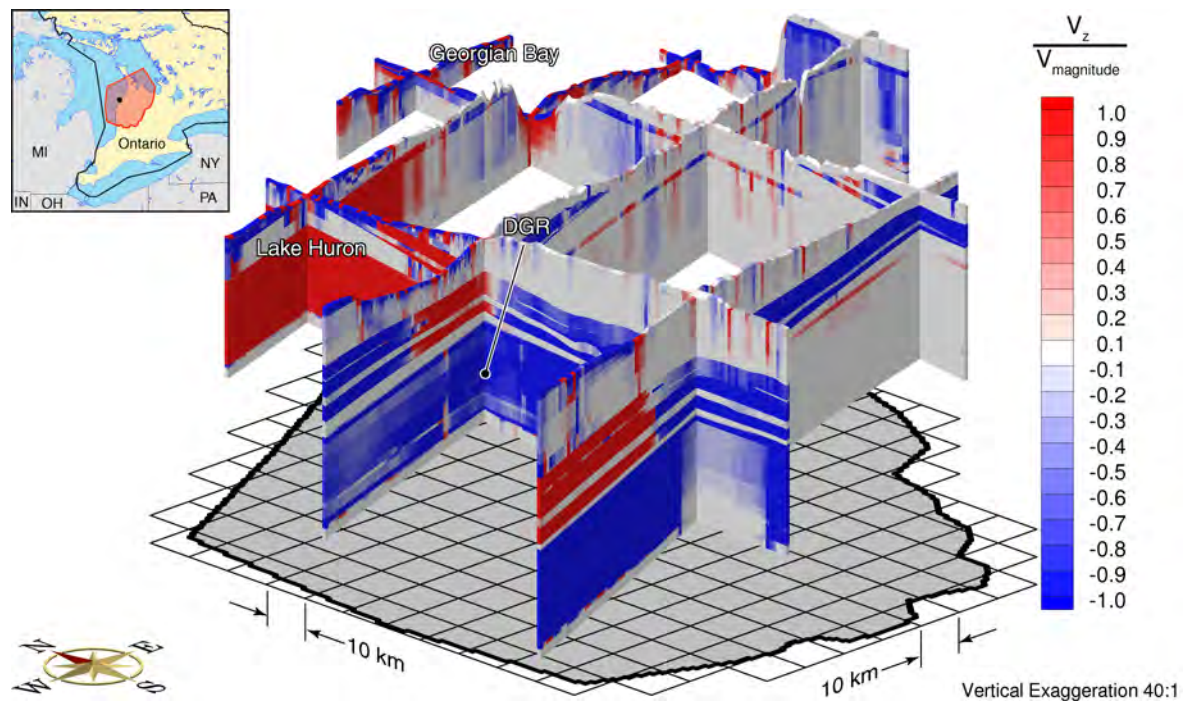


Figure I.10: Fence diagram of ratio of vertical velocity to velocity magnitude for base case parameters and site-scale sub-gridding.

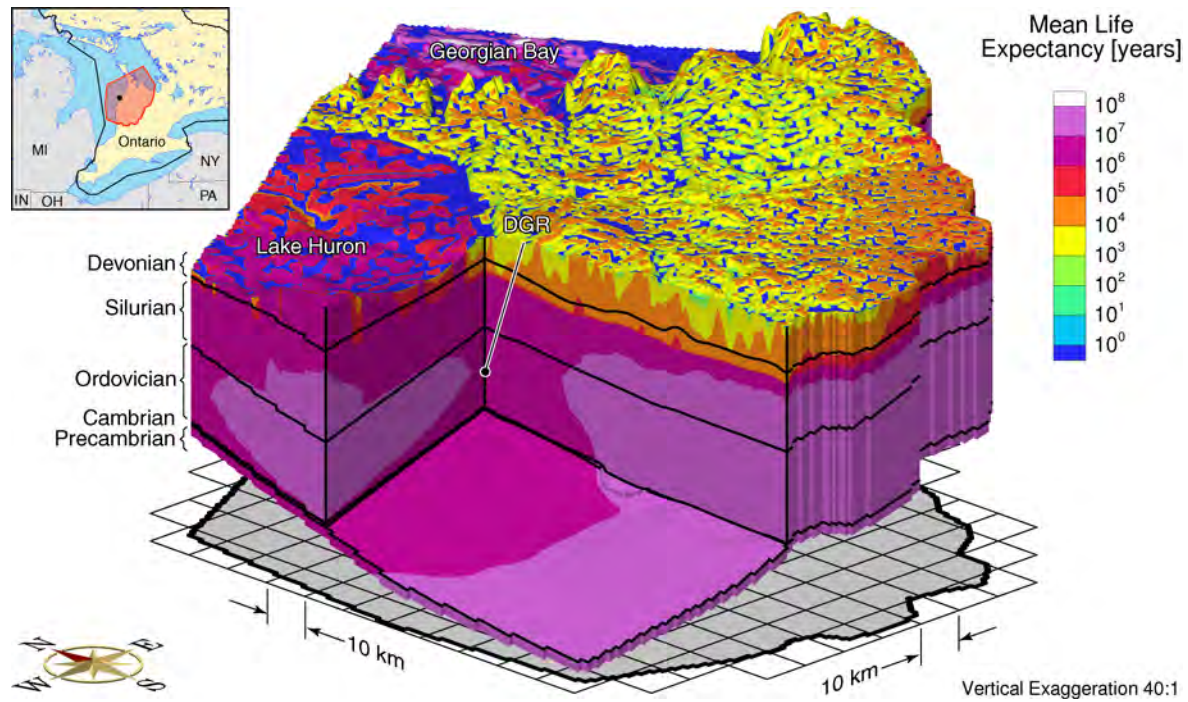


Figure I.11: Mean life expectancies for base case parameters and domain.

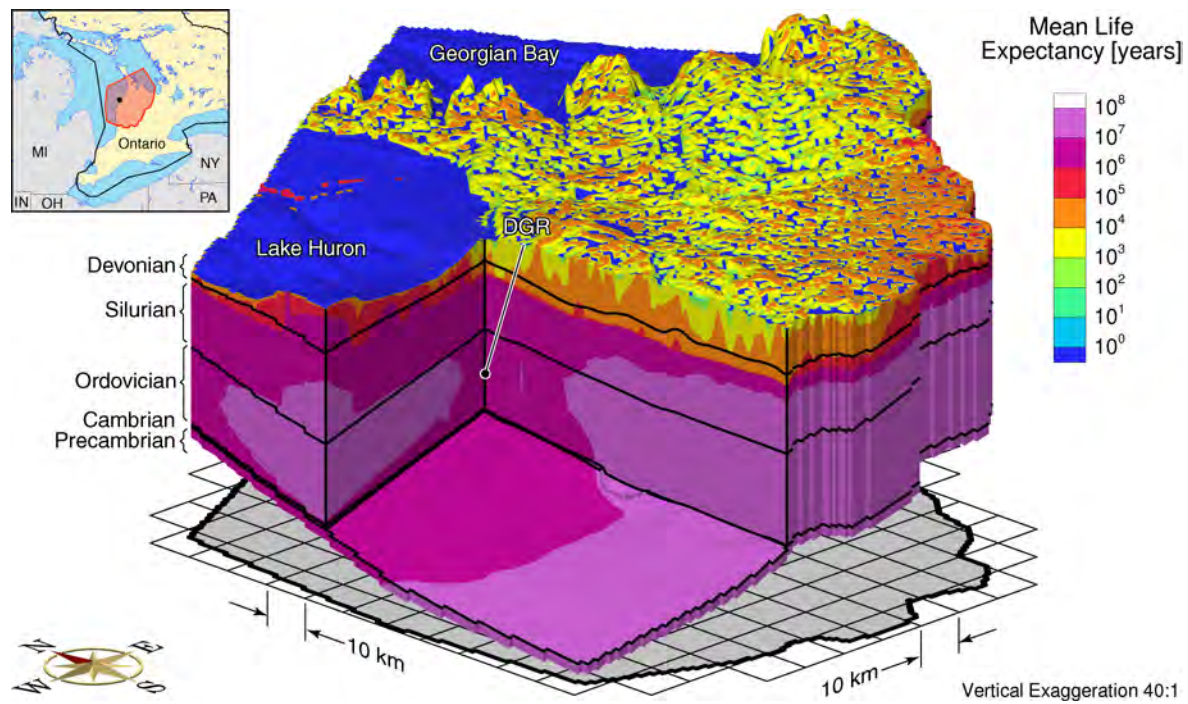


Figure I.12: Mean life expectancies for base case parameters and site-scale sub-gridding.

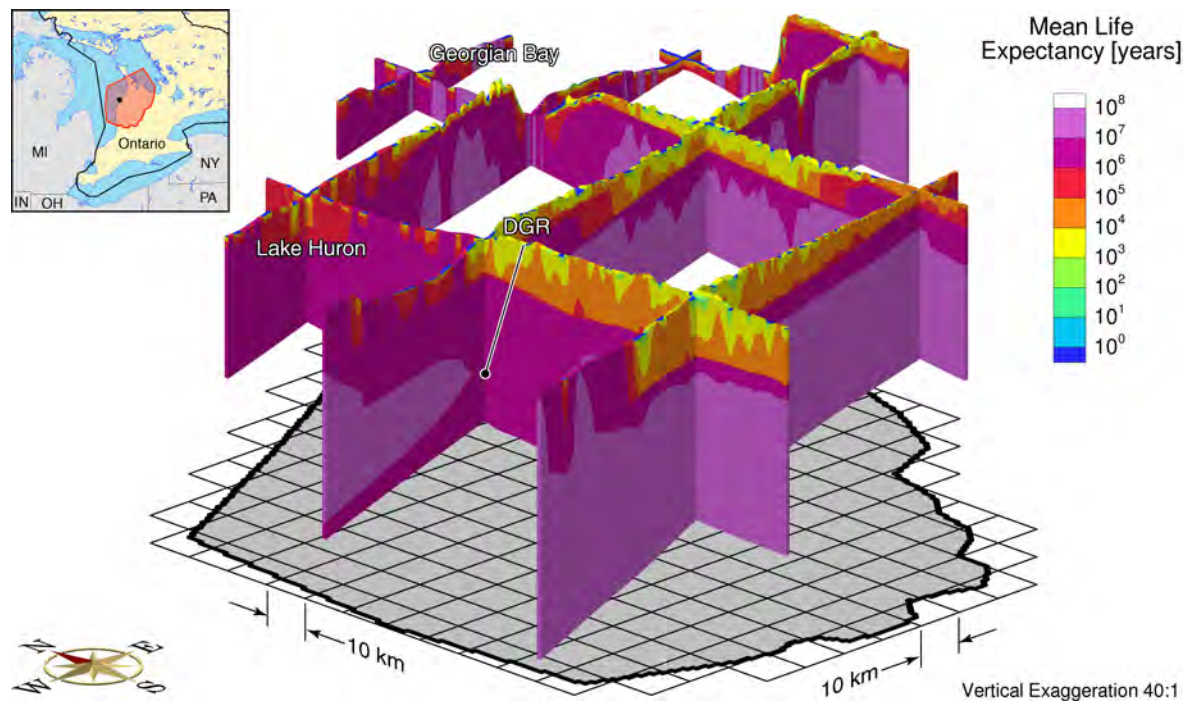


Figure I.13: Fence diagram showing mean life expectancies for base case parameters and domain.

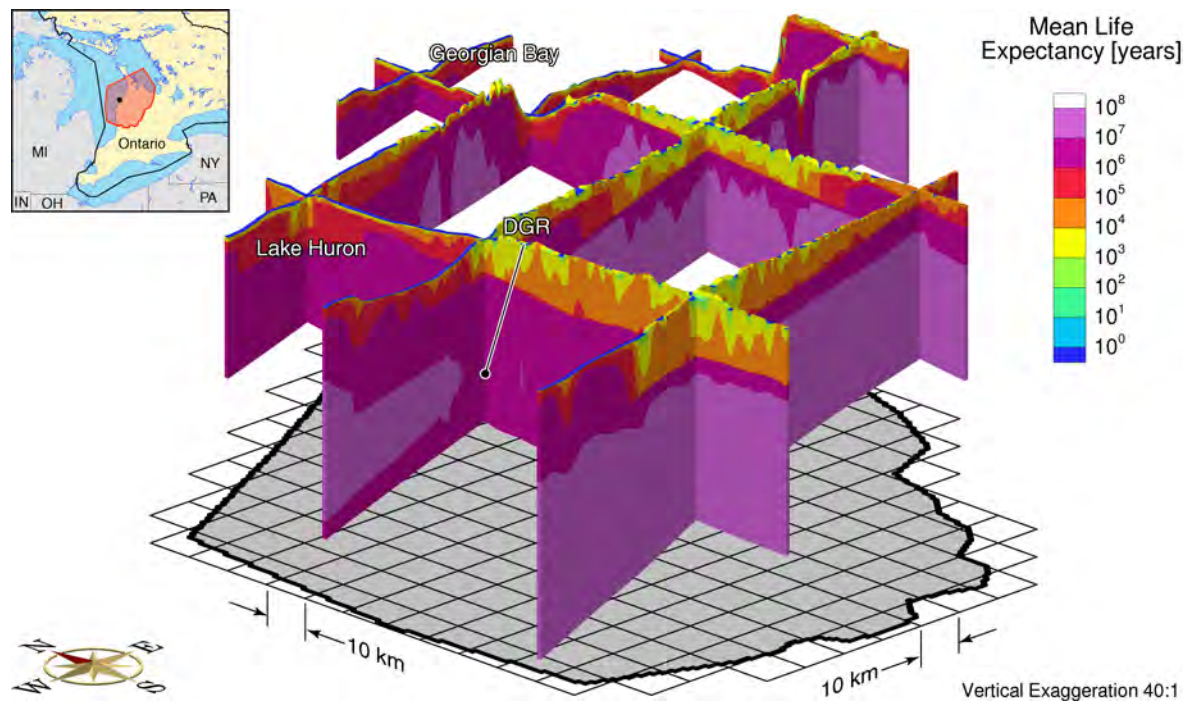


Figure I.14: Fence diagram showing life expectancies for base case parameters and site-scale sub-gridding.

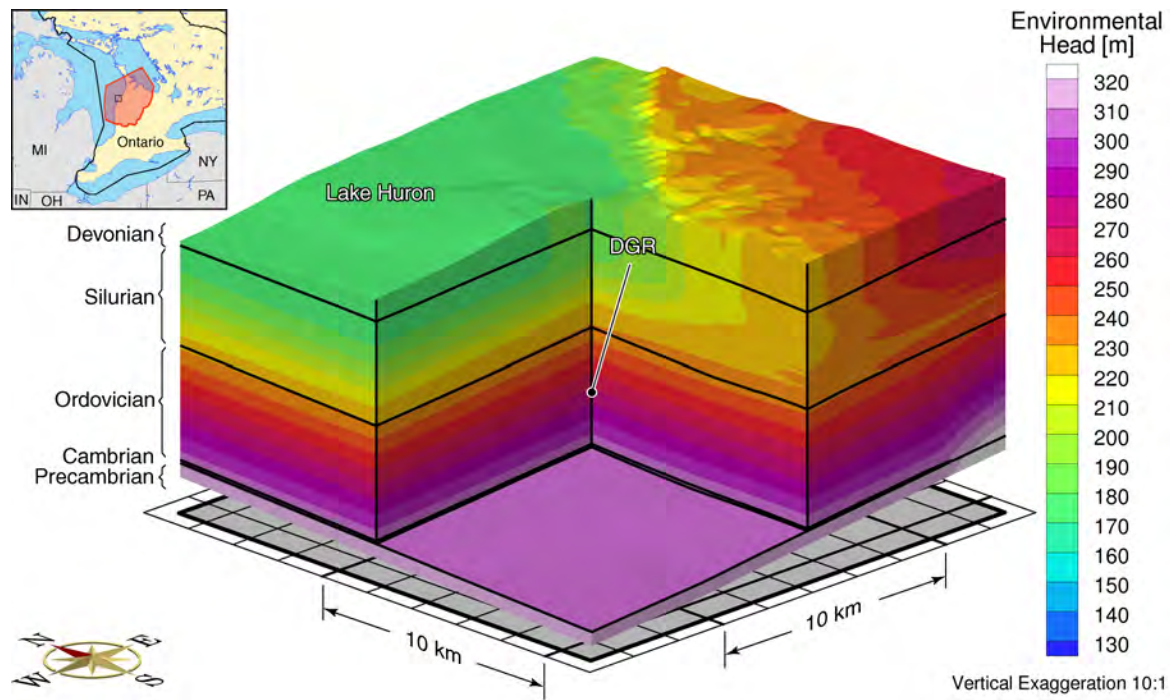


Figure I.15: Equivalent freshwater heads for the nested site-scale model and the base case parameters.

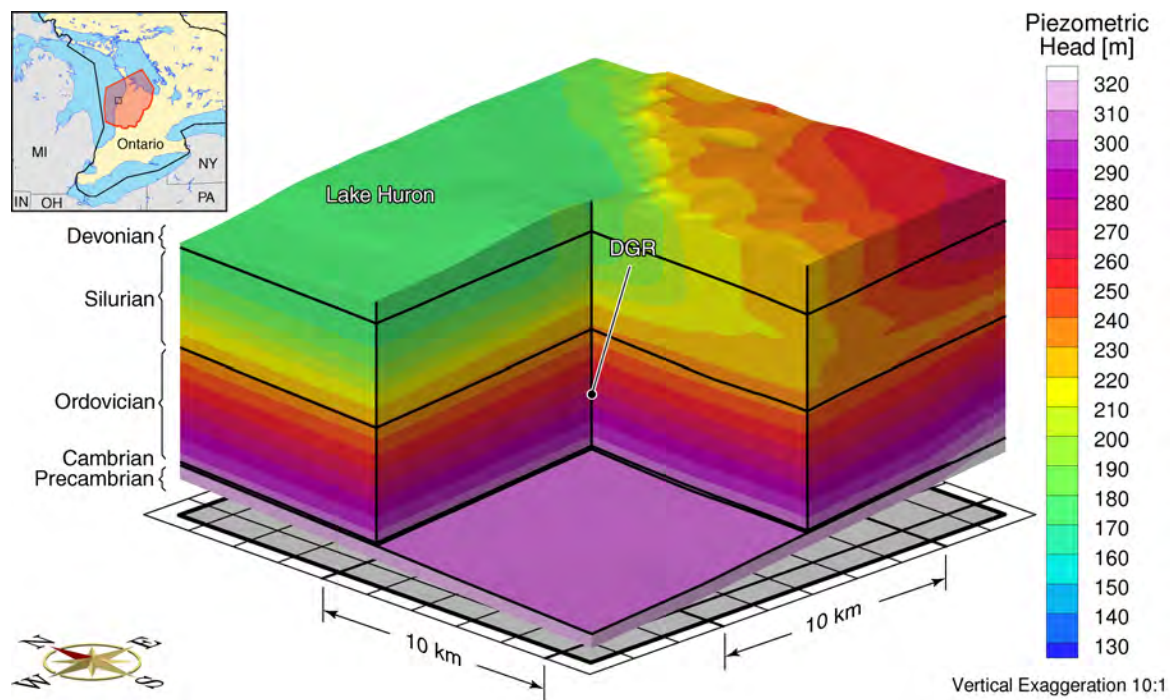


Figure I.16: Equivalent freshwater heads at the sub-gridded site-scale for the base case parameters.

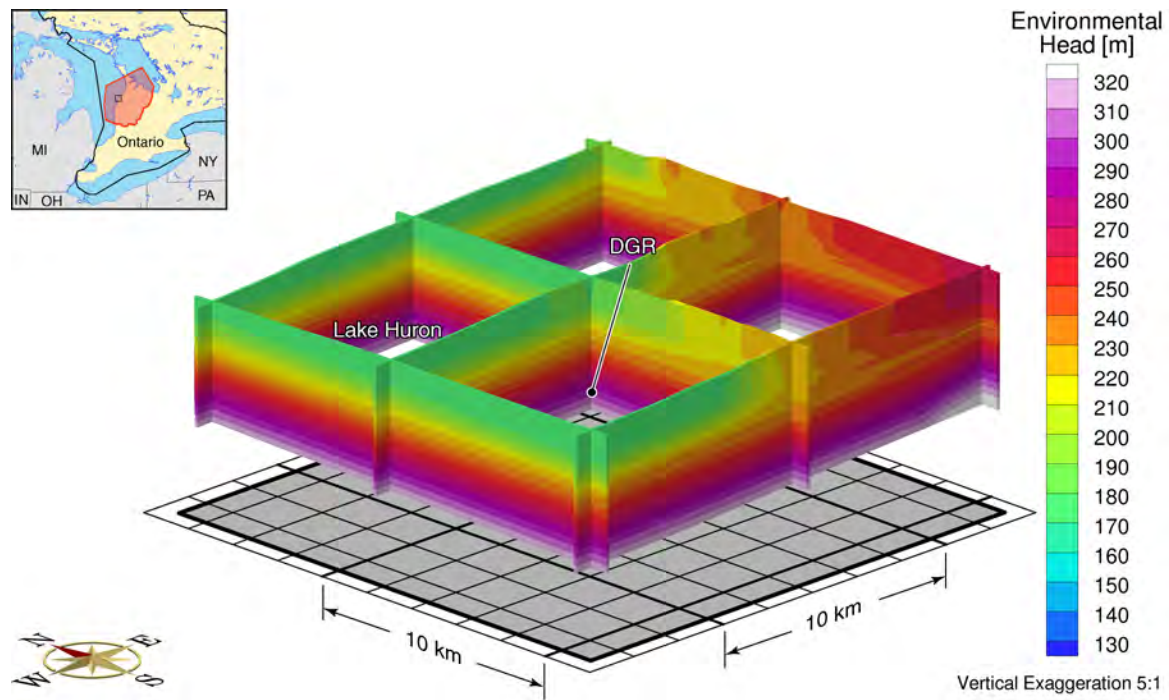


Figure I.17: Fence diagram of equivalent freshwater heads for the nested site-scale model and the base case parameters.

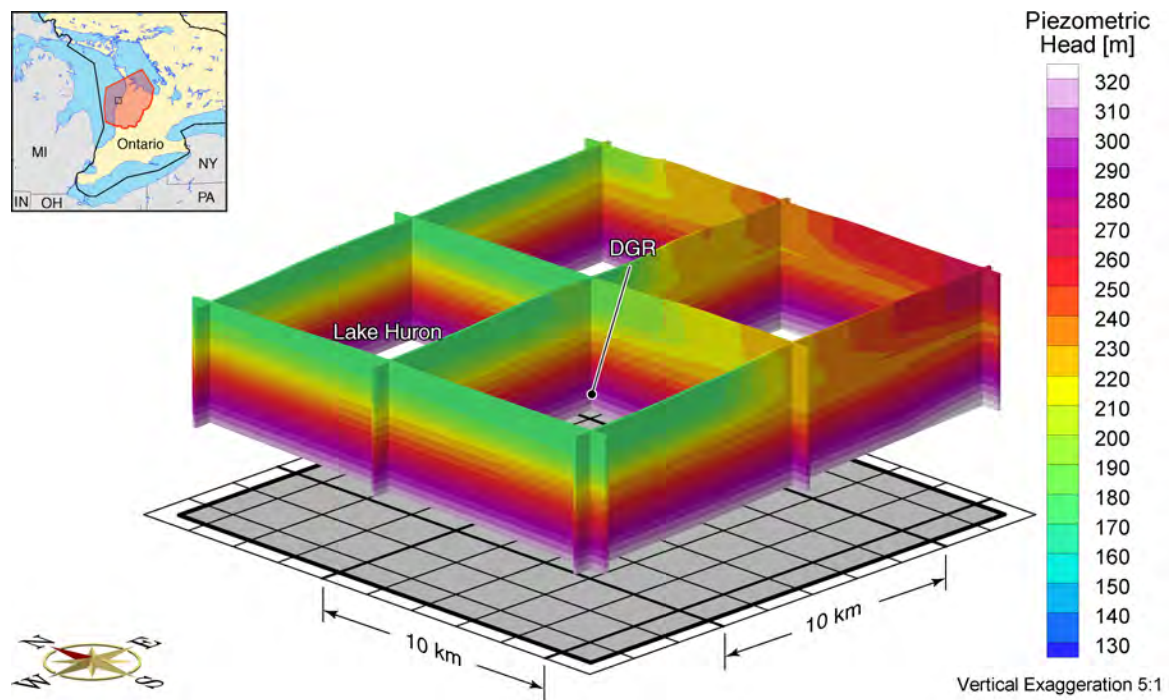


Figure I.18: Fence diagram of equivalent freshwater heads at the sub-gridded site-scale for the base case parameters.

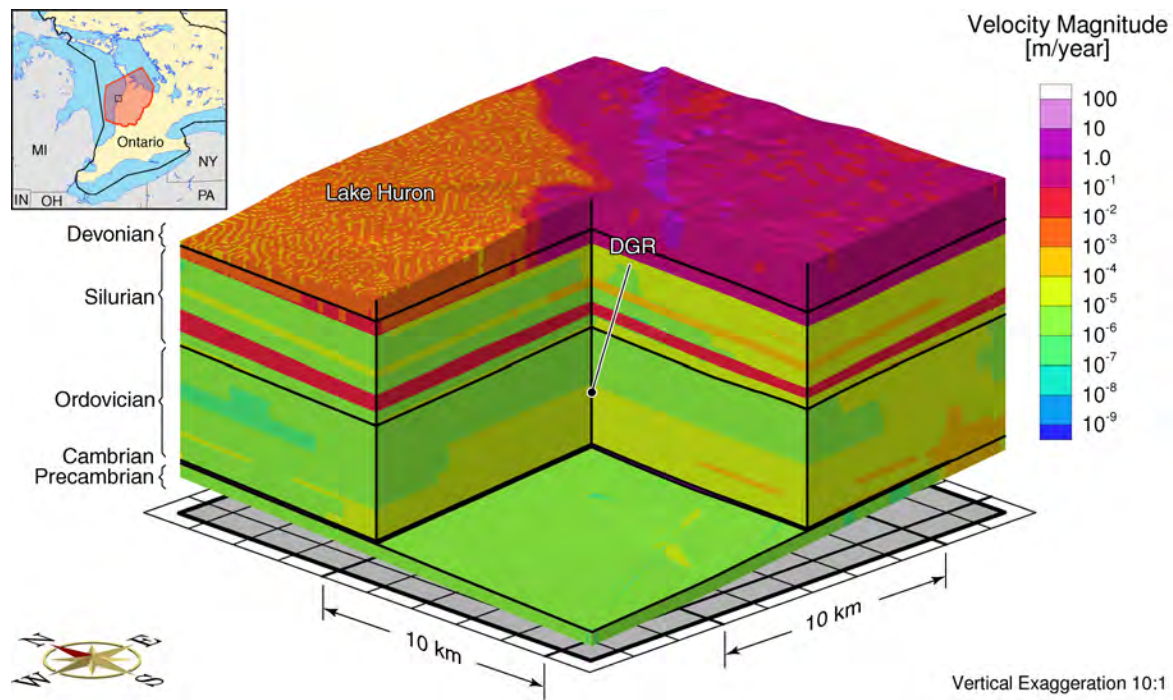


Figure I.19: Pore water velocity magnitude for the nested site-scale model and the base case parameters.

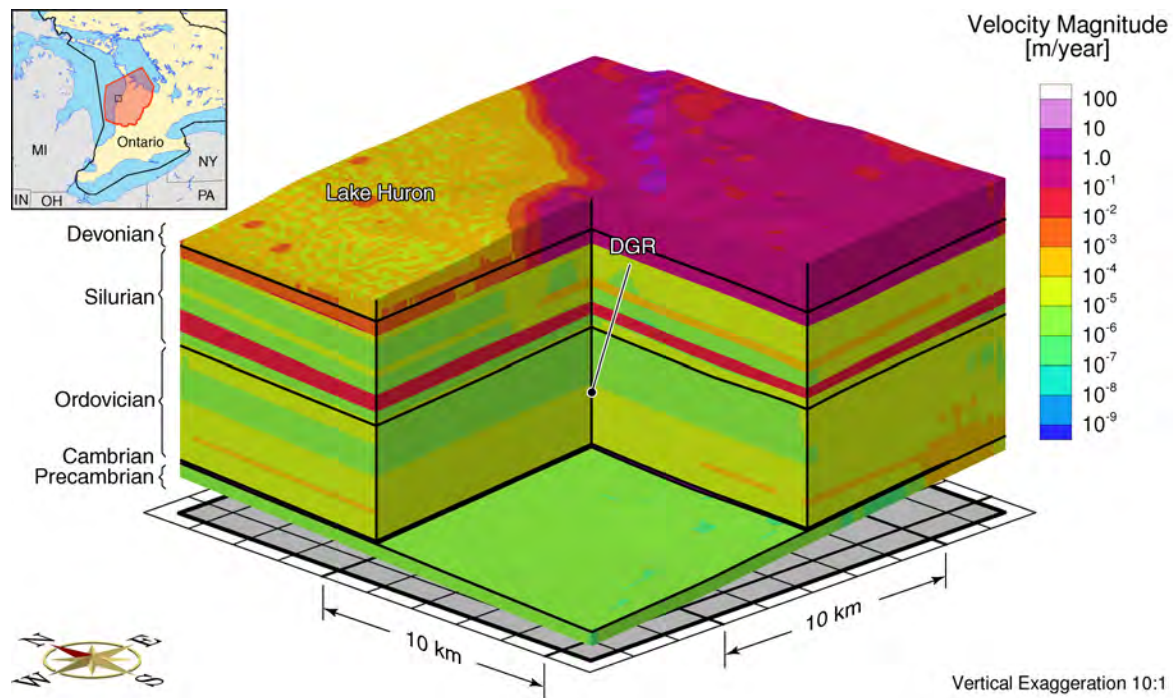


Figure I.20: Pore water velocity magnitude at the sub-gridded site-scale for the base case parameters.

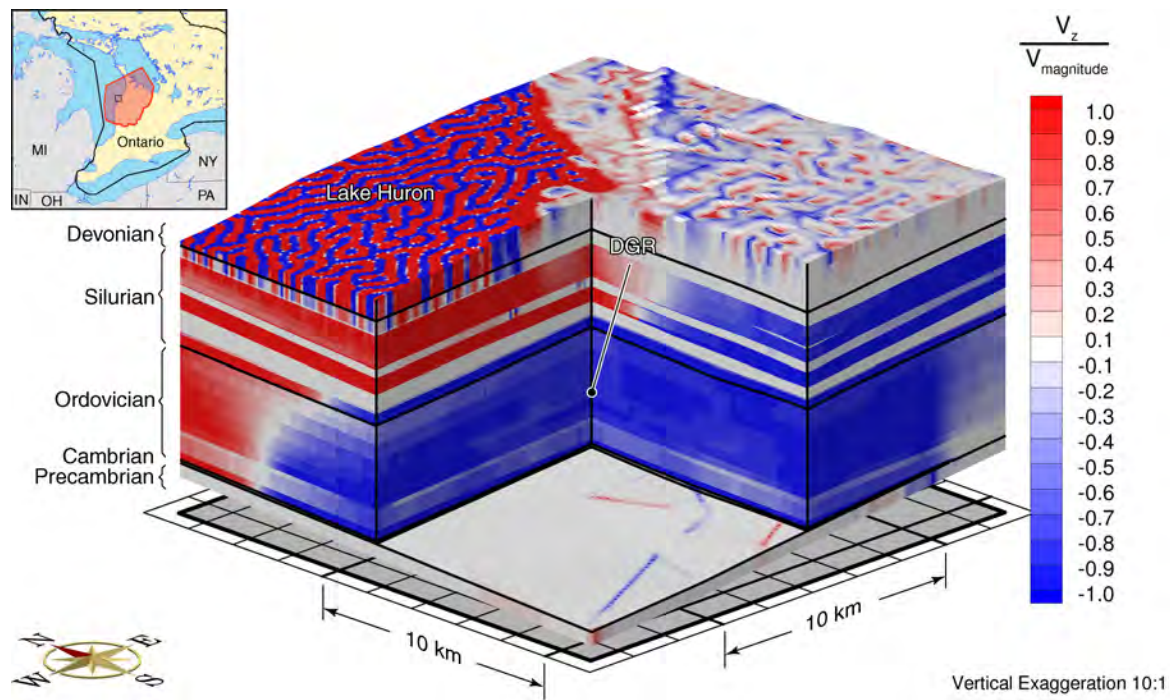


Figure I.21: Ratio of vertical velocity to the velocity magnitude for the nested site-scale model and the base case parameters.

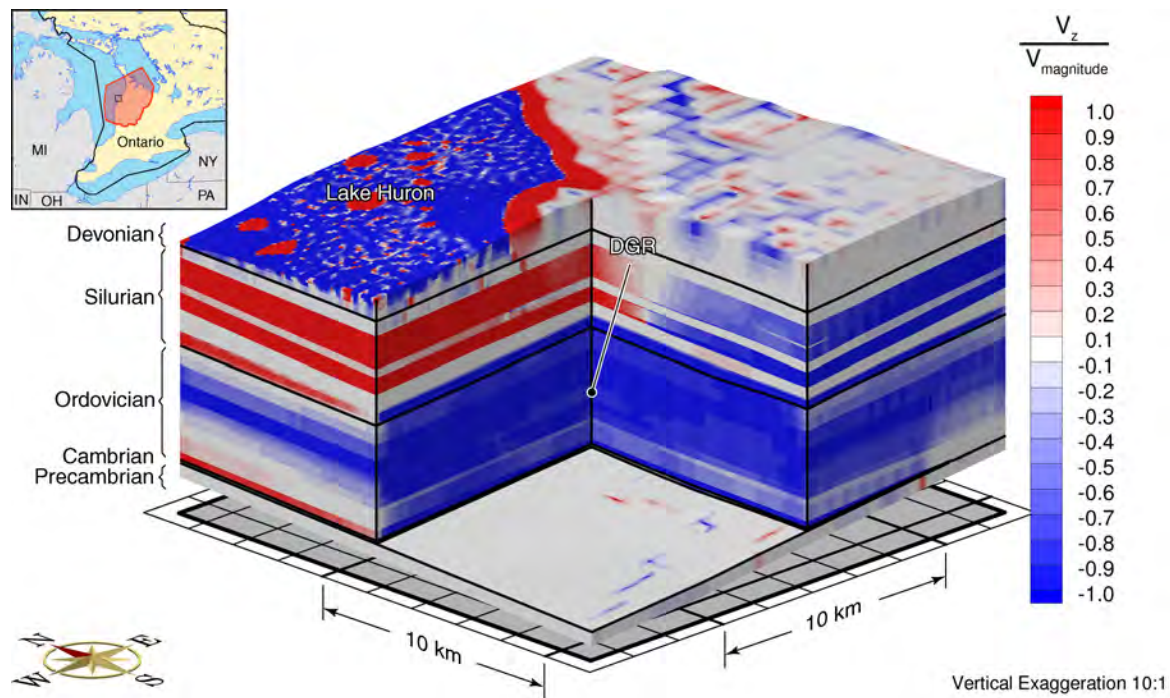


Figure I.22: Ratio of vertical velocity to the velocity magnitude at the sub-gridded site-scale for the base case parameters.

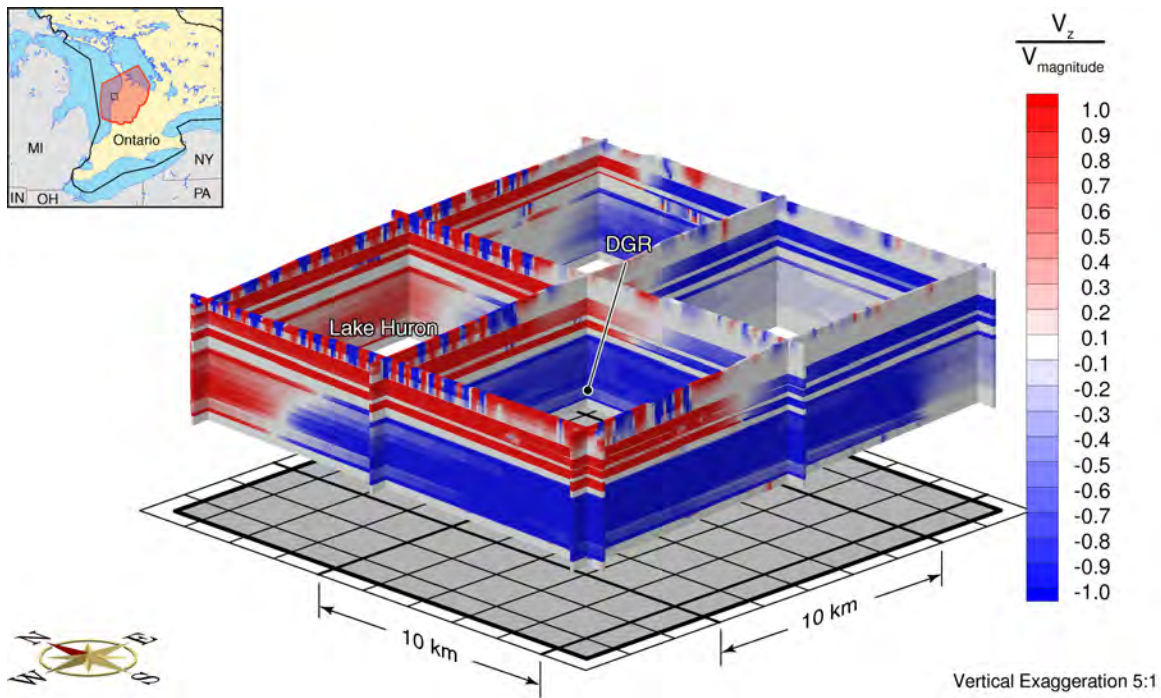


Figure I.23: Fence diagram of the ratio of vertical velocity to the velocity magnitude for the nested site-scale model and the base case parameters.

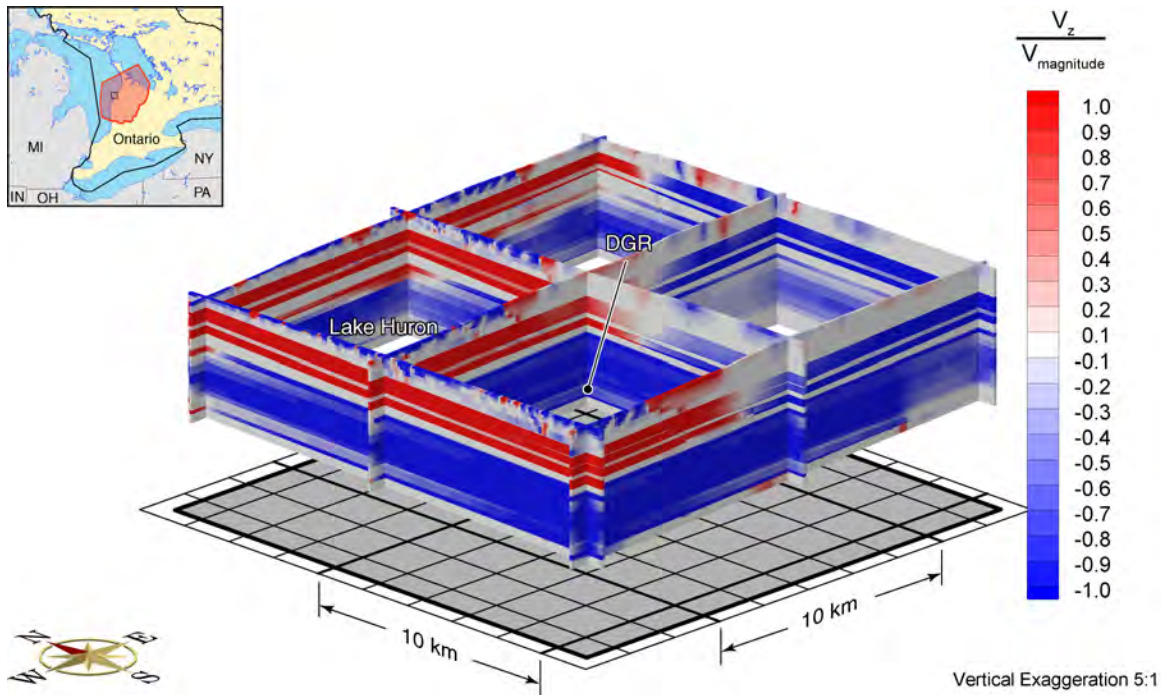


Figure I.24: Fence diagram of the ratio of vertical velocity to the velocity magnitude at the sub-gridded site-scale for the base case parameters.

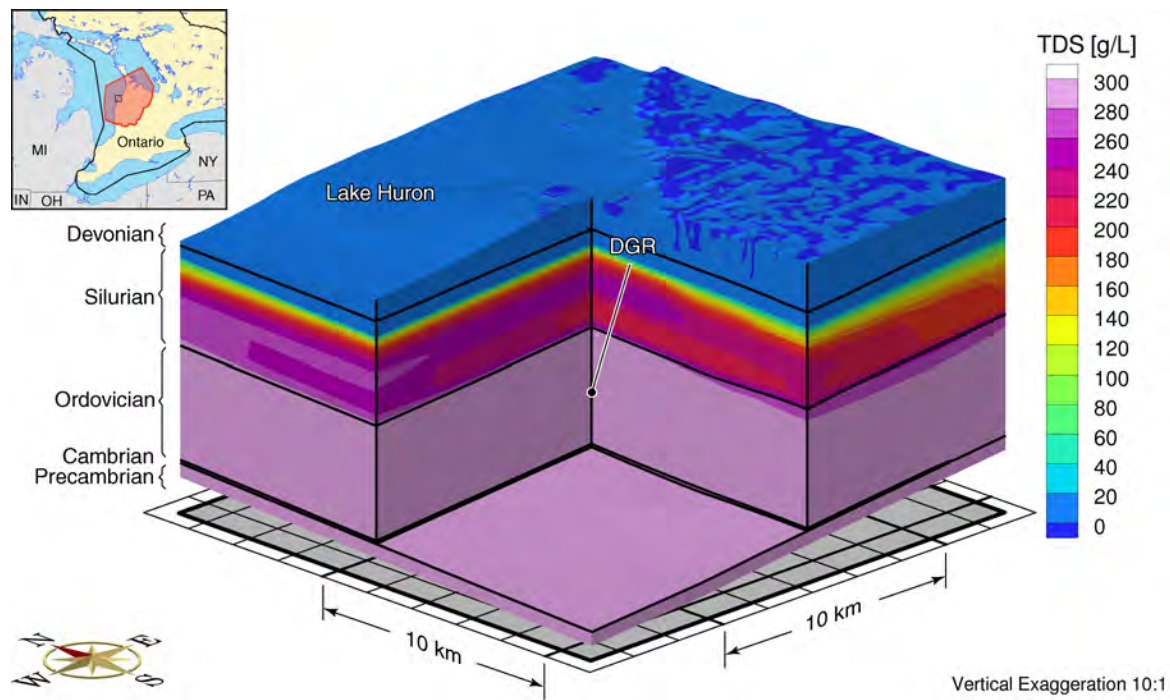


Figure I.25: Total dissolved solids concentration for the nested site-scale model and the base case parameters.

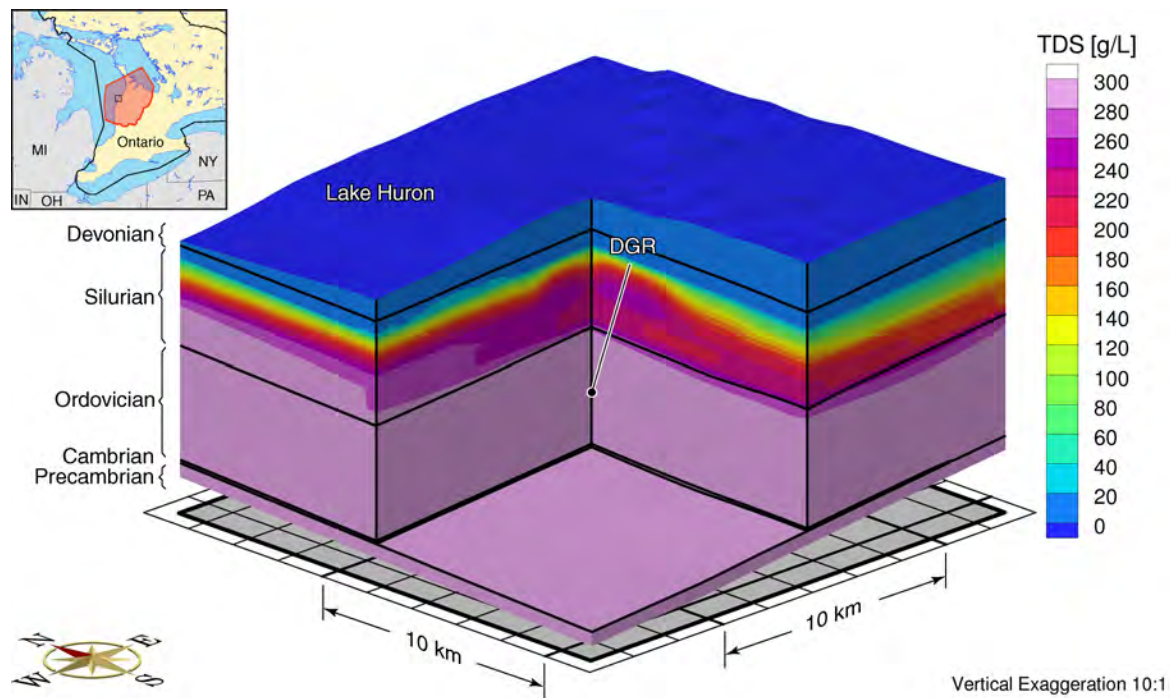


Figure I.26: Total dissolved solids concentration at the sub-gridded site-scale for the base case parameters.

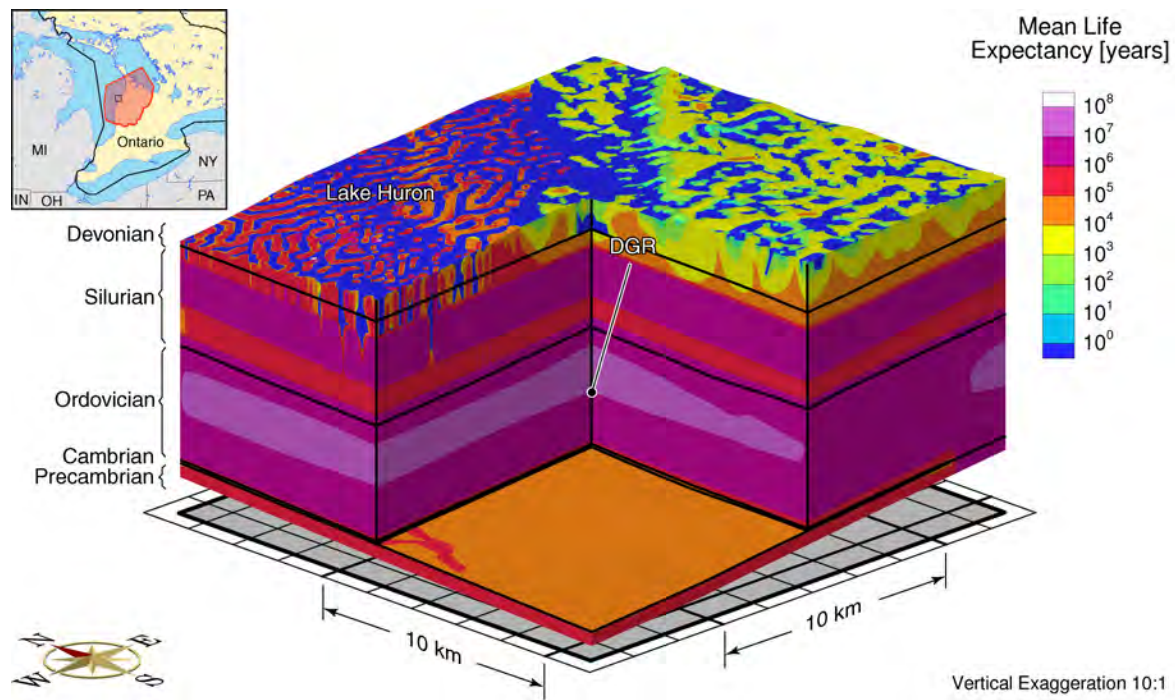


Figure I.27: Mean life expectancies for the nested site-scale model and the base case parameters.

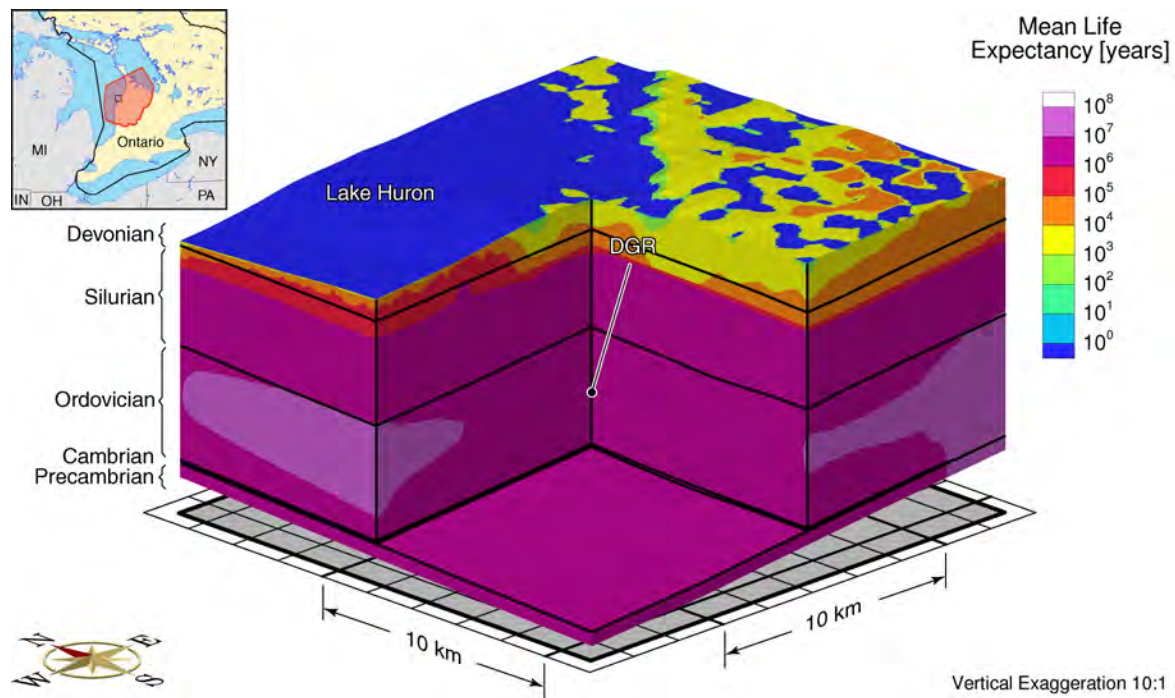


Figure I.28: Mean life expectancies for the sub-gridded site-scale model and the base case parameters.

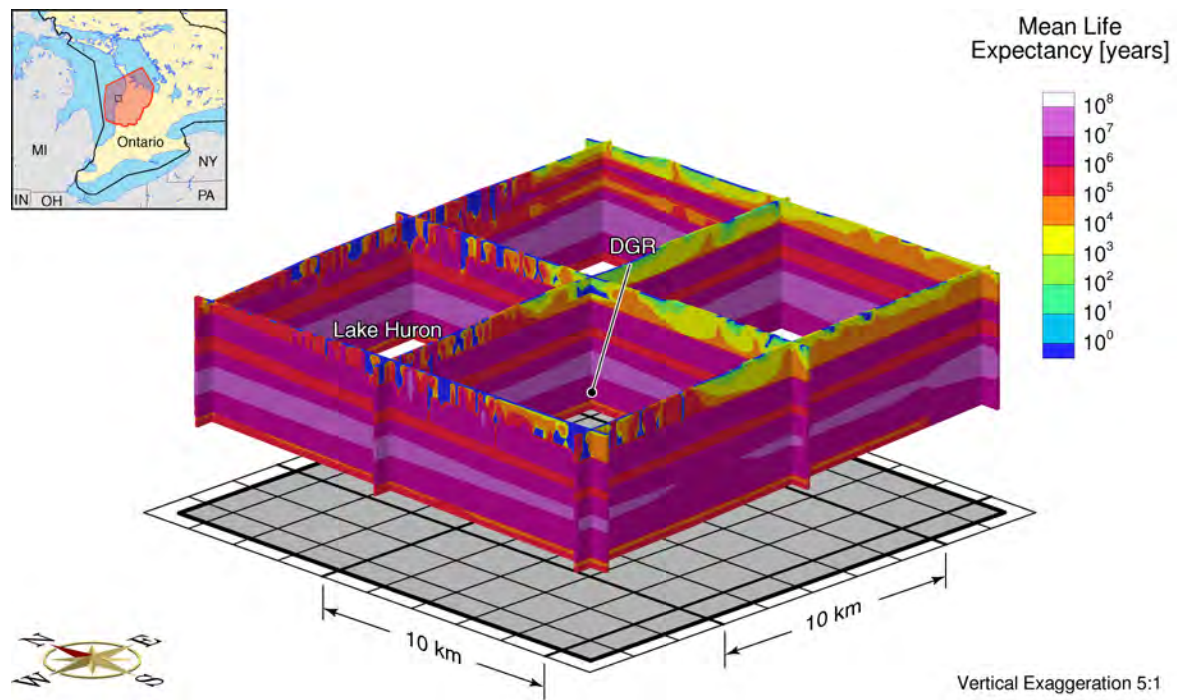


Figure I.29: Fence diagram showing the mean life expectancies for the nested site-scale model and the base case parameters.

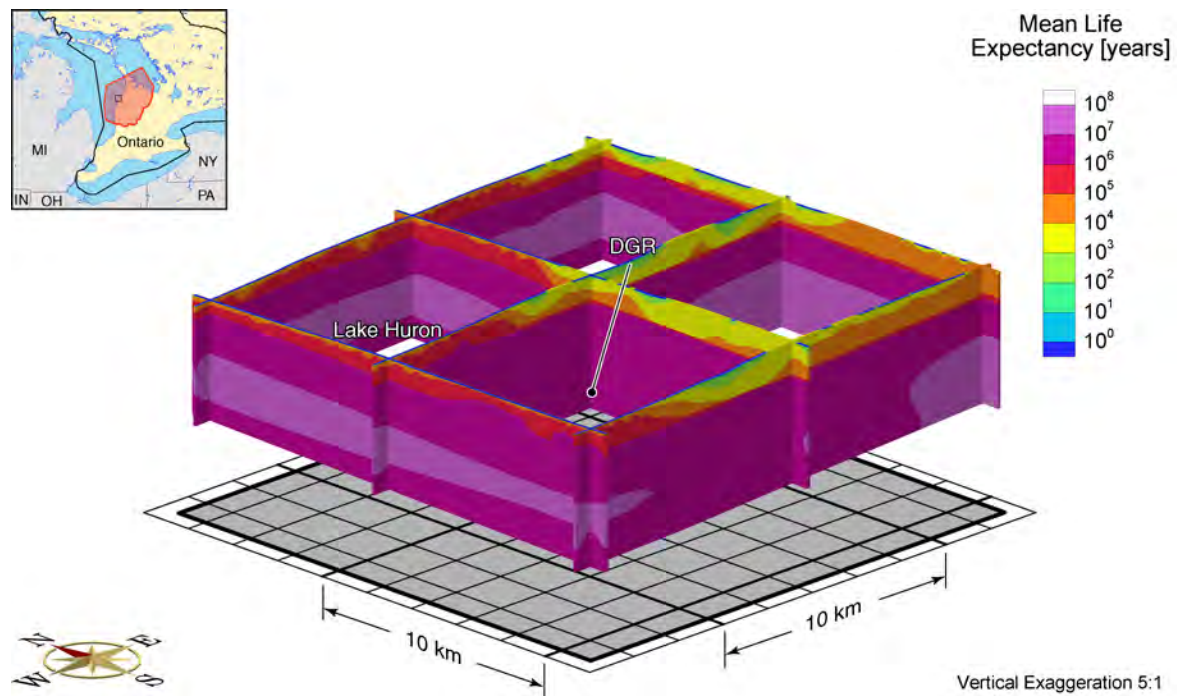


Figure I.30: Fence diagram showing the mean life expectancies for the sub-gridded site-scale model and the base case parameters.

APPENDIX J – ANALYSIS OF PRESSURE DISTRIBUTION AT DGR-1/DGR-2**LIST OF FIGURES**

| | Page |
|---|-------------|
| Figure J.1. Equivalent freshwater head profile at DGR-2 for base case parameters with anisotropy of 0.01; no pressure support for the Niagaran or Cambrian. . . . | 228 |
| Figure J.2. Environmental head profile at DGR-2 for base case parameters with anisotropy of 0.01; no pressure support for the Niagaran or Cambrian. | 228 |
| Figure J.3. Equivalent freshwater head profile at DGR-2 for base case parameters with anisotropy of 0.01; pressure support for the Cambrian and no pressure support for the Niagaran. | 229 |
| Figure J.4. Environmental head profile at DGR-2 for base case parameters with anisotropy of 0.01; pressure support for the Cambrian and no pressure support for the Niagaran. | 229 |
| Figure J.5. Equivalent freshwater head profile at DGR-2 for base case parameters with anisotropy of 0.01; pressure support for both the Niagaran and the Cambrian. | 230 |
| Figure J.6. Environmental head profile at DGR-2 for base case parameters with anisotropy of 0.01; pressure support for both the Niagaran and the Cambrian. | 230 |
| Figure J.7. Equivalent freshwater head profile at DGR-2 for base case parameters with anisotropy of 0.01; pressure support for the Niagaran and no pressure support for the Cambrian. | 231 |
| Figure J.8. Environmental head profile at DGR-2 for base case parameters with anisotropy of 0.01; pressure support for the Niagaran and no pressure support for the Cambrian. | 231 |
| Figure J.9. Equivalent freshwater head profile at DGR-2 for base case parameters with anisotropy of 0.001; no pressure support for the Niagaran or Cambrian. . . . | 232 |
| Figure J.10. Environmental head profile at DGR-2 for base case parameters with anisotropy of 0.001; no pressure support for the Niagaran or Cambrian. | 232 |
| Figure J.11. Equivalent freshwater head profile at DGR-2 for base case parameters with anisotropy of 0.001; pressure support for the Cambrian and no pressure support for the Niagaran. | 233 |
| Figure J.12. Environmental head profile at DGR-2 for base case parameters with anisotropy of 0.001; pressure support for the Cambrian and no pressure support for the Niagaran. | 233 |
| Figure J.13. Equivalent freshwater head profile at DGR-2 for base case parameters with anisotropy of 0.001; pressure support for both the Niagaran and the Cambrian. | 234 |
| Figure J.14. Environmental head profile at DGR-2 for base case parameters with anisotropy of 0.001; pressure support for both the Niagaran and the Cambrian. | 234 |
| Figure J.15. Equivalent freshwater head profile at DGR-2 for base case parameters with anisotropy of 0.001; pressure support for the Niagaran and no pressure support for the Cambrian. | 235 |
| Figure J.16. Environmental head profile at DGR-2 for base case parameters with anisotropy of 0.001; pressure support for the Niagaran and no pressure support for the Cambrian. | 235 |

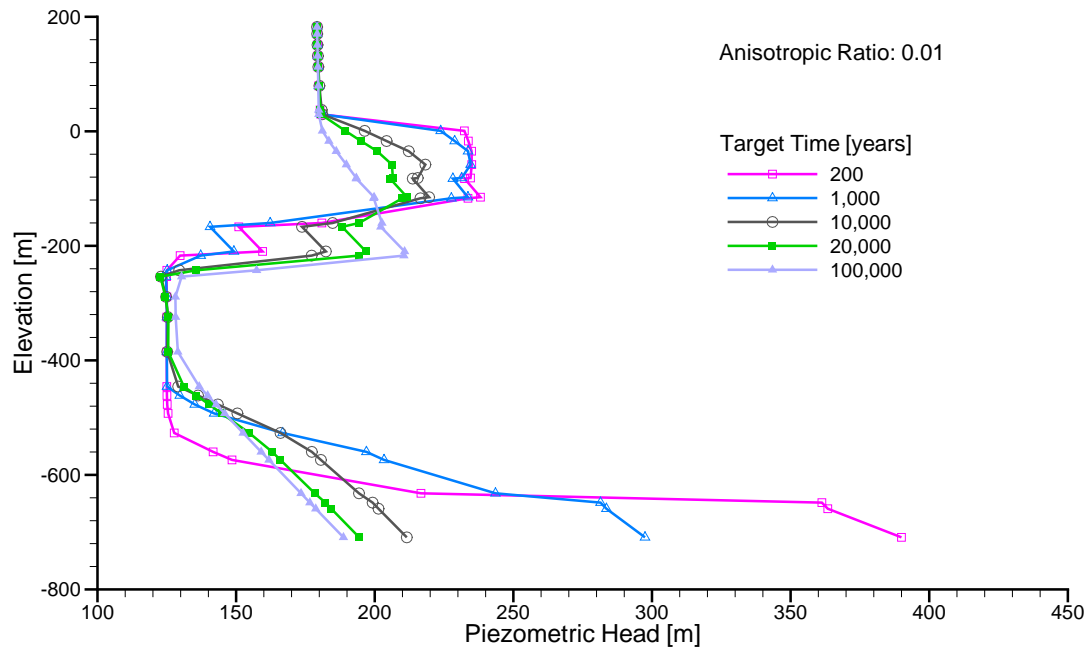


Figure J.1: Equivalent freshwater head profile at DGR-2 for base case parameters with anisotropy of 0.01; no pressure support for the Niagara or Cambrian.

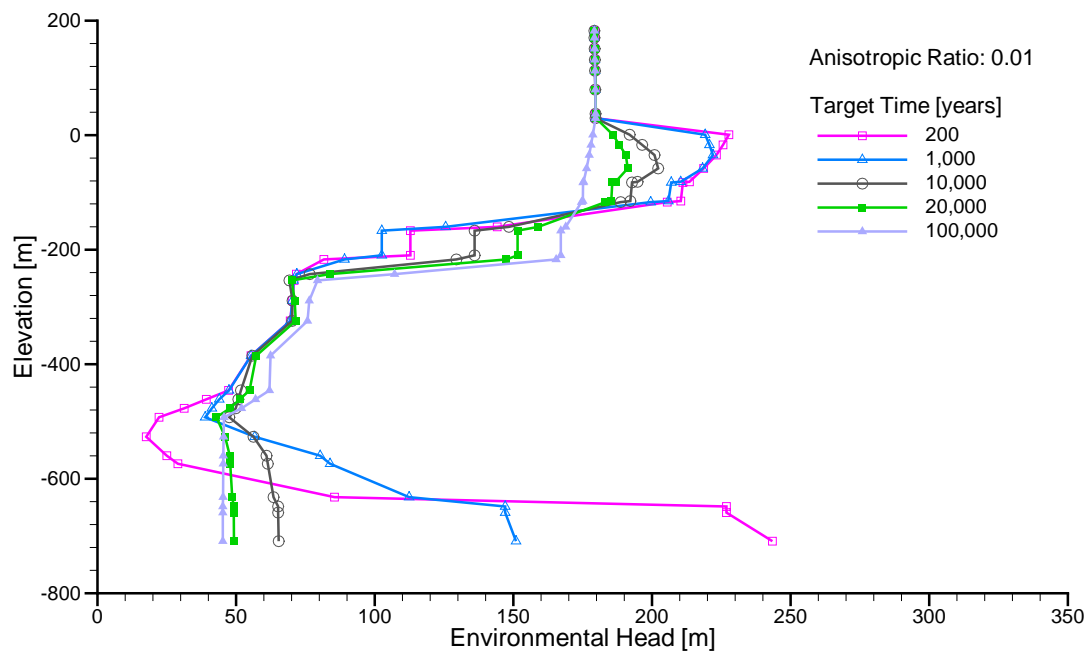


Figure J.2: Environmental head profile at DGR-2 for base case parameters with anisotropy of 0.01; no pressure support for the Niagara or Cambrian.

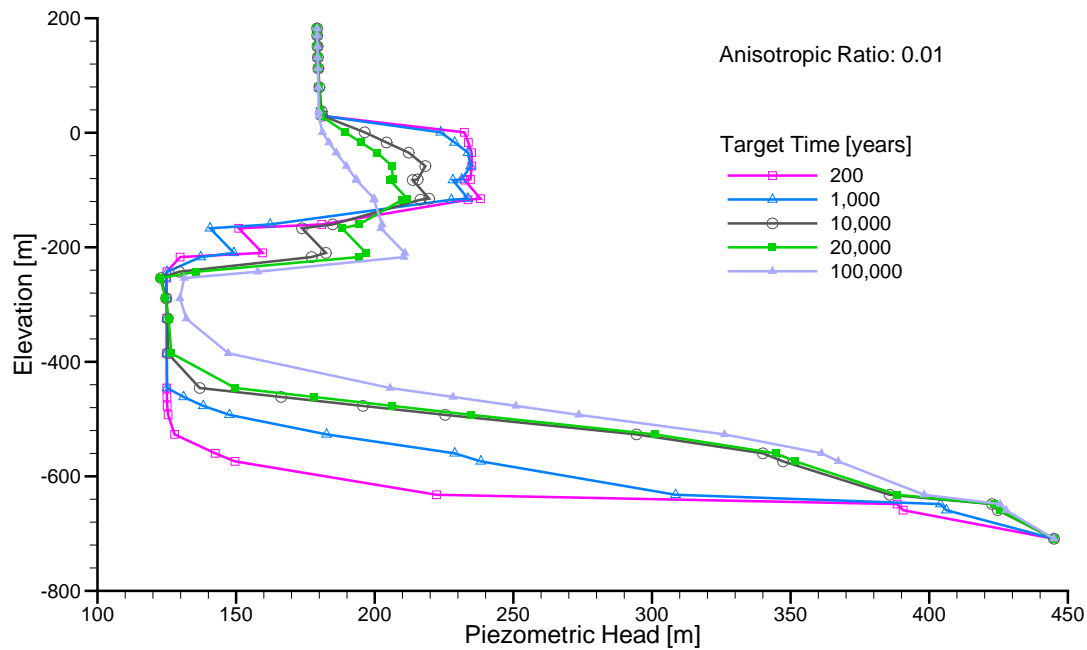


Figure J.3: Equivalent freshwater head profile at DGR-2 for base case parameters with anisotropy of 0.01; pressure support for the Cambrian and no pressure support for the Niagaran.

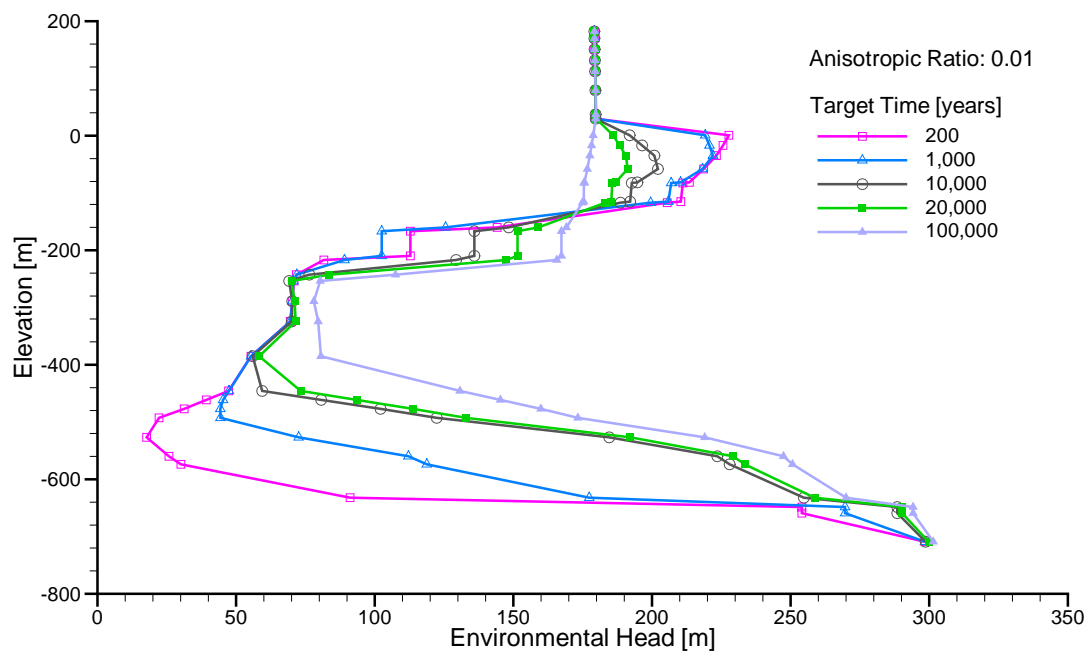


Figure J.4: Environmental head profile at DGR-2 for base case parameters with anisotropy of 0.01; pressure support for the Cambrian and no pressure support for the Niagaran.

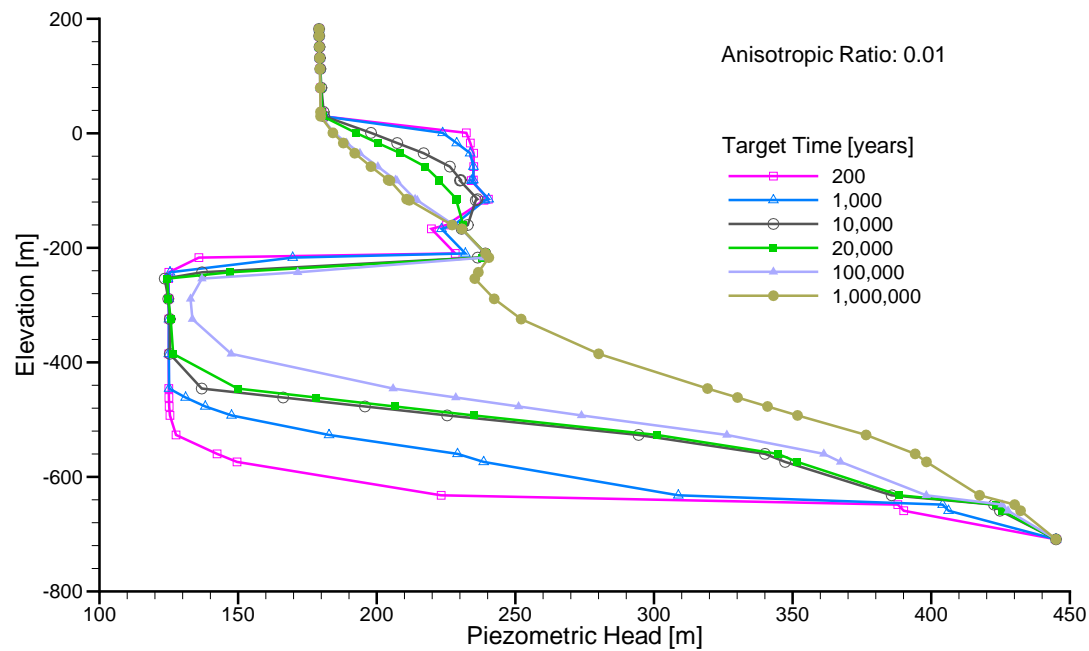


Figure J.5: Equivalent freshwater head profile at DGR-2 for base case parameters with anisotropy of 0.01; pressure support for both the Niagara and the Cambrian.

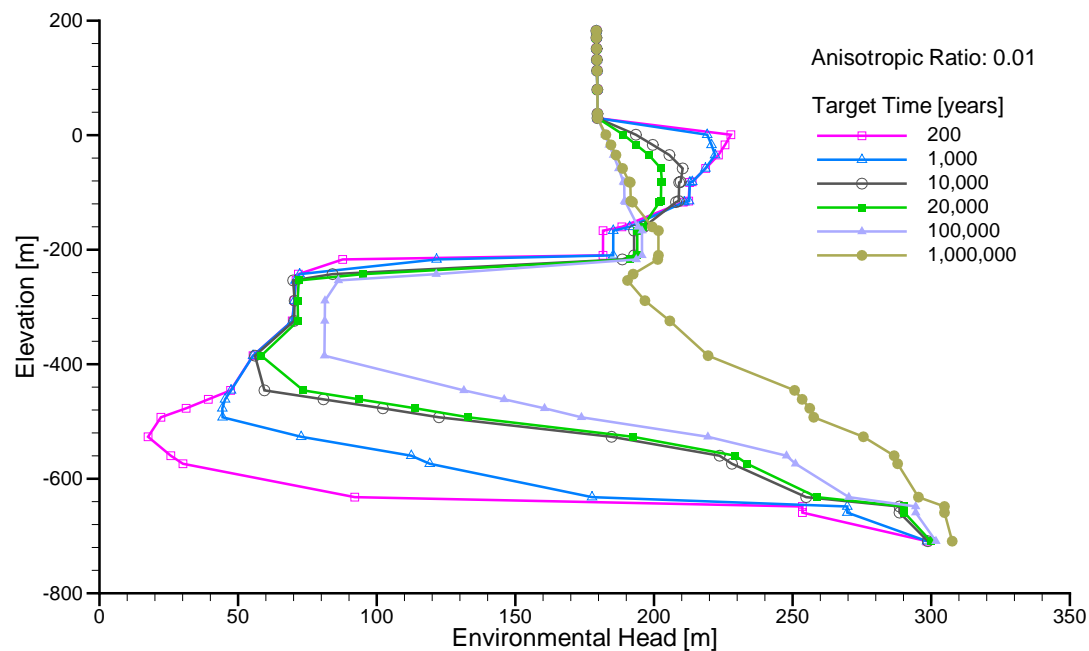


Figure J.6: Environmental head profile at DGR-2 for base case parameters with anisotropy of 0.01; pressure support for both the Niagara and the Cambrian.

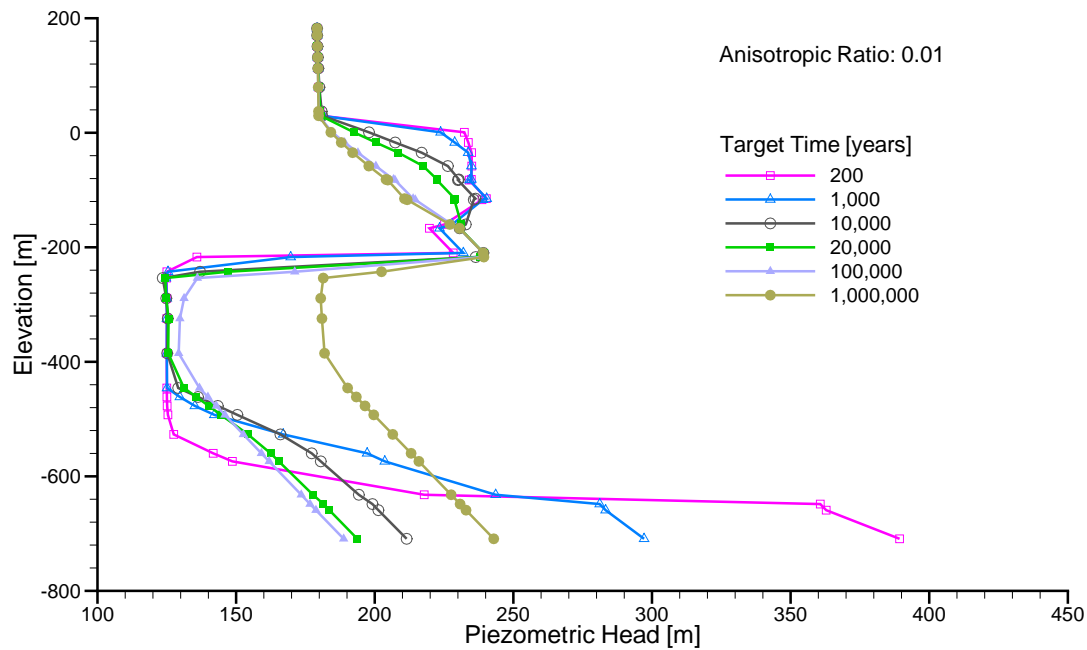


Figure J.7: Equivalent freshwater head profile at DGR-2 for base case parameters with anisotropy of 0.01; pressure support for the Niagaran and no pressure support for the Cambrian.

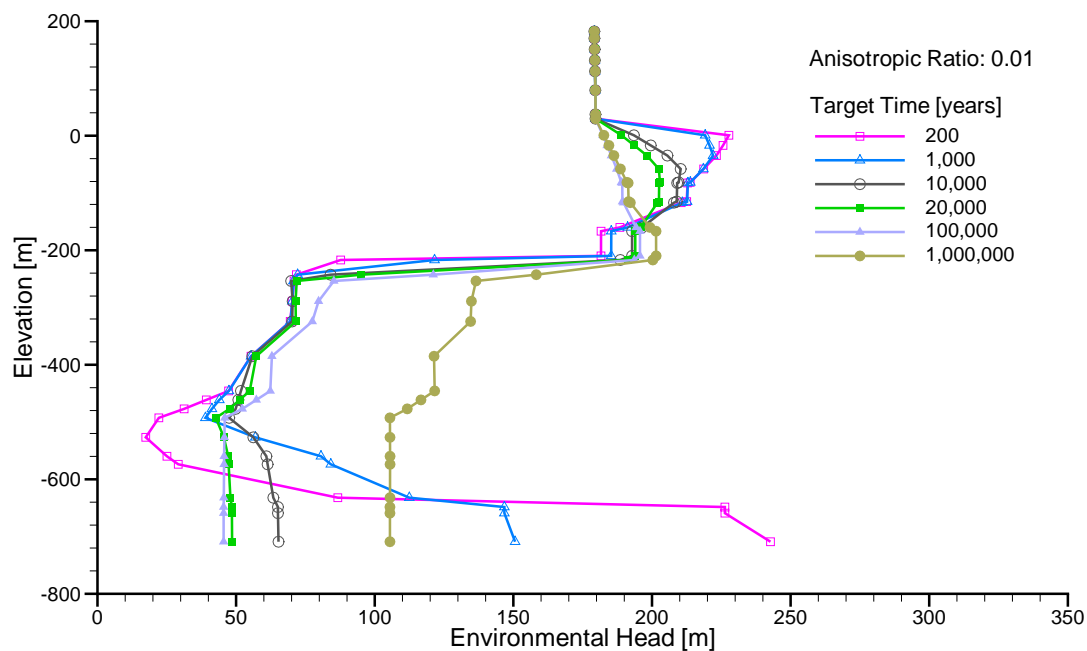


Figure J.8: Environmental head profile at DGR-2 for base case parameters with anisotropy of 0.01; pressure support for the Niagaran and no pressure support for the Cambrian.

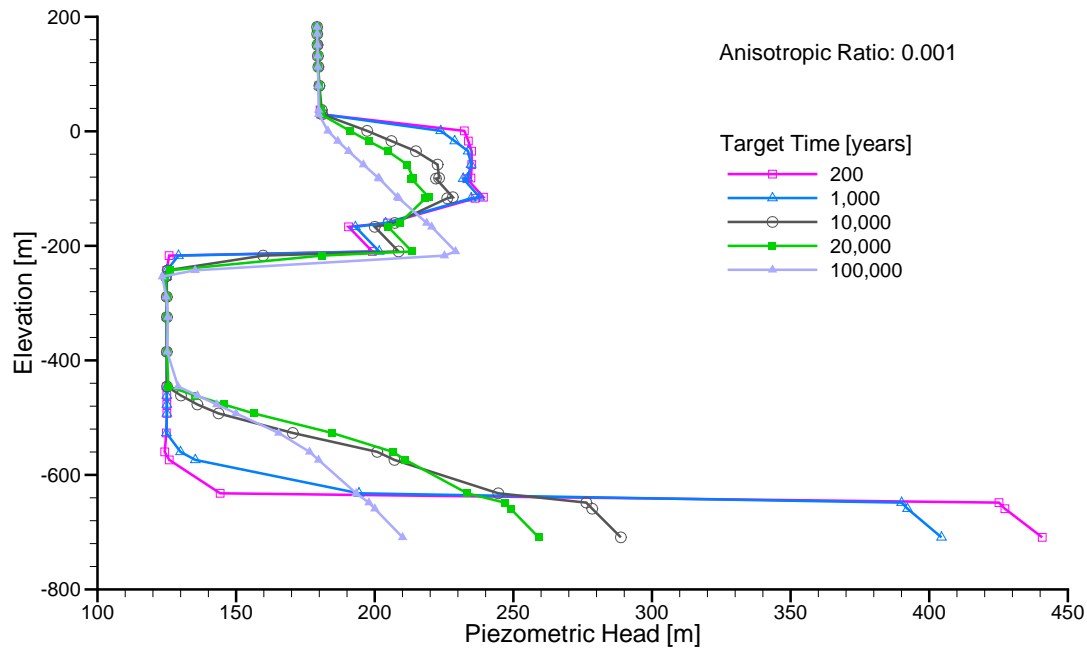


Figure J.9: Equivalent freshwater head profile at DGR-2 for base case parameters with anisotropy of 0.001; no pressure support for the Niagara or Cambrian.

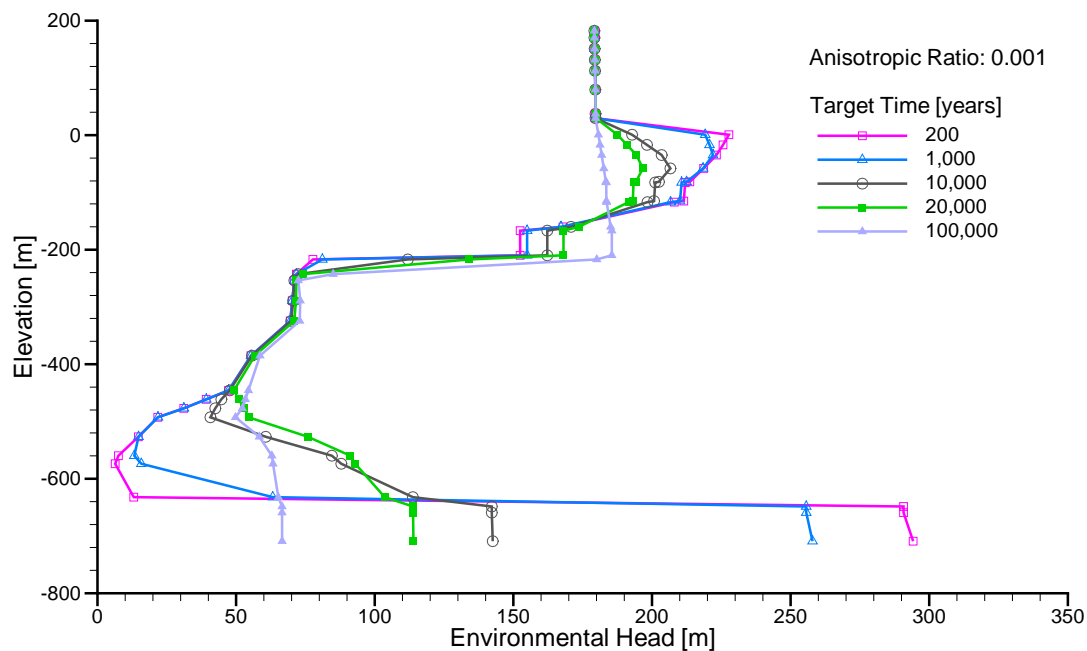


Figure J.10: Environmental head profile at DGR-2 for base case parameters with anisotropy of 0.001; no pressure support for the Niagara or Cambrian.

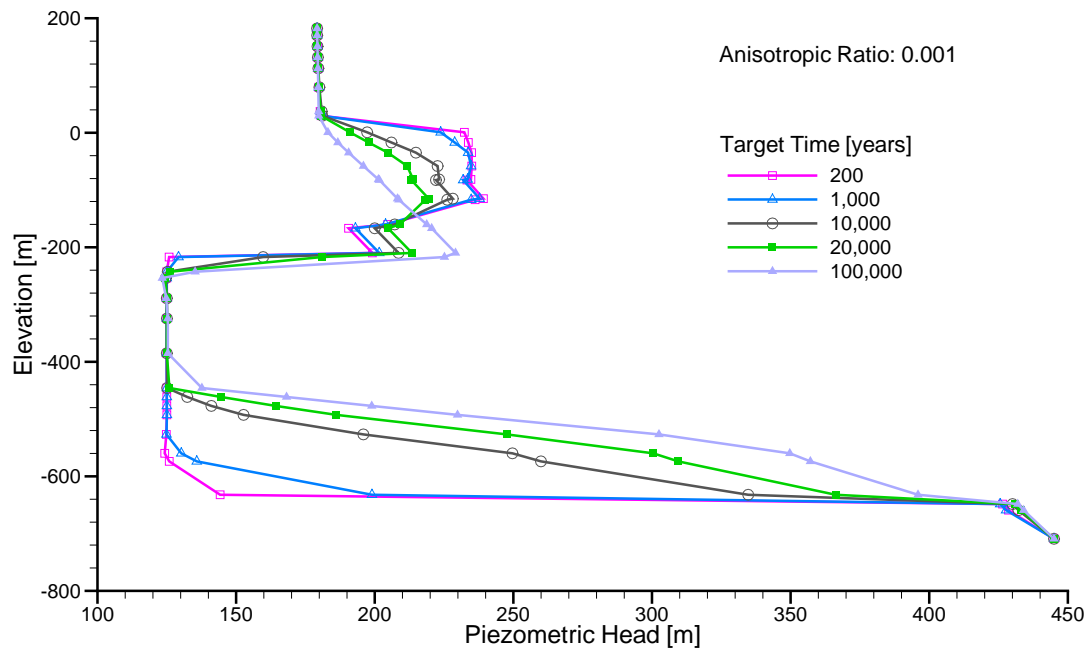


Figure J.11: Equivalent freshwater head profile at DGR-2 for base case parameters with anisotropy of 0.001; pressure support for the Cambrian and no pressure support for the Niagaran.

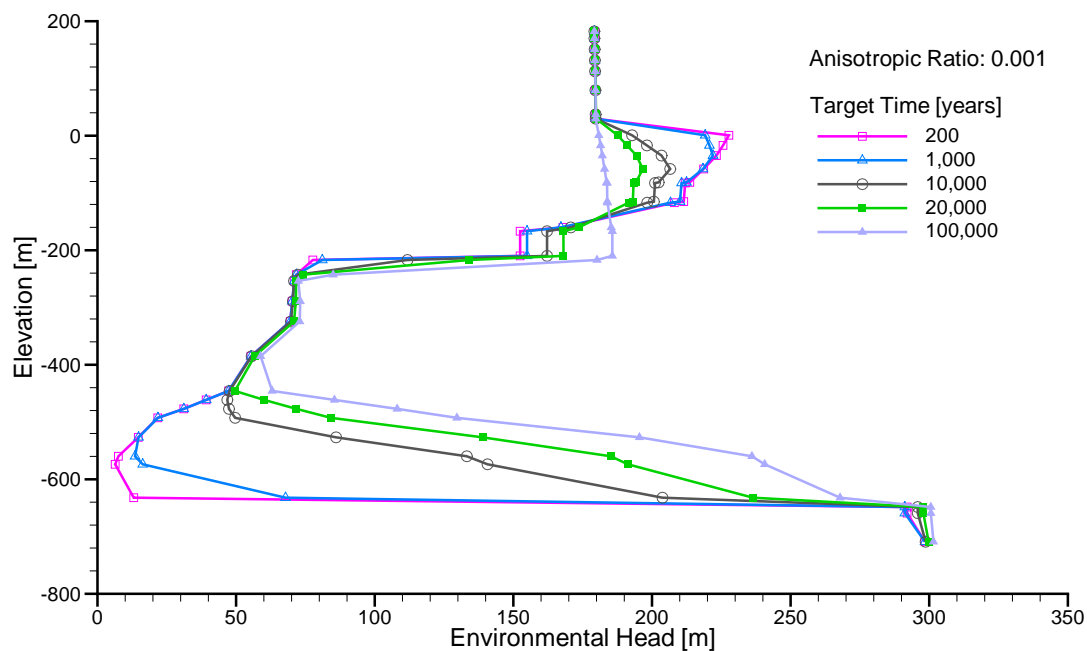


Figure J.12: Environmental head profile at DGR-2 for base case parameters with anisotropy of 0.001; pressure support for the Cambrian and no pressure support for the Niagaran.

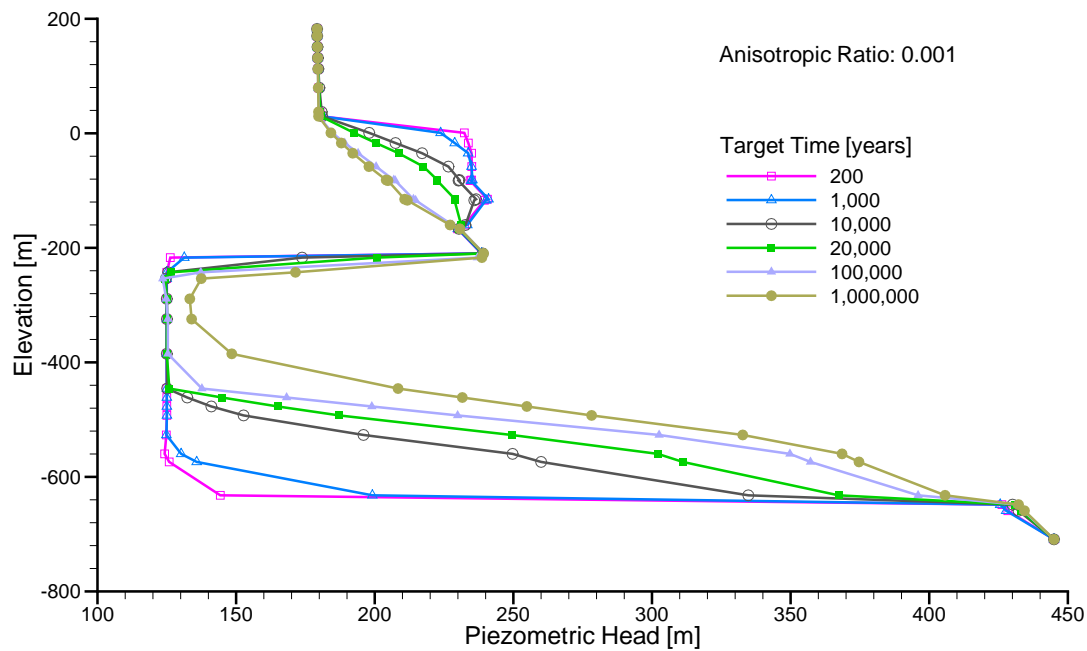


Figure J.13: Equivalent freshwater head profile at DGR-2 for base case parameters with anisotropy of 0.001; pressure support for both the Niagaran and the Cambrian.

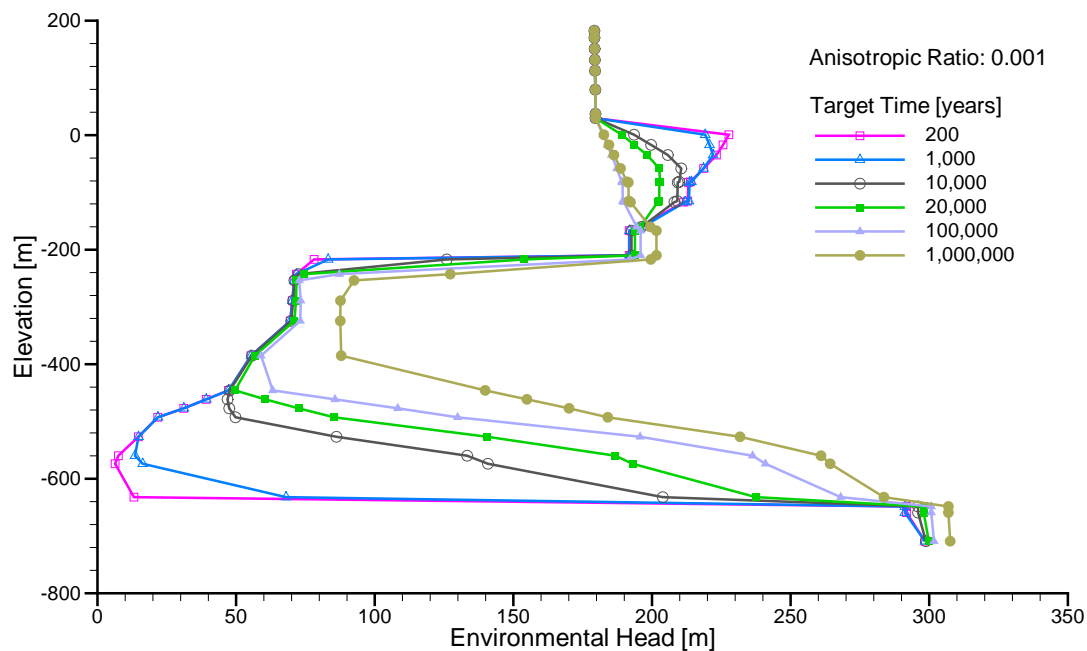


Figure J.14: Environmental head profile at DGR-2 for base case parameters with anisotropy of 0.001; pressure support for both the Niagaran and the Cambrian.

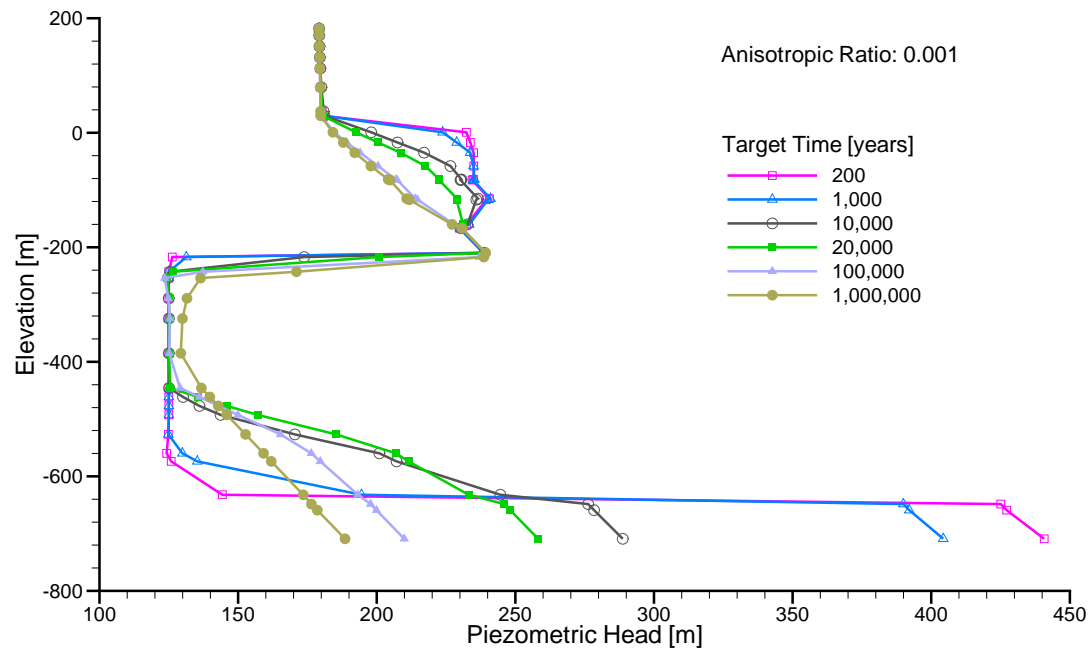


Figure J.15: Equivalent freshwater head profile at DGR-2 for base case parameters with anisotropy of 0.001; pressure support for the Niagaran and no pressure support for the Cambrian.

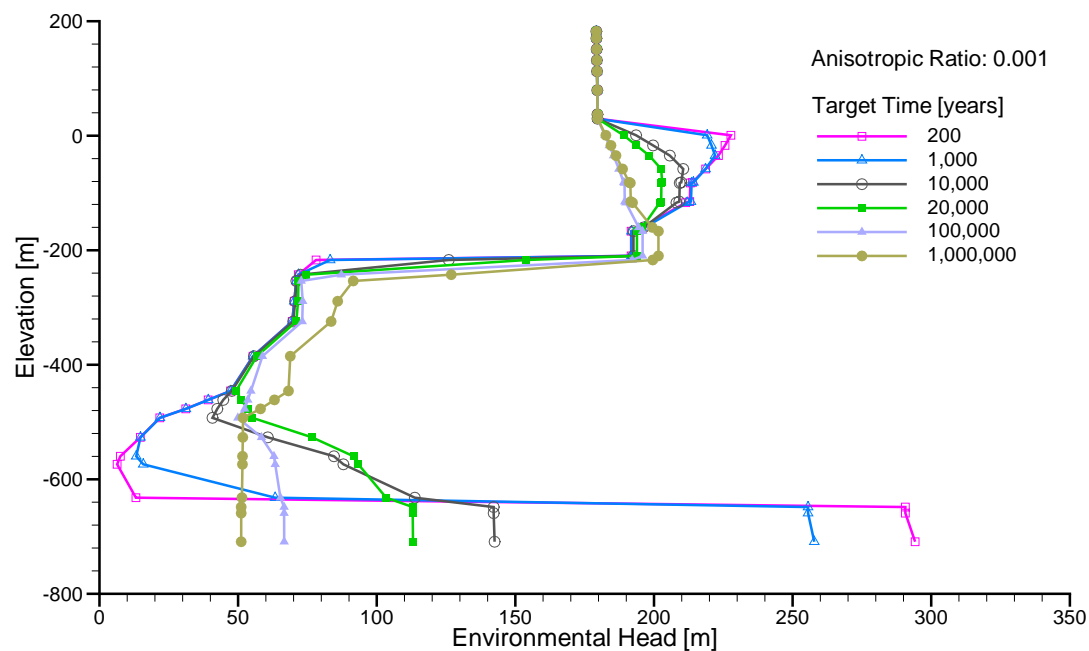


Figure J.16: Environmental head profile at DGR-2 for base case parameters with anisotropy of 0.001; pressure support for the Niagaran and no pressure support for the Cambrian.

